THE EFFECT OF BASE STOCK AND ADDITIVE PACKAGES IN AN AUTOMOTIVE OIL ON THE FRICTION AND WEAR BEHAVIOUR OF OVERHEAD CAMSHAFT AND FINGER FOLLOWER SYSTEMS

A THESIS SUBMITTED FOR THE DEGREE OF DOCTOR OF PHILOSOPHY

BY

JULIAN BENSON MSc

Department of Materials Technology
Brunel University

MAY 1987

CONTENTS

ABSTRACT

The introduction of overhead camshaft valve train systems some 25 years ago has resulted in improved engine performance and efficiency, this in turn however, has caused increased wear problems. In order to understand the tribological behaviour of overhead camshaft systems, test engines and dynamometer test methods have been extensively used. These are however, time consuming and expensive, a cheaper and quicker method of camshaft material and lubricant appraisal is therefore required and this has resulted in the design and construction of a simulative overhead camshaft test rig. A range of commercially available camshaft and follower materials have been tested using both a fully formulated and a mineral base equivalent. The most commonly encountered cam and follower wear failures of scuffing, pitting and polishing were reproduced.

Results showed scuffing wear to be associated with all of the camshaft materials using the mineral base oil under high load, boundary lubrication conditions. Scuffing also occurred under low load, mixed lubrication conditions using the case-hardened steel cam and chilled white iron follower combinations. The remaining cam materials, carbonitrided and induction hardened grey flake iron did not fail under similar test conditions due to the presence of free graphite in the microstructure. The fully formulated oil generally suppressed the onset of scuffing under all test conditions due to the presence of the zinc-dialkyldithiophosphate (Z.D.D.P) anti-wear additive in the oil.

Pitting failure was associated with the chilled white iron followers using the fully formulated oil under high load conditions. This failure could have been initiated by either a surface, sub-surface or stress corrosion mechanism. Analysis of this type of failure is complicated by the difference in both chill

depth and hardness and also the presence of cracks within samples prior to examination and testing. Standardisation of chilled white irons therefore needs to be carried out in order to understand fully the wear behaviour of such materials.

Polishing wear was associated with the fully formulated oil at low loads, and appeared to occur by a chemical reaction between the contacting surfaces and the additives present in the oil.

The use of the acetate replica technique proved a satisfactory method of analysing the change in surface topography of cam surfaces. Using the fully formulated oil the cam surface 'ran in' satisfactorily, by a process of plastic deformation and fracture, whilst the mineral base oil caused instanteous scuffing of the cam surface.

Once the surfaces had 'run in' satisfactorily by using either the additives in the oil or by a diamond lapping operation, the cams continued to run without scuffing in the mineral base oil under continuous, non stop test conditions. An intermittent, stop/start operating cycle however results in eventual scuffing due to additive film depletion and repeated surface interaction under boundary lubrication conditions.

From a range of 'new' materials tested for follower application the ceramics, with the exception of the toughened zirconia, exhibited the best wear characteristics using a case hardened steel cam as a standard and tested under mineral base oil conditions. The silicon carbide and sialon ceramics both exhibited a low frictional resistance and wear rate, whilst the metallic follower materials of cobalt and nickel base hard facing alloys and a ceramic fibre reinforced aluminium/silicon alloy all suffered some form of material

transfer against the steel cam, resulting in surface roughening and a correspondingly high frictional resistance.

CHAPTER ONE

1. INTRODUCTION

Valve train systems have been used for many years in both petrol and diesel engines, the design and utilization of materials for their construction are considered to be extremely important as they affect the performance and economics of the engine.

In recent years a change from the overhead pushrod to overhead camshaft valve system has brought about an improvement in engine efficiency and performance by the elimination of flexing and distortion of pushrods and their associated components. However, a review of the literature and the experience of those working in the automotive and oil industries has shown that problems are still encountered with the wear of these cam/follower systems. Even with the trend towards the use of overhead camshaft valve train designs which utilize finger follower actuating mechanisms, wear problems are still apparent. These wear problems are not fully understood, and are further complicated by metallurgy, lubricant chemistry and operating conditions, all affecting cam and cam follower performance.

Until recently the approach to the solution of wear problems in this area has been largely empirically based, and has accounted for the need to improve the understanding of the mechanisms of lubrication and wear that are responsible for tribological behaviour. A range of materials were selected for this study including steels and cast irons, enabling a preliminary but broad based investigation to be undertaken covering materials currently used in service, rig and bench tests. Also included in the study was the use of 'new' materials, brought about by

advances made in materials science research over the years. These include materials such as ceramics, oxyacetylene deposited hard-faced coatings and composite materials.

In this investigation interest has centered on the friction and wear behaviour of materials used in overhead camshaft and finger follower valve train designs. A practical approach to this study has been adopted and the lubricated wear tests reported in this thesis have been carried out under conditions which relate to those experienced in service.

The main aims of this investigation are to observe the effects of base stock oil and the additive formulation of automotive oil on the friction and wear characteristics of overhead camshaft and finger follower systems. Both conventional and new materials have been used to investigate specific areas of cam/cam follower wear behaviour such as 'running in' and the effect of lubricant chemistry on the satisfactory operation of such systems.

CHAPTER 2

2. LITERATURE REVIEW

2.1 Valve Train Types

2.1.1 Introduction

The modern high compression overhead valve engine has attained universal acceptance throughout the world. The valve actuating mechanisms used on this type of engine can be divided into two categories based on the camshaft location. The push rod - actuated system with the camshaft in the cylinder block, and the overhead system with the camshaft in the cylinder head.

2.1.2 Overhead Push Rod Mechanism

The push rod actuated mechanism consists of the camshaft located in the cylinder block. The camshaft actuates the valves by means of the lifter, push rod, and rocker arm. The rocker shaft supported in a bearing is mounted on the cylinder block and carries a row of rockers transmitting the motion from the top of the push rod to the end of the valve stem (Fig. 1.).

Due to large temperature variations, some provision for thermal expansion has to be included in the system. For this reason some engines employ mechanical valve lifters provided with a slight lash at the rocker arm. However, the latter can be a potential source of valve train noise and therefore hydraulic valve lifters have been

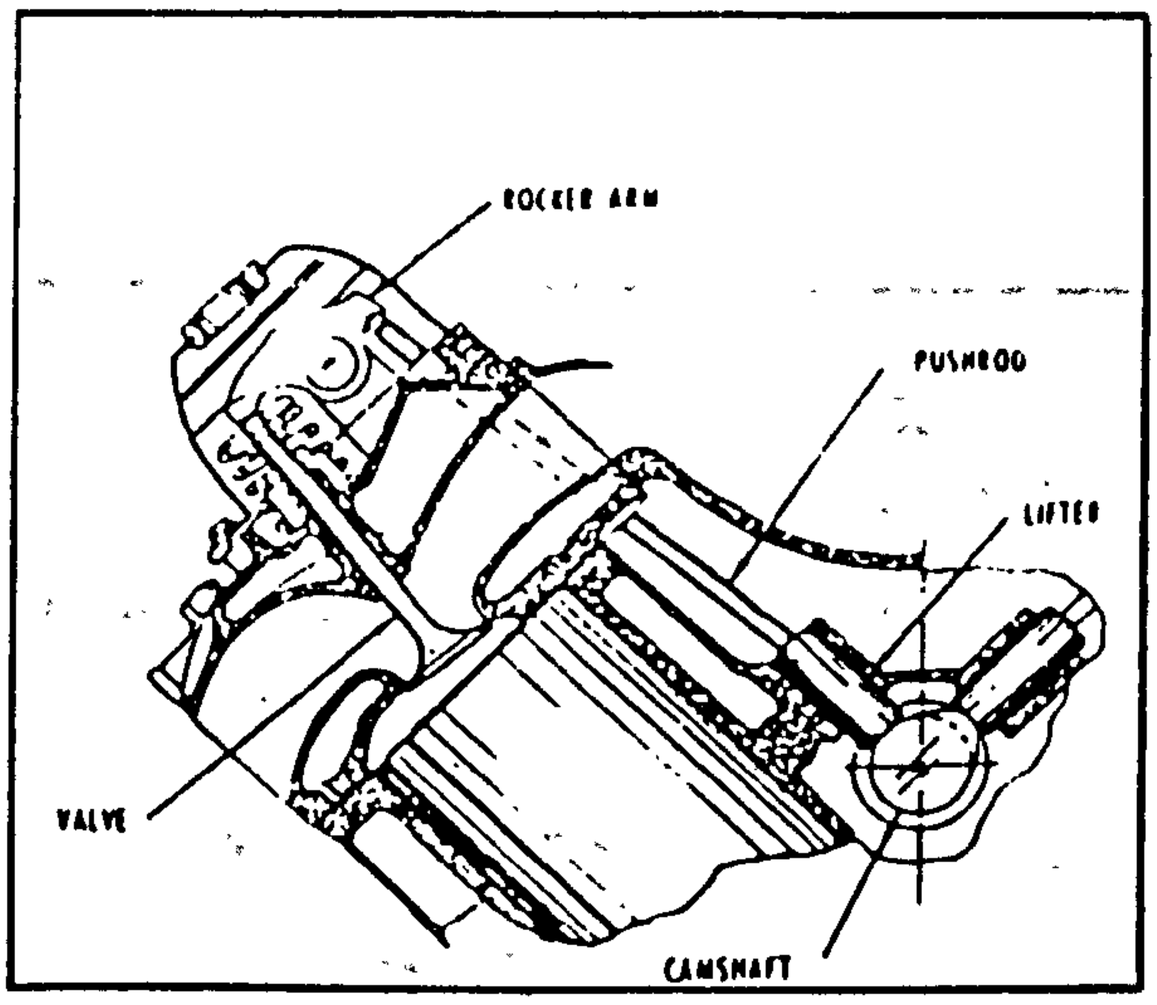

Fig. 1. TYPICAL PUSHROD-ACTUATED VALVE TRAIN

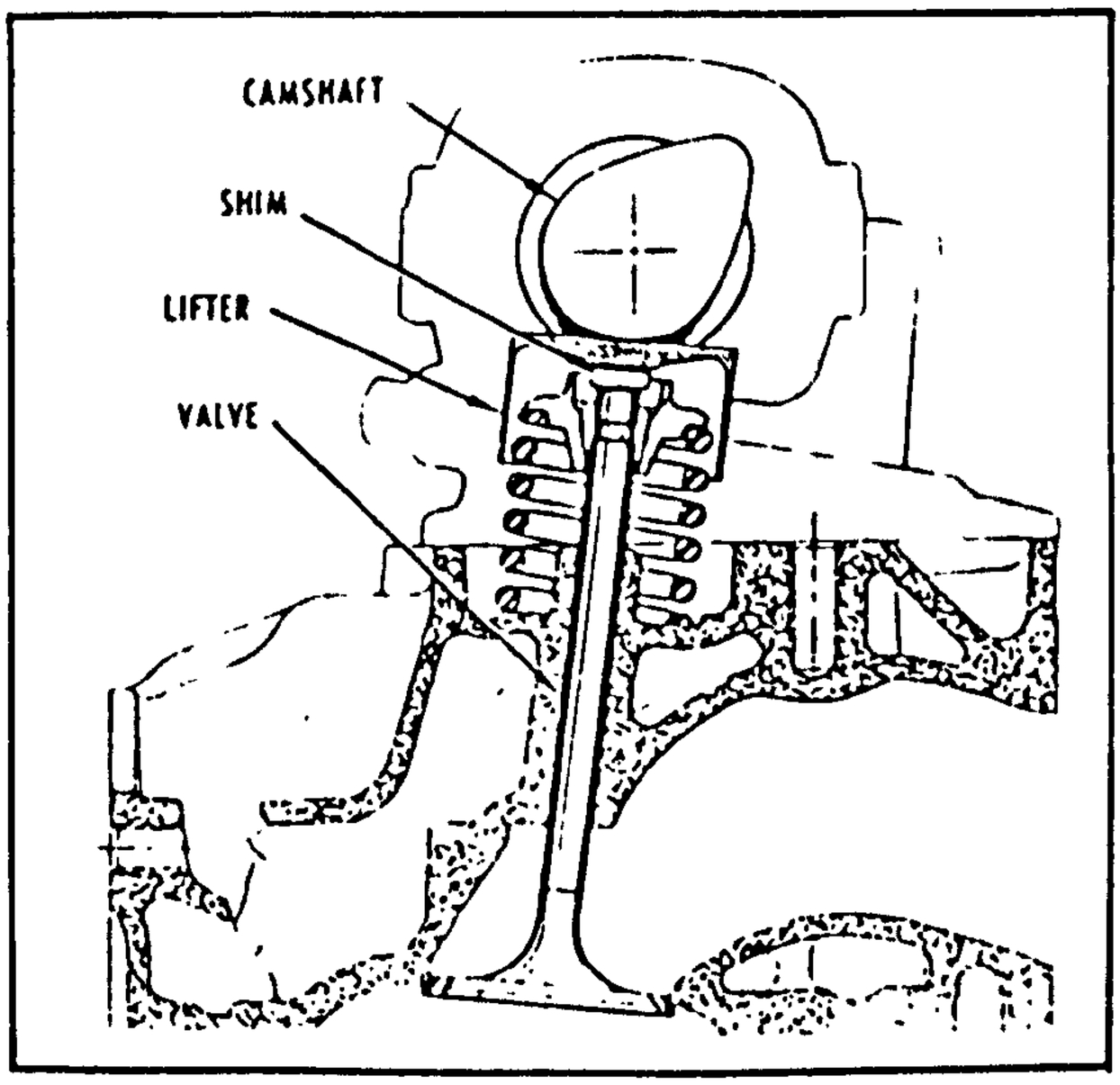

Fig. 2. DIRECT-ACTING OVERHEAD CAMSHAFT VALVE TRAIN WITH SHIM-TYPE LASH ADJUSTMENT

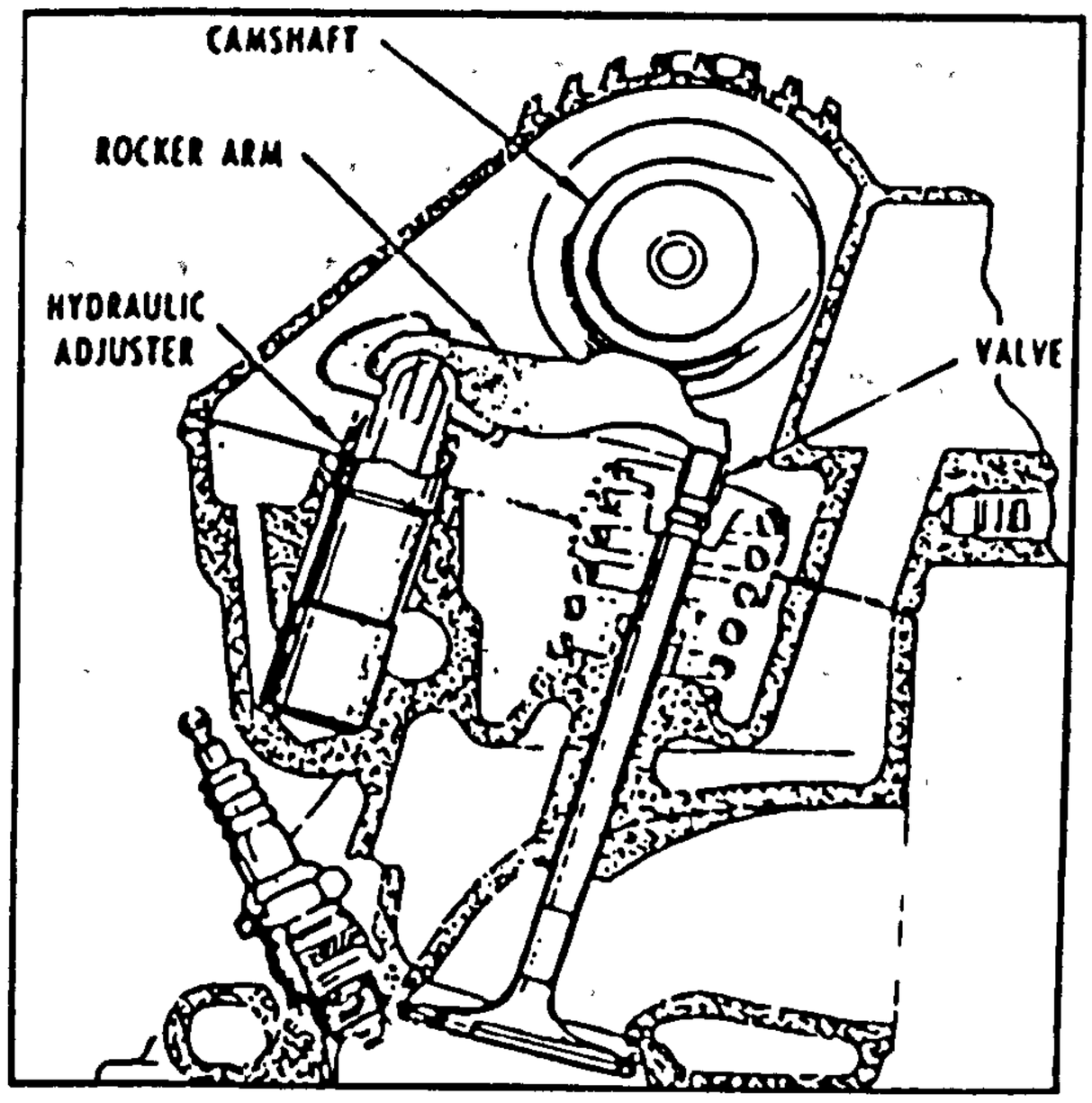

Fig. 3. ROCKER ACTUATED OVERHEAD CAMSHAFT

incorporated in some engines, thus compensating for thermal expansion as well as dimensional tolerances. Other factors that must be considered in the prevention of breakdown of such a system are the strength of the valve spring, required acceleration, deceleration and lift, choice of rocker (ratio of distance of rocker head to the two rocker ends) and adequate lubrication, particularly of the heavily loaded contact face. One of the most serious problems encountered was distortion of the long push rod, however, this was eliminated with the advent of short stroke engines using a shorter push rod or by arrangement of the camshaft in a location high up in the crankcase, thus reducing the distance travelled by the push rod.

2.1.3 Overhead Camshaft Mechanism

As an alternative to the use of push rods and their associated components, the overhead camshaft mounted in close proximity to the valves has many advantages. By eliminating a large number of components liable to flexing and unpredictable distortion under operating conditions, the overhead camshaft provides for a much greater consistency in timing and the desired requirement in regard to opening and closing periods and lift. Reduction of reciprocating motion inertia should also add to mechanical efficiency (Fig. 2).

The overhead camshaft allows a free choice in combustion space design. With a single shaft operating through suitable followers, the valves can be arranged either in a row similar to those in many push rod engines or at an angle in a hemispherical head, (Fig. 3). With two camshafts along the head the valves can be disposed at the desired angle without the use of long follower or cam levers. In this case the valve operation is

normally through inserted tappets with shim adjustment between the interior face of the tappet and the valve stem end. Other arrangements can be made where there is a single row of valves, in these engines all parts are brought out to one side of the head. There are also types having cam followers with the valves disposed at each side of the camshaft and in this case the followers are adjusted by the use of eccentric bushes on the follower shafts.

The principle advantage of the overhead cam over the overhead valve configuration is the increased natural frequency of O.H.C. valve trains, making possible the expansion of the operating ranges of an engine, this accounts for it's increased use in high speed engines. Other advantages include:-

1. An O.H.C. engine has fewer moving parts in the valve train, which permits the use of higher engine speeds.

2. The absence of push rods produces a valve train of increased stiffness. This in turn makes possible the following desirable characteristics:-

   a. Improved valve train durability.

   b. Reduced valve train noise level.

   c. More accurate reproduction of valve timings.

   d. The height of the cam quietening ramps can be reduced, improving idle quantity and lowering of hydrocarbon emission at idle.

3. The elimination of push rods and the mounting of the entire valve train on top of the cylinder head results in:

   a. Greater scope in the design of intake and exhaust ports, combustion chamber and valve arrangement for increased efficiency.

   b. A more symmetrical design of the cylinder block.

4. The adoption of a finger follower arrangement, allows the optimisation of the valve arrangement using only a single camshaft.

Disadvantages

1. It was thought that a direct change to O.H.C. would bring about a reduction in valve train weight(1). The use of direct acting overhead camshaft valve actuation reduces the effective valve train weight at the valve, compared to a push rod system, by about 5% at the maximum. However, depending on the type of follower used, the overhead camshaft may, in fact, incur a weight penalty of up to 35%. Only when a rocker actuated overhead camshaft mechanism is used does an appreciable weight saving of up to 20% occur(2). The effective valve train weight of an overhead camshaft mechanism therefore depends on the particular design, and the use of such a system does not necessarily result in an inherent weight reduction of the valve train.

2. Cams and tappets can be considered as the most sensitive working parts of an internal combustion engine, relying on satisfactory lubrication from crank case oil for efficient running. With an overhead camshaft arrangement these parts are extremely difficult to lubricate especially as engine speeds increase, hence the problem of wear becomes even more apparent.

2.2. Cam and Follower Materials and Method of Manufacture

There are a wide range of materials in current usage for both camshaft and cam followers. A survey carried out by Eyre and Crawley[3] showed that for the European market, camshaft and cam follower materials are listed as: chilled cast grey iron, hardened grey iron, hardened steel, hardened nodular and malleable iron, and carbonitrided grey flake and spheroidal graphite irons. Table 1 shows the materials and treatments commonly used for camshaft and cam follower components.

For cast camshaft production, green sand moulding is generally utilised although some shell moulding is used. For chilled camshafts, casting is carried out against iron chills to achieve a hardness range of 45-55 Rockwell Scale 'C' around the cam nose.

Material developments have included the use of grey iron with phosphorus contents of up to 0.7%. The matrix consists of hard iron-phosphide eutectic in pearlite with a fine dispersion of graphite brought about by secondary graphitisation. Iron containing controlled amounts of chromium and molybdenum are also used, these produce carbides, which improves wear resistance.

Nodular and malleable camshafts are cast in the same way as grey iron but with an added complication of a more expensive malleabilizing treatment carried out on the latter. Nodular and malleable irons are mainly found in O.H.C. systems where the use of a split bearing enables a larger cam nose radius to be used.

The most common materials used for cam follower component production are also cast irons, this is due to their ease of casting making the more complex shaped finger followers easier to produce particularly when compared to standard steel bucket followers which are machined from round bar stock.

2.3 Surface Treatments

The aim of surface treatments is to modify the chemical, mechanical and topographic characteristics of the surface so as to achieve the optimum conditions for wear resistance. The various types of surface treatment can be divided into two separate categories; those that have a life shorter than the life of the component, these treatments are commonly known as "running in" coatings and as the name suggests are concerned with successfully 'running in' and conforming of contacting surfaces to aid the satisfactory operation of engineering systems. The other coatings are those expected to last for the full life of the component. There is no clear distinction between the two groups and both treatments are often applied to a component, i.e. a gear with a carburised long life surface with a short life phosphate coating.

2.3.1 Short Life/'Running In' Treatments

These treatments involve the interposing of thin adherent layers between surfaces. They have a limited life span due to conditions of continuous movement and contact, causing rapid wear and eventual removal unless some form of renewal mechanism is introduced. The two most important instances of film/coating renewal is the use of 1) Oxide films on metals [4,5] and 2) the reaction between metals and E.P. additives in lubricating oils [6]. Limited life coatings with no renewal mechanisms, typically include phosphating and chemically formed oxide layers on steel and cast iron surfaces.

2.3.1.1 Phosphate Coatings

Phosphate coatings are used to reduce wear and prevent corrosion on cast iron and steel surfaces. These coatings are usually applied to the surfaces of contacting machine component such as gears, cams and tappets and piston rings[7]. Many coatings consist primarily of manganese phosphate crystals, with the composition, size and morphology of the crystals dependent in the operational conditions of the process. The resultant coating takes the form of channels and pits which improve oil retention thus assisting improved lubrication characteristics.

2.3.1.2 Oxide Films

Naturally formed oxide films are regarded as thin adherent layers interposed between surfaces. Wear resistant oxide films on steels for example, can be formed by both chemical and electrochemical techniques. A thick, crack free oxide can be produced on steel by annealing at 800 - 900°C in a weak oxidising atmosphere[8,9],

alternatively heating in steam between 260°C - 400°C will again produce a thick, well adhering oxide film commonly known as the ferrox treatment.

2.3.1.3 Thin Metal Films

These thin films are formed by electro or vapour deposition processes and are used to combat wear during running-in. The tin plating of both cast iron and aluminium alloy pistons is a prime example of such deposits with a typical thickness of 1-2 microns.

2.3.2 Long Life Treatments

Surface treatments having long life characteristics can be divided into three main areas:-

A) Surface Hardening - without changing the composition e.g. flame hardening and induction hardening processes, usually applied to medium carbon steels and cast irons.

B) Diffusion Treatments - the surface layer composition is changed by the diffusion of elements such as carbon, nitrogen, silicon, sulphur and boron into the surface. These diffusion processes are usually of a high temperature nature invariably requiring a specialised follow up heat-treatment.

C) Direct Application Coatings - applied by such techniques as electrodeposition, welding and metal spraying.

2.3.2.1 Surface Hardening Without Composition Change

Plain carbon, alloy steels and cast irons with combined carbon contents of over 0.35% can be surface hardened by flame and induction

hardening[10,11,12]. The surface is rapidly heated into the gamma phase region and quenched before the heat soaks through to the core of the component. The final result is a hard martensitic surface with a tough core. The volume expansion associated with the martensitic transformation induces compressive stresses in the surface layers thus improving fatigue and stress corrosion crack resistance.

2.3.2.2 Diffusion Treatments

One of the most widely used methods of improving the wear resistance of metals is by the diffusion of elements into the surface. The diffusion processes are of an atomic nature, by either interstitial or substitutional mechanisms. An example of substitutional solid solution hardening is provided by the diffusion of silicon into iron[13]. The silicon atoms replace iron atoms in the crystal lattice and introduces distortion into the lattice thus interfering with the slip processes and hardens the metal. On the other hand the diffusion of carbon or nitrogen into iron takes place by an intersitial mechanism. The solubility of these elements in ferrite however is extremely low, thus carbide or nitride compounds are soon precipitated. To promote the precipation of these hard carbides in steels elements such as aluminium, titanium and chromium are added to the steel during casting.

2.3.2.3 Carburization

This process is normally carried on steel with carbon contents less than 0.2%. The alloy in the austenitic condition is exposed to highly reducing conditions in the presence of carbon where well over 1% carbon can dissolve into the austenite. The rate of uptake and penetration of carbon depends mainly on the carburizing atmosphere,

the time and temperature of the operation and the composition of the steel. Diffusion rates increase markedly with temperature so diffusion times giving the same thickness of diffused layer decrease as diffusion temperatures increase. The thickness of diffused layers lies in the region of 0.25 to 2mm. After carburising the component is allowed to cool slowly thus retaining the softness of the core. Hardening is carried out by re-heating the component to about 780°C, this temperature being austenitic for the high carbon skin but not the lower carbon core. Quenching is then carried out so that the skin becomes martensitic leaving the core tough and ductile[10].

2.3.2.4 Nitriding

Traditional nitriding involves heating steels of special compositions in an atmosphere of cracked ammonia at about 550°C, and produces a fine, well dispersed, precipitate of hard nitrides in the surface layers. The formation of these nitrides is enhanced by the addition of elements in the steel with a high affinity for nitrogen such as molybdenum, vanadium, aluminium, chromium and titanium[10]. Nitrided layers are intrinsically hard and do not require quenching to develop their hardness. This factor coupled with the relatively low temperature required for nitriding, means that components suffer little distortion and therefore do not require additional machining after treatment[14]. Nitrided layers have also been found to have a greater resistance to thermal softening than carburized layers and therefore have a higher scuff resistance.

2.3.2.5 Carbonitriding

In this process carbon and nitrogen are taken up into the surface layers by gaseous diffusion. Carbonitrided layers are obtained by mixed about

10% ammonia with a normal carburizing gas at around 900°C. The proportion of nitrogen uptake decreases with an increase in temperature, the resultant surfaces are enriched with carbon and nitrogen resulting in improved resistance to adhesive wear compared to conventionally carburized surfaces. These mixed layers have a greater thermal stability giving a greater resistance to softening at elevated temperatures.

2.3.2.6 Sulfiniz Process (Soft Nitriding)

The sulfiniz treatment is carried out essentially in a nitriding salt bath into which an incompletely oxidized sulphur compound (sodium sulphide) is added[15]. The treatment is carried out at around 570°C for periods between 15 minutes and 2 hours. This gives a thin sulphur rich layer on top of a carbonitrided surface capable of increasing wear resistance, in particular, wear during running in. The sulfiniz process can be applied to a wide variety of ferrous alloys including mild steel, stainless steel and cast irons[16].

2.3.2.7 Tufftride Process

In this process the nitriding action of cyanide-based salt baths is accelerated by blowing compressed air through them. The process is similar to the Sulfiniz treatment except that it does not give a sulphur-rich surface depth range, instead, a thin-non-brittle surface layer of carbon bearing epsilon iron nitride is produced. The tufftride process can be applied to the same range of alloys as the sulfiniz process, however both these processes suffer a major disadvantage in that the operating temperatures of 550-600°C tend to soften hardened layers such as case-hardened, and if Sulfiniz and Tufftride are used alone, the

wear resistant surface skin often collapses under heavy load due to lack of support from the tough core. This is overcome by the use of the Noskuff Process[16,17].

2.3.2.8 Noskuff Process

This process is similar to Tufftriding with the exception of the operating temperature, of around 760°C followed by a quenching operation. This enables the carburized surfaces to retain their hardness and provides a greater depth of hardening allowing corrective grinding without the removal of the wear resistant layer.

2.3.2.9 Diffusion Layers - Ferrous Materials

The wear resistance of ferrous materials can be significantly improved by the diffusion of other metals into their surfaces. Some of these metal diffused layers can have specific advantages in overcoming both wear and corrosive conditions, an example being siliconizing[18] and chromizing[19,20]. In both processes the components for treatment are exposed to gaseous chlorides at temperatures of around 1000°C, silicon diffusion due to the presence of silicon carbide and chlorine or silicon chloride vapour and chromizing using chromium and chromous chloride.

2.3.2.10 Thermally Deposited Coatings

Coatings such as these can be applied by welding or spraying techniques and are primarily intended for use in the wear resistance of areas such as earth moving equipment[21,22,23,24,25]. These coatings however, cannot be laid down to fine tolerences and an expensive grinding operation usually follows. Nevertheless, these coatings are often used to build up worn surfaces and resist wear at high temperatures.

2.3.2.11 Electrodeposited Chromium

Electrodeposited wear resistant chromium more commonly known as hard chromium is a directly deposited chromium hydride coating in thicknesses ranging from 0.075 to 0.75 mm[10,26]. This differs appreciably to the decorative chrome plate commonly used, and has an as plated hardness of around 800 Hv. In order to enhance the lubrication characteristics of the chrome plate on such components as cylinder liners and tappet faces the plated surface is treated in some way to make it porous enabling oil retention to occur. An etching process can be carried out to produce this surface or alternatively techniques such as the Van der Horst or the Honey Chrome processes can be used. New processes such as plasma-sprayed chromium piston rings have found great success due to their inherent porosity which leads to improved oil retention.

2.4 New Materials

Improvements in Materials Science Research over the past 10 to 20 years has lead to a steady increase in the use of new materials for the prevention of wear in standard engineering systems, including the internal combustion engine (I.C.E.), both diesel and petroleum fuelled. These materials are both metallic and non-metallic and also combinations of the two.

Considerable development has occurred in utilising wear resistant coatings on cheap bulk materials. Processes such as arc, plasma and vapour deposited hard facing coatings are in current usage today.

Ceramic materials based on silica and alumina have become increasingly popular in the I.C.E. since the mid 1960's due partly to government legislation concerning engine emission standards, and improvements in ceramic technology and analytical design parameters. This has lead to the use of ceramics under severe environmental conditions[27,28,29]. The ultimate goal for designers and engineers being a fully adiabatic engine which does not require a conventional cooling or lubrication system[30]. Cummins Engineering Co in the U.S.A. have been involved in a joint project with the Propulsion Systems Division of the U.S. Army Tank Automobile Research and Development Command (TARADCOM) to produce an adiabatic diesel engine for use in the M60 series armoured tank.

Research into the combination of both metallic and non-metallic materials has resulted in advances in such processes as spray coated ceramics and more importantly advances in composite materials technology. A typical example of such a composite material is the ceramic fibre reinforced aluminium silicon alloy which has potential for piston crown applications in the I.C.E.

The area of new materials is indeed vast, the techniques and composition of these material conversion processes are numerous and are changing and becoming improved day by day. A resume of all new materials available and techniques currently under development would be virtually impossible to conduct within the scope of this thesis, therefore, only the new materials utilized for this research programme will be discussed in brief. These materials being:-

Hard face coatings	-	cobalt and nickel based
Ceramics	-	reaction sintered silicon carbide, sialon and partially stabilized 'toughened' zirconia.
Composite materials	-	ceramic fibre reinforced aluminium/ silicon alloy.

2.4.1 Hard Faced Coatings

With the present trend in increasing costs and shortages of strategic metals, protective coatings or facings are finding increasing usage in such applications as earth moving equipment and high temperature automotive components to improve wear and corrosion resistance. A typical example of these hard facing materials are the stellite alloys, first developed by Elwood Haynes circa 1900. These materials are cobalt based consisting initially, of a simple binary system with the addition of chromium, modified later by the additions of tungsten and/or molybdenum[31]. The price of cobalt has risen dramatically in the last few years however, making these popular hard facing alloys increasingly expensive. An alternative to these alloys are nickel rich hard facing coatings based in on the nickel-chromium solid solution with the additions of boron and silicon to lower the melting point. Carbon is also added to the alloy to increase carbide content by reaction with the chromium[32].

Both of these hard faced coatings can be applied by a variety of methods. Techniques such as metallic arc, plasma, gas and laser depositing are readily used to form and 'build up' worn component surfaces such as exhaust valve seats in the internal combustion engine. Their excellent wear and corrosion resistant properties are attributed to the large carbide networks present in the matrix.

2.4.2 Ceramics

2.4.2.1 Reaction Sintered Silicon Carbide

The sintering temperature required to form conventional silicon carbide ceramic powders is in excess of 2200°C, thus proving difficult and extremely expensive. This is overcome by a process know as reaction sintering, allowing temperatures of around 1400°C to be used. In this process a compacted body of α-SiC and graphite powder is heated in contact with liquid silicon, which impregnates the body converting the graphite to β-SiC which bonds the original alpha grains. With sufficient porosity present in the body, to accommodate both the volume change on reaction and cause complete silicon impregnation, a body of zero porosity can be obtained, the result and structure being areas of free silicon and α SiC grains in a β-SiC matrix[33].

The three key properties of reaction sintered silicon carbide in the field of engineering ceramics are it's resistance to high temperature, thermal stress/thermal shock, high temperature corrosion resistance in oxidising atmospheres and excellent wear resistance. Typical applications include fuel tubes in advanced gas cooled nuclear reactors, gas turbine components and non-lubricated bearings.

2.4.2.2 Sialon

The sialon range of ceramics are based upon silicon nitride Si_3N_4, the difference being the substitution of various elements in the ceramic powder mixture before processing. The main elements present in sialons are Si, Al, O_2, and N. The standard composition of silicon nitride is changed by the substitution of some of the silicon present with aluminium and some of the nitrogen present with oxygen, the final structure becomes $Si_3N_4 + Al_2O_3$ [34]. The presence of these elements

is thought to improve both fabricating and physical properties, thus proving superior properties to the already well estabilished silicon nitride ceramics for high temperature engineering and wear applications.

2.4.2.3 Partially Stabilised 'Toughened' Zirconia

Zirconia ceramics based on Z_rO_2 and stabilised using oxides such as M_gO, CaO and Y_2O_3 have found increasing use in wear resistant applications including use in the internal combustion engine. Zirconia alone exhibits three well defined polymorphs: monoclinic, tetragonal and cubic phases[35].

The temperatures at which these phase transformations occur is dependent upon the stabilising oxide used. The important feature of these ceramics is the tetragonal-monoclinic transformation which is associated with a large volume change (3-5%) causing cracking of individual particles in zirconia phases, the addition of these stabilising elements eliminates this volume change thus producing a fully stabilized ceramic. A satisfactory compromise is reached if an intermediate condition is adopted, thus producing a partially stabilized ceramic with, as will be explained, superior mechanical properties. If controlled, the tetragonal - monoclinic transformation helps to induce both directly and indirectly a toughening effect, thus improving the mechanical properties in particular fracture toughness, K_1C. This occurs by two mechanisms:-

1) Micro-cracking

Micro-cracking around ZrO_2 particles during the transformation, thus diverting and nullifying any external crack growth.

2) Stress induced transformation toughening

If for example the ZrO_2 is finely divided, zirconia particles can be retained in the metastable tetragonal form. The toughening mechanism arises due to the stress induced transformation of the metastable tetragonal particles to the monoclinic form under the action of external crack movement within the structure. The high tensile stresses induced at the crack tip causes this stress induced martensitic type transformation, thus forming compressive stresses around the transformed particles and arresting crack growth[36,37].

2.4.3 Composite Materials

2.4.3.1 Ceramic Fibre Reinforced Al/Si Alloy

The use of cast aluminium for pistons has frequently met with problems of ring sticking within the top ring groove of the piston body. This problem is alleviated by reinforcing the aluminium/silicon matrix with fibres, typically Titanate $K_2O\ (T_1O_2)_6$ and Pitch Carbon. Superior results however have been achieved by the development and subsequent use of ceramic fibres in the matrix giving excellent wear and seizure resistance against cast iron[38]. In addition, improved thermal conductivity and high temperature strength has also resulted giving increased performance without substantial rises in manufacturing costs. It is the considerable improvement in wear resistance however, that is leading to further research into the use of such materials for different component applications within the internal combustion engine.

2.5 Camshaft Requirements

The basic requirements of the camshaft material is to be compatable

with the follower material under operating conditions. With increase in engine power and speed, cam operating conditions have become more arduous. Increases in power have resulted in steeper cam ramps and smaller cam nose radii, resulting in higher contact stresses between cam and follower. Increases in speed require higher spring loads to offset increased valve train inertia loads, this has resulted in higher contact stresses when the engine is running at low speeds.

2.6 Lubrication

The purpose of introducing a lubricant into a system is to separate the moving parts with a film having a low shear resistance in an attempt not only to minimise friction and wear, but to perform a secondary function by removing heat and harmful wear debris away from contacting surfaces. The regimes which exist under highly loaded fluid lubricated conditions may be classified under four basic headings[39]. Boundary, mixed, elastohydrodynamic and fluid film.

Between 1900 and 1902, Stribeck[40], performed a series of experiments on the friction of sliding and rolling bearings measured as a function of load, speed and oil temperature. The result is the now familiar Stribeck curve representing the general characteristics of lubricated moving surfaces as a function of viscosity, normal load and velocity as seen in Fig. 4. This curve however does not clarify the effect of load and speed variables under conditions found in automotive valve train systems, in particular isothermal conditions controlled by heat generation at the cam/tappet interface. Thus the schematic diagram shown in Fig. 5, attempts to elucidate this effect and its subsequent consequences.

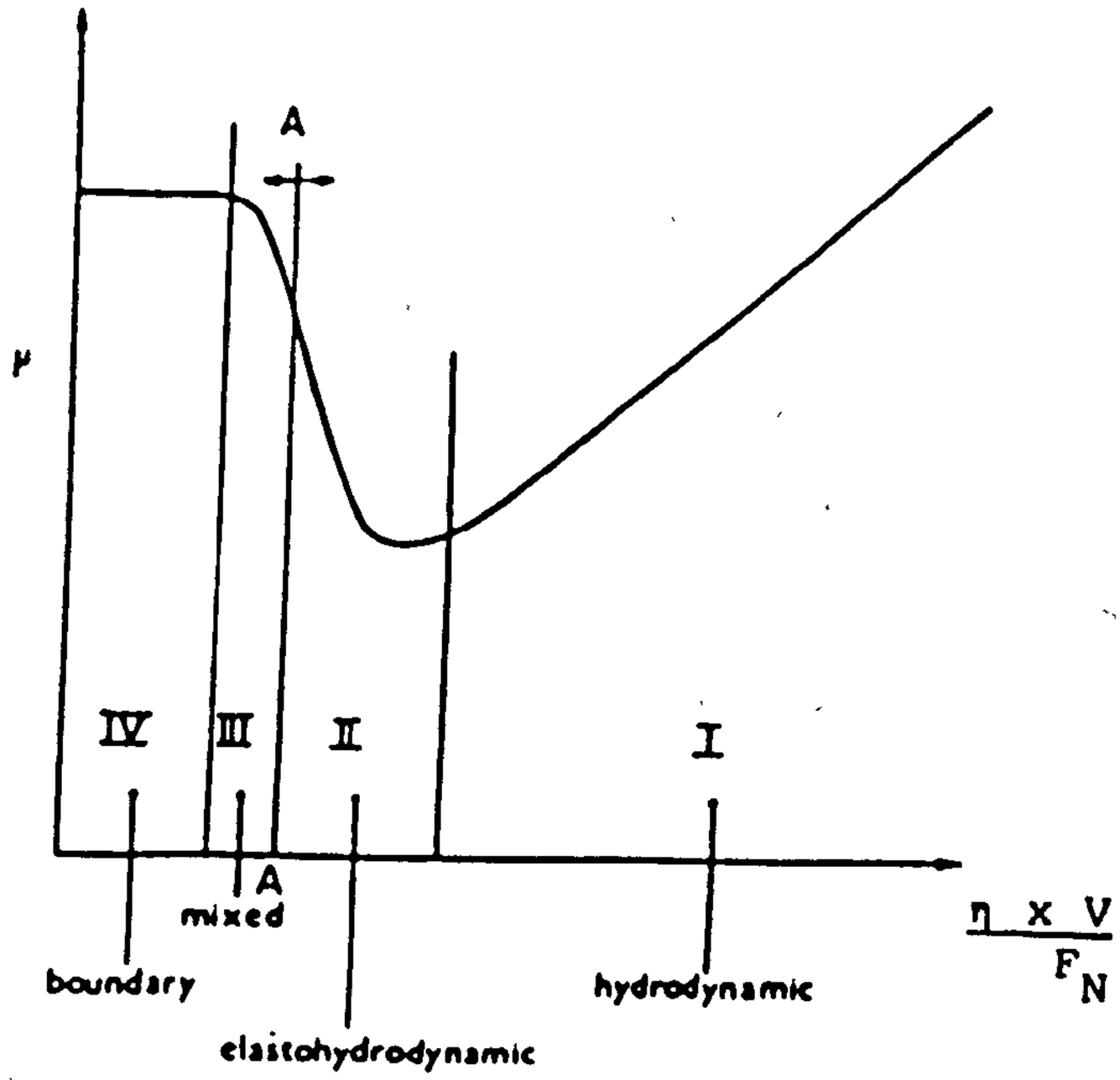

Fig. 4. LUBRICATION REGIMES

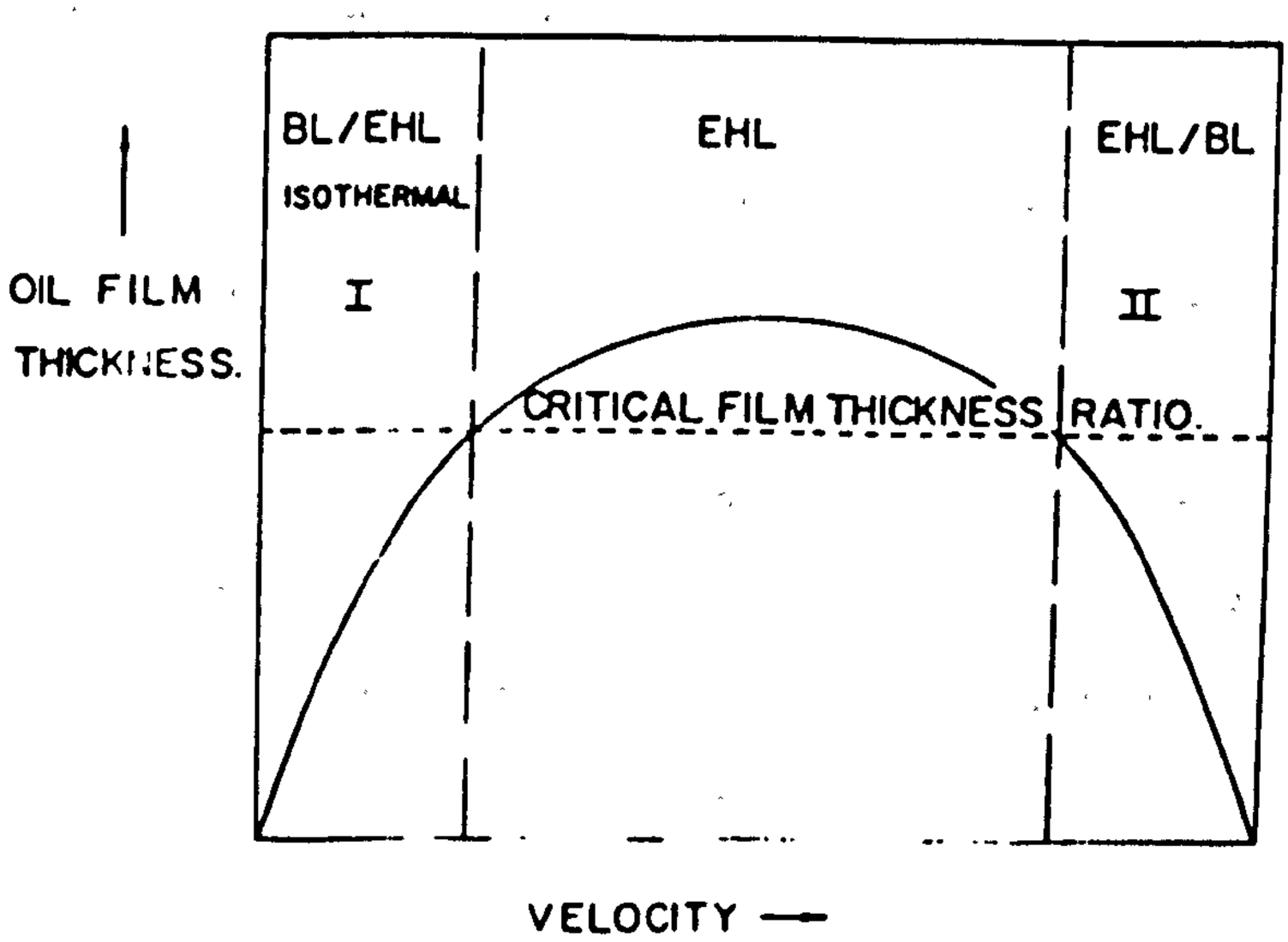

Fig. 5. LUBRICATION REGIMES FOR CAM/TAPPET SYSTEMS

2.6.1 Hydrodynamic Lubrication

This lubrication regime is represented by Region I of Fig. 4. Hydrodynamic or "Fluid Film" conditions are produced in systems where the viscosity, geometry and the relative motion of the surfaces are such that pressures are sufficiently high as to prevent surface contact. The separation of these surfaces by a lubricant film is produced by fluid adhering to the moving surfaces and being dragged into the converging zone in the direction of motion, thus building up a pressure sufficient to carry the load. The behaviour of the hydrodynamic regime is generally governed by the bulk physical properties of the lubricant as no direct physical interaction between the surfaces occurs, frictional characteristics therefore arise purely from the shearing of the viscous lubricant. The important geometrical features of these contacts, for example journal bearings, means the lubricating films are normally many times thicker than the surface roughness of the bearing surfaces.

2.6.2 Elastohydrodynamic Lubrication

The theory of elastohydrodynamic lubrication (EHL) has been established[41] to explain the fluid film lubrication of highly concentrated contacts such as gear teeth, round element bearings and cam-followers[42]. EHL is essentially an extension of hydrodynamic lubrication first described by Reynolds in 1886, with many of the fundamental concepts involved with hydrodynamic theory applicable to elastohydrodynamics. The basic difference between the two, is that in EHL the surfaces are not rigid but distort elastically to support a coherent hydrodynamic film. Providing this film is thick enough asperity interaction can be prevented. Fig. 6 shows the shape and pressure distribution associated with EHL films. The practical importance of EHL to cam-follower applications lies in the ability to express oil film

thickness in terms of operating conditions. An equation derived from theory[41] is given by:

$$h_m = \frac{2.65\,(\mu_o u)^{0.7}\alpha^{0.54}\,R^{0.43}}{E^{0.03}\,W^{0.13}}$$ (For a geometric line contact)

Where

h_m = film thickness at the rear constriction.

μ_o = viscosity at atmospheric pressure.

α = pressure-viscosity coefficient.

u = $\frac{1}{2}(u_1 + u_2)$ where u_1 and u_2 are the individual velocities of the moving surfaces.

R = radius of equivalent cylinder.

W = load per unit length

E = elastic modulus of equivalent cyclinder (flat surface assumed rigid).

Clearly before the oil film thickness can be measured in valve train systems using this equation, a series of other factors must be considered, including friction induced temperature effects, surface roughness, squeeze action and lubrication starvation. Barwell[43] reviewed these effects and concluded that a safety factor should be introduced in applying film thickness calculations to cams due to the many areas of uncertainty surrounding the direct application of EHL theory to design parameters.

The EHL regime occupies a domain to the left of hydrodynamic lubrication designated as region II of the Stribeck curve, Fig. 4.

The equation shows that the film thickness is most sensitive to velocity (u), the lubricant properties (μ_o and α) and the radius of curvature (R). The load (W) and the elastic modulus (E) have little influence on film thickness since their exponents are very small. These effects throw some doubt on the application of straight E.H.L. theory to cam-follower applications and has led to the concept of a third lubrication regime known as mixed lubrication or partial E.H.L. The onset of mixed then E.H.L. is shown by line AA in Fig. 4, there is no clear transition, and cannot be defined in terms of friction alone. Dowson [39] describes the transition in terms of multimolecular boundary layers working within the oil film thickness thus influencing the lubrication mechanism. Thus mixed lubrication would be expected when surface separation is reduced to 0.025 μm. This definition is difficult to relate to engineering surfaces, because the surfaces are assumed to be perfectly smooth. A further modification which accounts for surface roughness is now widely used. The general form of this parameter is given by:

$$\lambda = \frac{\text{Calculated film thickness}}{\Sigma \text{ Surface Roughness}}$$

Full E.H.L. conditions can be expected when λ is greater than five.

2.6.3 Mixed Lubrication

If a lubricated engineering system is running in regime III of Fig. 4 it is said to be operating in a condition of mixed lubrication. This lubrication mechanism is basically a compromise between E.H.L. and boundary effects, that is to say the lubricant films formed on surfaces are not

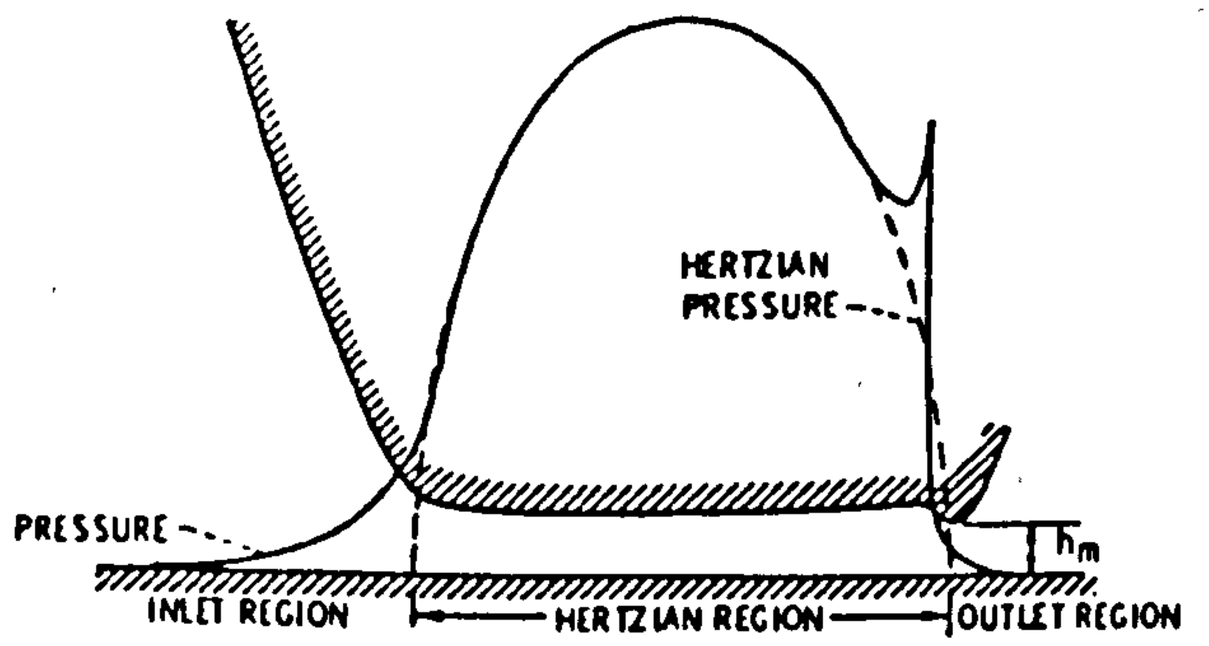

Fig. 6. ELASTOHYDRODYNAMIC LUBRICATION

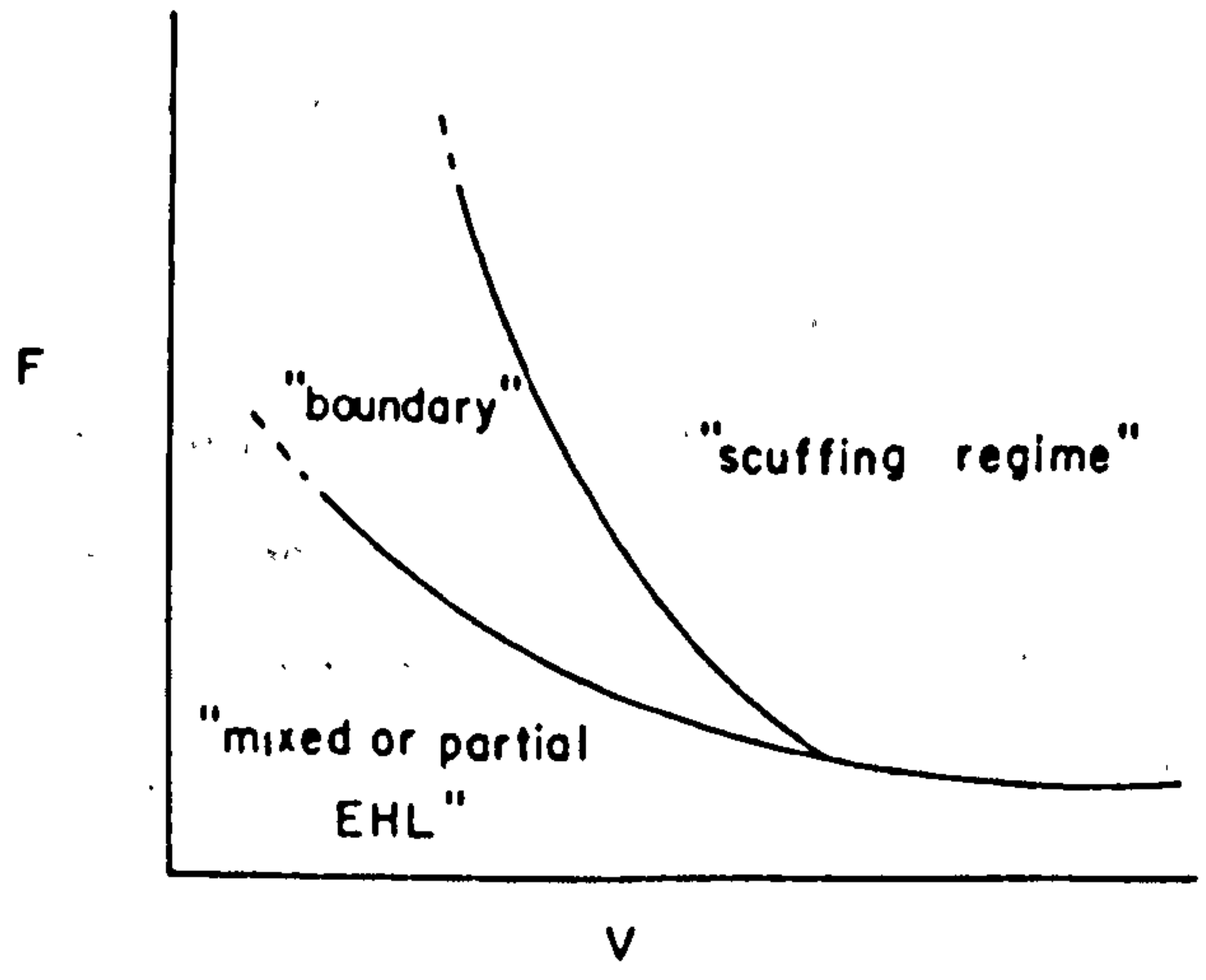

Fig. 7. AFTER BEGELINGER, REF 44

wholly responsible for the lubrication mechanism as the rheology of the oil also plays an important role. Surface separation is likely to be of molecular proportions, with the oil film thickness ratio in the range 1 to 5. Begelinger et al [44] have described this lubrication condition in terms of a transition diagram, shown in Fig. 7 related to the operating variables force (F), sliding speed (V) and temperature (T). The results of the experimental work showed that the load carrying capacity of the film is reduced with increasing speed, caused by a decrease in oil viscosity due to considerable heat generation in the film. Of course at the other extreme it has been established that low velocity conditions will also lead to a diminished oil film. It is extremely difficult to distinguish between these two forms of mixed lubricaton with reference to the Stribeck curve alone, however reference to the schematic hypothetical illustration in Fig. 5, clearly shows these two forms of mixed lubrication, the lubrication of cam-follower systems can be shown to be exclusively to the right hand side of this diagram. The material, additive type and base oil viscosity all have a significant role in wear behaviour under such lubrication conditions.

2.6.4 Boundary Lubrication

There have been many reviews on the subject of boundary lubrication[39]. Since the term was originated by Hardy, confusion has arisen as to the specific mechanisms involved because of the diversity of many authors experimental apparatus and techniques. It is generally agreed however, that the term describes lubrication by a liquid under conditions where solid surfaces come into appreciable contact with each other during operation. Under these conditions the bulk properties of the lubricants play little part in the friction and wear behaviour. The surface action

which dictates the behaviour of the system may be the result of physically or chemically adsorbed films or chemical reactions. The conditions under which these films are most effective varies according to the species, surface chemistry and operating parameters.

Experiments to evaluate boundary lubrication were initially confined to static and slow speed friction studies thus effectively evaluating the oiliness of a lubricant, that is the ability to reduce friction by mechanism of physical or chemical adsorption. The conditions under which cam follower systems operate however, are markedly different with sliding speeds typically three orders of magnitude higher and bulk temperatures in the region of 140°C[45]. Effective boundary lubrication is therefore more likely to be as a result of chemical reactions between the oil additives and the metals surface. Another effect the additive may have is to increase the load carrying capacity, in this case they are referred to as extreme pressure (EP) additives.

Although the lubrication mode of cam follower contacts is not exclusively boundary, evidence from the literature shows surface films influence the wear behaviour considerably. One such additive, of great importance for use in valve train system lubrication, zinc dialkyldithiophosphate is discussed in detail in the following section.

2.6.4.1 The Anti-Wear Mechanism of Zinc dialkyldithiophosphate

The high applied stress, sliding conditions and geometric design of many modern day valve train systems often makes the cam follower interface one of the most difficult areas in the engine to lubricate. The presence of additives in an internal combustion engine oil has been shown to play a

significant role in wear mitigation and the prevention of catastrophic failure of these components. The most widely used and useful additive for this purpose is zinc dialkyldithiophosphate (Z.D.D.P.)[46-49]. Over many years additive packages in automotive oils have become more complex to meet the needs of increased performance requirements and this has inevitably placed greater demands on the anti-wear behaviour of Z.D.D.P.s. There is considerable commercial interest to increase the effectiveness of Z.D.D.P.s, particularly as no other efficient substitute has yet been found.

It has generally been accepted that boundary lubrication is achieved as a result of the reaction between Z.D.D.P or its breakdown products and the metal surface[50]. Studies have tended to concentrate on two main areas of research, namely, decomposition of the additive in the bulk oil and analysis of surface films formed on contacting surfaces.

In the late 1950's it was realised that surface films formed at the mating cam follower interface was a significant factor in anti-wear behaviour[51]. The films observed were visible to the naked eye and it was concluded that the considerable differences in wear behaviour reflected the materials ability to form an anti-wear film. The most widely held view of the physical nature of these films is that they are soft and act as easily sheared layers on the rubbed surfaces, preventing metal-to-metal contact and seizure. An alternative model has been proposed by Martin et al[52,53], who suggests a paste is formed during frictional contact and this is the principal factor in wear characterisation. No direct evidence of the formation of this paste has been produced, the deduction of its formation being drawn from the presence of shallow tracks which coincide on opposing sliding surfaces.

Much work over the past 15 years has been concerned with the formation and composition of surface films in lubricated concentrated contacts. The films formed from Z.D.D.P. have been studied by a number of workers using electron probe microanalysis (EPMA), x-ray photo electron spectroscopy (XPS) and scanning auger spectroscopy (SAM). These films have in general been found to contain zinc, phosphorus and sulphur. A recent detailed analysis by Bird et al[54] using XPS and EPMA, has indicated that two types of film exist, a zinc thiophosphate and a ferrous sulphide, the latter found to be associated with high wear score marks on the surface.

As mentioned previously, published data on the anti-wear performance of additives operating under service conditions has shown significant differences depending on the cam or follower material, and although much work has been carried out related to the effect of metal structure and composition in lubricated tests, little work has been undertaken regarding surface film chemistry with respect to metal structure and wear performance. One exception to this has been the investigations carried out by Rounds[55]into the effects of steel composition on additive performance. Using x-ray flourescence (XRF), Rounds found considerable differences in the anti-wear behaviour of a range of materials with various types, although he found no differences in the case of Z.D.D.P. additive. He concluded that this was due to the mechanism by which Z.D.D.P. lubricates the contact, by adsorption not chemical reaction. The validity of this suggestion is questionable when one considers the majority of work was carried out on static immersion tests, and also the sensitivity of XRF is poor, typically analysing several millimetres in the sample.

Watkins[56] using XPS analysis of surface films on worn cam and follower components, also deduced the presence of two types of film. He suggests that sulphur reacts with iron at the surface to form a ternary eutectic with iron oxide and that the zinc polyphosphate is physically adsorbed. If zinc polyphosphate is physically adsorbed in the surface its role may be considered similar to that described by Cameron[57] in the lubrication of gears. His results with unreactive metals such as 18/8 austenitic stainless steel, have shown that physisorbed films have to desorb before sulphur can react with the surface, however, reactive metals such as carbon steels were found to behave differently. This has been attributed to a sufficiently long time period for the sulphur reaction to take place under slow running conditions, masking the deliterious effect of the physisorbed layer. Results obtained by Grew[58] and Begelinger et al [59] showed martensitic steels to be more reactive with sulphur additives than those containing retained austenite. Under conditions of partial EHL however, increasing retained austenite contents appeared to enhance the load carrying capacity, it follows therefore that any apparent discrepancies in results regarding austenite content produced by other authors can be attributed also be to differences in the lubricating regime.

2.7 Wear Mechanisms

Wear effects maintenance and economy due to it's affect on reducing efficiency and increasing power losses, oil consumption, and the rate of component replacement.

Wear may occur under various conditions of operation, therefore great care is needed in the choice of materials to suit the operating conditions. General metallurgical solutions cannot in many cases be

automatically applied to wear problems, for example, an increase in hardness does not necessarily mean a reduction in the wear rate as would be logically thought. Therefore the choice of materials for certain operating conditions is dependent on tests, specially devised so as to simulate as closely to provide the particular operating conditions.

Wear in industrial situations can be broadly divided into the following categories.

ABRASIVE	50%
ADHESIVE	15%
EROSION	8%
FRETTING	8%
CHEMICAL	5%

In a particular wear situation a combination of the above types of wear may operate together.

2.7.1 Abrasive Wear

Abrasive wear occurs when hard particles penetrate a surface and displace material in the form of elongated chips or 'swarf'. Abrasive wear occurs under 2 conditions, generally referred to as two and three body abrasive wear processes respectively.

Abrasive wear is very widely utilised in material finishing operations. The two body type of abrasive wear is made use of in files, abrasive paper, cloths and wheels, whilst three body wear is used for lapping and polishing.

In order to derive a quantitative expression for abrasive wear, consider a simple model where the asperities on the hard surface are conical (Fig 8). Considering a single asperity carrying a load ΔL, the extent to which it penetrates the softer surface is given by:

$$\Delta L = P\Delta A = P\pi r^2$$

Where P is the hardness of the softer surface.

The projected areas of the penetrating cone in the vertical plane is rX. Then when the cone moves through a distance dl it will sweep out a volume dV given by:-

$$dV = r\ X\ dl = r^2 \tan\theta\ dl = \frac{L \tan\ dl}{\pi\ P}$$

$$\frac{dV}{dl} = \frac{\Delta L \tan}{\pi\ P}$$

Now, by adding the contribution of all asperities we have

$$\frac{dV}{dl} = \frac{L \tan\theta}{\pi\ P}$$

Where, $\tan\theta$ is a weighted average of the $\tan\theta$ value of all the individual cones.

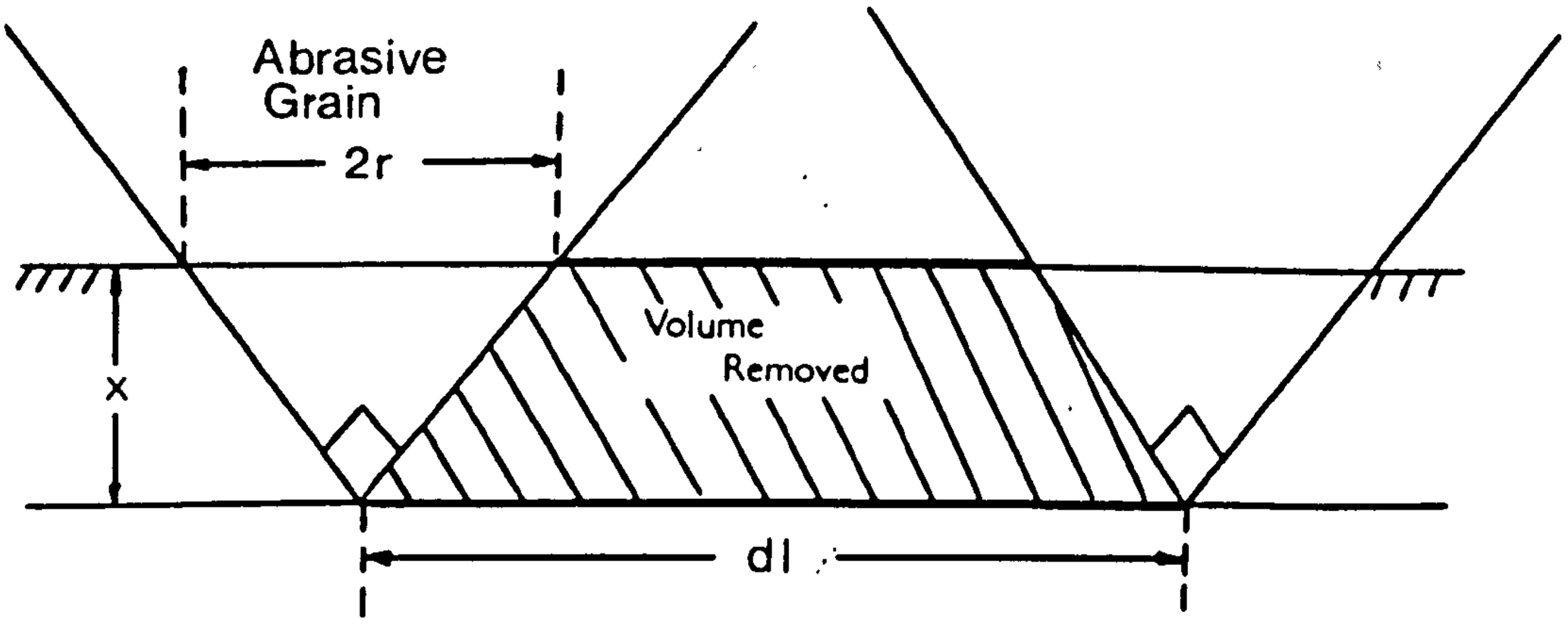

Fig. 8. ABRASIVE WEAR MECHANISM

In abrasive wear, particle penetration is given by

$$= \frac{\text{LOAD ON THE PARTICLE}}{\text{HARDNESS OF THE SURFACE } H_v} \cdot = \frac{W}{}$$

If A is the cross section of the groove, and L is the length, the volume of wear is:

$$\text{Wear Volume} = \frac{W}{H_v V}$$

From work carried out by Krushov[60] the relative wear resistance is defined as:

$$E = \frac{\text{Linear wear of a standard}}{\text{Linear wear of test material}}$$

which is usually greater than 1, since the standard has a relatively low hardness. E is proportional to hardness, but varies with the microstructure if the alloy is changed. Serpik[61] showed that E increases with carbon content in steel. Abrasive wear resistance can be considerably improved by refining the pearlite, this is due to the increased rate of work hardening produced. Popov[62] has shown in steels both the volume and composition of carbides have an affect on the wear properties.

It has been shown that the maximum hardness produced by wear, rather than the hardness of the unworn surface should be considered. Work carried out on white cast irons which do not work harden showed good correlation between wear volume and hardness. Steels that work harden give results in the worn condition that fall into the scatter band for other materials.

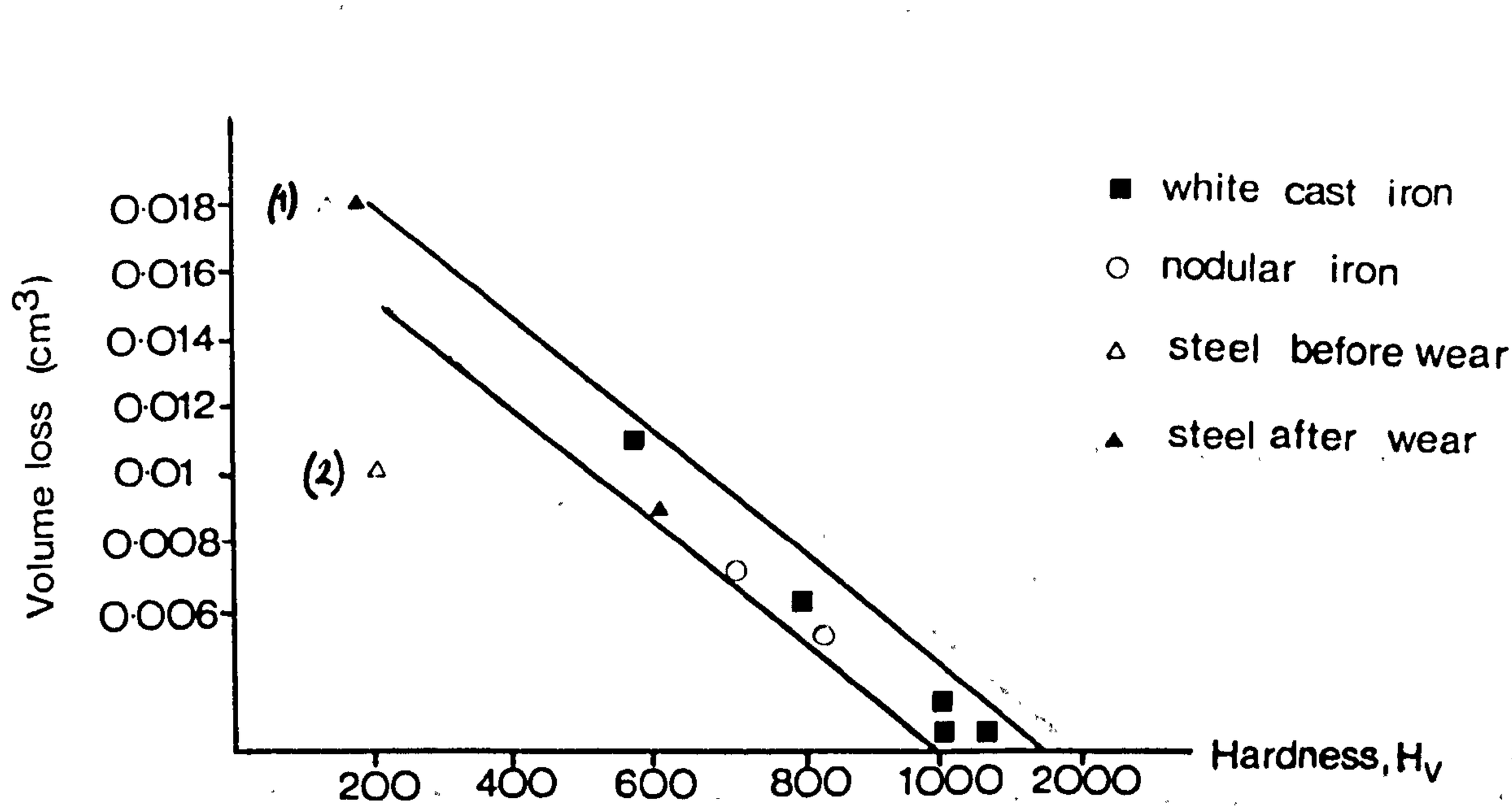

Fig. 9. ABRASIVE WEAR RATE DEPENDS ON THE HARDNESS OF THE WORN RATHER THAN THE UNWORN SURFACE.

There is no simple relationship between material hardness and wear resistance. Richardson[63] showed that the hardness of the surface resisting wear must be greater than half the hardness of the abrasive if any improvement in wear resistance is to be achieved.

$$KT = \frac{H_V \text{ of surface}}{H_V \text{ of abrasive}}$$

KT must be greater than 0.5. However an increase in the hardness of the material beyond 1.3 times that of the abrasive will produce no further significant improvement in wear resistance.

Data produced by Alenkov[64] shows a graph of wear rate/hardness against hardness, (Fig. 10), it shows a horizontal line up to a certain point and then drops drastically. The hardness value at which the abrasive wear rate drops reduces is approximately 0.65 the hardness of the abrasive.

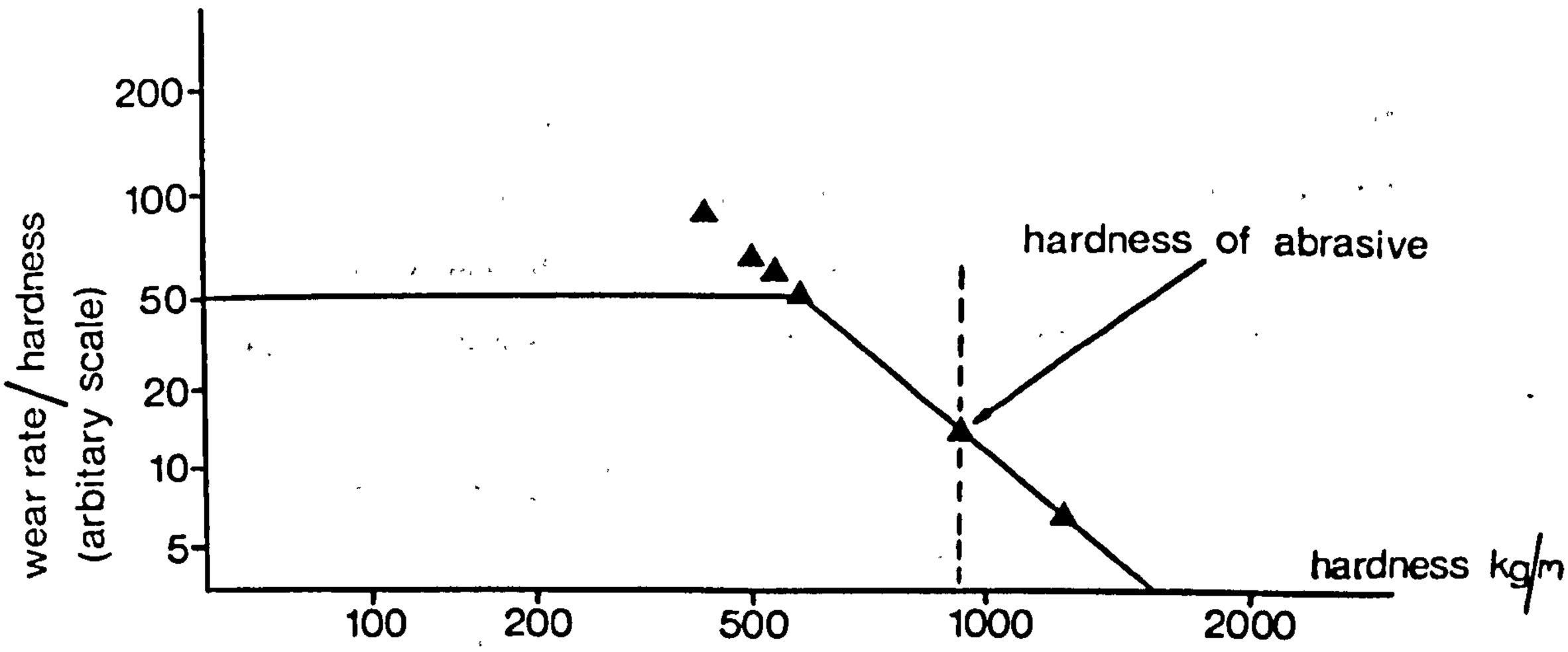

Fig. 10. THE WEAR RATE HARDNESS PRODUCT DROPS OFF DRASTICALLY WHEN THE MATERIAL BEING ABRADED IS HARDER THAN THE ABRASIVE

2.7.2 Adhesive Wear

This type of wear occurs when two surfaces slide against each other. The pressure produced by contacting asperities eventually reaches a rate sufficiently high enough to cause local plastic deformation, adhesion and in some cases welding of the asperities. Adhesion occurs between a few asperities which increase their size as motion continues. The junctions of the asperities eventually rupture causing metal transfer from one surface to another, but may in some cases come off in a loose form.

Adhesion is favoured by clean, non-oxidised surfaces and by chemical and structural simularities between the sliding couple. This is due to the attractive forces which exist between the surface atoms of the two similar materials[65]. If two surfaces are brought together and then separated, either normally or tangently the attractive forces act in such a way so as to attempt to pull material from one surface onto the other, thus increasing the likelyhood of bonding and welding[66].

Since the area of contact is inversely proportional to hardness, wear decreases with increasing asperity hardness. In some cases wear debris may become considerably harder due to work hardening, ultimately causing phase hardening and further wear by an abrasive mechanism.

According to Archard[67]

$$\text{Wear Volume} = \frac{KSP}{P_m}$$

Where K is a wear constant, S the sliding distance, P the applied load and P_m the flow stress of the wear surface.

The ability of pure metals to form solid solutions is related to their tendency for adhesion to occur[65]. For example, lead having a low solubility with cobalt, chromium, nickel and iron is therefore a good choice for a counterface material. Chemical contamination of a metal surface improves the wear resistance due to the non-adhesive, antiwelding properties of the contaminant.

From work carried out with various unlubricated materials, it is possible to write the laws of adhesion as follows[65]:

1. The amount of wear is generally proportional to the load.

2. The amount of wear is generally proportional to the sliding distance.

3. The amount of wear is generally inversely proportional to the hardness P of the surface being worn away.

Or, we can write the volume worn away in the form:

$$V = \frac{CLX}{P}$$

Where C is a constant depending on the materials in contact and their exact degree of cleanliness.

The volume of transferred fragments formed in sliding through a distance X was found to be

$$V = \frac{KLX}{3P}$$

In the case of the two bodies sliding over one another P is the flow pressure of the softer of the metals. This may be considered the fundamental law of adhesive wear, with K being the coefficient of wear.

Wear under adhesive conditions, unlike abrasive wear is subject to sharp transitions in behaviour. Variations in load and speed may bring about marked thermal changes which preceed, and cause, changes in wear[66].

Welsh[68] was one of the first to examine the concept of mild wear (oxidative) and severe wear (metallic) and the sharp transitions between them, referred to as T_1 and T_2 transitions respectively.

Wear below the T_1 transition load is due to the removal of oxide particles from an oxidised surface supported on a work hardened substrate. At T_1 severe wear occurs due to the break up of the oxide layer produced at lower loads. Plastic deformation occurs due to the lowering of the metals yield point caused by a higher bulk temperature, the wear rate increasing considerably with the production of metallic debris.

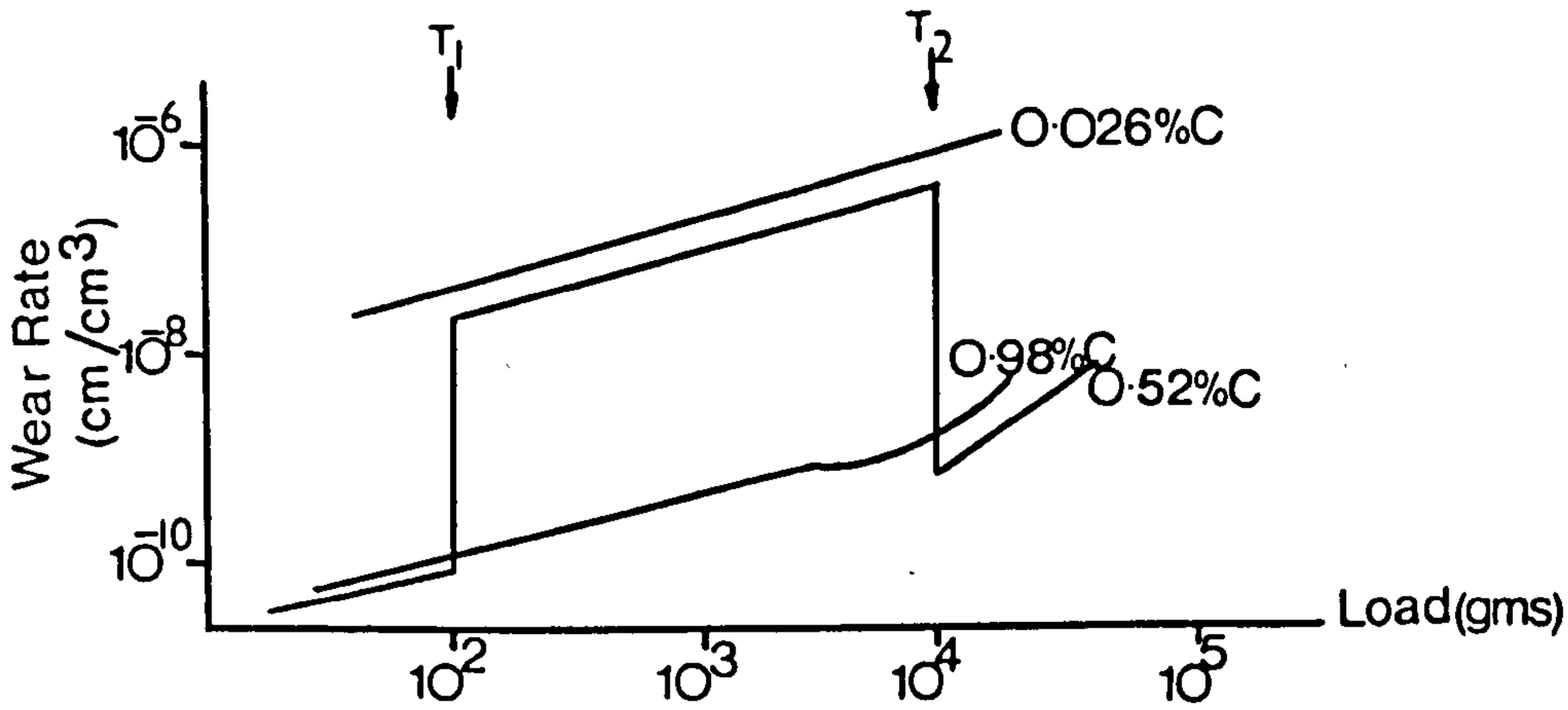

Fig. 11. TRANSITION WEAR BEHAVIOUR OF DIFFERENT STEELS.

Between T_1 and T_2 severe wear occurs. At the T_2 transition load the wear rate decreases due to a phase hardening process caused by higher friction induced surface temperatures. Phase hardening produces a hard 'white layer' structure which prevents deformation and helps to establish an oxidised surface once more.

During the early stages of rubbing under adhesive conditions, wear proceeds at a relatively high rate due to the surfaces being clean. Eventually, however, an oxidised surface forms. Under some conditions, particularly at loads close to the mild/severe (T_1) transition load, a particular form of wear called "scuffing" occurs, under such conditions the surface topography changes and a rough surface results. This roughening usually begins in localised narrow bands and gradually spreads along the rubbed surfaces.

2.7.3 Corrosive Wear

This form of wear occurs in situations in which the environment surrounding a sliding surface interacts chemically with it. If the products of reaction are worn off the surface, corrosive wear has occurred.

The first stage of corrosive wear involves the chemical attack of the surface, similar to that occurring in ordinary corrosion. Corrosion, initially rapid tends to slow down with time due to a film formation separating the reacting species. However, in some cases the initial reaction rate continues throughout the corrosion cycle either due to the lack or breakdown of the protective film.

The second stage of the corrosive wear process involves the wear of the reaction product film, as a result of sliding taking place. When this occurs, the naked surface is exposed and corrosive attack continues.

The corrosion products are usually harder and more brittle than the surface on which they form, and can cause additional abrasive wear.

2.7.4 Fatigue

Wear by a fatigue mechanism occurs on surfaces which come into repeated contact at stresses higher than the fatigue limit. Damage occurs in, or just below the surface, ultimately causing fracture and the production of surface pitting. Early fatigue failures may initiate from corrosion in the surface, or subsurface defects.

The metallurgy of the material plays a large role in the prevention of fatigue. For example, surface treatments that increase the hardness and form residual compressive stresses on the surface, enhance the fatigue resistance.

2.7.5 Delamination

Wear by delamination involves extensive deformation and fracture of the metal surface, producing a plate like debris. Observation of the debris shows it to be unlike the characteristic morphologies of abrasion (metal slivers) or of adhesion (particles with length to width ratios of 3.1), the plate-like debris has a length often exceeding 10 times the thickness.

This type of failure can be commonly found in automobile engine components for example cylinder liners and cam and tappet applications[66].

Delamination can occur under abrasive conditions if the cutting efficiency is low and under metal to metal sliding conditions if little adhesion occurs. Work carried out by Suh[69]showed that soft (ductile) layers enhanced a metals resistance to delamination. The effect of the deformation is very localised and it is sometimes possible to see these plates originating at impurities in the steel.

2.7.6 The Phenomena of Wear in the Cam and Tappet System

As already reported the lubrication of cam and tappets in overhead camshaft systems has become more difficult especially with the advent

of increased engine speeds. The most important factor governing the performance of cam and tappets is the metallurgy of these components, although the properties of the lubricating oil and cam/tappet geometry play an important role.

The majority of cam and tappet wear problems can be divided as follows:- Scuffing, Pitting, Polishing and Accelerated Normal Wear.

2.7.6.1 Scuffing

This form of wear is characterized by a roughening of the surfaces associated with the break down of oil films. The surface roughening is due to the rupture of small welds formed between the contacting surfaces and normally occurs fairly suddenly during the early stages of operation.

Under mild conditions, at low loads and temperatures the surfaces are completely separated by a lubricant film. However, if the load is increased, the bulk temperature increases, and a decrease in the oil film thickness occurs due to a lowering of the lubricant viscosity. At first the surface will be undisturbed, but gradually interaction and modification of the surfaces will occur. It is this interaction of the surfaces that if too severe, leads to surface damage. Associated with this damage are increases in the coefficient of friction, in some cases by a factor of 3 and the production of hard, white etch resistant phases commonly known as "white layer". These layers are claimed to be produced by an austenitic transformation with surface temperatures in excess of 723°C evident, the result is a hard brittle 'martensitic' type layer, leading to eventual failure by a spalling mechanism.

The theory of scuffing and associated white layer formation in ferrous alloys is dominated by Blok (1939) with his flash temperature concept[70]. Blok's hypothesis is based on the idea that a given system operating under given conditions will scuff if the maximum temperature in the contact area exceeds a critical value.

The temperature in the contact area is the steady bulk metal temperature of the rubbing parts added to the temporary rise in temperature of a point in the rubbing surface as it traverses the contact, this latter temperature is known as the flash temperature. This is the more important component of the contact temperature because of its thermal magnitude, but is however, extremely difficult to measure since it is of very short time duration and decays rapidly with both time after the surface has left the contact and with the depth below the surface. This theory is not of great practical use because it assumes single asperity contact with the material properties remaining constant. It does provide a general idea of the magnitude of the temperature rise and it's effect on phase transformations can therefore be predicted. More information is required before the method of calculation and the values obtained can be used to predict the systems behaviour.

The application of Blok's flash temperature concept to cam and tappet wear problems has been carried out by Dyson[71] who claims that the contact temperature reaches a maximum at three points in the valve operating cycle; at the cam nose and at the two points at zero tappet acceleration, the values obtained being dependant on cam contour, spring forces, materials of construction and other relevant factors.

2.7.6.2 Pitting

Pitting failure is readily recognised by an irregular distribution of pits

on the surface. Pitting failures in valve train components are experienced predominatly when manufactured from chilled white iron, the origin of the sub-surface cracks causing this type of failure being a subject of some dispute in which two opposing views are held. One theory considers that crack initiation occurs beneath the surface at a position corresponding to high shear stresses and is based on Herztian contact concepts. The other proposes that cracks are initiated at the surface and propogation occurs parallel to and beneath the wear surface until material is free to detach. Since there is evidence to show that pitting is both a stress and chemical dependant process it would seem likely that both mechanisms are possible, depending on the precise operating and environmental conditions.

The Motor Research Association[72] have reported failures initiating at the point of maximum Hertzian contact beneath the surface, and also concluded that crack propogation is assisted by oil pressure build up within the cracks during the operating cycle. Supportive evidence for this theory arises from observations that predominant crack orientation effects can be distinguished with respect to the direction of motion of the contacting surfaces.

The use of additives in lubricants such as zine dialkyldithiophosphate (Z.D.D.P.) has also been shown to influence the fatigue process. Caldicott[73] reported that chilled white iron running in a mineral base oil performed satisfactorily, whereas the addition of Z.D.D.P. resulted in increased pitting susceptability. Other authors have reported the migration of lubricant additive components along surface initiated cracks to depths of up to 150 microns thus possibly increasing the susceptability of accelerated fatigue crack growth by a stress corrosion mechanism(74).

2.7.6.3 Polishing Wear

This wear mode has been defined as a general attrition of the contacting surfaces[75] in which wear occurs progressively. The initial wear rate during 'running in' tends to diminish with time until a constant low rate is achieved, the higher the load the greater wear rate. There is no clear concensus of opinion as to the underlying mechanisms responsible for this phenomenon although many theories have been put forward.

Some workers have associated this type of wear with the flash temperature concept of correlating the severly worn areas of the surfaces to positions of maximum flash temperature[76]. Another theory assumes polishing wear to be formed chemically by additive interactions and corrosive means[77]. A third possibility is wear resulting from the abrasive action of dispersed solids less than 1 micron in size, typically found in crankcase oils. These particles are usually contaminants from one or two sources; particles of airborne dust such as SiO_2 and internally generated wear debris or combustion products.

2.7.6.4 Accelerated Wear

This severe form of wear is characterized by the appearance of the damaged parts, the only abnormality present is the very high rate of wear. In some cases the surface has the appearance of a machined surface which is typically associated with a worn cutting tool with a 'built up edge'.

2.8 Condition Monitoring

The introduction of condition based monitoring has increased considerably the efficiency and economy in machinery operation. Monitoring the condition of machinery can permit detection of potential breakdowns, thus allowing time for remedial action. When used in conjunction with improved design information and materials, condition monitoring can increase service life and reliability. In addition, condition monitoring can be used extensively for tribological wear analysis where wear rates are difficult to measure without the removal of reciprocating parts for analysis for instance those fully submerged in a lubricant.

The principle of condition monitoring is to select an appropriate indicator of a machines condition which can be monitored and measured successfully at different time intervals. The measurements, once recorded can be plotted against service time to indicate any deterioration of an operating system.

There are six basic methods of condition monitoring, these can be classified as follows:-

1. Visual Monitoring
2. Vibration Monitoring
3. Wear Debris Monitoring
4. Performance Monitoring
5. Corrosion Monitoring
6. Structural Integrity Monitoring

Wear debris monitoring being a widely used condition monitoring technique works on the principle that the working surfaces of a machine are washed by its lubricating oil, thus any damage occurring to the working surfaces should be detectable by analysis of the wear debris in the oil. If the debris consists of large particles they can be removed by magnetic plugs placed on the oil return lines. For smaller particles, analysis of the debris can be carried out by spectrometric analysis or microscopic examination of the debris after magnetic separation.

Wear debris analysis can be both quantitative and qualitative. QUANTITATIVE: giving information on the size, size distribution, concentration of the debris and the elemental composition. QUALITATIVE: state of the debris, e.g. oxidation, morphology and colour.

The objective of oil analysis is to provide:

1. Detection of abnormal wear indicating incipient failure.
2. Information on the morphology, location and wear mode of the debris and it's subsequent severity.
3. Prognosis of the future state of the machinery.
4. Action to be taken for maintenance rectification.

CHAPTER 3

3. EXPERIMENTAL PROCEDURE

3.1 INTRODUCTION

Test methods used in the study of friction, wear and lubrication are many and varied[78], their basic purpose being to study the effects of systems variables on tribological processes. The vast majority of test procedures used in determining the wear performance of automotive valve train systems[79-81] fall into the category of simulation to evaluate lubricants and/or materials. These techniques range from single cam lobe and follower systems, to fully fired engine tests. It is the cost however, of these fully fired engine tests, running sometimes into many thousands of pounds per test which has swung more emphasis onto the choice of cheaper laboratory bench rigs for the screening and evaluation of both lubricants and materials. Another important consideration in the selection of testing procedures is the significance of variables influencing the friction and wear processes, and the ability to control or measure these variables during testing.

The experimental work involved in this thesis is as the title suggests "The effect of base stock and additive package on the friction and wear behaviour of overhead camshaft and finger follower systems", and attempts to establish more confidence in laboratory based rig testing for the evaluation of materials and lubricants. The objectives of this work run in 3 main categories:-

Objective One

The main objective in this section is the evaluation of the laboratory based test rig for lubricant and material studies, in an attempt to introduce a cheaper and more convenient alternative to dynamometer and engine testing for the performance screening of lubricants and materials, for both design and quality assurance/control purposes. Secondary objectives can be divided into two main parts:

i) A pre-requisite to the success of laboratory bench rig testing is the reproduction of service failures commonly encountered under engine test and service conditions. This area of work is concerned with the reproduction of such service failures, the great advantage of rig testing being the elimination of variables encountered under fired engine conditions such as contamination from areas such as airborne dust and products of combustion and oil degredation due to engine atmosphere. These variables, to mention only a few, have served to confuse and mislead engineers and tribologists alike for many years. This has prevented a more fundamental understanding of wear mechanisms and surface interactions occurring in overhead camshaft systems and has only served to aggravate the already highly complex nature of these operating components. Rig testing therefore allows a more simplistic study of these components, thus attempting to give a more fundamental understanding of the wear behaviour of these components.

ii) To observe and examine the wear behaviour of well established camshaft and follower materials under fully lubricated conditions using a base stock oil and its full additive formulation. This is to

compare some of the effects of lubrication regime, oil rheology and additives on the friction and wear characteristics of these materials under well defined test conditions.

Objective Two

The importance of the wear mechanisms associated with the 'running in' of contacting surfaces, allowing the conforming and the successful operation of engineering systems has in the authors view been neglected by many, especially in the area of overhead camshaft and follower systems. The objective in this part of the experimental work therefore is to analyse and illustrate the importance of satisfactory 'running in' of surfaces and thus the formation of these surfaces. To compare the 'running in' characteristics with base and fully formulated oils for a standard material combination, using a variety of surface topographies, test conditions and analytical techniques.

Objective Three

This area of experiment work is concerned with the use of new materials for overhead camshaft systems. Samples of material have been supplied in insert form and consequently used for finger follower applications, and run against a standard ferrous cam material. Tests were conducted fully submerged in base oil (without additives) to observe and analyse the friction and wear characteristics of these new materials under low load conditions. The tests were of a 'screening' nature, the results obtained should be used to form the basis of further research work to be carried using these materials.

An important factor concerned with the experimental apparatus is the ability to obtain data, to provide a more fundamental understanding of the processes occurring during contact. The available literature classifies wear under generalised headings which relate to the mechanism or mechanisms responsible for a particular type of surface damage. There is little information in the field of valve train wear studies to explain the initiation and progress of many of these wear regimes. This can be achieved by the use of various techniques to monitor the state of a number of variables in the system. One variable which was easy to measure and partly fulfilled this testing objective was the coefficient of friction measurements. The study of the direct wear rate is difficult to achieve due to the geometric and operational constraints of the rig design. The use of indirect wear rate methods such as emission spectroscopy, ferrographic and rotary particle deposition techniques provides methods of accumulating wear data of a quantitative nature without detracting from the simulation design. The rig design also allows for accurate control of load, sliding speed and oil temperature throughout the duration of each experiment. This wide range of controllable operating conditions allowed service conditions to be reproduced.

The philosophy behind the rig design was to simulate an O.H.C. finger follower system as closely as such factors as economics and ease of operation would allow. For this purpose a cylinder on flat configuration was utilised to give nominal line contact conditions. Load is applied to this conjunction by the reaction of a spring to the eccentric motion of the cylinder. The layout of the configuration is based on the European Ford Finger Follower System, a comparison of which can be seen in Fig.12. This enabled a number of components from the production valve train to be utilised in the construction of the rig

and gave the additional advantage of superior surface alignment characteristics afforded by this design. The use of a cylinder on flat configuration allowed specimens to be produced in a wide range of materials and treatments and enabled the machining of the specimens from bar stock, thus keeping their manufacture under the author's control.

3.2 Description of Cam-Follower Test Rig

Wear testing has been carried out by loading a flat specimen, in line contact with an eccentrically rotating cylinder. The cylindrical cam specimens used throughout the experimental programme measured 32.00mm diameter by 20mm wide, a drawing of which can be seen in Fig. 13A. The follower specimen size and shape was chosen from considerations of suitability for insertion into a Cambridge S600 Scanning Electron Microscope and also ease of manufacture. The contacting face of the specimen measures 30mm by 16.5mm as shown in Fig. 13B. The use of hard materials for wear testing meant that the manufacture of specimens became difficult and uneconomic to produce. This was overcome by the use of inserts of size 17 x 12 x 3mm and were manufactured out of chilled white iron and all the new materials tested. A standard mild steel specimen was machined and a recess milled into the contacting surface of the follower. The insert was then epoxy bonded into this recess and allowed to cure, a specimen can be seen in Fig.13C. A specially hardened steel carrier was used to hold the test specimen within the apparatus, acting as a simulated follower arm. The carrier assembly is located in the rig between a spherically ended pivot and the top of a hardened silver steel valve stem by two spring retaining clips. By using a spherically ended pivot, the follower surface is free to align itself in the plane parallel to the line of contact.

Load is applied to the contacting surfaces when the rotation of the cam causes the carrier to arc downwards against a spring loaded valve stem. A standard Ford inlet valve spring was used for this purpose and was calibrated for load in the rig base block using a specially constructed compression jig.

The test configuration is totally enclosed in a rectangular container serving as an oil tank, associated with this is an independant filtration system. Lubricant temperatures in the rig are controlled by the use of two 2 KW heaters, thermostatically controlled in the rig base block. Friction measurements are obtained by the displacement of the pivot point with cam revolution. This displacement is measured by the use of an AC linear variable differential transformer (LVDT) linked to a signal conditioning module. The output signal from this unit is displayed on a Digital Storage Oscilloscope, from there the signal is fed into a B.B.C. microprocessor unit via a specially constructed interface and the friction measurements recorded continuously with time. The test rig and data logging system can be seen in Figs 14, 15 and 16. The program used for friction measurement in the microprocessor can be seen in Appendix 1.

3.3 Preparation of Cam and Follower Test Specimens

The 32mm diameter cam specimens were manufactured from cast or rolled bar stock in a range of materials listed in Table 3. After machining, the cam specimens were heat-treated using various methods depending upon the material and final properties required. After heat-treatment the periphery of each specimen was circumferentially ground to the final diameter of 32.0mm and a surface roughness of 0.35 -0.45 μm Ra.

The follower test specimens were milled from flat or bar stock to the dimensions given in Fig 16B and from the range of materials given in Tables 3 and 8.

3.4 Experimental Procedure

All the experimental work was carried out under fully flooded conditions within the oil tank, holding approximately one litre of test lubricant. Once the test temperature was reached, 10 minutes was allowed for temperature stabilization, and the computer program was loaded before testing commenced.

At periodic intervals throughout the duration of all experiments, a 10ml volume of lubricant was withdrawn from the oil tank by a pipette at a position corresponding to the lubricant exit point from the cam and follower interface. Fig. 14. These samples were then used to obtain diagnostic information on the character and severity of the wear process.

3.5 Experimental Techniques

3.5.1 Condition Monitoring

The lubricant samples removed during testing were used to determine wear rates indirectly, using emission spectroscopy and Ferrographic/R.P.D. techniques.

3.5.1.1 Atomic Emission Spectroscopy

Analysis of oil samples using emission spectroscopy was carried out using a Rank-Hilger medium quartz emission spectrometer with a FS165 source. The principle of atomic emission spectroscopy is to vapourize the oil sample by means of an electrical discharge, the energy for the discharge is provided by source units. Whilst the oil burns off, the atoms present in the remaining wear debris are excited by the discharge and emit light which is focussed onto a concave diffraction grating or prism, thus breaking down the emitted light into a spectrum containing, at discrete wavelengths, the spectral lines of all the elements present in the sample.

At least one line for each element whose concentration is to be determined is selected by passing the emitted light through a narrow exit slit after which it is focussed by a mirror onto the cathode of a photomultiplier tube. This converts the weak light signal into an electric current which can be measured. The luminous intensity of the line is related to the concentration of the relative element Fig. 17. The results are expressed in terms of parts per million of specific element and plotted graphically against test time[82].

3.5.1.2 Ferrographic And R.P.D. Analysis

The basic principle of ferrographic wear debris analysis is the magnetic separation of wear debris from lubricant samples taken from a recirculating system. One of the most well established techniques to date for the analysis of wear debris is ferrography, this consists of two stages, direct reading and analytical ferrography.

3.5.1.2.1 Direct Reading Ferrography

A 2 ml mixture of used oil and a fixer solution is siphoned through a glass precipitator tube place on a permanent magnet. Two fibre optic systems, 5mm apart, are situated near the front edge of the precipitator tube. The magnet is graded such that the ferromagnetic wear particles are precipitated at a position dependant upon their size, particles >5 microns are precipitated at the first fibre optic unit and particles <2 microns at the second fibre optic unit[82]. The units are connected to photodetectors which measure the light attenuation at these points. The reduction in light is proportional to the percentage area covered by the particles, Fig 18. The results are in a digital form D_L = large particles D_S = small particles.

$$\text{Total Wear} = D_L + D_S$$

$$\text{Severity of Wear} = D_L - D_S$$

A high number of large particles indicates a severe wear mode, thus giving a higher D_L value, and a correspondingly higher severity of wear value.

3.5.1.2.2 Analytical Ferrography

The standard ferrograph analyser consists of a peristatic pump to deliver the lubricant sample, a magnet that developes a high gradient magnetic field near its poles, and a treated transparent substrate for particle deposition. The lubricant sample, diluted with a solvent to promote the precipitation of wear particles, is pumped across the transparent substrate which is mounted at a slight incline. A washing

and fixing cycle is then carried out to remove residual oil leaving the wear particles adhering to the slide as a permanent record, Fig 19.

The adhered substrate particles are distributed according to their size and magnetic permeability. Large ferrous particles being deposited first with non-ferrous particles attached to small magnetic debris being deposited further down the substrate[83]. The deposited debris may range in size from sub-micron to several hundred microns.

Although the technique of ferrography is well established and extremely popular, doubts have been cast by Tribologists in two particular areas of ferrographic analysis:

(1) Dilution

(2) Debris deformation and fracture.

Exact dilutions are required in both direct reading and analytical ferrography to enable satisfactory investigation of debris quantity and morphology. Over dilution for example gives rise to debris 'pile up' and overlapping at both the precipitator tube in the direct reading, and the entry point of the treated substrate of the analytical method, leading to misleading and inaccurate analysis of the results obtained. Accurate and consistent dilution can prove extremely difficult without extensive experience in ferrography, especially when considering the reduced size of some oil samples taken from small recirculating oil system.

Debris deformation is confined to the analytical technique and occurs with the movement of the lubricant sample through the peristatic pump

arrangement. The small clearance allowed for debris passage in the pump are not big enough to allow free movement of large particles such as those produced in "scuffing", spalling and delamination. The resultant effect is mechanically deformed and fractured wear debris which may confuse investigators in the detection of the true wear mechanisms.

A relatively new technique developed by the Tribology Centre at University College Swansea U.K., has helped alleviate these problems by the use of a larger substrate area enabling improved debris spread and a straight syringe oil sample deposition method. This technique is called the Rotary Particle Depositor (R.P.D.) Fig. 20. The principle of the R.P.D. consists of depositing a fixed volume of a sample containing debris onto a substrate which is located within a magnetic field. The substrate/magnet system can be rotated by means of a variable speed motor such that the deposited sample fluid flows radially outward and the particulate content is deposited on the slide as a series of concentric rings. Washing of the slide is achieved using a syringe-pump system.

Slide preparation is achieved by a sequence of sample deposition, washing and drying. A 1cc sample of the warm, thoroughly shaken, bulk fluid is deposited in a controlled manner at the centre of the slide which is rotating at about 70 r.p.m. On completion of sample deposition, a washing procedure is carried out in which solvent is supplied to the slide using a syringe pump system whilst the rotational speed is increased up to 150 r.p.m. Drying of the slide is accomplished by rotation at about 200 r.p.m. for a few minutes, after which the slide is ready for optical and/or electron microscopic examination[84-86]. An additional piece of equipment called the Particle Quantifier (PQ)

enables a quantitative result from the debris deposited. This technique works on the principle of measuring the change in magnetic field intensity with increases or decreases in debris content. The results are in a digital form giving trends in wear rate with running times and thus can be plotted graphically Fig. 21.

Due to the ease of operation and interpretation the technique of Rotary Particle Deposition (R.P.D.) was used exclusively for this experimental work.

3.5.2 Wear Surface Examination

3.5.2.1 Optical and Scanning Electron Microscopy

Worn surfaces obtained from the experimental work have been examined using optical and scanning electron microscopic techniques. Scanning electron microscopy was carried out using both Cambridge S600 and S250 instruments equipped with energy dispersive x-ray analysis facilities. Photography of relevant wear features were taken at suitable magnifications. X-ray analysis of surfaces was extensively used to produce qualitative information on the distribution of elements in surface films. In addition the technique was used to obtain a semi-quantative assessment of film composition at selected points. This is somewhat limited by the fact that the surface films are thinner than the depth of sample being analysed. The presence of transferred material was also identified in a number of cases.

3.5.2.2 Surface Replication

This technique as the name suggests, allows the replication of wear surfaces using acetate films. The process of replication can be seen in Fig 22. and consists of flooding the wear surface with acetone, an acetate sheet is then placed on the flooded wear surface and allowed to soften. The softening of the film allows the contour of the wear surface to be reproduced on the acetate film and on drying, the film peeled off and inverted through 180° to give a replica of the wear surface, although 'back to front' Fig.23. This can be improved by the use of a carbon shadowing technique, dissolving the acetate replica and thus forming an exact replica of the wear surface in carbon.

3.5.2.3 Surface Profilometry

Surface roughness characteristics have been studied by the use of a Rank Taylor Hobson Talysurf. In addition, some of these surface roughness traces have been supplemented and subsequently compared with three dimensional surface plots produced by a computer aided talysurf machine used at C.E.G.B. Berkeley Laboratories, Glos.

3.5.3 Weight loss Measurements

Before testing commenced both the cam and follower specimens were weighed to an accuracy of 0.0001 gm. After testing, weight measurements were repeated to show evidence of weight loss and expressed as percentage weight loss from the original bulk specimen.

3.5.4 Metallography

3.5.4.1 Taper-Sectioning

The production of taper-sections enables relatively thin surface layers to be examined in more detail than would be possible with a normal 90° section.

The main stages of preparation involves the production of a taper section through the surface which is first protected with epoxy resin and then mounted in bakelite for metallographic examination. The polished and etched specimen can be examined metallographically and then removed from the bakelite, the protective epoxy resin film is then also removed from the surface prior to S.E.M. examination, Fig. 24.

Tapersections of cam and follower surfaces, both worn and as-ground were produced for metallographic and S.E.M. examination using this technique.

3.5.5 Lubricants and Additives

The range of lubricants used in the experimental programme consisted of a base stock oil and its full additive formulation. The base stock lubricant was a mineral base oil commercially known as Stanco 150, the properties of the oil and the nature of the additive package can be seen in Table 2.

3.6 Test Programme Description

3.6.1 Objective 1

As mentioned previously in this chapter, the introduction of more laboratory based test rigs to replace fired engine and dynonometer rigs for the evaluation and testing of lubricants and materials, requires the reproduction of failures occuring in engine test and service conditions. In addition, laboratory based test rigs should allow a more simplistic approach to understanding the fundamental mechanisms occuring during these wear processes.

This series of tests therefore, have been concerned with lubricant and material behaviour under well defined conditions with a base and fully formulated oil, using a range of well established production materials. The materials used include case hardened steel, chilled white cast iron, induction hardened grey flake iron, hardened and tempered nodular iron and carbonitrided grey flake iron. The test conditions can be seen in Table 3, the only variable being load. The different loads chosen, 80 kg and 120 kg were used to produce two different lubrication regimes, mixed elastohydrodynamic "thin film" and boundary lubrication conditions respectively, based on results from pilot tests.

3.6.2 Objective 2

The "running in" of cam and follower surfaces has, in this investigation been analysed using both fully formulated and a base oil. The material combination used exclusively for these tests was a case hardened steel cam and a chilled white iron follower, thus eliminating

the effects of free graphite in microstructures on the 'running in' characteristics of these materials. This series of experimental work consisting of five main test procedures, the conditions of which can be seen in Table 4.

i) The use of the replication technique to build up a surface topographical 'story' of how cam surfaces 'run in' and conform with time, using both fully formulated and base oils.

At periodic time intervals during testing, an oil sample was withdrawn from the lubricant tank for wear debris analysis and the test immediately stopped. When sufficiently cooled, a replica of the cam surface was taken without removing the cam specimen or dismantling the apparatus. Once the replica of the cam surface was formed and dried it was removed and logged for analysis and the test restarted for the next predetermined test time interval.

ii) The need for the use of E.P. additives in oils for the satisfactory 'running in' of cam/follower applications is well established, yet not fully understood. This test procedure attempted to analyse and illustrate whether such systems can operate satisfactorily with a non-additive base oil after the successful 'running in' of a cam/follower combination with a fully formulated oil. The combination was tested for 40 hours in a fully formulated oil, allowing satisfactory 'running in' of the surfaces, shown by a stabilised friction coefficient. The test was then stopped, the cam specimen removed and the surface analysed using energy

dispersive x-ray techniques. Once the presence of surface films had been established associated with the use of additives such as Z.D.D.P., the cam specimen was returned to the test rig apparatus and the fully formulated oil replaced with a base oil and the test continued for a further 60 hours. After the test was completed the cam surface was again analysed to establish the continued existence of these surface films from the fully formulated oil and its correlation with friction coefficient and debris formation.

iii) This test procedure was similar to ii) in that the surfaces of the cam/follower combination were 'run in' satisfactorily with a fully formulated oil, a stable coefficient of friction produced and the subsequent removal and analysis of the cam and the replacing of the fully formulated with a base oil and the recommencement of the test. In this test procedure however, the experiment was periodically stopped and both qualitative and semi-quantative x-ray dispersive analysis carried out on the cam and follower surfaces. This procedure was adopted in order to obtain information on additive film depletion under these stop/start boundary conditions, and its effect on the removal of these surface films.

iv) The use of E.P. additives to assist the 'running in' of surfaces works essentially by a mechanism of asperity fracture and plastic deformation without the formation, particularly in ferrous materials of scuffing and white layer production which could cause catastrophic failure by a spalling mechanism.

In this test procedure it was thought possible that a surface could be artificially formed so as to eliminate the 'running in' process during testing. Diamond lapping proved to be the most satisfactory method of producing the artificially run in surface. The cam and follower specimens were then tested in a base oil to analyse the behaviour of these materials and to ascertain the necessity of E.P. additives in such systems when surfaces can be artificially formed.

3.6.3 Objective 3

This experimental work involved the use of new materials for cam follower applications. The materials were in insert form 17 x 12 x 3 mm in size and epoxy bonded into a standard mild steel follower. The materials consisted of toughened zirconia, silicon carbide and sialon ceramics, oxyacetylene deposited nickel and cobalt rich hard facing alloys and a ceramic fibre reinforced aluminium silicon alloy, the chemical and physical properties of which can be seen in Tables 5, 6 and 7. The tests were conducted using an additive free base oil, the full test conditions can be seen in Table 8.

CHAPTER 4

4. RESULTS

4.1 INTRODUCTION

The results accumulated during the experimental work and subsequently reported in this section consist of at least three experiments per individual test sequence. This was carried out to ensure reproducability under the particular test conditions, thus eliminating any spurious individual results that could affect the final analysis. The number of results accumulated during the experimental work was considerable, and only those most relevant are presented.

The use of the weight loss measurement technique for the detection of wear rates was found to give unsatisfactory results, i.e. a lack of correlation with other wear diagnostic techniques. Reasons for this are varied, but are due mainly to the large effective surface area of the cam specimen, material transfer phenomena and the effect of a hot oil medium on epoxy resins used for the bonding of insert materials into follower specimen recesses.

The wear direction on the majority of photographs used in the results section, both optical and scanning electron, are left to right and top to bottom respectively, unless otherwise stated.

All specimens used for metallographic taper-sectioning were etched in 2% Nital for 15 seconds unless otherwise stated.

4.2 Results - Objective One; Tests 1A-1D

Material combination:- Cam - Case hardened steel

Follower - White cast iron

Test 1A - Fully formulated oil, 80 Kg peak load.

Test 1B - Base stock oil, 80 Kg peak load.

Test 1C - Fully formulated oil, 120 Kg peak load.

Test 1D - Base stock oil, 120 Kg peak load.

4.2.1 Friction Measurements

Coefficient of friction measurements versus test time are shown in Fig. 25, and it can be seen that the increase in friction coefficient is dependent upon the severity of the test conditions. Test 1A, with a load of 80 kg and the fully formulated oil possesses the lowest coefficient of friction, levelling off after 10 hours to a typical value of μ of around 0.16. This is in complete contrast to test 1D, with a load of 120 kg and the mineral base oil where the coefficient of friction rises continuously with test time up to the end of test at around 40 hours to a value of μ of 0.42. It is interesting to note that the tests with the fully formulated oil all initially have a high coefficient of friction which appear to level off after 6 to 10 hours testing, this was considered to be the 'running in' process and thus illustrates the effectiveness of additives in the oil, especially those of the extreme pressure 'EP' type.

4.2.2 Spectrometric Oil Analysis S.O.A.P.

Iron wear debris p.p.m. concentrations versus test time are shown in Fig. 26, and again shows a similar trend to the coefficient of friction results. At low loads using a fully formulated oil, test 1A, a maximum

concentration of 10 p.p.m. was found, this being typical of a normal wear rate and is in complete contrast to test 1D, where concentrations in excess of 50 p.p.m. were apparent after only 10-12 hours testing. An interesting feature was found for test 1B, using the mineral base stock at low loads which shows a high initial wear debris concentration upto 4 hours testing, of 30 p.p.m., followed by a gradual steady-state increase to the end of test, giving a maximum ferrous debris concentration after 40 hours of around 34 p.p.m. This appears to show that the majority of wear damage occurred in the early stages of operation and thus can be construed as a 'running in' problem. Test 1C, using a high load and fully formulated oil shows a high but steady increase in wear debris concentration with time, but appears to level off after about 25 hours testing.

4.2.3 Optical Examination

Optical examination of the wear surfaces of the low load tests, tests 1A and 1B can be seen in Figs. 27b, 28 and 34-36. In test 1A using the fully formulated oil the cam surface appears to have become smoother when compared with the 'as ground' cam surface shown in Fig. 27A. The manganese sulphide inclusions are still clearly present with evidence of slight abrasive wear running in the wear direction. Examination of follower surface at the worn/unworn interface shows what appears to be a corrosion/etching effect on the follower surface of a intercarbidic nature, where the pearlitic/bainitic matrix has been attacked.

The cam surface of test 1B using the mineral base stock oil can be seen in Figs. 34 and 35. After initial examination, the surface was etched in 2% nital for 10 seconds to observe any etch-resistant phases. The

general appearance of the cam specimen shows a typically 'scuffed' surface ie. extensive plastic deformation and successive layers of delaminated material. Fig. 34 shows small white etch resistant areas, which were considered unlikely to be 'white layer'. Fig. 35 shows the general morphology of white layered areas, which are banded following the circumference of the cam specimen, stopping only at inclusions. These small rounded etch resistant phase were considered to be due to carbide fracture from the chilled white iron follower causing transfer and embeddment into the cam surface. Examination of the follower surface, however, shows no immediate signs of carbide detachment. Fig. 36 shows the worn/unworn interface of the follower wear surface, with only evidence of slight staining of the wear surface caused by oxidation products from the oil during the test.

Optical examination of the wear surfaces of one of the high load tests, 1C can be seen in Figs. 44 and 45. The cam wear surface shows no obvious severe wear damage, shown again by the ease of which the manganese sulphide inclusions can be seen, running at 90° to the wear direction. What is evident however, is the chemical attack of the cam surface by the additives present in the oil, Fig. 44. Examination of the follower surface shows heavy pitting, with the detachment of large spalled areas. The remaining adjacent material is extensively 'craze cracked' to form small islands of material on the surface, and again the microstructure of the white cast iron is clearly visible due to additive etching effect, Fig. 45. Optical examination of wear surfaces in Test 1D, showed extensive damage and staining, to such an extent that no clear wear features could be readily identified.

4.2.4 Scanning Electron Microscopic Examination (S.E.M.)

S.E.M. examination of the wear surfaces of the low load tests, test 1A and 1B can be seen in Figs 29, 30 and 37, 38. In test 1A both the cam and follower surfaces show the same wear 'damage' as optical examination. The cam wear surface, Fig. 29 shows a smoother surface than the original 'as ground' surface as shown in Fig. 155A, with manganese sulphide inclusions clearly visible. The follower surface at the worn/unworn interface again shows the corrosive nature of the additive package, where intercarbidic attack of matrix microstructure is clearly seen leaving carbide in relief (Fig. 30). In test 1B, examination of the cam surface shows the heavily plastically deformed features typically associated with a scuffed surface (Fig. 37). The follower surface however, shows no evidence of any extensive wear damage, Fig. 38, which confirms the information gathered from optical examination.

S.E.M. examination of the high load tests, test 1C and 1D can be seen in Figs. 46, 47 and 51, 52. In Test 1C, the cam wear surface shows isolated areas of plastic deformation, similar to that found in scuffing (Fig. 46). The follower wear surface, Fig. 47, shows the extent of the surface pitting and the adjacent 'unspalled' areas with associated chemical attack of the matrix microstructure leaving carbide networks in relief. S.E.M. examination of the wear surfaces of Test 1D can be seen in Figs. 51 and 52. The cam wear surface shows extensive plastic deformation and severe delamination, typical of a scuffed surface (Fig. 51). The follower wear surface however, shows no sign of the 'pitting' wear shown in test 1C, Fig. 47, instead areas of what appears to be plastic deformation of the follower surface can be seen in Fig. 52. This is not frequently encountered with white cast irons due to the high

carbide content and their low ductility and was thus considered to be due to material transfer and 'smearing' from the cam surface.

4.2.5 Metallographic Examination

Taper microsections taken through both cam and follower specimens in the test series 1A to 1D can be seen in Figs. 31, 32, 39-42, 48, 49, 53 and 54. Under low load conditions with a fully formulated oil, test 1A, the cam specimen showed no deliterious surface/subsurface effects (Fig. 31). This is also the case with the follower specimen even though under optical examination the chemical attack of the surface appeared to be severe enough, it was not resolvable by standard optical techniques (Fig. 32). The cam specimen from test 1B, using low load conditions and the mineral base oil, however, showed different effects. Fig. 39, shows considerable white-layer production across the whole surface of the cam, with some areas of surface spalling and the band of tempered material progressing and gradually fading into the parent microstructure. Higher magnifications of the surface, Fig. 40, again shows this white layer and the associated carbide particles in the surface, and by focussing further into the epoxy resin surface in the same position, more areas of transferred carbide can be seen, (Fig. 41). The follower specimen showed no surface/subsurface damage (Fig. 42).

Under high load conditions with a fully formulated oil, test 1C, the cam specimen showed only isolated areas of white layer, (Fig. 48) the darker area in the sub surface being the higher carbon rich case. Examination of the follower specimen, Fig. 49, shows the extent of the surface/subsurface cracking. Cracking occurs throughout the section, the point of initiation being unkown, whether surface or subsurface initiated. Closer examination shows the cracking and

fracture to be of an inter-carbidic nature, with evidence also of some corrosive attack just below the surface. Test.1D, using a mineral base oil shows extensive damage to both the cam and follower specimens. The cam specimen, Fig. 53 shows again that without the presence of additives, scuffing and extensive white layer production occurs. This is again reflected by the examination of the follower specimen, which shows surface roughening and fracture and also the transfer and subsequent 'white layer' transformation of material from the cam (Fig. 54).

4.2.6 Wear Debris Examination

S.E.M. examination of the wear debris from the tests 1A to 1D can be seen in Figs. 33, 43, 50 and 55. The size, morphology and concentration of the debris again shows a similar trend to the coefficient of friction and spectrometric oil analysis results ie. the increase and concentration of debris is related to the severity of the test. The morphology and sizes range from small platelet type wear debris of typical size 2-3 microns from test 1A, low load and fully formulated oil, Fig. 33, to large 'chunky' type debris of typical size 25-30 microns from test 1D, high load and the mineral base stock oil (Fig. 55).

4.3 Results - Objective One, Tests 1E-1H

Material combination - Cam - Grey flake iron, induction hardened.
Follower - Case hardened steel.

Test 1E - Fully formulated oil, 80 Kg peak load.

Test 1F - Base stock oil, 80 Kg peak load.

Test 1G - Fully formulated oil, 120 Kg peak load.

Test 1H - Base stock oil, 120 Kg peak load.

4.3.1 Friction Measurements

Coefficient of friction measurements versus test time are shown in Fig. 56 and it appears that the final results for the coefficients of friction are independent of the severity of the test conditions. The corresponding values however are an order of magnitude lower than for tests 1A to 1D and appear to be due to the presence of free graphite in the cam microstructure acting as an addition to the E.P. additive. This is confirmed by the form of the friction curves under low load conditions, test 1E and 1F. Both curves exhibit the same high initial coefficient of friction followed by levelling off to lower steady state values of μ of 0.07 and 0.17 respectively. Tests under high load conditions, test 1G and 1H show a gradually increasing coefficient of friction for both tests up to 10 hours, then gradually decreasing to values of 0.1 and 0.15 respectively, an important point being that both of these values are below that of Test 1F under low load conditions.

4.3.2 Spectrometric Oil Analysis S.O.A.P.

Iron wear debris p.p.m. concentration versus test time are shown in Fig. 57, the results showing no correlation with coefficient of friction values μ. The curves produced, appear to follow the same trends as those obtained from test 1A to test 1B, the increases in debris concentration are dependent upon the increase in test severity, this ranges from 8 p.p.m. iron concentration after 40 hours for test 1E to 50 p.p.m. iron concentration 'off scale' after 9 hours for test 1H.

4.3.3 Optical Examination

Optical examination of the wear surface of the low load tests, tests 1E and 1F can be seen in Figs. 58, 59 and 65-67. In test 1E using the fully formulated oil the cam surface again appears to have become smoother

than the original ground surface, Fig. 58, clearly visible on the cam surface are the graphite flakes present in the microstructures and areas of slight abrasive wear. The follower surface has also become smoother, Fig. 59, although some chemical attack has occurred at the grain boundaries. Optical examination of the cam surface of Test 1F can be seen in Figs. 65 and 66, and shows a dark colouration covering the whole cam surface. It is important to note that this smearing effect only occurred with materials having free graphite in the microstructure, and therefore provided circumstantial evidence linking this effect to graphite smearing. Confirmation of this came on removal of the specimen for microscopic examination when the smeared coating was partly removed by passing a finger across the surface, the remainder of the coating removed by cleaning with a solvent immediately prior to S.E.M. examination. Also evident are areas of phosphide eutectic present in the microstructure and shown by small isolated white areas. The case hardened steel follower of test 1F can be seen in Fig. 67, and again shows graphite smearing over the surface, transferred from the free graphite present in the cam microstructure.

Visual examination of the cam wear surfaces from the high load tests, tests 1G and 1H showed extensive wear damage, removal of the induction hardened layer and the 'machining' away of the effective cam profile. The follower surface also showed extensive wear damage with deep recesses evident in the surfaces. The combination of the two forms of wear damage effectively resulted in two samples not acting as a cam and follower but a cylinder on a static block, hence the comparatively 'low' friction coefficient found for test 1G and 1H when compared with test 1F, Fig.56. The extent of the wear damage on closer examination was so great as to become unresolvable using

standard optical techniques.

4.3.4 Scanning Electron Microscopic Examination (S.E.M.)

S.E.M. examination of the wear surfaces of the low load tests, tests 1E and 1F can be seen in Figs. 60, 61, 68 and 69. S.E.M. examination of the wear surfaces of test 1E, using the fully formulated oil shows the same features as those evident from optical examination, the graphite structure and abrasive wear of the cam surface, Fig. 60, and the grain boundaries, caused by the chemical attack of additives on the follower surfaces (Fig. 61). Examination of the wear surfaces from Test 1F, using the mineral base oil can be seen in Figs. 68 and 69. Both the cam and follower surfaces show evidence of slight abrasive wear with the absence of any significant plastic deformation.

S.E.M. examination of the wear surface of the high load tests, test 1G and 1H can be seen in Figs. 73, 74, 78 and 79. Examination of the wear surfaces from test 1G, using the fully formulated oil shows extensive deformation of both the cam and follower surfaces (Figs. 73 and 74). Closer examination of the cam wear surface, Fig. 73, shows what appears to be pitting of the surface, the bottom of individual pits having morphologies similar to the matrixes of the graphite networks present in the microstructure. Examination of the wear surfaces of test 1H, using the mineral base oil shows extensive plastic deformation and what appears to be material transfer from both cam and follower surfaces (Fig. 78 and 79).

4.3.5 Metallographic Examination

Taper microsections taken through both cam and follower specimens in the test series 1E to 1H can be seen in Figs. 62, 63, 70, 71, 75, 76, 80 and 81. Under low load conditions using both fully formulated and

mineral base oil, tests 1E and 1F, no sub-surface damage or 'white layer' was present in either the cam or follower specimen samples, due to presence of free graphite in the cam microstructure, Figs. 62, 63, 70 and 71.

Under high load conditions with the fully formulated oil, test 1G, an important feature is the lack of any extensive white-layer production, although there is considerable wear damage. Examination of the cam specimen, Fig. 75, shows extensive material removal, the size and shape of the particles becoming detached from the surface are dependent upon the intergraphitic spacing of the microstructure. Examination of the follower surface shows considerable material transfer from the cam nose effectively building up the thickness of the surface with extensively transformed and plastically deformed material. Test 1H, using the mineral base oil shows, on the cam surface, evidence of extensive white layer running the whole length of the contact width, Fig. 80. The follower surface, Fig. 81, shows considerable sub-surface damage, running up to 2mm below the surface. This damage consists of both white layer and plastically deformed material, it is difficult to detect whether this material has been transferred from the cam, however, information gathered from test 1G, Fig. 76, concerning the follower specimen would suggest that this material is in fact, transferred and subsequently transformed material from the grey cast iron cam after the induction hardened layer had been removed.

4.3.6 Wear Debris Examination

S.E.M. examination of wear debris from the tests 1E-1H can be seen in Figs. 64, 72, 77 and 82. The wear debris from tests carried out under low load conditions, tests 1E and 1F, show sizes in both cases of 5μm max, Figs. 64 and 72, this being typical of steady state normal wear conditions. Tests 1G and 1H under high load conditions however, show

conflicting results to those normally expected. The general debris size from test 1G, using the fully formulated oil, Fig. 77, is in fact larger, with a chunkier morphology than the debris from test 1H, Fig. 82, using the mineral base oil.

4.4 Results - Objective One, Test 1I-1L

Material combination - Cam - Grey flake iron, carbonitrided.

Follower - Nodular cast iron, hardened and tempered.

Test 1I - Fully formulated oil, 80 Kg peak load.

Test 1J - Base stock oil, 80 Kg peak load.

Test 1K - Fully formulated oil, 120 Kg peak load.

Test 1L - Base stock oil, 120 Kg peak load.

4.4.1 Friction Measurements

Coefficient of friction measurements versus test time are shown in Fig. 83, and it can again be seen that the increase in friction coefficient is dependent upon the severity of the test conditions. Friction coefficients after 40 hours testing range from 0.1 for Test 1I to 0.45 for test 1L. It is important to note the 'running in' effects for tests 1I to 1K i.e. initially high but decreasing to lower steady state values. This shows in the case of tests 1I and 1K, the use of E.P. additive formulations in fully formulated oil to assist 'running in', but also in the case of test 1J, low load and a mineral base oil the possible effects of free graphite in the microstructure which appears to assist 'running in'. Test 1L, however shows a steady increase in the coefficient of friction to the end of the test at 40 hours to a value of μ of 0.45.

4.4.2 Spectrometric Oil Anaylsis S.O.A.P.

Iron wear debris p.p.m. concentration versus test time are shown in Fig. 84, and shows a similar trend to the coefficient of friction results. At low loads using a fully formulated oil, test 1I, a maximum concentration of 13 p.p.m. iron concentration was found, being typical of a normal wear rate is in complete contrast to test 1L where concentrations in excess of 50 p.p.m. were apparent after only 15 hours testing. Tests using the mineral base oil at low loads, test 1J and the fully formulated oil at high loads, test 1K gave iron concentrations after 40 hours of 16 and 41 p.p.m. respectively.

4.4.3 Optical Examination

Optical examination of the camwear surfaces of the low load tests, tests 1I and 1J can be seen in Figs. 85 and 91. In test 1I using the fully formulated oil, the cam surface has become smoother with the graphite structure clearly visible. Also apparent is evidence of slight abrasive wear, and etched areas caused by additives in the oil.

The cam surface of test 1J using the mineral base oil shows the graphite structure of the cast iron, however, there are areas of what appear to be spalling or pitting of the cam surface characterised by the dark areas randomly distributed across the surface (Fig. 91). Optical examination of the cam wear surfaces of the high load tests, tests 1K and 1L can be seen in Figs. 97 and 103. Using the fully formulated oil, test 1K, the cam surface again clearly shows the graphite network and the chemical attack of the surface by the additive formulation, (Fig. 97). The extent of this attack however is of a more severe nature than the corresponding test using a low load, test 1I, (Fig.85). Optical examination of the cam surface of test 1L, using the mineral base oil shows severe wear damage of the whole cam surface. Extensive plastic deformation is clearly evident with no microstructural

features visible. Cracks running at 90° to the wear direction can also be seen (Fig. 103).

4.4.4. Scanning Electron Microscopic Examination (S.E.M.)

S.E.M. examination of the wear surfaces of the low loads tests, test 1I and 1J can be seen in Figs. 86, 87, 92 and 93. Examination of the cam wear surface of test 1I, using the fully formulated oil shows again the graphite network apparent across the whole surface (Fig. 86). There is evident of slight plastic deformation, but this can be attributed to the initial grinding operation during the production of the cam specimens. Examination of the corresponding follower surface, Fig. 87, shows smoothing of the surface, with the graphite nodules, present in the microstructure, clearly evident. Close examination shows the removal of some of the graphite from the nodule cavities shown by smearing of the surface by the graphite. Examination of the cam surface of test 1J, using the mineral base oil, shows the graphite network present on the surface and a series of pits, the size and initial failure of which appears to be controlled by the spacing of these graphite networks, (Fig. 92). Examination of the corresponding follower surface, Fig. 93, again shows graphite smearing and the presence of the nodule cavities. It can be seen however, that plastic deformation has in fact occurred around these cavities when compared to the follower surface of test 1I, Fig. 87, giving some idea of the plastic deformation over the whole wear surface not shown by the affect of these surface discontinuities.

Examination of the wear surfaces of the high load tests, test 1K and 1L can be seen in Figs, 98, 99, 104 and 105. Examination of the cam surface of test 1K, using the fully formulated oil, shows the general

smoothing of the surface with the graphite structure clearly present, Fig. 98. Also evident are the surface films formed by additive interactions, shown by the grey areas on the wear surface. Examination of the follower surface from test 1K, again shows the general smoothing of the cam surface. The graphite present in the nodule cavities has been totally extracted leaving the empty cavities and it can be seen under closer examination, the dendritic nature of the graphite nodule clearly evident at the bottom of these cavities. Examination of both the cam and follower wear surfaces, using the mineral base oil, test 1L, show extensive plastic deformation, delamination and general severe wear damage associated with scuffed surfaces.

4.4.5 Metallographic Examination

Taper microsections taken through both cam and follower specimens in the test series 1I to 1L can be seen in Figs. 88, 89, 94, 95, 100, 101, 106 and 107. Examination of the cam and follower wear surfaces of the low load tests, tests 1I and 1J using the fully formulated and mineral base oils showed no significant surface or subsurface wear damage (Figs. 88, 89, 94 and 95). This lack of damage is also evident in test 1K, at high loads and the fully formulated oil in both the cam and follower specimens, Figs. 100 and 101. Examination of the surfaces from test 1L, using the mineral base oil however, shows extensive surface and subsurface wear damage and white layer production, running the whole width of the contacting surfaces, (Figs. 106 and 107).

4.4.6 Wear Debris Examination

S.E.M. examination of the wear debris from test 1I to 1L can be seen in Figs. 90, 96, 102 and 108. The size and morphology of the wear debris

again appears to be dependent upon the severity of the test conditions. The size and morphology ranges, start with the small platelet type debris, 2-3 microns in size from test 1I, to the large, angular debris, 20-25 microns in size from test 1K.

4.5 Surface Roughness Measurements

The use of surface profilometry as a wear diagnostic 'tool' is very well established, one of the most popular techniques and machine used is the Rank Taylor Hobson Talysurf which supplies a range of surface information in a two dimensional array. A relatively new technique has been developed however, which allows a three-dimensional surface topographical 'map' of a particular surface produced by the interfacing of a microprocessor system controlling a multi-trace talysurf needle movement.

This area of the results section is devoted to the comparison of these two techniques, and their relative advantages and disadvantages. With the range of wear failures and phenomena produced during the test series 1A to 1L, wear surfaces were selected and the surfaces analysed using both techniques, these surfaces were as follows:-

Characterization of Surface		Test No.	Figure No.
a)	'As Ground'		109
b)	Scuffing Wear	Test 1B (Base Oil, 80Kg Load)	110
c)	Pitting Wear	Test 1C (F.F. Oil, 120Kg Load)	111
d)	Severe Wear	Test 1H (Base Oil, 120Kg Load)	112
e)	Polishing Wear	Test 1A (F.F. Oil, 80Kg Load)	113

From the results obtained the relative advantages and disadvantages of both techniques are clearly evident. For instance, it can be seen that the use of a single talysurf trace does not allow the general, overall morphology and distribution of wear features to be clearly observed. An example of this is shown by reference to Fig. 109 of the 'as ground' surface. Using the '3D' talysurf technique the undulations in the surface, running at 90° to the wear direction and produced by the grinding operation can be clearly seen. This is caused by the abrasive ploughing nature of the grinding process and it can be seen that phenomena is not shown by the use of the conventional single talysurf trace. This is further highlighted with reference to the severe wear surface shown in Fig. 112. Using the 30 multi-trace technique the surface damage can be seen to be almost entirely of an abrasive nature, shown again by this ploughing effect giving an almost identical surface morphology along the wear direction. However, these wear features are in complete contrast to the pitting failure shown in Fig. 111, where the pitting is randomly distributed and orientated across the surface of the white cast iron specimen. The use of the 3D multi-trace technique obscures and hinders the calculation of the depth and the form of individual pits and thus relies on the conventional single talysurf trace to give us this additional information, and this is true for all of the surfaces analysed using both techniques.

4.6 Results - Objective Two, Tests 2A and 2B

4.6.1 Introduction

Material combination - Cam - Case hardened steel

Follower - White cast iron

Test 2A - Fully formulated oil, 80 Kg peak load.

Test 2B - Base stock oil, 80 Kg peak load.

The tests lasted for a duration of 80 hours in total. At periodic intervals oil samples were taken, and the test was immediately stopped and allowed to cool down. The cam surface was then cleaned and acetate replicas taken of the surface to monitor the change in surface topography with test time.

4.6.2 Friction Measurements

Coefficient of friction measurements versus test time are shown in Fig. 114, and it can be seen that for test 2A, using the fully formulated oil after an initial high coefficient of friction μ of 0.2, friction gradually decreased to a lower steady value of around 0.11 after 20 hours testing, and remained at this level to the end of the test at 80 hours. Test 2B, using the mineral base oil however, showed completely different results. After an initial large increase in the friction coefficient μ, the friction continued to rise to a value of 0.37 after 80 hours.

4.6.3 Spectrometric Oil Analysis (S.O.A.P.)

Iron wear debris p.p.m. concentrations versus test time can be seen in Fig. 115, and show a gradual increase in wear debris concentration for test 2A from 8 p.p.m. after 4 hours to a total of 11 p.p.m. after 80 hours testing, this being typical of a low or 'normal' wear rate. Test 2B using the mineral base oil however shows a very high initial in wear debris concentration, of around 30 p.p.m. after 5 hours, suggesting a high wear rate in the early stages of testing. This large increase in wear debris concentration tends to level off after 15 hours from there it increases gradually to a total of around 42 p.p.m. after 80 hours.

4.6.4 Semi-Quantitative Wear Debris Analysis (P.Q. Index)

The graph of wear particle index (PQ) versus test time can be seen in Fig. 116, and shows a similar trend to the curves obtained from spectrometric oil analysis. Test 2A shows a gradual increase in wear debris concentration with test-time, giving a maximum index value of around 20 after 80 hours of test. Test 2B however, again shows a large initial increase to around 200 after 10-12 hours, the increase then levelling off to around 220 after 80 hours again indicating a high wear rate during the early stages of testing.

4.6.5 Surface Replication

Cam surface replicas of both tests, test 2A and 2B with time can be seen in Figs. 117 to 121. Test 2A using the fully formulated oil, shows the cam surface becoming gradually smoother with test time. After 30 minutes it can be seen that slight abrasive wear starts to appear, Fig. 117e, typical of normal wear and it is apparent that after 2 hours, any reminants of the as ground surface had disappeared (Fig. 118e). The surface became increasingly smoother until at 70 hours a surface not dissimilar to a metallographically prepared surface had been produced (Fig. 121e). This is in complete contrast to test 2B, using the mineral base oil where after only 15 minutes extensive surface damage had occurred. Closer examination of the replica after 15 minutes testing, Fig. 117d, shows actual wear debris attached to the replica itself, thus illustrating the amount of wear debris being produced during the early stages of testing. It can then be seen that the surface becomes progressively damaged with test time, with the depth of wear damage increasing, characterized by the darker contrast of the wear features in the photographs, and this is illustrated by comparing for instance Fig. 117d, after 15 minutes with Fig. 121, at 70 hours.

4.6.6 Optical Examination

Examination of the cam surface of test 2A, using the fully formulated oil, showed the surface to have become increasingly smoother, similar in fact to a surface that had become metallographically polished. A standard unworn cam was then prepared metallographically to a 1µm diamond finish for comparison with the cam of test 2A, and showed in the 'as polished' conditions, considerable similarities between the two. Both surfaces were subsequently etched in 2% Nital for 10 seconds, the 'as polished' cam surface can be seen in in Fig. 122, clearly showing the martensitic microstructure. The cam surface from test 2A after subsequent etching is not dissimilar and a martensitic transformed type of structure can be seen, Fig. 123. although it is not as clear as Fig. 122.

4.6.7 Wear Debris Examination

S.E.M. examination of the wear debris from both tests and from different times during testing can be seen in Fig. 124. Wear debris obtained from the tests after 5 minutes duration can be seen in Figs. 124a and 124b. Debris from the fully formulated oil, test 2a, Fig. 124a, show thin platelets in the size region of 5 microns, with some evidence of spheroidal debris commonly found during 'running in'. This is in complete constrast to the wear debris from the mineral base oil, test 2B, Fig. 124b, after 15 minutes, where platelet debris sizes ranging up to 40 microns, illustrating the initial severe wear damage during the early stages of testing. The size of wear debris from test 2A after 50 hours, has in fact decreased to an average platelet size of around 2-3 microns, Fig. 124c, typical of a low wear rate. It can be seen however, that the wear debris from test 2B after 50 hours has become more angular and 'chunky' in morphology with particles of up to 50 microns in

size clearly evident, Fig. 124d, suggesting, a spalling type of wear mechanism.

4.6.8 Metallographic Examination

Taper microsections taken through the cam surfaces of both test 2A and 2B, can be seen in Fig. 125. A section taken through test 2A, using the fully formulated oil after 75 hours shows no surface or sub-surface damage, the microstructure is unaffected. A cam tapersection taken through test 2B, using the mineral base oil, after only 1 hour testing shows considerable white layer formation and the associated tempered layer. Fig. 125b, also shows evidence of cracking of this white layer, which leads to the spalling of particles in excess of 50 microns, after 75 hours as shown in Fig. 125c. These observations confirm the wear debris results.

4.7 Results - Objective Two, Tests 2C to 2E

4.7.1 Introduction

Material combination - Cam - Case hardened steel.

Follower - White cast iron.

Test 2C - 0-40 Hrs, fully formulated oil, 40-80 Hrs, Base stock oil.

Test 2D - 0-40 Hrs, fully formulated oil, 40-80 Hrs, Base stock oil.

Test 2E - 0-80 Hrs, Base stock oil.

Test 2C The test lasted 80 hrs in total and comprised of running the test for 40 hrs in a fully formulated oil, stopping the test, draining the oil and replacing with the mineral base oil for the duration of test.

Test 2D The test lasted 80 hrs in total and comprised of running the test 40 hrs in a fully formulated oil, stopping the test, draining the draining the oil and analysing the cam surface by EDAX X-Ray dispersive techniques for the presence of additive film formation on the cam surface. The fully formulated oil was then replaced with the mineral base oil and the test recommenced. At periodic intervals the test was stopped, and EDAX analysis carried out on the cam surface to observe any depletion in the surface films with test time.

Test 2E The test lasted 80 hrs in total and comprised of artificially 'running in' both the cam and follower specimen by diamond lapping the surface to a 1μm finish, and testing in a mineral base oil.

4.7.2 Results, Test 2C

4.7.2.1 Friction Measurements

Coefficient of friction measurements versus test time are shown in Fig. 126. In test 2C, the high initial friction coefficient is again present, which is typical of the use of fully formulated oils and decreases to a lower steady state value of around 0.1, up to 40 hours. After replacing the fully formulated with the mineral base oil the friction increases very slightly for the remaining 40 hours to a maximum μ value of around 0.13.

4.7.2.2 Spectrometric Oil Analysis S.O.A.P.

Iron wear debris p.p.m. concentrations versus test time can be seen in

Fig. 127, and shows a wear debris concentration of 10 p.p.m. after 2 hours, reaching around 11 p.p.m. at 40 hours when the oil was changed. From there the concentration increases from 1 to 3 p.p.m. after 10 hours testing in the mineral base oil (50 hours in total) and rises to a maximum of around 4 p.p.m. after 80 hours testing, indicating no significant wear damage occurring after the substitution of the mineral base oil.

4.7.2.3 Semi-Quantitative Wear Debris Analysis (P.Q. Index)

The graph of wear particle index (PQ), versus test time can be seen in Fig. 128, and shows for test 2C, the same general trend as the spectrometric oil analysis. A gradual increase from an index of around 12 at 2 hours to an index of 15 at 40 hours testing. The fall and then gradual increase in index number can be seen between 40 and 50 hours testing from 2 to 10 PQ index rising to a maximum index number of around 11 after 80 hours testing.

4.7.2.4 Scanning Electron and X-Ray Dispersive Surface Analysis (EDAX)

S.E.M. examination of the cam and follower surfaces can be seen in Figs. 129a and 129b. Both wear surfaces show no appreciable wear damage, with the cam surface becoming smoother than the original ground finish (Fig. 144). The follower surface shows some signs of the chemical etch attack from the fully formulated oil, Fig. 145, and in both samples surface films are still evident even after solvent cleaning. EDAX analysis of the cam surface confirms the presence of these films. Fig. 129c shows x-ray energy spectra for phosphorus, sulphur, zinc and calcium, these elements being present in zinc dialkyldithiophosphate (Z.D.D.P), the extreme pressure additive, and calcium sulphonate the dispersant.

4.7.2.5 Metallographic Examination

Taper-microsections of both the cam and follower surfaces from Test 2C can be seen in Figs 130 and 131. These surfaces show no evidence of any surface/subsurface damage or in the case of the cam surface, white layer formation.

4.7.2.6 Wear Debris Examination

S.E.M. examination of the wear debris from test 2C can be seen in Fig. 132. The debris has a platelet morphology in the size range 3-10 microns.

4.7.3 Results, Test 2D

4.7.3.1 Friction Measurements

Coefficient of friction measurements versus test time are shown in Fig. 126. Test 2D shows the same general trend as test 2C, a high initial coefficient of friction, levelling off to a lower steady state value of μ of 0.12. This value increases after the addition of the mineral base oil at 40 hours to a maximum value of 0.14 μ after 80 hours testing.

4.7.3.2 Spectrometric Oil Analysis S.O.A.P.

Iron wear debris p.p.m. concentration versus test time can be seen in Fig. 127, and again shows a similar trend to test 2C. After 2 hours the iron concentration is 12 p.p.m, slowly increasing to around 14 p.p.m. after 40 hours. After the addition of the mineral base oil and the stopping of the test after 50, 60 and 70 hours for cam surface elemental analysis a decrease and increase can be seen, at each of the points of test stoppage and is probably caused by the lubricant not mixing and or the gravitational movement of the wear debris through the oil. Extrapolation of the curve further would show that the wear debris content increases gradually and appears to be independent of the form or rheology of the lubricant, and reaches a maximum of around 16 p.p.m. after 80 hours.

4.7.3.3 Semi-Quantitative Wear Debris Analysis (P.Q. Index)

The graph of wear particle index (PQ) versus test time can be seen in Fig. 128, and again shows the same trend as spectrometric oil analysis with a gradual increase with test time and the decrease or increase effects due to test stoppage. After an initial increase in the wear particle index to around 18 after 2 hours the increase then becomes less pronounced, reaching around 20 after 40 hours and a maximum of 30 after 80 hours.

4.7.3.4 Scanning Electron Microscopic Examination (S.E.M.)

S.E.M. examination of the follower surface after 40, 50, 60 and 70 hours testing can be seen in Figs. 133, 135, 137, and 139 respectively. Immediately prior to surface examination and analysis, the follower specimen was degreased by immersion in a petroleum ether solution for 10 seconds, thus removing the oil and leaving any additive films present on the surface. Examination of all the surfaces shows the general chemical attack caused by the additives present in the fully formulated oil. Also present on all of the follower surfaces is the presence of additive film formation shown by the dark colouration of the surface. Closer examination of the surfaces show these additive films to be less apparent with test time, suggesting the gradual removal of these films with test time.

4.7.3.5 X-Ray Dispersive Surface Analysis (EDAX)

The EDAX energy spectra for the follower surfaces after 40, 50, 60 and 70 hours can be seen in Figs. 134, 138 and 140 respectively. The scan for each follower surface shows the characteristic spectra for additive films ie. the presence of elements such as phosphorus, sulphur, zinc and calcium. Closer examination shows the qualitative decrease in the amount of these elements present on the surface with test time, and is

confirmed by the semi-quantitative analysis shown in Tables 9 to 12. This shows generally a decrease in elements such as P, S, Zn and Ca with a corresponding increase in Fe content, although the accuracy of EDAX analysis can be a the subject of some debate due to the effect of variables affecting operation.

4.7.3.6 Metallographic Examination

The micro-sections of both the cam and follower surfaces from Test 2D can be seen in Figs 141 and 142. Although the follower surface, Fig. 142, shows no apparent surface/subsurface wear damage, the cam surface shows evidence of white layer formation, (Fig. 141). This is only slight however, with a very thin band of associated tempered material. The white layer was present in only isolated areas on the cam surface with no evidence of cracking or spalling of this white layer.

4.7.3.7 Wear Debris Examination

S.E.M. examination of the wear debris shows small platelets, 3-4 microns in size, Fig. 143.

4.7.4 Results, Test 2E

4.7.4.1 Friction Measurements

Coefficient of friction measurements versus test time can be seen in Fig. 126, and shows a gradual increase in the coefficient of friction to 40 hours testing to a value of around 0.18μ. After 40 hours and up to the end of test the friction coefficient rises slowly to a maximum of 0.19 at 80 hours.

4.7.4.2 Spectrometric Oil Analysis S.O.A.P.

Iron wear debris p.p.m. concentration versus test time can be seen in

Fig. 127, and shows a gradual increase, high initially, to a maximum of 25 p.p.m. after 80 hours of tests.

4.7.4.3 Semi-Quantitative Wear Debris Analysis (P.Q. Index)

The graph of wear particle index (PQ) versus test time can be seen in Fig. 128, and shows the same general trend as the results from spectrometric oil analysis, a high initial increase up to an index number of 70 after 15 hours, then gradually increasing up to a maximum index number of 80 after 80 hours of tests.

4.7.4.4 Scanning Electron and X-Ray Dispersive Surface Analysis (EDAX)

S.E.M. examination of the cam and follower surfaces can be seen in Figs. 144 and 145 respectively. Wear surfaces show no appreciable wear damage, the polished nature of the artifically formed surface is still clearly evident. EDAX analysis of the cam surface shows no evidence of any film formation, the scan showing energy spectra for iron, manganese and sulphur only.

4.7.4.5 Metallographic Examination

Taper microsections taken through the cam and follower surfaces can be seen in Figs. 147 and 148 respectively, and show no signs of surface/subsurface damage or white layer formation.

4.7.4.6 Wear Debris Examination

S.E.M. examination of the wear debris from test 2E can be seen in Fig. 149, and shows debris in a platelet form in the size range 2-10 microns.

4.8 Results - Objective Three, Test 3A-3D

Material combination - Cam - Case hardened steel

Follower - Test 3A - White cast iron

Test 3B - Toughened zirconia

Test 3C - Silicon carbide

Test 3D - Sialon

Test 3A - Base stock oil, 80 Kg, peak load.

Test 3B - Base stock oil, 80 Kg, peak load.

Test 3C - Base stock oil, 80 Kg, peak load.

Test 3D - Base stock oil, 80 Kg, peak load.

4.8.1 Introduction

The tests lasted for a duration of 20 hours, and were designed to test the suitable of ceramics in the form of inserts for use in finger follower applications, run against a standard case hardened steel cam. The test conditions, eg. the use of a mineral base oil, were delibertately chosen so as to produce a high wear condition with the metallic combination, and this formed a standard to which the ceramics could be compared. The wear direction for both optical photographs and scanning electron micrographs in this result section is from top to bottom.

4.8.2 Friction Measurements

Coefficient of friction measurements versus test time can be seen in Fig. 150, and it can be seen that after an initial high peak the three ceramics settled to a lower steady state value after about 3 hours testing. For both the silicon carbide and sialon follower combinations, the friction decreases considerably to values of μ of 0.12 and 0.08 respectively. The toughened zirconia follower high frictional value, being 0.32 at the end of test. The chilled cast iron follower however rose further than the initial high peak value and continued to rise to a

maximum of 0.43 at the end of test, indicating a particularly severe form of wear.

4.8.3 Surface Roughness Measurements

Talysurf traces of both the cam and follower specimen from tests 3A to 3D can be seen in Fig. 151. The chilled white iron combination showed extensive roughening and damage to the surfaces shown numerically by comparing the centre line average values (CLA) for the 'as ground' and worn conditions. The silicon carbide and sialon combinations however produced smoother surface finishes in the worn than in the 'as ground' conditions. The cam surface worn against the toughened zirconia follower also showed extensive roughening of the surface, however, the zirconia follower surface itself did not exhibit the same extent of surface damage. The silicon carbide and sialon combinations produced smoother surface finishes in the worn than in the 'as ground' conditions.

4.8.4 Optical Examination

Optical examination of the cam and follower surfaces can be seen in Figs. 152-154. Examination of the cam nose surfaces confirms the results obtained from surface roughness measurements, the cams from both the white cast iron and toughened zirconia follower combinations have become badly worn. Fig. 152b shows the cam surface from the white cast iron follower combination, Test 3A, and it can be seen that the surface has become severly scuffed and delaminated. The cam surface from the toughened zirconia follower combination, test 3B, shows wear damage of an abrasive nature with some plastic deformation shown by the plastic flow of the material over the manganese sulphide inclusions running at 90° to the wear direction, (Fig. 152c). However both the cam nose surfaces from the silicon carbide and sialon follower combinations, tests 3C and 3D, Fig. 152d and 152e have

become smoother than the original ground surface as shown in Fig. 152a. Optical examination of the follower surfaces can be seen in Figs. 154 and 155. The white iron and toughened zirconia followers can be seen in Fig. 154 and show the extent of the wear damage. The wear damage on the white iron follower, test 2A, Fig. 154b is partly disguised by the products of oil oxidation staining the surface, but is confirmed by the results from surface roughness measurements. Fig. 154d of the toughened zirconia wear surface test 3b shows what appears to be a micro-pitting type mechanism on the surface with, what appears to be material transfer from the cam nose. Optical examination of the silicon carbide and sialon follower surfaces can be seen Fig. 154 and show in both cases smoothing of the surfaces and minimal material removal shown by the existance of the original grinding marks running at 90° to the wear direction. Also evident on both surfaces are the presence of free silica particles in the matrix (light), that should theoretically have reacted during the sintering process.

4.8.5 Scanning Electron Microscopic Examination (S.E.M.)

S.E.M. examination of the cam and follower surfaces from tests 3A to 3D can be seen in Figs. 155-157. Examination of the cam surfaces confirms the results gathered from optical examination, and show the extent of cam nose wear damage from the white cast iron and toughened zirconia followers, test 3A and 3B. Fig. 155b shows the extensive plastic deformation and delamination of the cam nose from test 3A, this being typical of a scuffing failure. Examination of the cam nose from the toughened zirconia follower combination, test 3B is shown in Fig. 155c and shows the abrasive nature of the wear damage running circumferentially around the cam nose which would appear to be caused by the impingement of loose abrasive particles. Examination of the cam noses from the silicon carbide and

sialon follower combinations, test 3C and 3D, show the extent of the effective polishing of the cam noses, Figs. 155d and 155e, with the manganese sulphide inclusions clearly evident. This being in complete contrast to the as-ground surface shown in Fig. 155a.

S.E.M. examination of the follower surfaces can be seen in Figs. 156 and 157. Fig. 156 shows both the white cast iron and toughened zirconia surfaces, the true extent of the wear damage occurring on the white cast iron follower, test 3A, obscured somewhat by the products of oil oxidation, (Fig. 156b). The toughened zirconia follower from 3B however, shows the extensive micro-pitting of large areas over the surface, Fig. 156d. Examination of both the silicon carbide and silicon followers, tests 3C and 3D, again shows polishing with minimal material removal from the surface shown by the existence of original grinding marks, Figs. 157b and 157d.

4.8.6 Metallographic Examination

Taper microsections taken through the cam nose from test 3A to 3D can be seen in Fig. 158. Examination of the cam from test 3A shows extensive white layer and an associated tempered region, Fig. 158a. White layer formation is less pronounced on the cam surface from test 3B worn against the toughened zirconia follower combination and is confined to isolated areas of the cam surface, Fig. 158b. The cam nose surfaces from tests 3C and 3D worn against the silicon carbide and sialon follower combinations can be seen in Figs. 158c and 158d, and show no associated sub-surface damage.

4.8.7 X-Ray Dispersive Surface Analysis

X-ray dispersive analysis of the toughened zirconia follower was carried out to confirm whether material transfer had occurred from the cam surface as suggested during optical examination, (Fig. 154d). Fig. 159,

shows an iron line scan across the follower and clearly shows peaks indicating variable iron content across the surface, thus confirming that material transfer occurred.

4.9 Results - Objective Three, Tests 3E-3G

Material combination - Cam - Case hardened steel.

Follower - Test 3E - Ceramic Fibre reinforced Al/Si alloy.

Test 3F - Cobalt iron, hard facing alloy.

Test 3G - Nickel rich, harding facing alloy.

Test 3E - Base stock oil, 80 Kg, peak load.

Test 3F - Base stock oil, 80 Kg, peak load.

Test 3G - Base stock oil, 80 Kg, peak load.

4.9.1 Introduction

The tests lasted for a duration of 20 hours, and were designed to test the suitability of these 'advanced' materials for use in finger follower applications, run against a standard case hardened steel cam.

4.9.2 Friction Measurements

Coefficient of friction measurements versus test time are shown in Fig. 160, and show that after high initial peak values of friction, the coefficients for all three tests decreased to lower steady state values, although the two hard facing alloy follower test combinations were considered to be high under such lubricated condition. Test 3E, the ceramic fibre reinforced aluminium/silicon alloy exhibited the lowest coefficient of friction, levelling out to a steady state value of around

0.13 after 10 hours testing. The two hard facing alloys, test 3F the cobalt rich alloy and test 3G the nickel rich alloy had friction coefficients decreasing to steady state values of μ after 3 hours testing, of 0.24 and 0.27 respectively.

4.9.3 Optical Examination

Optical examination of the cam and selected follower surfaces can be seen in Figs. 161, 162, 169 and 176. Examination of the cam and follower surfaces from test 3E, Figs 161 and 162, shows some plastic deformation of the cam surface which is exaggerated by the staining of some areas (Fig. 161). The follower surface is also stained somewhat, however there is clear evidence of material transfer over the whole follower surface, (Fig. 162). Examination of the cam surface from test 3F, using the cobalt hard facing alloy shows extensive plastic deformation and some areas of material transfer (Fig. 169). The cam nose surface from test 3G, the nickel hard facing alloy shows extensive staining of the surface, obscuring what little plastic deformation had occurred, however, there is clear evidence of material transfer from the follower.

4.9.4 Scanning Electron Microscopic Examination, S.E.M.

S.E.M. examination of both cam and follower surfaces from test 3E to 3G can be seen in Figs. 163, 164, 170, 171, 177 and 178. The cam and follower surfaces from test 3E show a general lack of wear damage on the surfaces, Figs. 163 and 164, however material transfer is evident on both surfaces and is especially extensive on the follower surface, (Fig.164). Examination of the cam and follower surfaces from test 3F can be seen in Figs. 170 and 171 respectively. The cam surface shows plastic deformation and a general scuffed appearance with evidence of material transfer. The follower surface however, shows no material transfer, but what is clearly evident is the wear of the solid solution

matrix of the cobalt surface, leaving the carbide networks clearly discernable and in some areas are in relief, (Fig. 171). Examination of the cam surface from test 3G shows again a general lack of plastic deformation, but extensive material transfer as seen in Fig. 177. The follower however, shows no immediate signs of material transfer but extensive wear by delamination (Fig. 178).

4.9.5 X-Ray Energy Dispersive Analysis Of Wear Surfaces E.D.A.X.

X-ray energy dispersive analysis was carried out on the follower wear surface from test 3E, the ceramic fibre reinforced Al/Si follower to identify the nature of the transferred material. The results of the analysis was in the form of x-ray dot image scans, the density of the image dependent upon the elemental composition of the material. The results can be seen in Fig. 165. Fig. 165a shows the general area viewed in the S.E.M. with the x-ray image for iron (Fig. 165b) and aluminium (Fig. 165c). This evidence clearly shows iron transfer from the case hardened steel cam nose to the follower surface.

4.9.6 Metallographic Examination

Taper microsections through both cam and follower surfaces from tests 3E to 3G can be seen in Figs. 166, 167, 172, 173, 179 and 180. Examination of the cam and follower surfaces from test 3E, Figs. 166 and 167 show no signs of any surface/subsurface damage although under closer examination some deformation of the ceramic fibres in the follower subsurface has occurred, (Fig. 167).

Examination of the cam surface from test 3F, shows white layer formation over the whole width of the cam nose, Fig. 172. The cobalt follower surface after etching in 2% nital showed evidence of material impingement into its surface, transferred from the cam nose, (Fig. 173).

Examination of the cam and follower surfaces from test 3G can be seen in Figs. 179 and 180. The cam surface on first examination appears to have transformed to white layer but on closer examination this is seen as nickel material transferred from the follower which 'builds up' on the cam surface, (Fig. 179). The adjacent tempered areas are then produced by the frictional heating caused by interaction of chemically similar species. The follower surface after etching in 2% nital again shows what appears to be ferrous material impingement into it's surface, Fig. 180, and under closer examination this material appears to have become mixed or alloyed into the nickel matrix.

4.9.7 X-Ray Energy Dispersive Analysis Of Follower Taper Microsections

X-ray energy dispersive analysis was carried out on the follower taper sections from test 3F and 3G with the cobalt and nickel alloys to identify the nature of the transferred material. Examination of the cobalt follower, test 3F, can be seen in Fig. 175, and clearly shows the impingement of iron debris into and on the surface of the follower, (Fig. 175b). This is not as obvious for the nickel follower, test 3G, and only under closer examination can the local concentrations of iron be seen, (Fig. 182). This effect is due to the mixing or alloying of the steel debris and the nickel matrix previously shown under optical examination (Fig. 180).

4.9.8 Wear Debris Examination

S.E.M. examination of the wear debris from test 3E to 3G can be seen in Figs. 168, 174, and 181. Examination of the debris from test 3E shows debris in the range of 15 to 20 microns, the thickness of debris particles in some cases being up to 2-3 microns (Fig. 168). Debris accumulated from tests 3F and 3G can be seen in Figs. 174 and 181 and are of the same size and morphology, very thin platelets 5-10 microns maximum size.

CHAPTER 5

5. DISCUSSION

5.1 OBJECTIVE ONE - SERVICE REPRODUCABILITY TESTS - "THE EFFECTS OF THE MINERAL BASE OIL AND ADDITIVE PACKAGES ON THE WEAR BEHAVIOUR OF CONVENTIONAL CAM AND FOLLOWER MATERIALS.

5.1.1 Introduction

As mentioned previously, the objective of the experimental work described here is to reproduce cam and follower wear failures similar to those encountered in service. This would enable the test rig to be used as a cheaper and faster method of material and oil evaluation, thus complimenting the more expensive and time consuming test engine and dynomometer test methods.

The wear mechanisms commonly encountered in cam and follower arrangements in service were reproduced during this test procedure. A more simplistic and fundamental analysis of these failures under controlled test variables was thus possible, effectively eliminating the uncontrolled variables encountered in engine and dynomometer test methods.

The author does not attempt to form any new theories about such cam and follower failures but instead attempts to provide information to aid further discussion of such failures and their solutions.

5.1.2 Case Hardened Steel Cam/White Cast Iron Follower Combination

Test 1A using the fully formulated oil under low load conditions produced a low wear rate shown by spectrometric oil analysis and complimented by the friction result (Figs 25-26). Surface analysis using both optical and scanning electron microscopy techniques show the cam surface at the end of test to be smoother than the original ground surface. The surface is polished and manganese sulphide inclusions (MnS) can clearly be seen orientated at 90° to the wear direction. The reasons for no significant wear damage, is the formation of surface films from additives in the oil produced under the predominatly boundary lubrication conditions at the start of test.

Polishing wear of the cam surface is commonly found in such systems, the literature states that this polishing wear becomes progressively more severe, resulting in considerable material removal with time. The amount of wear occurring within the test duration used in this investigation however, suggests polishing wear to be in the early stages of initiation. The actual mechanism of polishing wear is discussed in more detail later in this chapter, but it appears to be affected by additives in automotive oils. Chemical effects produced by these additives however are clearly evident on the white iron follower surface. Both optical and S.E.M. examination of the follower surface shows preferential attack in the wear scar region. This appears to be chemical attack of an intercarbidic nature whereby the pearlitic/martensitic matrix is effectively corroded away leaving the carbide networks in relief. Prolonged attack by the additives can lead to carbide fracture with surface interaction and

cause further wear by abrasion. The short time duration and the test parameters have prevented this form of wear reaching an advanced stage, and this is confirmed by examination of the tapersections and wear debris after 40 hours (Figs 31-33).

Under the same general test conditions but using the mineral base oil, test 1B, the wear behaviour of this material combination differed significantly. In this test the cam surface became scuffed with extensive plastic deformation of the surface. Subsequent etching of the cam wear surface in 2% nital showed small white etch resistant areas distributed within isolated bands across the surface (Fig. 34). These areas were considered to be carbides that had broken away from the surface of the chilled white iron follower surface and became embedded in the cam surface, probably during the very early stages of the test, under the boundary conditions that prevailed at the start of testing. General Motors in an S.A.E. communique[87] have attributed this phenomenon to a momentary breakdown in the lubricating oil during the early stages of testing. This permitted metal contact, with the attendant heat generated leading to localised softening of the martensitic chilled white iron matrix phase. This in turn allowed the removal of the carbide present in the structure and it's subsequent transfer. It can be seen however that the presence of these carbide particles are in relatively smooth undamaged areas and could improve the wear resistance of these areas by acting as an effective bearing surface. The scuffed morphology of the cam surface can be seen more clearly in Fig. 35 and shows, apart from the plastic deformation, evidence of white layer formation in the form of thin bands running in some cases, around the circumference of the

cam specimen. There is no significant wear damage on the follower surface with only a slight etching effect of the surface caused by products of oil oxidation. There is however a random distribution of small black areas on the surface but these were difficult to resolve even by S.E.M. examination.

The failure of the cam by a scuffing mechanism was further confirmed by tapersection examination. Fig. 39 shows extensive white-layer formation and the associated tempered regions within the cam sub-surface. Examination at a higher magnification shows the carbide transfer phenomenon and thermally cracked regions. By further focussing into the epoxy resin protecting the surface this random distribution of embedded carbide can be seen (Figs. 40-41). The follower sub-surface confirms that the majority of the wear damage occurred on the cam nose and the platelet morphology of the wear debris produced (Fig. 43) also confirms this observation.

A change to boundary lubrication conditions using the fully formulated oil showed significantly different wear behaviour using this same material combination. With test 1C, excessive wear of the chilled iron follower occurred whereas the cam was less worn. Friction measurements appeared relatively high although there is a decrease from the start of test indicating some form of 'running in' to have occurred. Spectrometric oil analysis however, indicates a severe form of wear during the whole test sequence when compared to the wear debris concentration for Test 1A at lower loads.

Examination of the cam showed the only significant wear feature to be isolated areas of plastic deformation. This was confirmed by

examination of the tapersection which showed no white layer formation and hence eliminates the possibility of scuffing. This confirms the effect of anti wear additives such as Z.D.D.P. in the oil preventing scuffing.

Examination of the follower shows failure by the classic pitting mechanism. Using optical techniques the pitting can be seen to be randomly distributed across the surface in a crazed pattern, with the microstructure of the white cast iron clearly visible on the unpitted surfaces (Fig. 45). Fig. 47 is a view of a pitted/unpitted region and again shows the chemical attack of the microstructure revealing the carbide networks. The extent and depth of the pitting is also shown. Taper-sectioning of the follower surface shows some interesting features. Fig. 49 shows cracks running both parallel and at 90° to the surface and there is also evidence of corrosion shown by the circular nature of some of the areas of the pitting failure. It is these different wear features that make the analysis of this form of pit formation in white cast iron extremely difficult. Available literature is conflicting, some scientists suggest cracks form by a surface initiation process, caused by the corrosive nature of E.P. additives which cause cracks by stress corrosion. Oil pressure builds up between carbide networks which propogate these cracks. Others have determined the cause of failure to be due to subsurface cracks parallel to the surface, initiated and controlled by the Hertzian stresses present under by mixed rolling/sliding conditions. Chinese workers[88,89] postulate a stress fatigue mechanism of pit formation and the direct application of general fatigue theory to it's solution. It can be seen from the literature that these scientific workers suggest that the formation of these failures is controlled by the individual hypothesises that they attempt to put forward. However it

can be seen from the work carried out by the author, that any one or, in fact, all of the mechanisms postulated can contribute to pitting failure. The author does not attempt to discredit any of these postulations but there appears to be a distinct lack of research into the chilled white iron itself. In particular for cam and follower components prior to the commencement of their operation. For example, a hardness survey carried out on 6 commercially available automobile tappets (Fig. 183-184) show differences in both hardness and chill depth. Chill hardnesses ranging from 540 Hv 5gm for a B.L.M.C. 'Mini' tappet, to 795 Hv 5gm for a Ford 'Dover' tappet. It is agreed however, that the operating conditions of the two vehicles differ. However, a hardness difference of 250 Hv is considerable, with the associated strength also expected to differ considerably. Indeed a survey of similar components from a single production batch, showed hardness differences of up to 70 Hv. There appears to be no hardness standards for white iron tappet production, yet standards exist for other hardening treatments such as carburising and carbonitriding. On sectioning several of the components for hardness testing, cracks were observed which emminated from various positions within the chilled area. Some cracks emminated at a 90° angle to the surface (Fig. 185a) whilst others were more random, (Fig. 185b) These cracks might have originated from sectioning on the abrasive wheel due to thermal cycles causing mechanical cracks to occur. Close examination of some of the cracks however, shows evidence of oxide present within the crack which must have formed prior to installation in the valve train. The cracks on this occasion probably arise from solidification against graphite chills during casting and the associated thermal shock effects, (Fig. 185c).

A more thorough and meaningful investigation must be carried out in order to understand the pitting mechanism of chilled white iron valve train components. This should commence firstly by standardising the hardnesses of the tappets prior to a full investigation into the pitting mechanism and secondly, some form of quality system should be established involving non destructive testing techniques such as ultrasonics and radiography to test for the presence of cracks prior to testing. Only when a test sequence is fully standardised can a meaningful investigation into the effect of differences in chilled hardness and depth be carried out.

Test 1D using the mineral base oil at high loads, showed typically high wear rates (Figs 25-26). The cam surface showed evidence of severe plastic deformation and delamination consistent with failure by a scuffing mechanism (Fig. 51). This is confirmed by tapersection examination showing white layer formation across the width of the cam nose (Fig. 53). Preliminary examination of the follower wear surface also shows evidence of plastic deformation of the surface (Fig. 52), however tapersection examination shows this plastic deformation effect to be material transfer from the cam surface, shown by the light areas on the follower surface. This smeared material, transferred from the cam produce a 'like on like' adhesive situation initiating further wear.

To conclude the results from the test procedures 1A to 1D, it can be seen that a variety of wear mechanisms were observed within the duration of the test sequences. Using the material combination of a case hardened steel cam and a white cast iron follower, the most commonly encountered forms of wear in cam/follower systems were

reproduced. Using the fully formulated oil at low loads a polishing form of wear was apparent with the cam, whilst the follower surface suffered chemical attack in the wear scar area, contributing to pitting commonly found in white cast irons. At higher loads this pitting wear fully manifested itself and the surface degenerated. The mechanism for this form of pit formation appears to be mainly of a three fold nature, with stress corrosion, surface and subsurface crack initiation being the dominant catalysts. Analysis of these failures becomes extremely difficult however when considering the hardness differences between cast iron tappets, and also the presence of cracks in tappets prior to installation.

Using the mineral base oil at both low and high loads, the classic scuffing form of wear occurred with the cam. Associated with the typical plastic deformation and delamination at low loads, was carbide transfer from the follower surface and circumferential white layer band formation. At high loads scuffing again occurred with the cam, which caused material transfer to the follower surface. This produced a 'like on like' adhesive situation contributing to frictional heating and further increases in wear rate.

5.1.3 Induction Hardened Grey Flake Iron Cam /Case Hardened Steel Follower Combination

Test 1E using the fully formulated oil under mixed lubrication conditions show with reference to the coefficient of friction and spectrometric oil analysis (Figs 56-57) low wear rates typically associated with satisfactorily operating systems. This is confirmed by surface examination, which show the worn areas to be

smoother than the as ground surfaces, (Figs 58-61), this being beneficial to the production of elastohydrodynamic oil films which eliminate surface asperity interaction. This surface smoothing is best illustrated in Fig. 58 which clearly shows the graphite flake structure on the cast iron cam surface. This effect is similar to the 'bore polishing' phenomena found in the cylinder liners of highly rated diesel engines. This is detrimental in such applications as too smooth a surface results in oil breakdown and scuffing. However, as already mentioned smoother surfaces in cam/follower applications are considered advantageous and thus show the importance of additive packages in automotive oils. There are some detrimental aspects associated with the use of such additives however, one of these being their corrosive nature. Examination of the follower surface (Figs 59 and 61) shows the corrosive nature of the additive package preferentially attacking the grain boundaries. However this attack was again considered negligible over the relatively short test duration, with examination of the tapersections and the wear debris confirming the low wear rate and the satisfactory running of the system.

Test 1F using the mineral base oil exhibited much lower wear rates when compared to testing under similar conditions using the case hardened steel cam and white cast iron follower combination. This is shown by reference to the coefficient of friction and spectrometric oil analysis results (Figs 56 and 57). Further confirmation of these low wear rates is shown by optical and S.E.M. examination of both the cam and follower surfaces (Figs 65-69). The surfaces show no evidence of any significant wear damage, instead there is present on both the cam and follower surfaces evidence of graphite smearing.

Also present on the cam surface was evidence of phosphide eutectic shown by the small white areas distributed over the surface, (Figs. 65 and 66).

The possible reasons for the general resistance to plastic deformation and scuffing using this material combination, under conditions where the previous material combination failed by scuffing are two fold:-

i) The use of graphite as an 'anti-seizure' lubricant is well established. For example, a graphite suspension in rape oil is a common lubricant used in the hot working and forging of carbon steels, and has been used successfully for many years. It appears therefore, that the free graphite present in the form of graphite networks in the cast iron cam matrix again acts as an anti-seizure additive, thus preventing surface interaction and metal to metal contact. Indeed Sugishita and Fujiyoshi[90] have shown under rolling, sliding conditions that cast irons with free graphite present in the microstructures have favourable wear properties compared to those without free graphite. The principle works on a squeeze/smear action caused by contacts between the surfaces. The higher the percentage of free graphite in the microstructure the lower the wear rate.

ii) The presence of hard phosphide eutectic in cast irons can according to Eyre and Williams[91], act as bearing surfaces minimising metal to metal contact. It is likely that the phosphide eutectic evident at the cam surface found by optical examination, (Figs 65-66) acts in such a way. Tapersectioning of the cam surface shows this effect, (Fig. 70).

The use of the induction hardened grey cast iron cam and case hardened steel follower combination under high load conditions, resulted in excessive wear rates using both the fully formulated and mineral base oils. The extent of the wear damage was such that the wear features were unresolvable using conventional optical techniques. Visual examination however, showed that a form of accelerated wear had occurred resulting in the removal of the induction hardened layers of the cam specimens. The extent of wear damage became apparent under S.E.M. examination, where the cam and follower surfaces from both tests 1G and 1H showed extensive plastic deformation and scuffing (Figs 73-74 and 78-79). Further examination of the wear surfaces from test 1H using the mineral base oil showed in addition extensive material transfer and smearing (Figs 78 and 79). This is important when considering the rate and mode of wear using the two different oils. Visual examaintion of the cam surfaces showed that although in general the wear features were similar the rates of material removal differed significantly, the wear couple tested in the mineral base oil showing the highest material removal rate.

The reason for the difference in material removal rates becomes clear on tapersection examination, and shows these dissimilar removal rates to be due to differences in the actual mechanism of material removal. Figs 75 and 76 show the cam and follower tapersections from 1G using the fully formulated oil and it can be seen that although there is considerable wear damage and material transfer and build up, there is no evidence of any significant white layer formation on either surface. This evidence indicates a different mechanism of wear occurring than the scuffing

type of wear typically found under these conditions. This suggests that the additive package present in the oil has prevented asperity welding and the generation of temperatures associated with white layer formation. The failure of the cam specimen in the fully formulated oil appears to have been caused by a fatigue mechanism controlled by sub-surface stresses. Close examination of the cam subsurface (Fig. 75) shows a network of cracks eminating from the ends of graphite flakes. These graphite flakes acts as stress raisers within the matrix, thus increasing the likelyhood of failure by a pitting mechanism. Eyre and Zhu[92] have reported that crack propogation and the morphology of the wear debris subsequently produced under reciprocating wear conditions, is dependant upon the size and distribution of the graphite networks present in the microstructure. This form of pitting can be clearly seen on the cam surface from test 1G (Fig. 73) and would appear to show that the predominant cam nose failure using the fully formulated oil is by fatigue. This fatigue mechanism is brought about by an affective failure in the 'damping' capacity of the grey flake iron under repeated and heavily loaded rolling/sliding conditions.

Examination of the cam and follower tapersections from tests 1H using the mineral base oil (Figs 80 and 81) confirmed the evidence gathered from S.E.M. examination of the wear surfaces. The tapersections again showed extensive plastic deformation of both the cam and follower subsurfaces and extensive white layer formation on both surfaces. It was considered therefore that failure in the mineral base oil was due to the classic 'scuffing' mechanism, with additional wear occurring by the spalling of the brittle white layer under fatigue conditions.

5.1.4 Carbonitrided Flake Iron Cam/Hardened And Tempered Nodular Iron Follower Combination

Test 1I, using the fully formulated oil at low loads showed this material combination to have excellent wear properties shown by the low wear rates indicated by coefficient of friction and spectrometric oil analysis (Fig 83-84). This was confirmed by both optical and S.E.M. examination of the cam and follower surfaces which showed the wear surfaces to be smoother than the original ground finish. The cam surface was smoothed to such an extent that graphite networks were clearly visible on the surface (Fig. 86). The lack of any subsurface wear damage and a wear debris size range of 1-5 microns confirms a satisfactorily running system being established with the aid of the anti-wear additives present in the oil formulation.

Analysis of the cam surface used in the mineral base oil (Test 1J) again shows a general smoothing of the cam surface, however, there is an irregular distribution of pits across the surface as shown inFig. 91. S.E.M. examination of the surface shows the pitting to be of a shallow form (Fig. 92), the actual size of which, appears to be dependant upon the size of the graphite networks themselves. The wear debris comprises of small platelets of up to 10 microns in size, suggesting this shallow pit formation to be an accumulation of these small platelets, the sizes being governed by the intergraphitic spacings of the networks, because closer examination of Fig. 92 shows no pit formation in areas of low flake network concentration. The follower surface from test 1J agains shows no significant bulk wear damage, however, Fig. 93 shows a general ripping out of the graphite nodules from the surface of the nodular iron. These nodules

constituted the graphite films which were still present after solvent cleaning. These are shown by the remnants of dark areas present around empty nodule cavities. Examination of the tapersections showed no deliterious subsurface white layer transformations or plastic deformation. However, some plastic deformation did occur on the surface, mainly around the nodule cavities of the follower surface (Fig. 93).

Under high loads, using the fully formulated oil, the carbonitrided flake iron cam and hardened and tempered nodular iron follower combination, exhibited superior wear characteristics to any of the other material combinations tested under the same experimental conditions. Examination of both the cam and follower surfaces from test 1K show no significant wear damage. What is evident however is the presence of surface films remaining on the surface after thorough solvent cleaning. This illustrates the tenacity of these anti-wear films under extreme load conditions. These surface films together with the effect of graphite film formation enabled this material combination to run satisfactorily under these arduous conditions. this is further confirmed by examination of the tapersections of both the cam and follower, showing no subsurface damage or white layer formation.

In the mineral base oil the results were predictable and showed high wear rates that were confirmed by an unsatisfactory coefficient of friction and spectrometric oil analysis results. Plastic deformation and scuffing was found on examination of both the cam and follower surfaces along with extensive white layer (Figs 103-105). Although the wear rates were high they were of a lower magnitude than those obtained using the other material combinations. The results

therefore illustrate the superior wear properties of carbonitrided grey flake iron and hardened and tempered nodular iron over the other material combinations used in this test program.

5.1.5 Surface Roughness Measurements

It can be seen from the results of surface profilmetry the relative advantages and disadvantages of both the conventional single trace talysurf machine and the 3D computorised multi-trace system. The use of the multi-trace system is advantageous when analysing the general morphology and distribution of wear features on particular surfaces. This became extremely useful in the characterisation of surfaces produced in this first test objective. The general morphologies of the scuffing, pitting and severly worn surfaces were clearly distinguishable and showed for instance, the random distribution of pits from the pitted follower surface (Fig. 111), whilst the severely worn surface showed an abrasive form of wear mechanism occurring. This was shown by the reproduction of similar surface characteristics along the wear direction, likened to furrows in a 'ploughed' field. The use of the 3D multitrace system however appears to hinder the calculation of the depth and form of individual wear 'valleys' and 'peaks', an important factor in the analysis of single point abrasive wear tests for instance. This form of surface profilometry analysis therefore relies on the single trace talysurf technique. It becomes generally apparent therefore, that both of these methods of surface profilometry are invaluable in the monitoring of wear surfaces, and both systems should be employed to ensure maximum information is obtained.

To conclude this part of the discussion section, it can be seen that the cam/follower rig has proven to be a useful test apparatus for both material and lubricant appraisal. The test rig can act as a cheaper and faster alternative to the more expensive and time consuming dynomometer and test engine systems. The test rig discriminated between the fully formulated and mineral base oil by reproducing the most commonly encountered cam follower wear problems of scuffing, pitting and polishing wear. No new theories have been put forward regarding the mechanism of these failures, instead the author has presented information which he hopes will aid further discussion regarding these failures and hopefully contribute to their eventual elimination from service. This information has included such areas as chilled white iron pitting failure, where the hardness ranges of commercially available automobile tappets differ considerably, and also the presence of cracks evidence in components prior to operation. Other work has included the role of free graphite in cast iron microstructures preventing the onset of scuffing under low load, mineral base oil conditions, and the superior wear properties of carbonitrided grey flake iron.

5.2 OBJECTIVE 2

5.2.1 The 'Running In' Of Cam Surfaces Using The Replication Technique

The use of acetate replicas during the test procedures 2A and 2B shows the versatility and distinct advantages of using this simple but effective surface analysis technique. Using a fully formulated oil and it's base stock it was possible to produce a surface topographical 'story' of how cam surfaces 'run-in'. Replicas of the cam surfaces show in the case of the fully formulated oil (Fig. 117 to 121) a gradual smoothing of the surface with test time. From the start of test, ie. the 'as ground' surface (Fig. 117a) to the surface after 1 hour of testing (Fig. 118C) show the grinding marks to have been all but removed, with evidence of abrasion becoming the predominant wear feature. This abrasive wear, like the original grinding marks, then became less evident as the test was concluded. After 70 hours the surface had become highly polished with very little evidence of abrasive wear apparent on the cam surface. In constrast, the replicas of the cam surface using the mineral base oil showed instantaneous surface roughening as shown in Fig. 117d, after 15 minutes testing. Closer examination shows small light areas on the replica surface, these were small wear particles that had become detached from the surface with relative ease and had become embedded in the acetate sheet after removal from the surface. Damage of the surface then became increasingly severe with test time shown by the darker, constrasting areas of the replica indicating deeper sub-surface wear of the cam (Fig. 121F). It was therefore evident that scuffing had occurred and was a 'running in' problem.

The sequence of surface events leading to the formation and in the case of the mineral base oil the scuffing of the surface are best described with reference to the coefficient of friction and condition monitoring graphs (Figs 114-116) and metallographic and wear debris examination (Figs 122-125). Using the fully formulated oil the surfaces of the cam in conjunction with the white cast iron follower surface begin to 'run in' immediately. In this process the asperities or 'high spots' are removed from the mating surfaces with the Z.D.D.P. additives present in the oil causing instantaneous reaction film formation and the subsequent prevention of welding of these asperities and thus the prevention of scuffing. The high spots on the surface are removed by a process of adhesive wear and plastic deformation and cause an initially higher wear rate than would be expected during normal running, shown by an initially high coefficient of friction (Fig. 114). The iron concentration, and wear particle index obtained from spectrometric oil and semi-quantative debris analysis Figs 115 and 116 respectively, show a steady state increase in wear debris concentration with immediately high concentrations in oil samples taken after 2 minutes testing, showing material removal to haved occurred almost immediately. The gradual decrease in friction with time is due to the continuing process of plastic deformation of the asperities, thus lowering the real area of contact towards the design contact area. This higher rate of material removal during the very early stages of 'running in' can be seen with reference to Fig. 124a, and shows the relative wear debris size increase during 'running in' when compared to the debris size range under normal wear conditions, as seen in Fig. 124C. Also evident during 'running in' is the occurrence of spherical debris commonly associated with rolling contact fatigue. The formation of this spherical wear debris morphology is open to much discussion.

The sequence of surface events leading to the formation and in the case of the mineral base oil the scuffing of the surface are best described with reference to the coefficient of friction and condition monitoring graphs (Figs 114-116) and metallographic and wear debris examination (Figs 122-125). Using the fully formulated oil the surfaces of the cam in conjunction with the white cast iron follower surface begin to 'run in' immediately. In this process the asperities or 'high spots' are removed from the mating surfaces with the Z.D.D.P. additives present in the oil causing instantaneous reaction film formation and the subsequent prevention of welding of these asperities and thus the prevention of scuffing. The high spots on the surface are removed by a process of adhesive wear and plastic deformation and cause an initially higher wear rate than would be expected during normal running, shown by an initially high coefficient of friction (Fig. 114). The iron concentration, and wear particle index obtained from spectrometric oil and semi-quantative debris analysis Figs 115 and 116 respectively, show a steady state increase in wear debris concentration with immediately high concentrations in oil samples taken after 2 minutes testing, showing material removal to haved occurred almost immediately. The gradual decrease in friction with time is due to the continuing process of plastic deformation of the asperities, thus lowering the real area of contact towards the design contact area. This higher rate of material removal during the very early stages of 'running in' can be seen with reference to Fig. 124a, and shows the relative wear debris size increase during 'running in' when compared to the debris size range under normal wear conditions, as seen in Fig. 124C. Also evident during 'running in' is the occurrence of spherical debris commonly associated with rolling contact fatigue. The formation of this spherical wear debris morphology is open to much discussion.

There are a number of basic hypotheses that have been advanced to account for the occurrence of these spherical particles. The first is that they result in some way from the interaction of the lubricant and surface cracks that continually open and close[93]. A second theory associates them with melting as a resulting of high instantaneous surface temperature during sliding followed by subsequent freezing in the oil[94,95] a third theory is that they result from the rolling up of flat wear particles[96]; whilst a fourth theory states that they are formed by a subsurface mechanism associated with fatigue crack development[97]. The fifth and in this particular case the most tangeable explanation is that in order to produce spherical particles, chunky particles must be formed as a result of an adhesive wear process ie. "running in", and then become rounded and polished as a result of a form of burnishing process[98]. Close examination of the spherical debris shown in Fig. 124a illustrates this burnished effect at one end showing an apparent axis of revolution around which the debris formed.

Once the surface had become satisfactorily run-in, the size range of the wear debris decreased to an average platelet size of around 1-2 microns as shown in Fig. 124C. Examination of the cam tapersection in Fig. 125a shows no subsurface damage and this again illustrates satisfactory 'running in'. The extent of cam surface smoothing was such that there were strong similarities between the cam surface test and a metallographically prepared surface. A cam surface in the initial 'as ground' condition was diamond lapped to a metallographic 1μm finish and etched in 2% Nital. The worn cam surface was then also etched under the same conditions and the two compared. Fig. 122 shows the 'as ground', polished and etched cam specimen and

the martensitic structure and the grain boundaries present in the hardened steel case can be clearly seen. The surface of the worn cam surface although not showing the grain boundaries in the structure, does show a martensitically transformed microstructure not dissimilar to the metallographically prepared surface. It appears therefore that the 'running in' using the fully formulated oil is a two stage phenomena. Firstly, during the early stages of testing, plastic deformation and fracture of the asperities occurs, which, under the influence of the anti-wear additive (Z.D.D.P.), prevents any welding and rupture of the asperities under the initial high contact stress conditions operating in a mixed elastohydrodynamic lubrication regime. Further plastic deformation of the surface moves towards the ideal contact area from the real area of contact, thus lowering the contact stress towards the ideal design stress. This gradual smoothing of the surface then allows full elastohydrodynamic conditions to exist governed by the surface roughness factor in the formation of elastohydrodynamic films - postulated by Wellaner[99] and Barwell[100]. No mention has been made in this series of tests into microscopic elastohydrodynamics whereby analysis of individual asperities is carried out. Further smoothing of the surface after the elastohydrodynamic film is formed occurs by a chemical polishing mechanism by the additive package in the oil, whether antiwear, dispersant, detergent or any other of the many additives added to produce the full oil formulation. Further evidence of the chemical polishing is already shown in Fig. 61. A case hardened finger follower processed under exactly the same heat treatment conditions and run under identical test conditions, Test 1E, again shows the same form of polishing on the surface. Although in this case attack of the

ferrite grain boundaries had occurred thus further showing the reactivity of certain additives in contact with ferrous materials. The lack of any sub-surface damage present, shown by the tapersection from the cam surface in Fig. 125a again shows satisfactory 'running in'. Much work has been carried out on the polishing of cam and tappets which has generally been considered beneficial. Few investigators have suggested that the polishing of internal combustion engine components is a chemical process, and have mainly attributed this form of polishing to a fine abrasive action caused by the products of combustion, ie. hard carbon and airborne particles such as silica ingressing into the valve train arrangements and ultimately to the piston rings and cyclinder liners, leading to bore polishing of turbo-charged diesel engines[101]. The presence of this polishing is considered to be detrimental due to possible oil film thickness reductions leading to surface interaction, scuffing and blow-by of exhaust gases. Polishing of valve train components however, as mentioned previously, is considered to be beneficial due to the ease of elastohydrodynamic film formation with 'smooth' surfaces. Evidence of this is shown by reference to Fig. 58, showing the graphite flake structure on the surface of the cam from test 1E using a fully formulated oil. The mechanism of this type of polishing however appears not to be of a fine abrasive nature as the test rig is completely enclosed and is therefore 'airborne' contaminant free and since the apparatus is not 'fired' unlike an engine, there are no products of combustion such as hard carbon to assist in the polishing operation. The mechanism of polishing therefore appears to be of a chemical nature confirmed somewhat by examination of the surface of the case hardened follower from test 1E, (Fig. 59) which shows not only general polishing of the surface,

but also chemical attack of the ferrite grain boundaries shown more clearly by S.E.M. examination, (Fig. 61). This mechanism of polishing appears to be in part agreement with Onion[102] who found highly polished areas on components of diesel fuel injection systems, and postulated that surface films are produced by reaction between additives in the oil and steel surfaces. These films prevent wear, but also cause chemical polishing of the surface.

The use of the mineral base oil in test 2B, showed completely different effects in the forming of a cam surface. Examination of the cam replica, as seen in Fig. 117d, shows surface roughening occurring during the very early stages of testing, this damage is considered to be instantaneously produced, of test and is confirmed by an initially high friction coefficient shown in Fig. 114. The actual friction after 5 seconds testing, as measured and recorded by the microprocessor system was 0.29μ. Close examination of the replica surfaces in Fig. 117d and 117F, show the damage to be of a very shallow surface nature shown by the lack of any sharp contrast that would differentiate between surface and severe subsurface wear. The detachment of the material from the cam surface up to 30 minutes testing is predominantly of a thin-platelet form as shown in Fig. 124b, after only 5 minutes testing. The size in some cases however is up to 50 microns in width although some particles are in the size range of 2-5 microns. Re-examination of the replica surface in Fig. 117F shows wear debris particles embedded in the replica itself, shown by the very bright areas. It can be seen therefore that surface damage occurs during the early stages of operation and this is confirmed by S.O.A.P. analysis and the PQ index shown in Figs 115

and 116 respectively. Both graphs show high initial debris levels, suggesting the majority of damage occurring in the first 10 hours of testing, this however is not strictly correct. Examination of the replicas from 119F (7 hours) to 121F (70 hours) show a steadily increasing depth of wear shown by the darker areas on the replica surfaces, and a subsequent increase in debris size and morphology. This is confirmed by examination of the wear debris after 50 hours, Fig. 124d. This shows particle sizes of the same length as those obtained after 5 minutes testing, however the morphology of the debris has changed to a large 'chunky' type morphology, consistent with a pitting/spalling failure mechanism. This effect was not clearly evident by S.O.A.P. analysis or the PQ index. They show only a gradual increase in debris concentration from around 7 to 10 hours to the end of test after 80 hours. The reasons for this are two-fold. Firstly spectrometric oil analysis has a normal particle size limit of around 10 microns, any particles above this size are incapable of being detected. The formation of these large spalled debris would go undetected, hence the apparent decrease in wear debris production after around 10 hours testing as shown in Fig. 115. Secondly, the Particle Quantifying Technique (PQ Index), relies on changes in magnetic field intensity caused by the debris deposited on the RPD slide. The PQ machine cannot differentiate debris morphologies, hence a change over to fewer, but much chunker wear debris production by a fatigue type mechanism is shown as an apparent decrease in wear debris production as shown in Fig. 116, however SEM examination of the wear debris suggests that the wear has increased. The wear pattern adopted by the cam using a mineral base oil appears to be basically a two stage process, and is confirmed by examination of the tapersections shown in Figs. 125B and C.

i) At the start of the test, instantaneous asperity interaction occurs, leading to welding, rupture, and material transfer. The temperatures generated at the contacting surfaces ie. the hot spots, are sufficiently high to cause white-layer and associated adjacent tempered areas (Fig. 125b. The mechanical properties of the white layer produced are of a very hard, brittle nature thus the susceptability to cracking of both a mechanical and thermal nature are high.

ii) The mechanical/thermal cracking that occurs, under continued cyclic fatigue stressing under the rolling/sliding conditions, will cause detachment of large spalled particles, the size controlled to a certain extent by the hertzian stress patterns created under such contact conditions. This results in a pitted surface shown in Fig. 125C, leading to the commonly encountered increases in cam-tappet clearance and operating noise commonly associated with a scuffing failure.

5.2.2 The Effect of Surface Film Formation

The results obtained from test 2A and 2b formed the basis of the test procedure in test 2c. It was shown with tests 2a and 2b the effects of the two oils on the 'running in' and formation of hardened steel cam surfaces and showed the gradual smoothing of the surface using

the fully formulated oil (test 2a) whilst the mineral base oil caused instantaneous scuffing and subsequent spalling of the cam surface.

It was then thought that if a cam system was 'run in' satisfactorily with a fully formulated oil, the lubricant could be replaced with it's mineral base oil and the system could continue to run successfully. Test 2c was based on this idea and the test was run for an 80 hour duration, 40 hours 'running in' with the fully formulated oil, the test then stopped and the fully formulated oil replaced with the mineral oil and the test restarted for the remaining 40 hours to observe and examine the effectiveness of 'running in' and surface film formation.

The friction results from test 2c can be seen in Fig. 126 and show only a slight and gradual increase from 0.11 to 0.14 at the moment of test stoppage after 40 hours and replacing the fully formulated oil with the mineral oil. Spectrometric analysis however showed a slow steady state increase in ferrous debris content from a concentration of 10 ppm after 1 hour test to a maximum of around 11-12 ppm after 40 hour testing. Changing the fully formulated oil with the mineral base and the recommencement of the test up to the 80 hours total test duration met with minimal increase in ferrous debris concentration, 4 ppm to the end of test, thus emphasising the lack of wear damage and material removal. This was also the case using the particle quantifying technique, the PQ index rose very slightly over the test period 40 to 80 hours to a maximum of 8. SEM examination of both the cam and follower surface showed no significant wear damage, the cam surface, (Fig. 129a) shows evidence of slight abrasive wear, which is consistent with satisfactorily operating

systems and the follower surfaces exhibit the corrosion effect of the fully formulated oil etching the white cast iron surface partly revealing the microstructure (Fig. 129b). Edax analysis of the cam surface shows evidence of film formation remaining on the surface, shown by elemental concentration peaks of S, P, Ca, Zn, these being consistent with work carried out by Watkins on the composition of these surface films. Tapersectioning of the cam and follower surfaces showed no evidence of surface or subsurface wear damage (Fig 130 and 131). SEM examination of the wear debris shows particle sizes in the range of 3-5 microns (Fig. 132).

To conclude, it can be seen during this experimental procedure that the cam and follower ran satisfactory in base oil conditions where previously these conditions would result in incipient scuffing and spalling of the cam surface as shown by results from test 2B. The reason for the satisfactory operation of the cam/follower couple was the previously satisfactory 'running in' of the surface using the fully formulated oil and the EP additive Z.D.D.P. present in the oil formulation. This allowed fracture and plastic deformation to occur without the welding and rupture of asperities, and enabled a smoother surface to form thus enabling elastohydrodynamic lubrication conditions to prevail. The lack of metallic contact is shown by the continued presence of the additive film at the end of the test (Fig. 129c). To conclude, the ability of cam/tappet systems, once satisfactorily 'run in' to operate with a mineral base oil with no significant additive additions, is due to two main reasons:-

1) The formation of surface films from Z.D.D.P. additives in

the fully formulated oil restricted surface interactions that might occur during operation.

2) The general smoothing of the surface during 'running in' with the fully formulated oil illustrated the relevance of the surface roughness safety factor, which is extremely important in elastohydrodynamic lubrication.

This test ran however from at least the 40 hours period at which the fully formulated oil was changed with the mineral base to the end of test at 80 hours 'non stop' under predominantly elastohydrodynamic conditions with negligble surface interaction. This was considered unrealistic when comparing with service conditions in the internal combustion engine where 'stop/start' conditions are frequently encountered in general motoring, with substantial boundary lubrication periods during an operating cycle. This lead to a test sequence adopting stop/start conditions commonly encountered during operation, and became the basis of test 2D, where again the surfaces were 'run in' satisfactorily with a fully formulated oil for 40 hours. The oil was then drained and replaced with a mineral base oil and the test recommenced and stopped at 10 hourly intervals and the surfaces analysed. This was to observe the effect of stop/start boundary conditions on surface films produced on cam surfaces by the fully formulated oil whilst running in a mineral base oil.

5.2.3 Surface Film Depletion Under Stop/Start Conditions

The friction results from test 2D (Fig. 126) show the same general trend as test 2C, ie. a high initial friction coefficient, decreasing to a lower steady state value of 0.12 up to 40 hours testing, then a gradual increase to the end of test of 0.14. This was again apparent with spectrometric oil analysis and PQ index. A slow gradual increase in debris concentration is apparent after an initial steep rise in the first few hours of testing and this is consistent with a satisfactorily running system. After changing the two oils, the results for both SOAP and PQ index show another slow increase in wear debris concentration up to the end of test, S.O.A.P analysis rising from around 6 ppm at 41 hours testing immediately after changing of the oil up to a maximum of 9 ppm at the end of test, whilst the PQ index rose from 10 to 20 after 80 hours. The reason for the presence of wear debris concentrations at the start of the second half of the test commencing at 40 hours using the clean mineral base oil is due to the gravitational movement of the wear debris in the fully formulated oil sinking to the sump of the oil bath, and subsequently disturbed by the addition of the mineral base oil causing turbulence, thus agitating the debris in the bulk oil, and giving again the high initial increase.

The increase in wear debris concentration in test 2D between 40 and 80 hours testing shown by S.O.A.P. and PQ analysis (Fig. 127-128) is higher than the wear debris concentrations of test 2C incurred during the same test period. This is confirmed by SEM and Edax analysis of the surfaces with test time. Figs 133 to 140 and Tables 9 to 12 show a gradual depletion in the distribution and concentration of

surface films on the follower surface. This can be seen with reference to the electron micrograph of the follower surface. After 40 hours testing in the fully formulated oil, the surface films are clearly evident, shown by the dark smeared areas. These become progressively less apparent under the repeated stop/start boundary conditions, until after 70 hours testing the surface films are bearly visible and are replaced with evidence of abrasive wear (Fig. 139). This is further confirmed by examination of the concentration peaks from EDAX analysis (Fig. 134, 136, 138 and 140), and show a gradual and general decrease in the concentration of the elements in the surface constituting the anti-wear film, these elements being P, S, and Zn. Quantitative analysis of these films can be seen in Tables 9-12 and these again show a decrease in the elemental concentration of the relevant elements in the surface films. The actual quantitative results fluctuate slightly due to the scanning span of the electron beam used in EDAX analysis not exactly analysing the same area during each analysis. There is also a variation in film concentration traversing across the follower surface itself. There appears to be however a surface film depletion or removal mechanism occurring under these stop/start conditions where boundary lubrication occurs at regular intervals during the second half of the test sequence. The mechanism of this surface film removal appears to be of a predominatly mechanical nature and is best shown by the cam specimen tapersection (Fig. 141). Present on, and within the subsurface is evidence of white layer formation and associated tempered regions. The white layer however is intermittently spread across the surface with no sharp boundaries between white layered areas and the adjacent tempered and parent microstructures. Also evident is the lack of any deliterious crack formation or spalling of

the surface. This white layer has formed under boundary lubrication conditions where surface interaction has occurred immediately after the combination of mechanical removal and/or thermal decomposition of the surface films at asperity contacts, due to the intense pressures and temperatures generated at these surfaces. The relative 'smoothness' of the surface after 'running in' makes the real contact stress as near to or equal to the design stress. This reduces the likelyhood of plastic deformation, welding and rupture of the surface using the mineral base oil. The production of this crack free white layer and the lack of any associated plastic deformation and wear damage of the surfaces, along with the generally small wear debris in the size range 2-5 microns, shows the actual wear occurring in this system, under these test conditions to be negligble. Although it is known that the production of white layer is detrimental to fatigue[103] and stress corrosion[104]the surface hardening that occurs can in fact improve the wear resistance[105, 106]. Griffiths and Furze[107] have carried out wear tests on surfaces where white layer had been deliberately produced and found a superior wear resistance of these white layered surfaces. However, in the authors view further running of this system would inevitably result in extensive wear damage under stop/start conditions if the test procedure was allowed to progress for long operating periods due to the removal of these surface films. The Z.D.D.P. additives in the system appeared to be of a sacrificial nature, replenishment of these films would need to occur by the addition of further anti-wear additives for the system to continue to run satisfactorily.

5.2.4 The Effect of Artificially 'Run In' Surfaces

The 'ability' of successfully 'run in' cam and follower surfaces to operate under a mineral base oil conditions rely on satisfactory thin-film lubrication to prevent surface contact, assuming continuous, non-deviating operating conditions ie. not 'stop/start' conditions with lubrication regimes fluctuating between elastohydrodynamic and boundary. It was thought that if surfaces could be artificially 'run in' it might be possible to eliminate the use of E.P. additives and their deliterious effects on cam/follower systems such as pitting. This idea formed the basis of test 2E in which both cam and follower surfaces were artificially 'run in' prior to testing. The 'running in' process consisted of diamond lapping both the cam and follower surface to produce a metallographically smooth surface. Friction results for test 2E can be seen in Fig. 126 and show a gradual increase in the coefficient of friction to 0.18 after 30 hours which remained at this constant value up to the end of test. Spectrometric oil analysis and PQ index also showed this same general trend. The wear rates of the diamond lapped surfaces were overall slightly higher than the tests run in the fully formulated oil. The initial wear rates of these diamond lapped surfaces were not as severe as the as-ground surfaces used with the fully formulated oil, this is due to the artificial 'running in' process produced by this diamond lapping operation. The overall wear rates are higher however with the diamond lapped surfaces. These higher wear rates are shown by reference to Figs 127 and 128 and indicate that although the surfaces are metallographically smooth, they are still triboligically

rough and a considerable amount of microscopic plastic deformation and material removal has to occur to complete the 'running in' cycle. The majority of wear of the diamond lapped surfaces occurred within the first 20 hours of testing and this was of a gradual nature, and is best indicated by the coefficient friction results in Fig. 126. The amount of visible wear damage however was negligible and appeared to be confined to areas of abrasive wear as shown in Figs 144 and 145, with no evidence of surface film formation. The extent of the initial surface lapping operation is still evident, in the case of the cam surface where the manganese sulphide inclusions present these can still be seen (Fig. 144). Edax analysis of the cam surface shows no characteristic peaks which would provide evidence of surface film formation. The only significant concentrations on the surface apart from the typical iron peak were peaks for manganese and sulphur, however, the lack of any surface films showed that both the manganese and sulphur concentrations were due to the inclusions present in the steel. Tapersections taken from both the cam and follower wear specimens showed no evidence of any subsurface wear damage (Figs. 147 and 148) and SEM examination of the wear debris showed morphologies and sizes of the debris of a platelet form in the size range 1-8 microns. The results obtained from test 2E must not be allowed to mislead readers into thinking that diamond lapping of cam follower surfaces can be a commercial proposition in the motor industry. Test conditions again were undeviating and thus meant the system ran under predominantly elastohydrodynamic lubrication conditions throughout the test period. Under service operation,

stop/start conditions would prevail, leading to boundary lubrication which in the absence of additives and associated surface films would lead to catastrophic wear damage if run through a typical operating cycle.

To conclude this part of the dicussion section, the author has illustrated the importance of satisfactory 'running in' of surfaces, with surface film formation of cam and follower systems. Using the relatively simple technique of acetate replication a surface topographical 'history' showing the sequences of 'running in' and 'scuffing' using a fully formulated oil and it's mineral base equivalent has been established. Results show satisfactory 'running in' using a fully formulated oil occurs by a process of plastic deformation and fracture of asperities gradually resulting in smoother surfaces and satisfactory operation of the cam/follower system. However surface interaction, asperity welding and scuffing occurs using the mineral base oil, leading ultimately to catastrophic wear by a spalling mechanism. Other results show the importance of surface film formation during 'running in' in fully formulated oils leading ultimately to satisfactory operation in the mineral base oil under continuous, non-stop test conditions. Intermittent testing under stop/start conditions in the mineral base oil after surface film formation leads however, to gradual surface film depletion by a mechanical and/or thermal mechanism. This leads to sporadic white layer formation and eventual failure by scuffing. Satisfactory running was also possible in a mineral base oil by artificially 'running in' the surface by a diamond lapping process. However, satisfactory operation was only possible under continuous running conditions, with

scuffing likely to occur under stop/start boundary conditions if these conditions were to predominate.

5.3 OBJECTIVE THREE

5.3.1 New Materials

5.3.1.1 Ceramics

This work only arose very late in the research period and very little time was available and only preliminary results are reported here.

The test procedure selected for this piece of work was deliberately chosen therefore to produce an unacceptable wear condition for the metallic couple and this was achieved by the use of mineral base oil with no significant anti-wear additives present and a mixed lubrication regime.

In the case of the metallic couple, test 3A, Fig. 150 shows the very high coefficient of friction generated through the test duration and this is supported by the rough cam wear surfaces shown in Fig. 151, 152b and 155b which are associated with scuffing shown by the 'white layer' present in Fig. 158a. These results were completely predictable and therefore formed the basis for the examination of the ceramics. In the case of Silicon Carbide and Sialon, the surfaces generated were smoother than the 'as produced' surfaces and this is very well illustrated by the visual examination of the ceramic surfaces themselves. Figs. 154b and d show the Silicon Carbide and Sialon surfaces respectively and in both cases particles of silicon can be seen in the matrix shown by the small white areas. The presence of this unfused silicon is due to unsatisfactorily fabrication techniques and although thought to be deliterious to the bulk mechanical properties of the ceramics the

presence of these particles highlights clearly the extent of the polishing of the ceramic surfaces. The polished morphology of both the cam and follower surfaces from tests 3C and 3D is reflected by the very low frictional resistance, again suggesting a change to elastohydrodynamic lubrication from the initially mixed lubrication regime conditions at the start of test.

As far as test 3B is concerned using the toughened zirconia the frictional resistance was higher than the other two ceramic tests but lower than for the metallic couple (Fig. 150). The cam surface showed only slight evidence of scuffing (Fig. 155b) although it showed significant evidence of wear of an abrasive nature. The reason for this becomes apparent when Fig. 156d is examined, which shows general grooving of the zirconia surface suggesting a loose abrasive wear debris being produced which subsequently wears the cam surface by a three body wear mechanism. The mechanism of the micro - pitting on the zirconia follower surface shown in Fig. 156d, can best be explained by reference to zirconia/yttrium phase diagram shown in Fig. 191. The transformation toughening mechanism of zirconias are only possible by the addition of stablising elements, in this case yttrium in molecular percentages of around 2-3, shown by the broken line on the left hand side of the phase diagram. On cooling ZrO_2 from above 1200°C to room temperature the tetragonal - monoclinic transformation occurs. If however the ZrO_2 is finely divided, or a constraining pressure is exerted on it by the matrix, then the zirconia particles can be retained in the metastable tetragonal form. The mechanism of toughening is considered to be a stress induced transformation of the metastable tetragonal particles

to the monoclinic form. If a crack is made to extend under stress, large tensile stresses are generated around the crack, especially ahead of the crack tip. These stresses release the matrix constraint on the tetragonal zirconia particle and if sufficiently large results in a net tensile stress on the particle, which under the new conditions will transform to a monoclinic symmetry. The volume expansion (> 3%) and shear strain (1.7%) developed in the particle causes the martensitic reaction, with a resultant compressive strain being generated in the matrix. Since this occurs in the vicinity of the crack, extra work would be required to move the crack through the ceramic, thus accounts for the increase in toughness and hence strength (Fig. 186). This toughening mechanism however assumes fracture initiation temperatures ranging from 0°C to a maximum temperature of around 500°C to ensure a satisfactory transformation, whereas hot spot temperatures at asperity points on contacting surfaces have been, in some cases calculated to be in excess of 1000°C. Reference to the phase diagram, (Fig. 187) shows these temperature dependent transformations to be reversible, including the phases with yttrium contents in the 0-4% region. It is postulated therefore that the micro pitting which is apparent on the zirconia surfaces is due to the hot spot temperatures of the zirconia asperities when in contact with the steel cam which may be high enough to reverse the tetragonal/monoclinic transformation. This places the ceramic surface in the fully tetragonal phase form, thus completely eliminating the possibilities of a stress induced strengthening transformation occurring.

Another significant feature associated with the zirconia surface are the bright areas shown in Fig. 154d which appear to be metallic

transfer particles orientated in the direction of rubbing. Microprobe analysis shown in Fig. 159 clearly indicates the presence of iron transferred to it's surface, thus stimulating a like on like adhesive wear situation contributing to a higher friction resistance, Fig. 150.

To summarize, this work shows the possible advantages of using certain ceramics for the use in finger follower applications in overhead camshaft systems. The results show the increased wear performance of the silicon carbide and sialon ceramics when compared with a standard steel and cast iron combination and the zirconia ceramic. This also further illustrates the importance of surface roughness criteria in determining the predominant lubrication regime during operation, ie the decreasing surface roughness of the silicon carbide and sialon/steel combinations leading to elastohydrodynamic lubrication and 'zero' wear and the increasing surface roughness of the white cast iron and zirconia/steel combinations leading to boundary lubrication and high wear scuffing conditions. These were based on predominatly mixed lubrication conditions at the commencement of testing, with the absence of any significant additives in the test oil. The hypothesis postulated by the author regarding the failure mechanism for the zirconia ceramic should be given serious consideration in the early design stages when considering these forms of ceramics for wear applications in such areas as the internal combustion engine where the possibility of oil starvation and surface interaction with ferrous materials is all too likely to occur.

5.3.1.2 Ceramic Fibre Reinforced Aluminium Silicon Alloy

The use of the ceramic fibre reinforced Al/Si alloy gave a lower friction coefficient than the hard faced alloys, reducing to a steady state value of around 0.13 after 10 hours which is consistent with a low overall wear rate. The wear that did occur was mainly from the cam nose as shown in Figs. 161 and 163 where evidence of slight delamination and material removal was clearly visible. Examination of the follower surfaces (Figs 162 and 164) shows the wear features of a material transfer nature. This was confirmed by EDAX and dot image analysis, Fig 165 a to c shows cam material impingement into the surface, producing a like on like adhesive wear situation which would inevitably lead to an to increase in the frictional resistance. Wear debris produced from contacting surfaces shows the size and morphology of these large ferrous wear platelets contributing to this transfer and impingement phenomena. Examination of the tapersections from both the cam and follower, Fig. 166 and 167 respectively show in the case of the cam no white layer production or sub surface deformation and cracking. The follower subsurface however showed a small amount of deformation indicated by the of individual ceramic fibres. Examination of a specimen in the 'as ground' condition however showed this deformation to be due to the original grinding operation.

Donomoto and his fellow workers[38] have worked on these composite alloys for piston crown applications in high performance diesel engines and found such materials to have excellent seizure resistance against cast iron, good thermal conductivity and high strength

at elevated temperatures when compared to many other candidate fibres such as carbon and titanate. The processing of such materials is carried out by casting the aluminium piston such that the ceramic fibres are impregnated in and around the piston crown and ring groove. The fibre reinforced section of the alloy however, does not, during a general operating cycle have any direct interaction with any other surface and appears only to strengthen the piston ring groove. This indirectly increases the rigidity of the piston ring, giving high overall strengths at the elevated temperatures clearly apparent in the combustion zone of the cylinder block. Its low bulk hardness however, when compared to other standard wear resistant materials and surface treatments means it's resistance to wear by modes such as abrasion, commonly encountered during the interaction of surfaces such as cam and follower systems in fired engines to be generally low. It was not possible however to simulate exactly such conditions in the test rig, but the ease with which ferrous debris became embedded in the surface and the subsequent 'cratering' left in the composite surface after detachment of the transferred material (Fig. 164) shows the disadvantages of using such materials even though the materials themselves did not contribute directly to the general mechanism of wear.

5.3.1.3 Hard Faced Cobalt and Nickel Alloys

After an initial increase, a lower steady state friction coefficient of around 0.25 after 20 hours was obtained (Fig. 160). The surfaces of both the cam and cobalt alloy follower specimens showed extensive wear damage with material transfer onto both surfaces. The cam surface examined by both optical and scanning electron techniques

showed extensive plastic deformation, consistent with a scuffing type failure. Also apparent is evidence of the transfer of cobalt matrix from the follower in a thin platelet form, (Fig. 169 and 170). Examination of the follower surface also shows evidence of material transfer shown by the small white areas shown in Fig. 171. However, by far the most prominent wear feature is the attack of the cobalt alloy surface leaving what appears to be evidence of the microstructure itself, caused by the removal of the solid solution matrix, leaving in some areas the carbide networks in relief. The majority of the published literature on the wear of these cobalt based alloys has concentrated on the excellent abrasive wear resistance of such alloys. This is due to the morphology and volume fraction of the carbide (Cr_7C_3) present in the microstructure. Adhesive wear of such alloys has been mainly concerned with wear under dry conditions, ranging from mild, oxidative wear at low loads, to severe metallic wear at higher loads[31]. There is however no readily available literature of the wear of such materials under lubricated conditions, in particular for use in cam and tappet applications. Examination of the tapersections from both the cam and follower specimens shows extensive white-layer production on the cam surface, (Fig. 172), indicating hot-spot temperatures in excess of 1000°C being produced. The follower specimen tapersection shows extensive ferrous material transfer and embeddment, (Fig. 173), and this is confirmed by x-ray dot image analysis, (Fig. 175 a to c). The evidence of ferrous particle embeddment into the surface is shown by the overetched pitted areas on the surface caused by the reaction of the ferrous particle during the electrolytic etching of the cobalt matrix in 10% oxalic acid. Also evident is the smearing of ferrous

material over the cobalt surface shown by the x-ray image plot for iron in Fig. 175b. The morphology of the ferrous wear debris shown in Fig 174, having a thickness of up to 4 microns confirms this material transfer phenomena.

The use of the hard-faced Nickel based alloy gave the overall highest friction coefficient, this being 0.28 after 20 hours testing, and again gave the same deliterious wear characteristic as the cobalt based alloy. Material transfer occurred on both the cam and follower surface Fig. 176-178. The nickel follower surface also showed a delamination type of wear occuring (Fig. 178). Tapersections taken through both the cam and follower surfaces confirmed this material transfer phenomena, shown by the brilliant white area on the cam surface, (Fig. 179), this being the smearing of the softer nickel matrix onto the cam surface. This would consequently cause a 'like on like' adhesive situation, resulting in the higher frictional resistance, increased temperatures and the characteristic darker tempered band evident within the cam sub-surface, (Fig. 179). Examination of the follower subsurface shows ferrous material impingement and embeddment into the nickel follower surface, (Fig. 180). Closer examination however shows the ferrous material present in the follower surface has started to diffuse into the nickel matrix forming in effect an iron/nickel alloy and this is confirmed by the faintness of the traces obtained from x-ray dot image analysis of the follower surface as shown in Fig. 182 a to c.

The excessive wear rates that are apparent using both the cobalt and nickel hard faced alloys may be explained by reference to Table 13, of

the compatability of metal pairs to form alloys with each other. The higher the relative number the easier it is to achieve alloying between the two metals and it can be seen that for both the cobalt and nickel alloys that alloying with iron appears to be easy, both registering 4 on the chart. Reference to figs 188 and 189, the iron/cobalt and iron/nickel phase diagram again shows the ease at which solid solutions between the metals can occur, especially when considering temperatures of 1000°C being generated at the asperity hot spots.

These results show that for the range of new materials tested for the applications of finger followers in valve train systems, the use of ceramics proved the most satisfactory. With the exception of the toughened zirconia the ceramics gave, under mineral base oil conditions, a lower frictional resistance, and smoother surfaces thus enabling elastohydrodynamic lubrication conditions to develop after the predominatly mixed lubrication conditions at the start of test. Test on the metallic combinations resulted in plastic deformation, material transfer and phase transformations and clearly showed a necessity for additive additions to be made if these systems were to run satisfactorily. However, the tests were carried out under non-deviating test conditions, changes in these conditions could have resulted in different wear behaviours of the materials. The materials used were obtained from commercial source and were not characterised prior to wear evaluation. This factor combined with the standard test conditions used and time constraints meant that these results constituted an exploratory investigation only providing a stimulus for further work involving the characterization of such materials.

CHAPTER SIX

6. CONCLUSIONS

6.1 The cam/follower test apparatus has proven to be a satisfactory and inexpensive complimentary technique to both dynomometer and fired test engine methods, for the appraisal of both materials and lubricants.

6.2 Scuffing, pitting and polishing, which are the commonly encountered cam and follower wear failures were reproduced.

i) **Scuffing** - The general scuffing form of wear with associated white layer formation, predominated in the mineral base oil under high load, boundary lubrication conditions. Scuffing occurred at low load, mixed lubrication conditions using the case hardened steel cam and chilled white iron follower combination. Subsequent tests using material combinations with free graphite present in the microstructure did not fail under similar test conditions. The fully formulated oil generally suppressed the onset of scuffing at both high and low loads, due to the presence of anti-wear additives such as zincdialkyldithiophosphate (Z.D.D.P.) present in the oil.

ii) **Pitting** - This form of failure was associated with the chilled white iron follower, using the fully formulated oil at high loads. Evidence showed the failure could have been initiated by either a surface, sub-surface or a stress corrosion mechanism.

iii) <u>Polishing</u> - This form of wear is associated with the fully formulated oil at low loads. The mechanism appeared to be associated with a chemical reaction between the contacting surfaces and the additives present in the oil.

6.3 The test rig differentiated between the mineral base and the fully formulated oil.

6.4 The use of the acetate replica technique proved a satisfactory method of analysing the dynamic change in surface topography of contacting surfaces.

i) Using the fully formulated oil, the surfaces 'ran-in' satisfactorily by a process of plastic deformation and fracture. The surfaces became gradually smoother, allowing elastohydrodynamic oil films to form, thus eliminating surface contact.

ii) Using the mineral base oil, the surfaces scuffed instantaneously. The mechanism of failure occurred by a two stage process.

6.5 Results have shown that surfaces that have 'run-in' with a fully formulated oil can continue to run satisfactorily without scuffing failure, in a mineral base oil under continuous, non-stop conditions.

6.6. Artificially 'run-in' surfaces, produced by a diamond lapping operation prior to testing, operate satisfactorily in a mineral base oil under continuous, non-stop conditions.

6.7 Surfaces that have 'run in' satisfactorily with a fully formulated oil

and subsequently tested in a mineral base oil under stop/start boundary lubrication conditions, will ultimately fail by a scuffing mechanism.

6.8 From the range of new materials tested, the ceramics, with the exception of toughened zirconia, proved the most satisfactory materials under mineral base oil conditions.

7. SUGGESTIONS FOR FURTHER WORK

1. Areas of this research work have dealt with materials which are not yet fully characterised with particular reference to structure/property relationships and their effect on wear behaviour. This becomes evident with reference to the work carried out on the pitting of chilled white iron. No unified solution to this particularly serious wear problem can be sought whilst large differences in hardness and chilled depth, and the presence of cracks in components prior to testing exist. It is because of this that standardisation of chilled white irons becomes extremely important. Much more characterisation work also needs to be carried out on ceramics. The work carried out in the experimental section showed the possible advantages on using certain ceramics for components in the internal combustion engine. The work was however, considered only to be a preliminary study and further work, in particular the characterisation of these ceramics needs to be carried out before ceramics can become economically viable for commercial automobile usage.

2. Further work should be carried out in the area of 'running in', with particular reference to the effect of different surface finishes applied to cams and follower, and observe their effect on producing a successfully running cam/follower, thus optimizing the surface characteristics of such components.

3. Much interest has been shown recently on the continuous condition monitoring of machinery, especially in the light of a helicopter gear box failure resulting in loss of life. The use of this form of monitoring can also be an advantage in the cam/follower rig where a

reliance on wear debris analysis is made for the detection and monitoring of wear rates, as no direct method of wear rate monitoring is readily available. Recent advances in continuous monitoring techniques such as improved magnetic plug detectors and on-line wear debris monitors could lead to a better understanding of the wear rates occurring in such simulative rig applications. It is envisaged that experimental work could be carried out whereby such monitoring aids could be attached to the rig during operation and compared with existing off-line techniques. Advice from this work would be invaluable to engineers concerned with selecting the most appropriate technique for their particular requirement.

PAGES MISSING IN ORIGINAL

8. ACKNOWLEDGEMENTS

I would like to thank Dr T.S. Eyre who initiated and supervised this project for his helpful guidance and encouragement. I gratefully acknowledge the support provided by the Ministry of Defence. The assistance and co-operation of the technical staff in the Department of Materials Technology was greatly appreciated. Thanks are also due to my parents for their moral and financial help, and Julia for her unending support.

Finally I would like to thank Miss L. Rolph for her patience in the typing of this thesis.

9. REFERENCES

1. Dyson, A., Trib. Int., (1980), 13,121-132.

2. Bakaonyi, S.M., SAE Paper No. 680028, (1968).

3. Crawley, B.W., T.S. Eyre., Trib. Int., (1978), 11, 91-96.

4. Bowden, F.P., Tabor, D., The friction and lubrication of solids. Part I, 1950, Part II, 1964, Clarendon Press, Oxford.

5. Wilson, R.W., Proc. Phys. Soc., (1955), 68, 625-641.

6. Paleavi, C., Girelli, A., and Sinivanred, C., J. Inst. Petrol., (1958), 44, 178-181.

7. Keller, H., Metallur. Ind., (1957), 48, 443-447.

8. Wiederholt, W., Robert Draper Ltd, Teddington, (1965), Commercial Handbook.

9. Schenk, H., Kuppersbusch, H., Stahl and Eisen., (1963), 83, 154-161.

10. Metals Handbook, (1964), 2, 8th Edition, 531-547.

11. Zaat, J.H., Technische Hogeschool, Eindhoven, (1967), Paper No.2

12. Morgan, H.L., B.C.I.R.A. Report No. 1047, (1971).

13. Ihrig, H.K., U.S. Patent No. 2, (1938), 109, 485.

14. Chesters, W.T., J. Iron and Steel Inst., (1970), 208, 982-987.

15. Marshall, L., Mansell, S.J., Engineering, (1956), 181, 425-428.

16. Gregory, J.C. Tribology Int, (1970), 3, 73-83.

17. Waterfall, F.D., Metallurgia, (1967), 76, 98-100.

18. Kanter, J.J., Metals Handbook, (1964), 8th Edition, 2, 529-530.

19. Drewett, R., Journal of Anti-Corrosion Methods and Materials, (1969), 16, 10-14.

20. Ullman, D.K.O., Eng. Mat. Design., (1969), 12, 897-900.

21. Proceedings of conference on the science and technology of surface coatings. Imperial College, London, (1972).

22. Ballard, W.E., (1963), 4th Edition, (Griffin, London).

23. Metals Handbook, (1961), 1, 820-833.

24. Metals Handbook, (1971), 6, 424-427.

25. Donovan, M., et al., Trib. Int., (1972), 5, 205-224.

26. Greenwood, J.P., "Hard Chromium Plating", Robert Draper Ltd, Teddington, (1971), Commercial Handbook.

27. Godfrey, D.J. May, E.R.W., "Ceramics in severe environments", Ed. W.W. Krieger and H. Palmour, Plenum Press, New York, (1971), 149.

28. Godrey, D.J., Trans SAE, (1974), 2, 1036.

29. Timoney, S.G., (Ed), Diesel Engines: EUR 7660EN, European Community, Brussels, (1981).

30. Kamo, R., "Cycle and performance studies for advanced diesel engines". Presented at conference on ceramics for High Performance Applications, Newport, Rhode Island, (1977).

31. Antony, K.L., Journal of metals, (1983), 2, 52-60.

32. Hickl, A.J., Journal of metals, (1983), 1, 6-12.

33. Moore, J.C., Powder Metallurgy, (1984), 4, 229-230.

34. Jack, K.H., J. of Mats. Science., (1976), 11, 1135-1158.

35. Stevens, R., Introduction to Zirconia, Pub Magnesium Elektron, Publication No. 113.

36. Evans, A.G., Heuer, A.H., J. Amer. Ceram. Soc. (1981), 63, [5-6], 241-248.

37. McMeeking, R.M., Evans, A.G., J. Amer. Ceram. Sco., (1982), 65 [5], 242.

38. Donomoto, T., et al. SAE paper no. 830252, (1983).

39. Dowson, D., 'Boundary Lubrication - An appraisal of world literature', (1969), Chaper 11. Ed. Ling, Klaus & Fein.

40. Stribeck, R., Die Wesentlichen Eigenschaften der gleit - und rollenloger, VDI - Zeitschrift, (1902), 46, 1341, 1432, 1463.

41. Dowson, D., Proc. Instn. Mech. Engrs., (1967-68), 182, Pt 3A, 151-167.

42. Wedeven, L.D., Journal ASLE, (1975), 31, 6, 291-296.

43. 'Cams and cam mechanisms', Proc. Mechanisms 74' conference of I.Mech.E., Pub. MEP., (1974).

44. Begelinger, A., De Gee, A.W.J., Wear, (1974), 28, 103-114.

45. Morgan, J.A., Stojek, P.J., SAE Trans., (1971), 80, 546-573.

46. Pless, L.G., Rodgers, J.J., SAE paper no. 770087, (1977).

47. Torii, Kyozo, Chida, Hitoshi, et al., SAE paper no. 770635, (1977).

48. Watkins, R.C., Spedding, H., Trib. Int., (1982), 15, 9-12.

49. Waddey, W.E., Pearce, A.F., SAE paper no. 690774, (1969).

50. Sakurai, T., J. Lub. Technology., (1980), 103, 473-485.

51. Robinson, G.H., et al, SAE Journal, (1959), 80-83.

52. Georges, J.M., Martin, J.M., et al., Wear, (1979), 53, 9-34.

53. Kapsa, P.H., Martin J.M., et al, J. Lube. Tech., (1981), 103, 486-496.

54. Bird, R.J., Coy, R.C., Halton, J.F., ASLE. Trans. (1978), 23, 2, 121-130.

55. Rounds, F.G., SAE Paper No. 770829, (1977).

56. Watkins, R.C., Trib. Int., (1982), 15, 13-15.

57. Cameron, A., ASLE Trans., (1979), 23, 4, 388-392.

58. Grew, W., Cameron A., Nature, (1968), 217, 481-482.

59. Begenlinger, A., DeGee, A.W., Salomon, G., ASLE Trans., (1978), 23, 1, 23.

60. Kruschov, M.M. Proc. Conf. Lab. Wear. (1957), 655.

61. Serpik, N.M., Kantor, M.M. Friction and wear in machinery, (1965), 19, 28.

62. Popov, V.S., Nagormyi, P.L., Rumanian Casting Production, (1969), 8, 337.

63. Richardson, R.C., Wear, (1968), 11, 245.

64. Alienkov., F.K., Soviet Physics - Technical Physics Journal, (1956-57), 2, 2529-2538.

65. Rabinowicz, E., 'Friction and wear of materials' (1965) J. Wiley (Ed), New York.

66. Eyre, T.S., Trib. Int., (1978), 11, 91-96.

67. Archard, J.F., Wear, (1959), 2, 6, 438-455.

68. Welsh, N.C., Trans. Roy. Soc., (1965), 257, 31-70.

69. Suh, N.P., Wear, (1977), 44, 1-16.

70. Blok, H., Wear, (1963), 6, 483-494.

71. Dyson, A., Naylor, H., Proc. Inst. Mech. Engrs. (1960-61), 8, 255-262.

72. Wykes, F.C., (1970), 'Summary report on the performance of cam and cam follower material combinations' Report No. 1970/73.

73. Caldicott, B., (1960), Symposium on wear in the petrol engine, Shell Res., 227-234.

74. Jahanmir, S., (1984), 'Examination of wear mechanisms in automotive camshafts'., Exxon Res. and Eng. Co. New Jersey, USA.

75. Neale, M.J., 'Tribology Handbook' (1973) A.23. Butterworths.

76. Dyson, A., Naylor, H., Proc. Instn. Mech. Engrs. (1960-61), (AD), 8, 255-280.

77. Schilling, A., 'Automobile Engine Lubrication', Scientific Pubn. (1971).

78. Benzing, R., et al., "Frictional Wear Devices" ASLE (1976).

79. Just, E., Metal Progress, (1970), Aug., 110-114.

80. Slater, B.B., Lane, G., Weston, J., Co-ordinating European Council. 'International Symposium on the Performance Evaluation of Automotive Fuels and Lubricants'. EL/2/4, 1981.

81. Slater, B.B., SAE paper no. 750866 (1975).

82. Pocock, G., Brit. Journal N.D.T., (1979), 5, 125-130.

83. Mills, G.H., Davis, F.A., 'A Ferrographic Case Study Applied to Hydraulic Systems". Private Communication.

84. Price, A.L., Roylance, B.J., "The Rotary Particle Depositor - a response to problems experienced with wear particle deposition". Proc. Intl. Conf. Cond. Monit. (1984) Ed, Mervin Jones 11 596-608.

85. Yardley, E.D., "The use of wear debris analysis to monitor gear transmissions used underground". Proc. Intl. Conf. Cond. Monit. (1984) Ed. Mervin Jones.

86. Price, A.L., Yardley, E.D., "The evaluation of the rotary particle depositor in the monitoring of gear transmissions used underground". Proc. Intl. Conf. Cond. Monit. (1984) Ed. Mervin Jones, 12, 608-617.

87. Etchells, E.B., Thomson R.F. "What we know about cams and tappets" S.A.E. Journal, (1955) September, 56-65.

88. Jiajun, L., Fuxing, W., Zhouping, C., "Research on the pitting mechanism of chilled white iron". Tsinghua University, Beijing, China. 1985. To be published.

89. Jiajun, L., Zhiqiang, L., "A wear failure analysis of a chilled cast iron tappet". Mechanical Engineering Department, Tsinghua University, Beijing, China. 1985. To be published.

90. Sugishita, J., Fujiyoshi, S., Wear, (1982), 77, 181-193.

91. Eyre, T.S., William, P., Wear, (1973), 24, 337/349.

92. Eyre, T.S., Zhu, Y.M. "The lubricated Wear of Flake Graphite Cast Iron". Brunel University, U.K., 1985. To be published.

93. Scott, D., Mills, G.H., Wear (1970) 16 234-237.

94. Hack. K., Feller, H.G., Z. Metallkd, (1970), 61, 394-400.

95. Swain, M.V., Jackson, Wear (1976) 37 63-68.

96. Scott, D., Mills, G.H., Wear (1973) 24 235-242.

97. Loy, B., McCallum, R., Wear (1973) 24 219-228.

98. Rabinowicz, E., Wear (1977) 42 149-156.

99. Wellaver, E.J., Symp. Japan. Soc. Mech. Engrs, 1967.

100. Barwell, F.T., Roylance, B.J., "Tribological Considerations In The Design and Operation of Cams" - A Review of the Situation. 1975. Ed. J. Rees Jones.

101. Eyre, T.S., Al-Khalidi, G.F., "Bore Polishing - Indentification and Simulation" Trib. Int. (1987) Feb. 20, 1, 18-24.

102. Onion, G. 'Reaction Film Lubrication' Journal of Chartered Mechanical Engineers, July 1979.

103. Field, M., Kahles, J.F. "Review of Surface Integrity of Machined Components", Annals of C.I.R.P, (1971) Vo. 20/2 153-162.

104. Field, M., Koster, W.P., Kohls, J.B., Snider, R.E., Maranchick, J. "Machining of High Strength Steels with Emphasis Surface Integrity". American Air Force Machinability Data Center Report AFMOC 70-1, 1970.

105. Griffiths, B.J., Furze, D.C., "White layers at machined surfaces". Proc. Inst. Metals. Conf. London, 14-16 May 1986.

106. Eyre, T.S., Baxter, A., Metals and Materials (1972), 6, 435-439.

107. Griffiths, B.J., Furze, D.C., "Tribological Advantages of White Layers Produced by Machining" Proc.Conf. Joint ASME-ASLE Oct. 20-22, 1986.

Table 1. Materials and Treatments Commonly Used for Camshaft and Cam Follower Components

CAMSHAFT	CAM FOLLOWER
Alloy Flake Cast Iron Induction Hardened	Chilled Nodular Cast Iron
Chilled Cast Iron	Chilled Cast Iron
Spheroidal Graphite Cast Iron Induction Hardened	Spheroidal Graphite Cast Iron Induction Hardened and Tufftrided
Pearlitic Malleable Cast Iron Induction Hardened	Hard Chromium Plating
0.1% Steel Case Carburised	Carbo-nitrided 1½% Manganese Molybdenum Steel
0.35% C Steel Induction Hardened	0.1% C Steel Case Carburised
0.7% Phosphorus Flake Cast Iron Induction Hardened	Alloy Flake Cast Iron Induction Hardened
Carbo-Nitrided Grey Flake Cast Iron	Hardened and Tempered Chilled Cast Iron
	Carbo-Nitrided Spheroidal Graphite Cast Iron

LUBRICANT	DENSITY @ 15°C	FLASH POINT °C	VISCOSITY CS @ 40°C	VISCOSITY CS @ 100°C	VISCOSITY INDEX	POUR POINT °C	CARBON RESIDUE	ELEMENTAL ANALYSIS % W		
								Ca	P	ZN
MINERAL BASE OIL	0.877	222	33	5.5	102	-9	.08	\	\	\
FULLY FORMULATED	0.884	207	63	11	167	-30	\	0.16	0.08	0.08

TABLE 2. PROPERTIES OF TEST OILS

TEST NUMBER	CAM MATERIAL	FOLLOWER MATERIAL	LUBRICANT	SPEED (R.P.M.)	LOAD (Kg)	TEST TIME (HRS)	TEMP (°C)	PURPOSE OF TEST
1A	CASE HARDENED STEEL	CHILLED WHITE CAST IRON	FULLY FORMULATED OIL	1500	80	50	100	EFFECT OF BASE STOCK AND ADDITIVE PACKAGE ON THE WEAR BEHAVIOUR OF CONVENTIONAL CAM AND FOLLOWER MATERIALS.
1B	"	"	MINERAL BASE OIL	"	80	"	"	" "
1C	"	"	FULLY FORMULATED OIL	"	120	"	"	" "
1D	"	"	MINERAL BASE OIL	"	120	"	"	" "
1E	GREY FLAKE IRON INDUCTION HARDENED	CASE HARDENED STEEL	FULLY FORMULATED OIL	"	80	"	"	" "
1F	"	"	MINERAL BASE OIL	"	80	"	"	" "
1G	"	"	FULLY FORMULATED OIL	"	120	"	"	" "
1H	"	"	MINERAL BASE OIL	"	120	"	"	" "
1I	GREY FLAKE IRON CARBO - NITRIDED	NODULAR CAST IRON HARDENED AND TEMPERED	FULLY FORMULATED OIL	"	80	"	"	" "
1J	"	"	MINERAL BASE OIL	"	80	"	"	" "
1K	"	"	FULLY FORMULATED OIL	"	120	"	"	" "
1L	"	"	MINERAL BASE OIL	"	120	"	"	" "

TABLE 3. TEST CONDITIONS OBJECTIVE ONE

TEST NUMBER	CAM MATERIAL	FOLLOWER MATERIAL	LUBRICANT	SPEED (R.P.M.)	LOAD (Kg)	TEST TIME (HRS)	TEMP (^{o}C)	PURPOSE OF TEST
2A	CASE HARDENED STEEL	CHILLED WHITE CAST IRON	FULLY FORMULATED OIL	1500	80	75	100	THE USE OF THE REPLICATION TECHNIQUE TO OBSERVE THE 'RUNNING IN' CHARACTERISTICS OF FULLY FORMULATED OIL.
2B	"	"	MINERAL BASE OIL	"	80	75	"	THE USE OF THE REPLICATION TECHNIQUE TO OBSERVE THE 'RUNNING IN' CHARACTERISTICS OF MINERAL BASE OIL.
2C	"	"	FULLY FORMULATED OIL AND MINERAL BASE OIL	"	80	80	"	'RUN IN' SURFACES FOR 40 HRS WITH FULLY FORMULATED OIL, REPLACE WITH MINERAL BASE OIL TO OBSERVE THE EFFECT OF RUNNING WITH A BASE OIL ON FULLY 'RUN IN' SURFACES.
2D	"	"	FULLY FORMULATED AND MINERAL BASE OIL	"	80	80	"	'RUN IN' SURFACES IN FULLY FORMULATED OIL FOR 40 HRS, REPLACE WITH A BASE OIL AND CONTINUE STOPPING AT PERIODIC INTERVALS AND ANALYSING THE SURFACES FOR SURFACE FILM DEPLETION.
2E	"	"	MINERAL BASE OIL	"	80	80	"	OBSERVE EFFECT OF MINERAL BASE OIL OR THE WEAR BEHAVIOUR OF ARTIFICIALLY 'RUN IN' SURFACES

TABLE 4. TEST CONDITIONS OBJECTIVE TWO

MATERIAL	DENSITY	GRAIN SIZE (μm)	ELASTIC MODULUS (GPa)	HARDNESS (GPa)	FRACTURE TOUGHNESS (MPa)$m^{\frac{1}{2}}$	POISSON'S RATIO
SILICON CARBIDE	3.40	5-10	410	33	4.1	0.16
SIALON	3.20	1-5	300	20	5.4	0.26
TOUGHENED ZIRCONIA	5.7	40-50	200	14	10	0.29
WHITE CAST IRON	7.7	-	207	435-550 (DPN)	-	-

TABLE 5. FOLLOWER MATERIAL PROPERTIES

MATERIAL	Ni	Co	Cr	B	Si	C	Fe	W
NICKEL 'RICH'	BALANCE	—	11.5	2.5	3.75	0.65	4.25	—
COBALT 'RICH'	—	BALANCE	29	—	1.25	1.0	—	4.5

TABLE 6. CHEMICAL COMPOSITION OF HARD FACED COATINGS

FIBRE	COMPOSITION	DIAMETER (μM)	DENSITY (g/cm^3)	STRENGTH (MPa)	MODULUS (MPa)
Aluminia Silica	Al_2O_3: 51% SiO_2: 49%	2.8	2.6	1,300	120,000

TABLE 7. PHYSICAL PROPERTIES OF REINFORCED FIBRE IN Al/Si ALLOY

Test Number	Cam Material	Follower Material	Lubricant	Speed R.P.M.	Load (Kg)	Test Time (Hrs)	Temp (°C)	Purpose of Test
3A	Case Hardened Steel	Chilled White Iron	Mineral Base Oil	1500	80	20	100	Comparison for New Materials
3B	"	Toughened Zirconia Ceramic	"	"	"	"	"	The Use of New Materials For Finger Followers, Applications, Using a Mineral Base Oil.
3C	"	Silicon Carbide Ceramic	"	"	"	"	"	" "
3D	"	Sialon Cermic	"	"	"	"	"	" "
3E	"	Ceramic Fibre Reinforced Al/Si Alloy	"	"	"	"	"	" "
3F	"	Hard Faced Cobalt Alloy	"	"	"	"	"	" "
3G	"	Hard Faced Nickel Alloy	"	"	"	"	"	" "

TABLE 8. TEST CONDITIONS OBJECTIVE THREE

Compatability of Metal Pairs

	Re	W	Mo	Be	Pl	Cr	Co	Ni	Fe	Pt	Cu	Ti	Nb	Zr	Zn	Au	Ag	Al	Cd	Mg	Sn	Mn	Pb
In				1			2	3			3	3		4	3	4	4	1	4	4	4		4
Pb		3	2			1	1	1	1	4	1	4	1		1	2	3	1	3	3	4		
La						1		2	2	4			1	1					4				
Sn	2	3		1	4	1	3	3	2	4	3	4	2	3	3	4	4	2	4	2			
MG				2				2	2		4	2		4	3	4	4	4	4				
Cd				3		3	3	2	2	4	3			4	4	4	4	1					
Al	3	4	3	2	4	4	3	4	4	3	4	4	4	3	4	4	4						
Ag	2	1		4	2	1	1	1	1	4	3	4		3	4	4							
Au	2		3	4	2	4	3	4	4	4	4	3			4								
Zn			3		4	4	4	4	4	4	4	3	2	2									
Zr		3	4		4	3	4	3	2	3	4	4	4										
Nb	4	4	4			4		4	2	4	4	4											
Ti	4	4	4	4		4	3	4	4	4	3												
Cu	3	2	1	4	4	1	4	4	3	4													
Pt	4	4	4	4	4	4	4	4	4														
Fe	4	4	4	4	4	4	4	4															
Ni	4	4	4	4		4	4																
Co	4	4	4	4	4	4																	
Cr	4	4	4	4	4																		
Pl	4	4	4																				
Be	4		3																				
Mo	4	4																					
W	4																						

TABLE 13. THE COMPATABILITY OF METAL PAIRS TO FORM SOLID SOLUTIONS

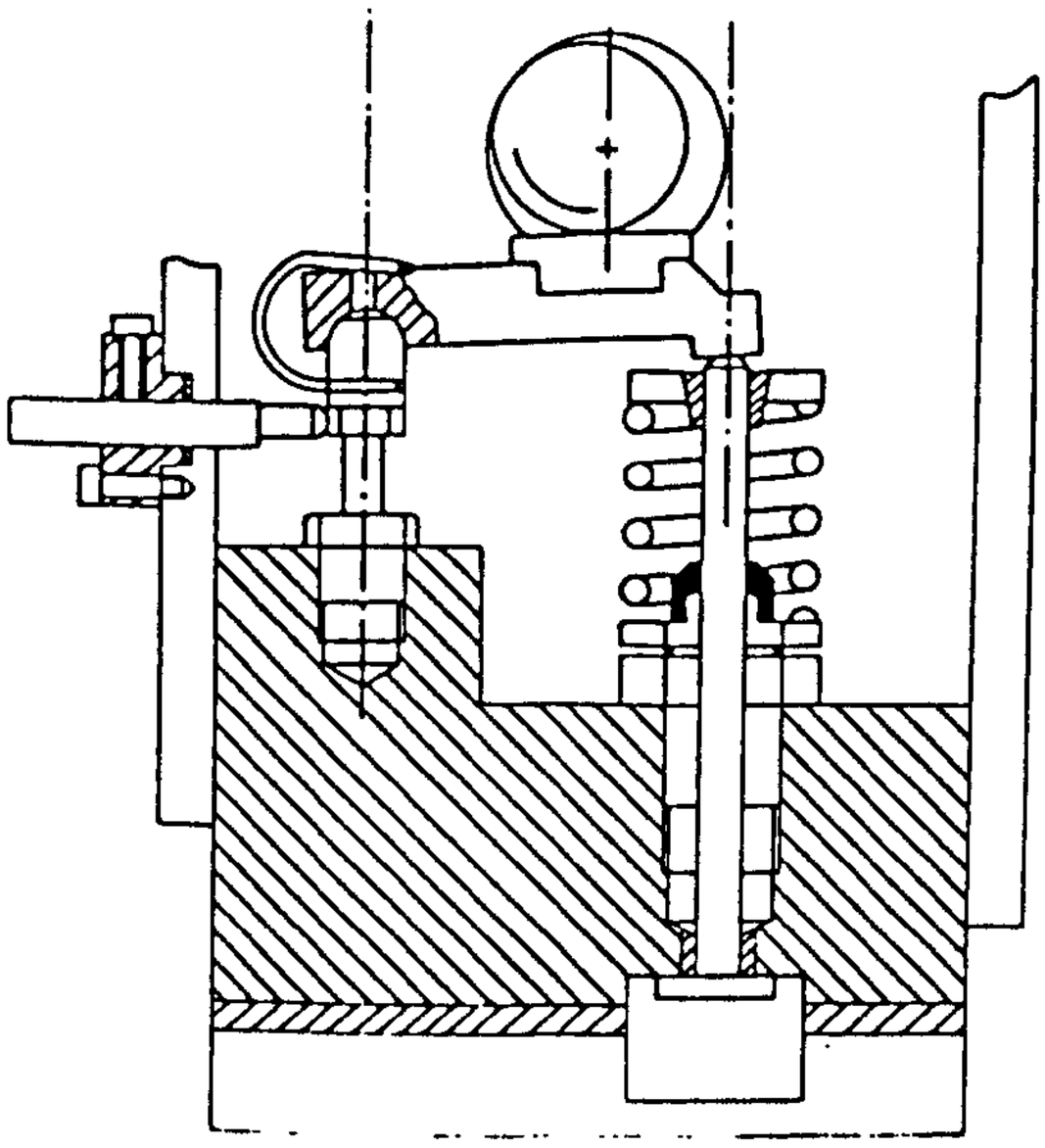

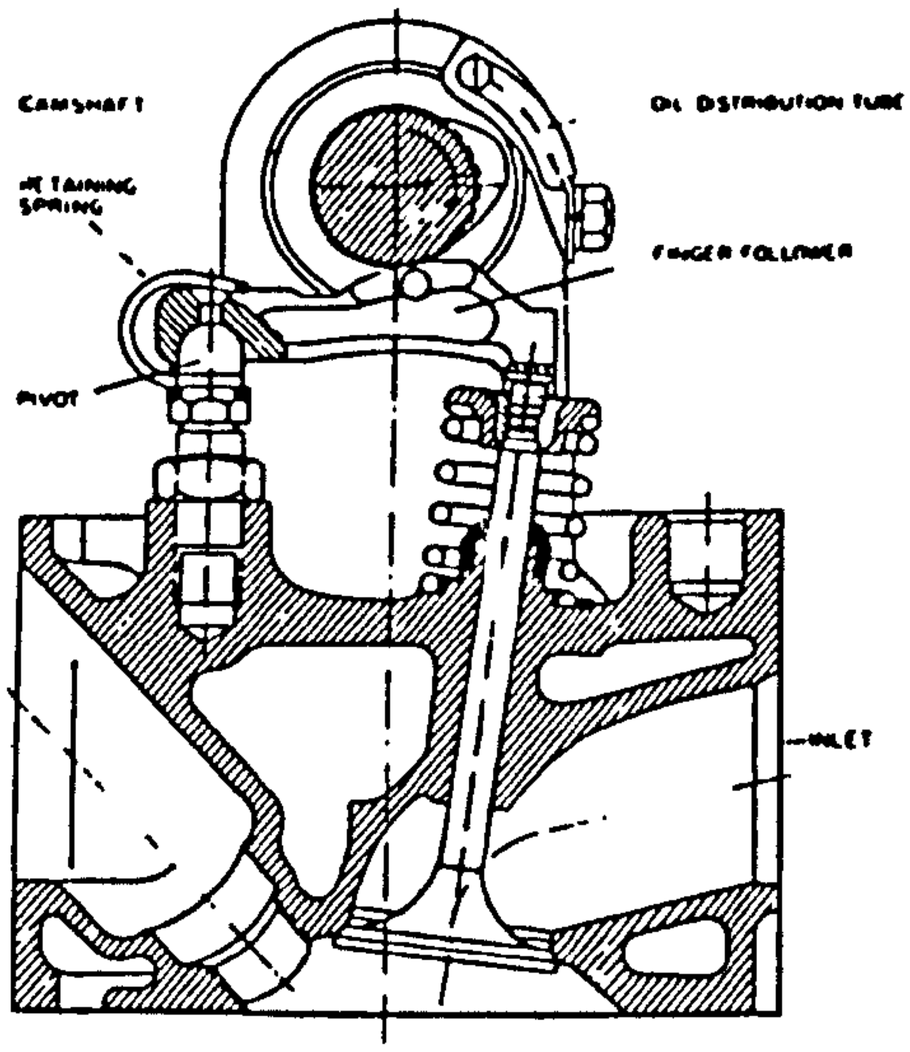

FIG. 12. COMPARISON OF TEST RIG AND EUROPEAN FORD FINGER FOLLOWER SYSTEM.

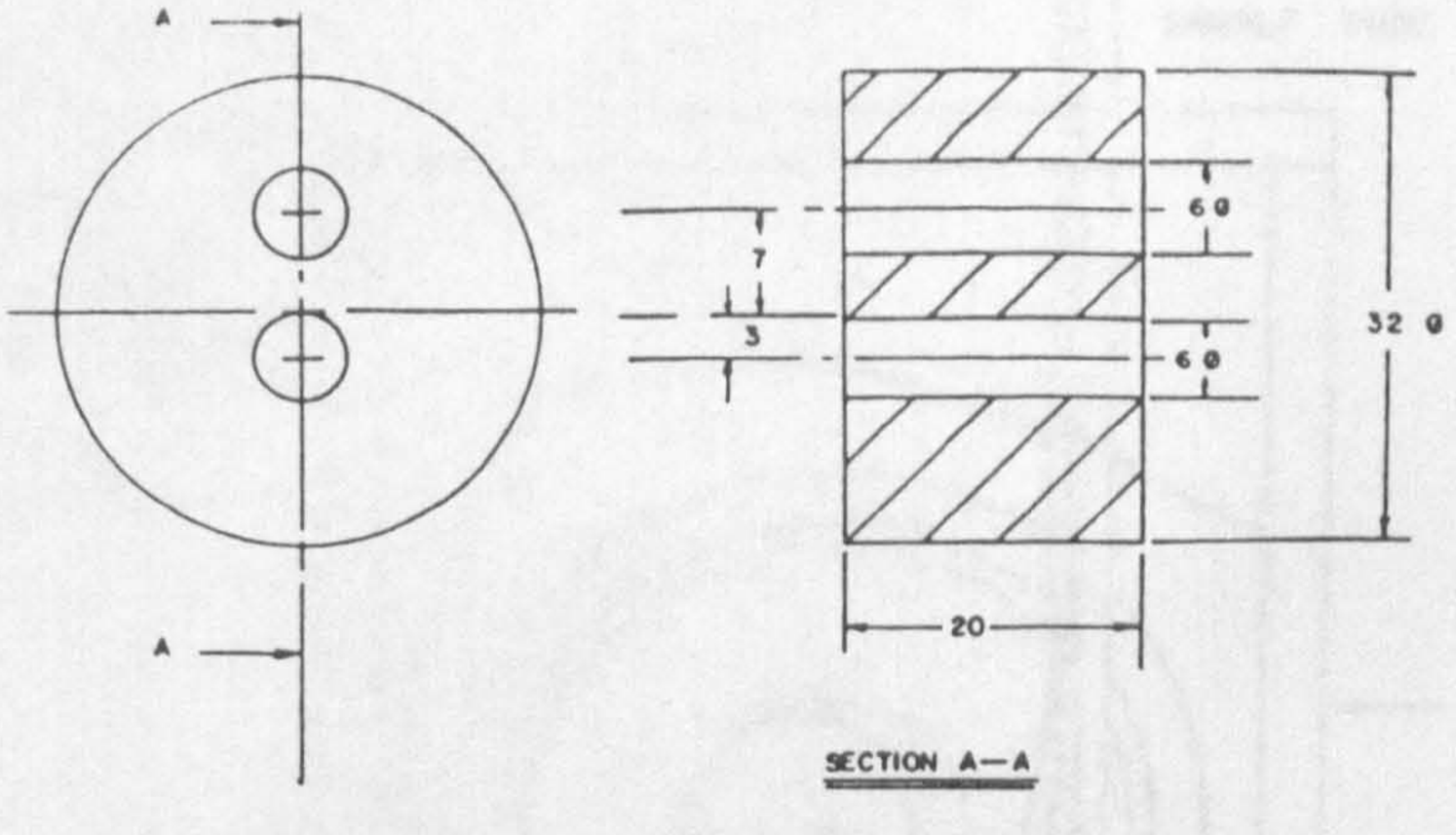

CAM SPECIMEN DIMENSIONS IN MM

FIG. 13A. CAM SPECIMEN DIMENSIONS.

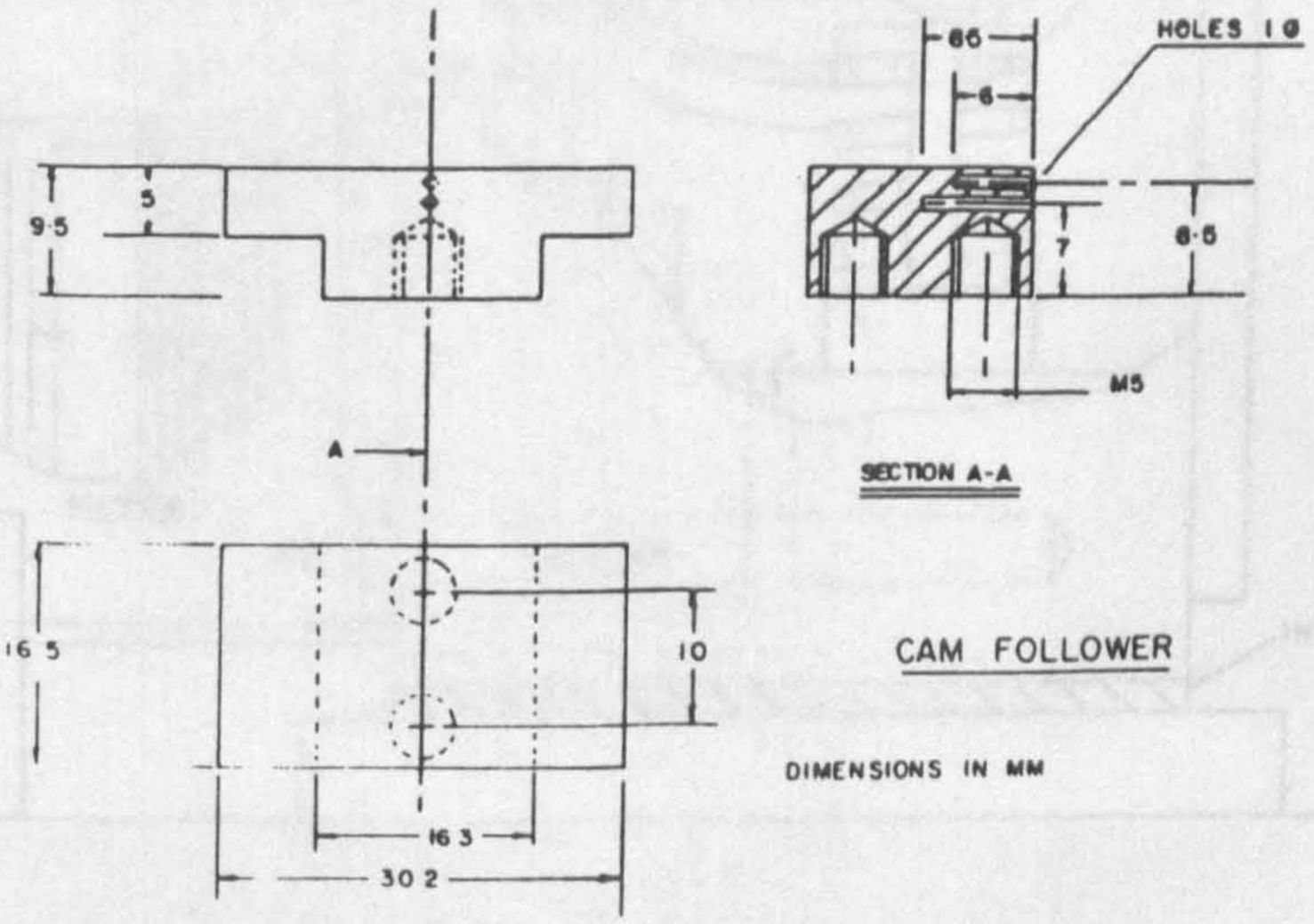

FIG. 13B. FOLLOWER SPECIMEN DIMENSIONS.

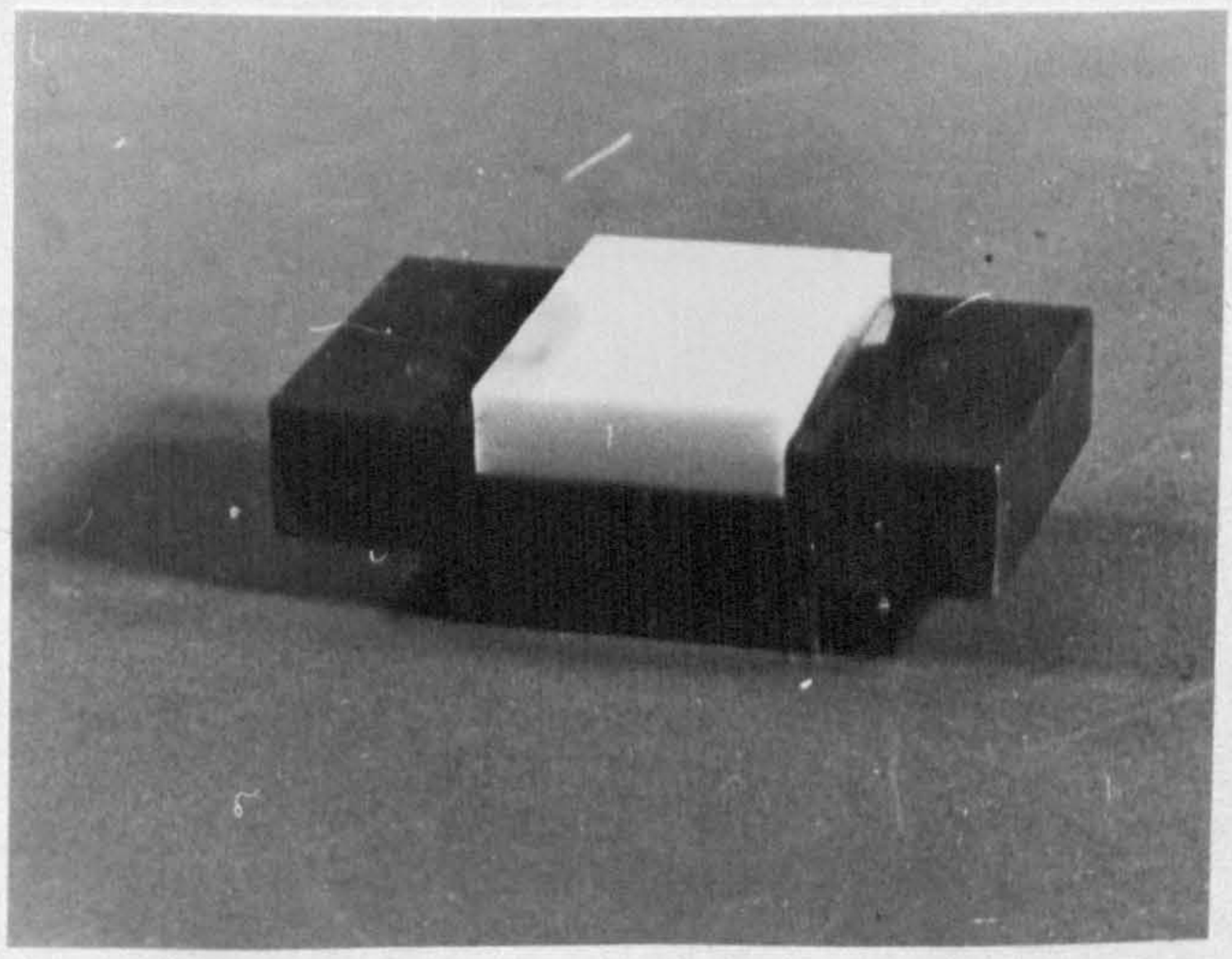

FIG. 13C. INSERT FOLLOWER SPECIMEN.

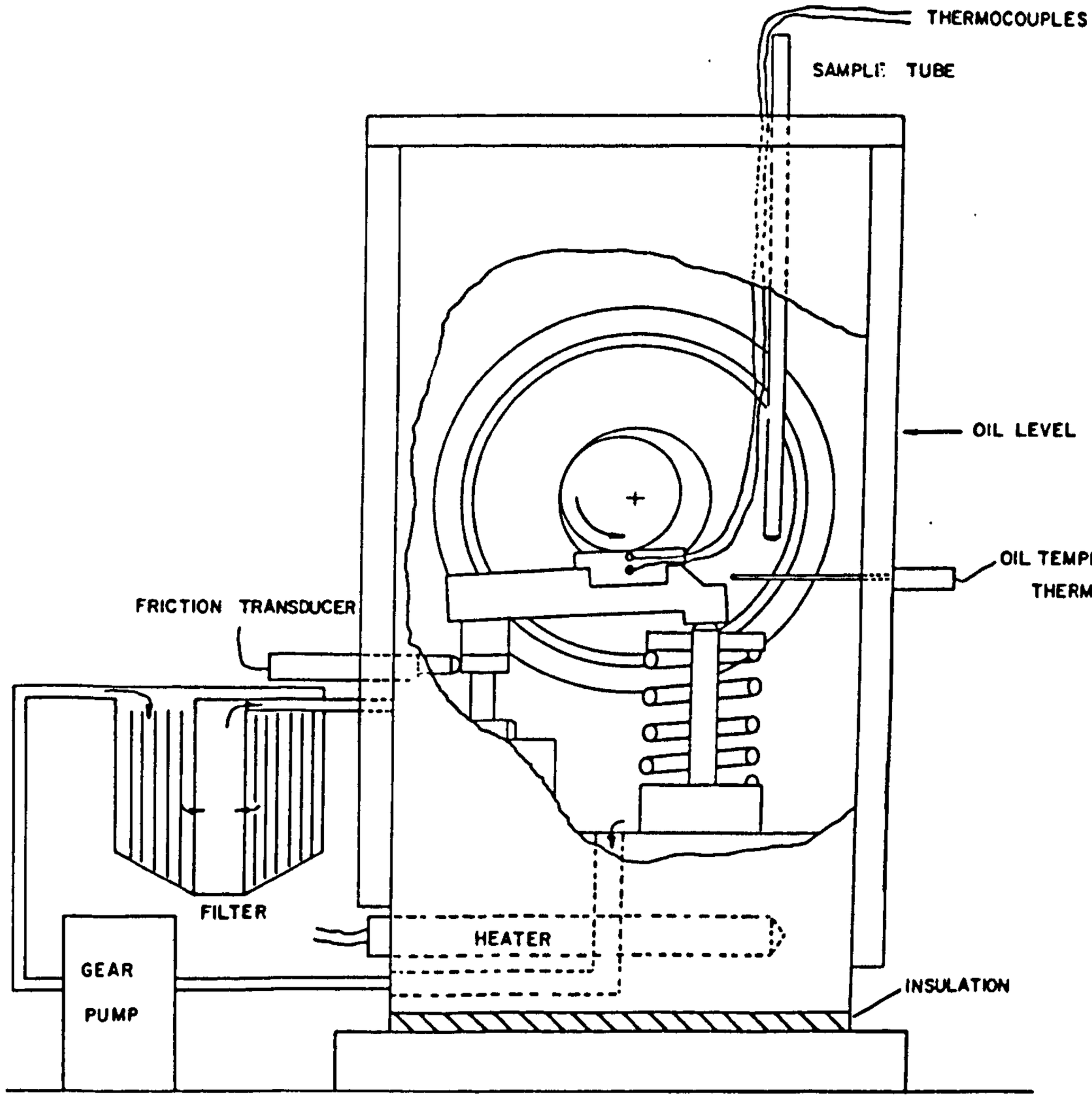

FIG. 14. TEST RIG CONFIGURATION.

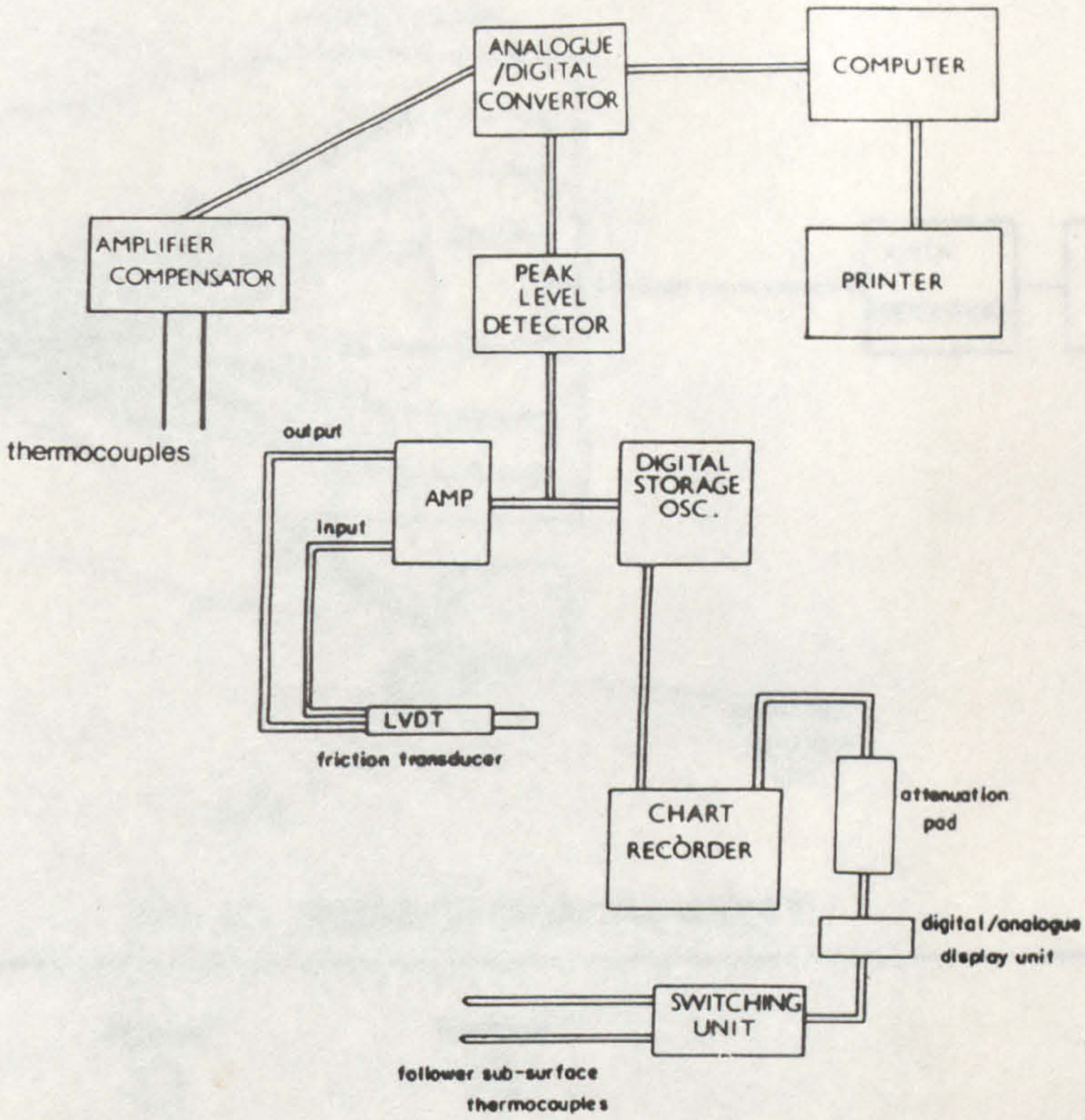

FIG. 15. DATA LOGGING SYSTEM.

FIG. 16. DATA LOGGING AND TESTING LAYOUT.

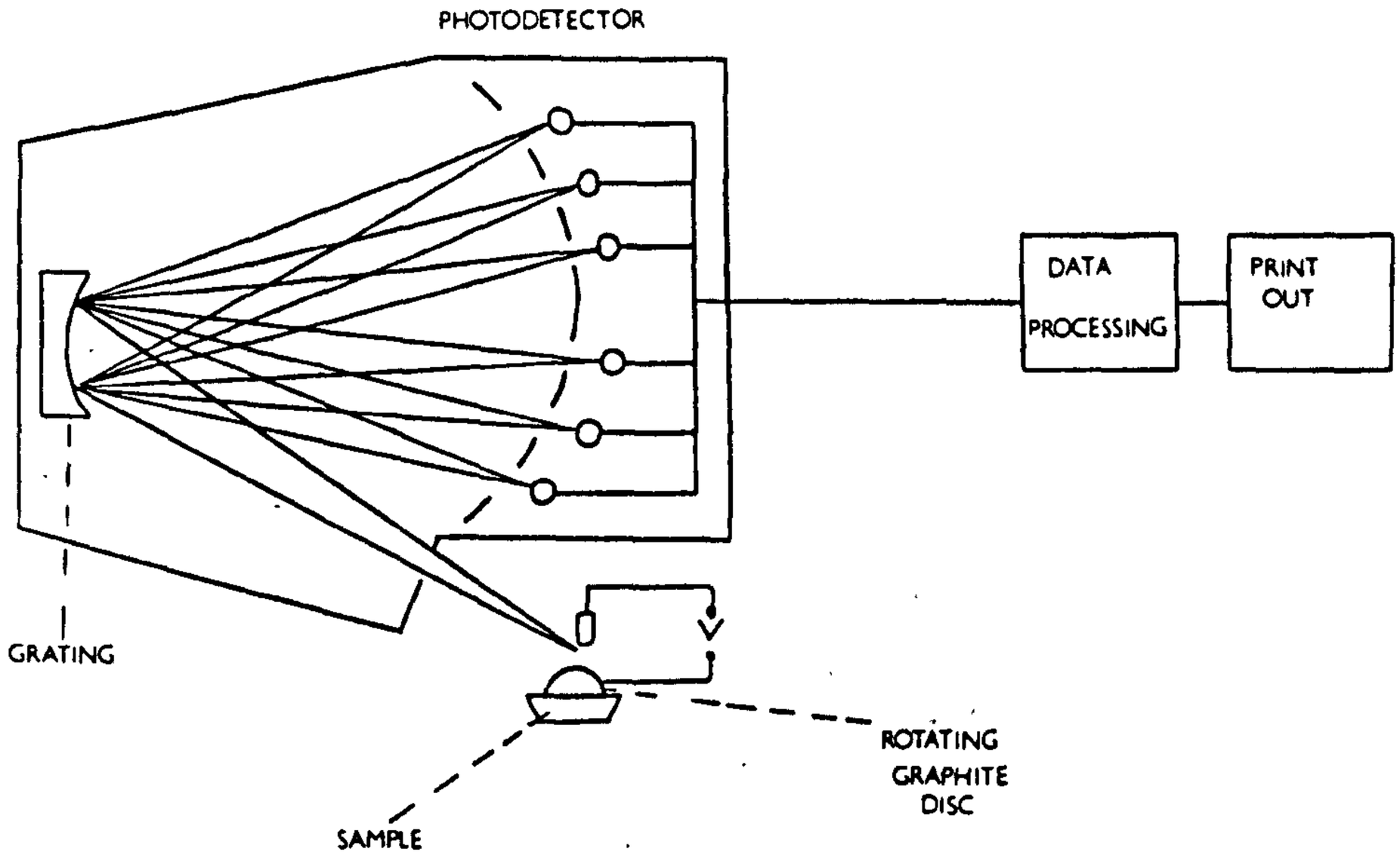

FIG. 17. EMISSION SPECTROMETRY

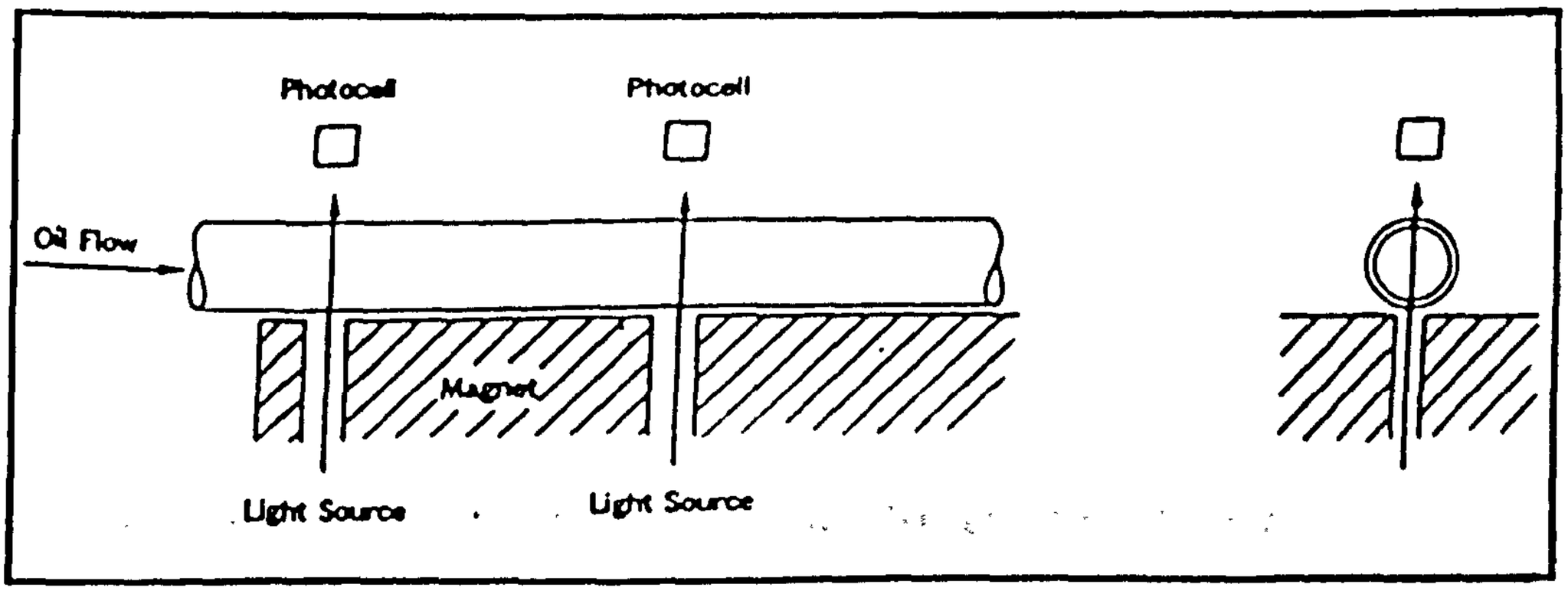

FIG. 18. DIRECT READING FERROGRAPH.

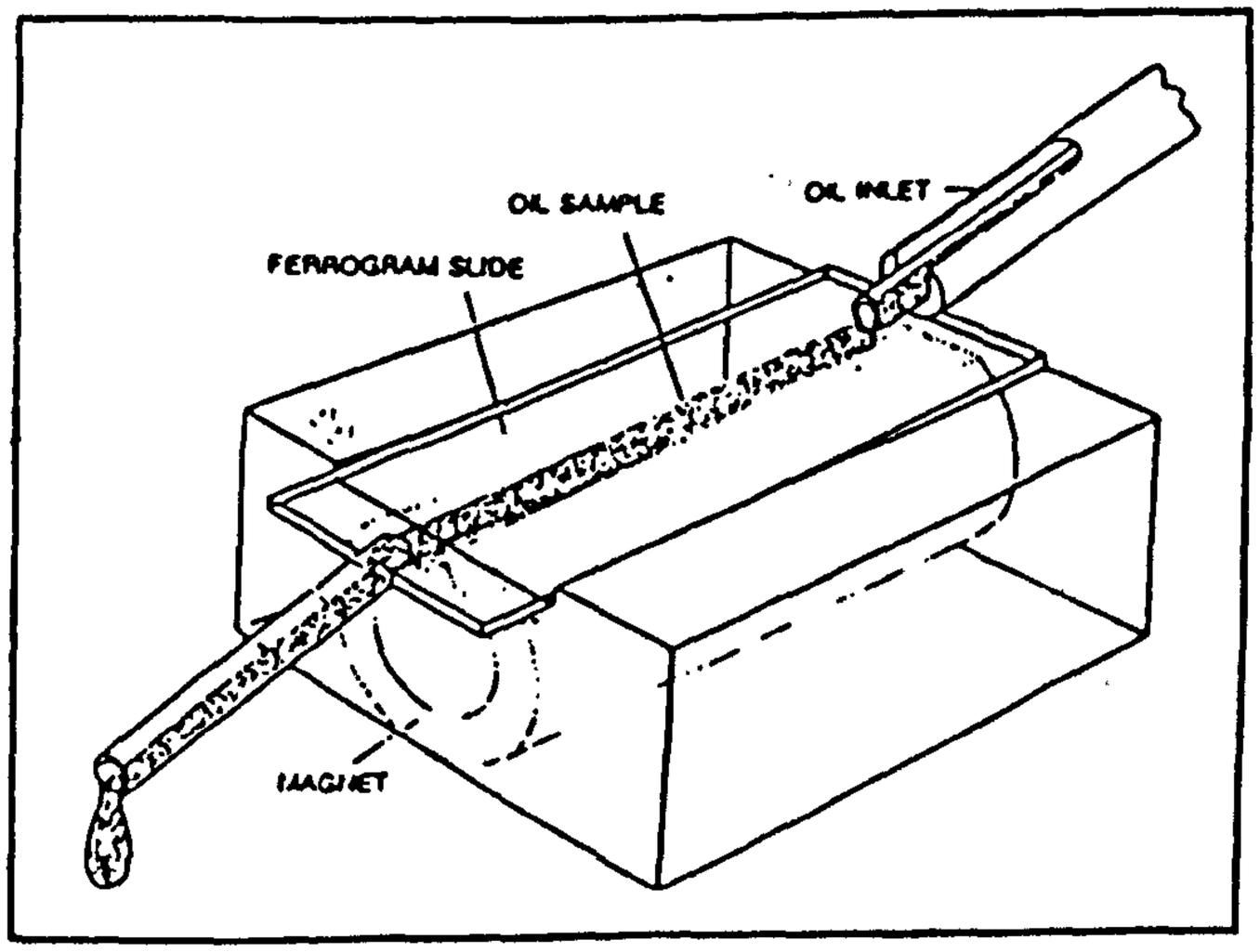

FIG. 19. ANALYTICAL FERROGRAPH.

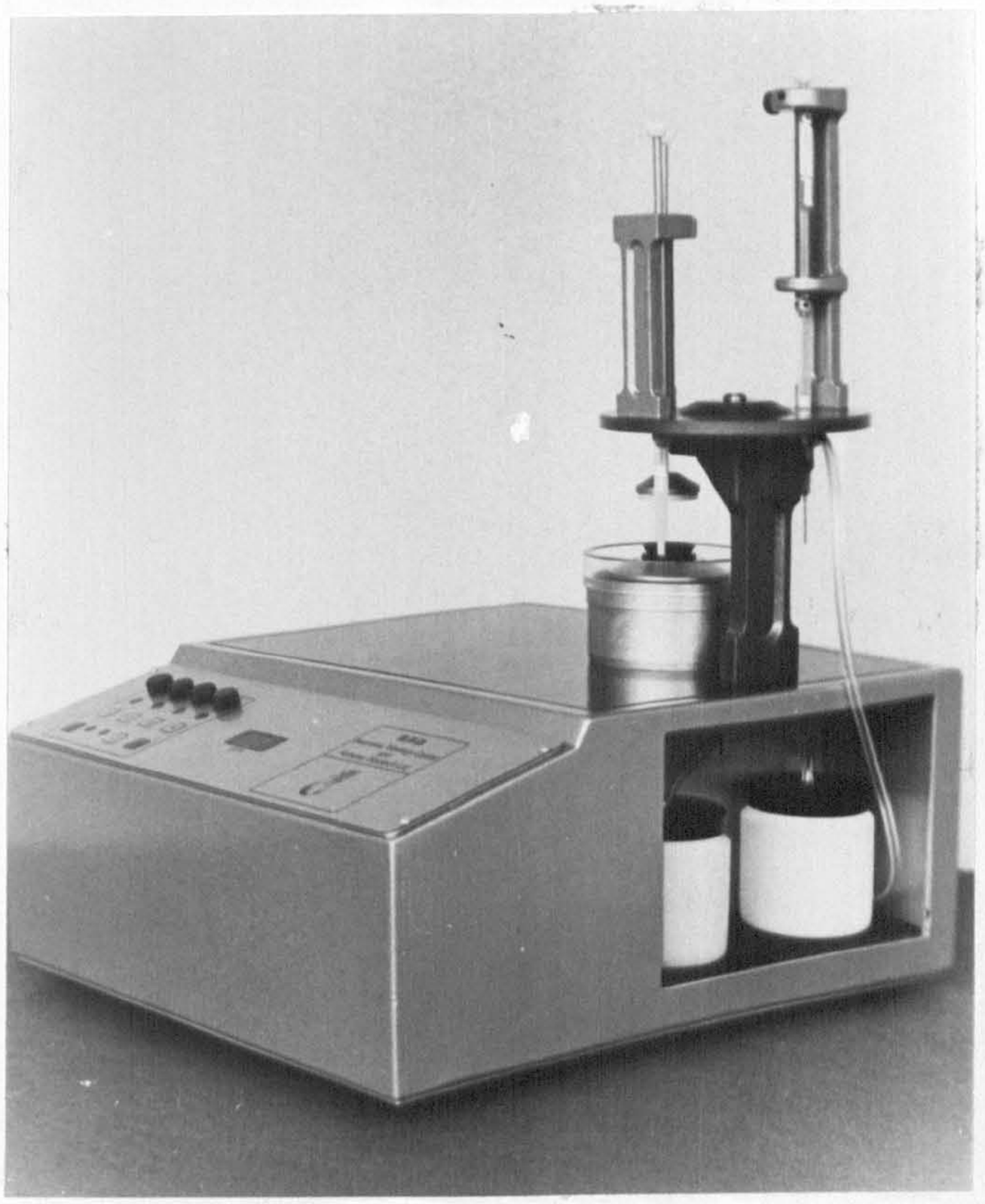

FIG. 20. ROTARY PARTICLE DEPOSITOR (R.P.D.)

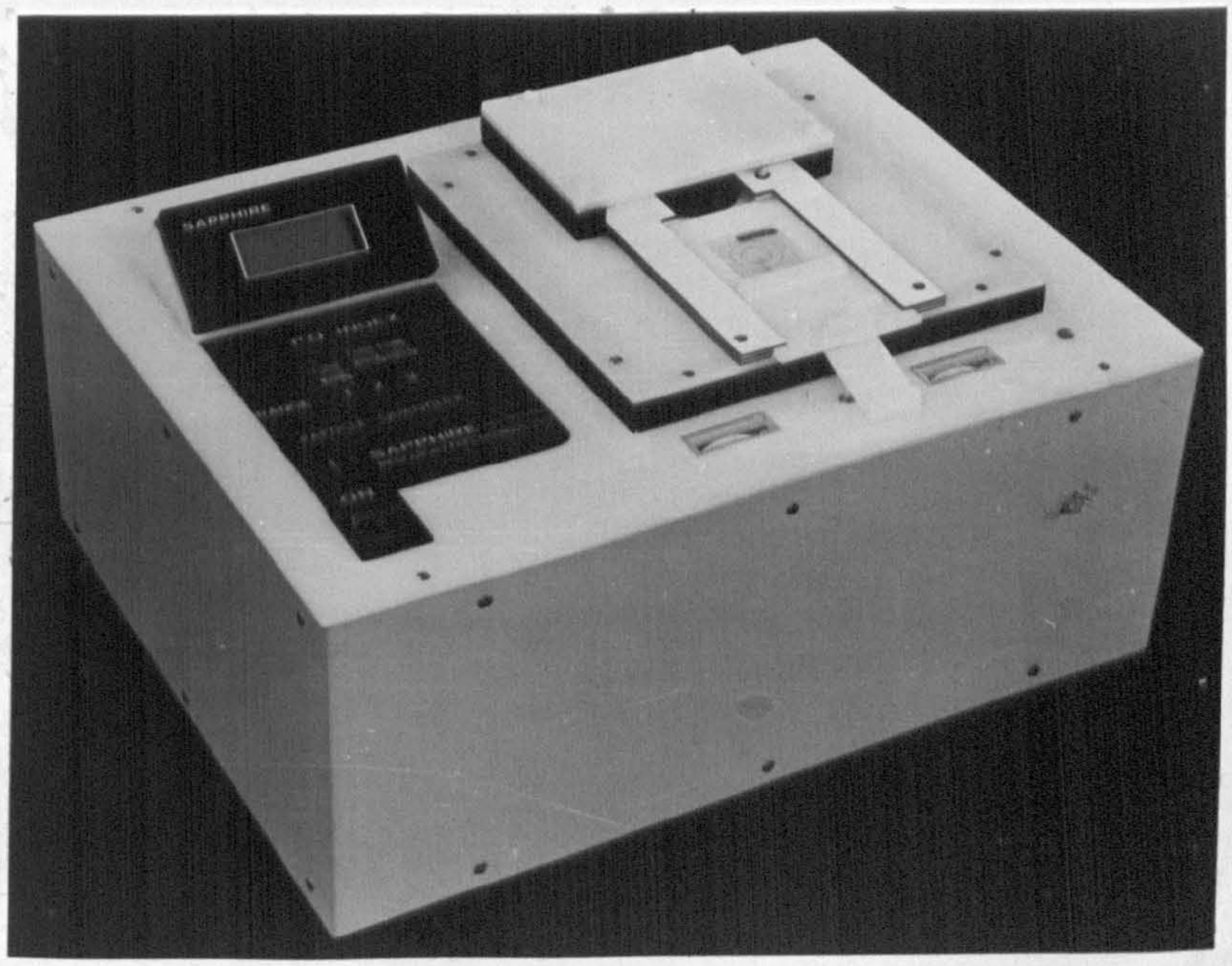

FIG. 21. PARTICLE QUANTIFIER (PQ)

REPLICATION TECHNIQUE.

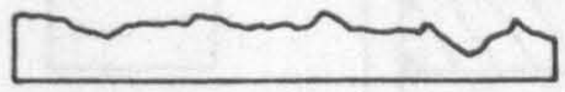

WEAR SURFACE.

CELLULOSE ACETATE.

FLOOD SURFACE WITH ACETONE.

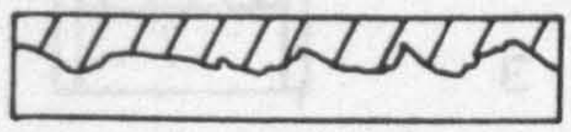

ACETONE SOFTENS & ADOPTS CONTOUR OF WEAR SURFACE.

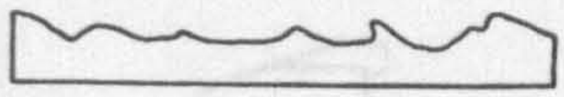

ALLOW TO DRY, PEEL OFF, & INVERT THROUGH 180°.

FIG. 22. REPLICATION TECHNIQUE

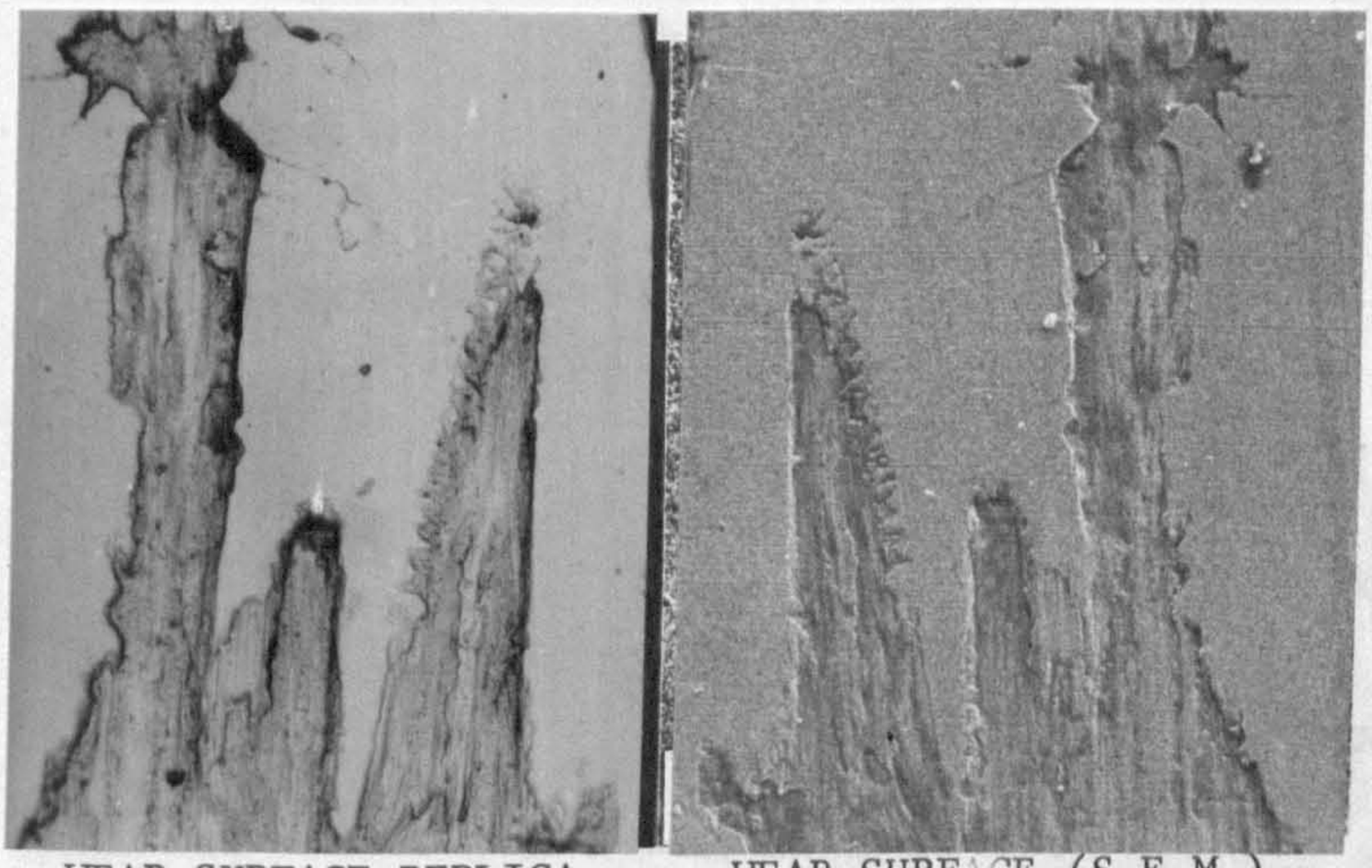

WEAR SURFACE REPLICA (OPTICAL)

WEAR SURFACE (S.E.M.)

FIG. 23. COMPARISON OF REPLICATED AND S.E.M. WEAR SURFACES.

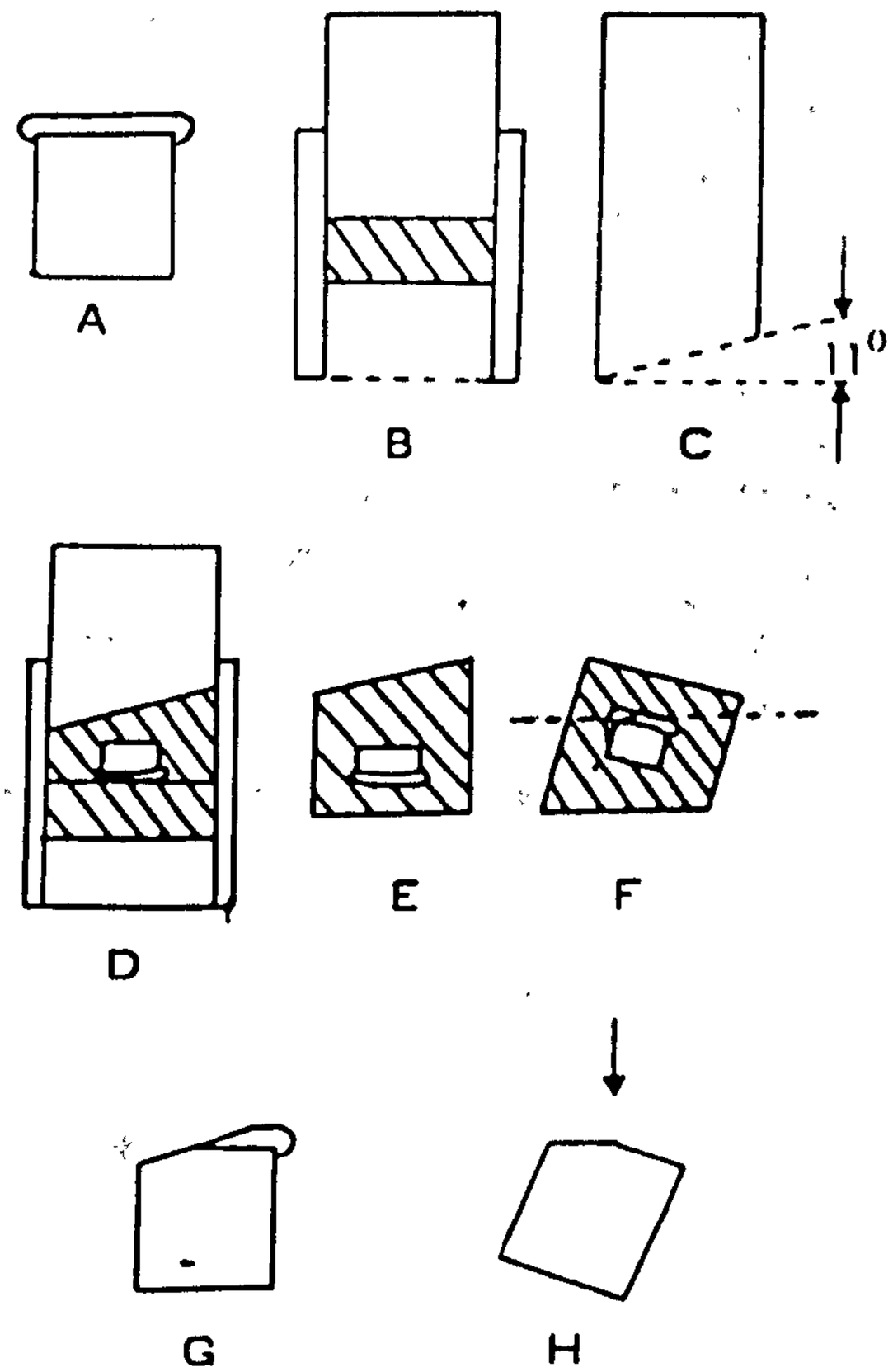

FIG 24. PREPARATION OF A TAPER SECTION THROUGH A WEAR SURFACE FOR BOTH OPTICAL MICROSCOPY AND SEM EXAMINATION.

a. Epoxy resin applied to the wear surface.

b. Preparation of a block of uncured bakelite.

c. Eleven degree angle ram.

d. Final mounting of the wear specimen.

e. Mounted specimen removed from the pressure cylinder.

f. Specimen inverted through 180^{o}, top surface ground, polished and etched. At this stage optical metallographic examination is carried out.

g. Wear specimen removed from the bakelite and epoxy coating is then removed.

h. Wear surface topography and metallurgical substrate ready for simultaneous viewing in the SEM.

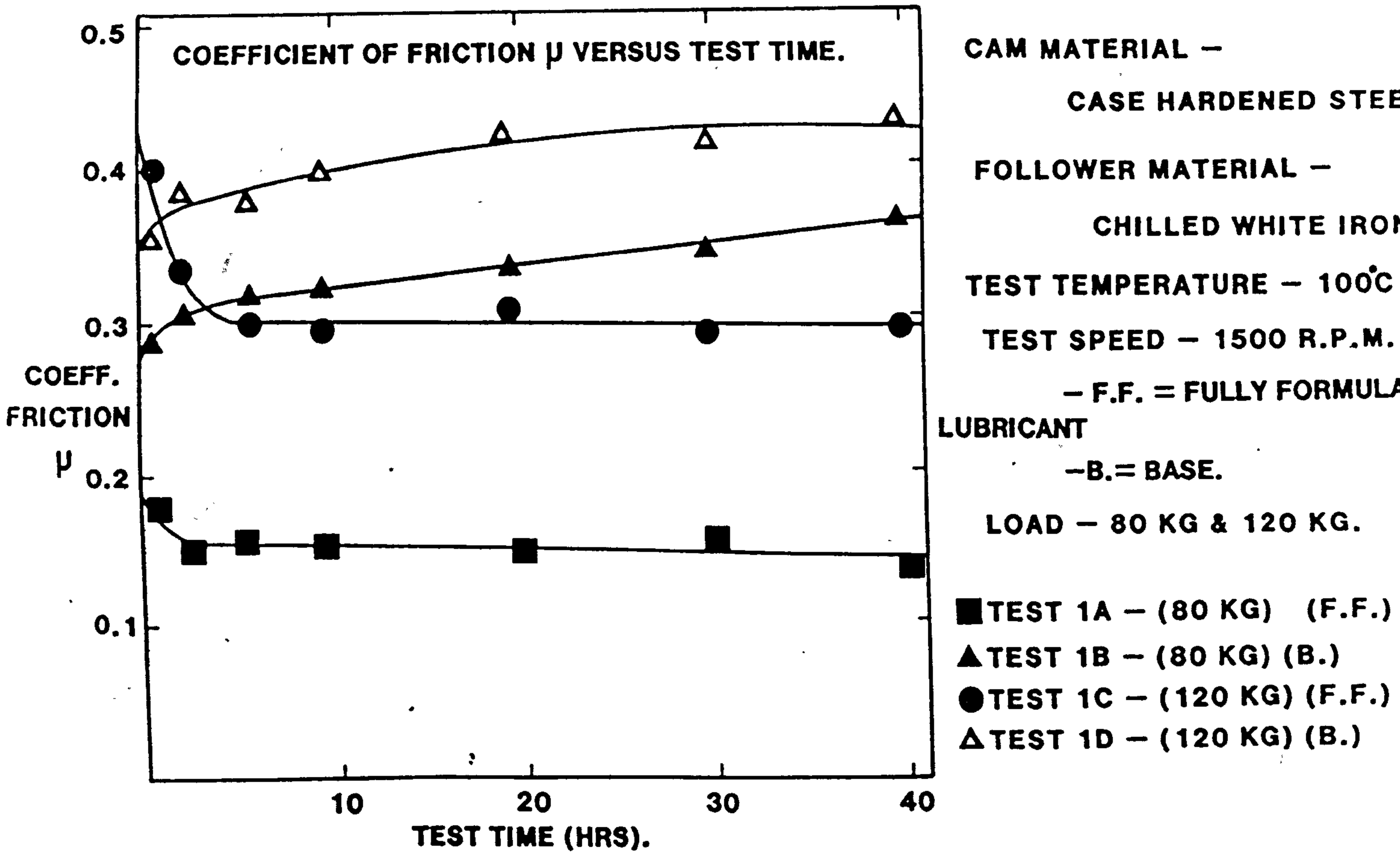

FIG. 25. GRAPH OF COEFFICIENT OF FRICTION VERSUS TEST TIME.

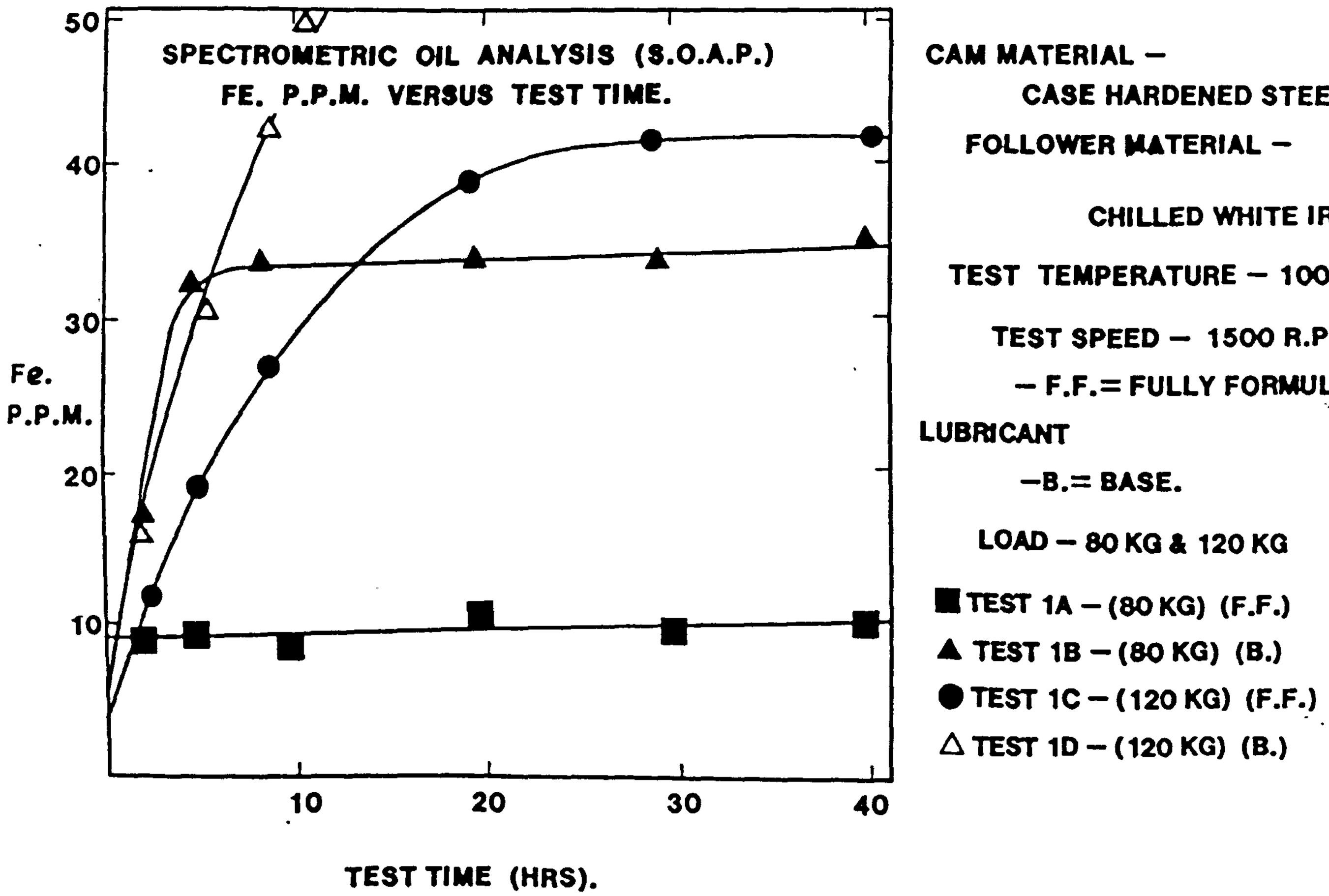

FIG. 26. QUANTITATIVE WEAR DEBRIS ANALYSIS, SPECTROMETRIC OIL ANALYSIS. GRAPH OF WEAR DEBRIS CONCENTRATION VERSUS TEST TIME.

FIG. 27a. CAM SURFACE, 'AS GROUND' OPTICAL.

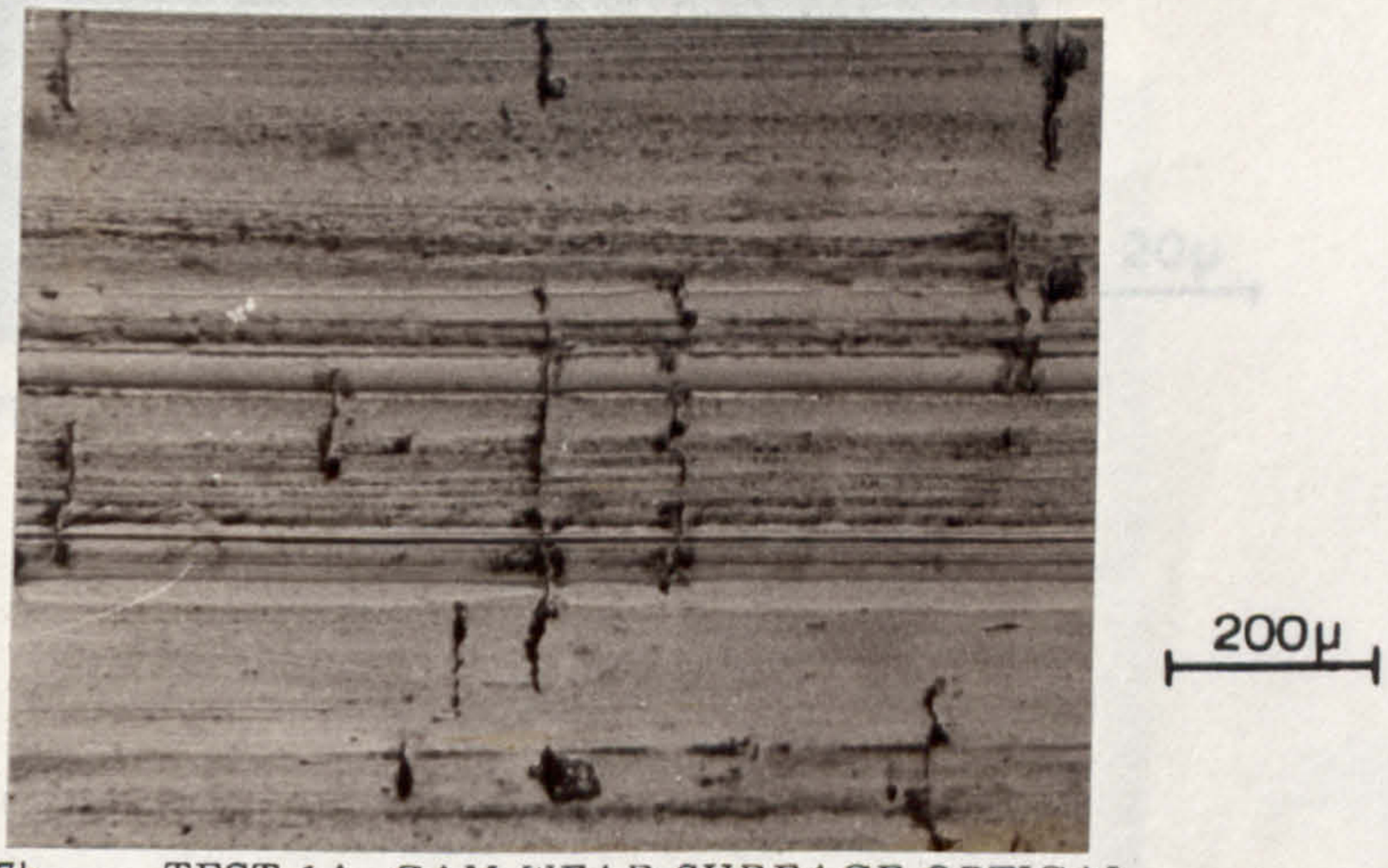

FIG. 27b. TEST 1A, CAM WEAR SURFACE OPTICAL.

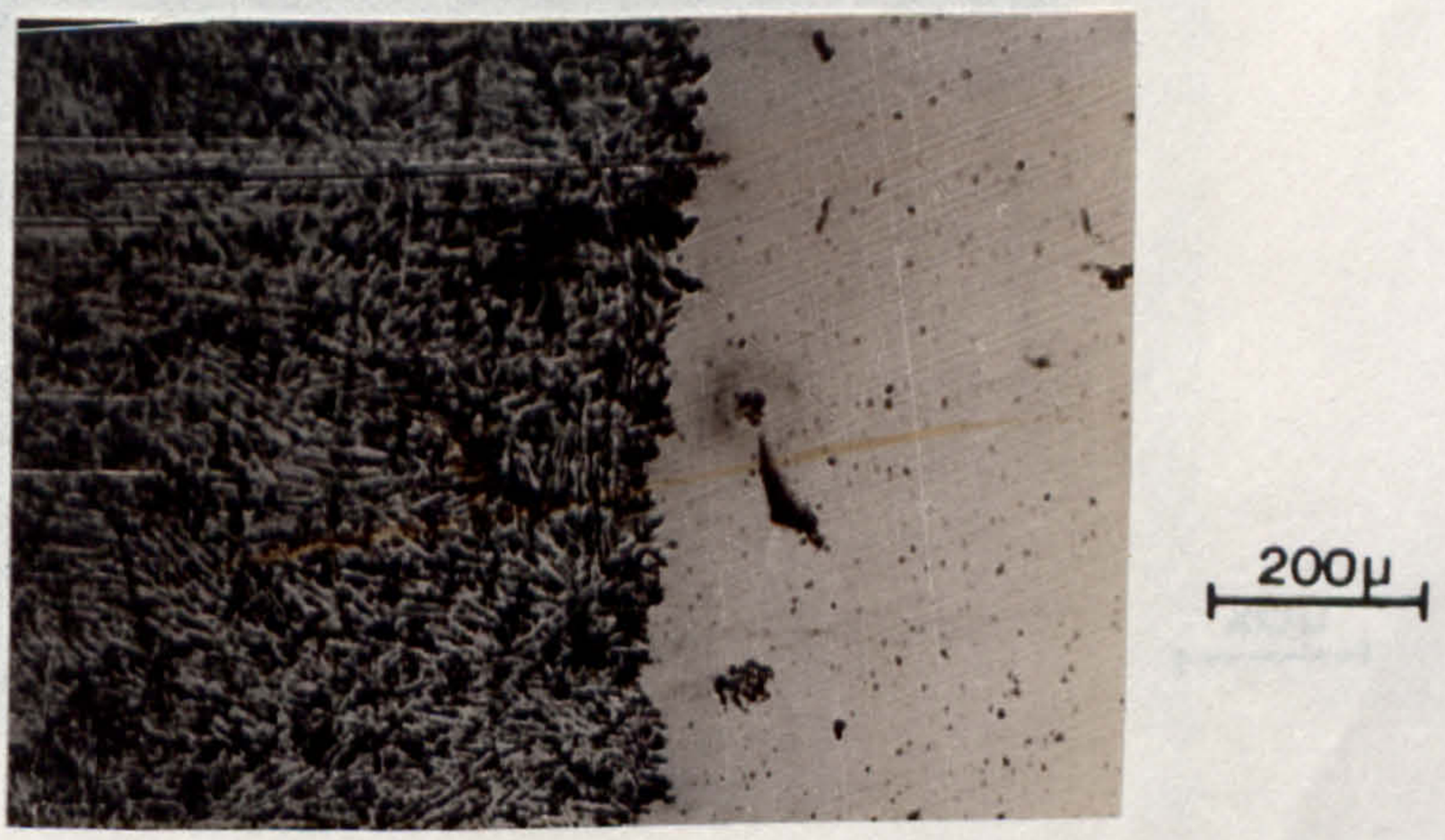

FIG. 28. TEST 1A, FOLLOWER WEAR SURFACE, WORN/ UNWORN INTERFACE, OPTICAL.

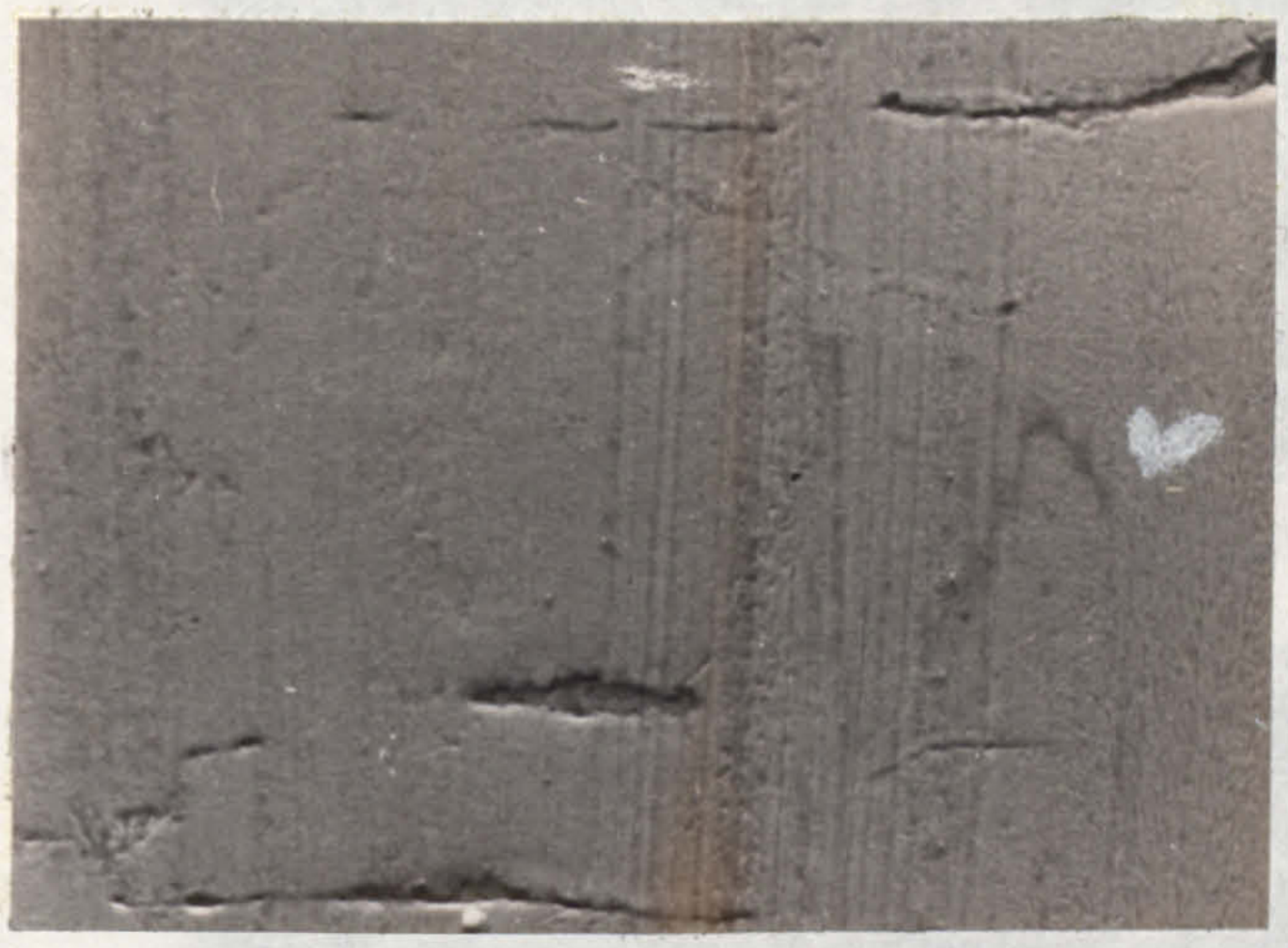

FIG. 29. TEST 1A, CAM WEAR SURFACE,

ELECTRON MICROGRAPH

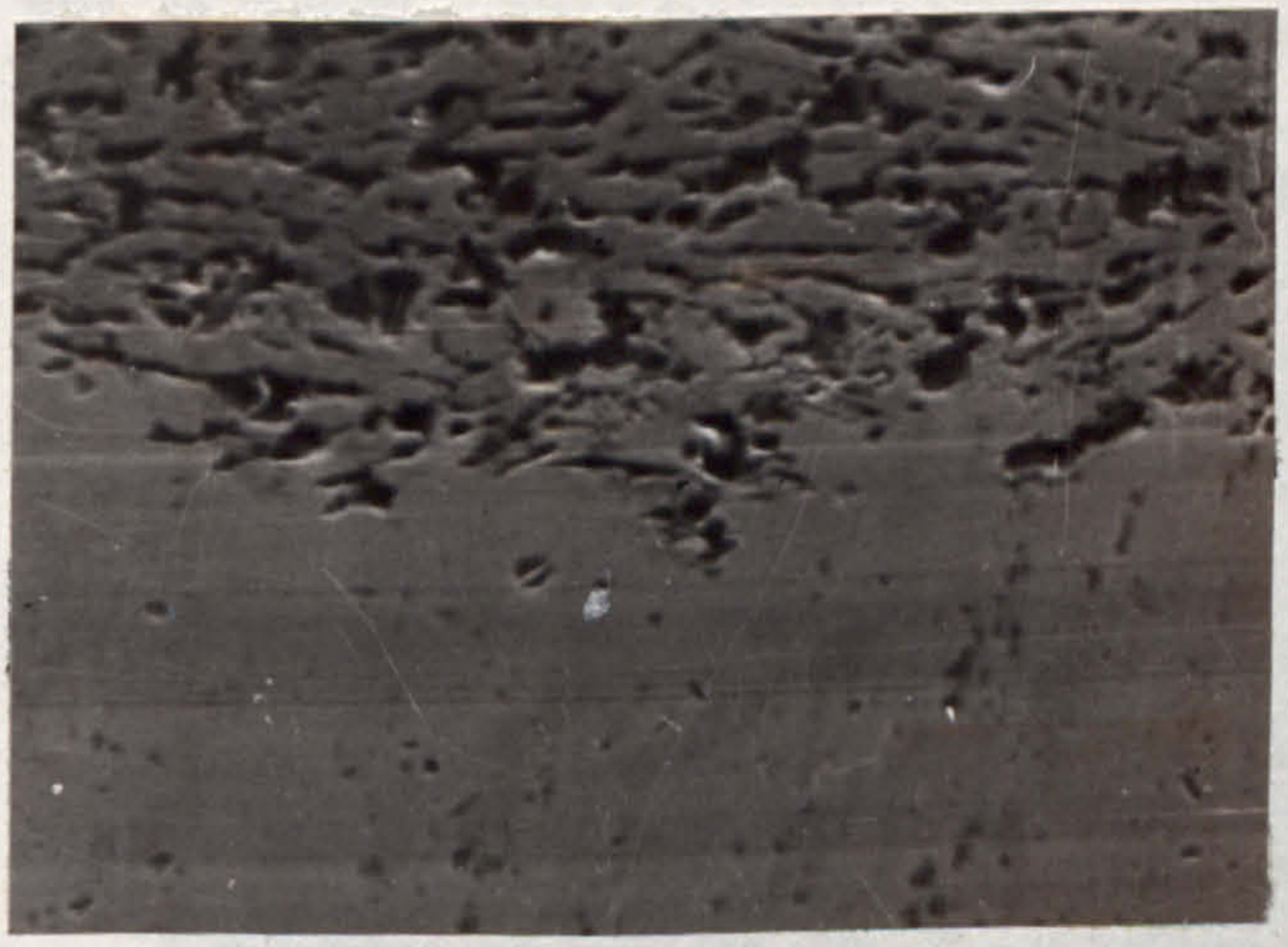

FIG. 30. TEST 1A, FOLLOWER WEAR SURFACE,

WORN/UNWORN INTERFACE, ELECTRON MICROGRAPH.

FIG. 31, TEST 1A, CAM SPECIMEN TAPER SECTION.

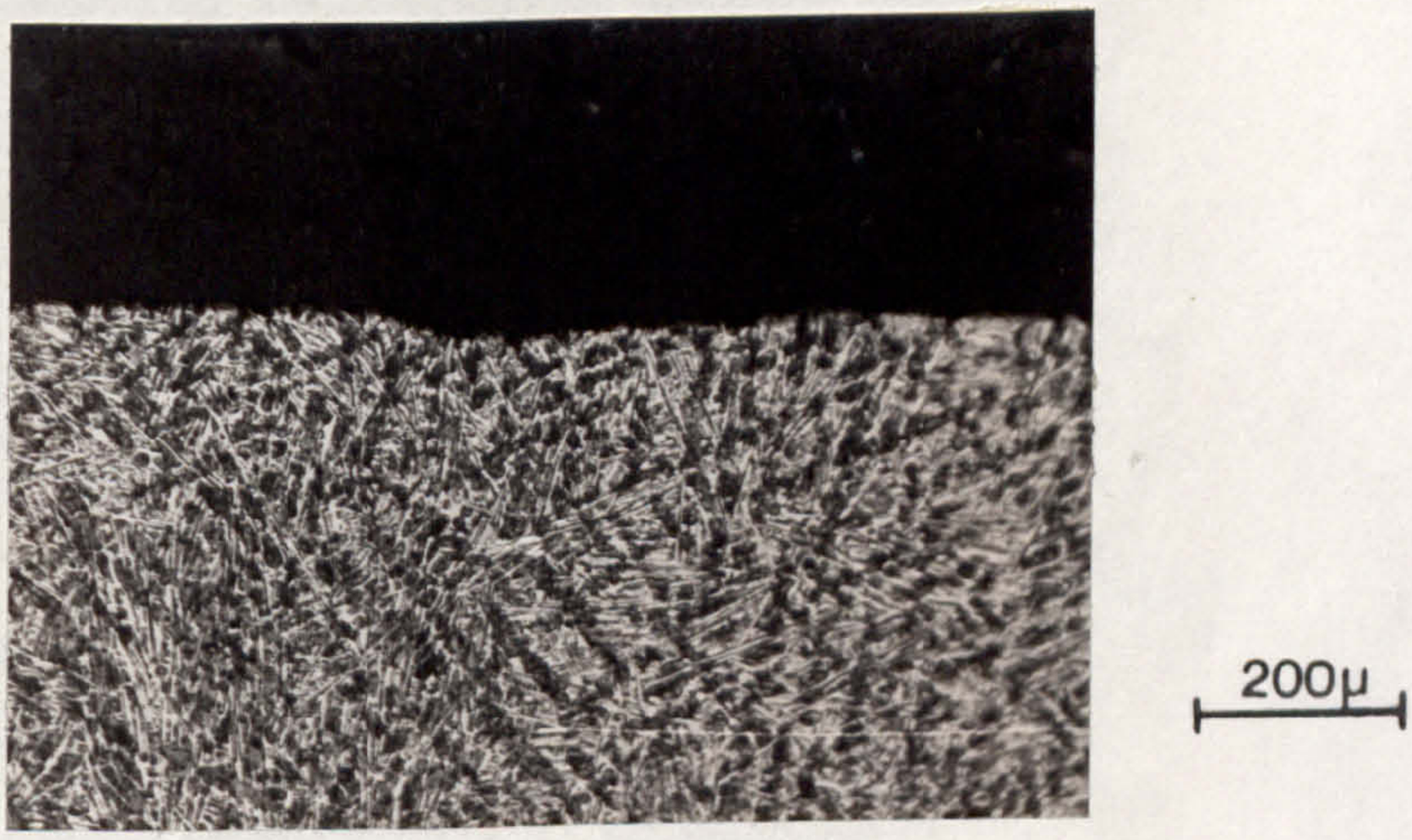

FIG. 32, TEST 1A, FOLLOWER SPECIMEN TAPERSECTION.

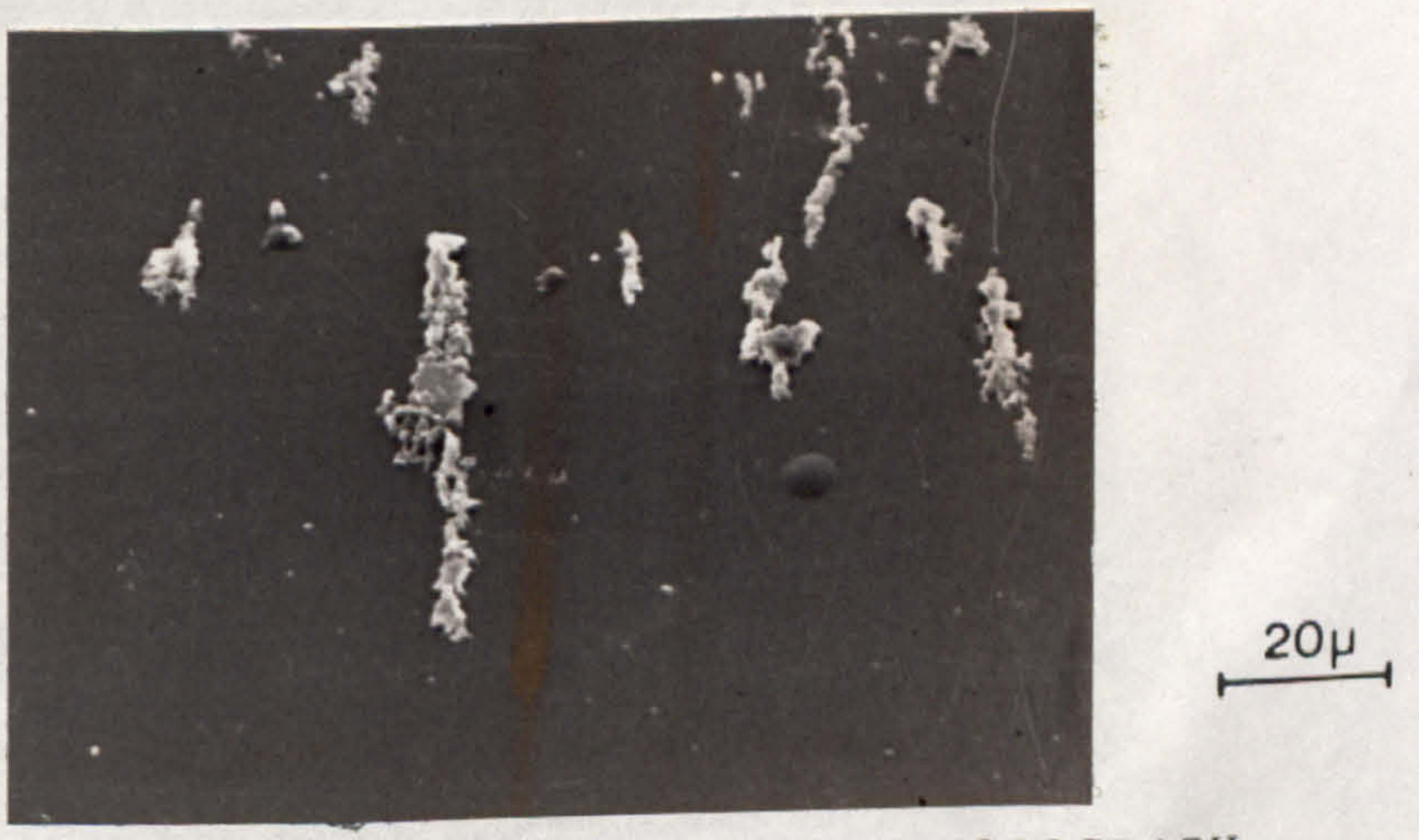

FIG. 33, TEST 1A, WEAR DEBRIS, ELECTRON MICROGRAPH.

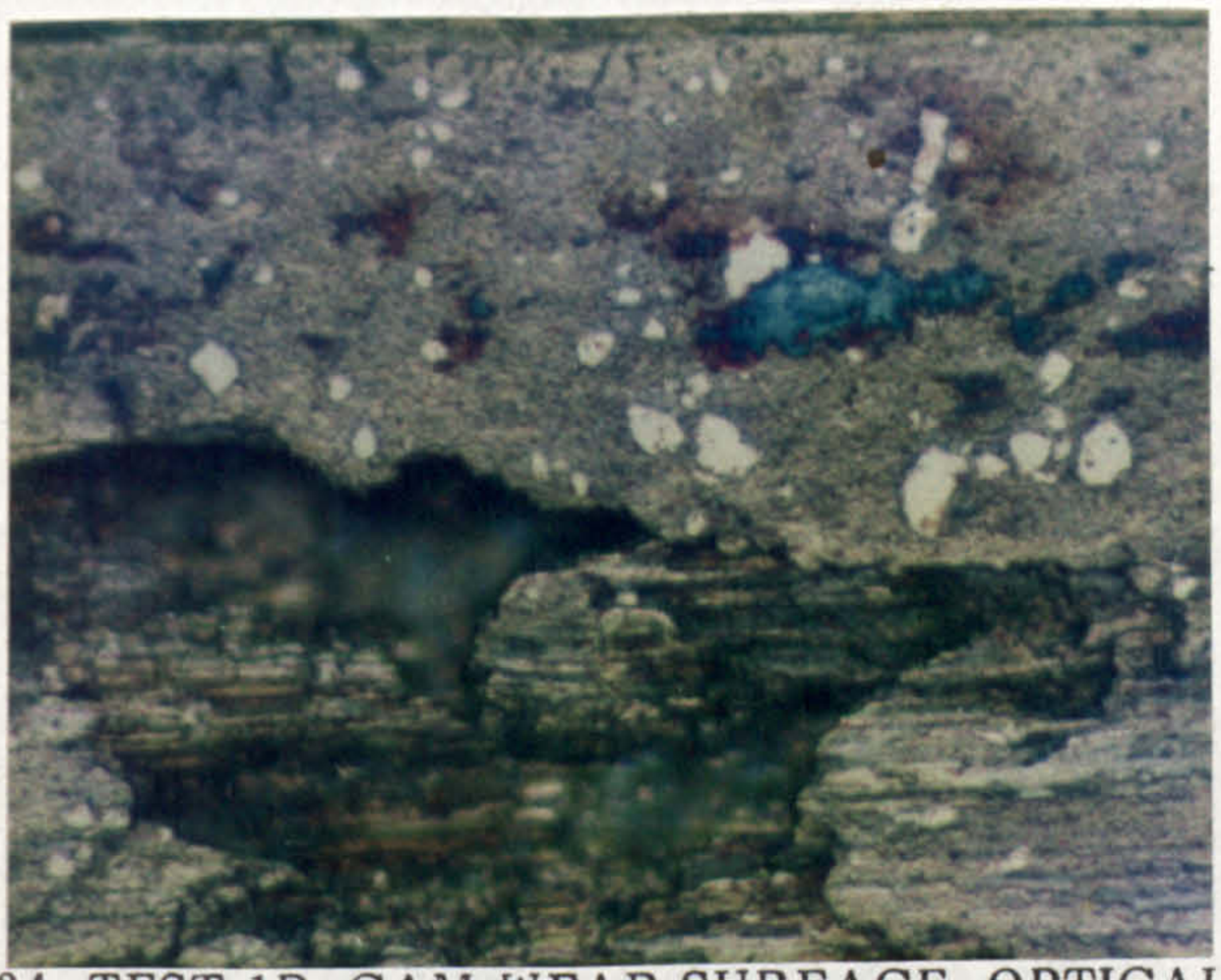

FIG. 34, TEST 1B, CAM WEAR SURFACE. OPTICAL.

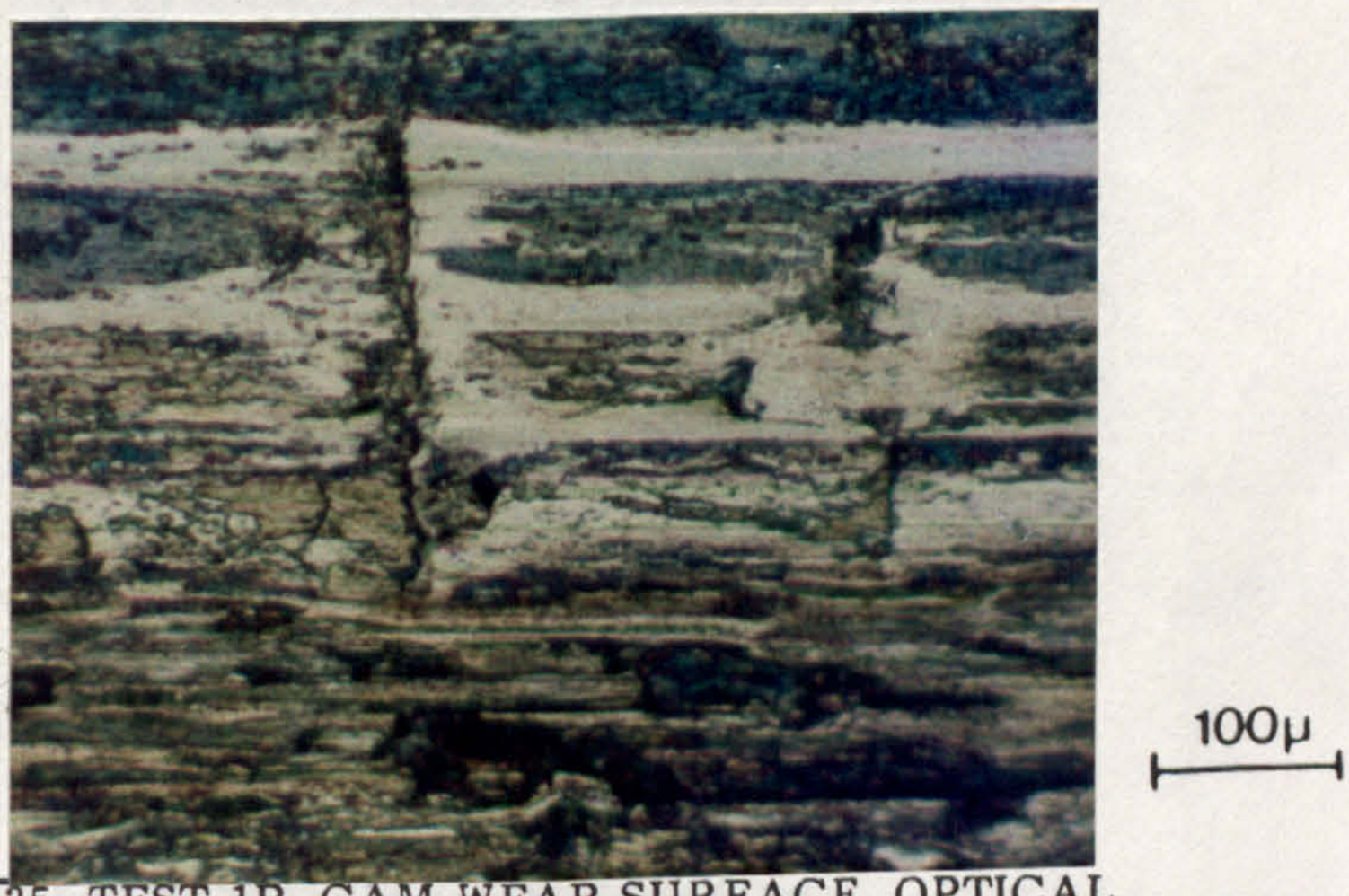

FIG. 35, TEST 1B, CAM WEAR SURFACE, OPTICAL.

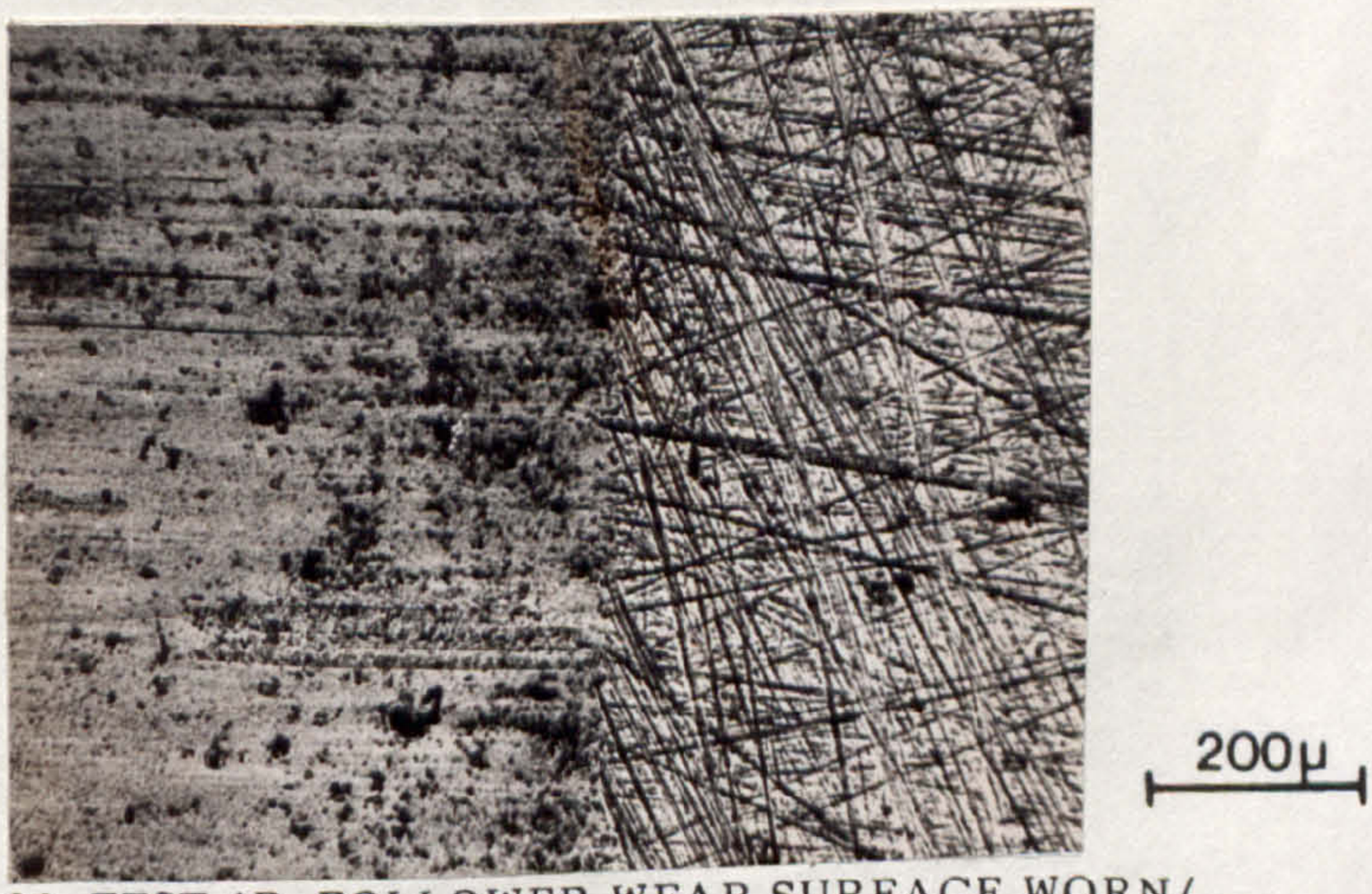

FIG. 36, TEST 1B, FOLLOWER WEAR SURFACE WORN/ UNWORN INTERFACE, OPTICAL.

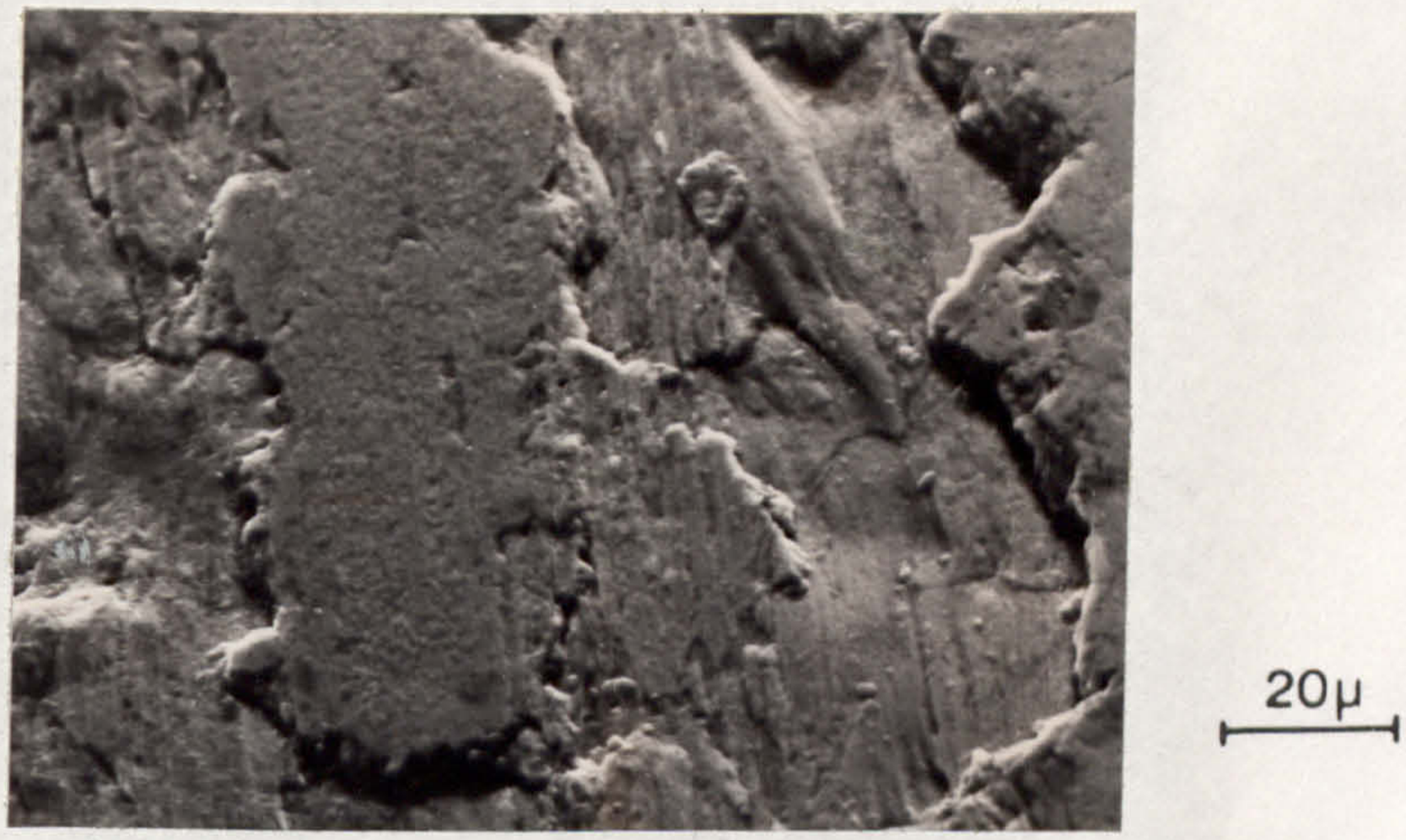

FIG. 37. TEST 1B, CAM WEAR SURFACE, ELECTRON MICROGRAPH.

FIG. 38. TEST 1B, FOLLOWER WEAR SURFACE, ELECTRON MICROGRAPH.

FIG. 39. TEST 1B, CAM SPECIMEN TAPERSECTION.

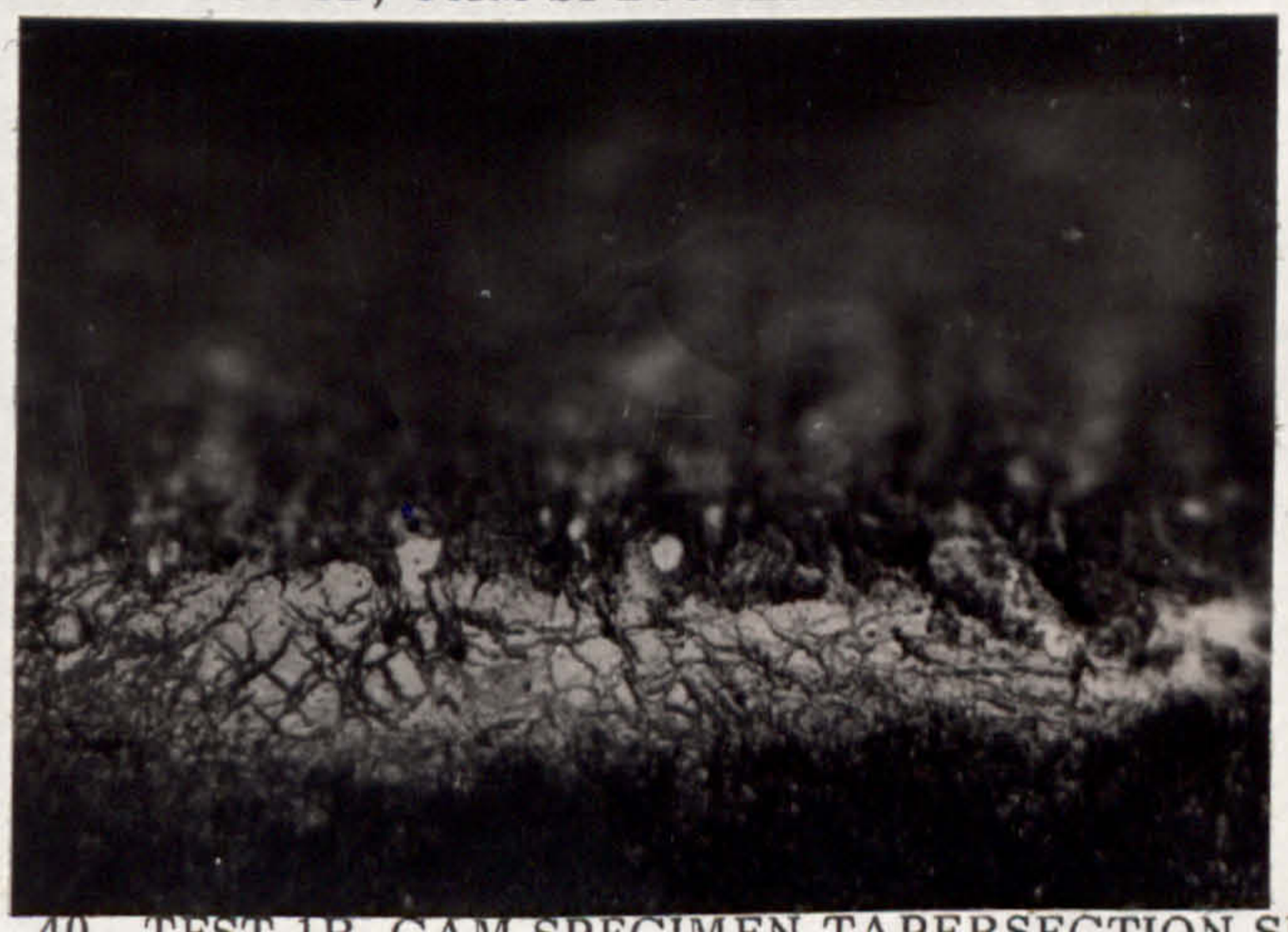

FIG. 40. TEST 1B, CAM SPECIMEN TAPERSECTION SHOWING CARBIDE TRANSFER AND EMBEDDMENT.

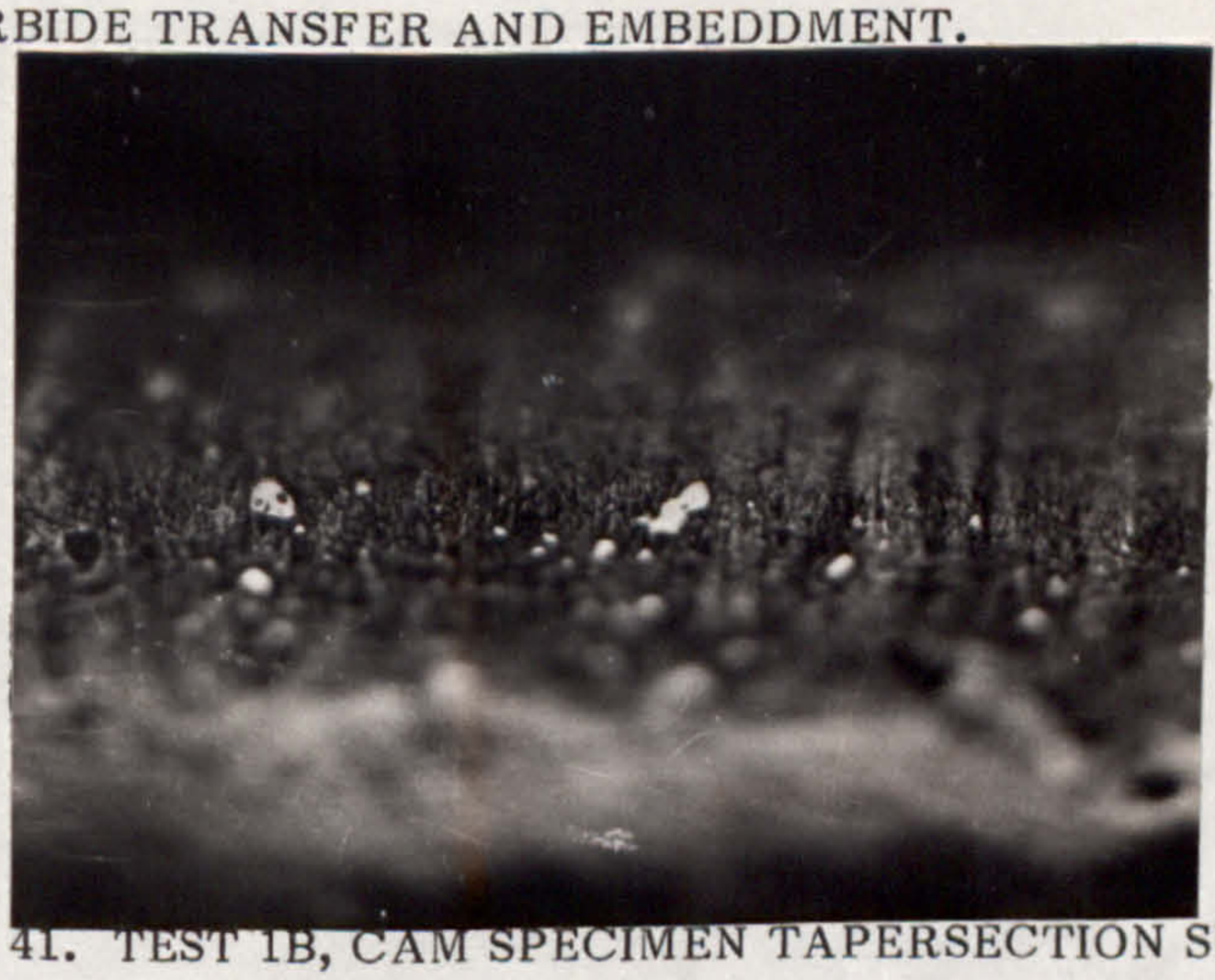

FIG. 41. TEST 1B, CAM SPECIMEN TAPERSECTION SHOWING CARBIDE TRANSFER AND EMBEDDMENT ON WEAR SURFACE.

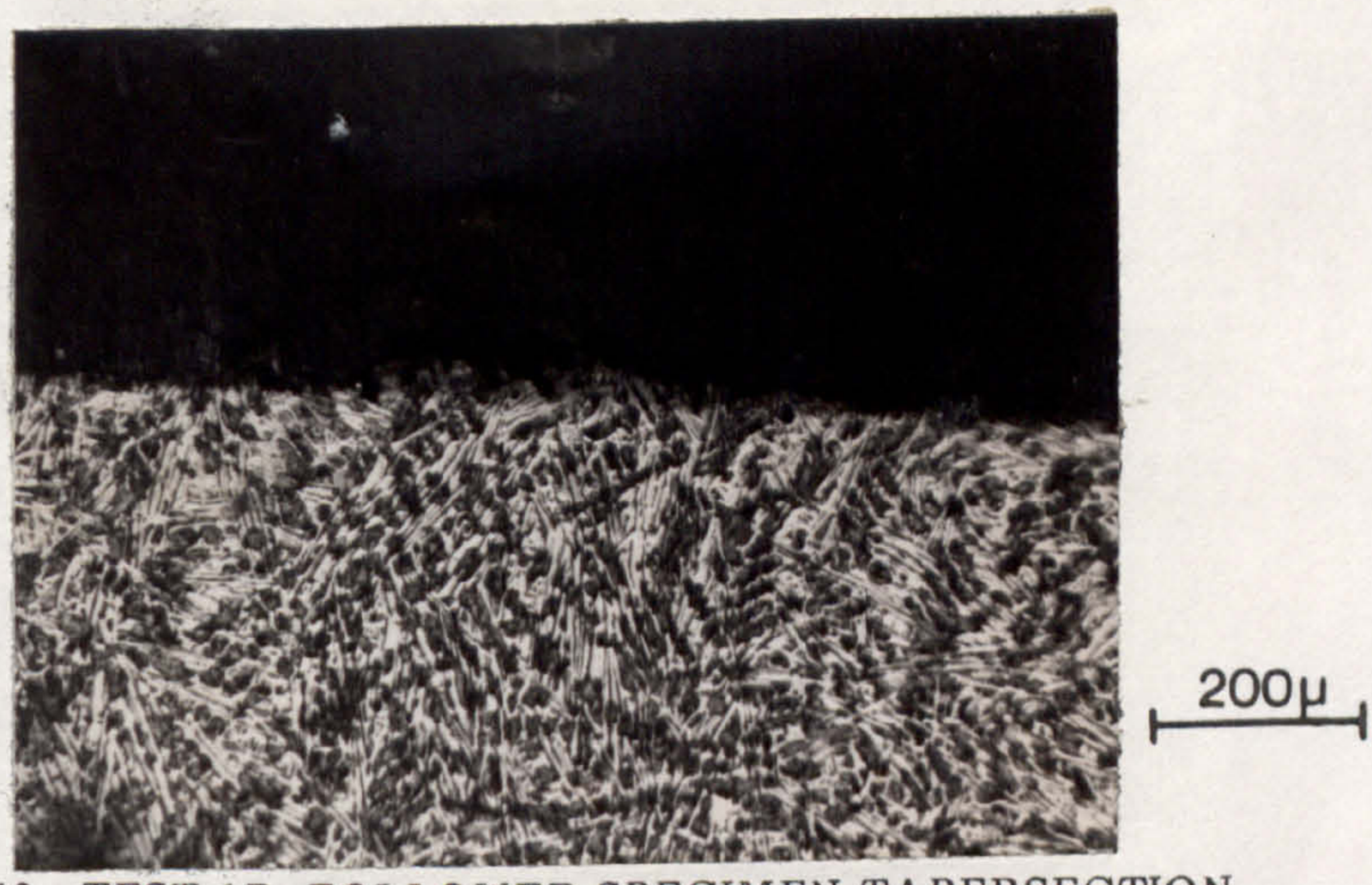

FIG. 42. TEST 1B, FOLLOWER SPECIMEN TAPERSECTION.

FIG. 43, TEST 1B, WEAR DEBRIS, ELECTRON MICROGRAPH.

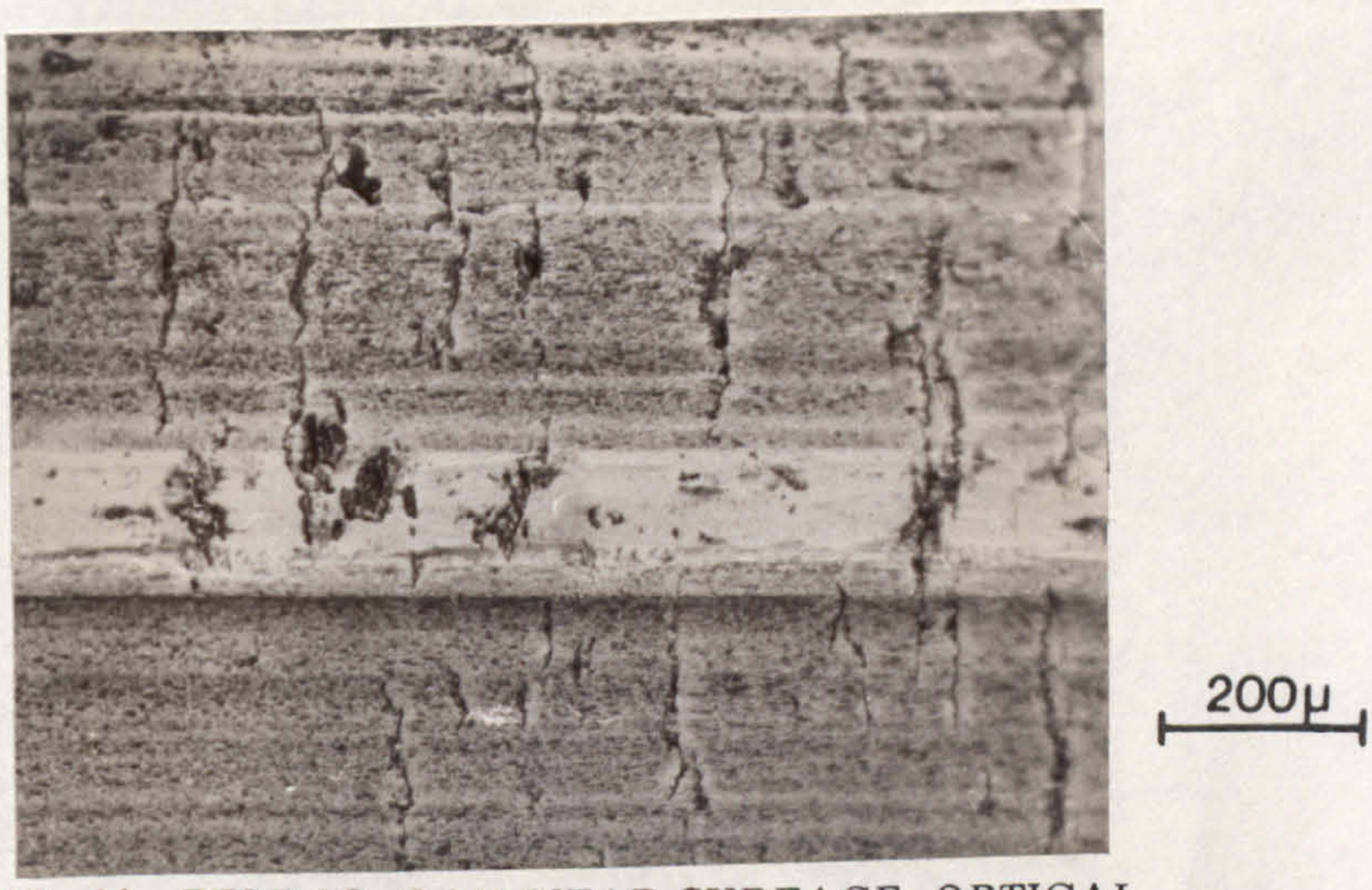

FIG. 44. TEST 1C, CAM WEAR SURFACE, OPTICAL.

FIG. 45, TEST 1C, FOLLOWER WEAR SURFACE, OPTICAL.

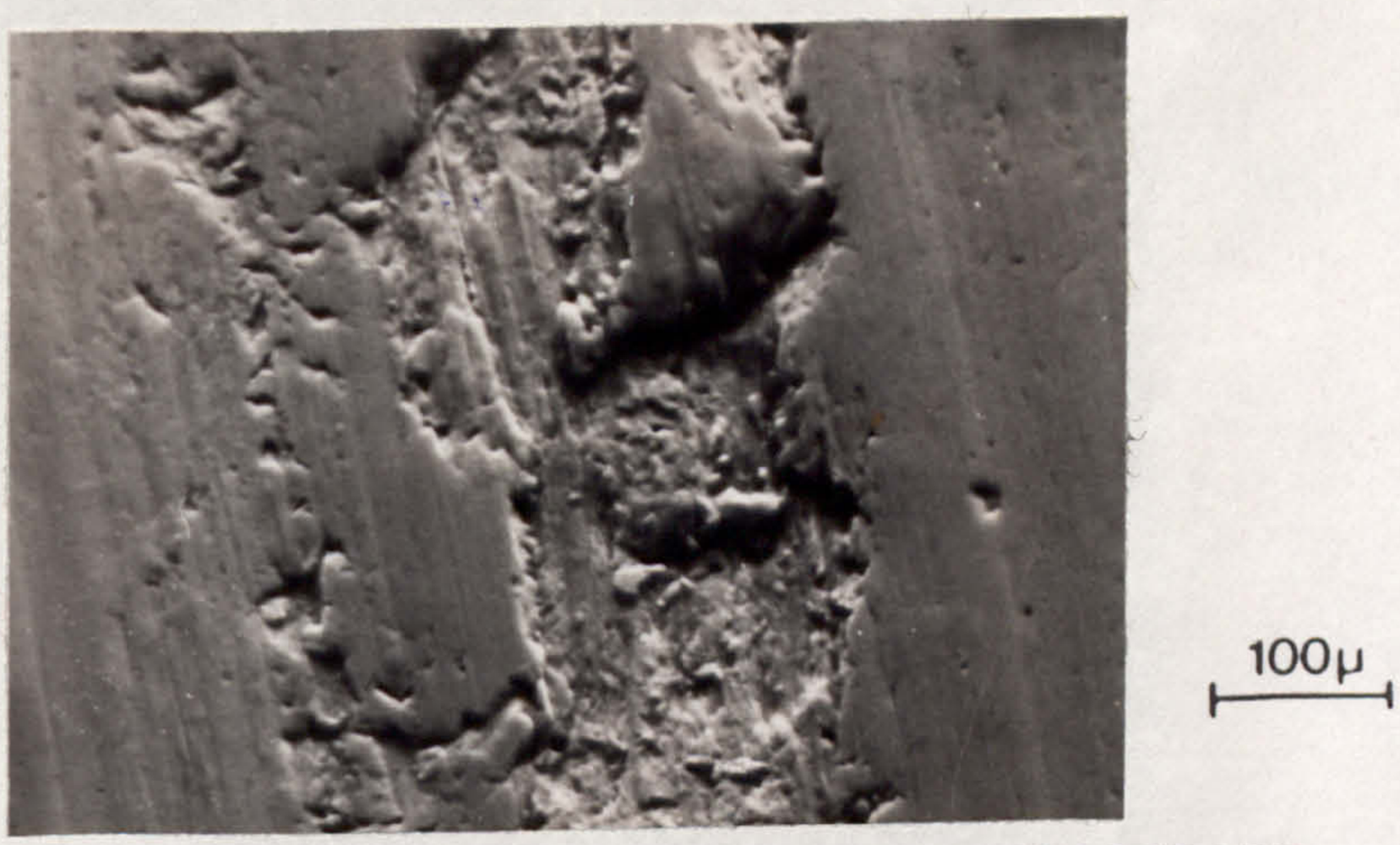

FIG. 46. TEST 1C, CAM WEAR SURFACE, ELECTRON MICROGRAPH.

FIG. 47, TEST 1C, FOLLOWER WEAR SURFACE ELECTRON MICROGRAPH.

FIG. 48. TEST 1C, CAM SPECIMEN TAPERSECTION.

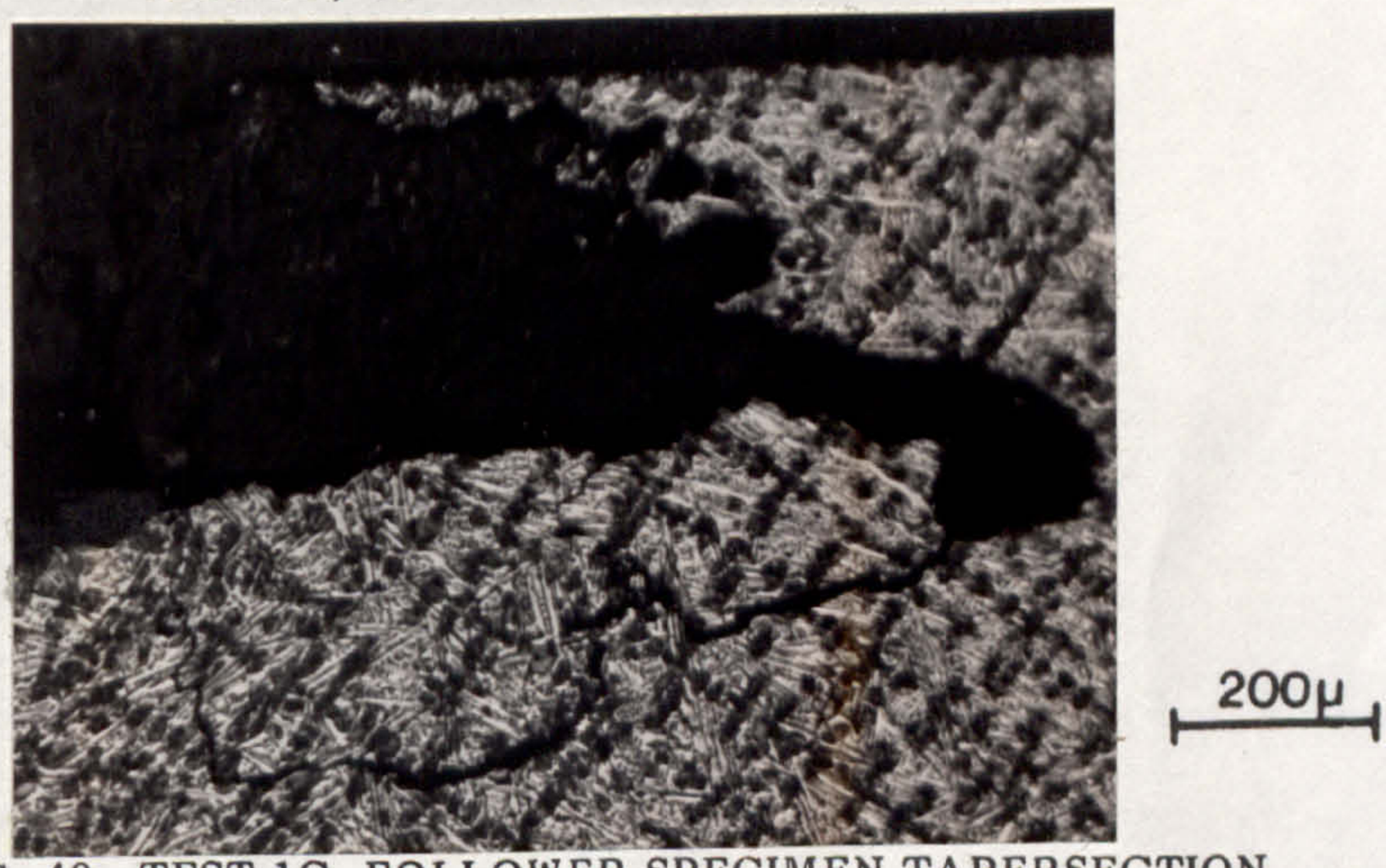

FIG. 49. TEST 1C, FOLLOWER SPECIMEN TAPERSECTION.

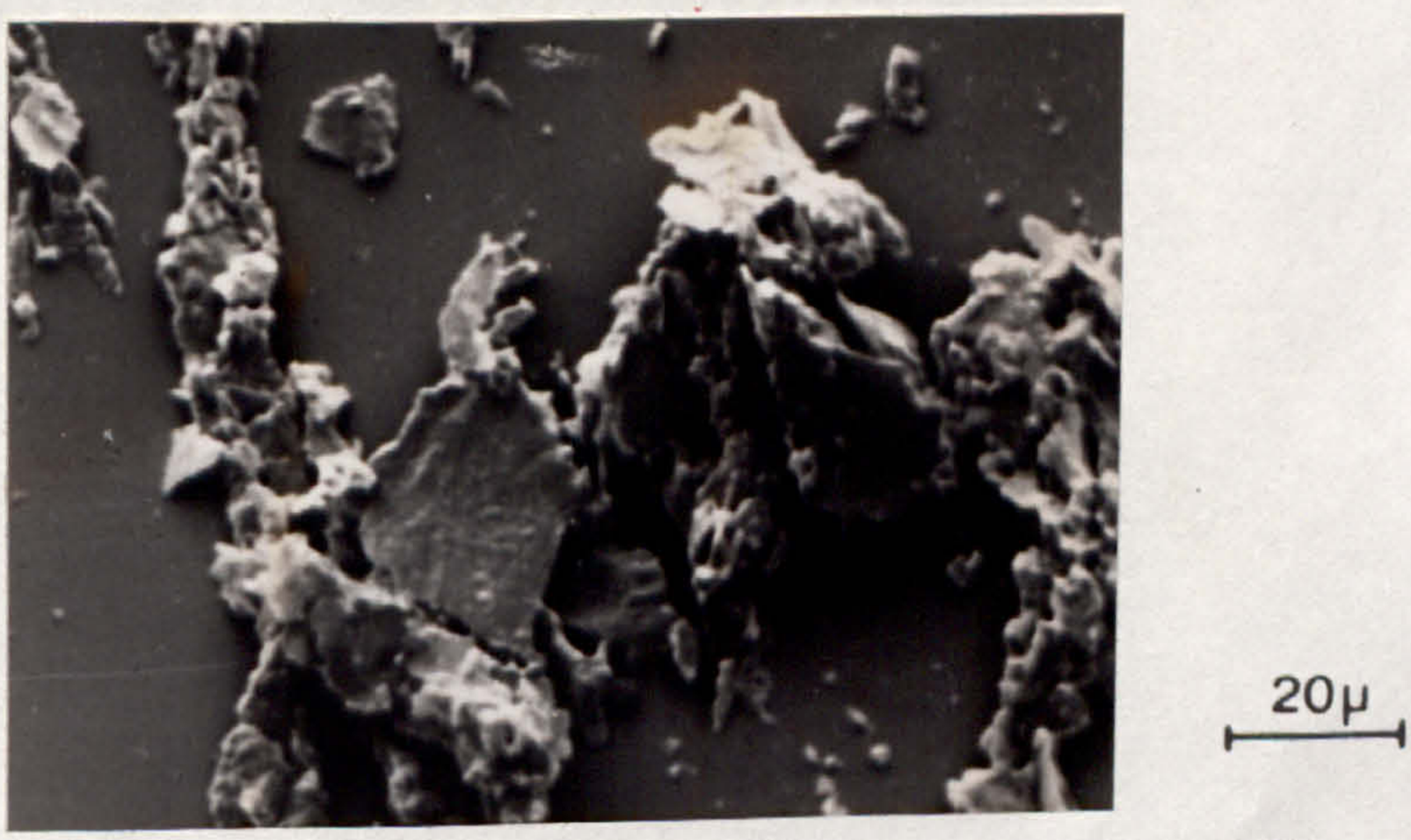

FIG. 50, TEST 1C, WEAR DEBRIS, ELECTRON MICROGRAPH.

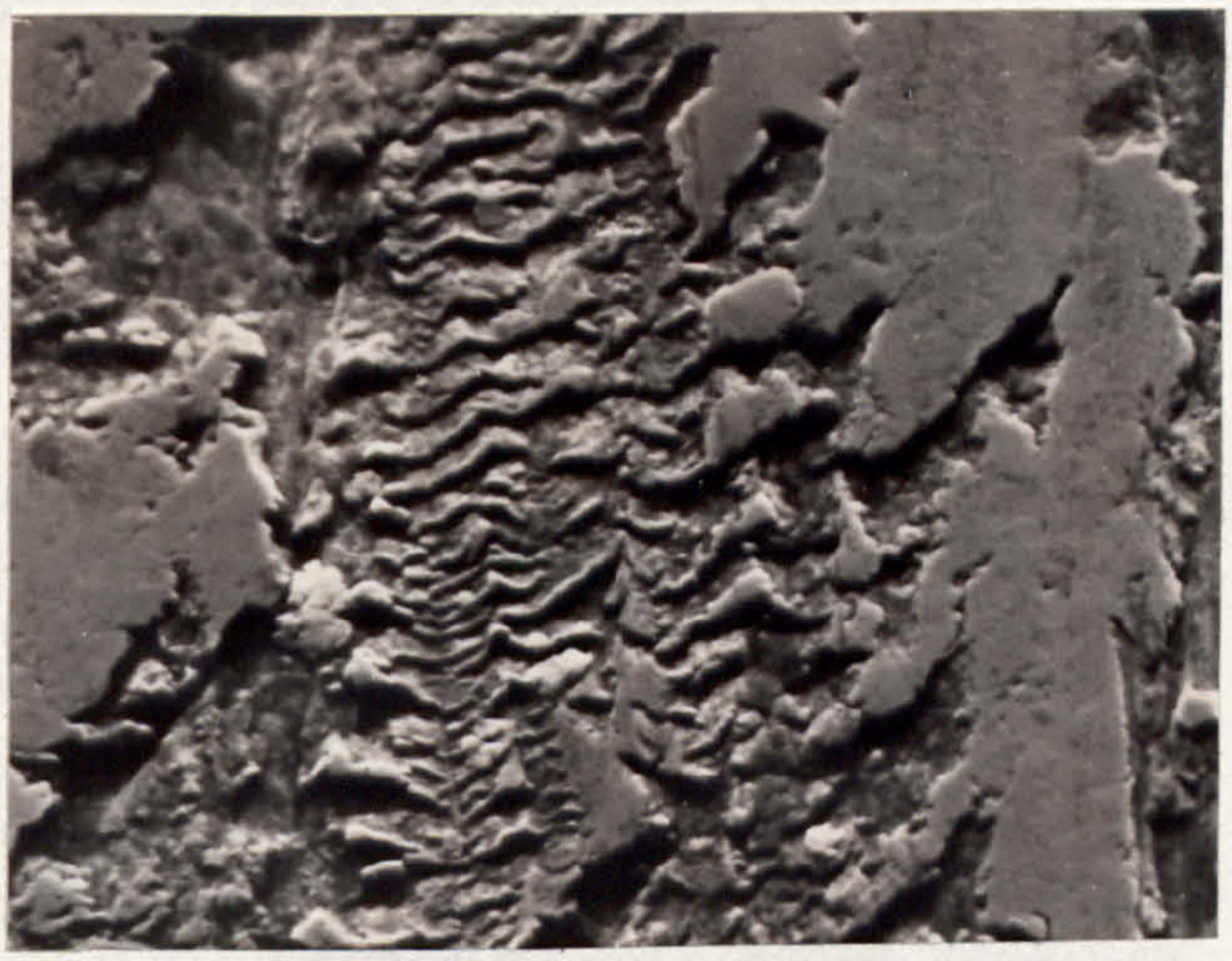

FIG. 51. TEST 1D, CAM WEAR SURFACE, ELECTRON MICROGRAPH.

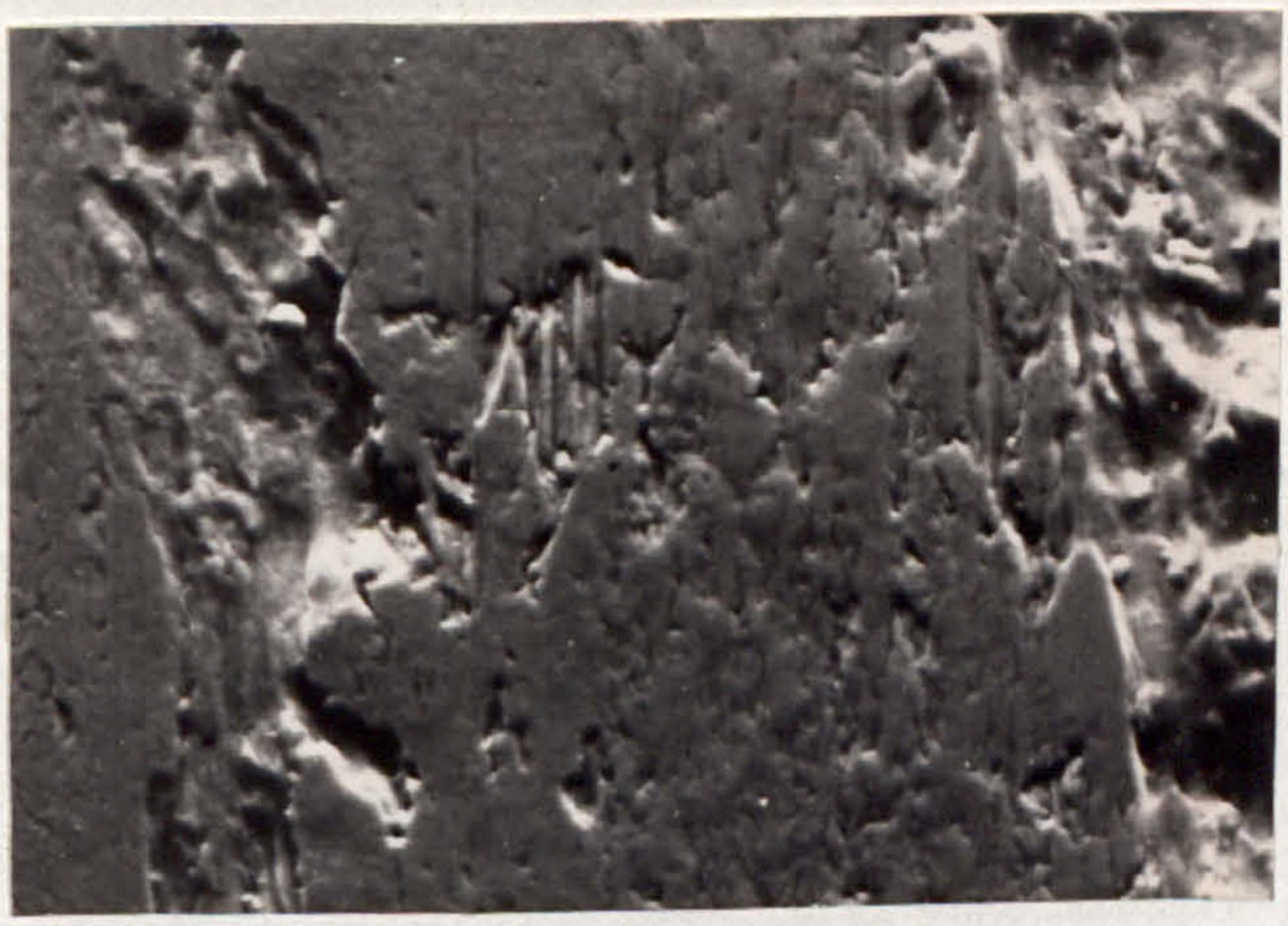

FIG. 52. TEST 1D, FOLLOWER WEAR SURFACE, ELECTRON MICROGRAPH.

FIG. 53. TEST 1D, CAM SPECIMEN TAPERSECTION.

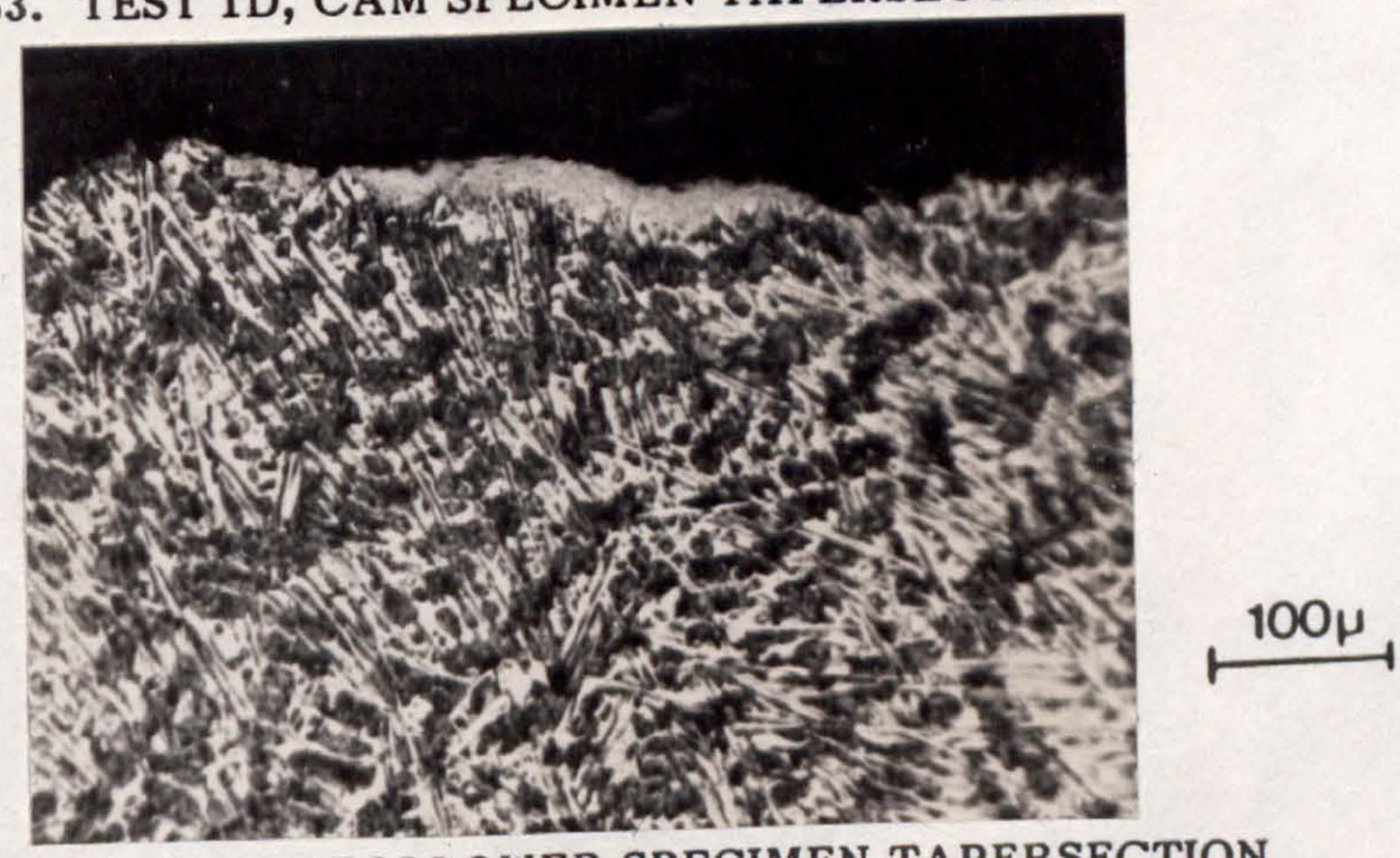

FIG. 54. TEST 1D, FOLLOWER SPECIMEN TAPERSECTION.

FIG. 55. TEST 1D, WEAR DEBRIS, ELECTRON MICROGRAPH.

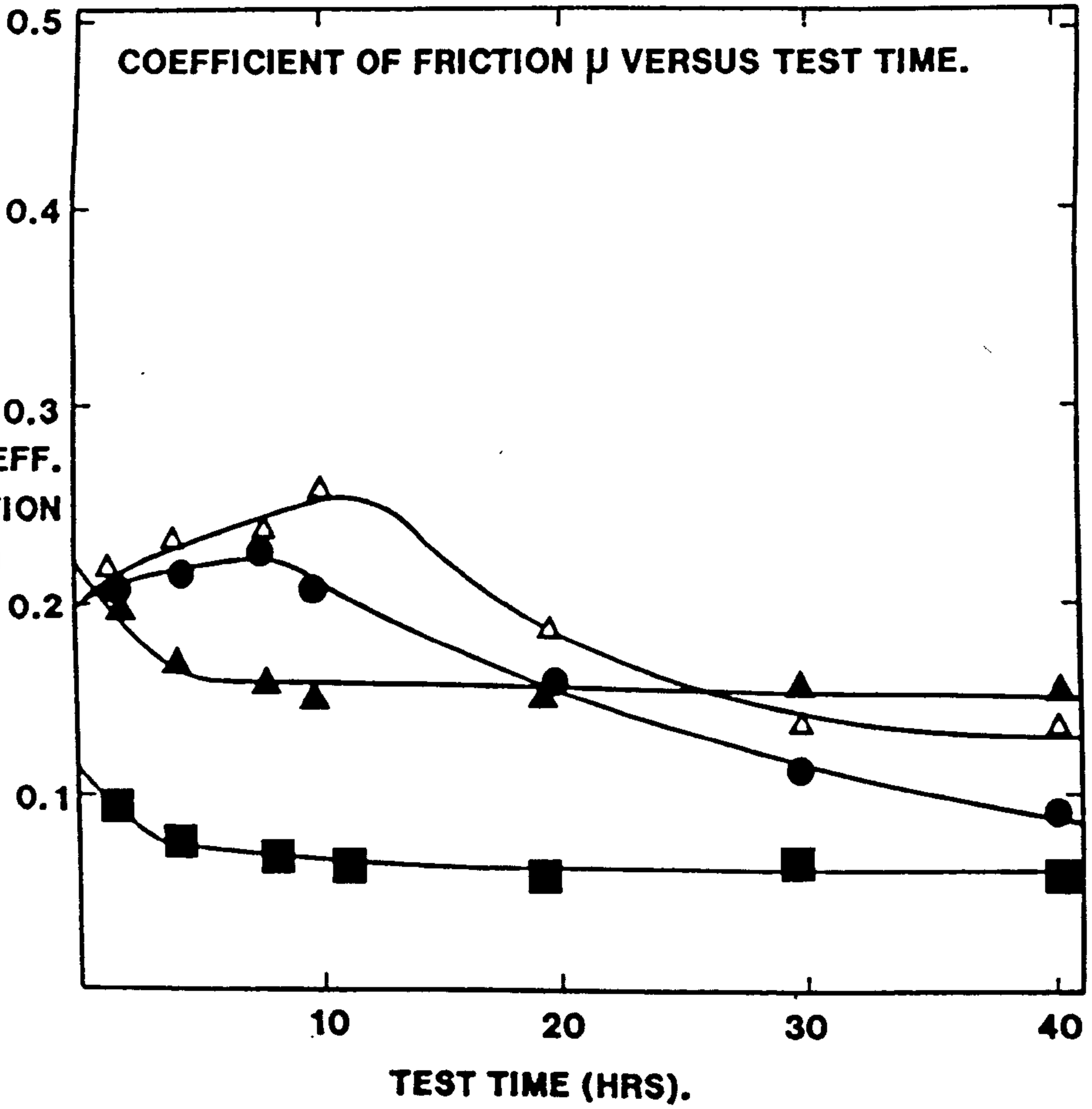

CAM MATERIAL –

GREY FLAKE IRON

INDUCTION HARDENED.

FOLLOWER MATERIAL –

CASE HARDENED STEEL.

TEST TEMPERATURE – 100°C

TEST SPEED – 1500 R.P.M.

– F.F. = FULLY FORMULATED LUBRICANT

–B. = BASE.

LOAD – 80 KG & 120 KG.

■ TEST 1E – (80 KG) (F.F.)

▲ TEST 1F – (80 KG) (B.)

● TEST 1G – (120 KG) (F.F.)

△ TEST 1H – (120 KG) (B.)

FIG 56. GRAPH OF COEFFICIENT OF FRICTION VERSUS TEST TIME.

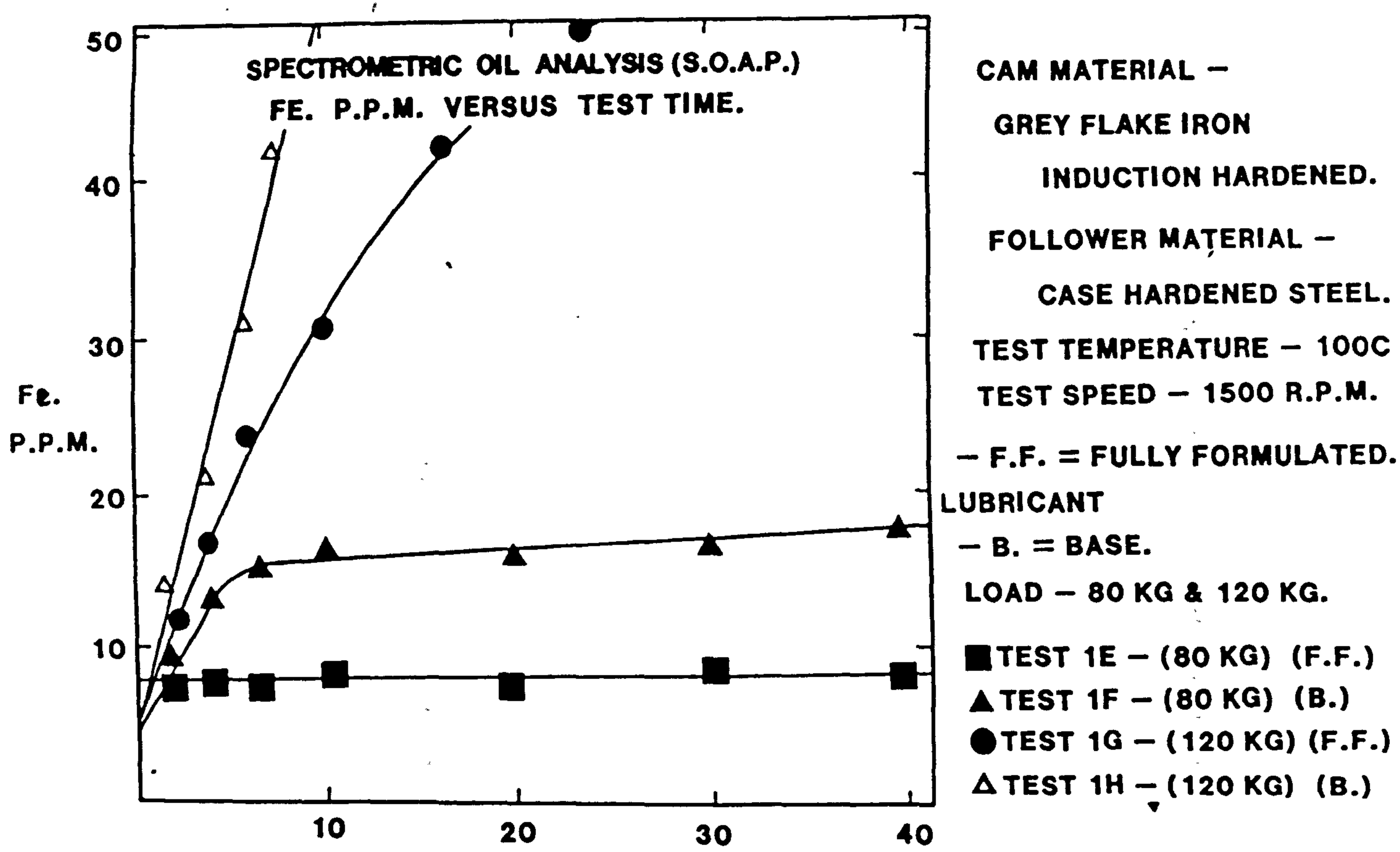

FIG. 57. QUANTITATIVE WEAR DEBRIS ANALYSIS, SPECTROMETRIC OIL ANALYSIS. GRAPH OF WEAR DEBRIS CONCENTRATION VERSUS TEST TIME.

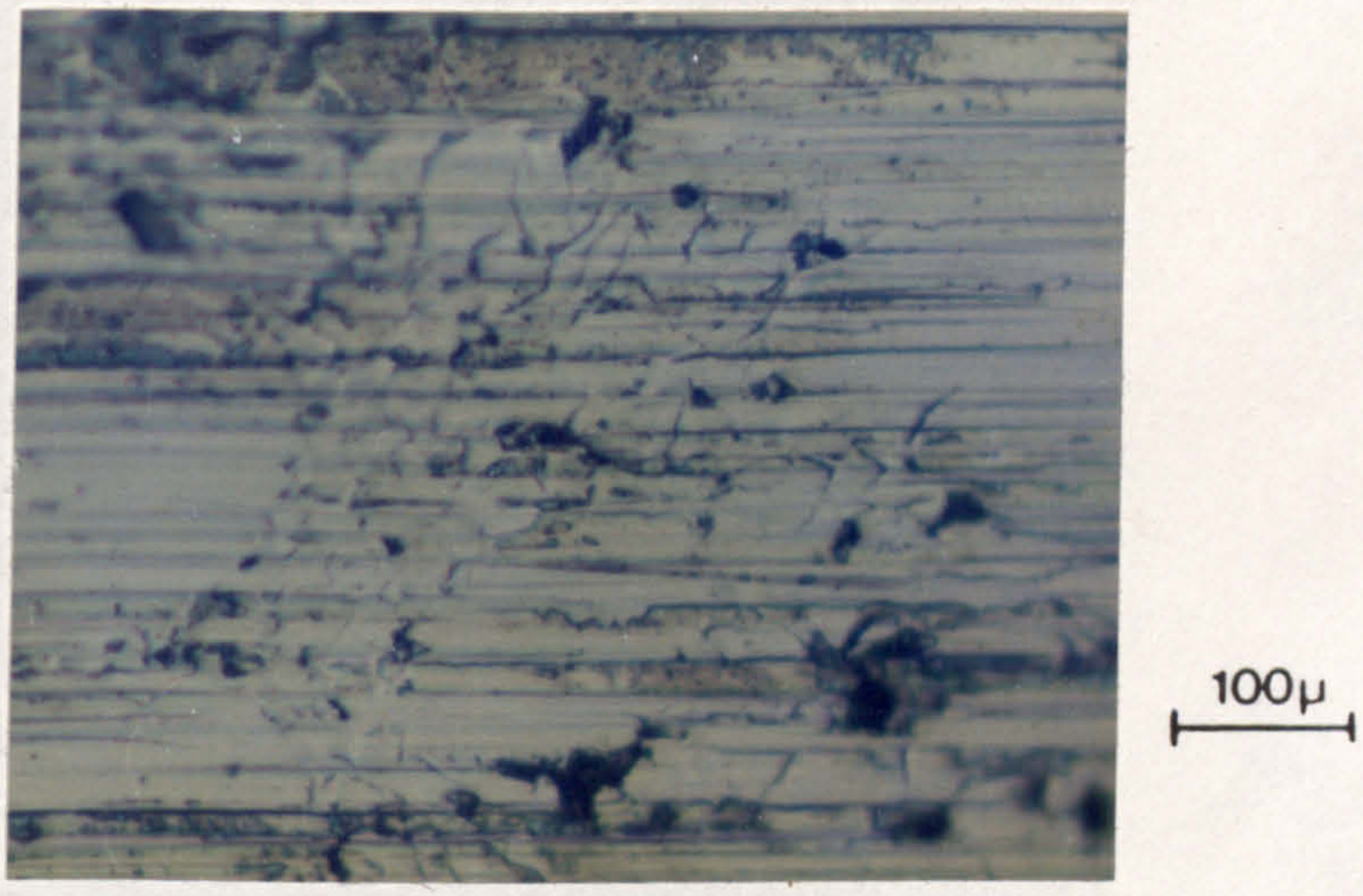

FIG. 58. TEST 1E, CAM WEAR SURFACE, OPTICAL.

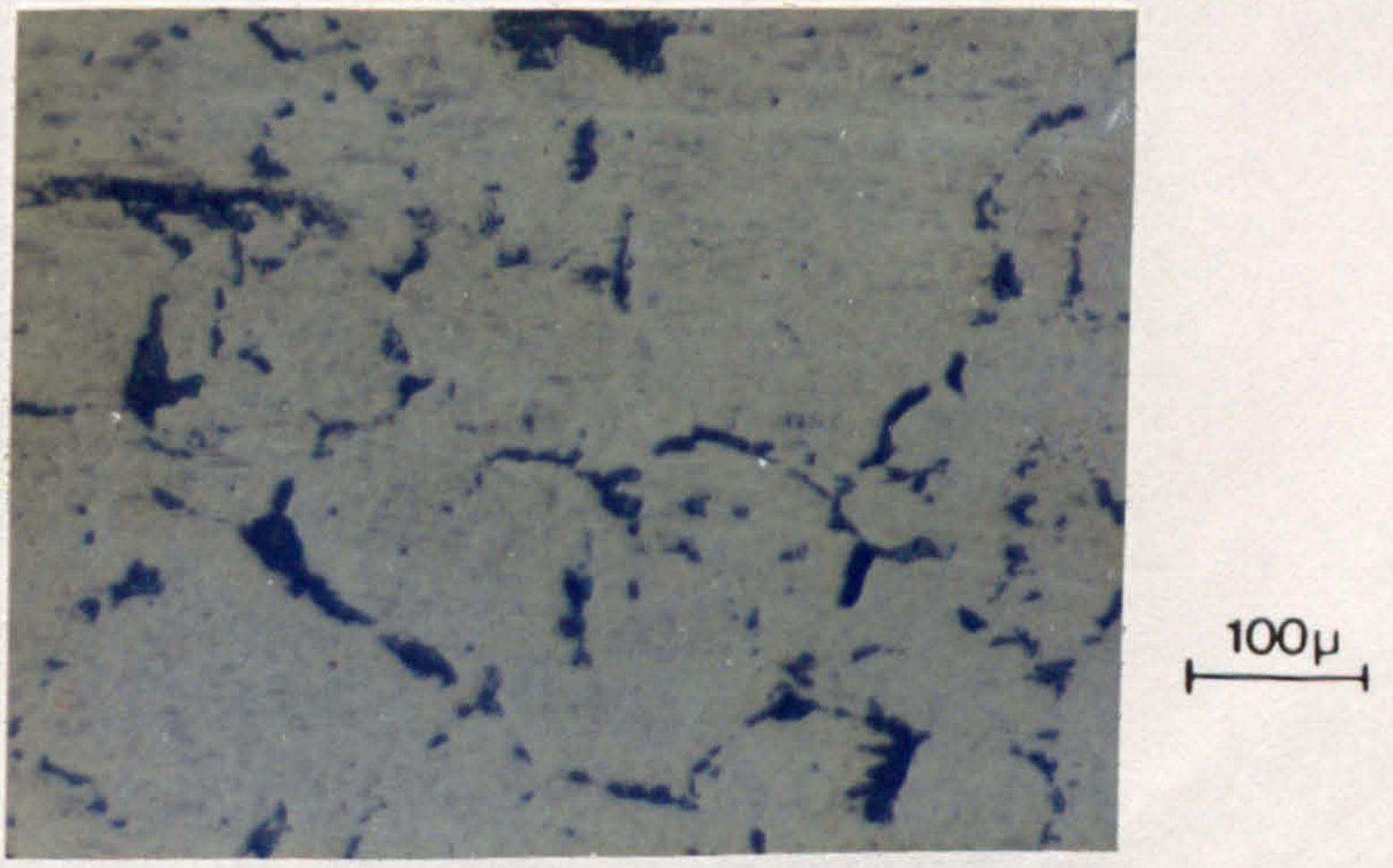

FIG. 59. TEST 1E, FOLLOWER WEAR SURFACE, OPTICAL.

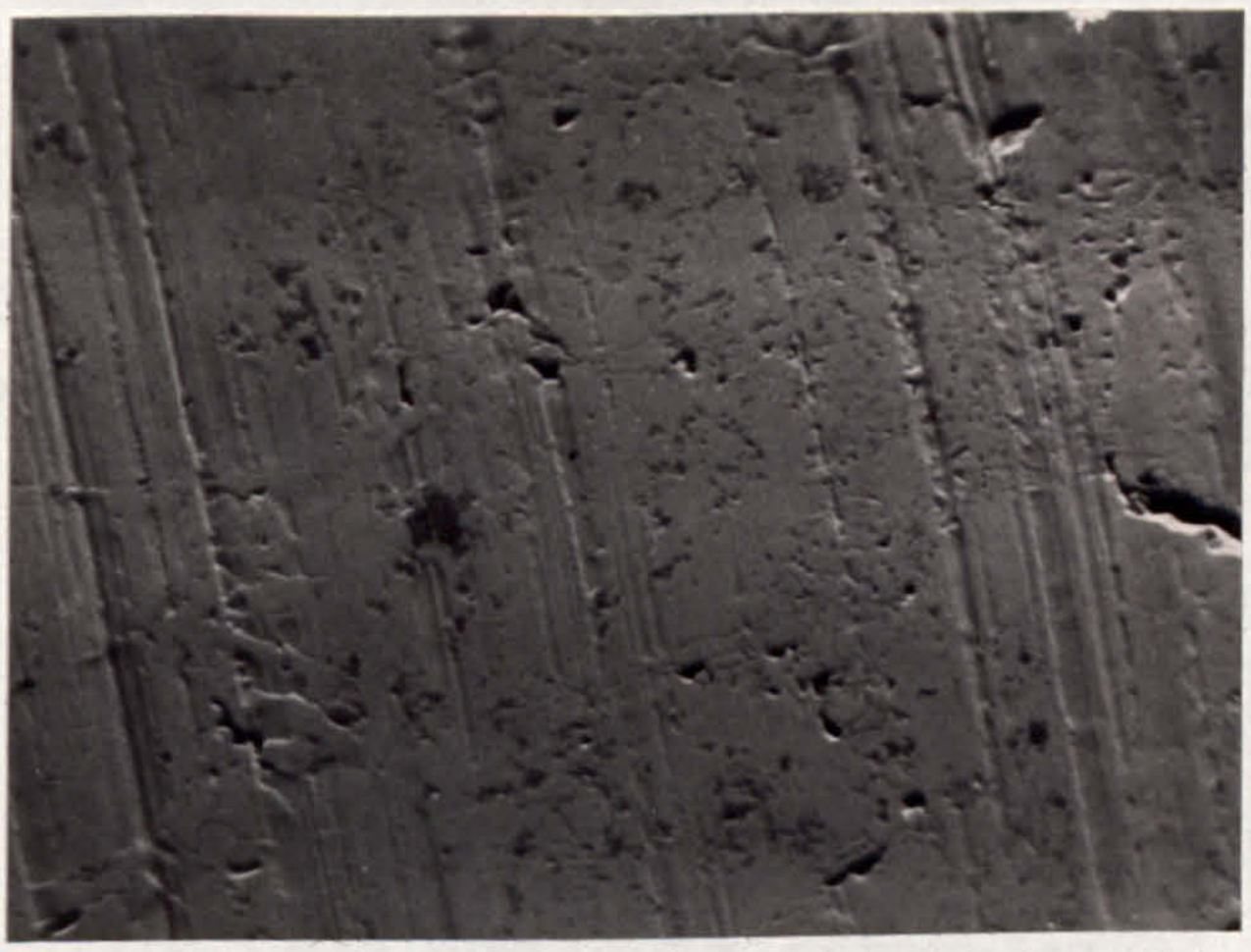

FIG. 60. TEST 1E, CAM WEAR SURFACE, ELECTRON MICROGRAPH.

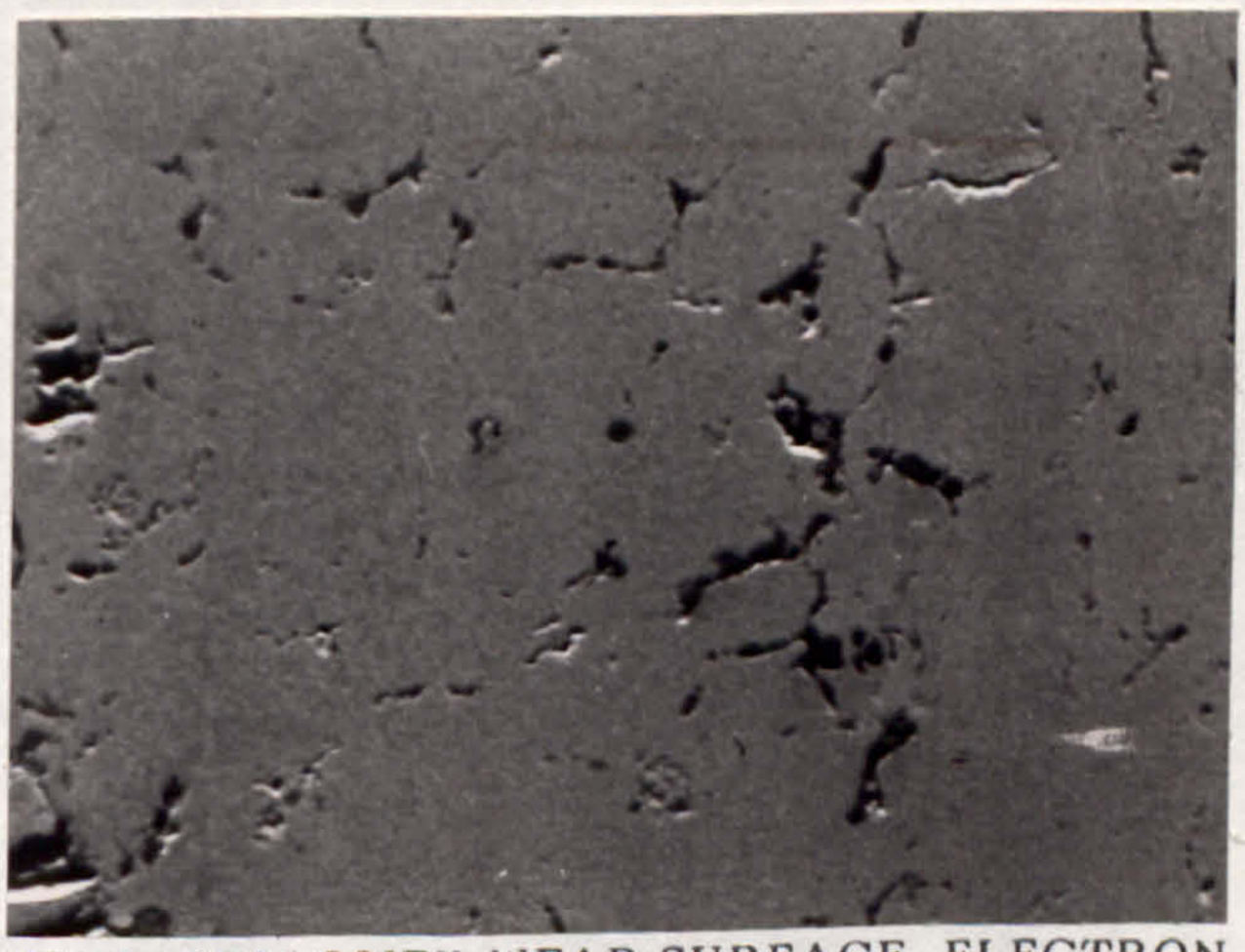

FIG. 61. TEST 1E, FOLLOWER WEAR SURFACE, ELECTRON MICROGRAPH.

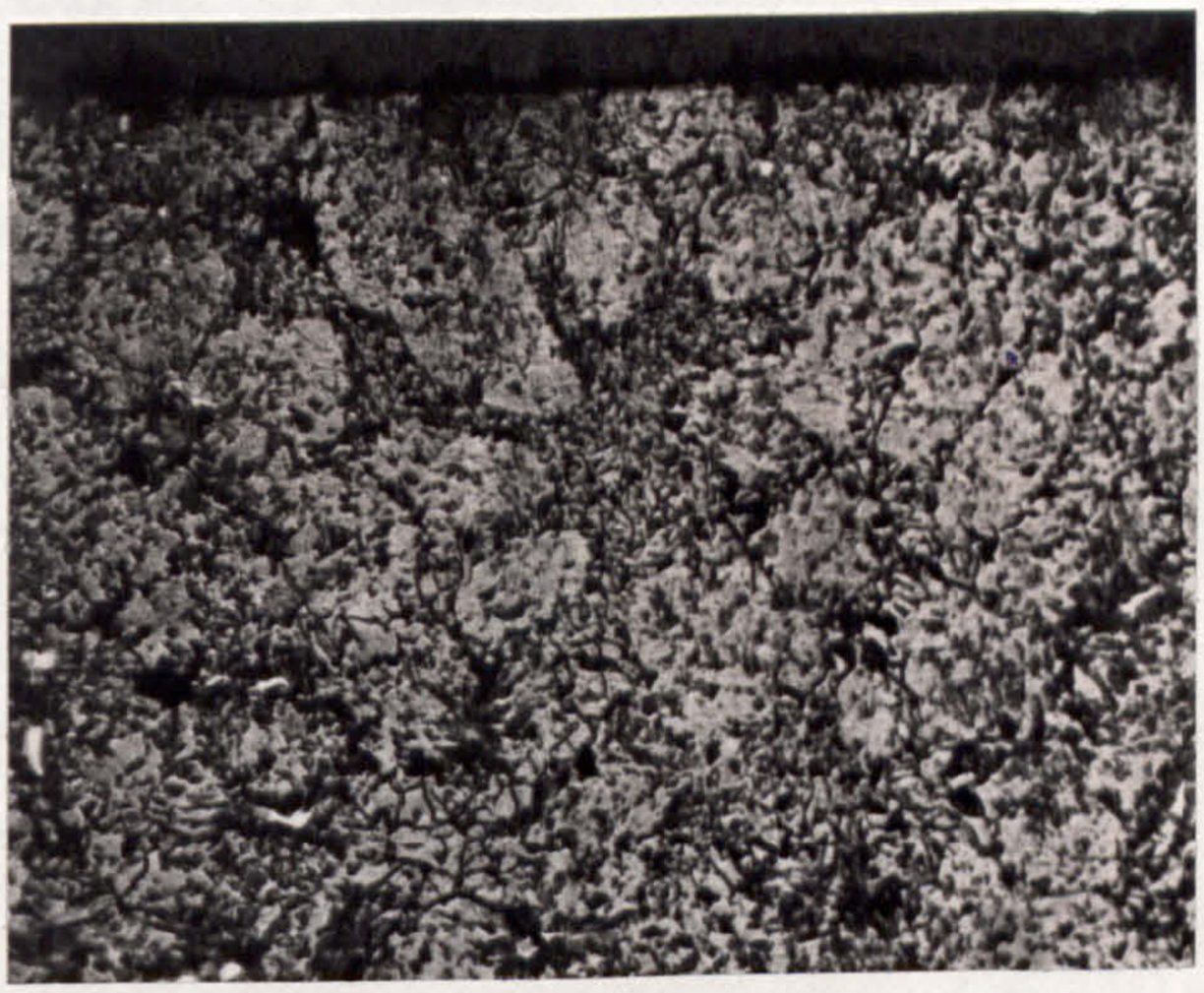

FIG. 62. TEST 1E, CAM SPECIMEN TAPERSECTION.

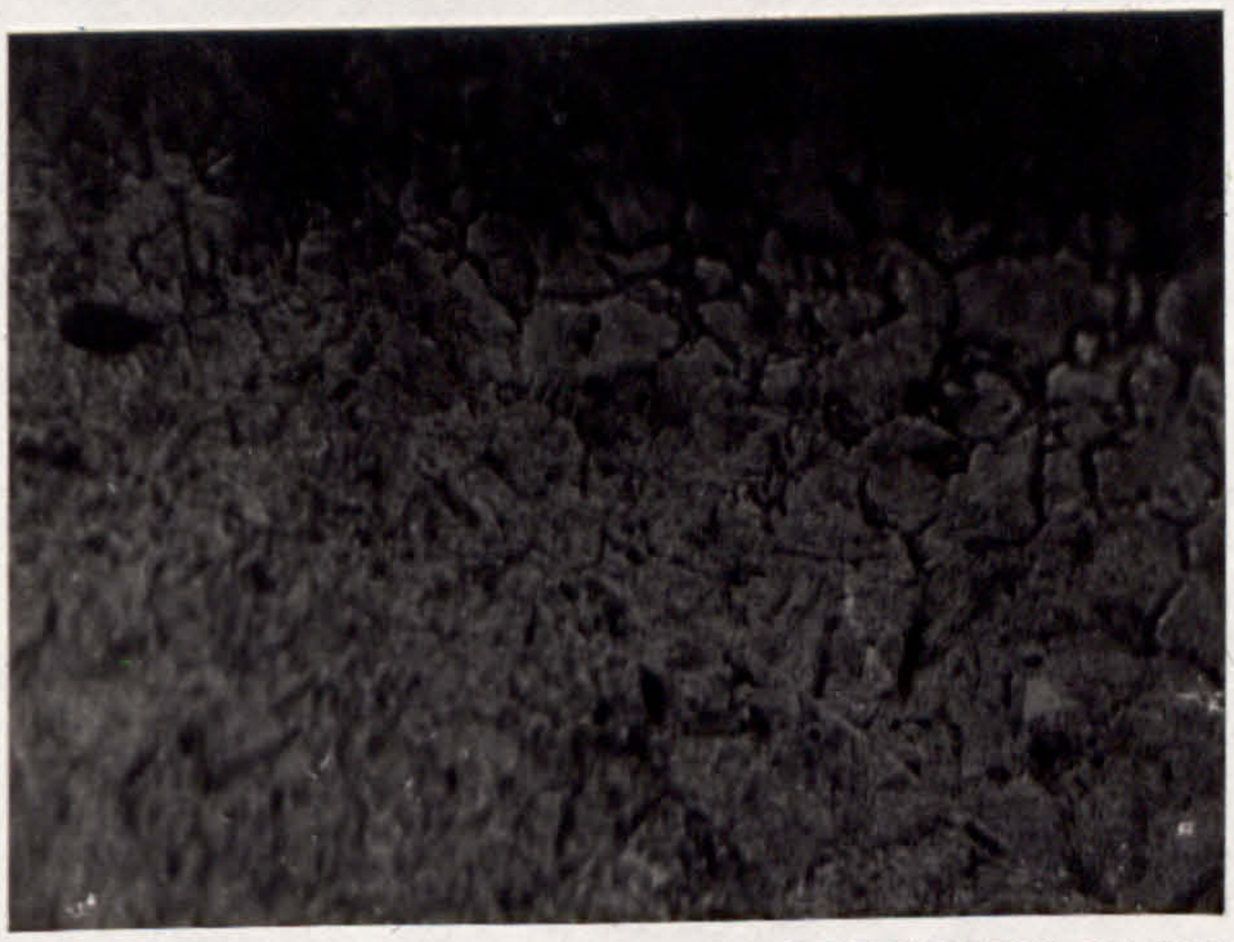

FIG. 63. TEST 1E, FOLLOWER SPECIMEN TAPERSECTION.

FIG. 64. TEST 1E, WEAR DEBRIS, ELECTRON MICROGRAPH.

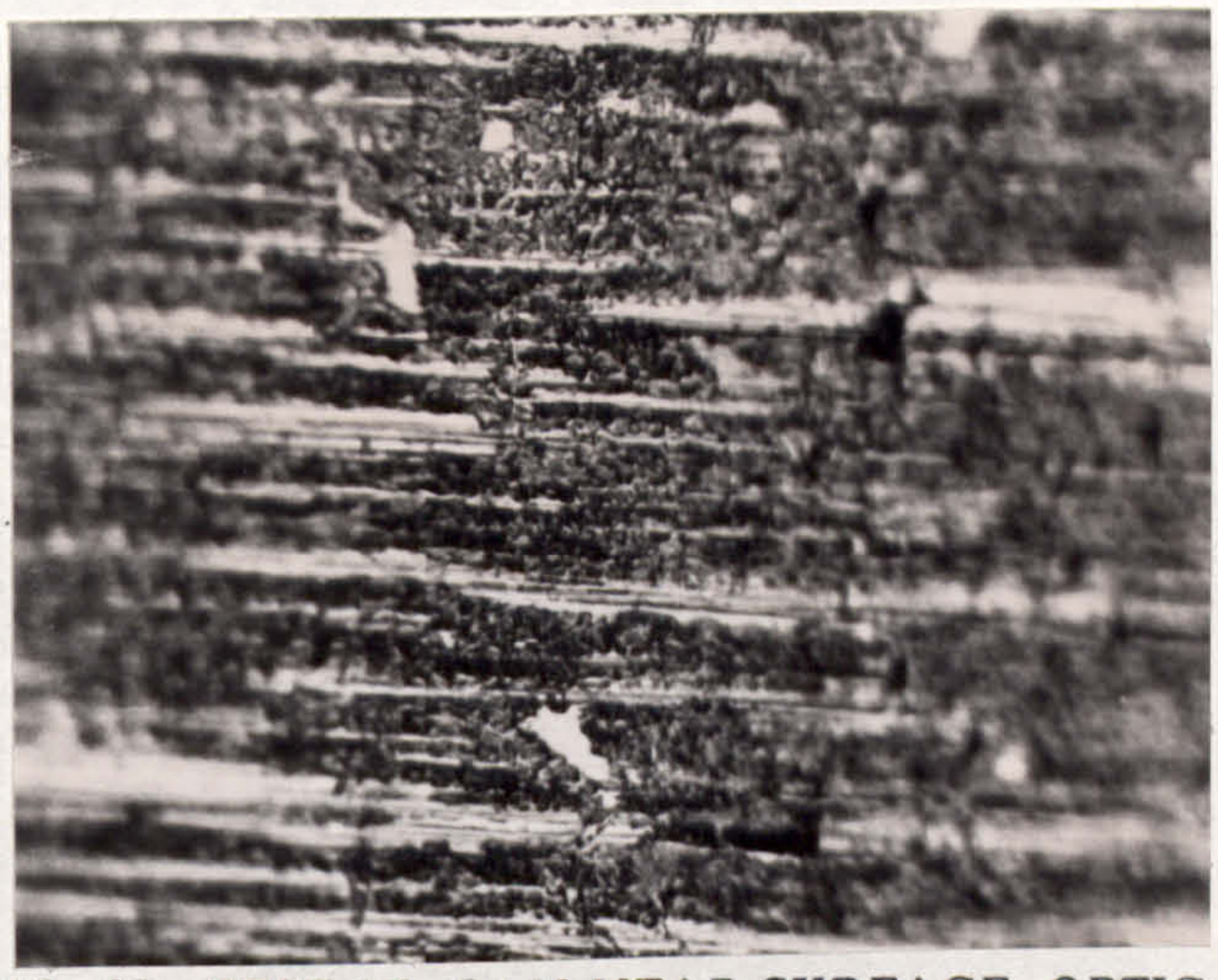

FIG. 65. TEST 1F, CAM WEAR SURFACE, OPTICAL.

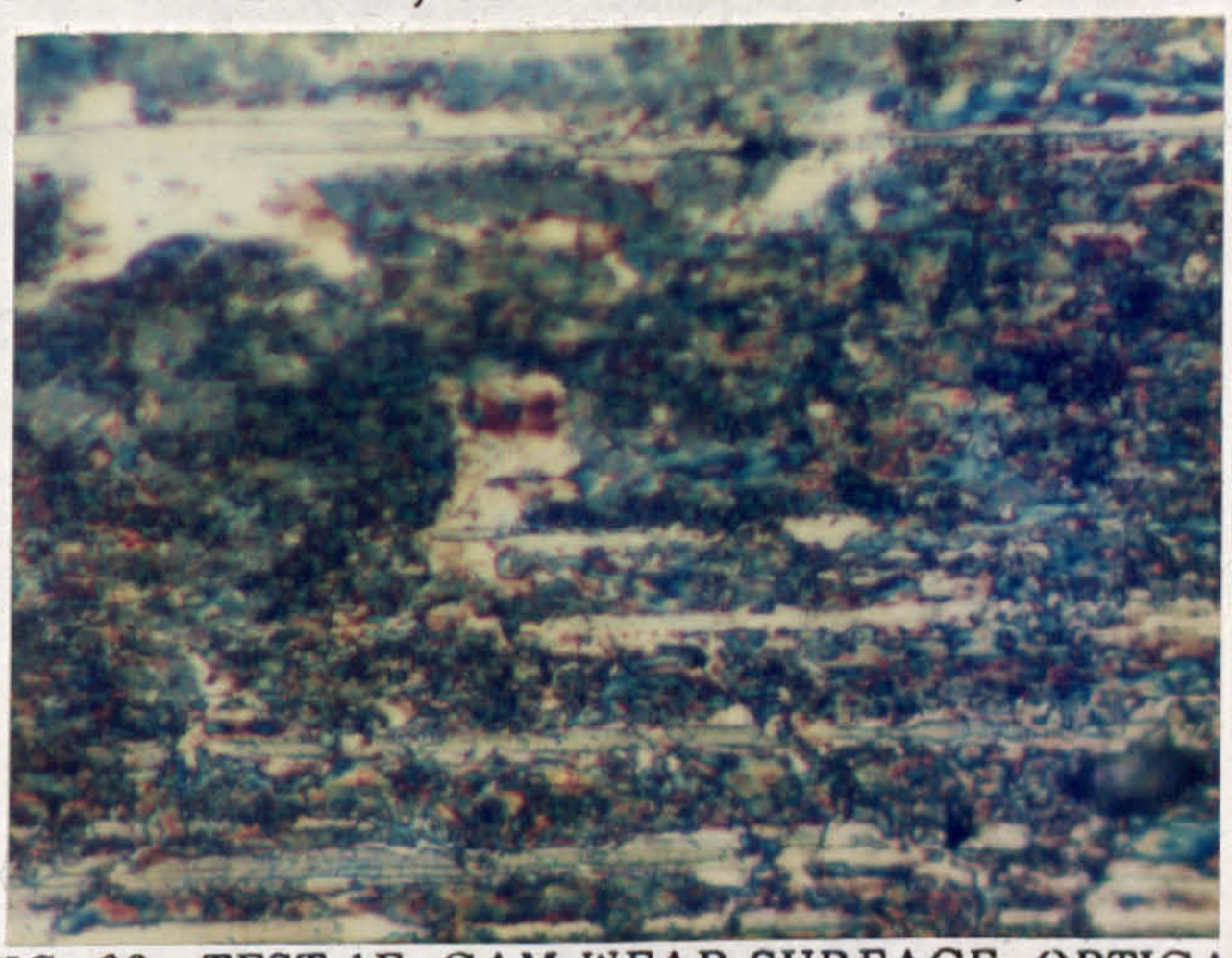

FIG. 66. TEST 1F, CAM WEAR SURFACE, OPTICAL.

FIG. 67. TEST 1F, FOLLOWER WEAR SURFACE, OPTICAL.

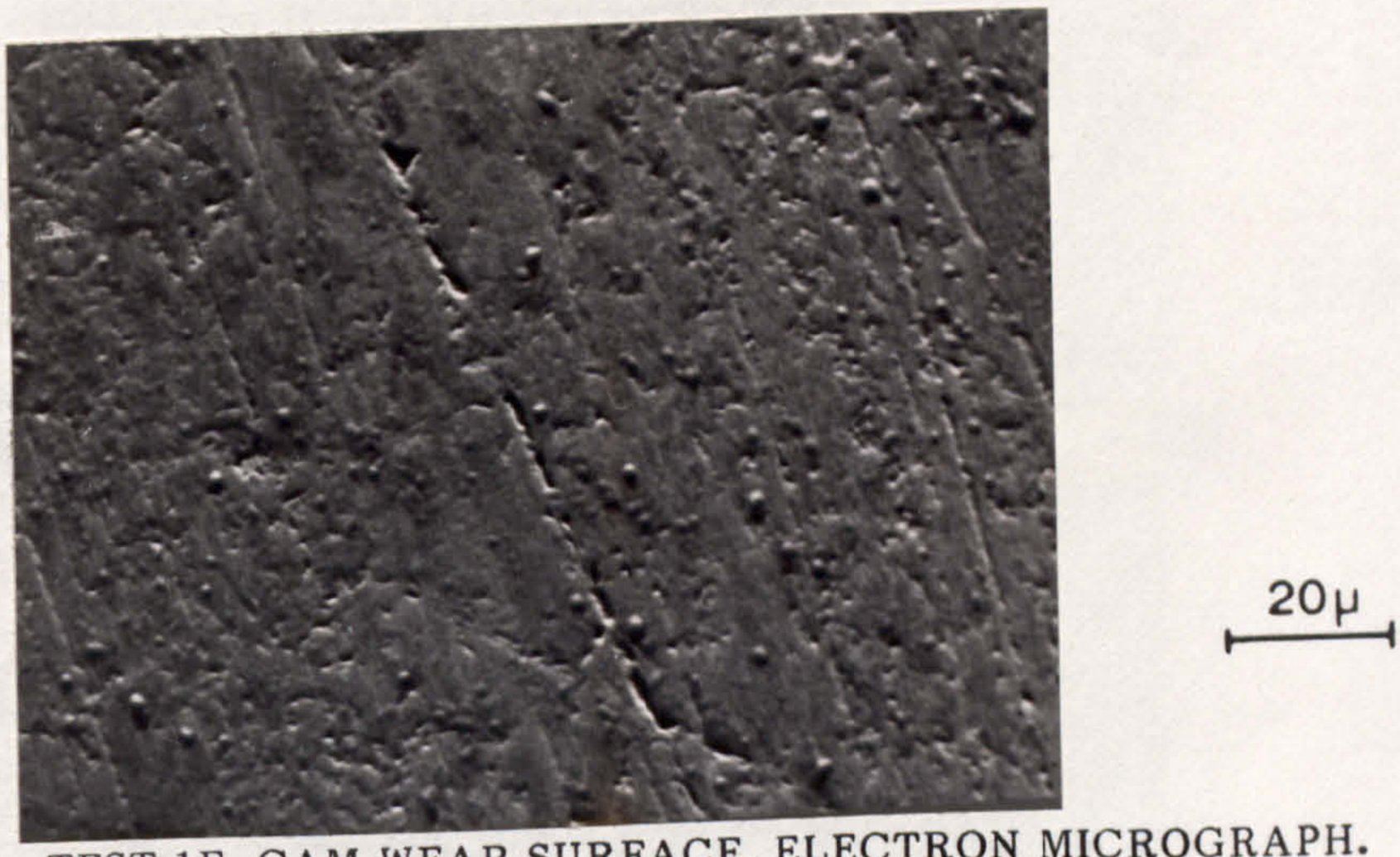

FIG. 68. TEST 1F, CAM WEAR SURFACE, ELECTRON MICROGRAPH.

FIG. 69. TEST 1F, FOLLOWER WEAR SURFACE, ELECTRON MICROGRAPH.

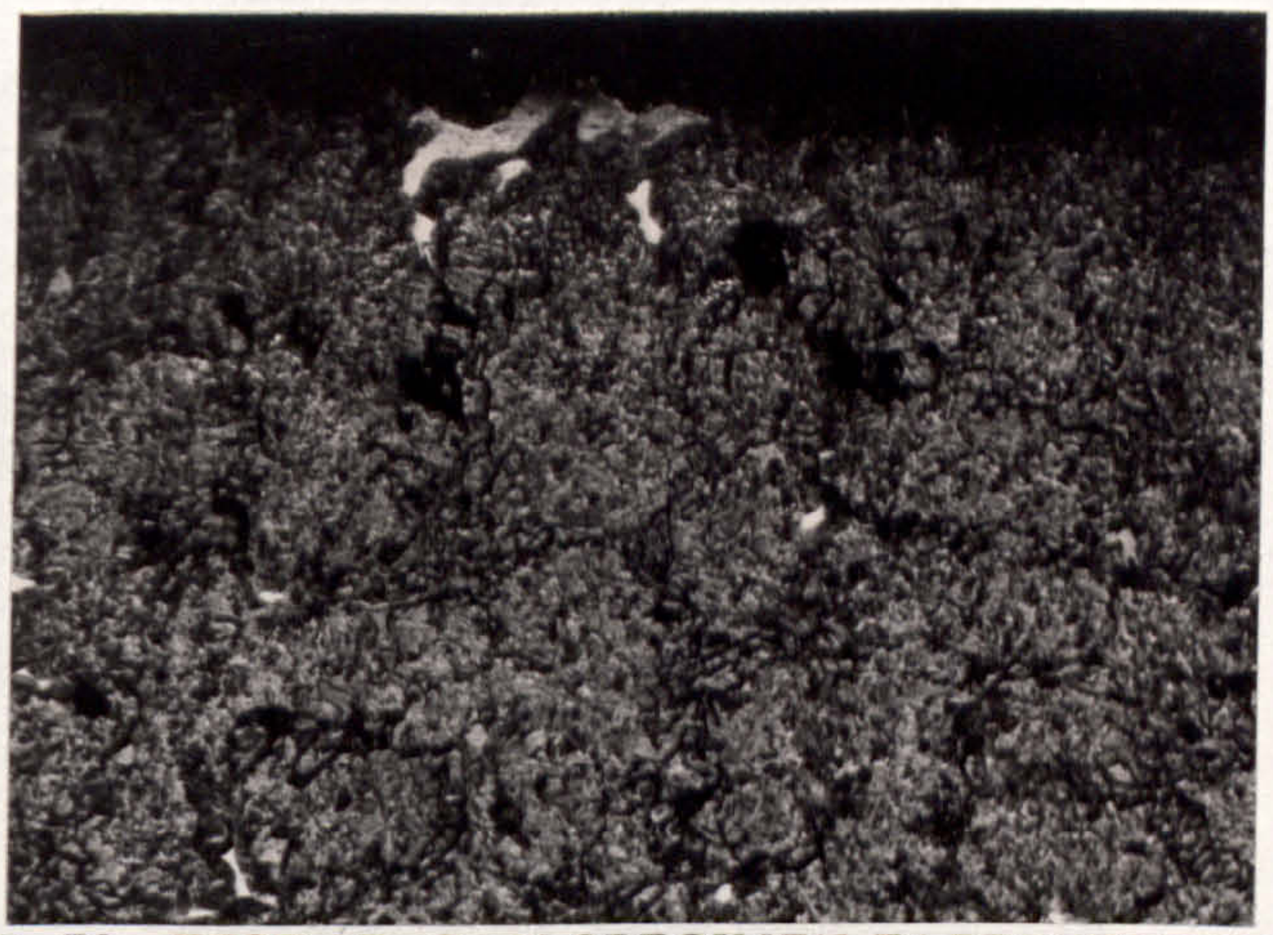

FIG. 70. TEST 1F, CAM SPECIMEN TAPERSECTION.

FIG. 71. TEST 1F, FOLLOWER SPECIMEN TAPERSECTION.

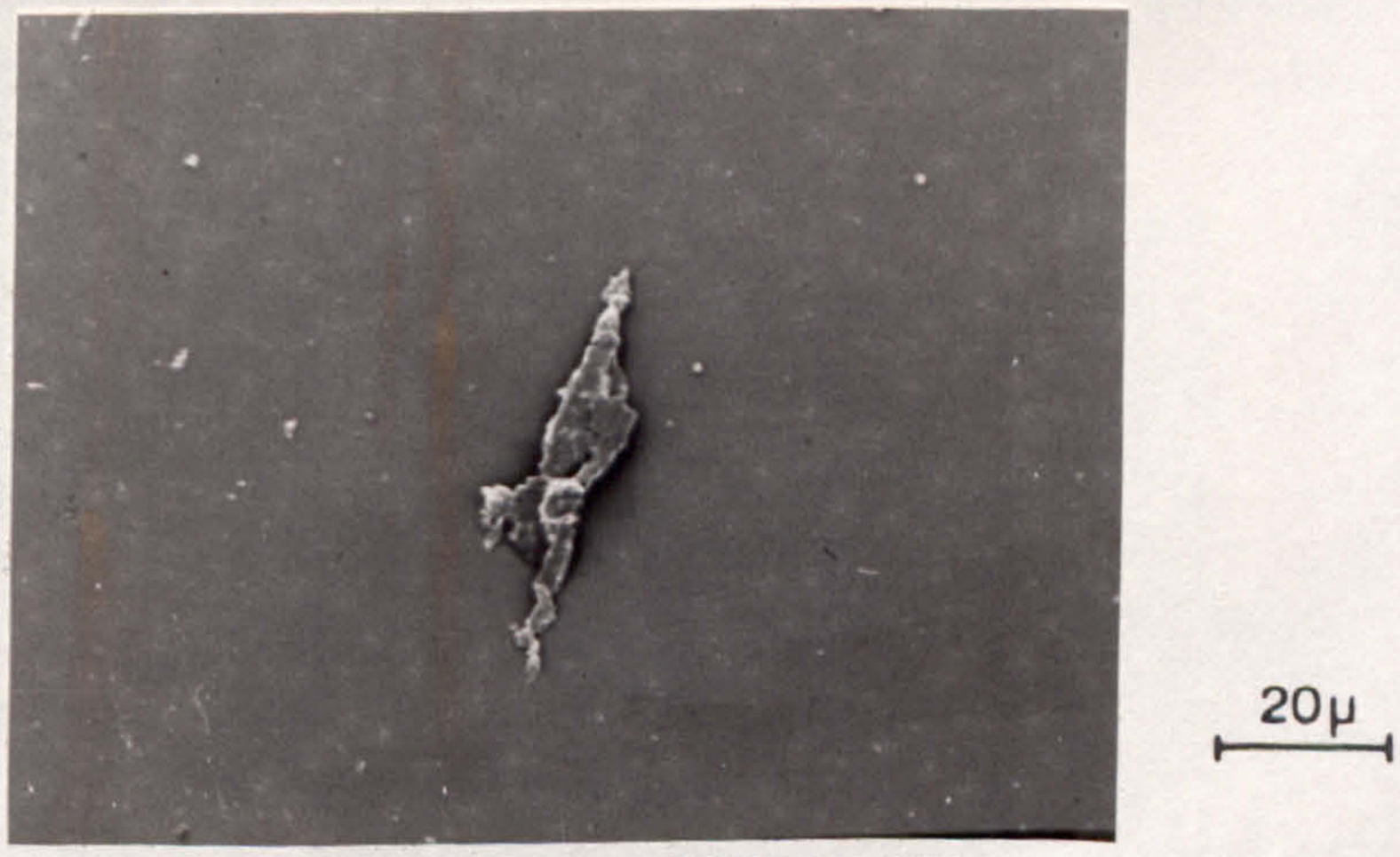

FIG. 72. TEST 1F, WEAR DEBRIS, ELECTRON MICROGRAPH.

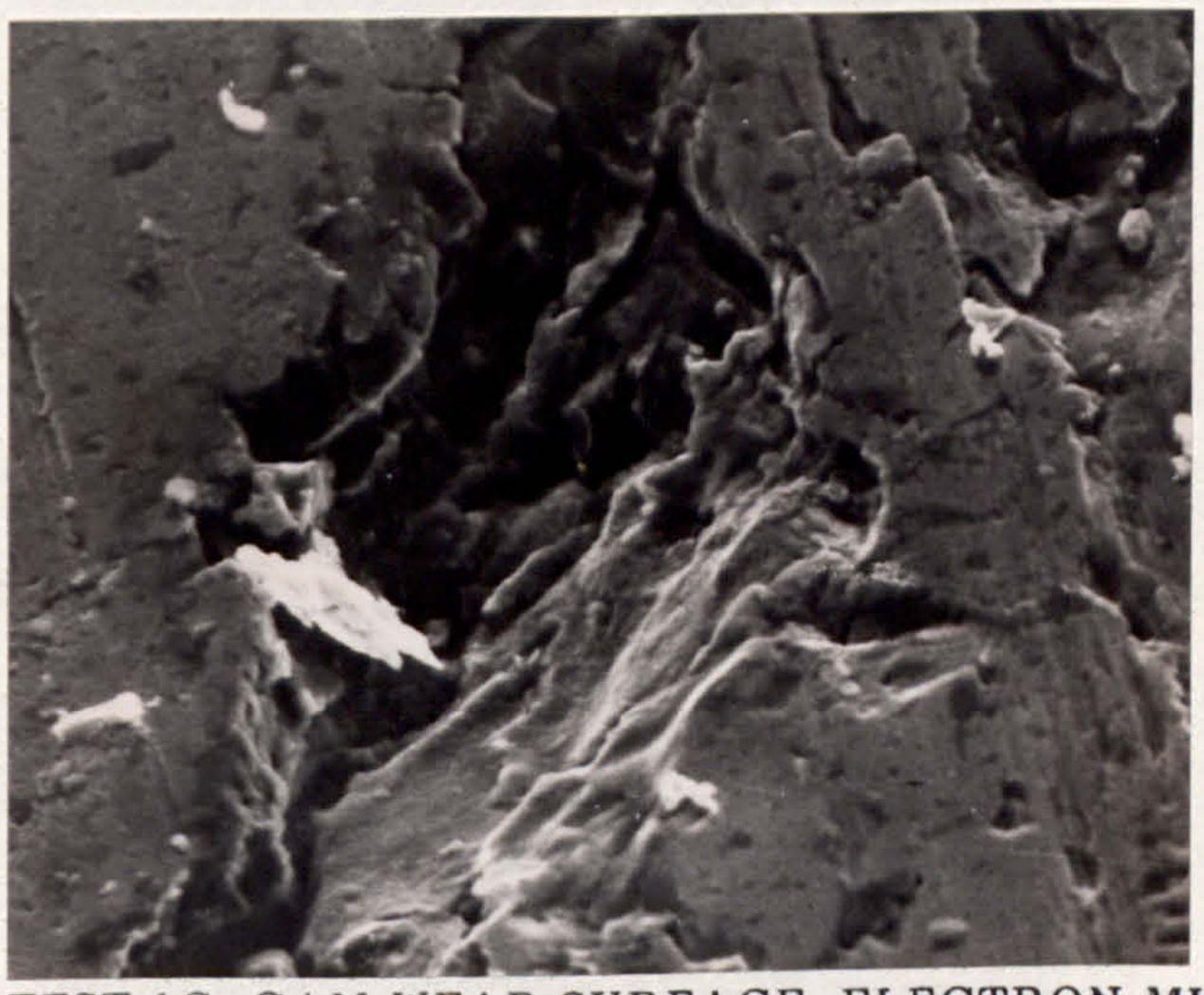

FIG. 73. TEST 1G, CAM WEAR SURFACE, ELECTRON MICROGRAPH.

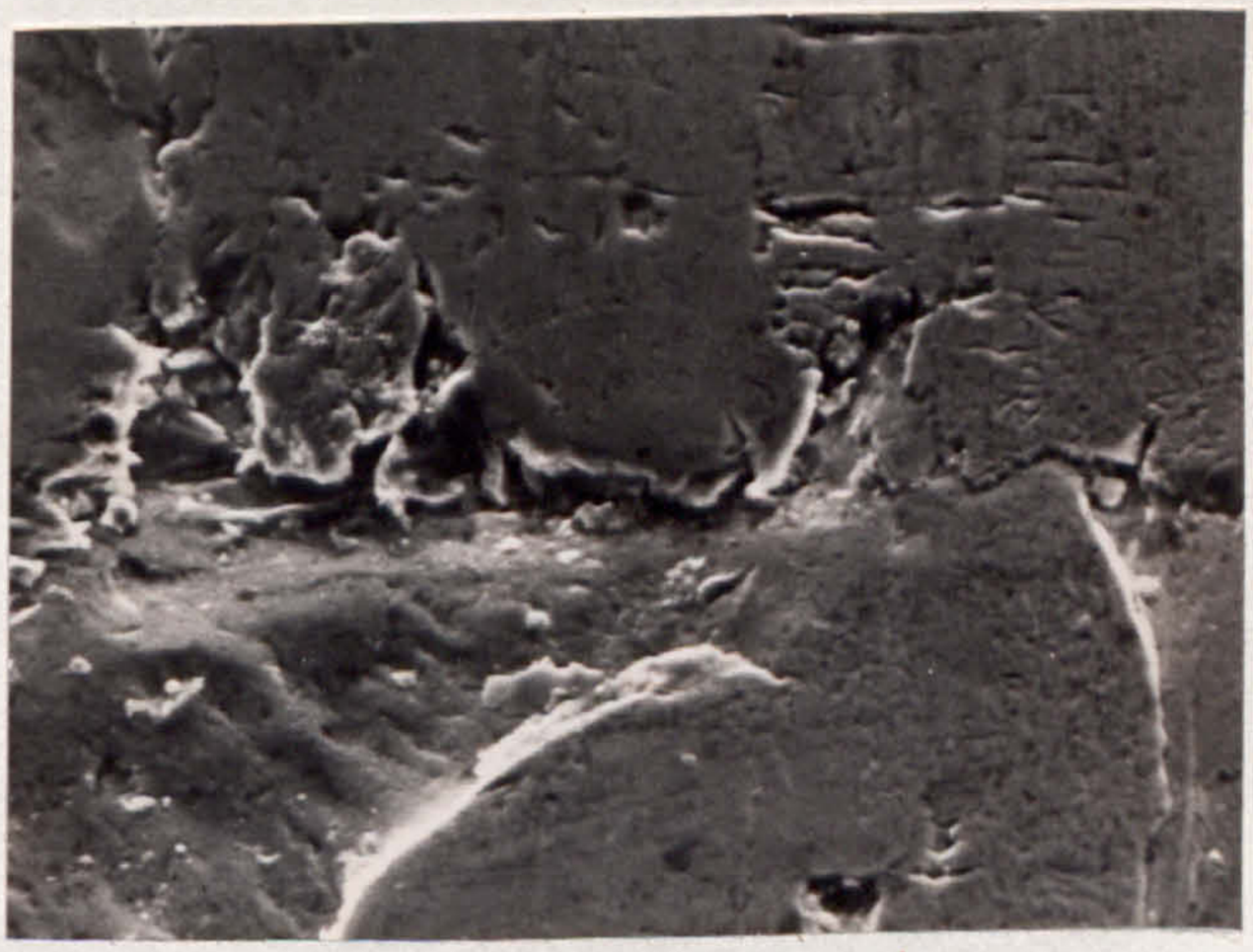

FIG. 74. TEST 1G, FOLLOWER WEAR SURFACE, ELECTRON MICROGRAPH.

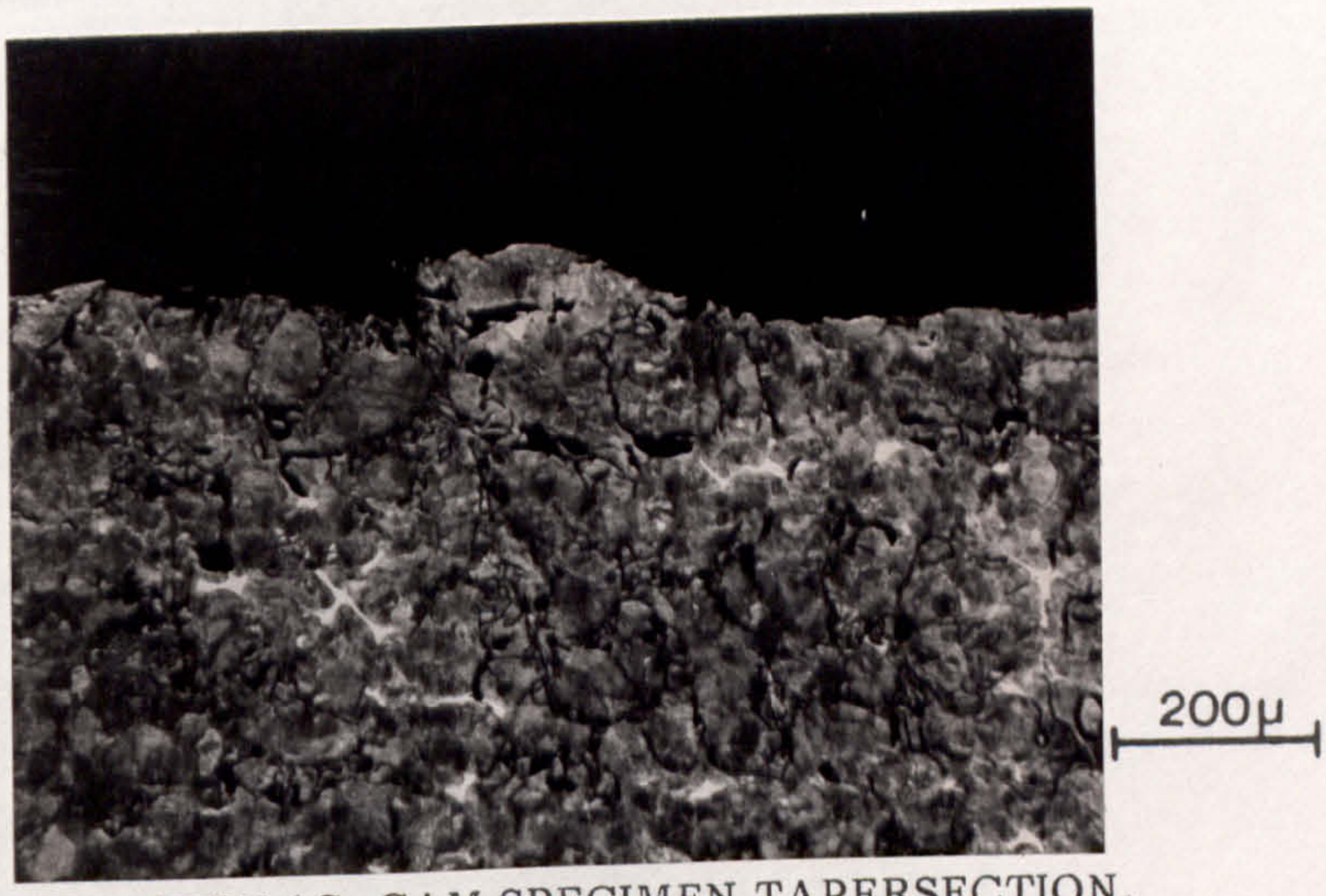

FIG. 75. TEST 1G, CAM SPECIMEN TAPERSECTION.

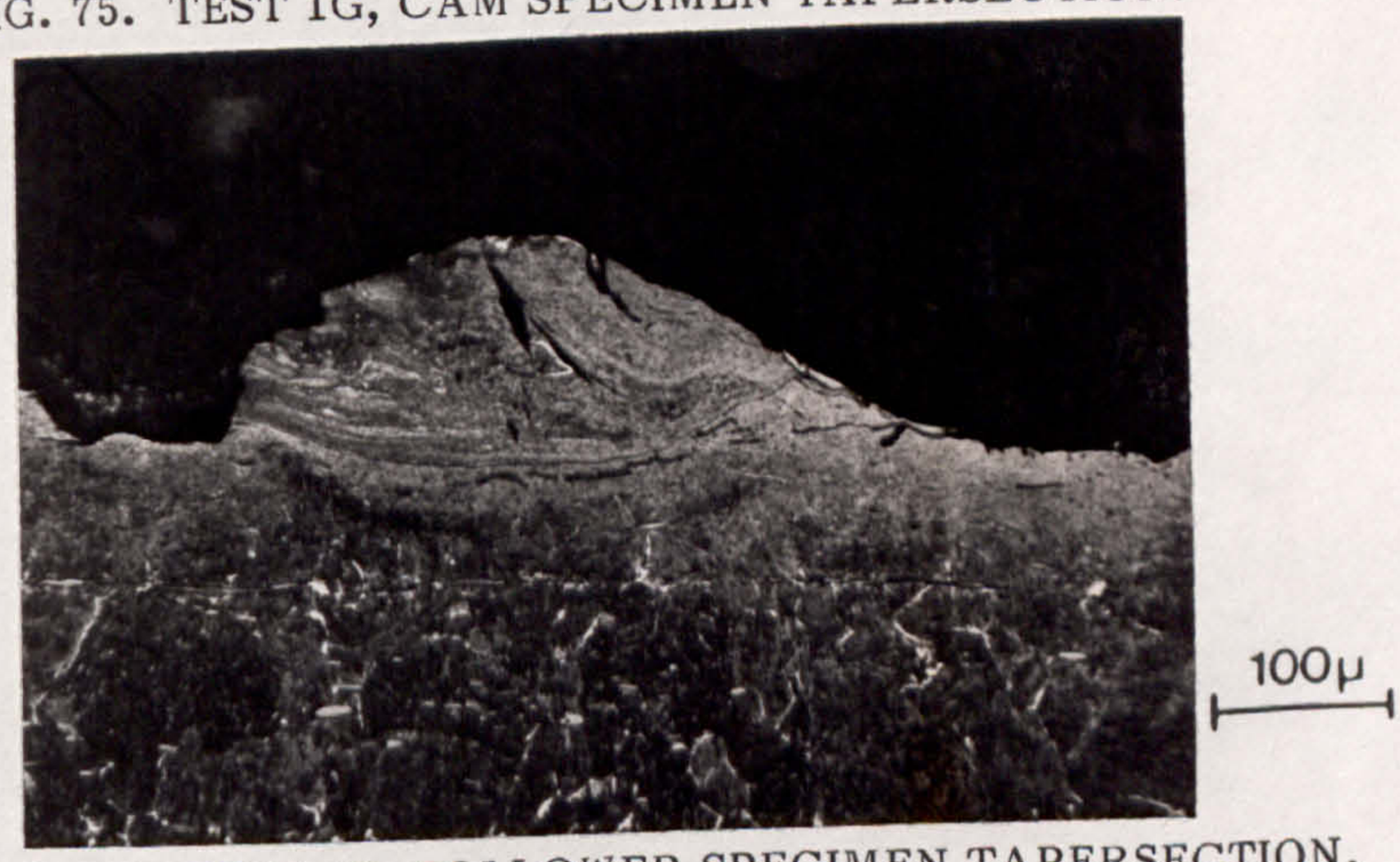

FIG. 76. TEST 1G, FOLLOWER SPECIMEN TAPERSECTION.

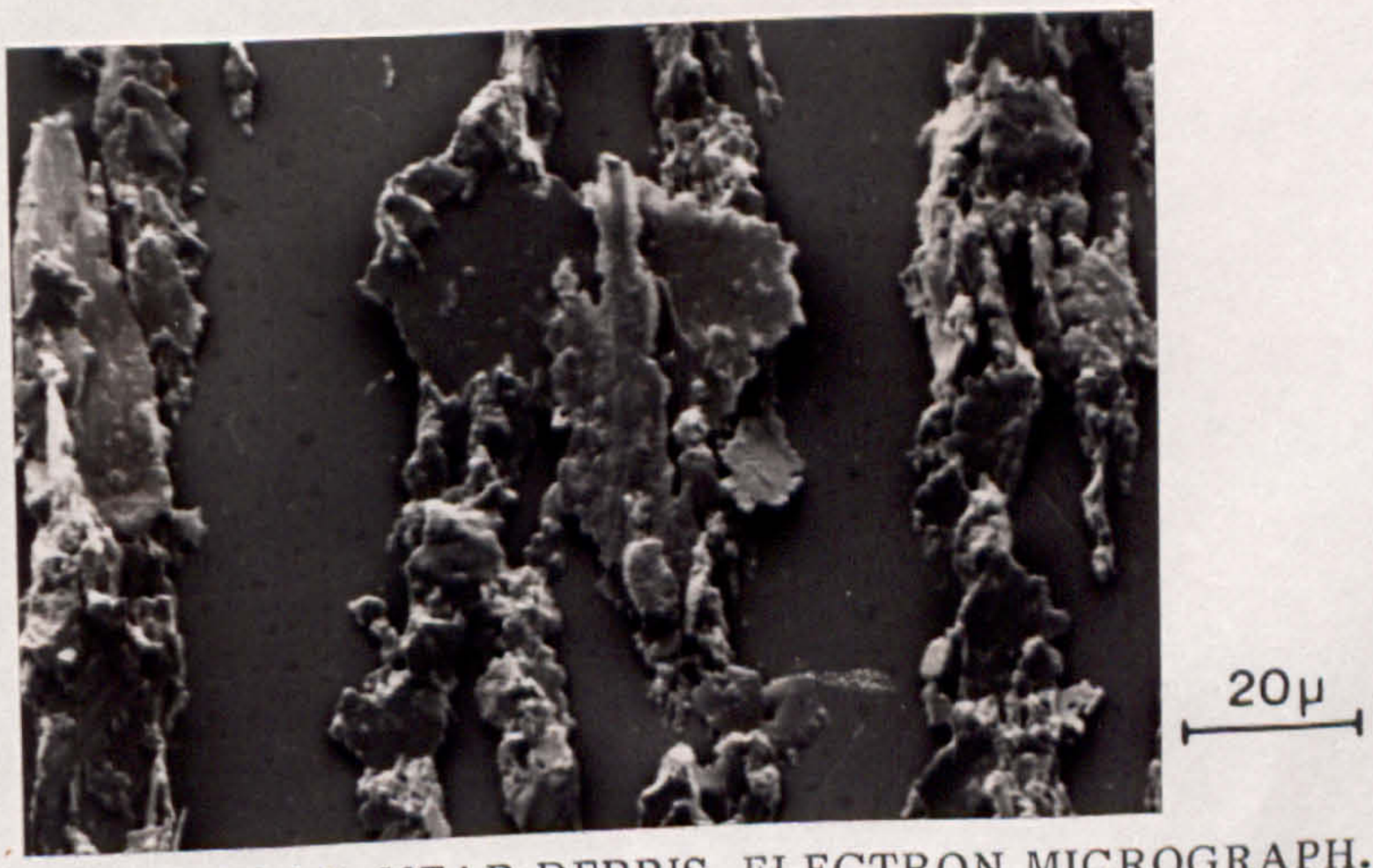

FIG. 77. TEST 1G, WEAR DEBRIS, ELECTRON MICROGRAPH.

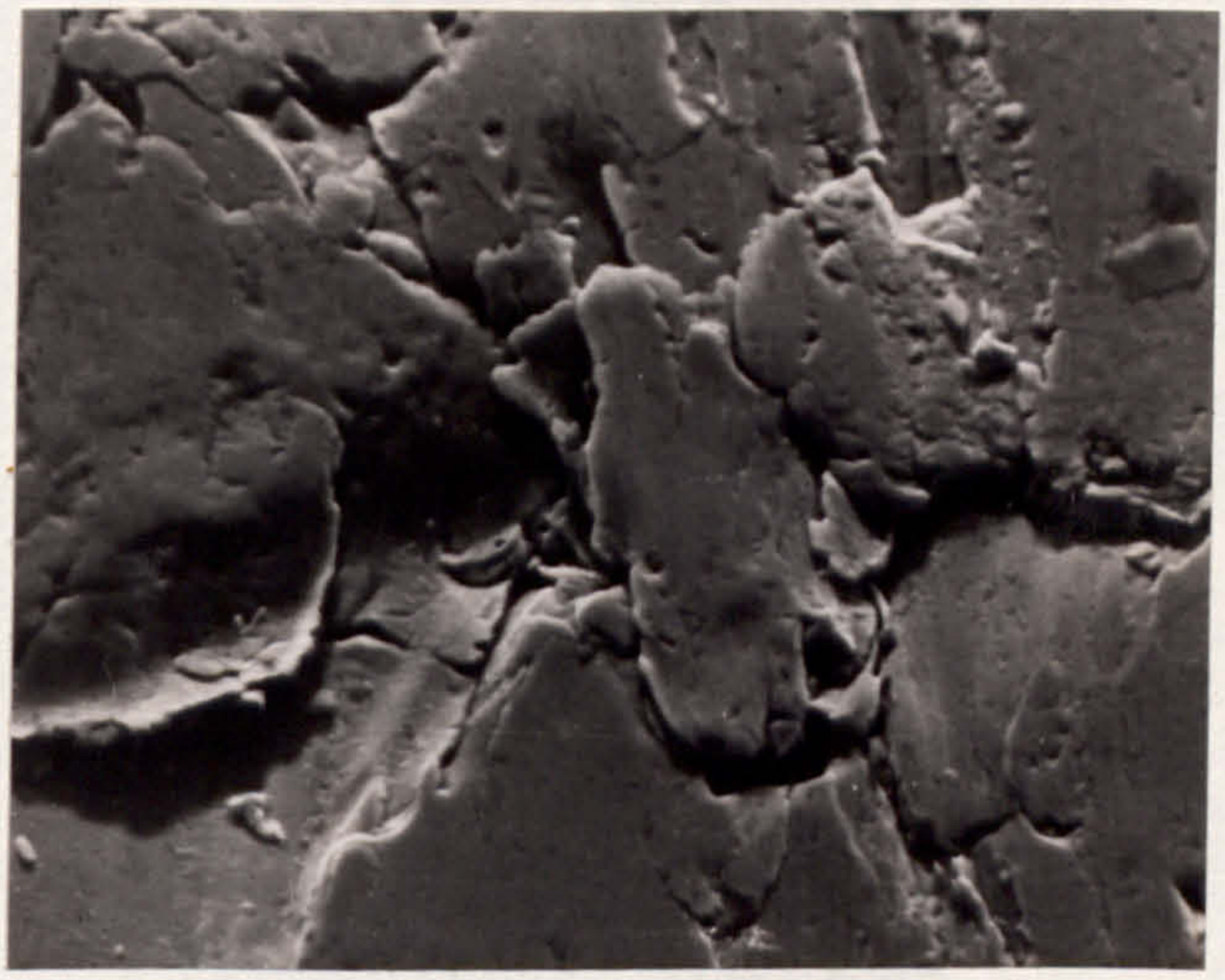

FIG. 78. TEST 1H, CAM WEAR SURFACE, ELECTRON MICROGRAPH.

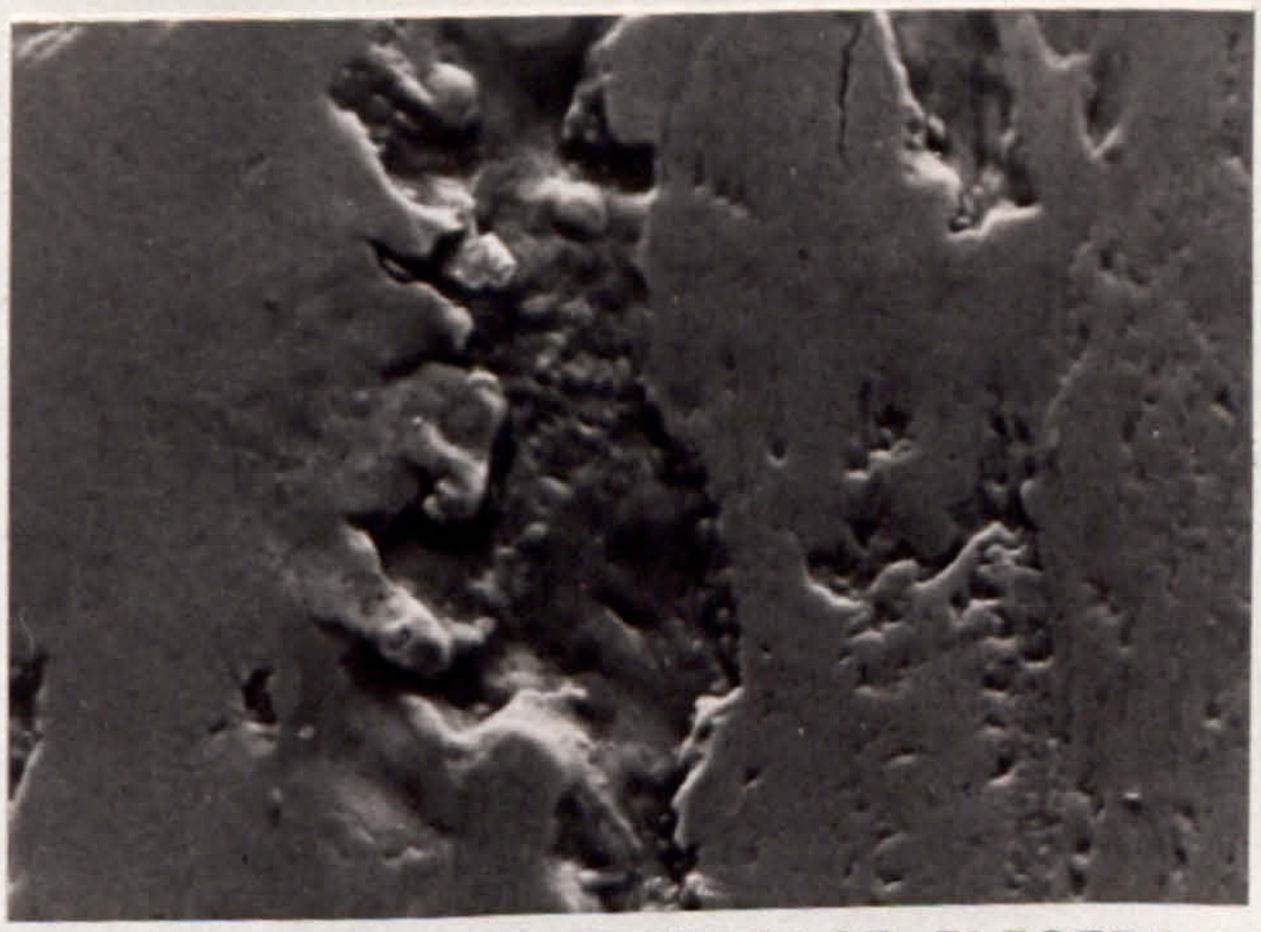

FIG. 79. TEST 1H, FOLLOWER WEAR SURFACE, ELECTRON MICROGRAPH.

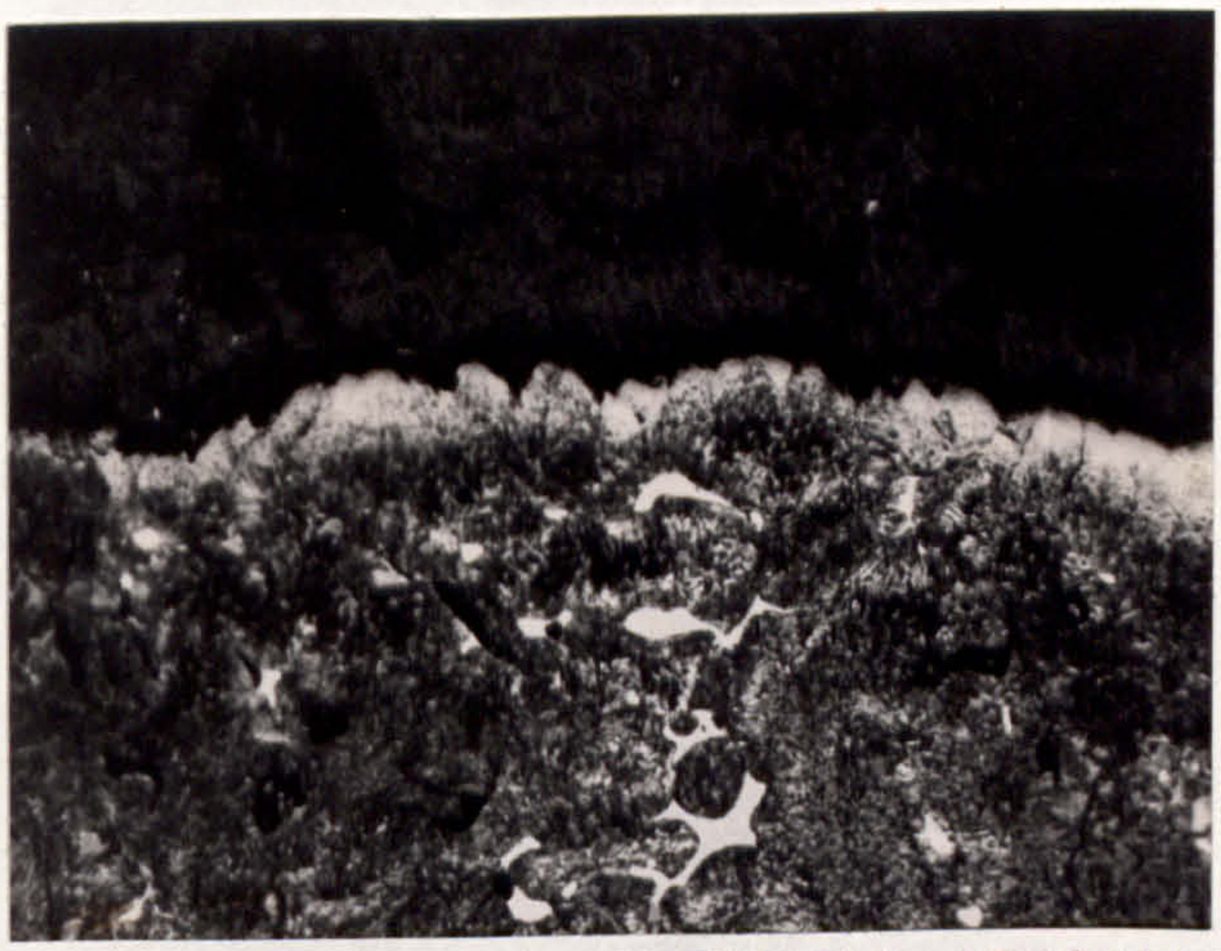

FIG. 80. TEST 1H, CAM SPECIMEN TAPERSECTION.

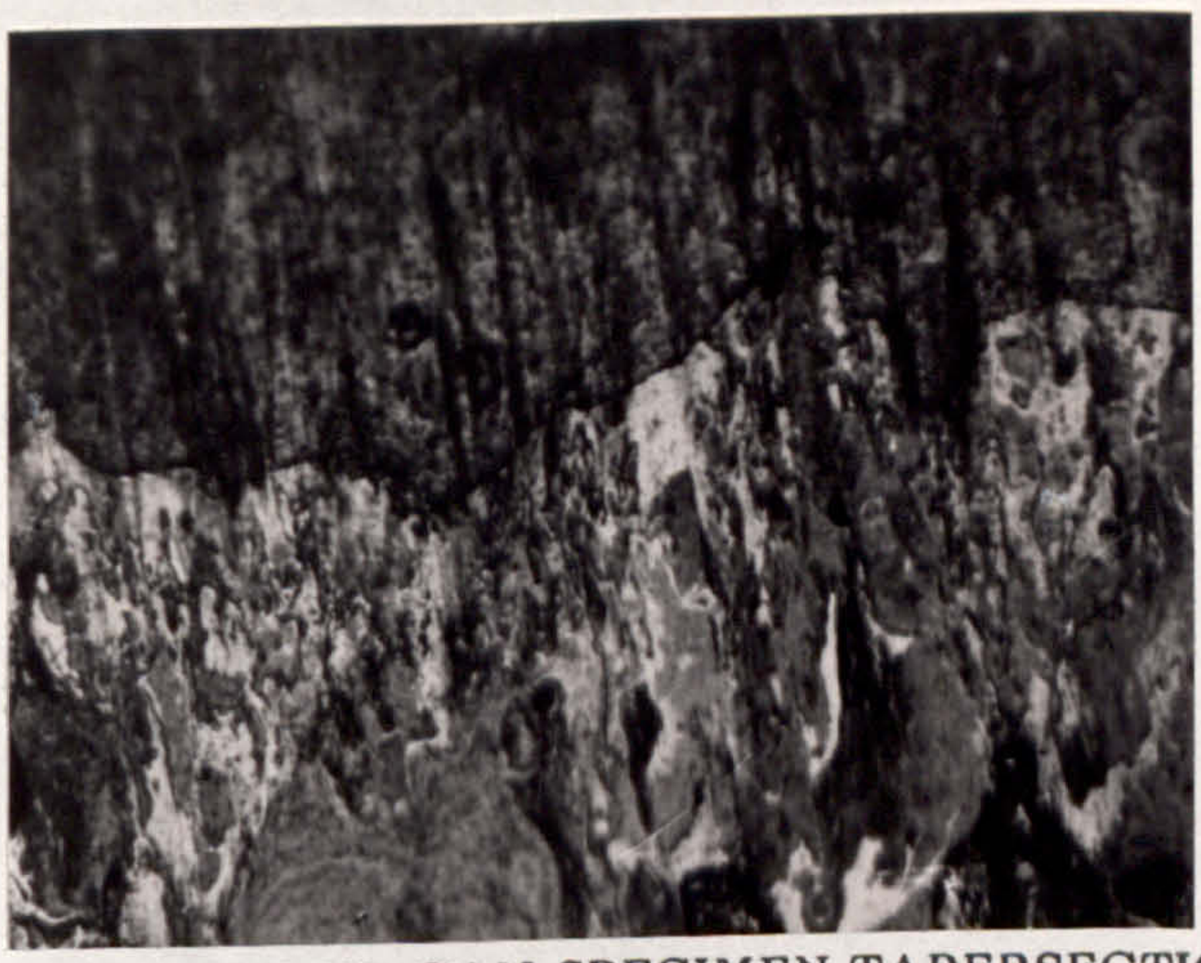

FIG. 81, TEST 1H, CAM SPECIMEN TAPERSECTION.

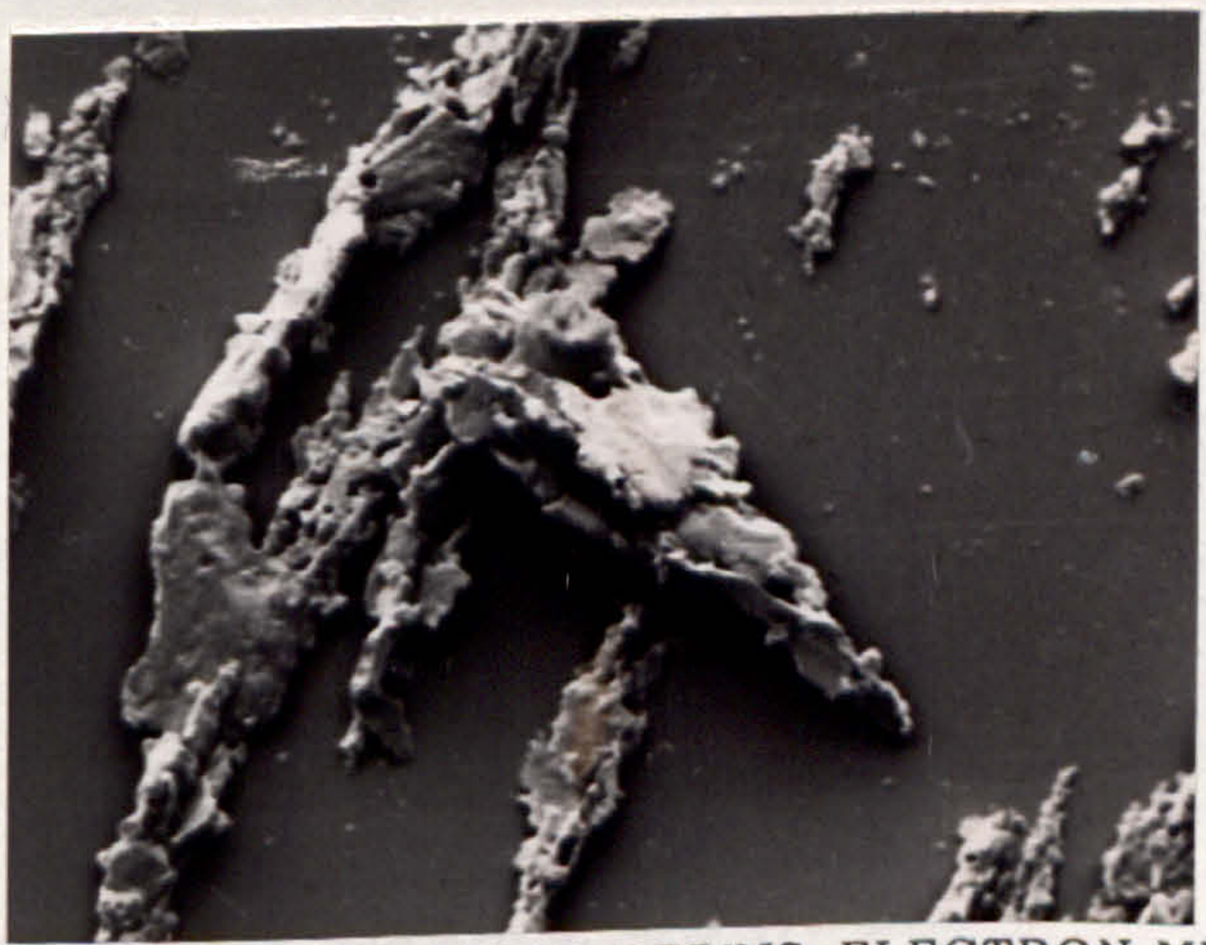

FIG. 82. TEST 1H, WEAR DEBRIS, ELECTRON MICROGRAPH.

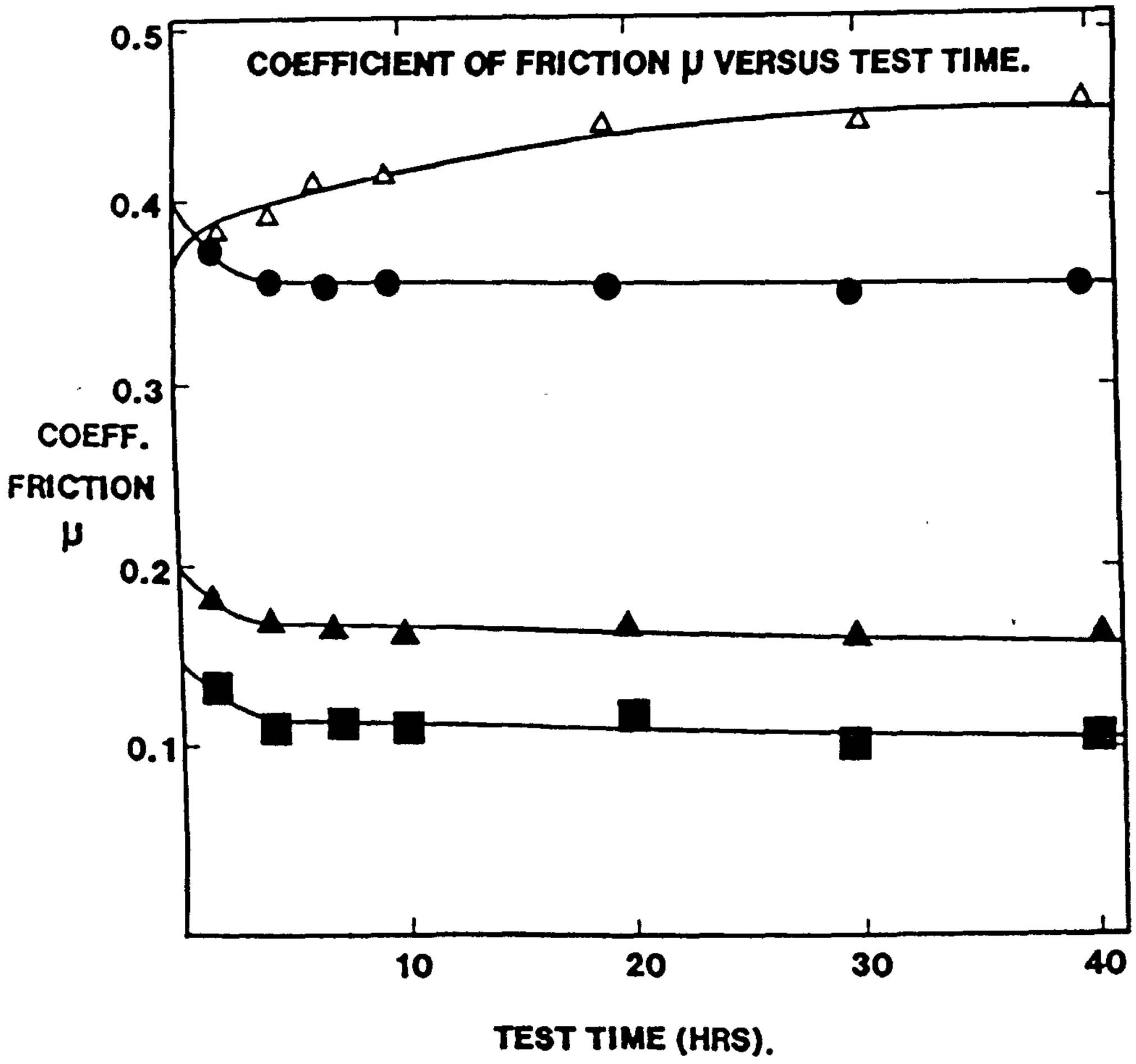

FIG. 83. GRAPH OF COEFFICIENT OF FRICTION VERSUS TEST TIME.

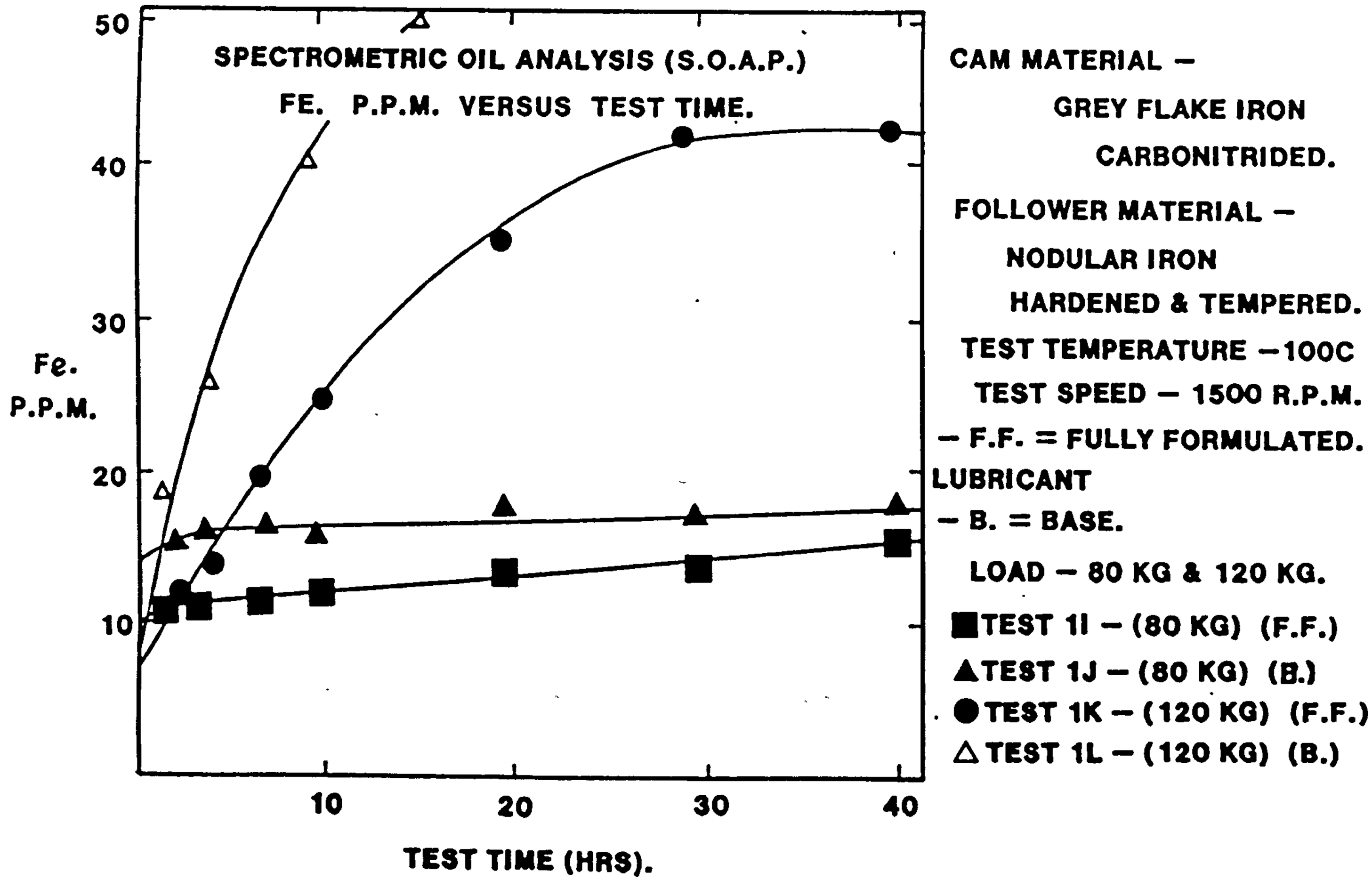

FIG. 84. QUANTITATIVE WEAR DEBRIS ANALYSIS, SPECTROMETRIC OIL ANALYSIS. GRAPH OF WEAR DEBRIS CONCENTRATION VERSUS TEST TIME.

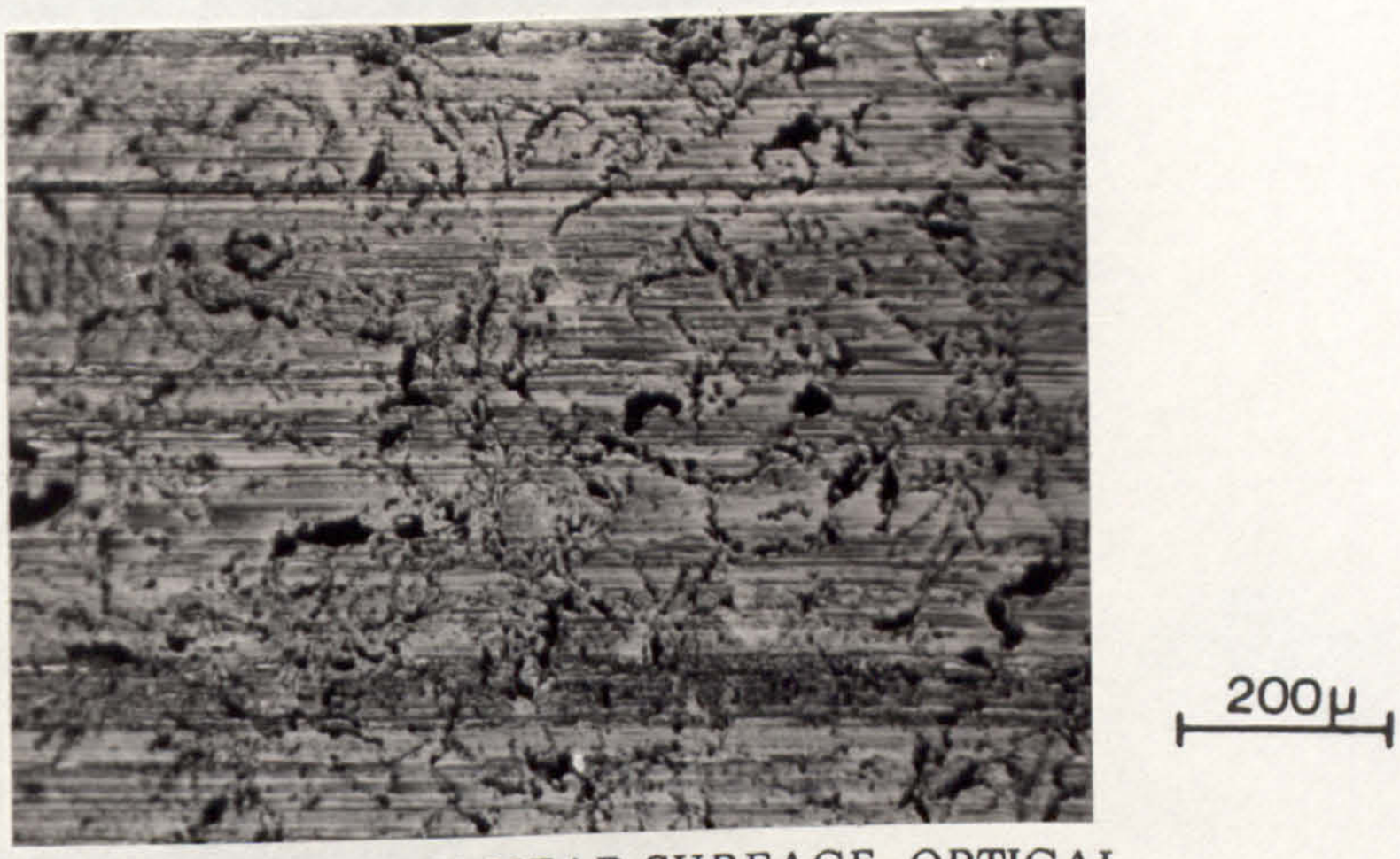

FIG. 85. TEST 11, CAM WEAR SURFACE, OPTICAL.

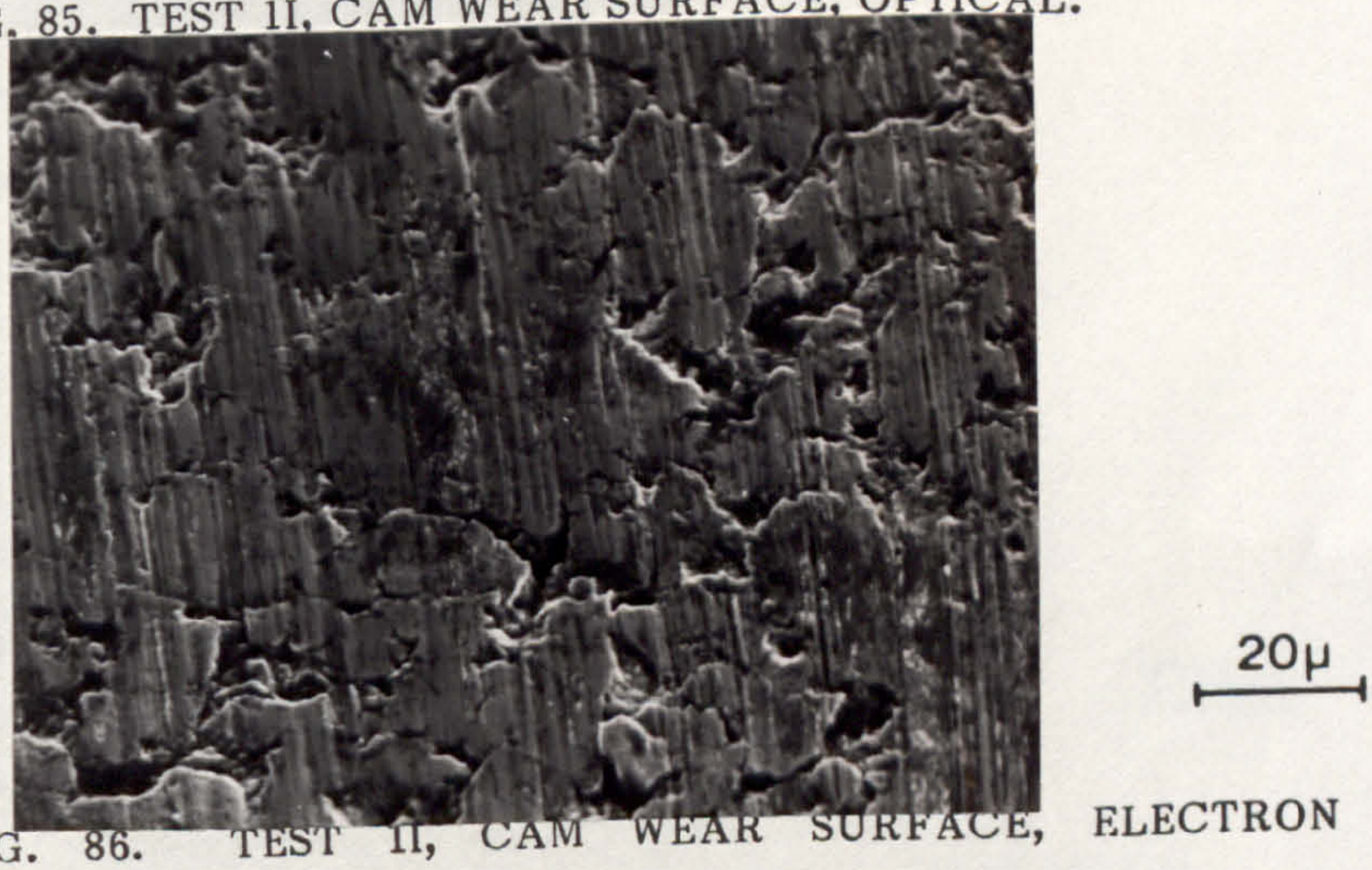

FIG. 86. TEST 11, CAM WEAR SURFACE, ELECTRON MICROGRAPH.

FIG. 87. TEST 11, FOLLOWER WEAR SURFACE, ELECTRON MICROGRAPH.

FIG. 88. TEST 1I, CAM SPECIMEN TAPERSECTION.

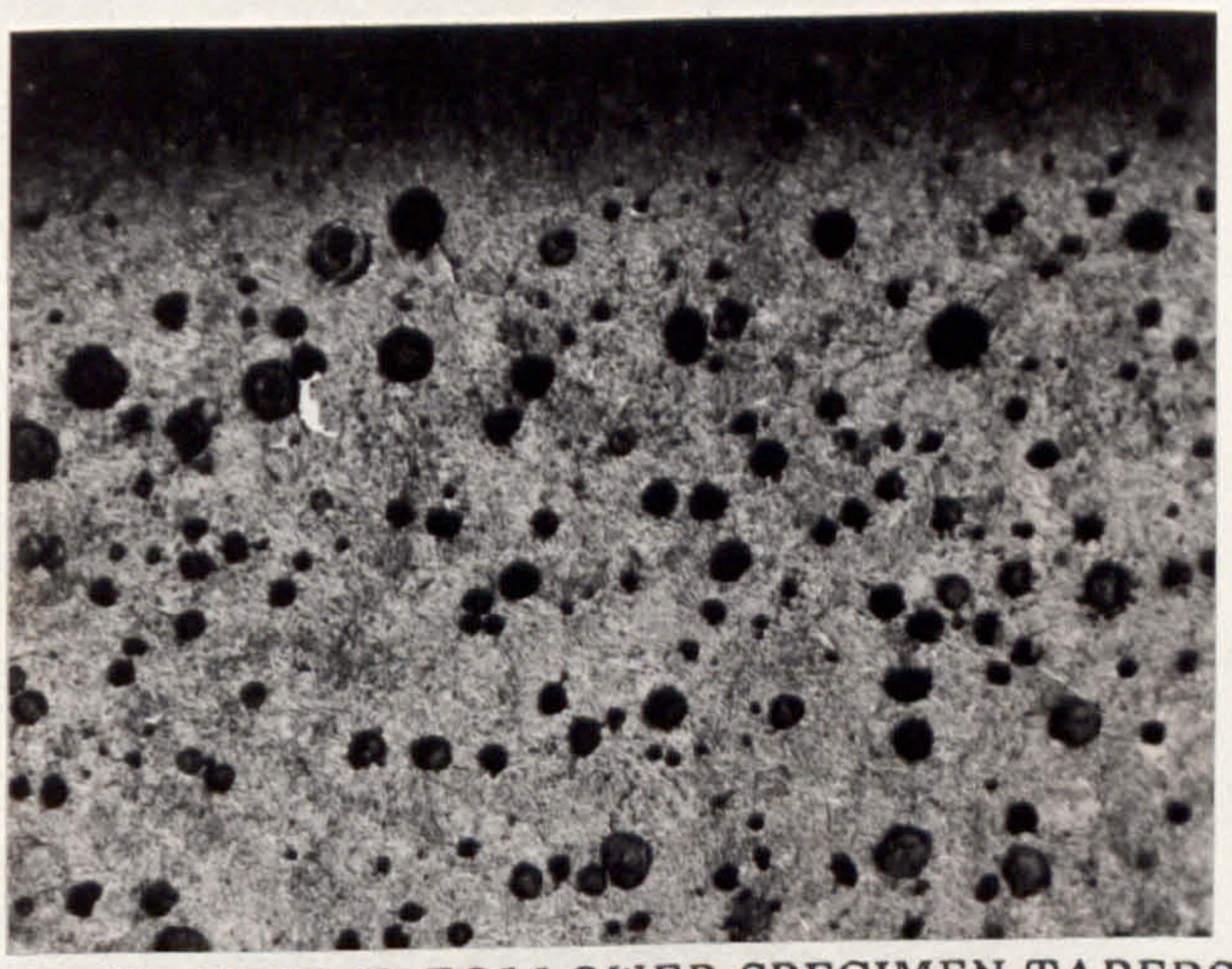

FIG. 89. TEST 1I, FOLLOWER SPECIMEN TAPERSECTION.

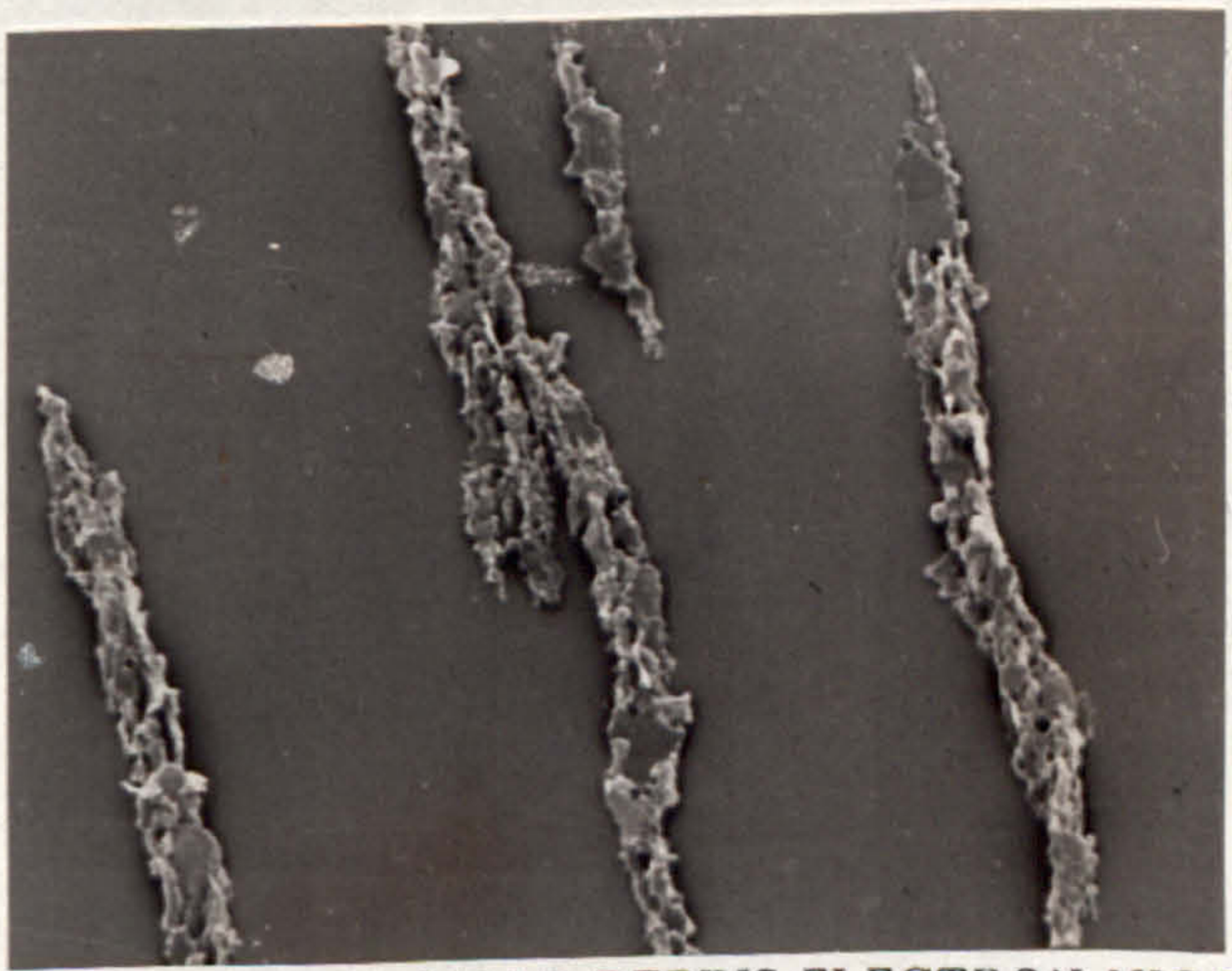

FIG. 90. TEST 1I, WEAR DEBRIS ELECTRON MICROGRAPH.

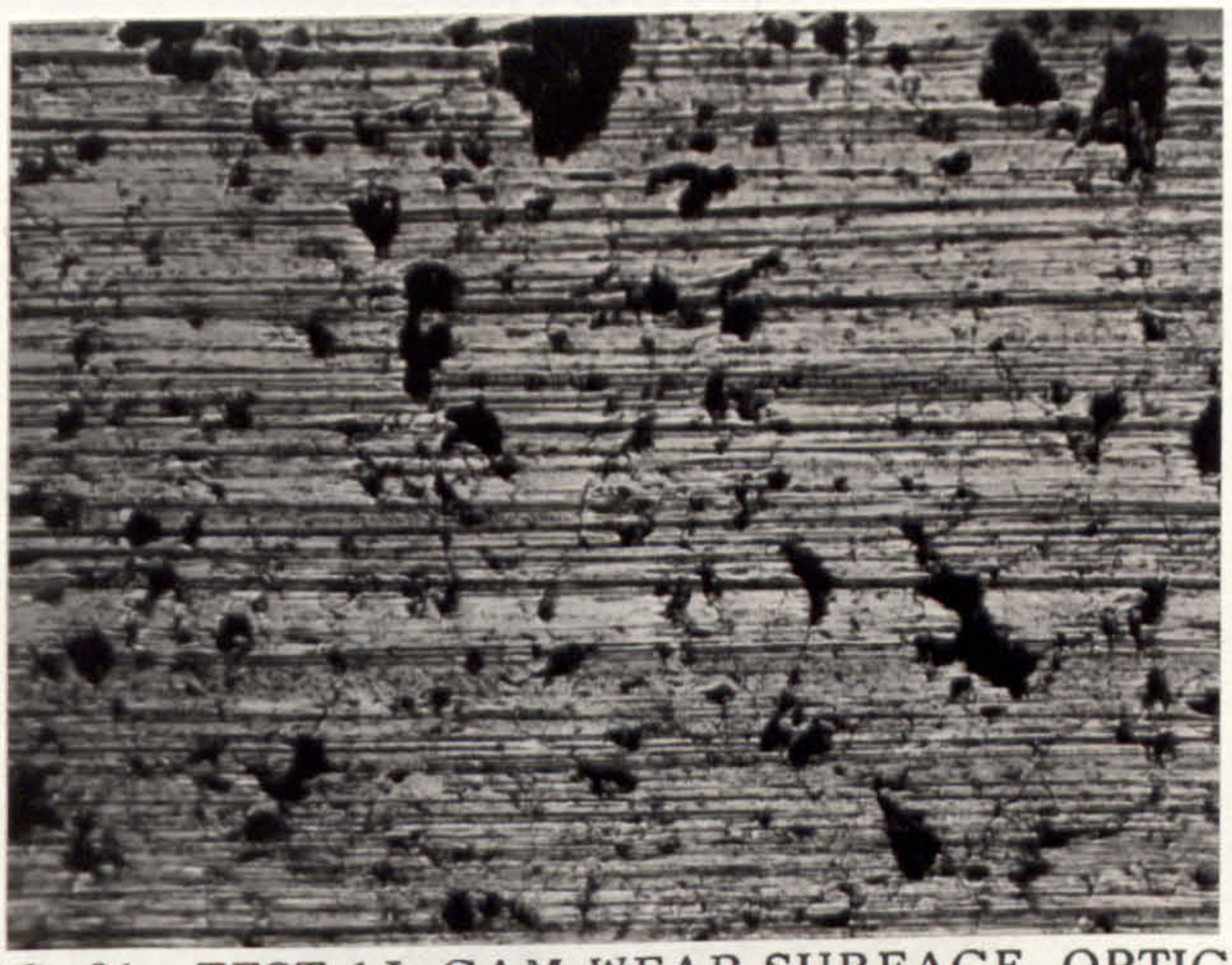

FIG. 91. TEST 1J, CAM WEAR SURFACE, OPTICAL.

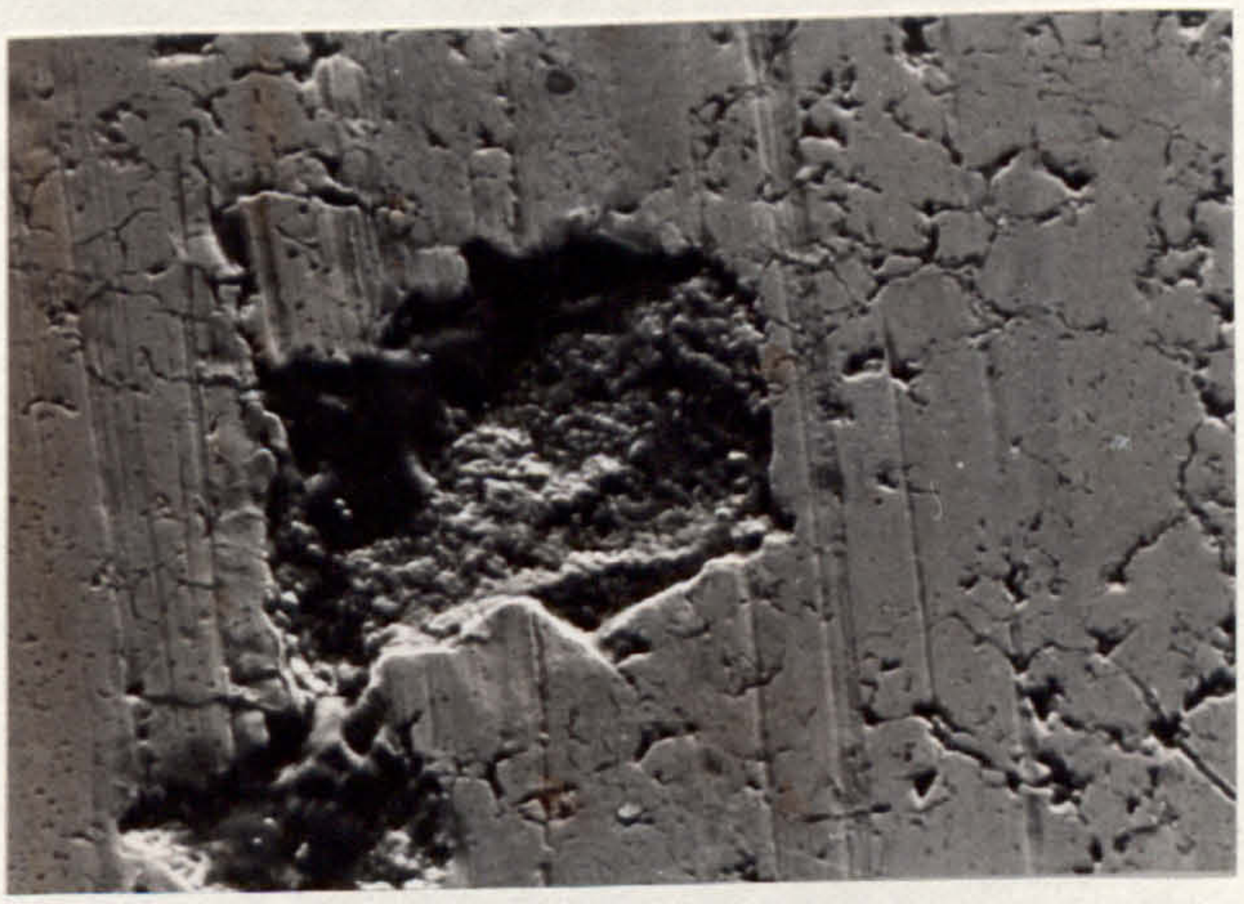

FIG. 92. TEST 1J, CAM WEAR SURFACE, ELECTRON MICROGRAPH.

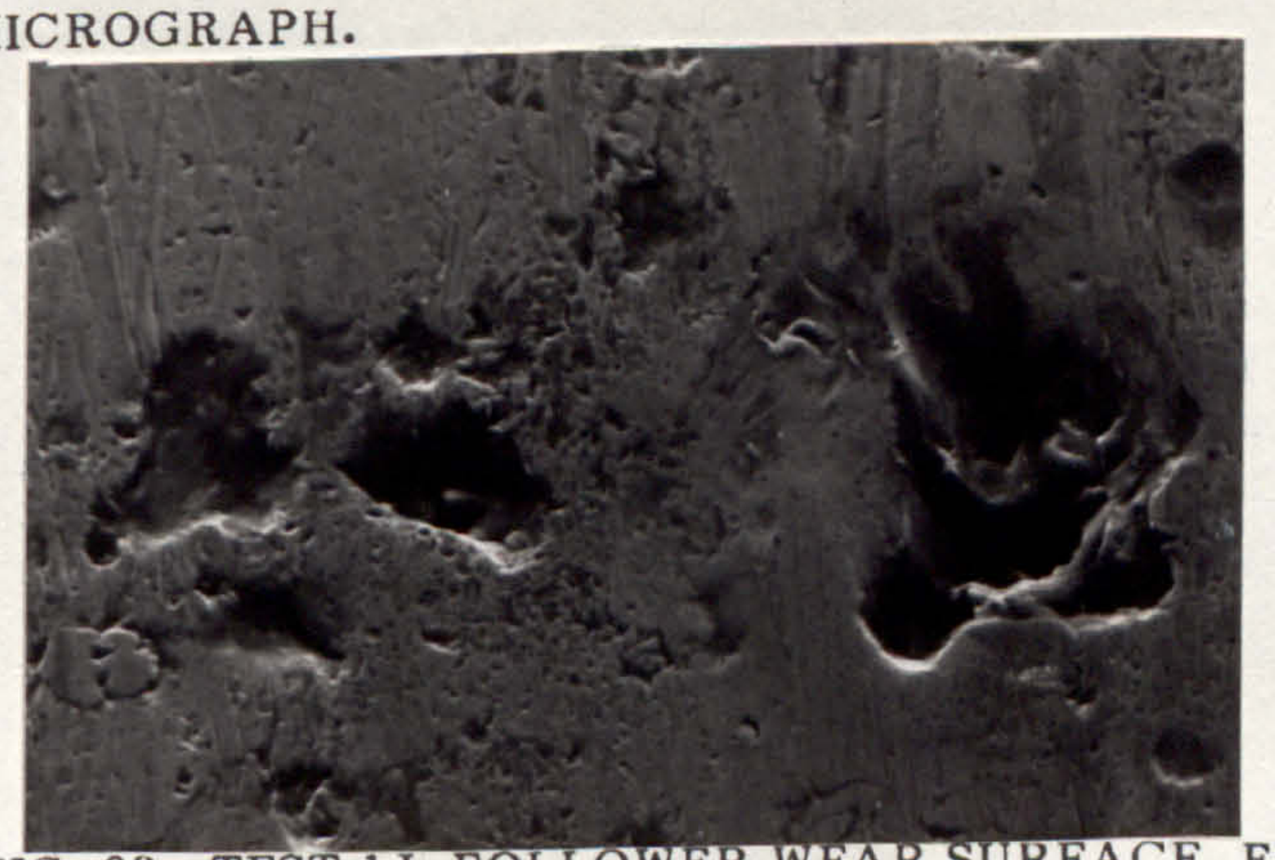

FIG. 93. TEST 1J, FOLLOWER WEAR SURFACE, ELECTRON MICROGRAPH.

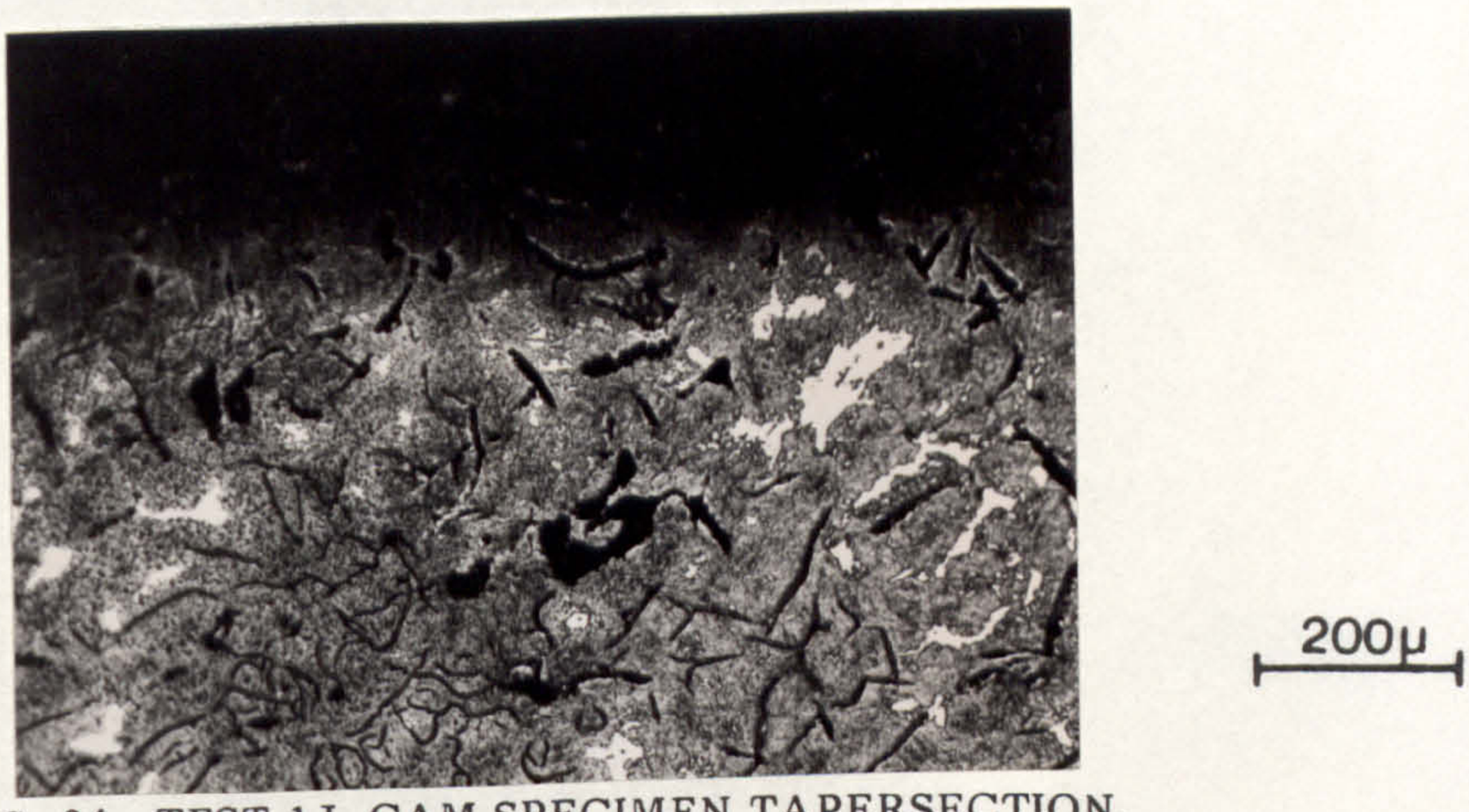

FIG. 94. TEST 1J, CAM SPECIMEN TAPERSECTION.

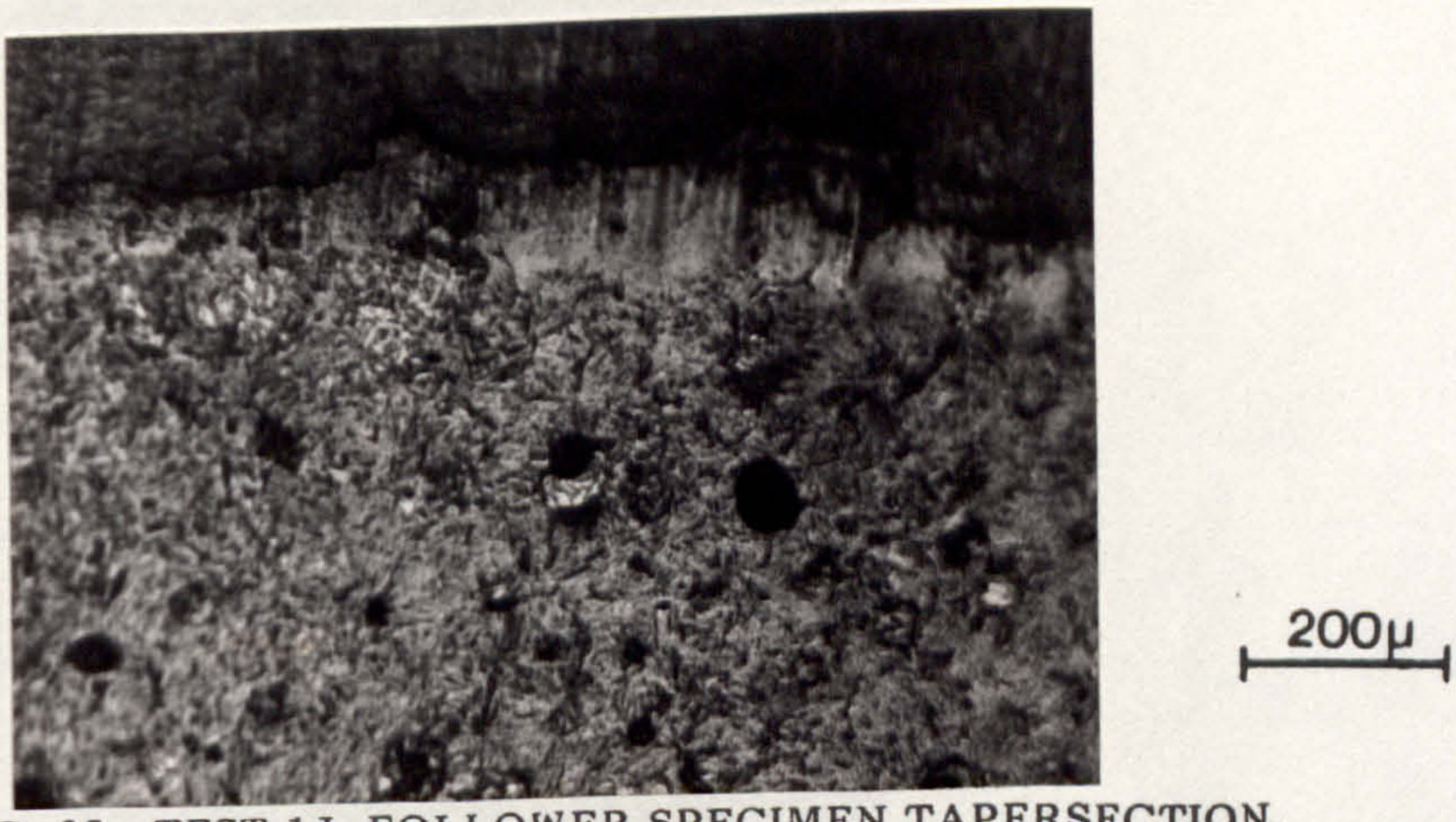

FIG. 95. TEST 1J, FOLLOWER SPECIMEN TAPERSECTION.

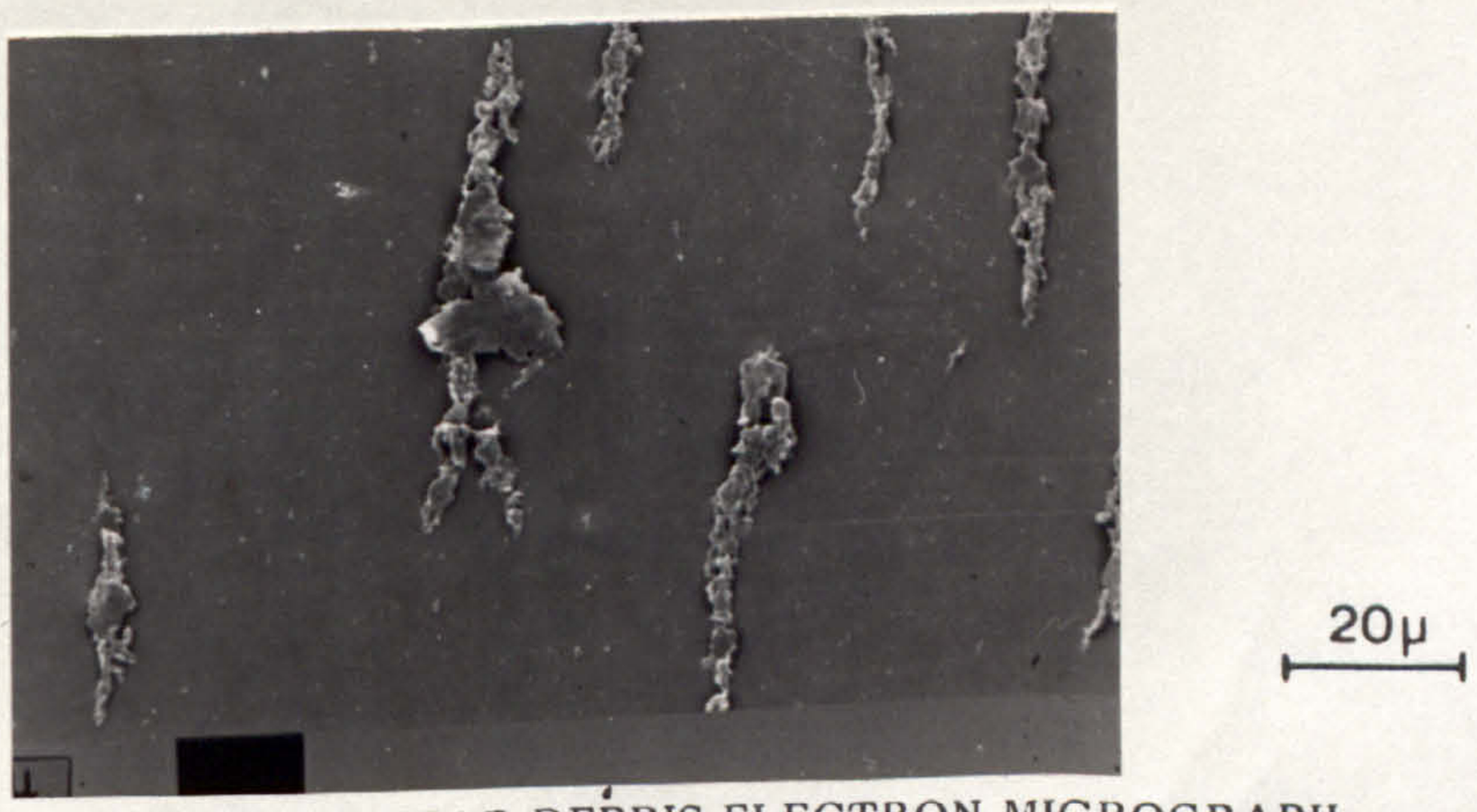

FIG. 96. TEST 1J, WEAR DEBRIS ELECTRON MICROGRAPH.

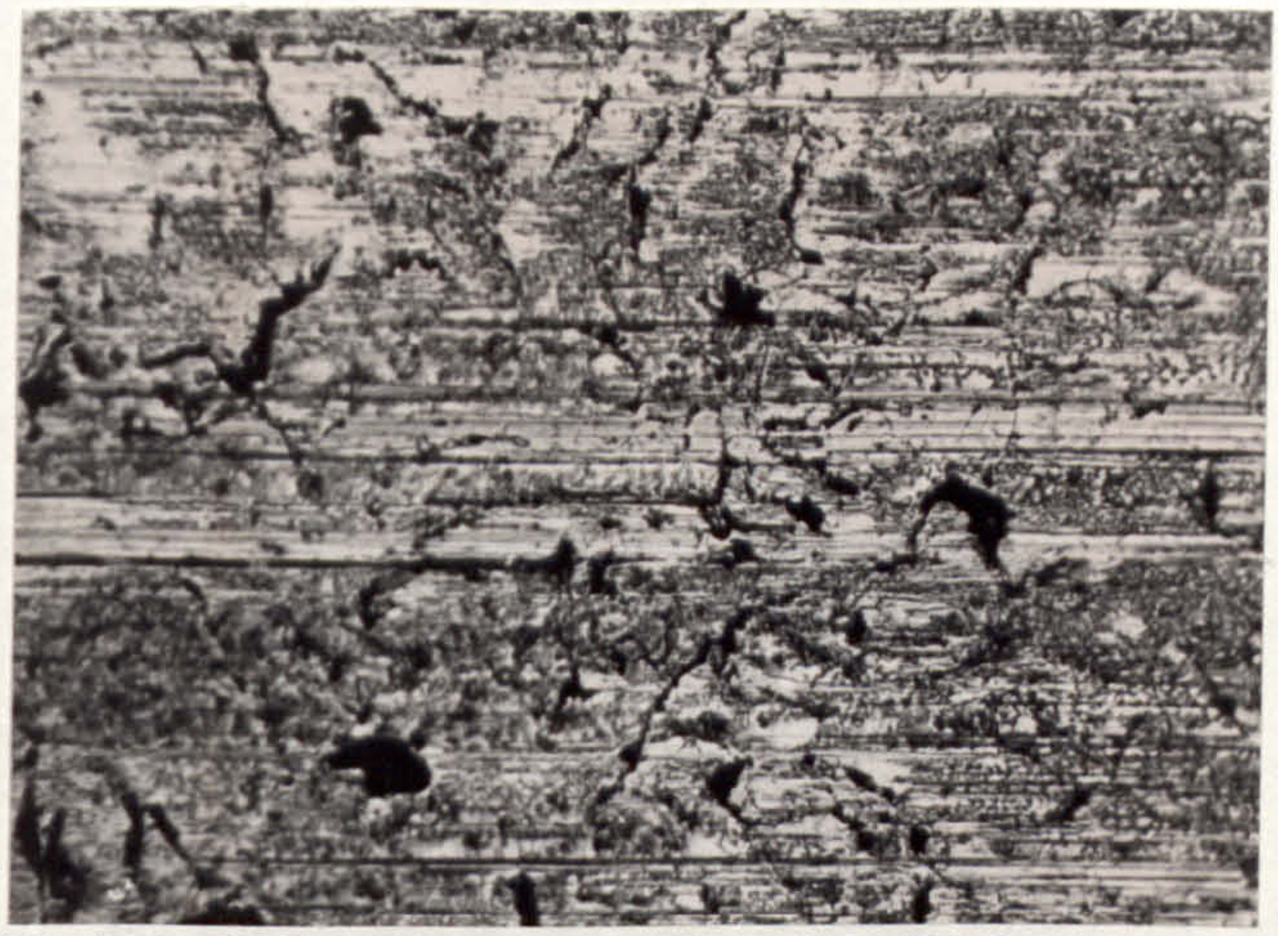

FIG. 97. TEST 1K, CAM WEAR SURFACE, OPTICAL.

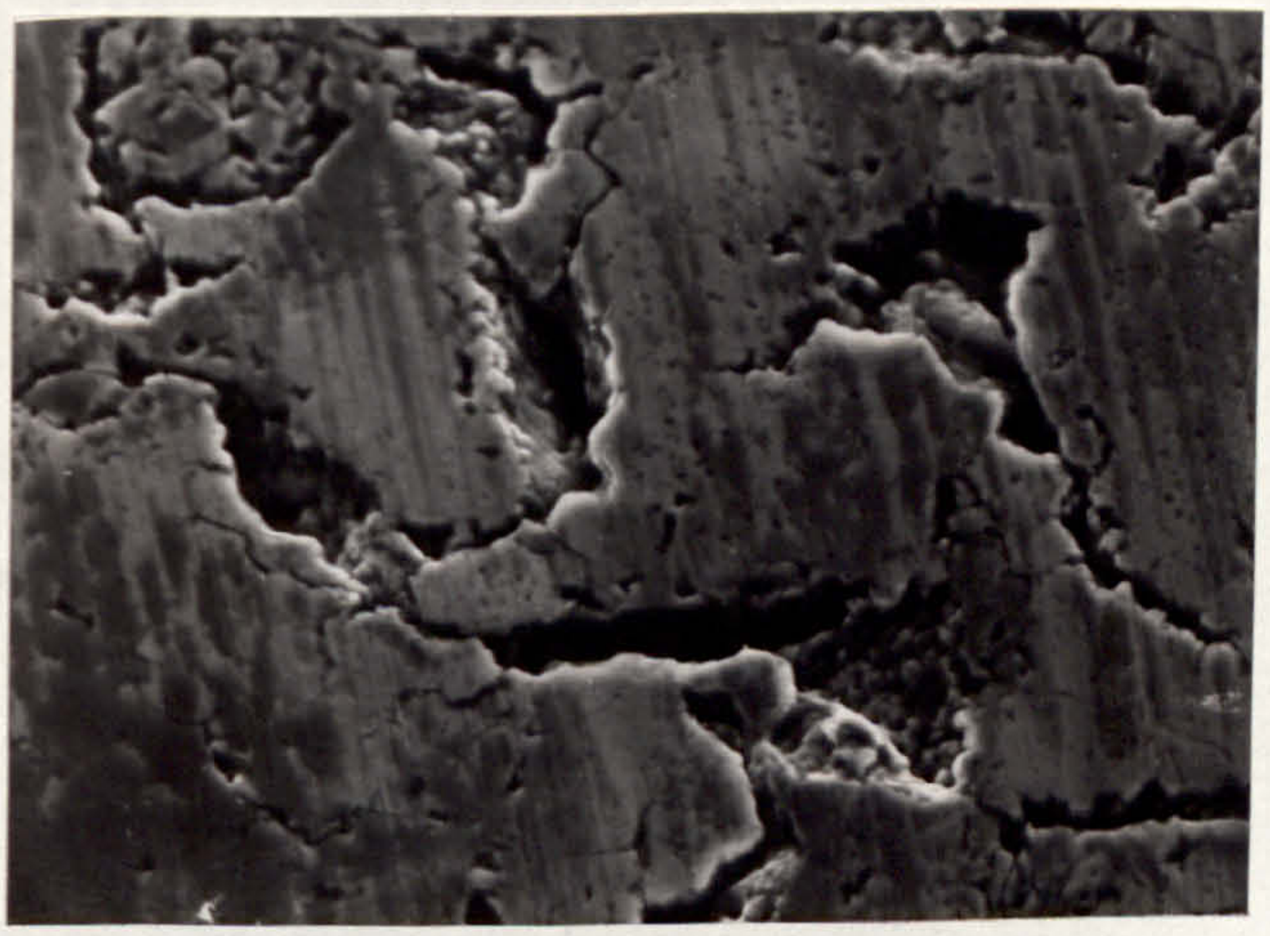

FIG. 98. TEST 1K, CAM WEAR SURFACE, ELECTRON MICROGRAPH.

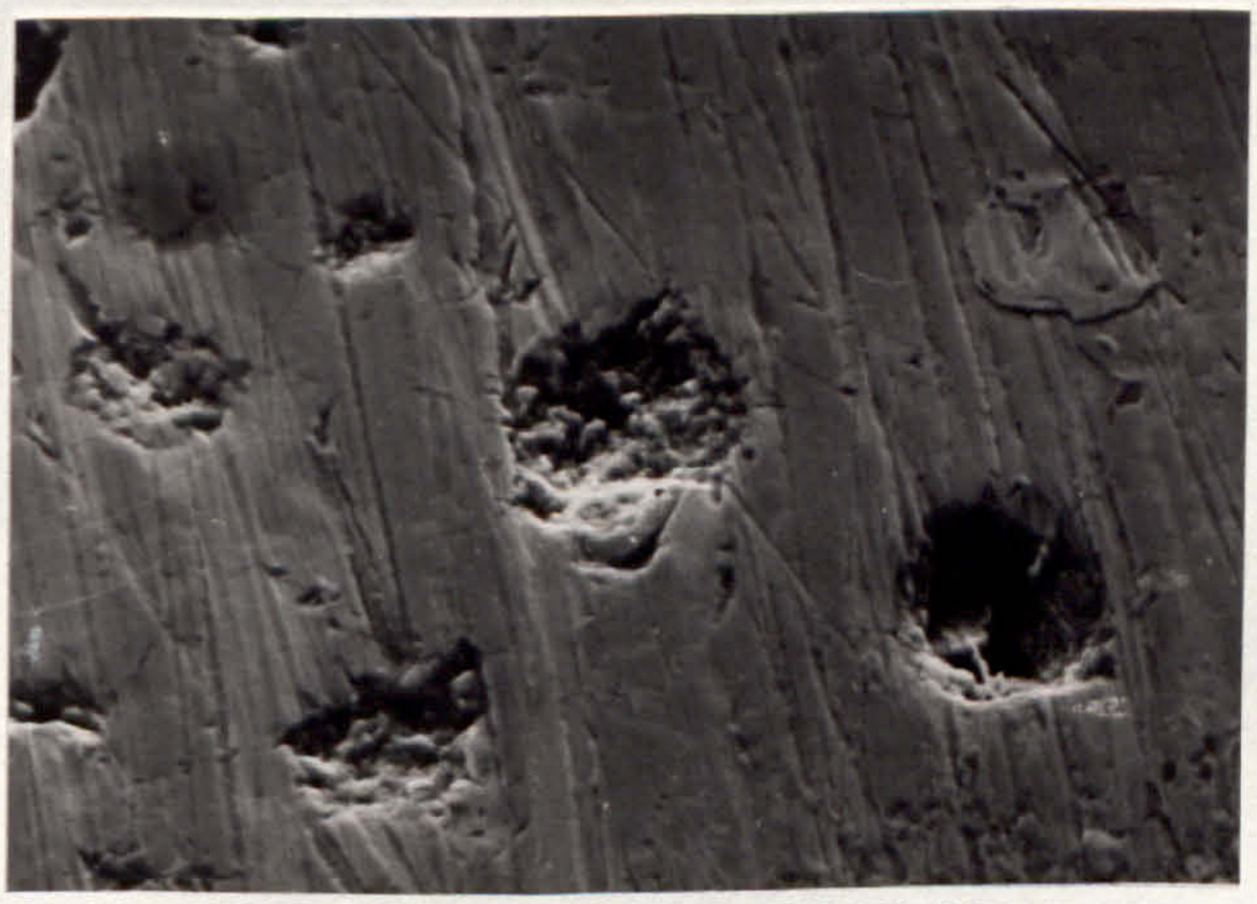

FIG. 99. TEST 1K, FOLLOWER WEAR SURFACE, ELECTRON MICROGRAPH.

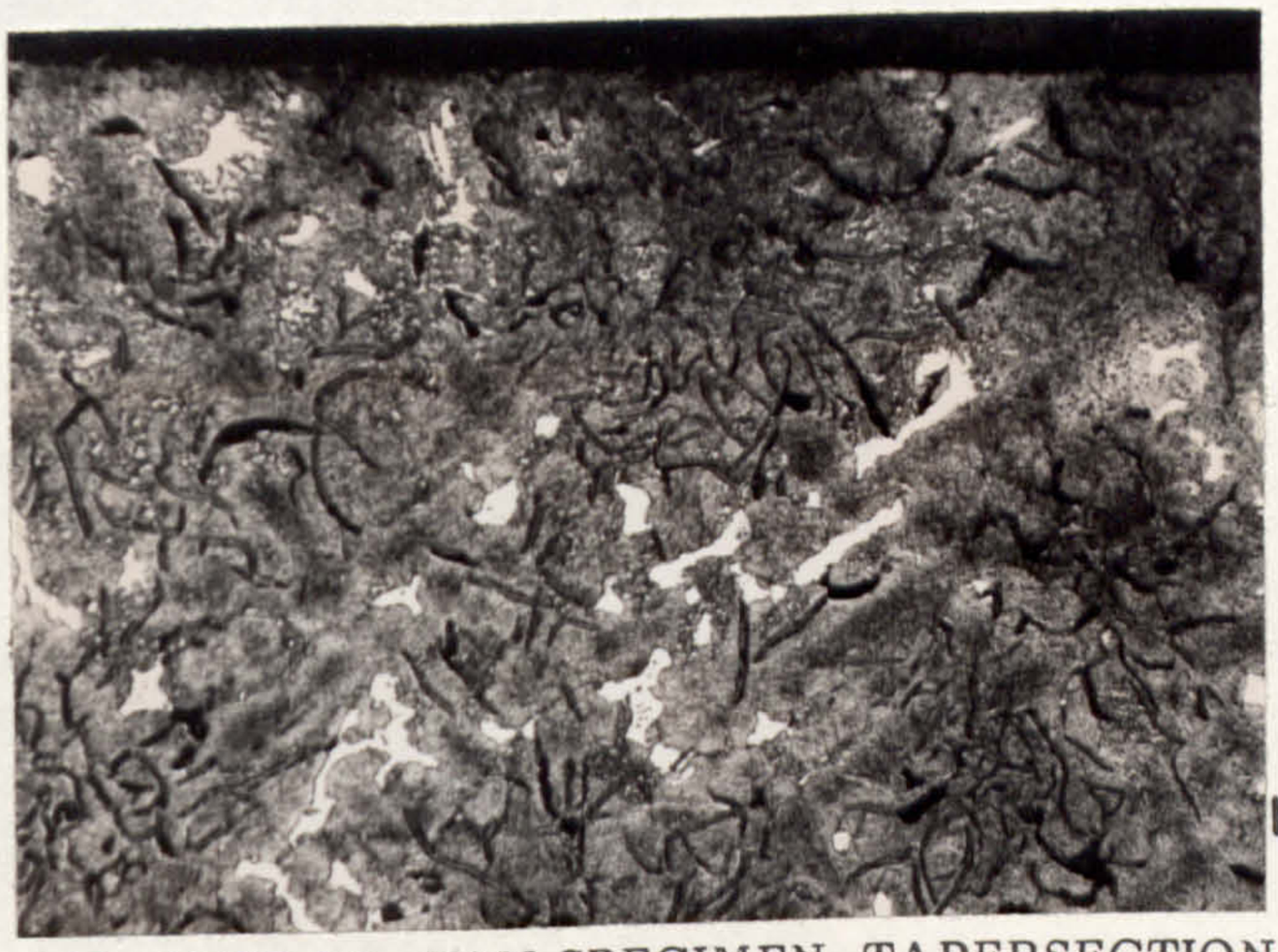

FIG. 100. TEST 1K, CAM SPECIMEN, TAPERSECTION.

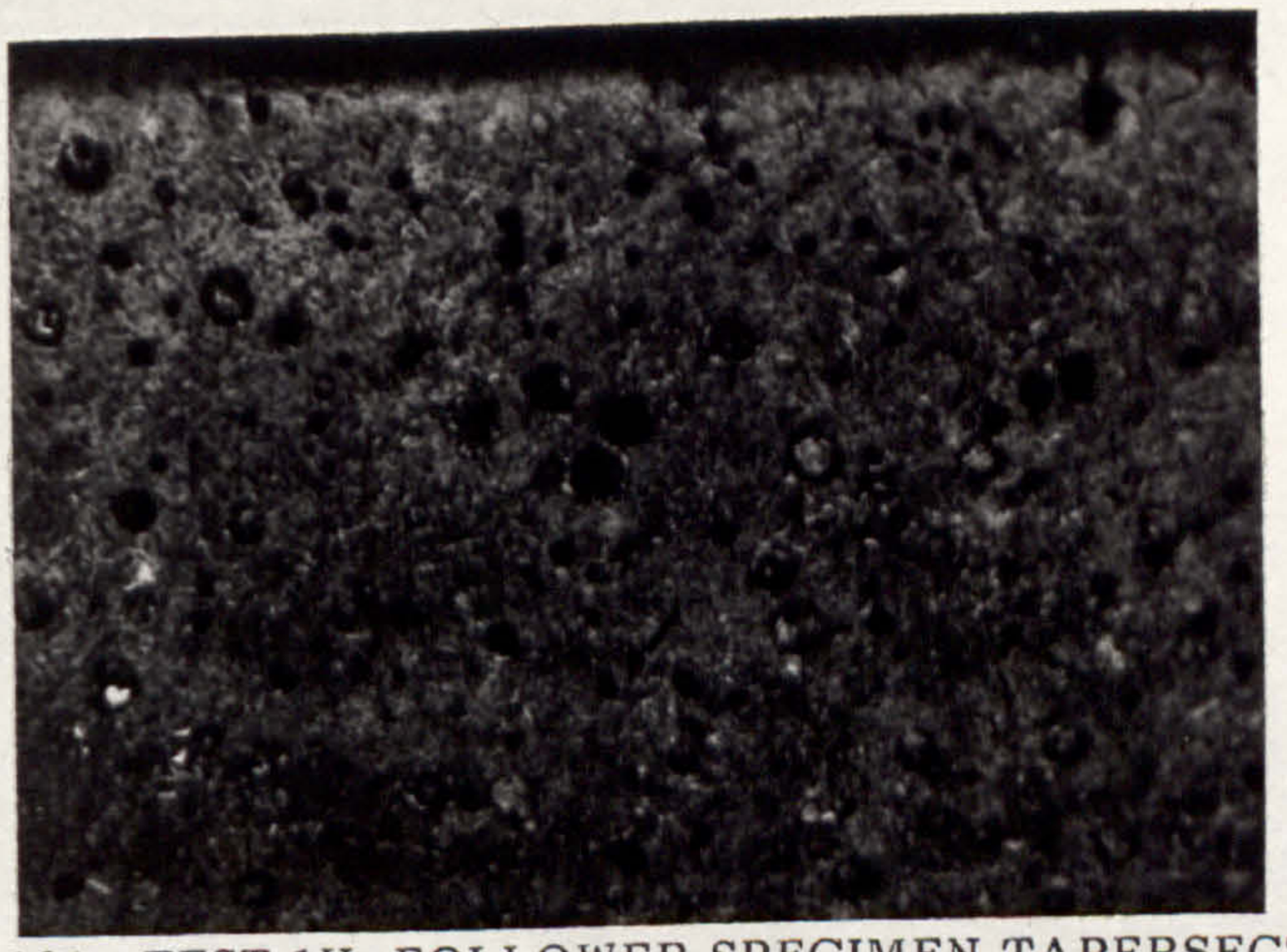

FIG. 101. TEST 1K, FOLLOWER SPECIMEN TAPERSECTION.

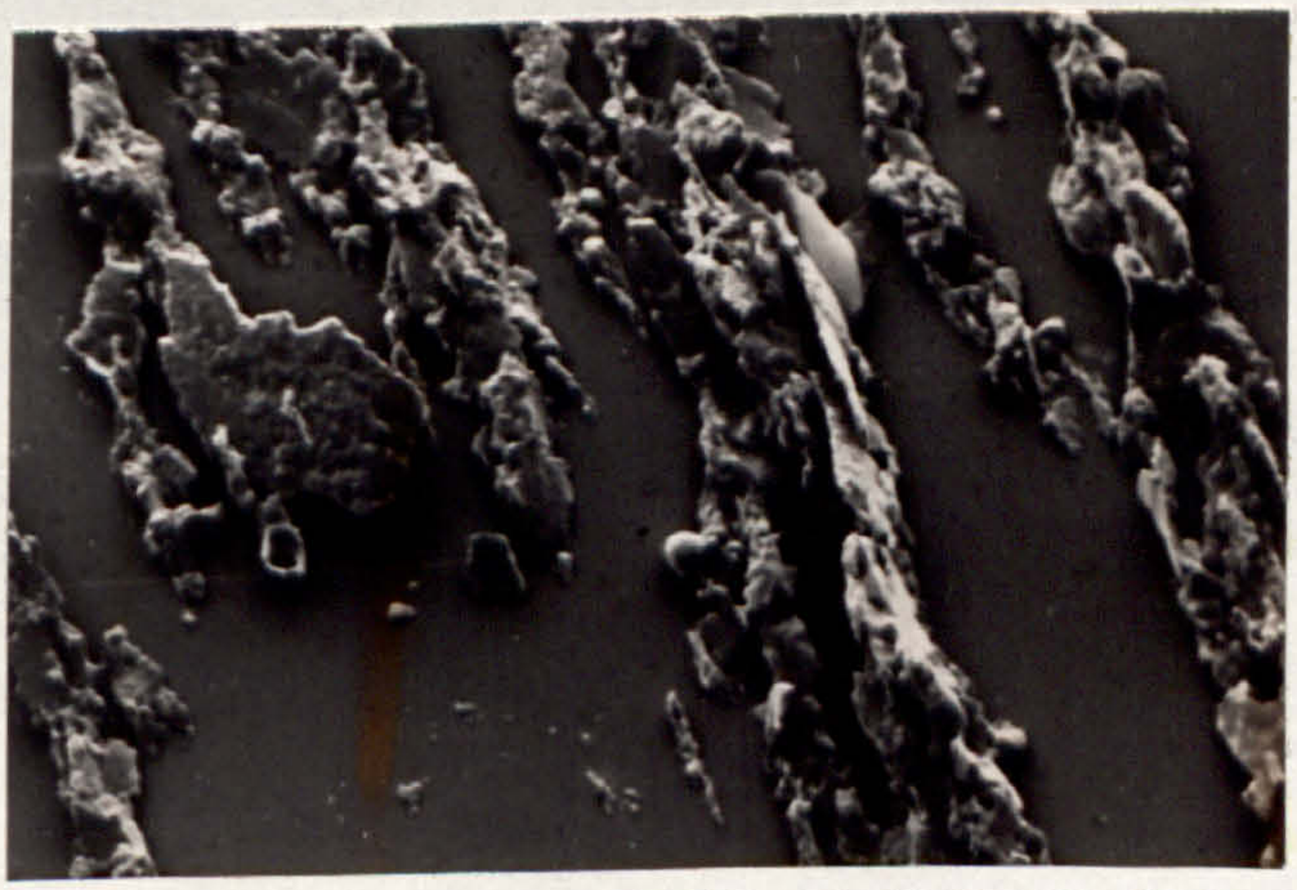

FIG. 102. TEST 1K, WEAR DEBRIS, ELECTRON MICROGRAPH.

FIG. 103. TEST 1L, CAM WEAR SURFACE, OPTICAL.

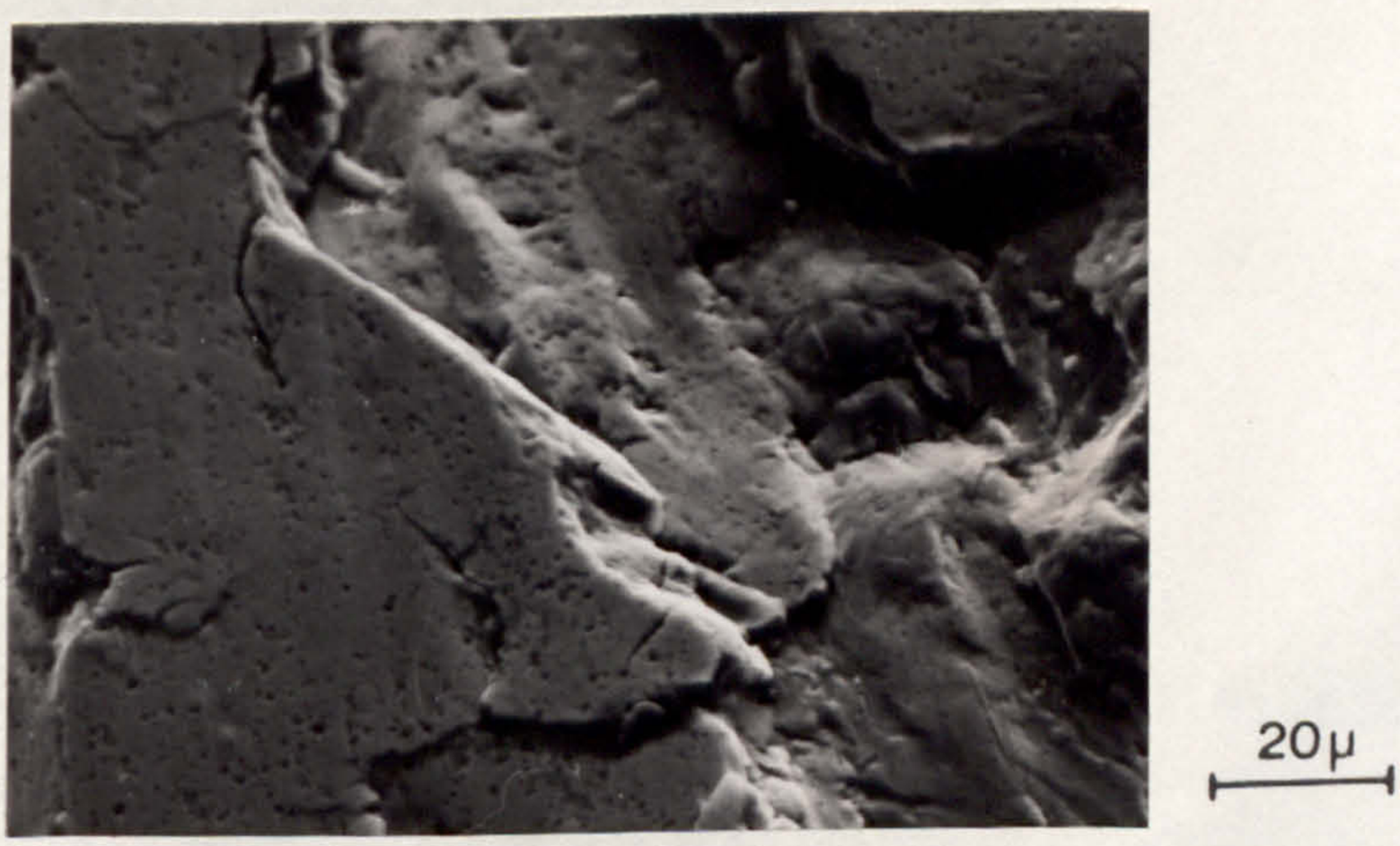

FIG. 104, TEST 1L, CAM WEAR SURFACE, ELECTRON MICROGRAPH.

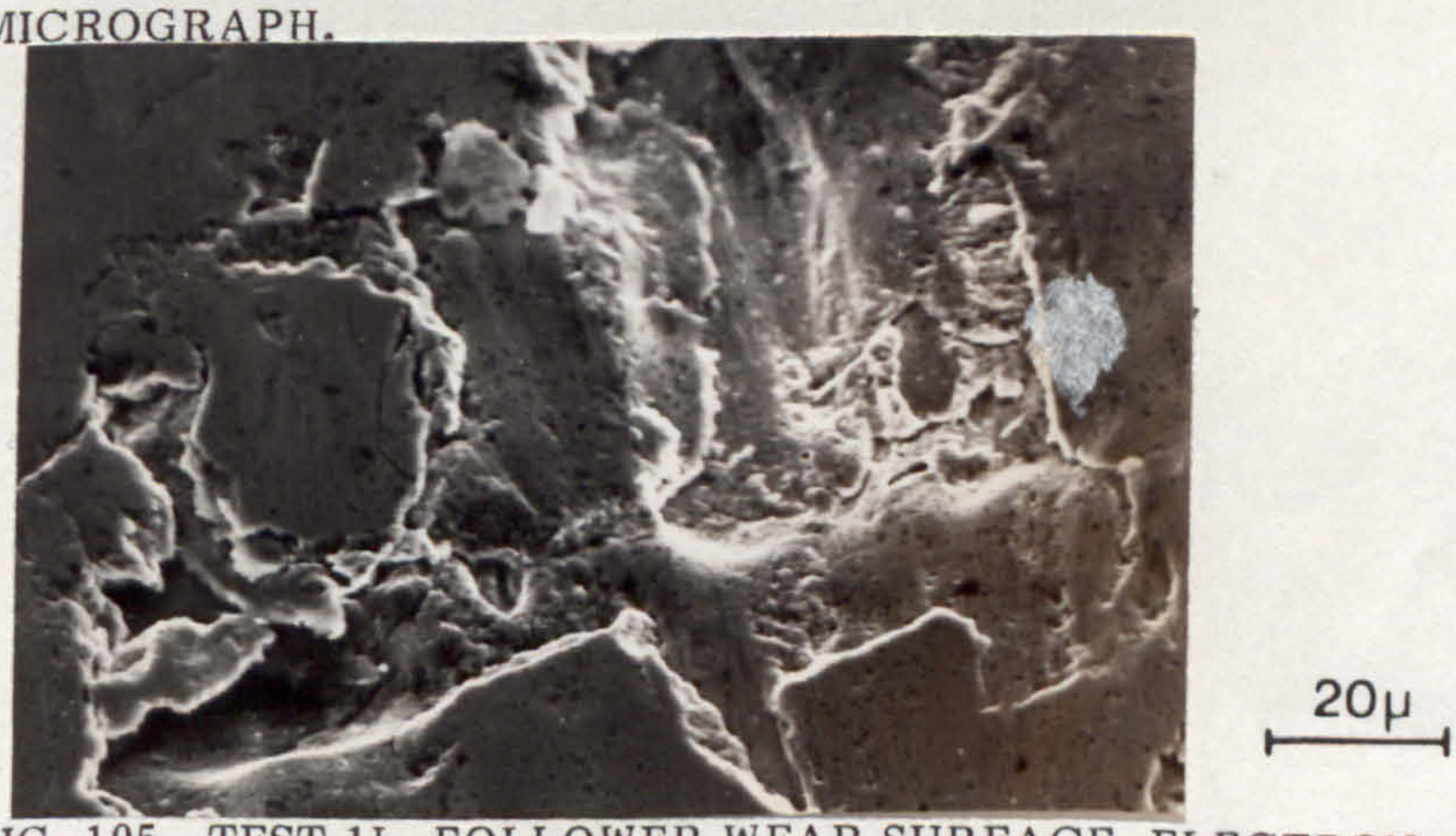

FIG. 105. TEST 1L, FOLLOWER WEAR SURFACE, ELECTRON MICROGRAPH.

FIG. 106. TEST 1L, CAM SPECIMEN TAPERSECTION.

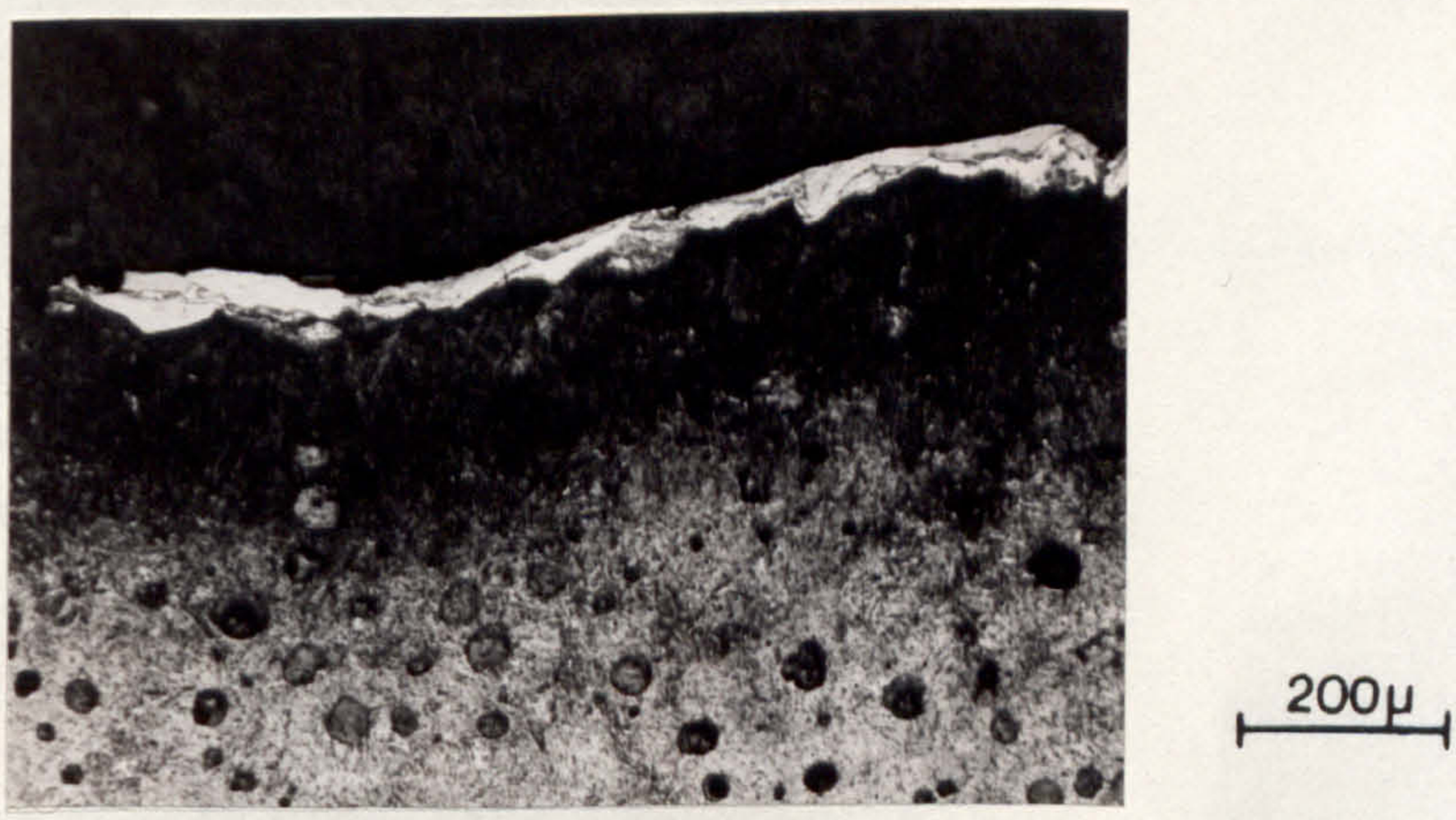

FIG. 107. TEST 1L, FOLLOWER SPECIMEN TAPERSECTION.

FIG. 108. TEST 1L, WEAR DEBRIS, ELECTRON MICROGRAPH.

AS GROUND 6μ"CLA

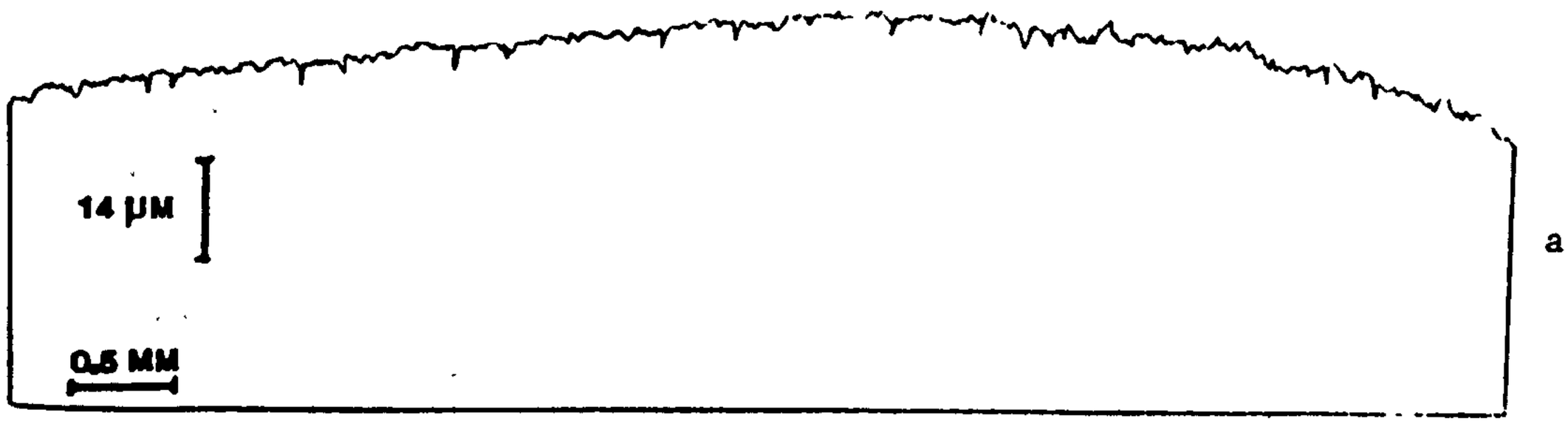

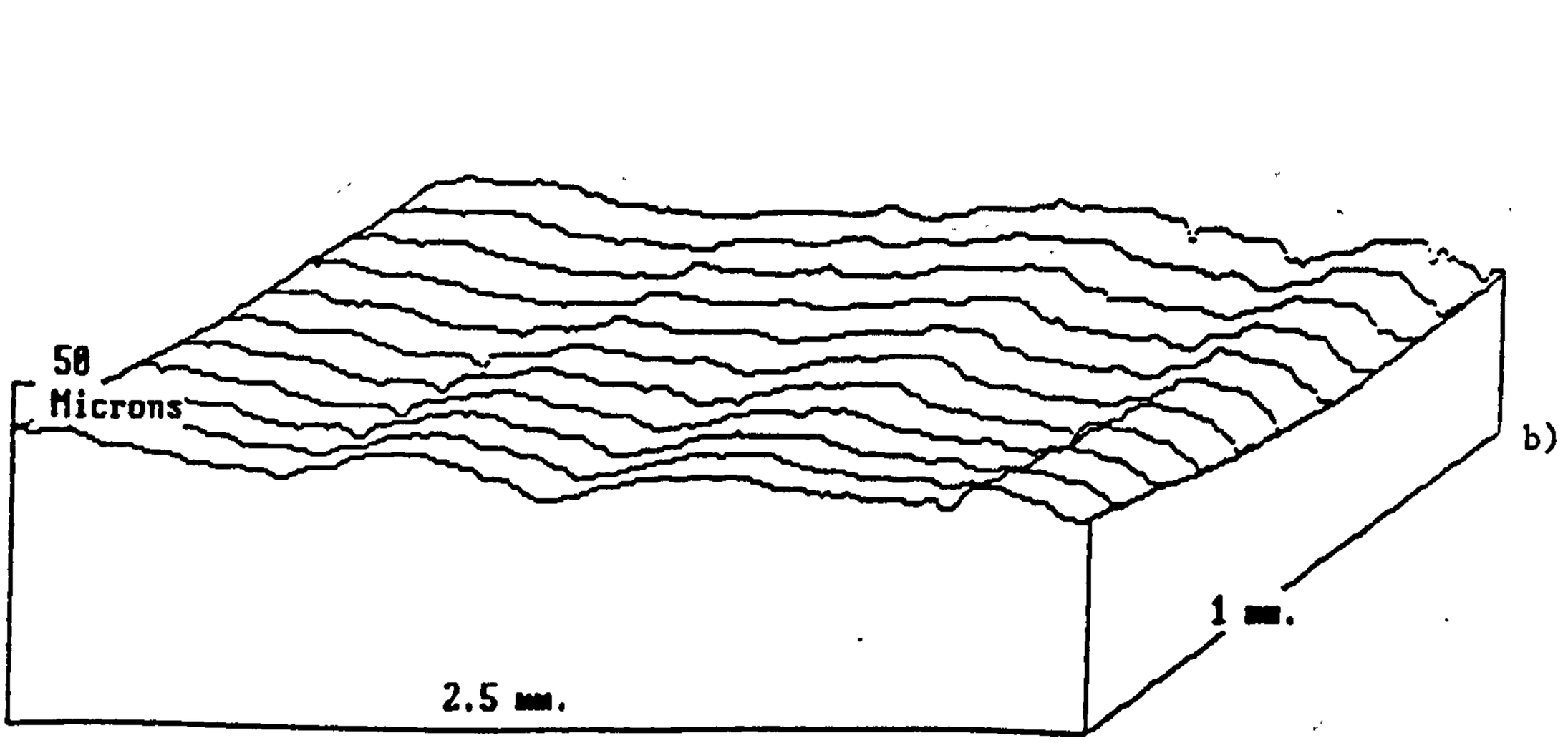

FIG. 109. COMPARISON OF SURFACE ROUGHNESS TRACES USING A CONVENTIONAL SINGLE TALYSURF TRACE. a) WITH A '3D' COMPUTORISED MULTI-TRACE. b) "AS GROUND SURFACE" (NOT TO SCALE).

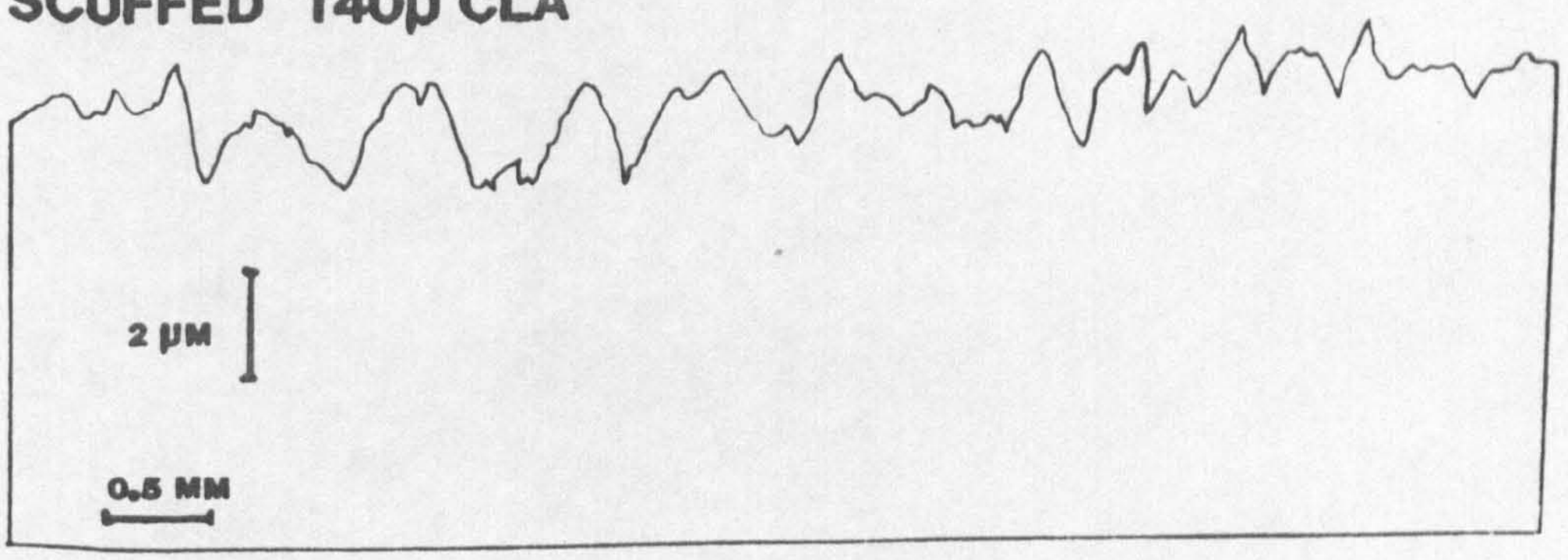

a)

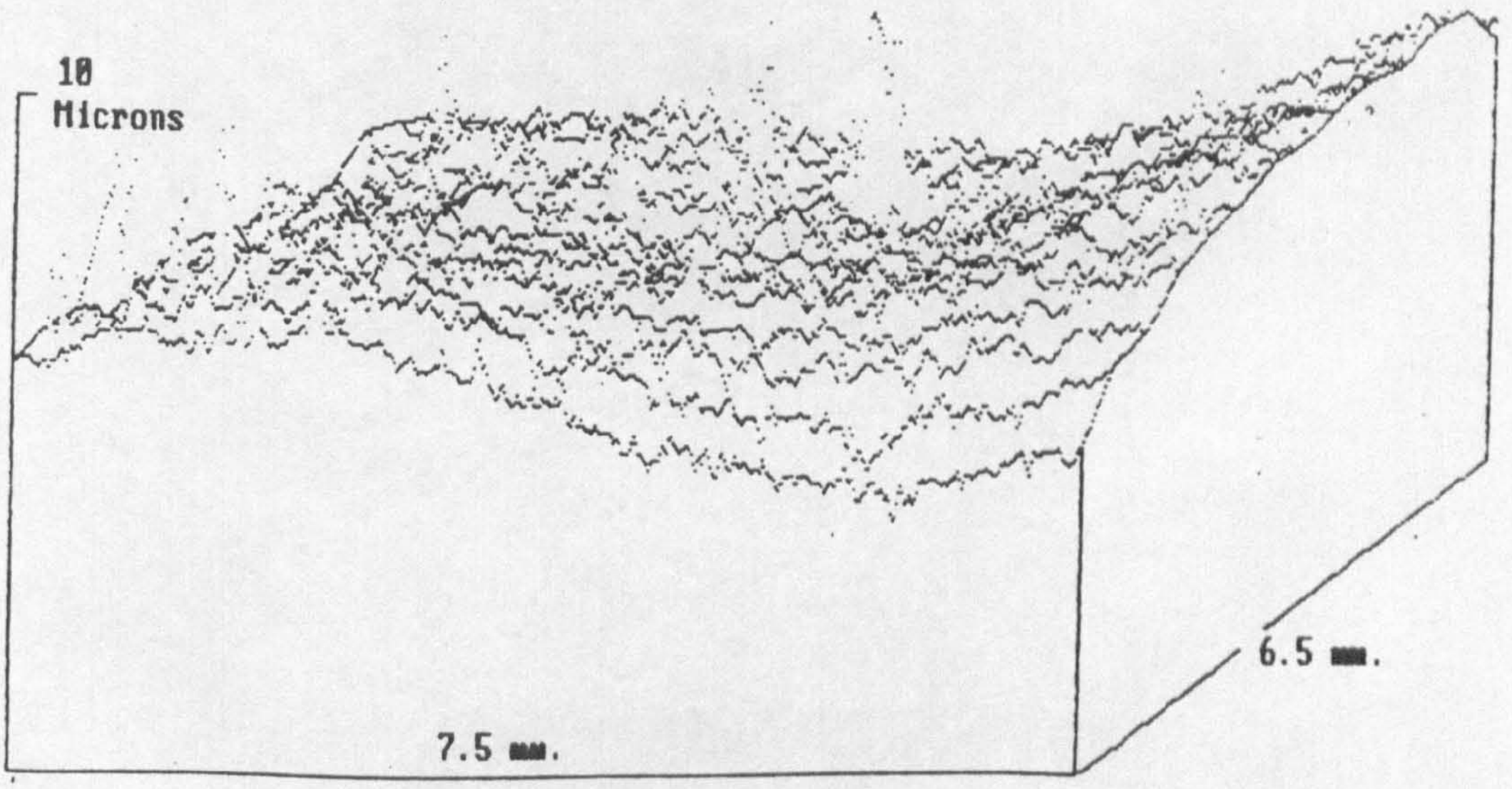

b)

FIG. 110. COMPARISON OF SURFACE ROUGHNESS TRACES USING A CONVENTIONAL SINGLE TALYSURF TRACE. a) WITH A '3D' COMPUTORISED MULTI-TRACE. b) "SCUFFED SURFACE". (NOT TO SCALE).

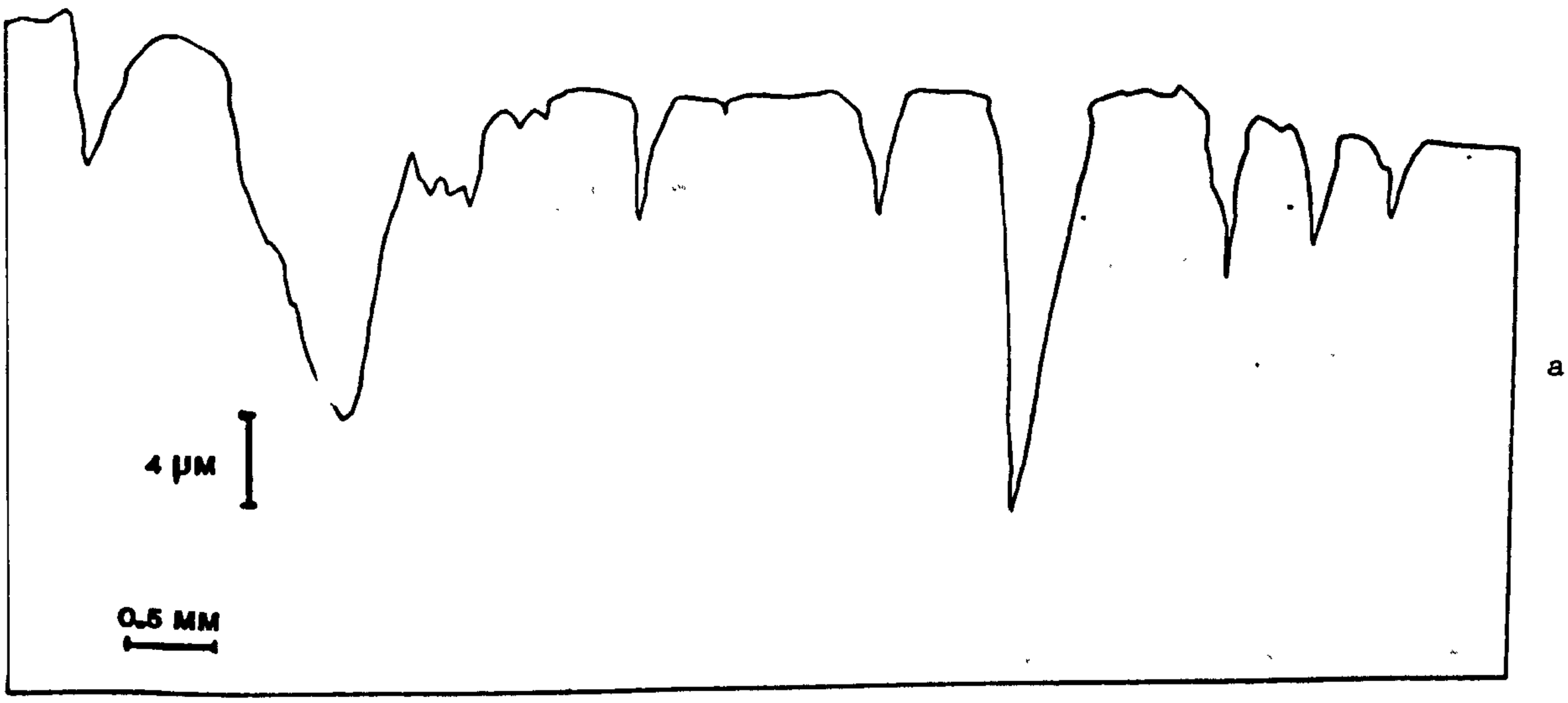

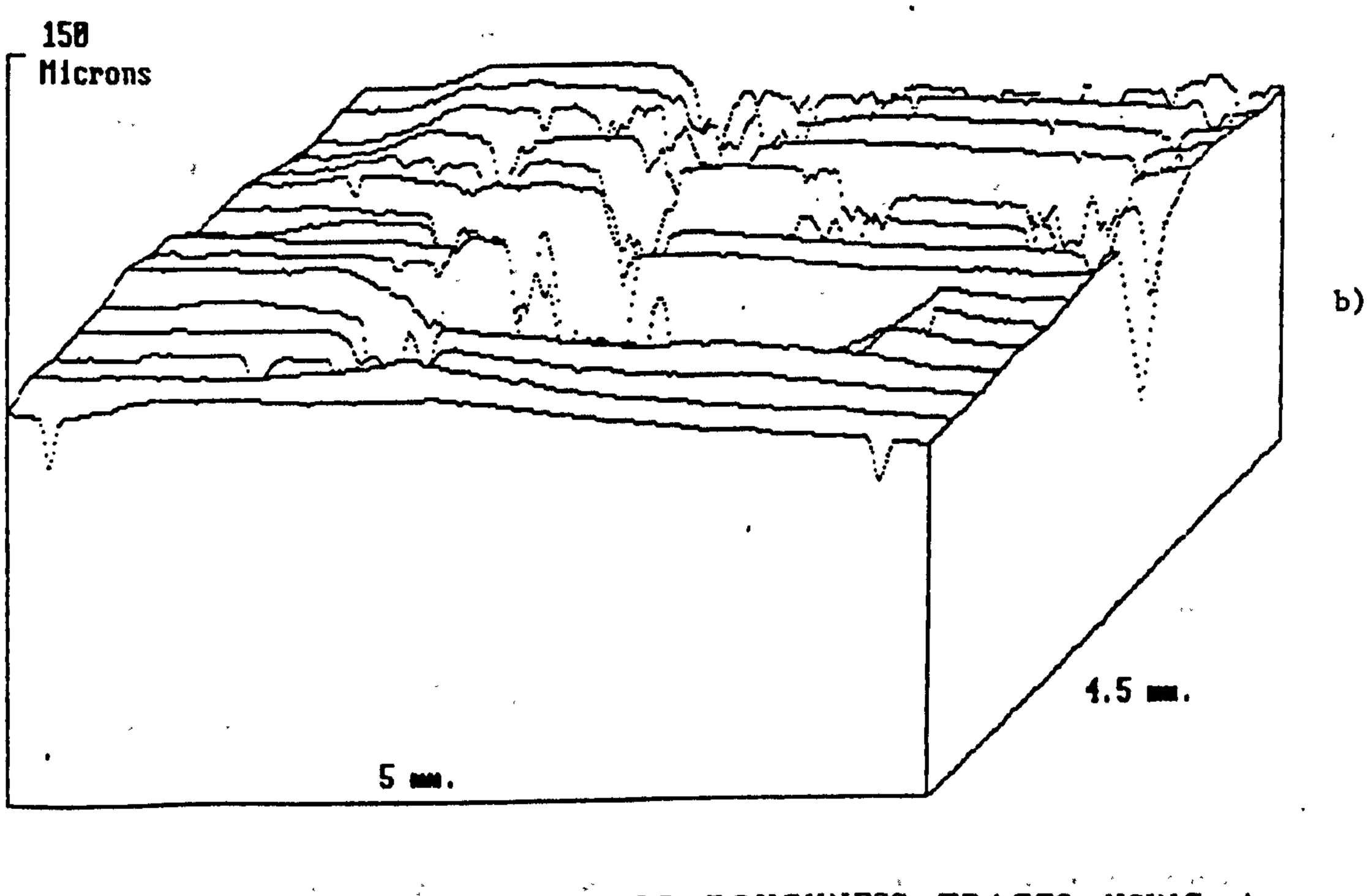

FIG. 111. COMPARISON OF SURFACE ROUGHNESS TRACES USING A CONVENTIONAL 'SINGLE' TALYSURF TRACE. a) WITH A '3D' COMPUTORISED MULTI-TRACE. b) "PITTING WEAR" (NOT TO SCALE).

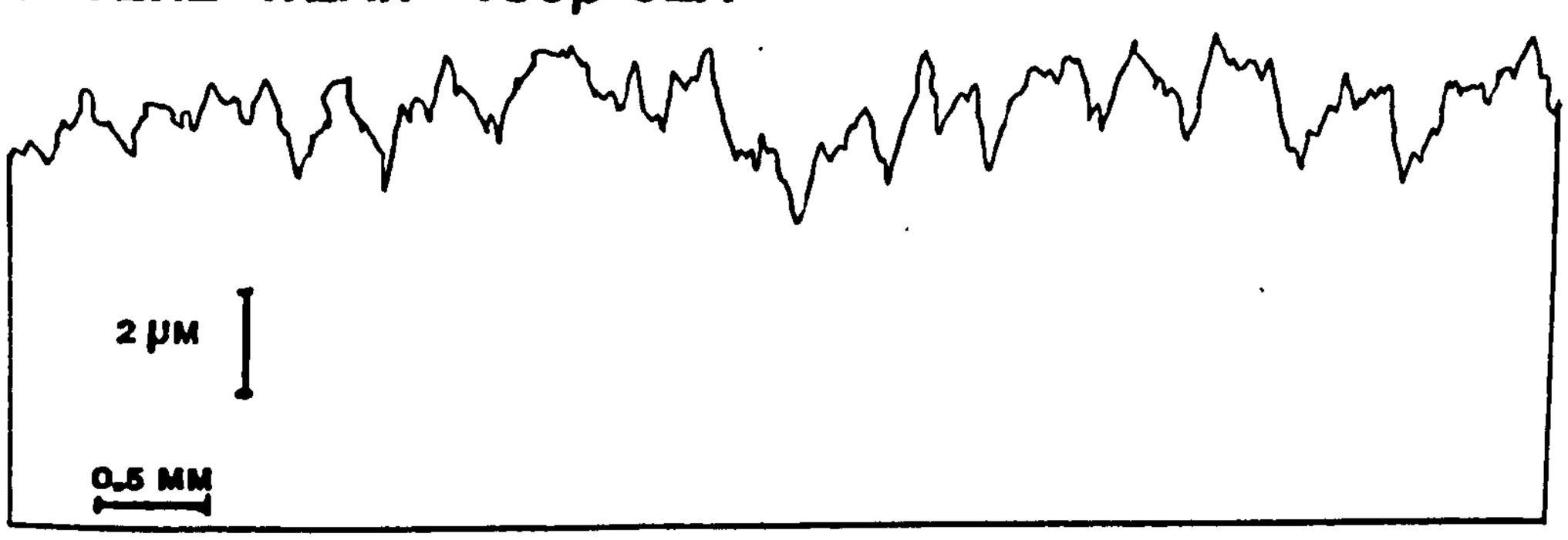

FIG. 112. COMPARISON OF SURFACE ROUGHNESS TRACES USING A CONVENTIONAL 'SINGLE TALYSURF TRACE. a) WITH A '3D' COMPUTORISED MULTI-TRACE b) "SEVERE WEAR". (NOT TO SCALE).

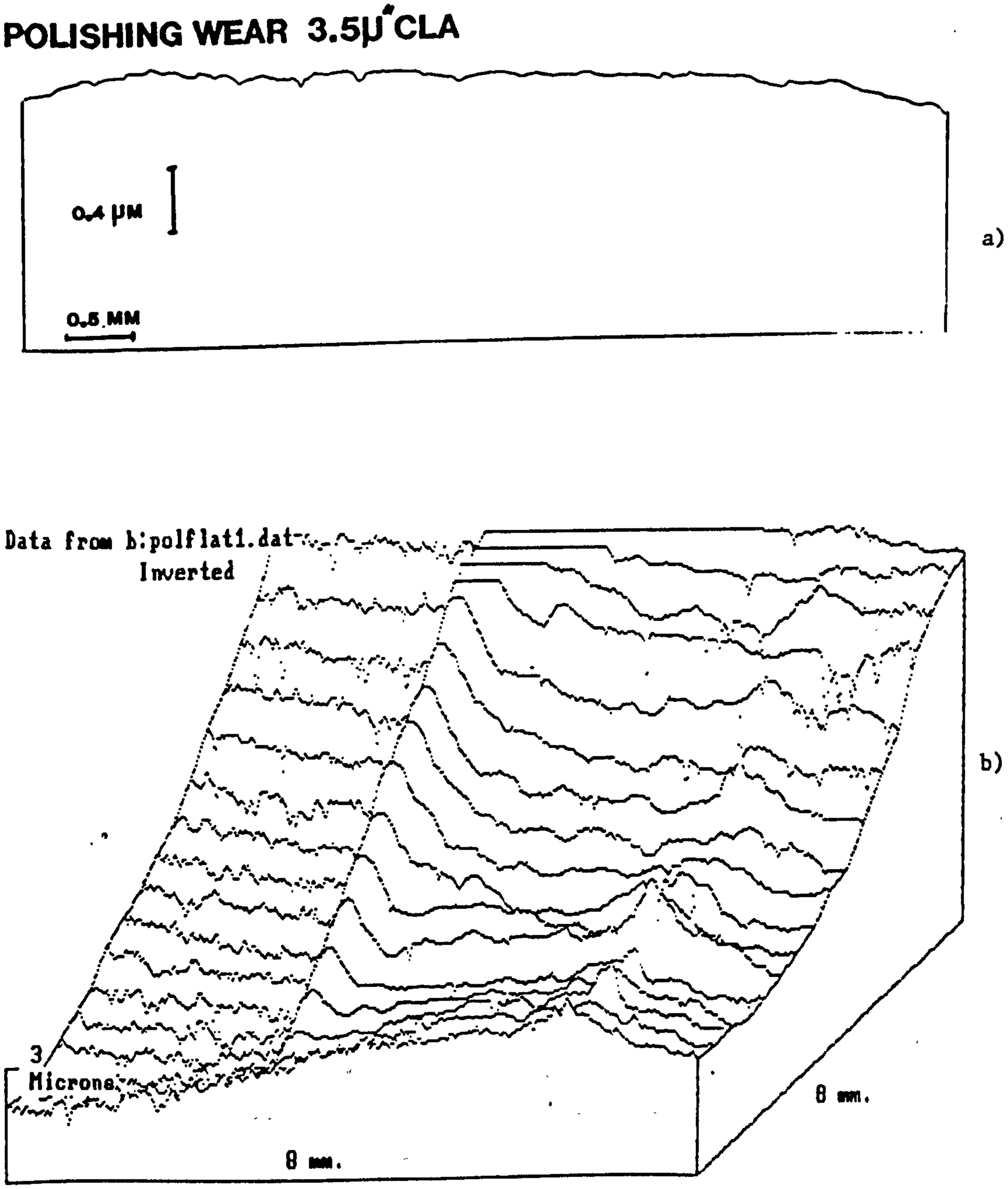

FIG. 113. COMPARISON OF SURFACE ROUGHNESS TRACES USING A CONVENTIONAL 'SINGLE TALYSURF TRACE a) WITH A '3D' COMPUTORISED MULTI-TRACE b) "POLISHING WEAR". (NOT TO SCALE).

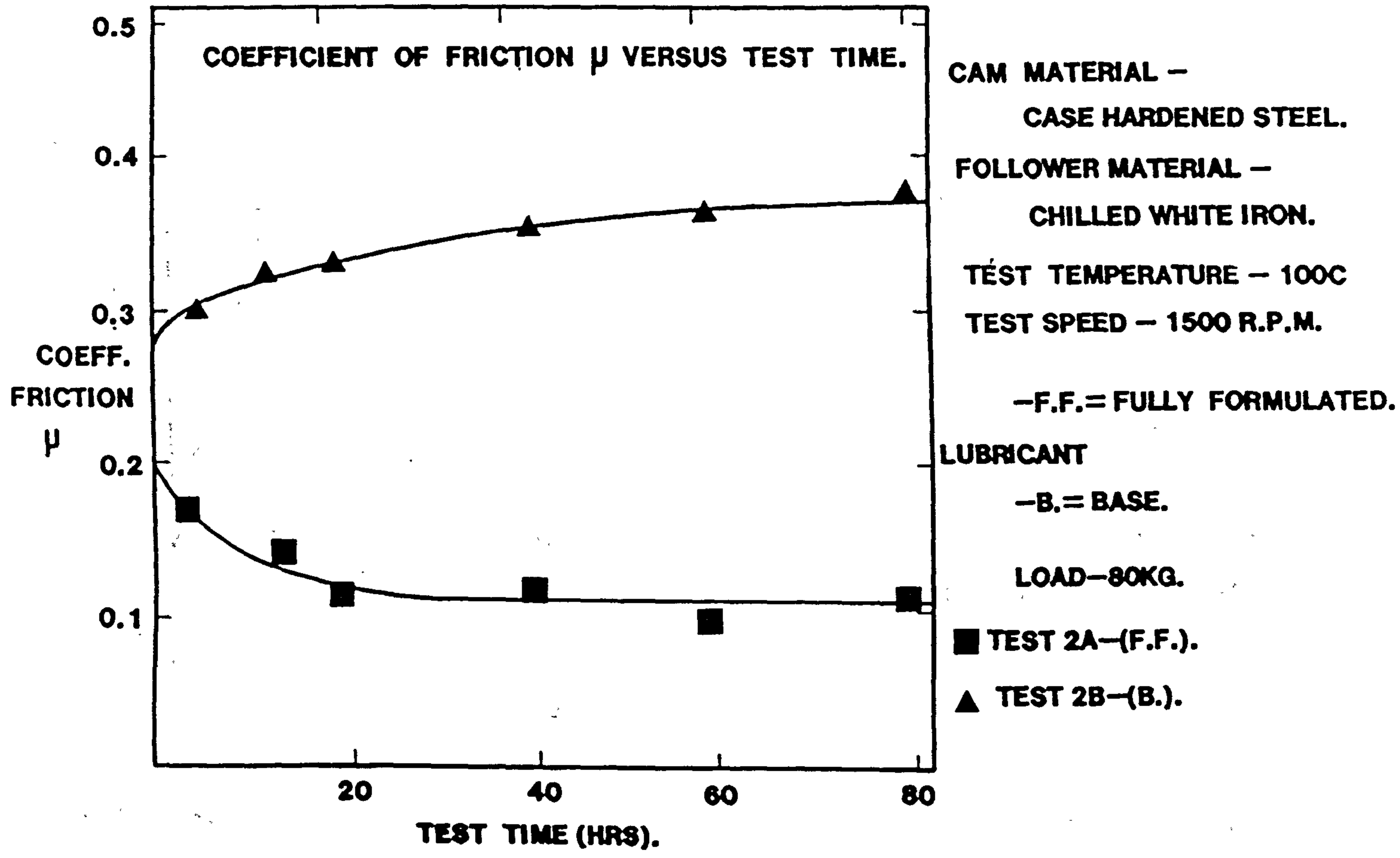

FIG. 114. GRAPH OF COEFFICIENT OF FRICTION VERSUS TEST TIME.

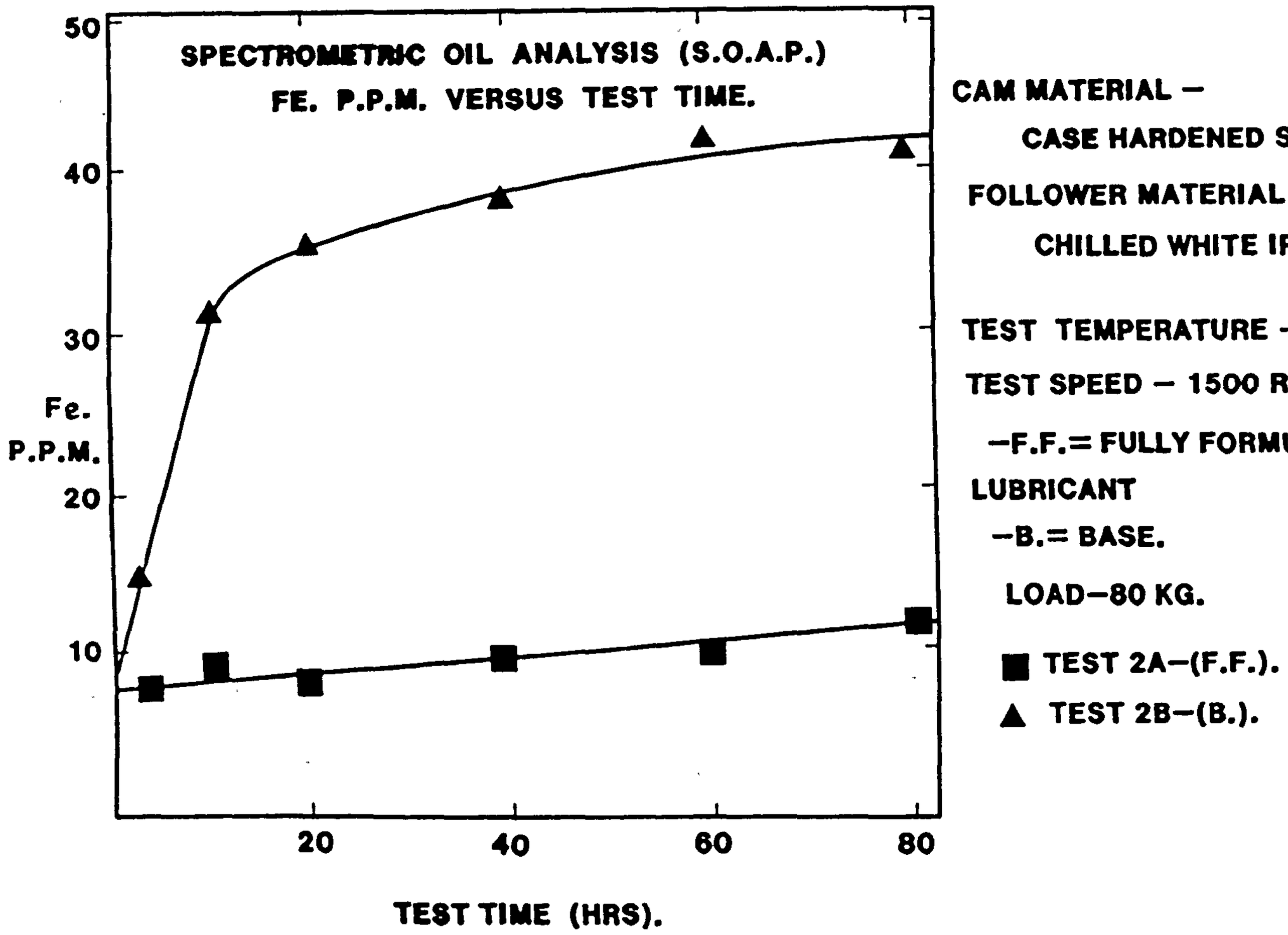

FIG. 115. QUANTITATIVE WEAR DEBRIS ANALYSIS, SPECTROMETRIC OIL ANALYSIS. GRAPH OF WEAR DEBRIS CONCENTRATION VERSUS TEST TIME.

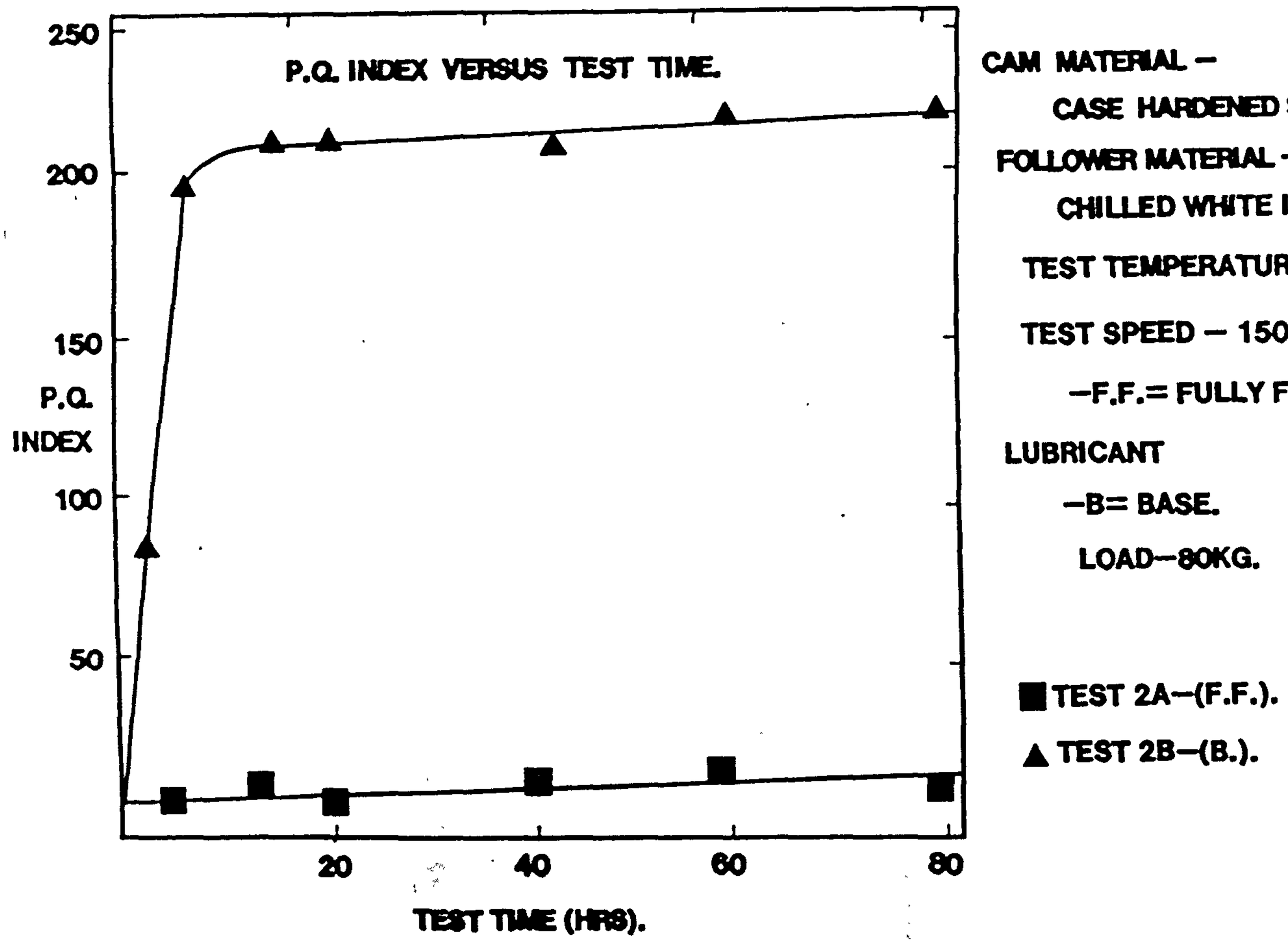

FIG. 116. SEMI-QUANTITATIVE WEAR DEBRIS ANALYSIS. GRAPH OF WEAR PARTICLE INDEX VERSUS TEST TIME.

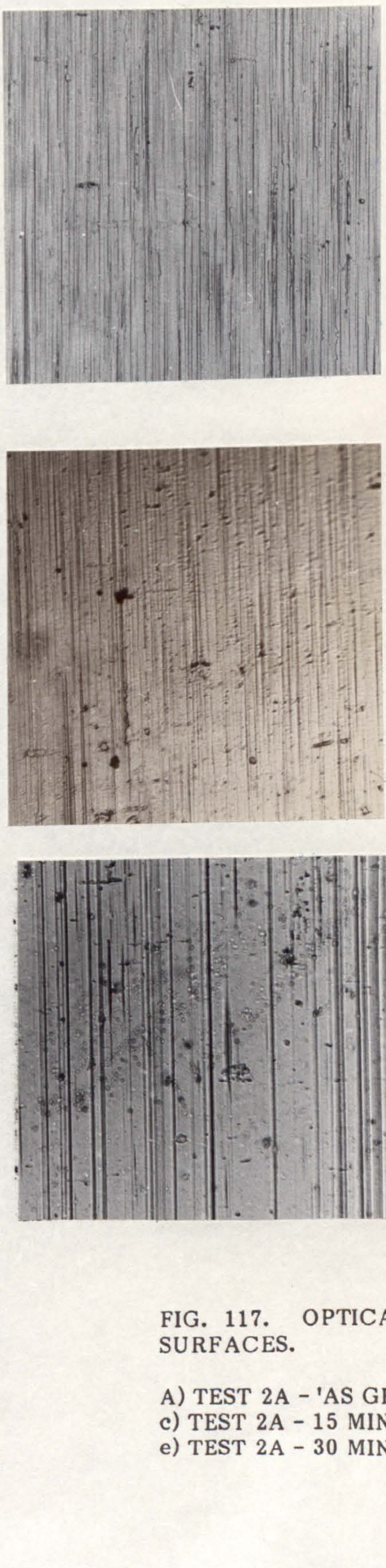

a)

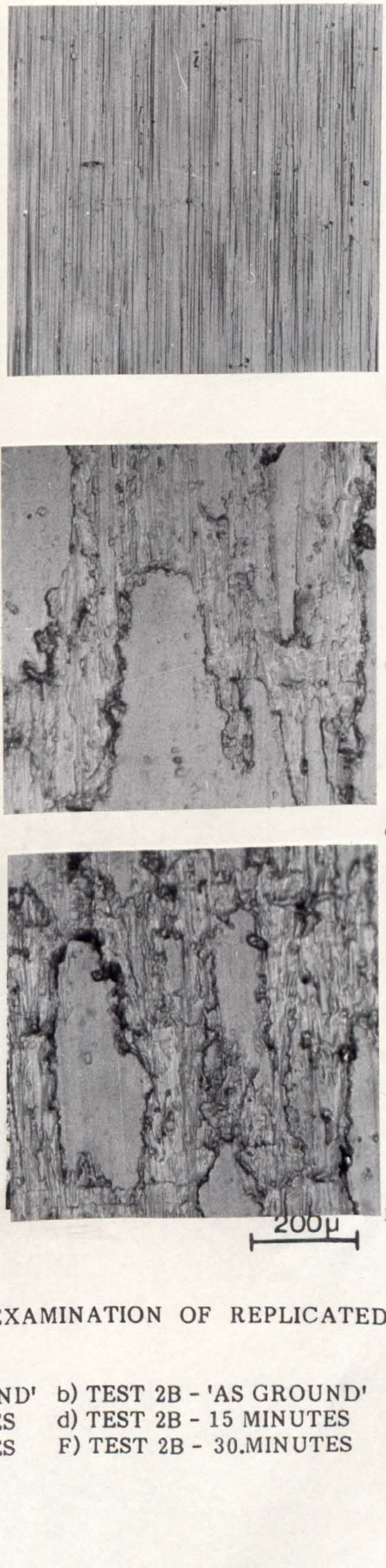

b)

c)

d)

e)

f)

200μ

FIG. 117. OPTICAL EXAMINATION OF REPLICATED CAM SURFACES.

A) TEST 2A - 'AS GROUND' b) TEST 2B - 'AS GROUND'
c) TEST 2A - 15 MINUTES d) TEST 2B - 15 MINUTES
e) TEST 2A - 30 MINUTES F) TEST 2B - 30.MINUTES

a)

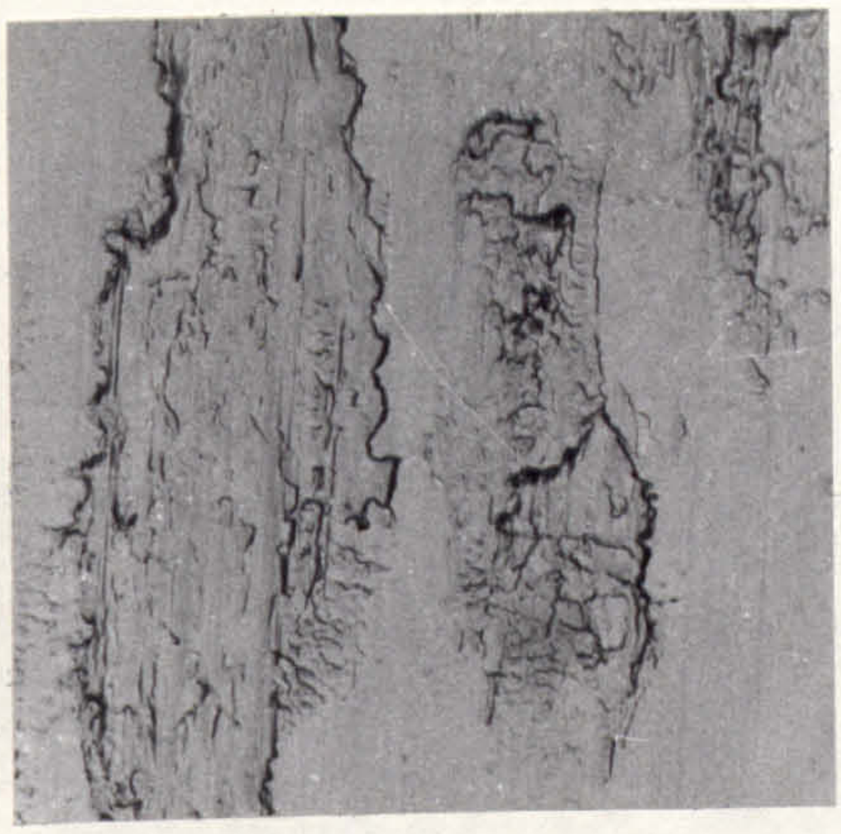

b)

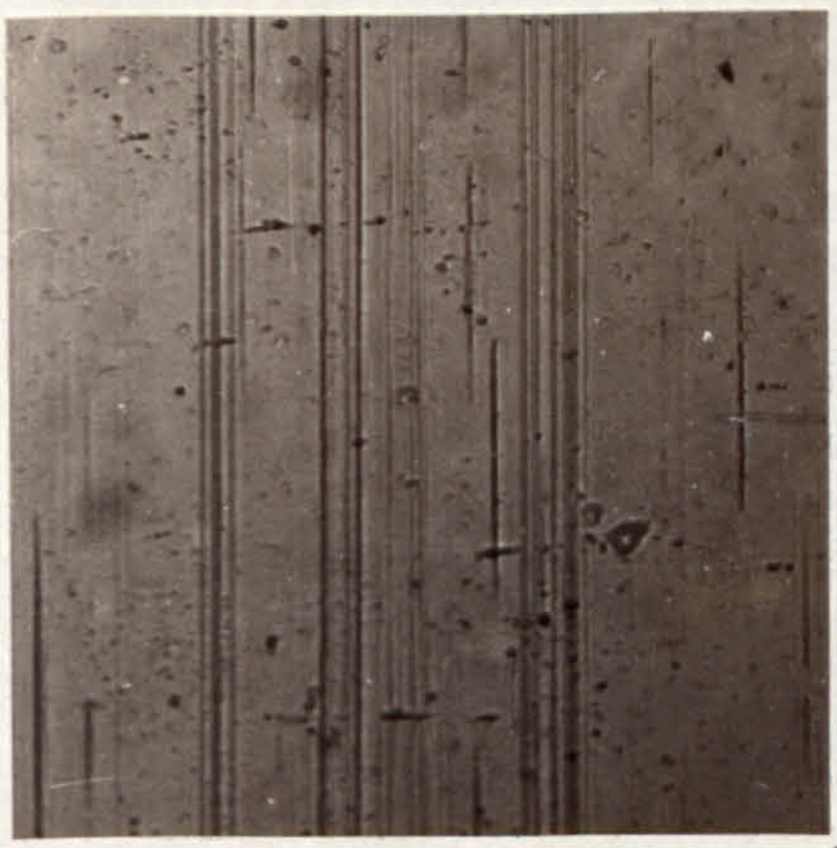

c)

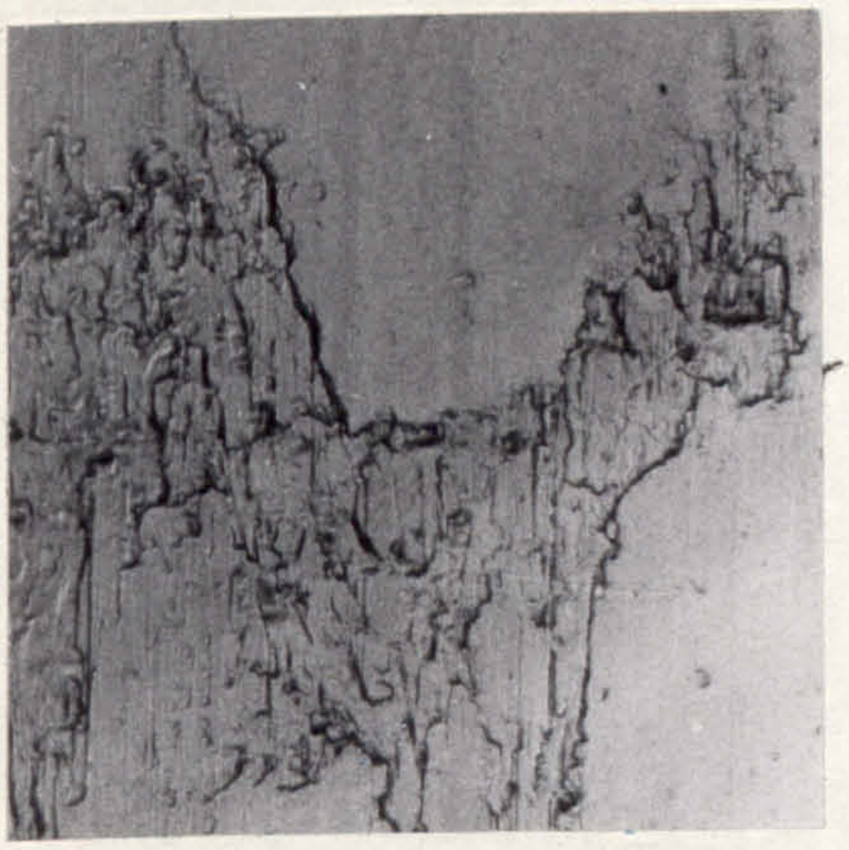

d)

e)

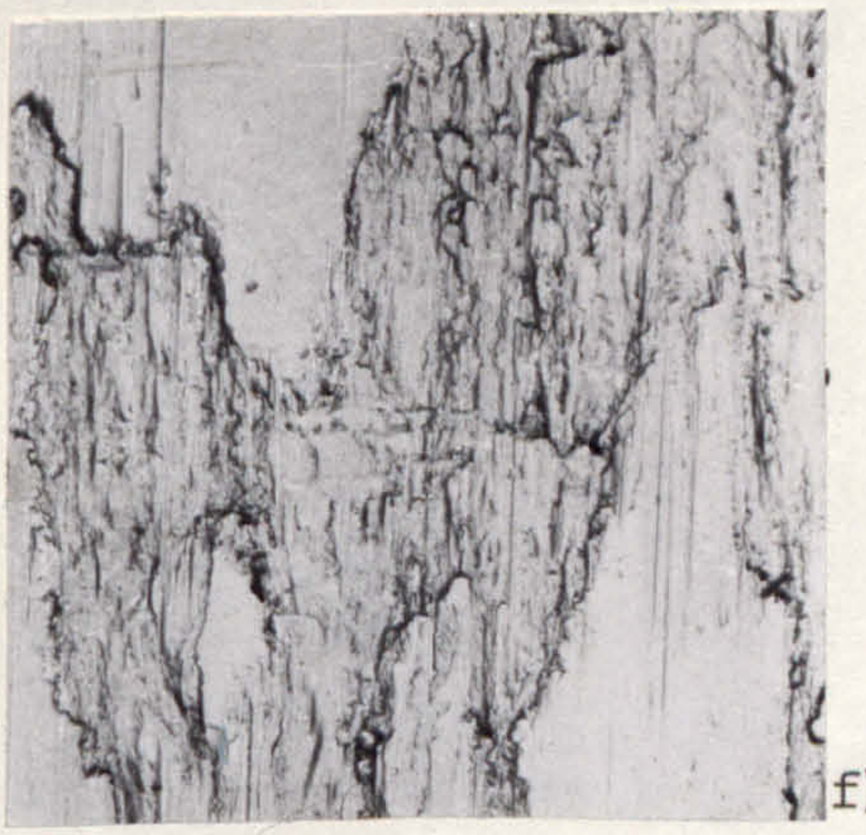

f)

200μ

FIG. 118. OPTICAL EXAMINATION OF REPLICATED CAM SURFACES.

a) TEST 2A - 45 MINUTES
b) TEST 2B - 45 MINUTES
c) TEST 2A - 1 HOUR
d) TEST 2B - 1 HOUR
e) TEST 2A - 2 HOURS
f) TEST 2B - 2 HOURS

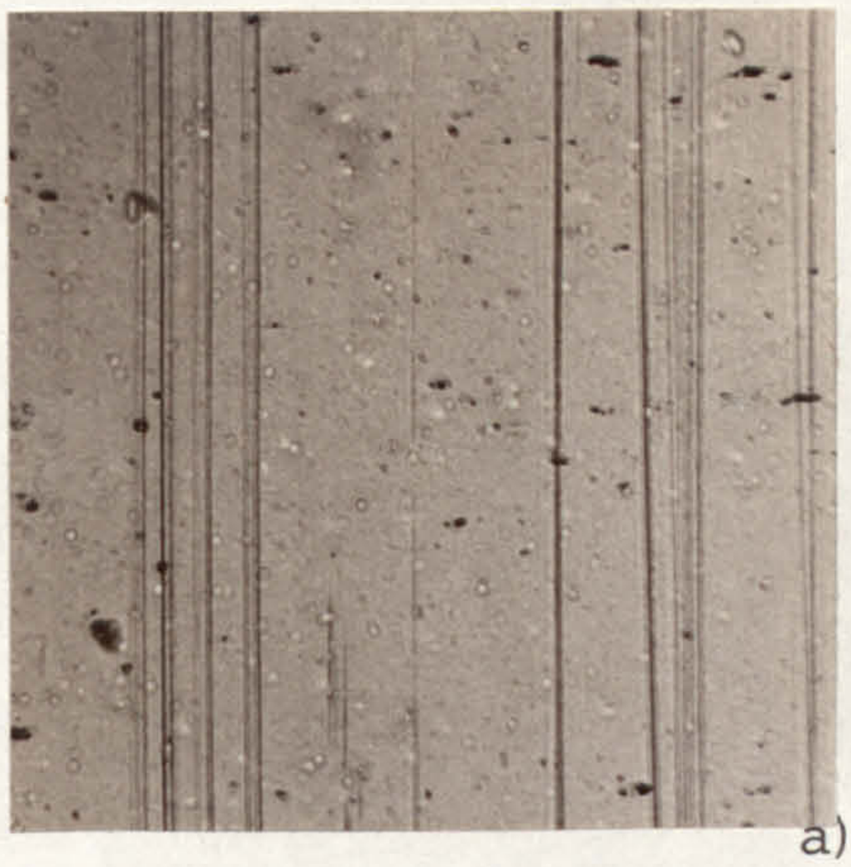

a)

b)

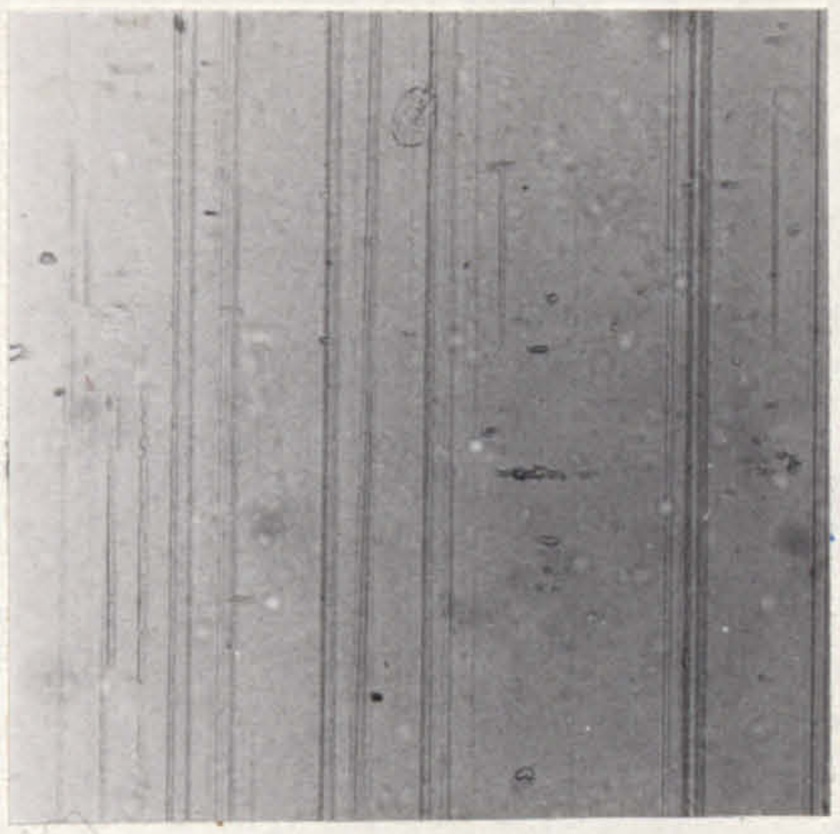

c)

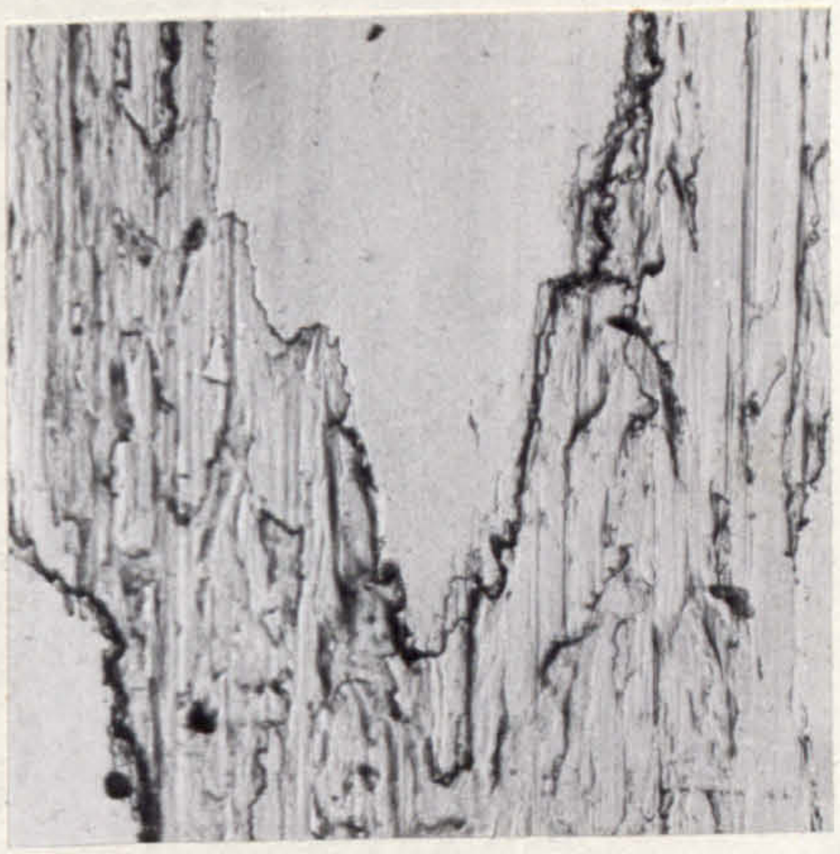

d)

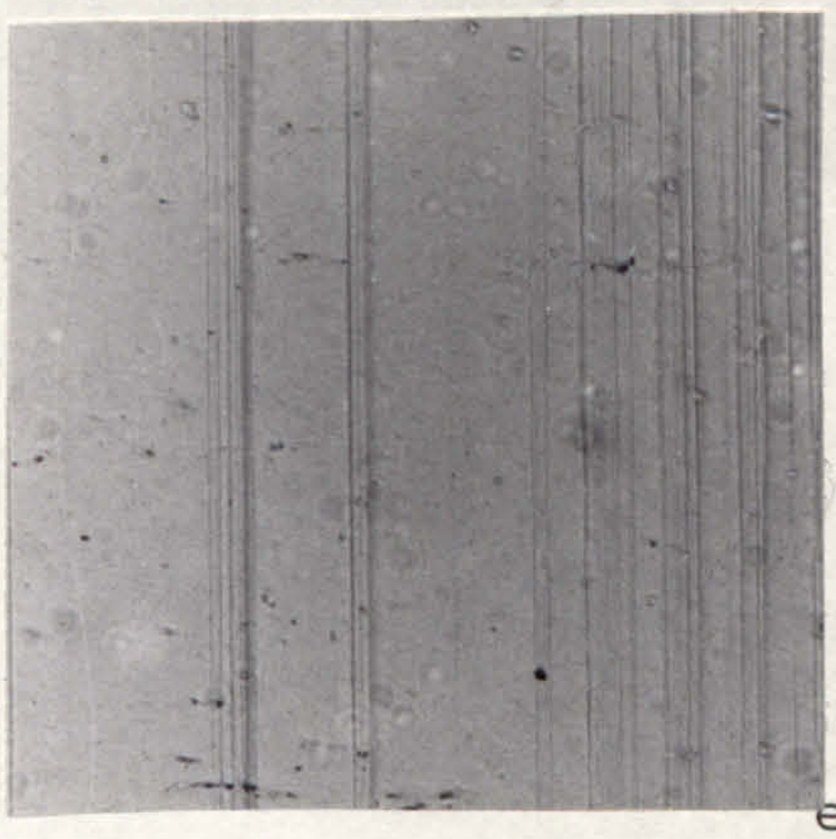

e)

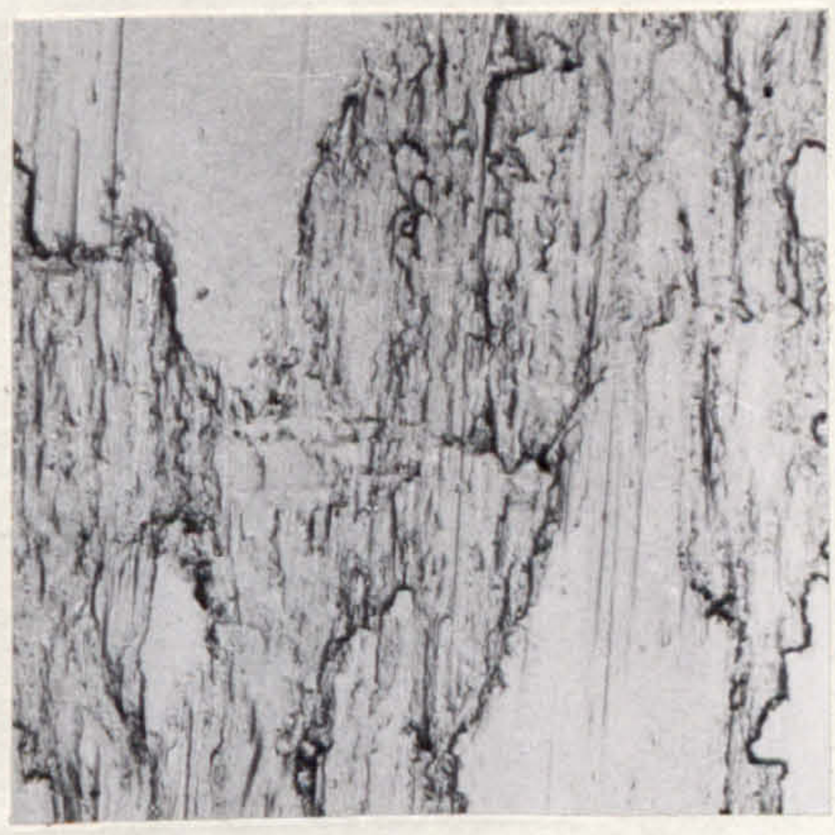

f)

200μ

FIG. 119. OPTICAL EXAMINATION OF REPLICATED CAM SURFACES.

a) TEST 2A - 3 HOURS
b) TEST 2B - 3 HOURS
c) TEST 2A - 4 HOURS
d) TEST 2B - 4 HOURS
e) TEST 2A - 7 HOURS
f) TEST 2B - 7 HOURS

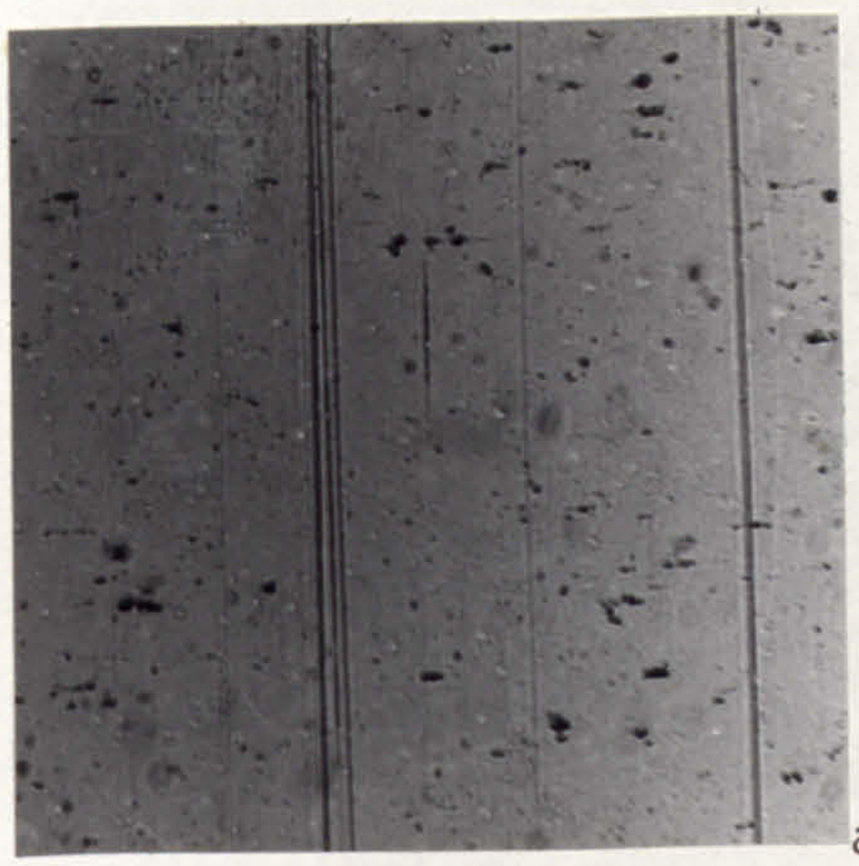

a)

b)

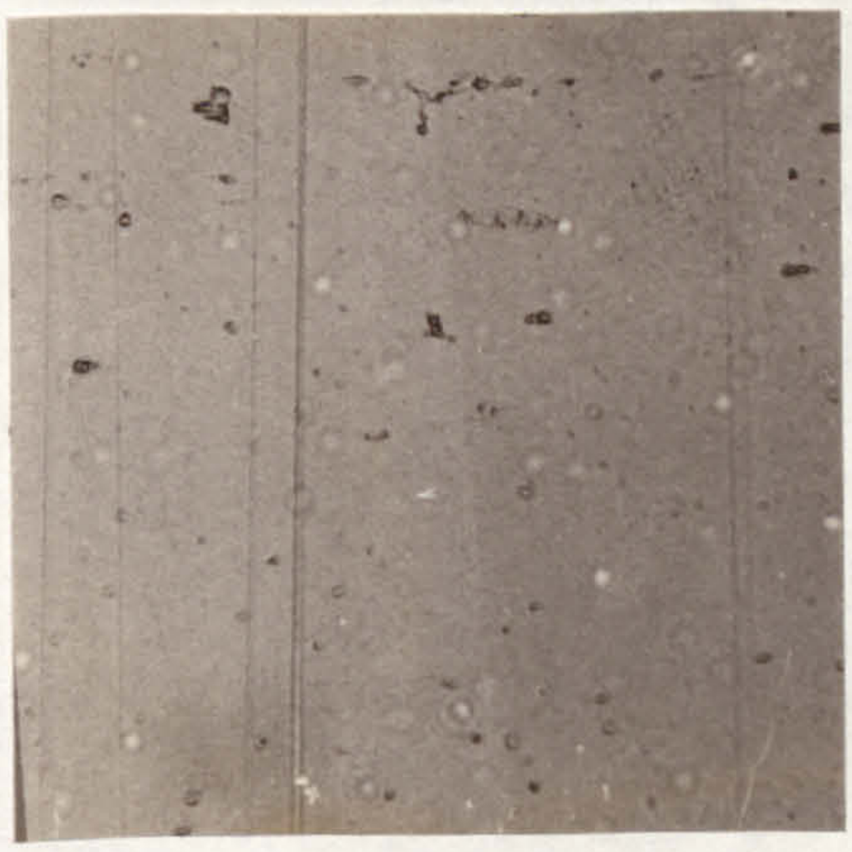

c)

d)

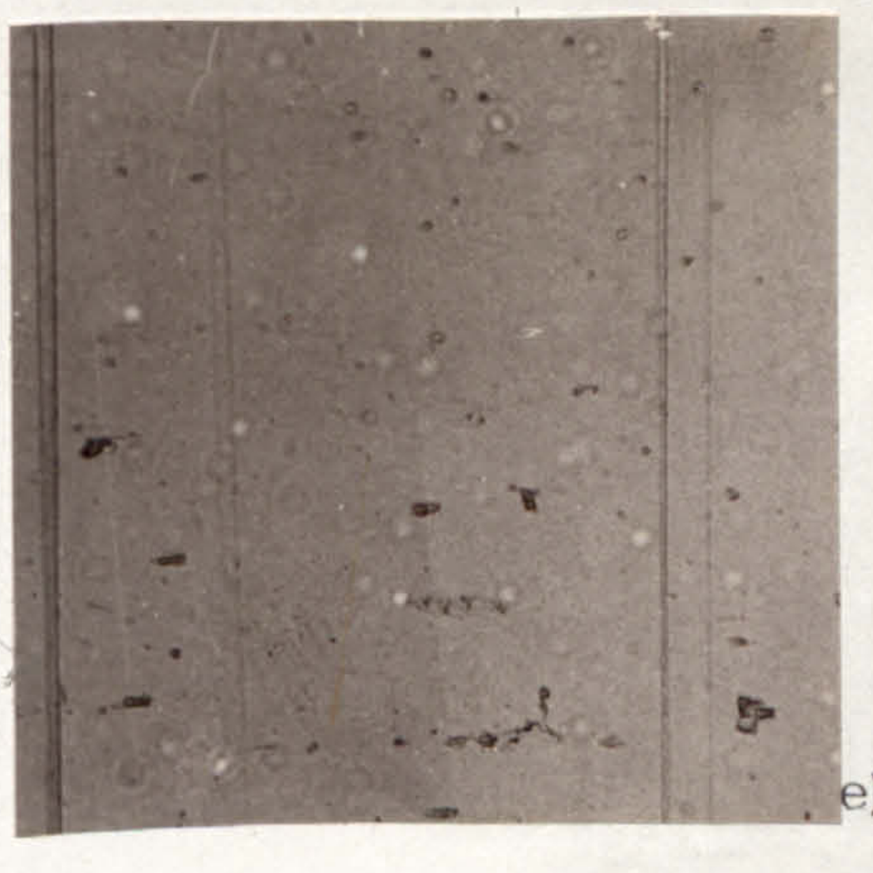

e)

f)

200μ

FIG. 120. OPTICAL EXAMINATION OF REPLICATED CAM SURFACES.

a) TEST 2A - 11 HOURS
b) TEST 2B - 11 HOURS
c) TEST 2A - 19 HOURS
d) TEST 2B - 19 HOURS
e) TEST 2A - 24 HOURS
f) TEST 2B - 24 HOURS

a)

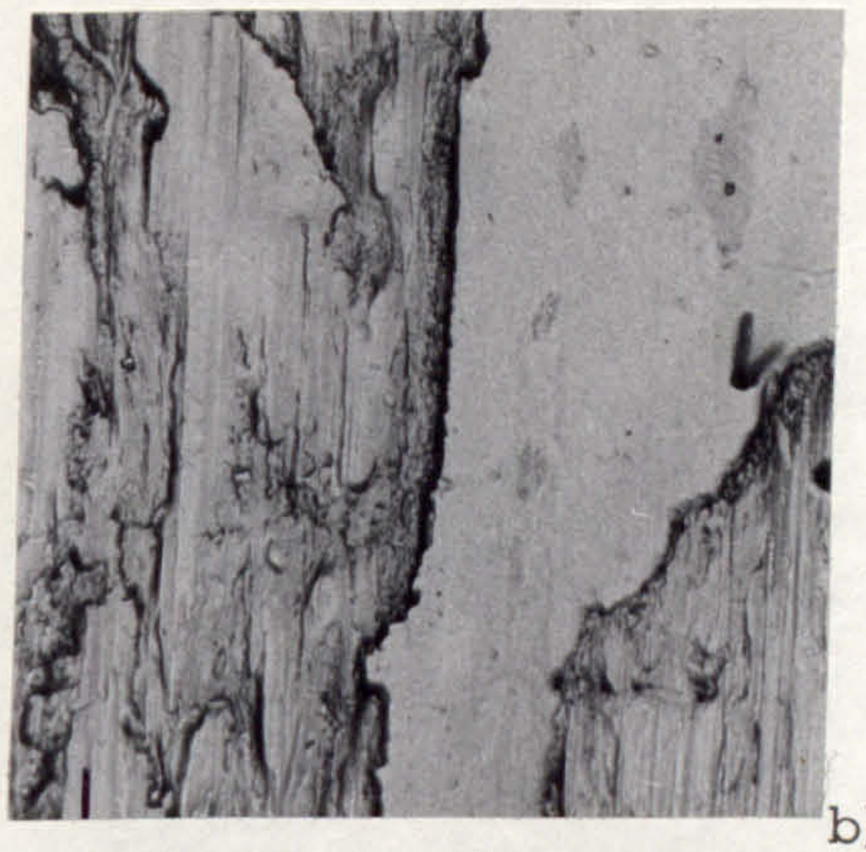

b)

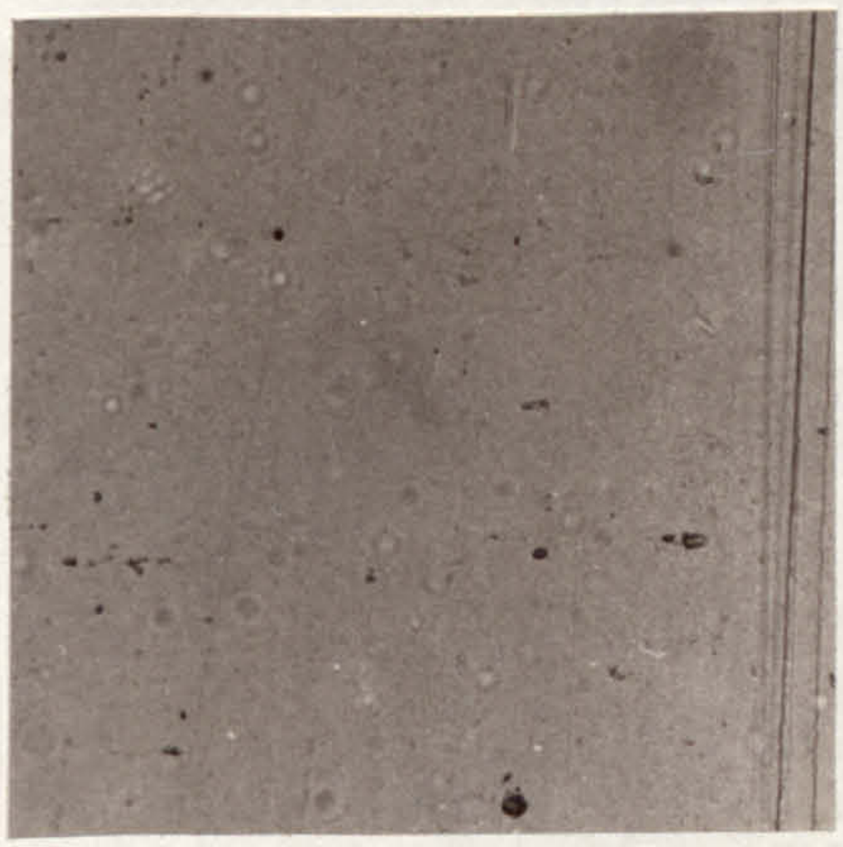

c)

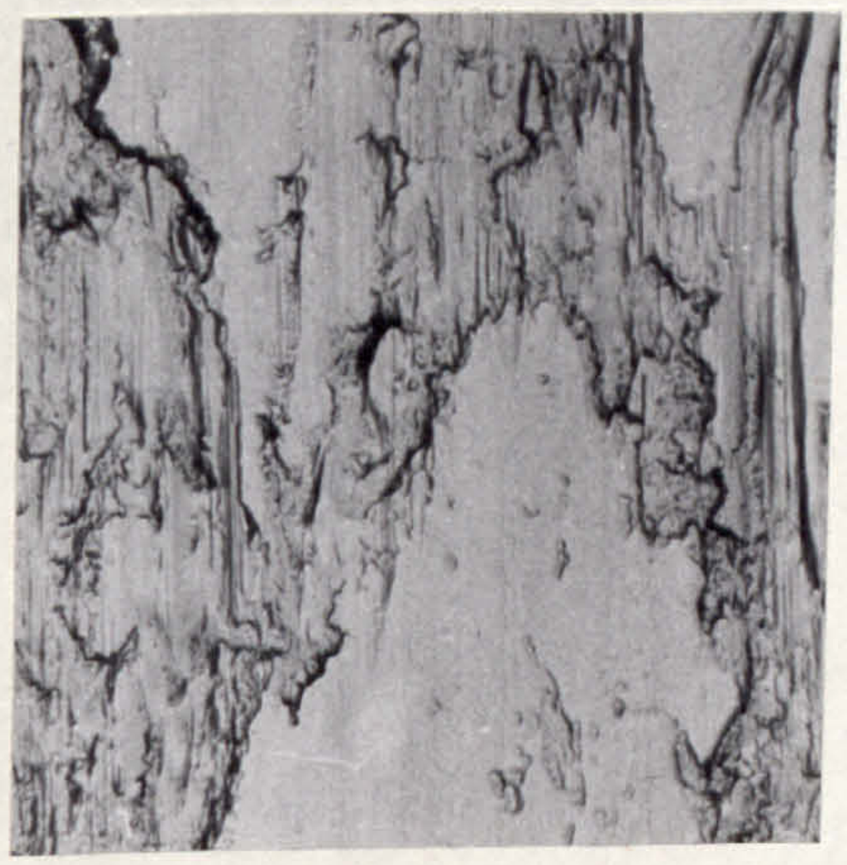

d)

e)

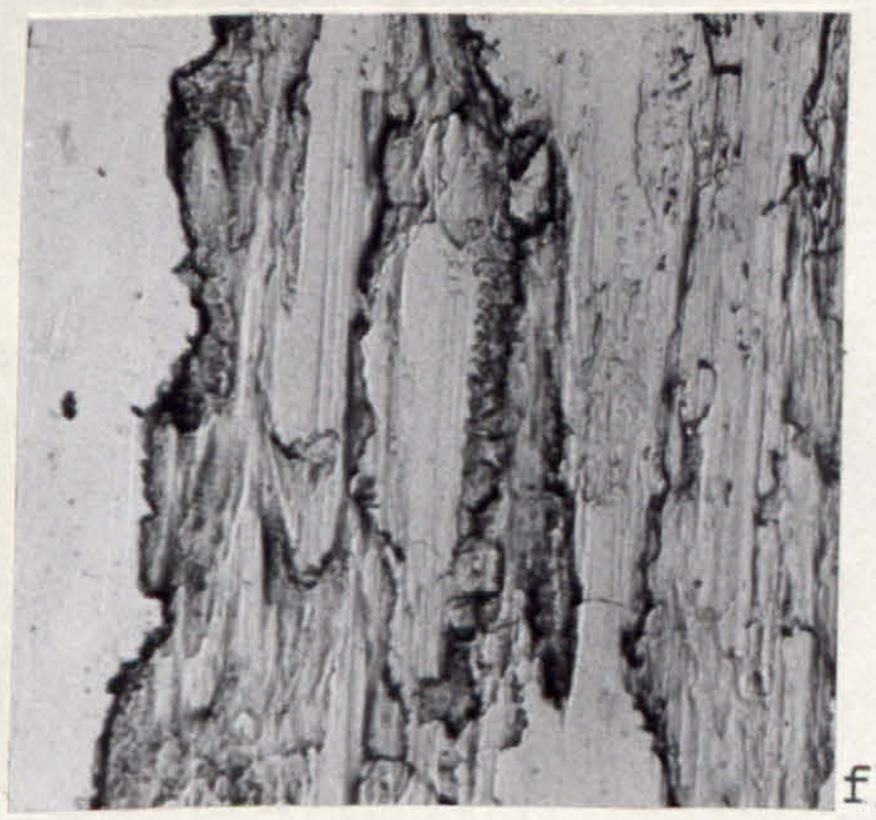

f)

200μ

FIG. 121. OPTICAL EXAMINATION OF REPLICATED CAM SURFACES.

a) TEST 2A - 30 HOURS
b) TEST 2B - 30 HOURS
c) TEST 2A - 45 HOURS
d) TEST 2B - 45 HOURS
e) TEST 2A - 70 HOURS
f) TEST 2B - 70 HOURS

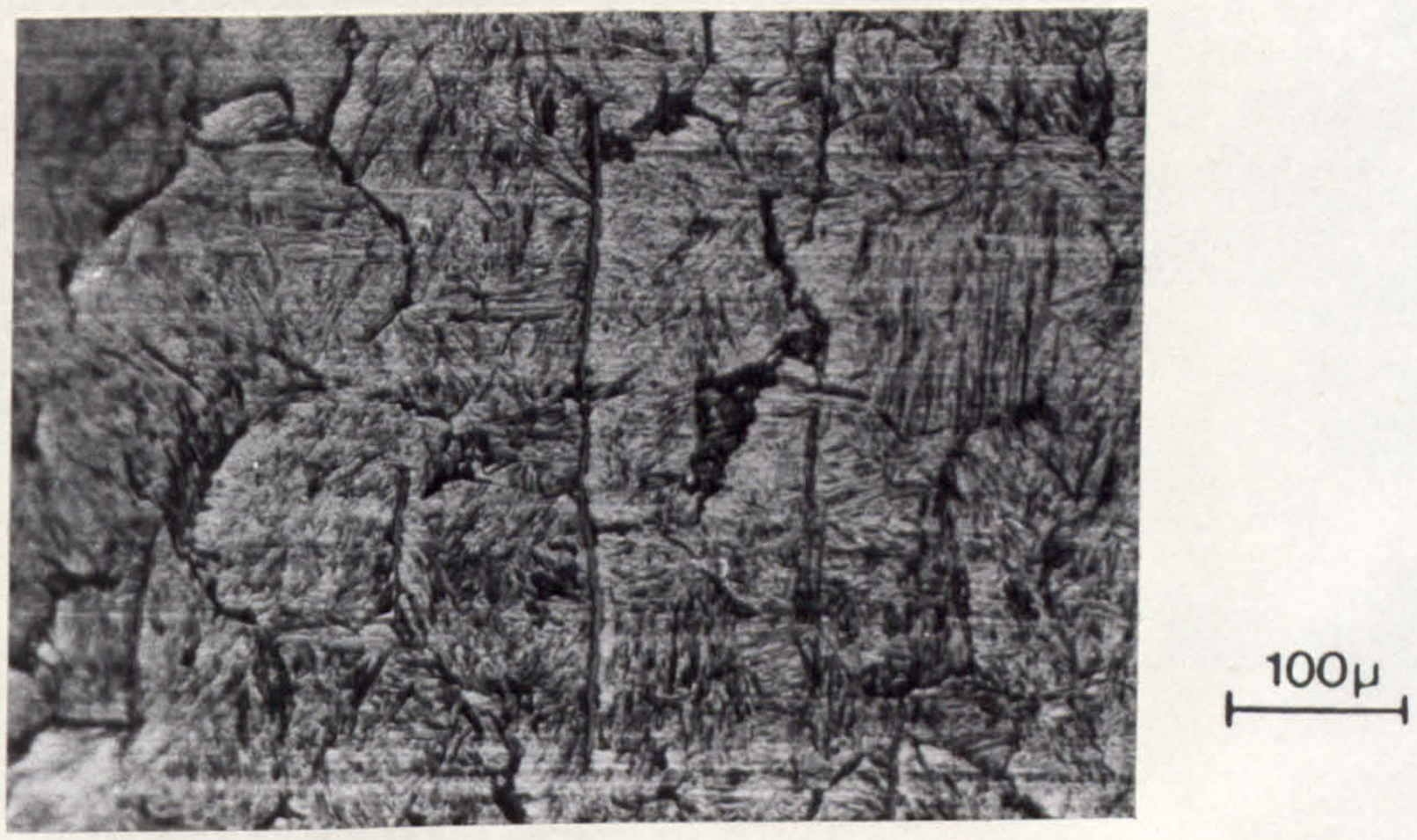

FIG. 122. CAM SURFACE, AS POLISHED AND ETCHED 2% NITAL.

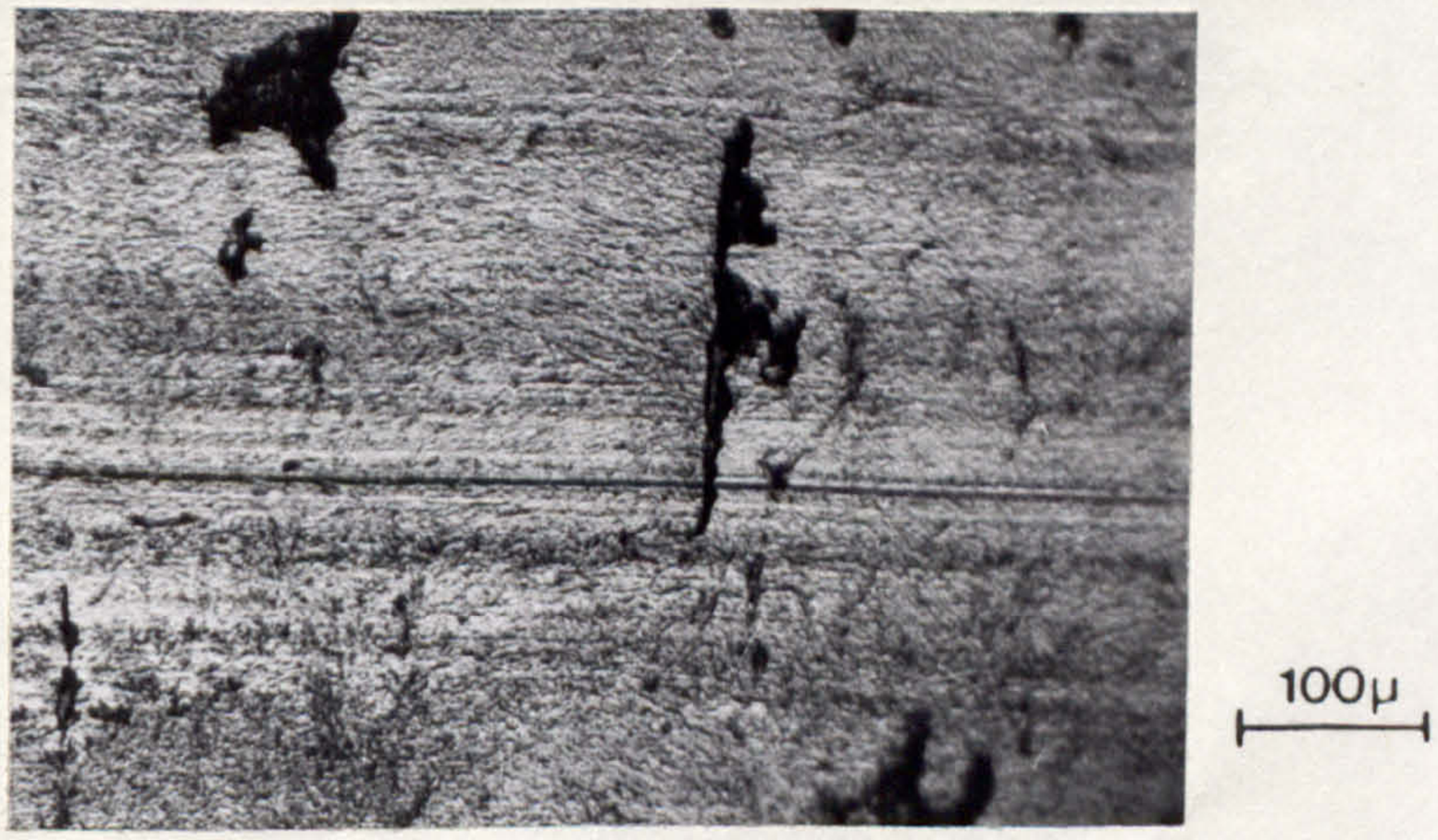

FIG. 123. TEST 2A, CAM SURFACE, FULLY FORMULATED OIL. 75 HOURS, ETCHED 2% NITAL.

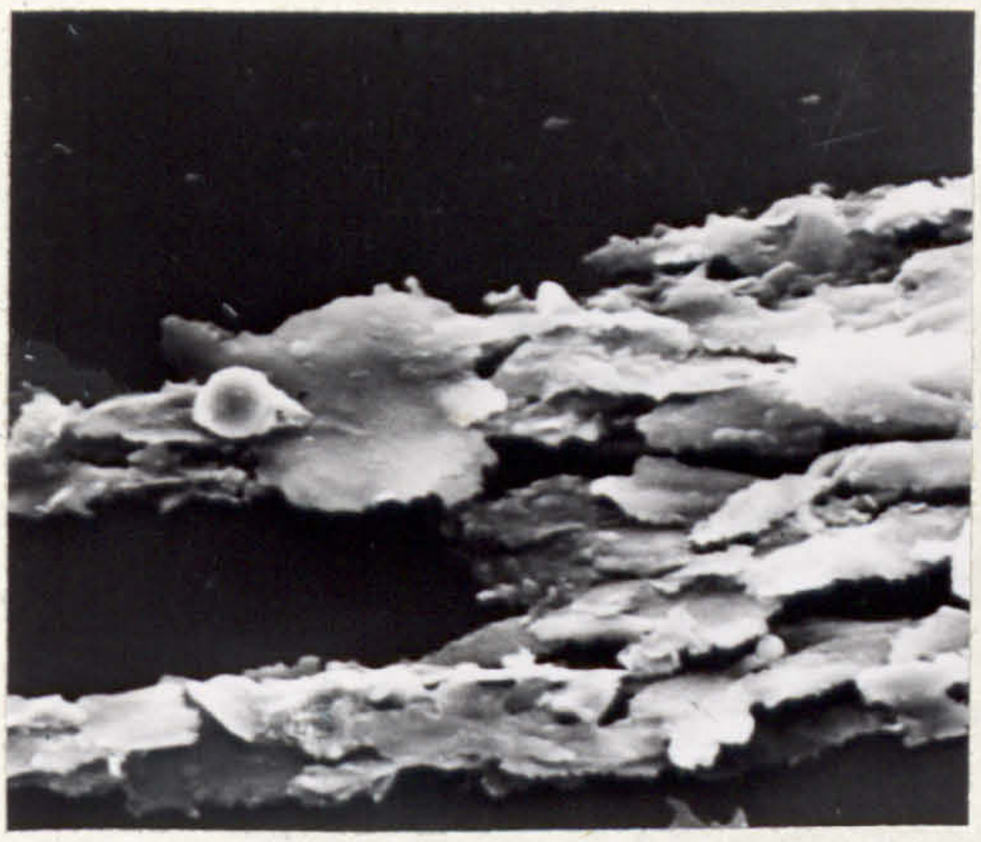

a) WEAR DEBRIS, FULLY FORMULATED
5 MINUTES

b) WEAR DEBRIS, BASE OIL
5 MINUTES.

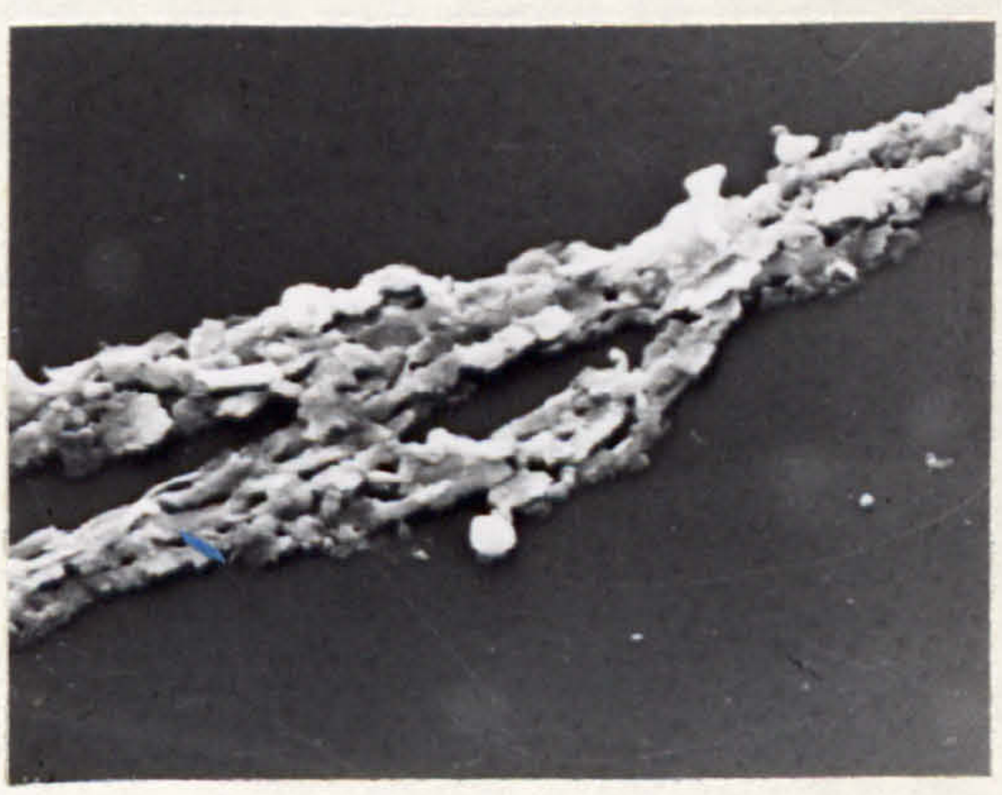

c) WEAR DEBRIS, FULLY FORMULATED
50 HOURS

d) WEAR DEBRIS, BASE OIL
50 HOURS

10μ

FIG. 124. WEAR DEBRIS - ELECTRON MICROGRAPHS.

a) TEST 2A - 5 MINUTES
b) TEST 2B - 5 MINUTES
c) TEST 2A - 50 HOURS
d) TEST 2B - 50 HOURS

a) CAM TAPERSECTION, FULLY FORMULATED OIL. 75 HOURS

b) CAM TAPERSECTION, BASE OIL. 1 HOUR.

200μ

c) CAM TAPERSECTION, BASE OIL. 75 HOURS.

200μ

FIG. 125. OPTICAL EXAMINATION OF CAM SPECIMEN TAPERSECTIONS.

a) TEST 2A - CAM TAPERSECTION 75 HOURS

b) TEST 2B - CAM TAPERSECTION 1 HOUR

c) TEST 2B - CAM TAPERSECTION 75 HOURS.

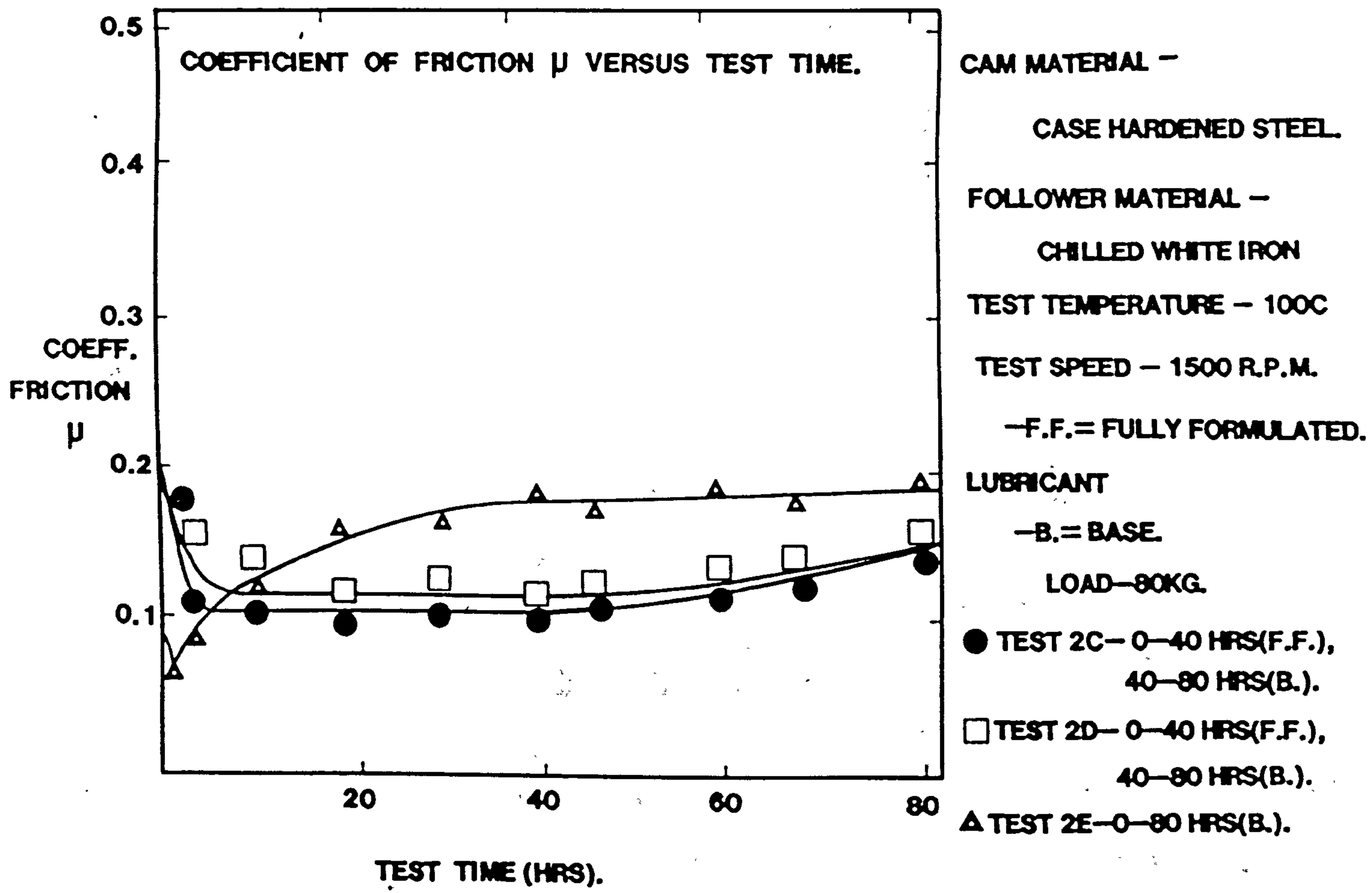

FIG. 126. GRAPH OF COEFFICIENT OF FRICTION VERSUS TEST TIME.

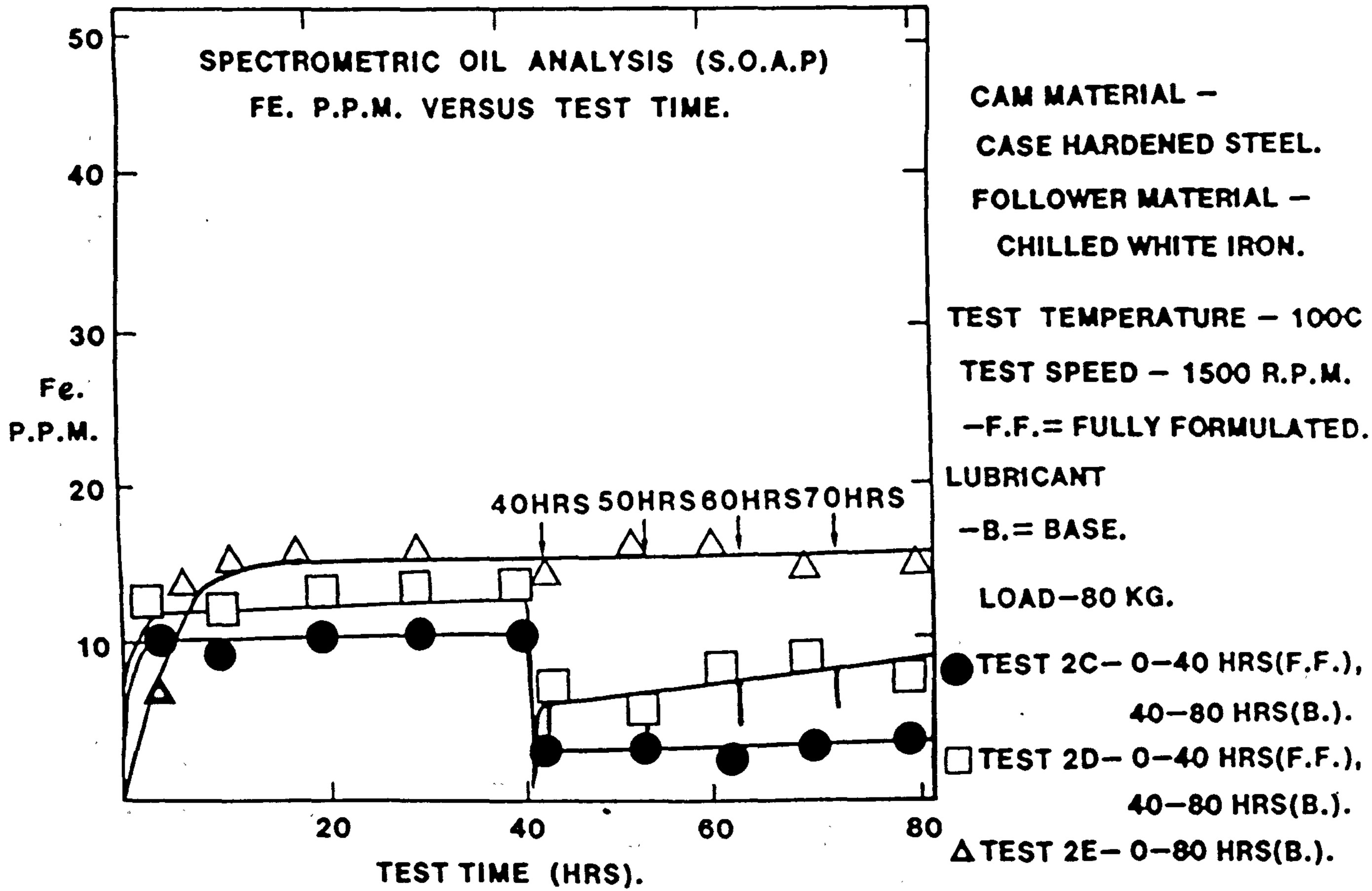

FIG. 127. QUANTITATIVE WEAR DEBRIS ANALYSIS, SPECTROMETRIC OIL ANALYSIS. GRAPH OF WEAR DEBRIS CONCENTRATION VERSUS TEST TIME.

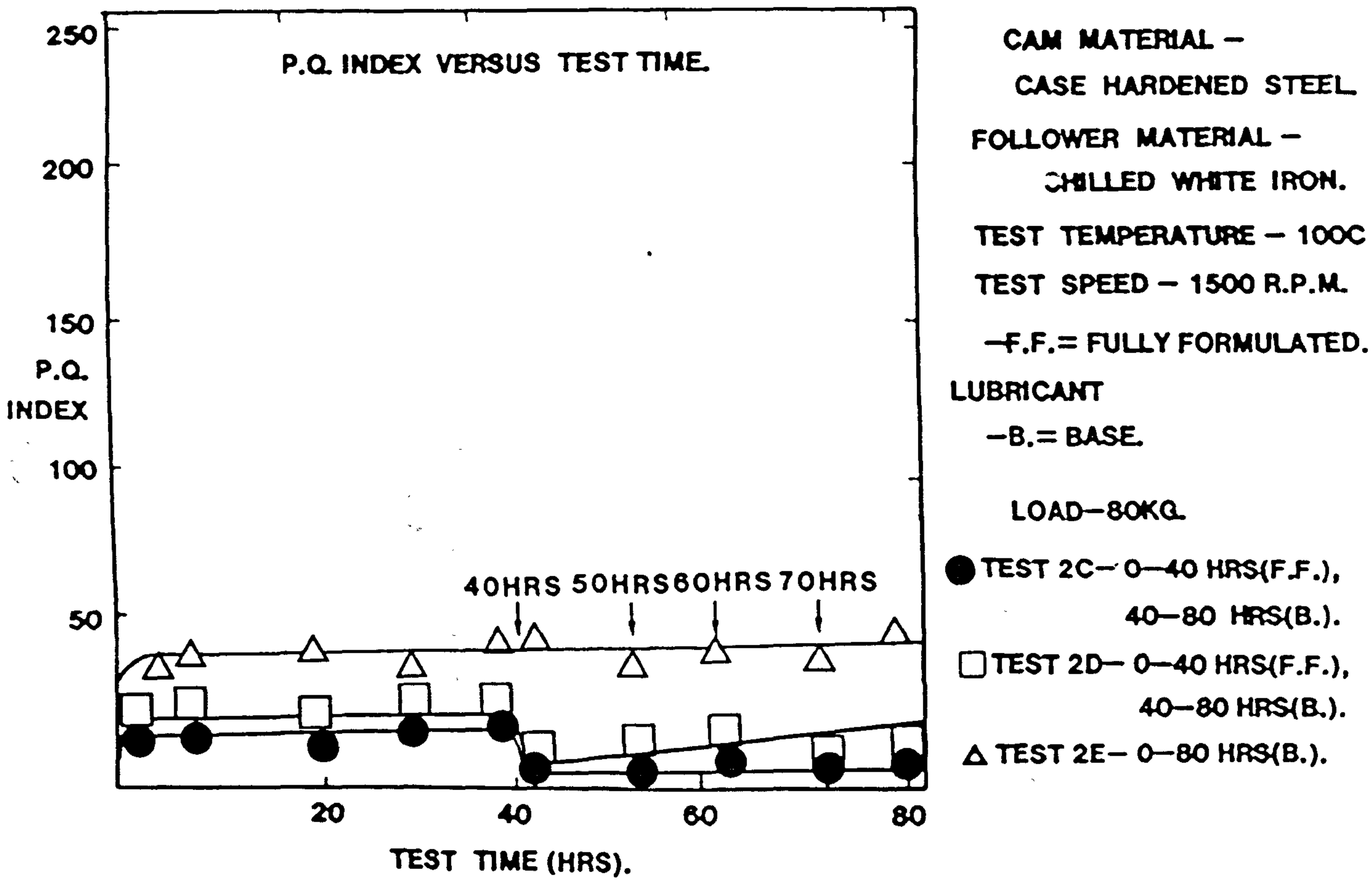

FIG. 128. SEMI-QUANTITATIVE WEAR DEBRIS ANALYSIS. GRAPH OF WEAR PARTICLE INDEX VERSUS TEST TIME.

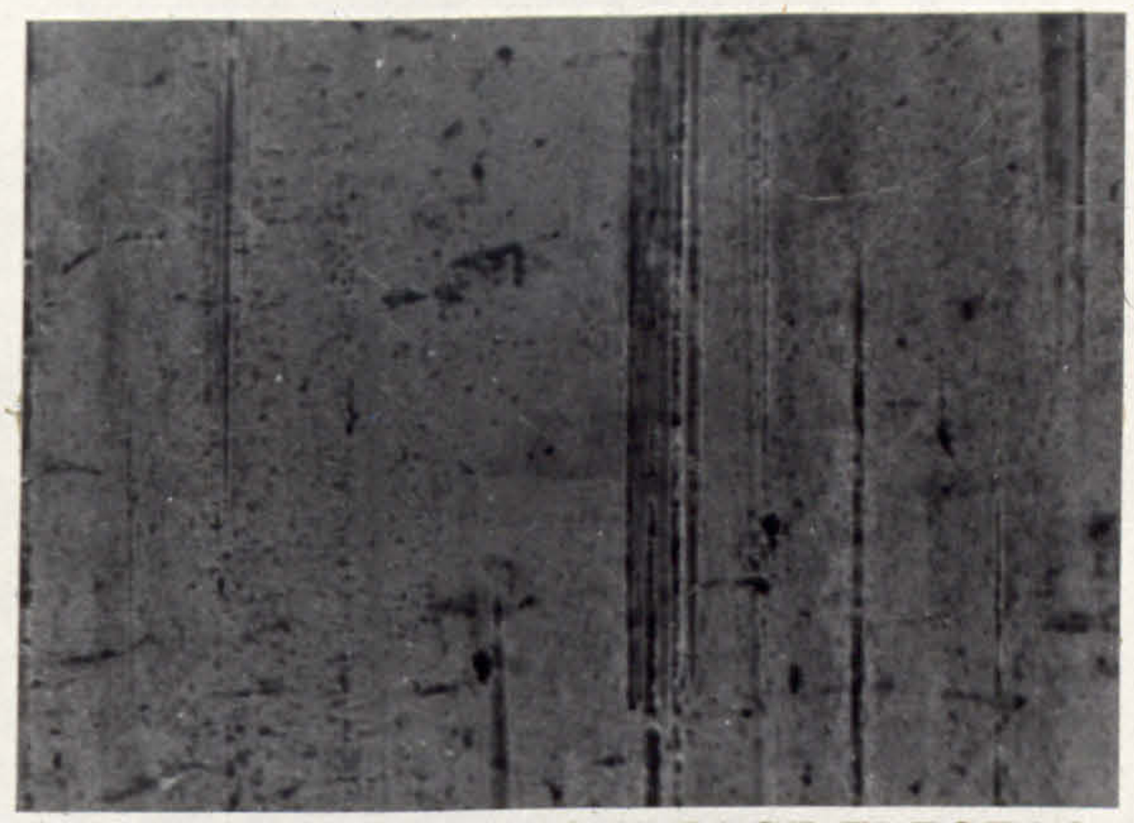

FIG. 129A. TEST 2C - CAM WEAR SURFACE ELECTRON MICROGRAPH

FIG. 129B. TEST 2C - FOLLOWER WEAR SURFACE ELECTRON MICROGRAPH.

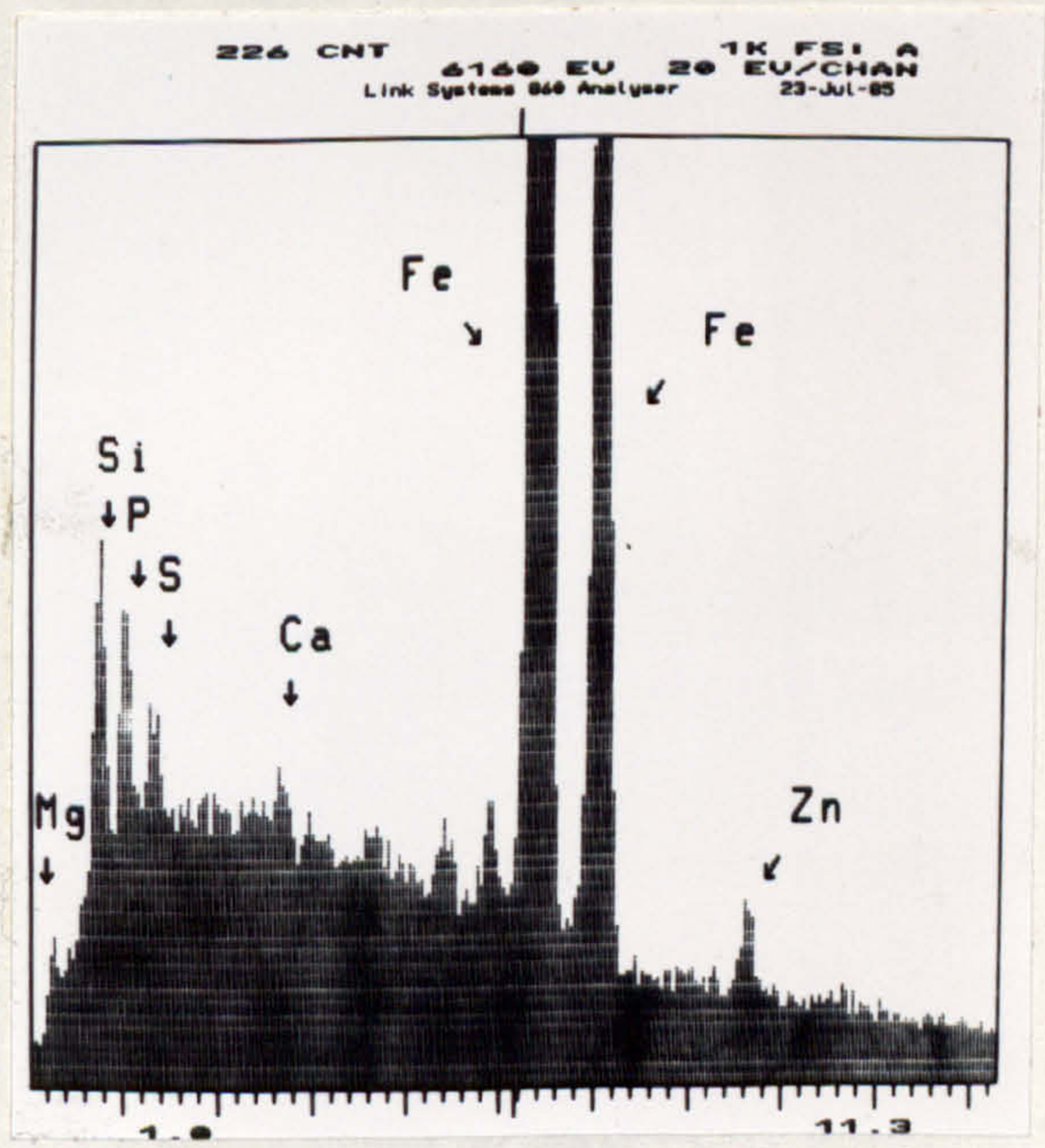

FIG. 129C. TEST 2C - CAM WEAR SURFACE X-RAY ENERGY SPECTRA.

FIG. 130. TEST 2C - CAM SPECIMEN TAPERSECTION.

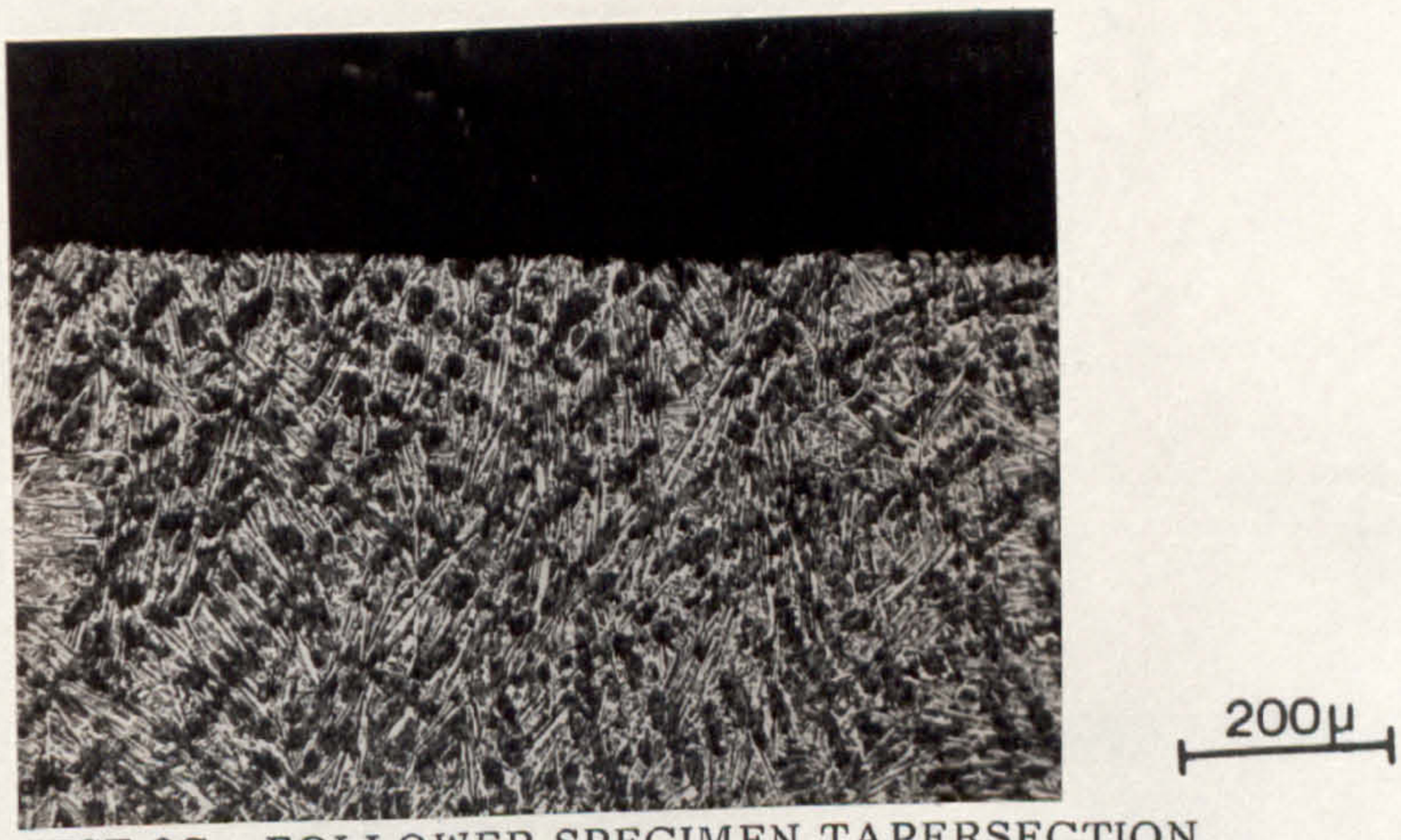

FIG. 131. TEST 2C - FOLLOWER SPECIMEN TAPERSECTION.

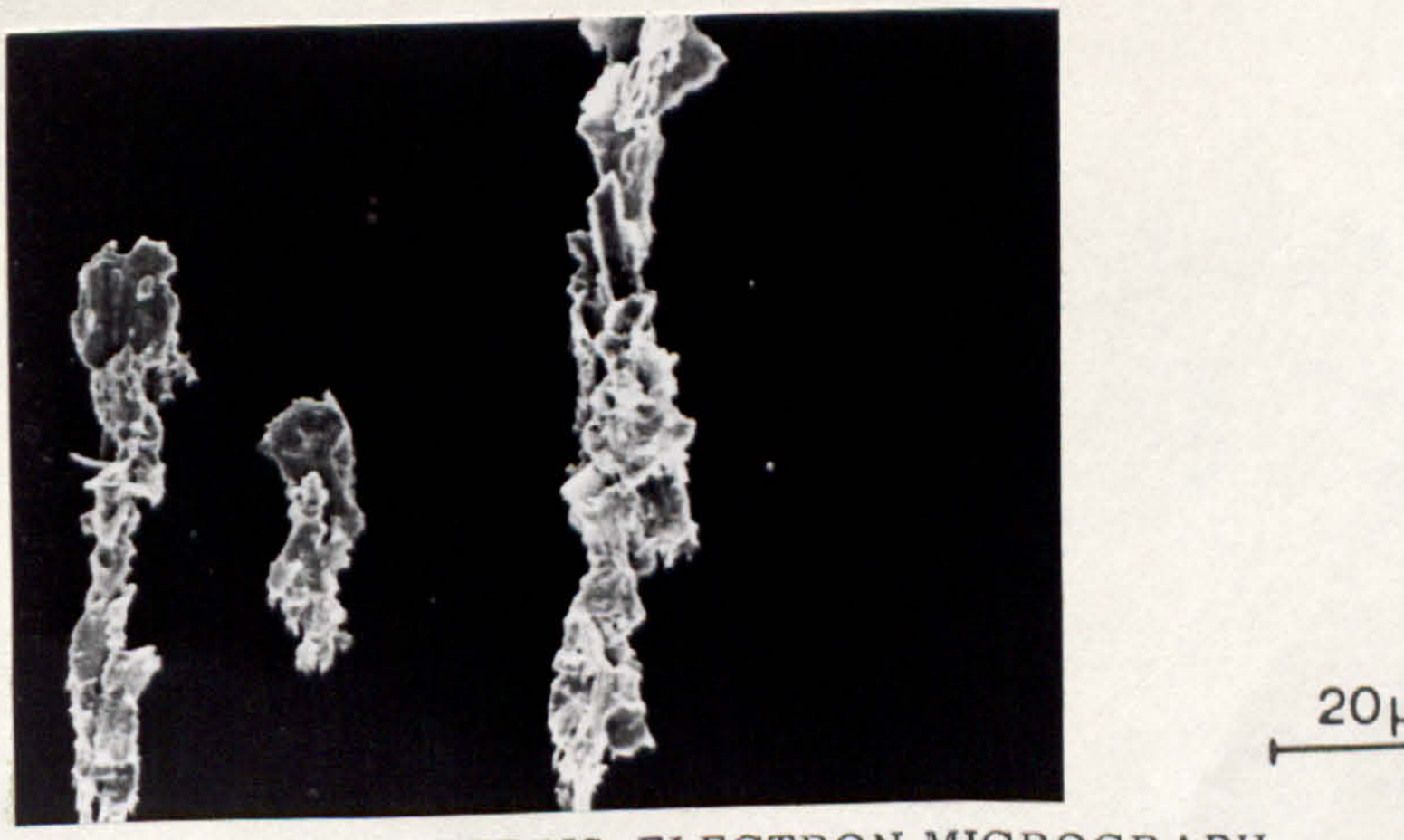

FIG. 132. TEST 2C - WEAR DEBRIS, ELECTRON MICROGRAPH.

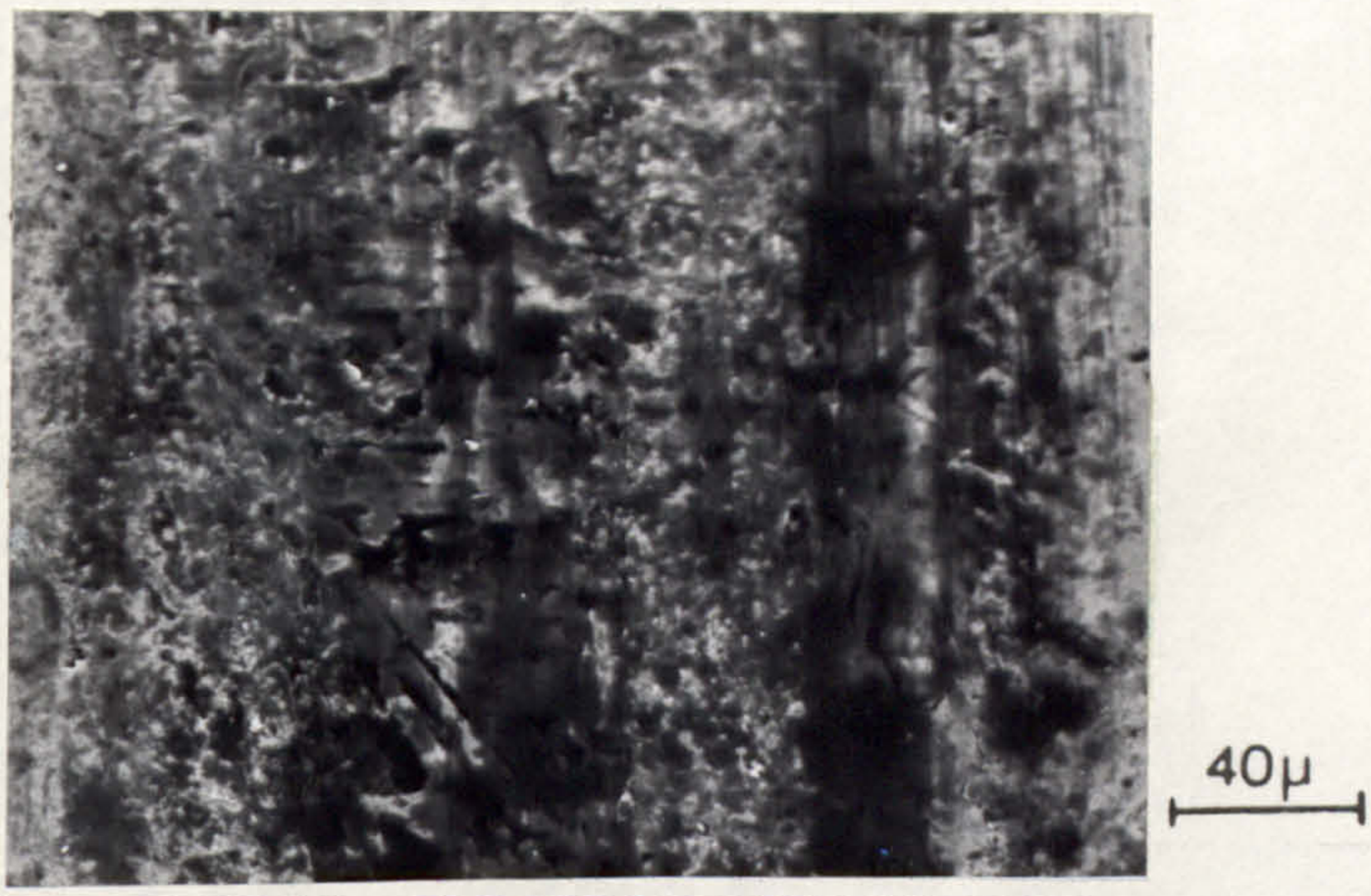

FIG. 133. TEST 2D - ELECTRON MICROGRAPH, FOLLOWER WEAR SURFACE, 40 HOURS.

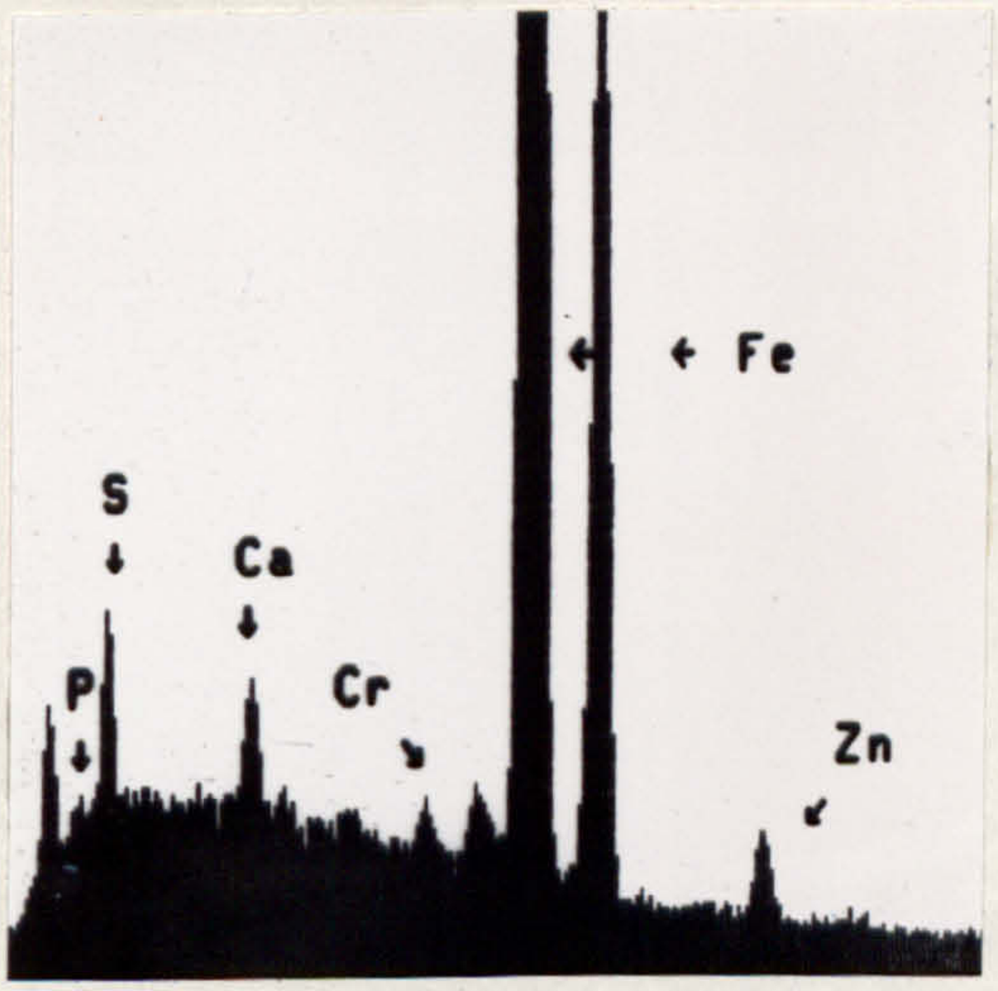

FIG. 134. TEST 2D - X-RAY ENERGY SPECTRA, FOLLOWER WEAR SURFACE, 40 HOURS.

WINDOW LABEL	WINDOW CENTRE	FIRST CHAN	LAST CHAN	NET INTEGRAL	EFF. FACTOR	XAGE TOTAL
P	2060	1980	2160	222	1.00	0.17
S	2320	2220	2440	1724	1.00	1.30
CA	3700	3600	3800	1188	1.00	0.90
FE	6380	6140	6640	128220	1.00	96.77
ZN	8600	8480	8740	1143	1.00	0.86

TABLE 9. SEMI-QUANTITATIVE ELEMENTAL ANALYSIS, FOLLOWER WEAR SURFACE, 40 HOURS.

FIG. 135. TEST 20 - ELECTRON MICROGRAPH FOLLOWER WEAR SURFACE, 50 HOURS.

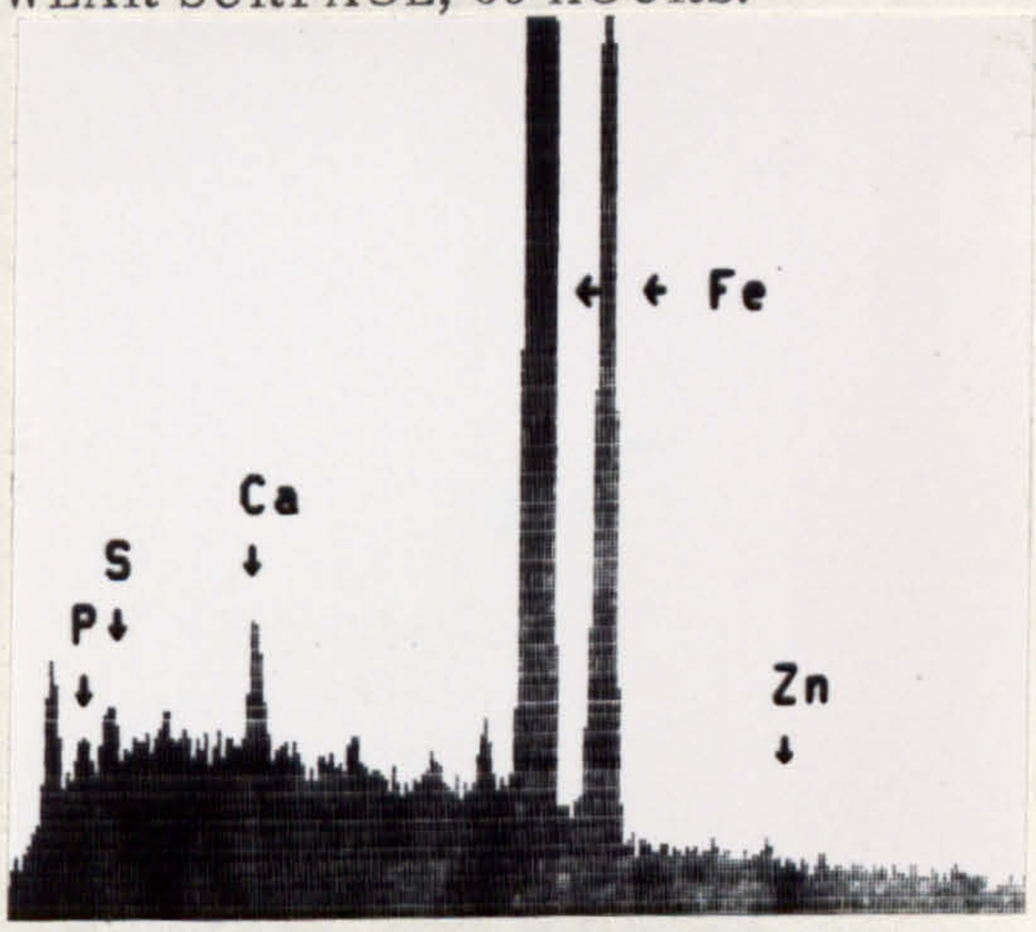

FIG. 136. TEST 20 - X-RAY ENERGY SPECTRA, FOLLOWER WEAR SURFACE, 50 HOURS.

WINDOW LABEL	WINDOW CENTRE	FIRST CHAN	LAST CHAN	NET INTEGRAL	EFF. FACTOR	XAGE TOTAL
P	2040	1960	2140	291	1.00	0.24
S	2300	2200	2420	681	1.00	0.57
CA	3680	3580	3780	864	1.00	0.72
FE	6360	6120	6620	117354	1.00	98.21
ZN	8580	8460	8720	301	1.00	0.25

TABLE 10. SEMI-QUANTITATIVE ELEMENTAL ANALYSIS FOLLOWER WEAR SURFACE, 50 HOURS.

FIG. 137. TEST 2D - ELECTRON MICROGRAPH, FOLLOWER WEAR SURFACE, 60 HOURS.

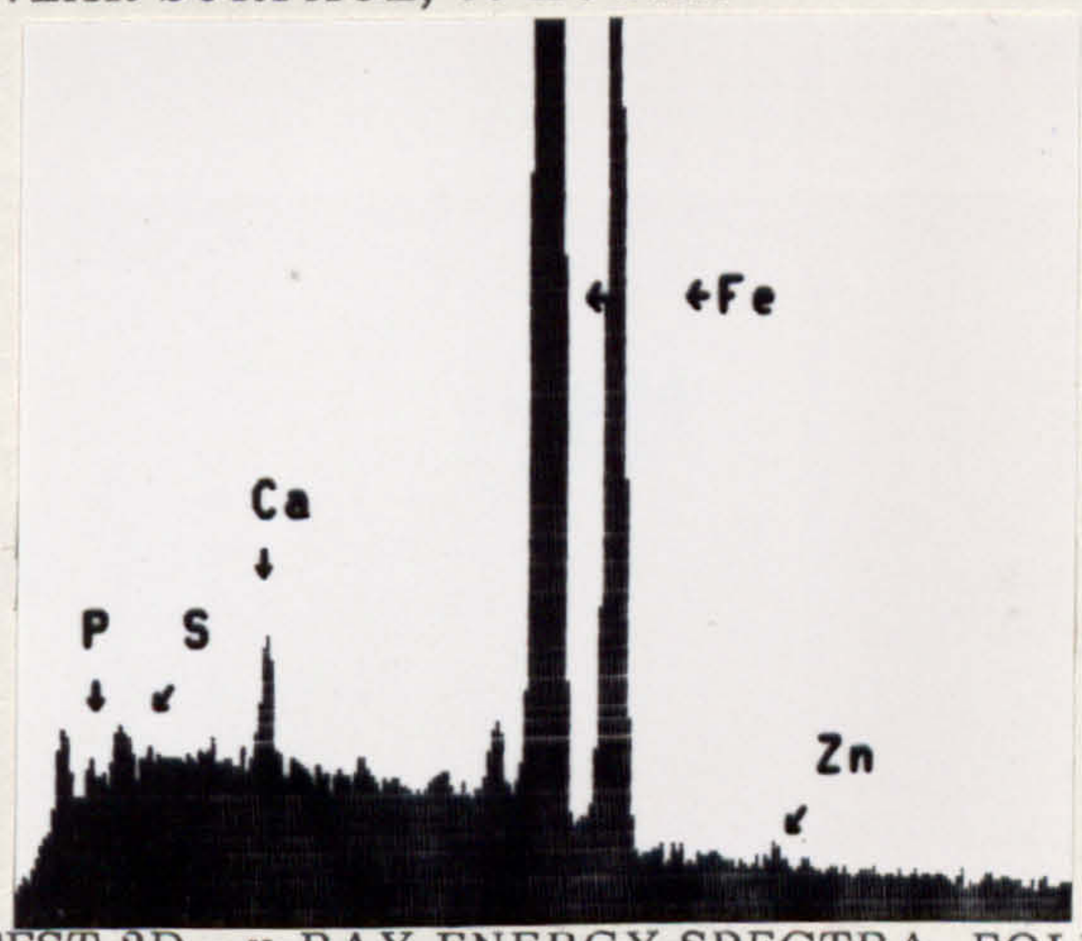

FIG. 138. TEST 2D - x-RAY ENERGY SPECTRA, FOLLOWER WEAR SURFACE, 60 HOURS.

WINDOW LABEL	WINDOW CENTRE	FIRST CHAN	LAST CHAN	NET INTEGRAL	EFF. FACTOR	XAGE TOTAL
P	2040	1960	2140	312	1.00	0.24
S	2300	2200	2420	561	1.00	0.44
CA	3680	3580	3780	992	1.00	0.78
FE	6360	6120	6620	125593	1.00	98.44
ZN	8580	8460	8720	123	1.00	0.10

TABLE 11. SEMI-QUANTITATIVE ELEMENTAL ANALYSIS, FOLLOWER WEAR SURFACE, 60 HOURS.

FIG. 139. TEST 2D - ELECTRON MICROGRAPH FOLLOWER WEAR SURFACE, 70 HOURS.

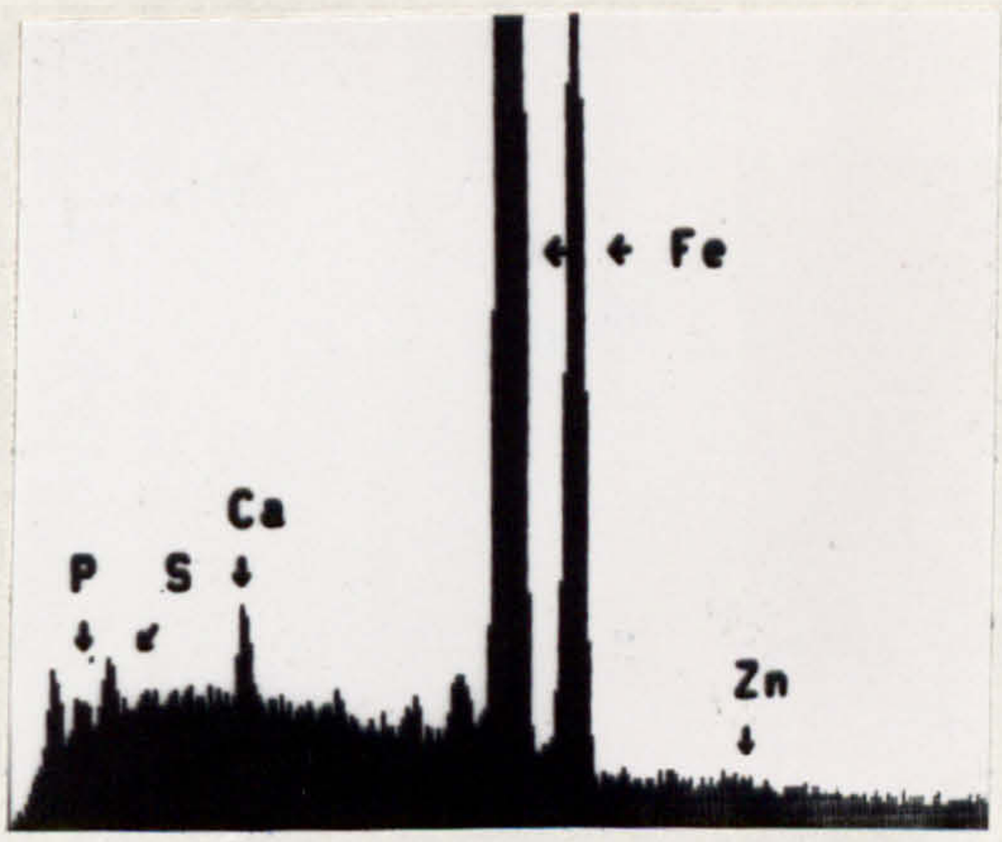

FIG. 140. TEST 2D - X-RAY ENERGY SPECTRA FOLLOWER WEAR SURFACE, 70 HOURS.

WINDOW LABEL	WINDOW CENTRE	FIRST CHAN	LAST CHAN	NET INTEGRAL	EFF. FACTOR	XAGE TOTAL
P	2040	1960	2140	770	1.00	0.16
S	2300	2200	2420	940	1.00	0.19
CA	3680	3580	3780	2856	1.00	0.59
FE	6360	6120	6620	481740	1.00	98.82
ZN	8580	8460	8720	1211	1.00	0.25

TABLE 12. SEMI-QUANTITATIVE ELEMENTAL ANALYSIS FOLLOWER SURFACE, 70 HOURS.

FIG. 141. TEST 2D - CAM SPECIMEN TAPERSECTION.

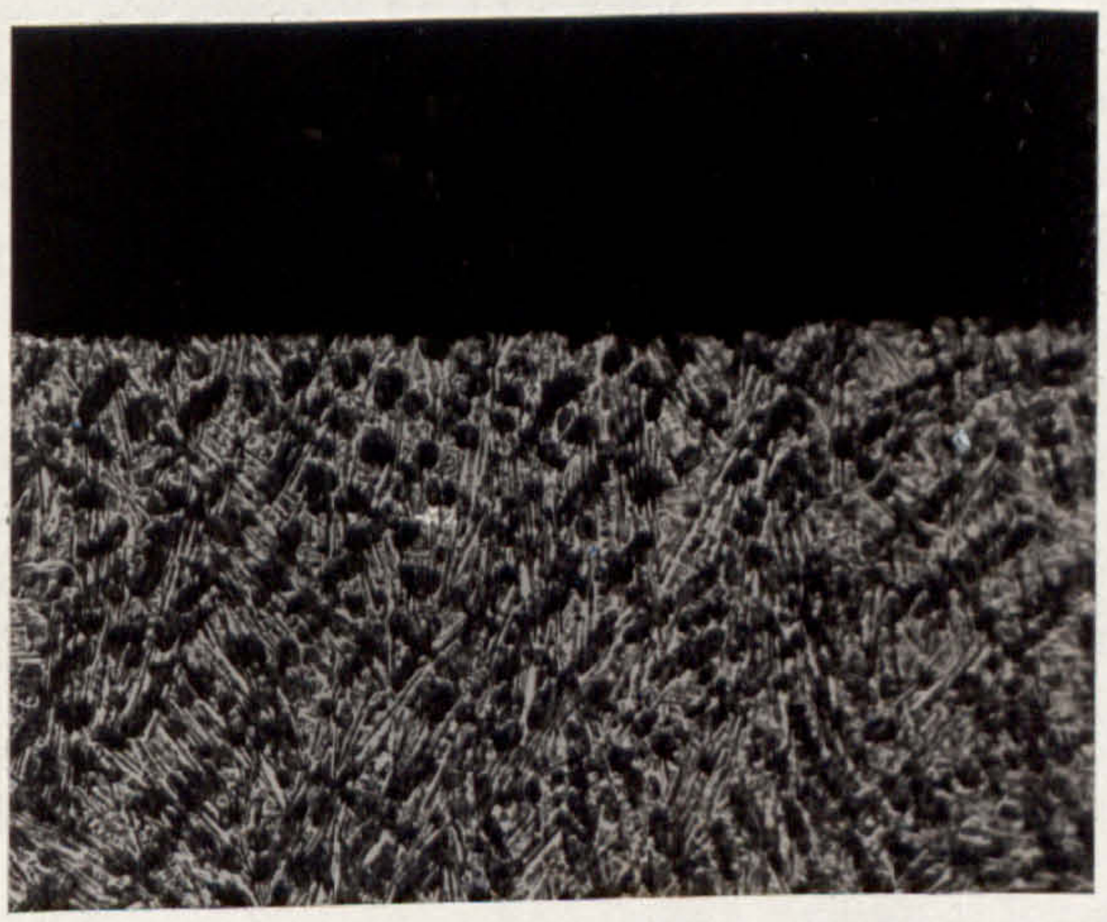

FIG. 142. TEST 2D - FOLLOWER SPECIMEN TAPERSECTION.

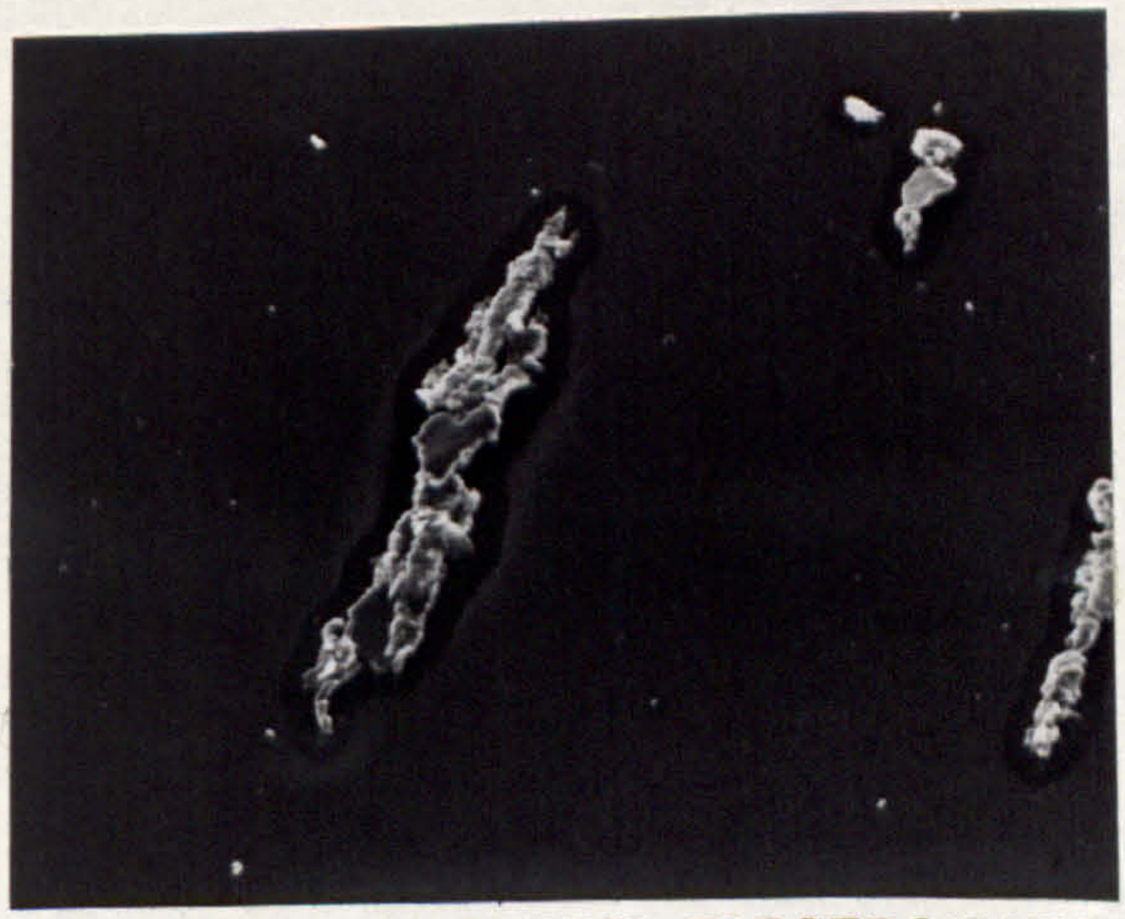

FIG. 143. TEST 2D - WEAR DEBRIS, ELECTRON MICROGRAPH.

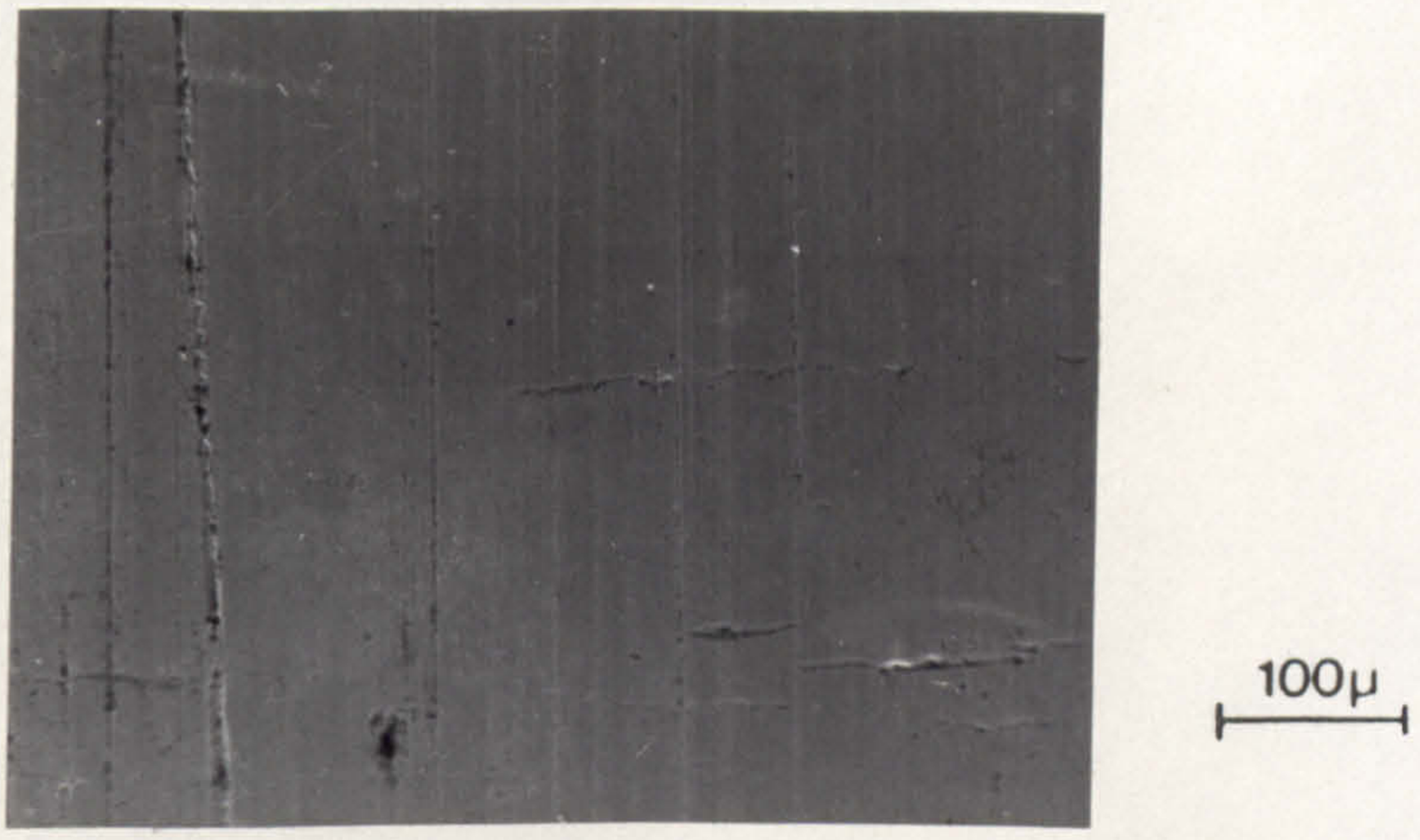

FIG. 144. TEST 2E - ELECTRON MICROGRAPH CAM WEAR SURFACE.

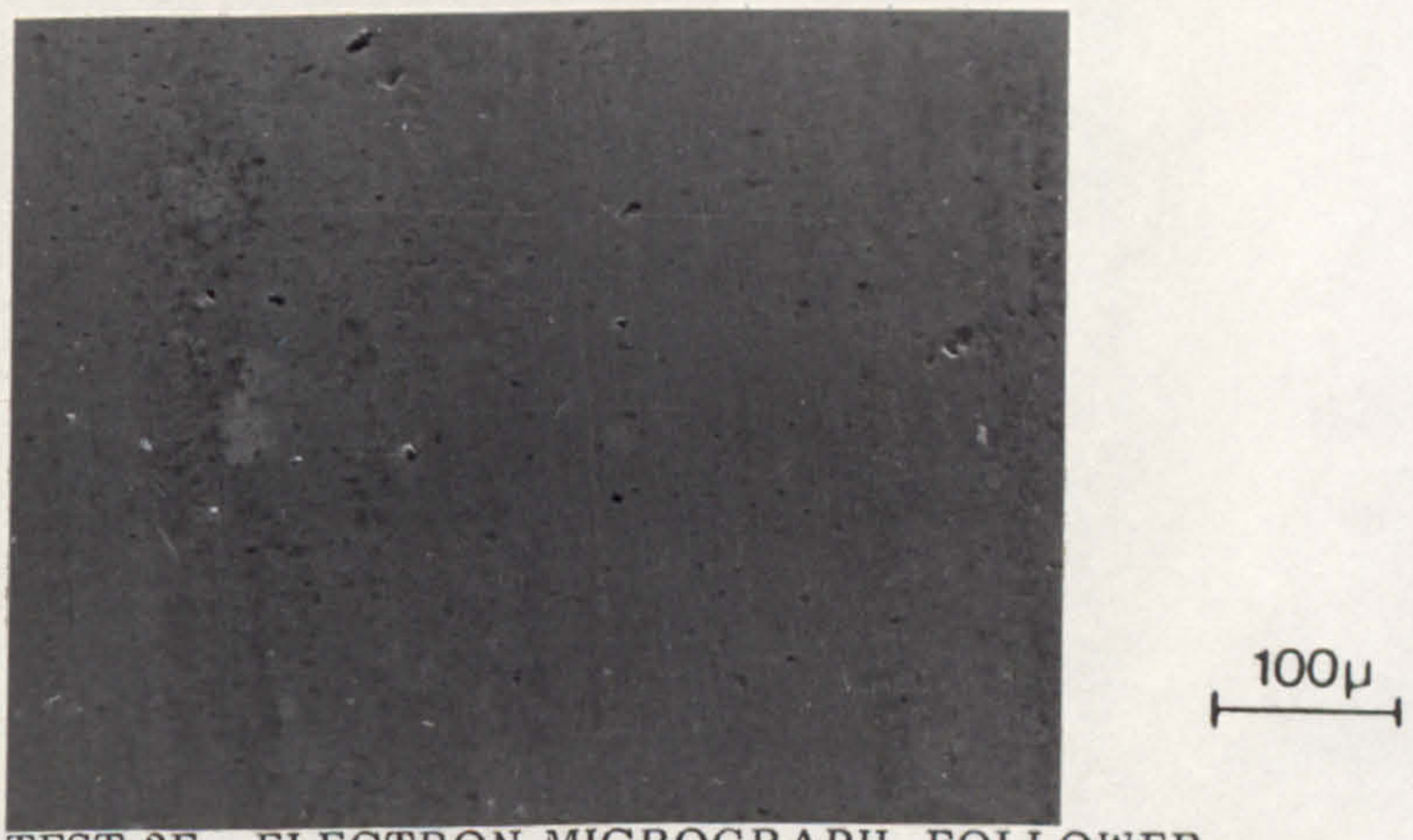

FIG. 145. TEST 2E - ELECTRON MICROGRAPH, FOLLOWER WEAR SURFACE.

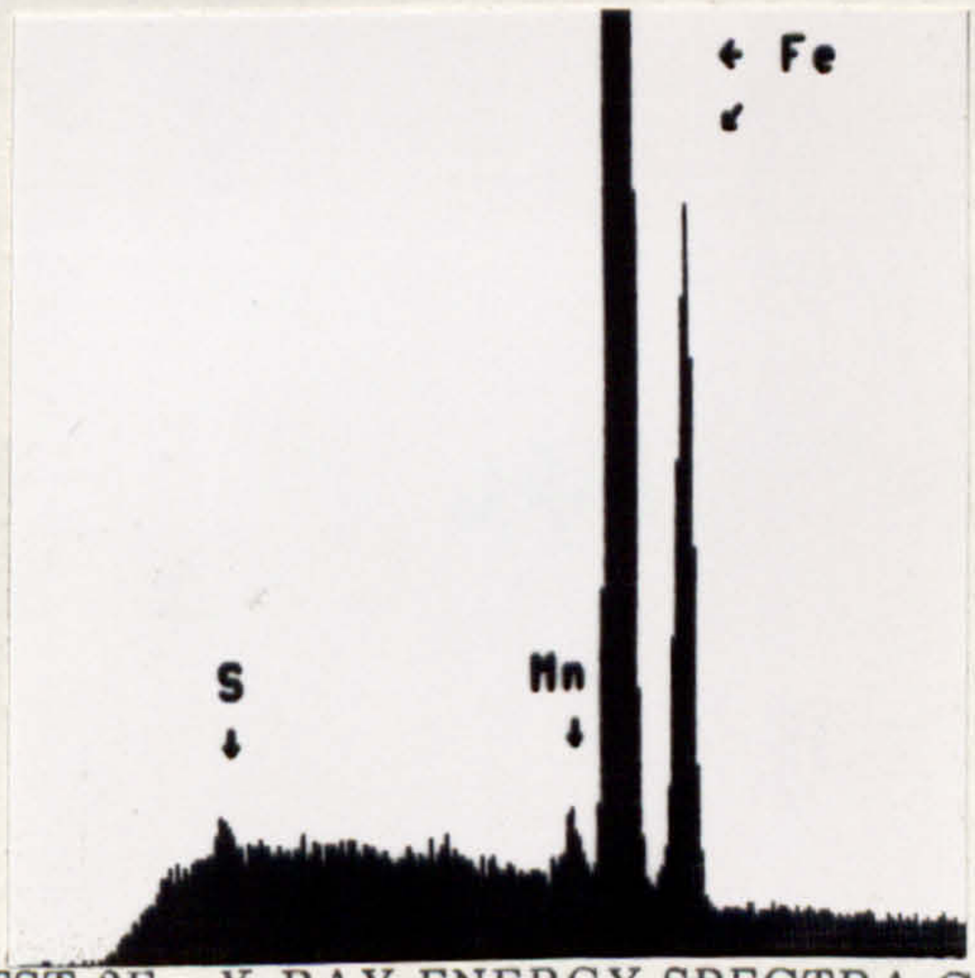

FIG. 146. TEST 2E - X-RAY ENERGY SPECTRA CAM WEAR SURFACE.

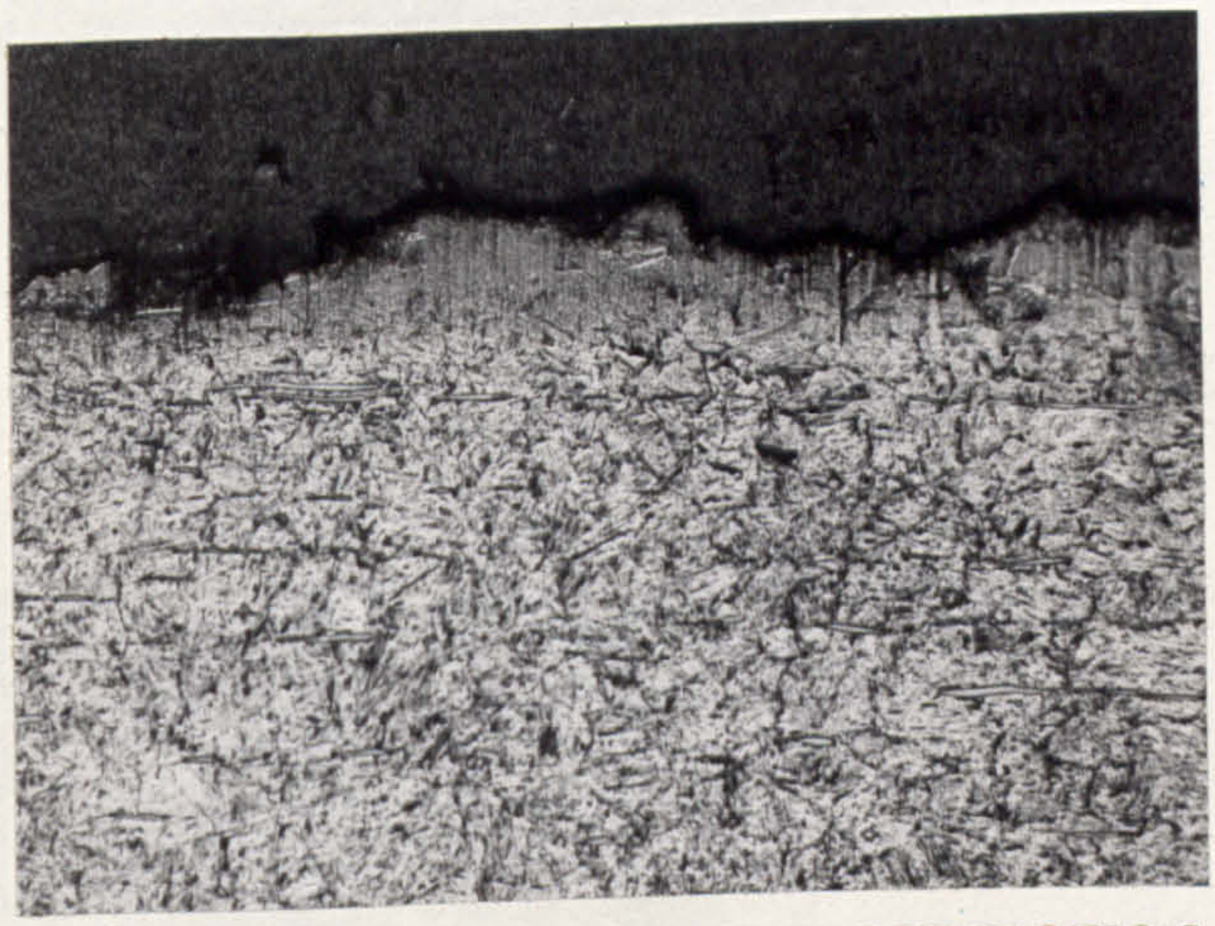

FIG. 147. TEST 2E - CAM SPECIMEN TAPERSECTION.

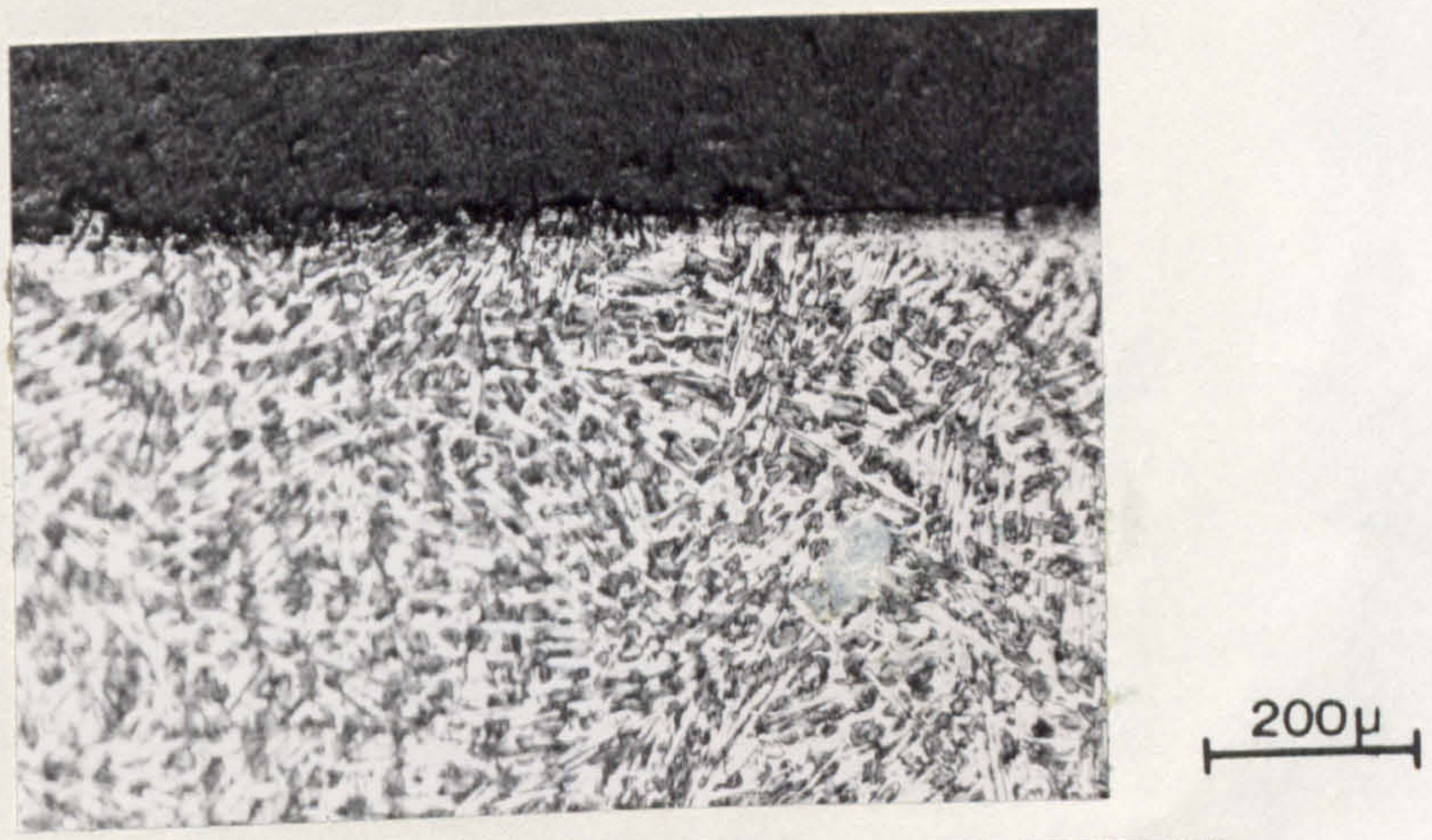

FIG. 148. TEST 2E - FOLLOWER SPECIMEN TAPERSECTION.

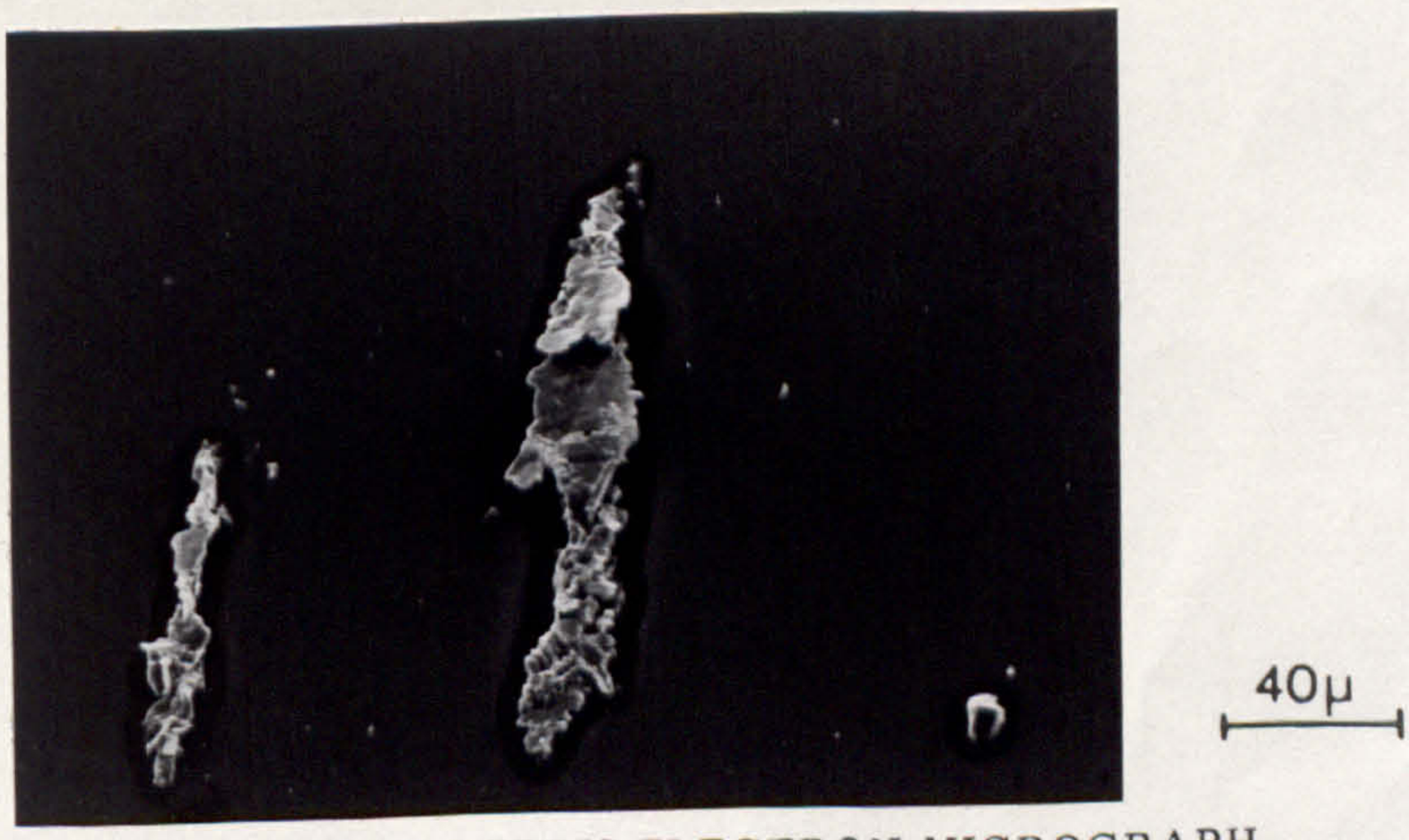

FIG. 149. TEST 2E - WEAR DEBRIS ELECTRON MICROGRAPH

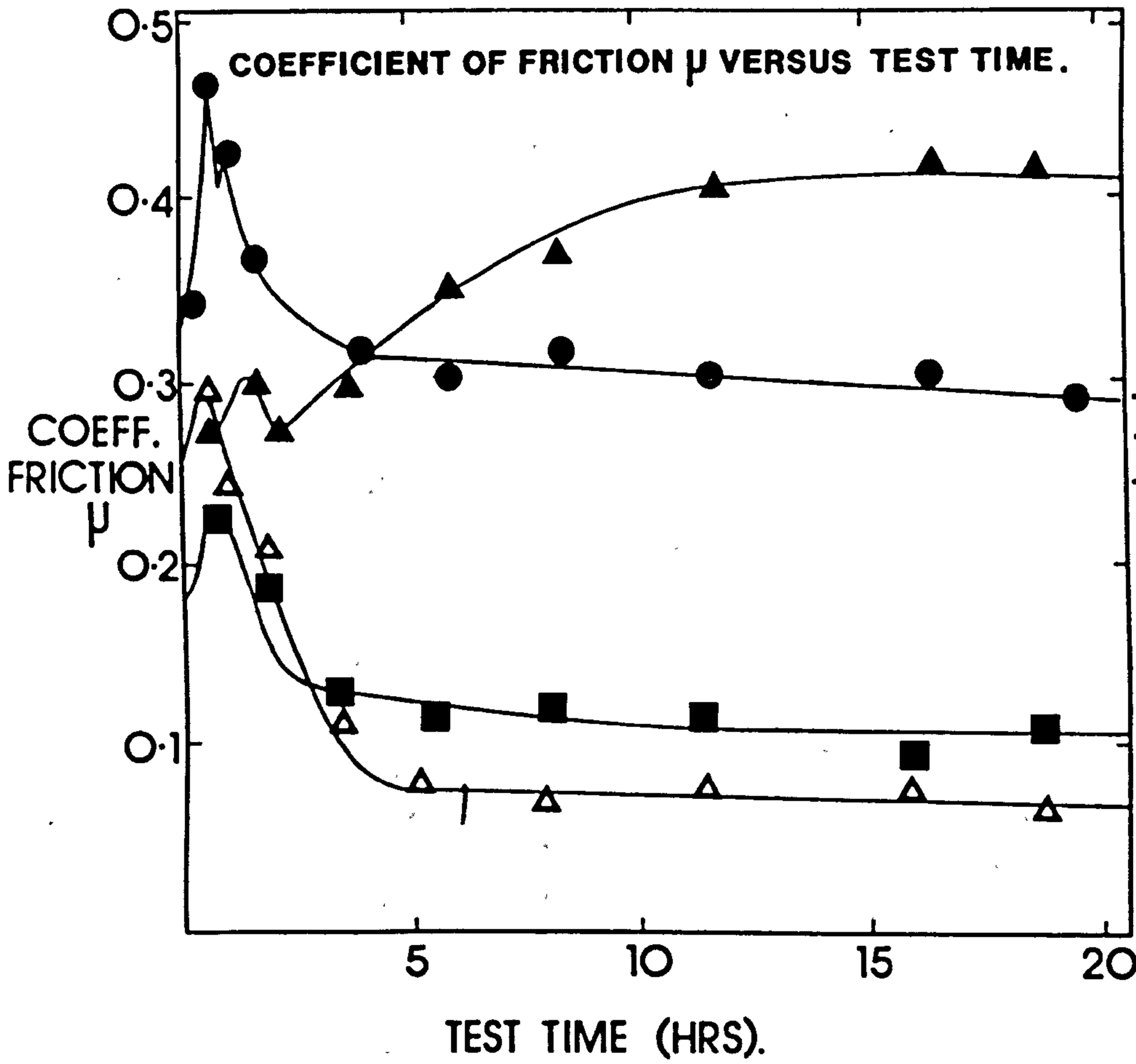

FIG. 150. GRAPH OF COEFFICIENT OF FRICTION VERSUS TEST TIME.

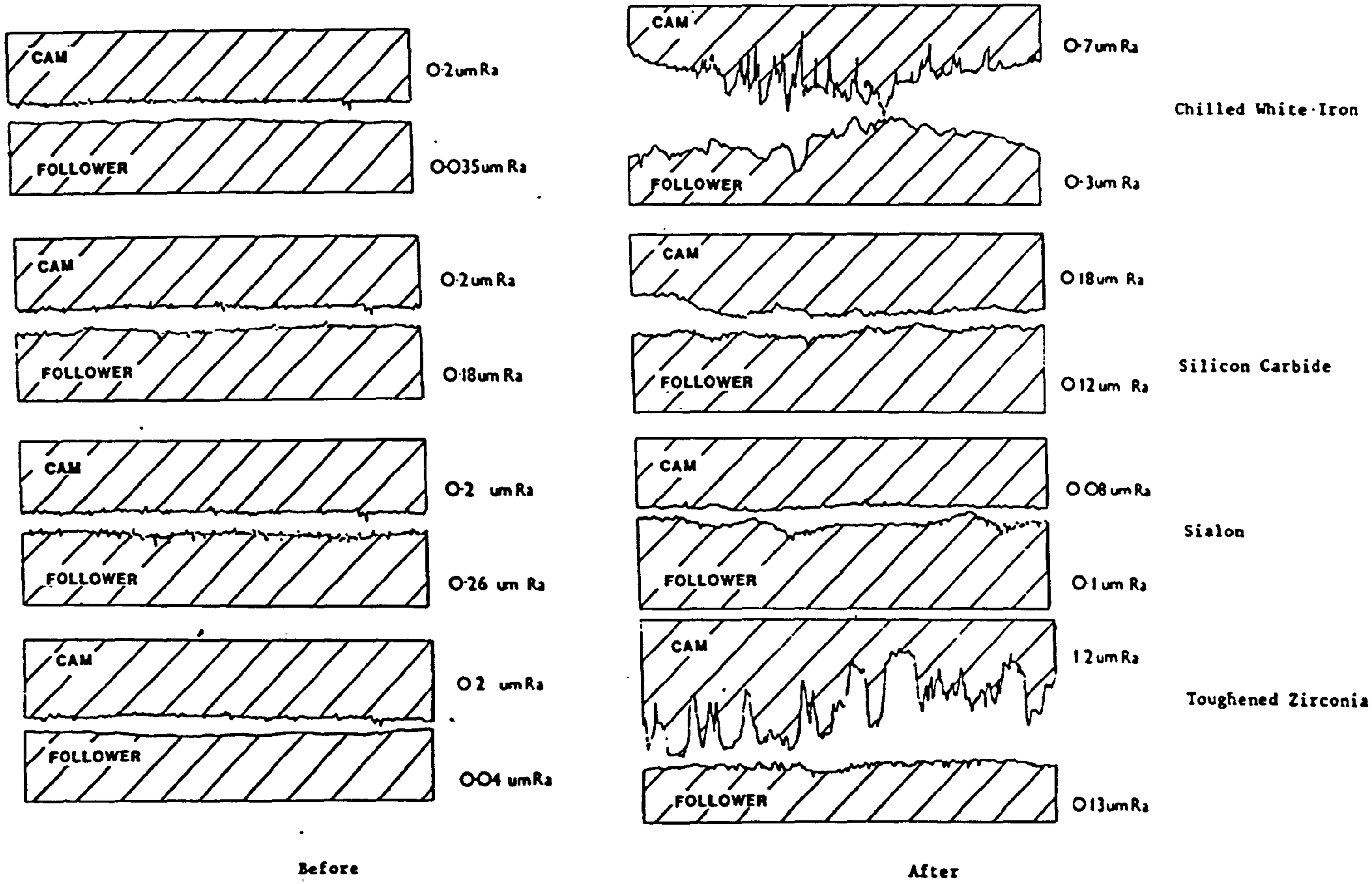

FIG. 151. TEST 3A-3C SURFACE ROUGHNESS MEASUREMENTS.

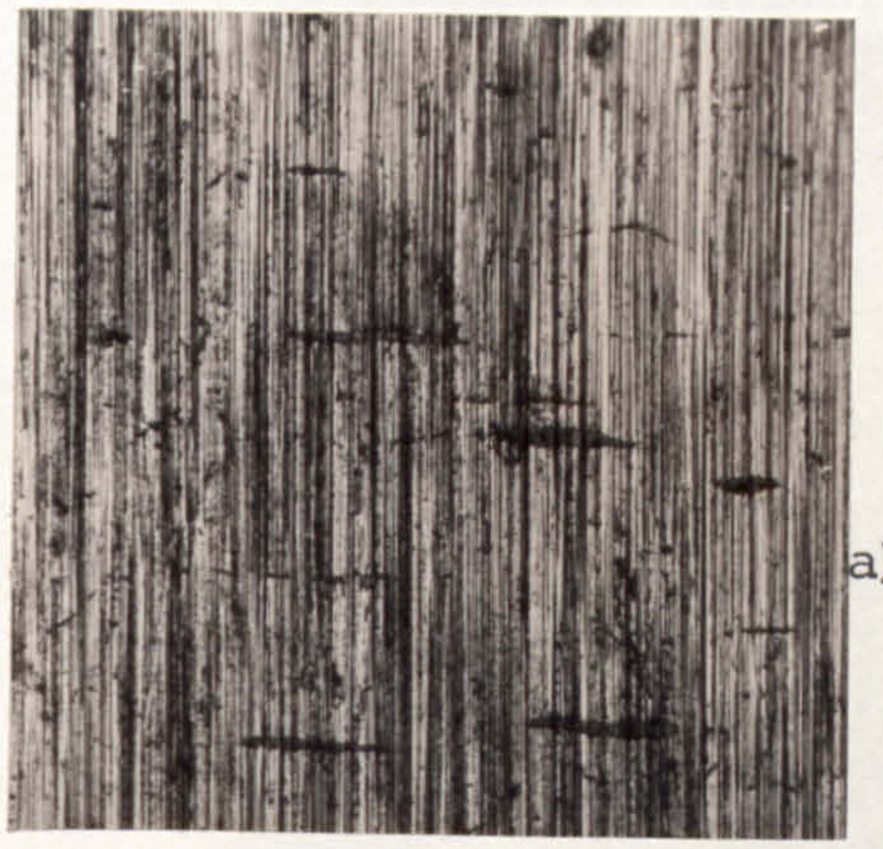

a)

b)

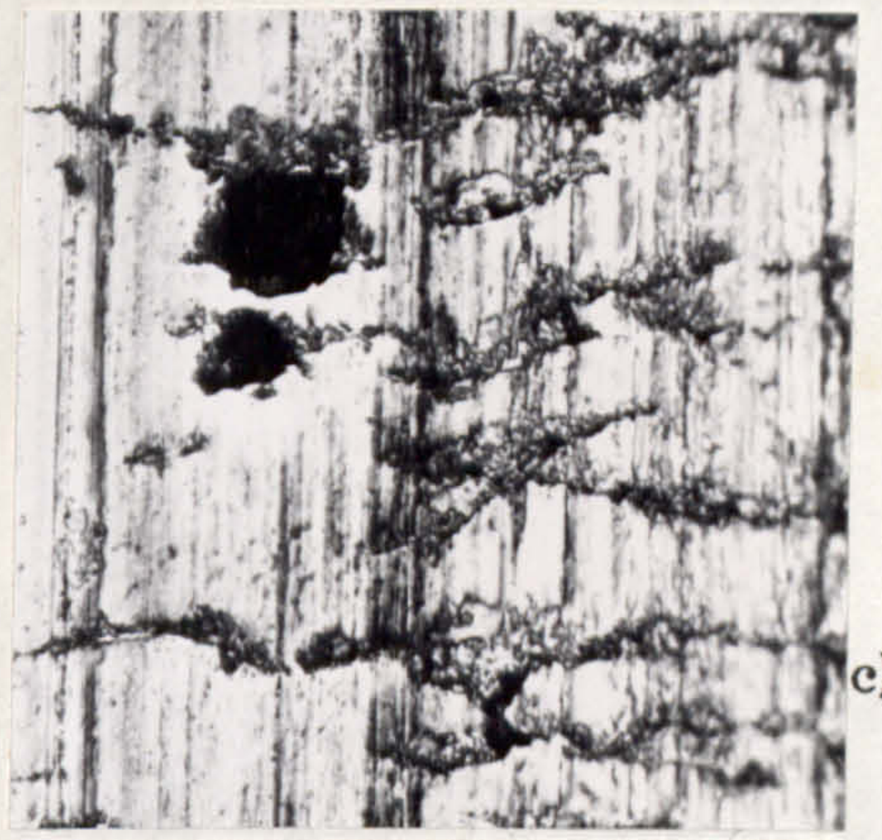

c)

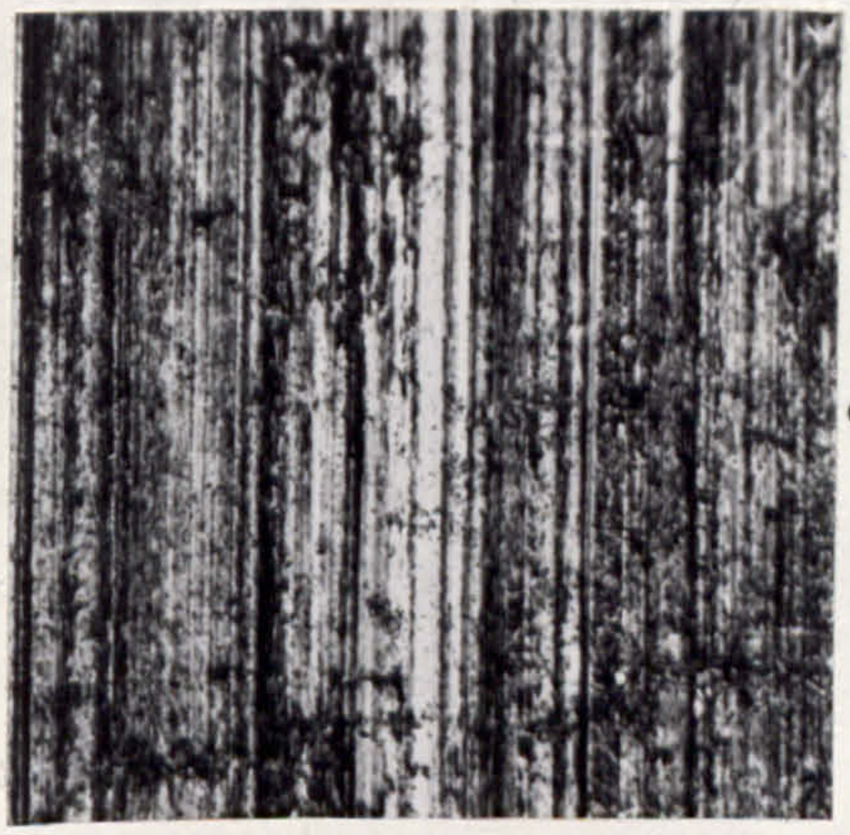

d)

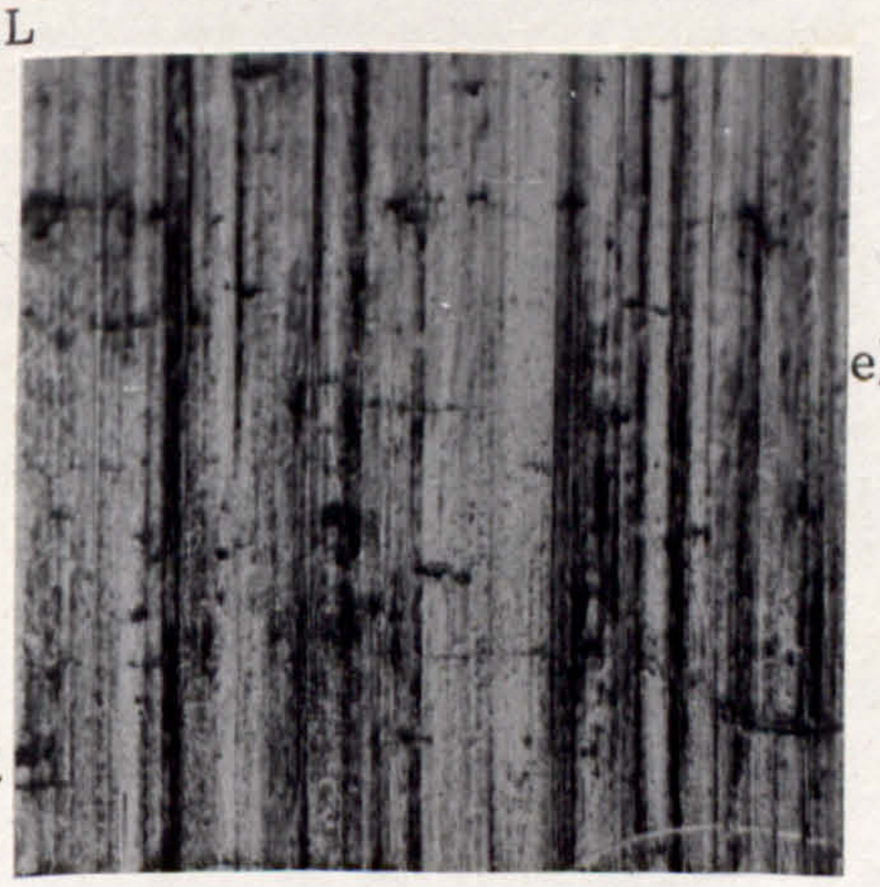

e)

200μ

FIG. 152. CAM SURFACES, OPTICAL EXAMINATION.

a) 'AS GROUND'

b) TEST 3A - WORN AGAINST A CHILLED IRON FOLLOWER

c) TEST 3B - WORN AGAINST A TOUGHENED ZIRCONIA FOLLOWER

d) TEST 3C - WORN AGAINST A SILICON CARBIDE FOLLOWER

e) TEST 3D - WORN AGAINST A SIALON FOLLOWER

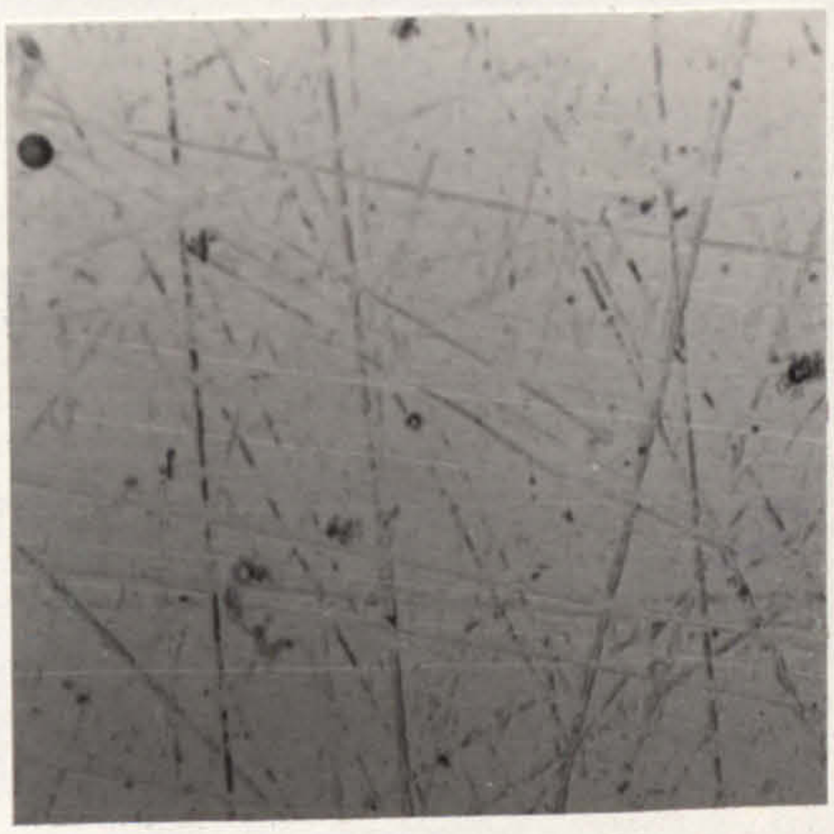

a)

b)

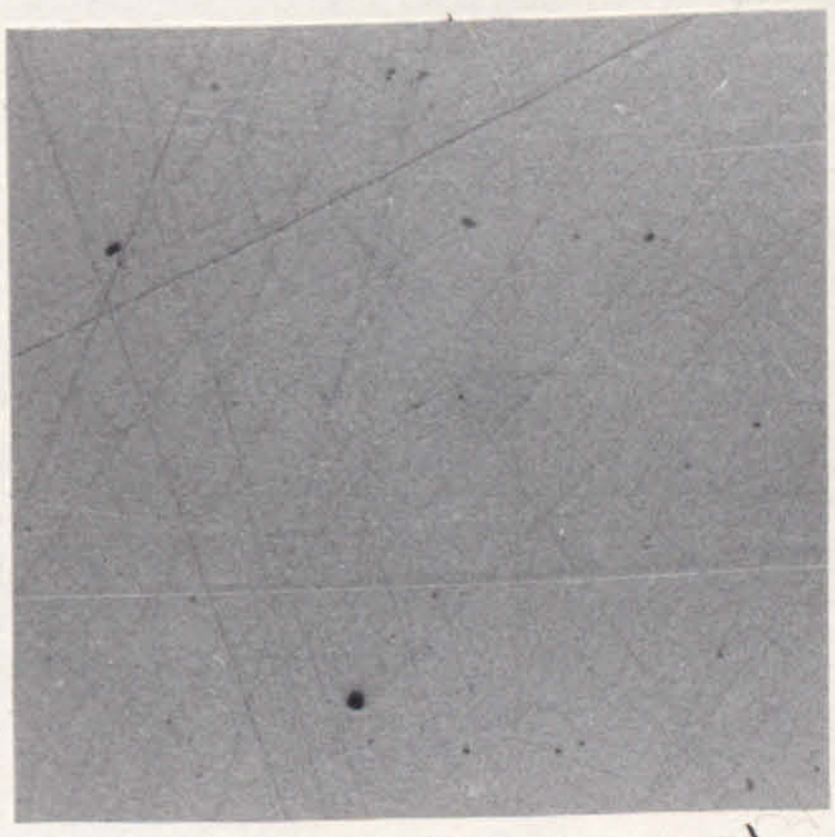

c)

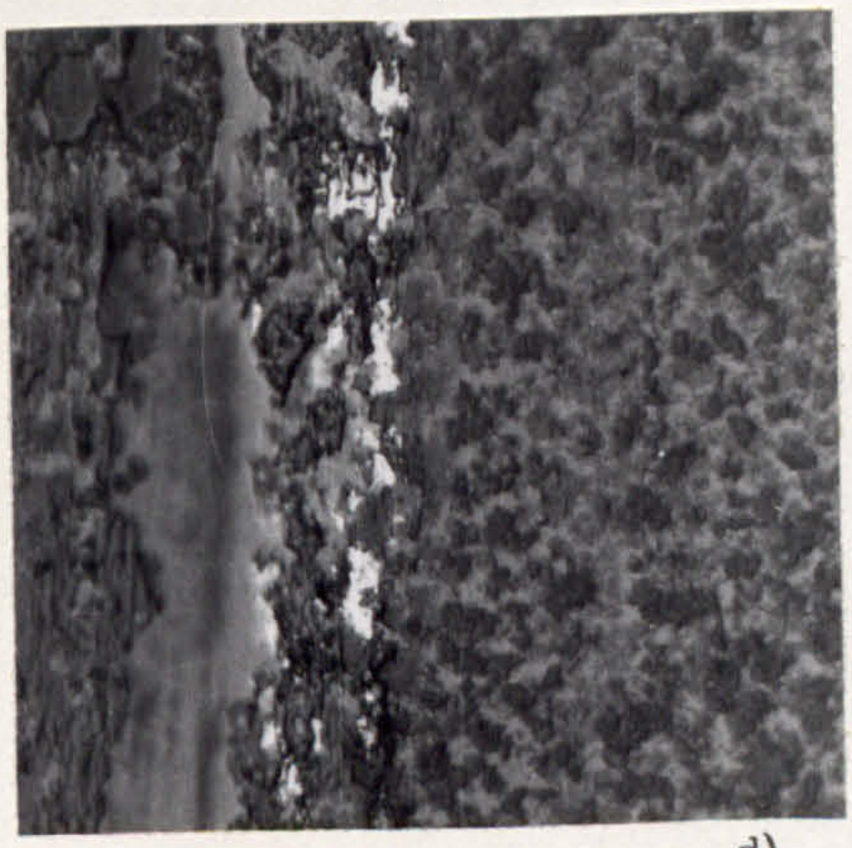

d)

200μ

FIG. 153. FOLLOWER SURFACES, OPTICAL EXAMINATION.

a) TEST 3A - CHILLED WHITE IRON, 'AS GROUND'.

b) TEST 3A - CHILLED WHITE IRON, 'WORN'.

c) TEST 3B - TOUGHENED ZIRCONIA, 'AS FINISHED'.

d) TEST 3B - TOUGHENED ZIRCONIA, 'WORN'.

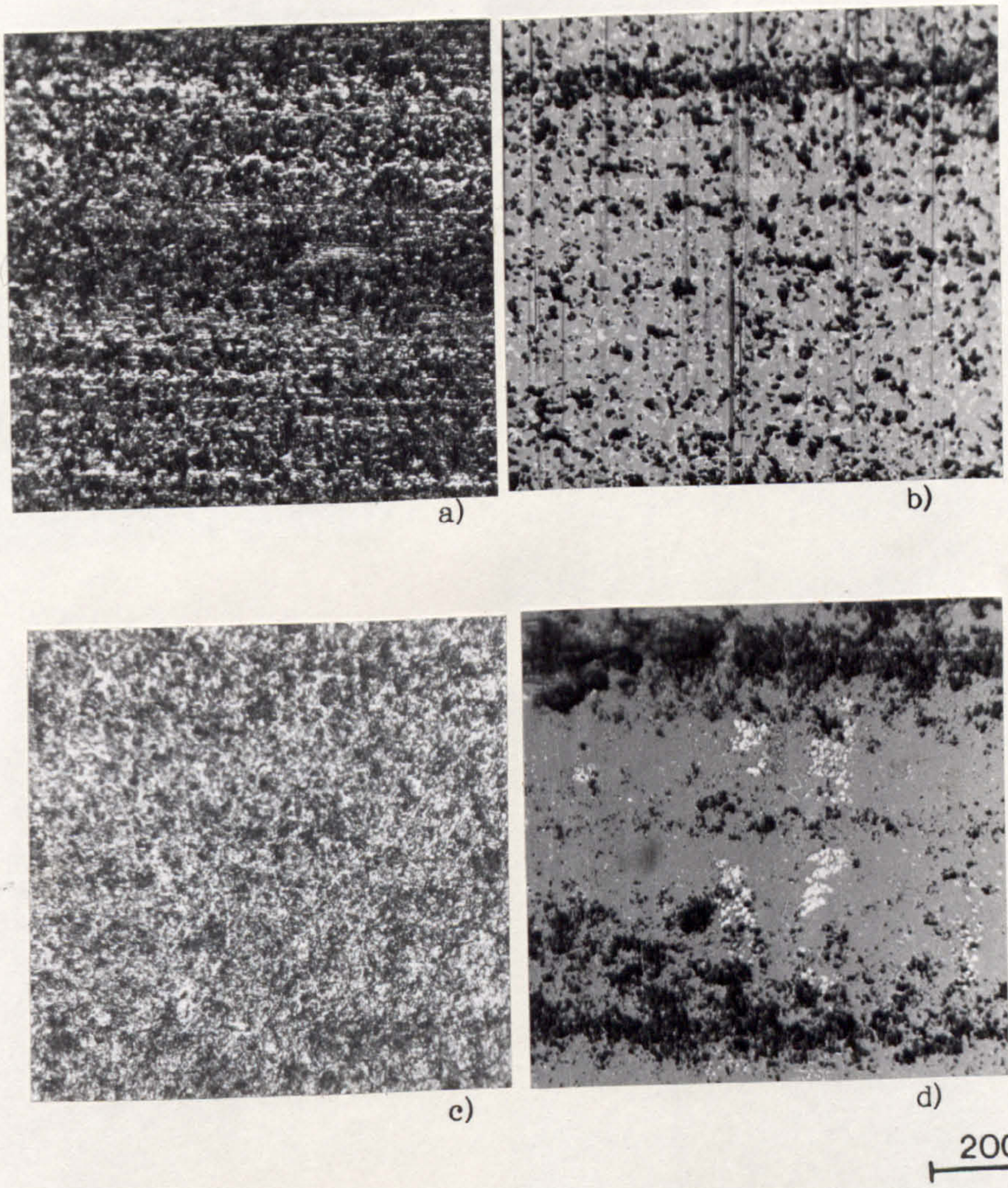

FIG. 154. FOLLOWER SURFACES, OPTICAL EXAMINATION.

a) TEST 3C - SILICON CARBIDE, 'AS FINISHED'.

b) TEST 3C - SILICON CARBIDE, 'WORN'.

c) TEST 3D - SIALON, 'AS FINISHED'.

d) TEST 3D - SIALON, 'WORN'.

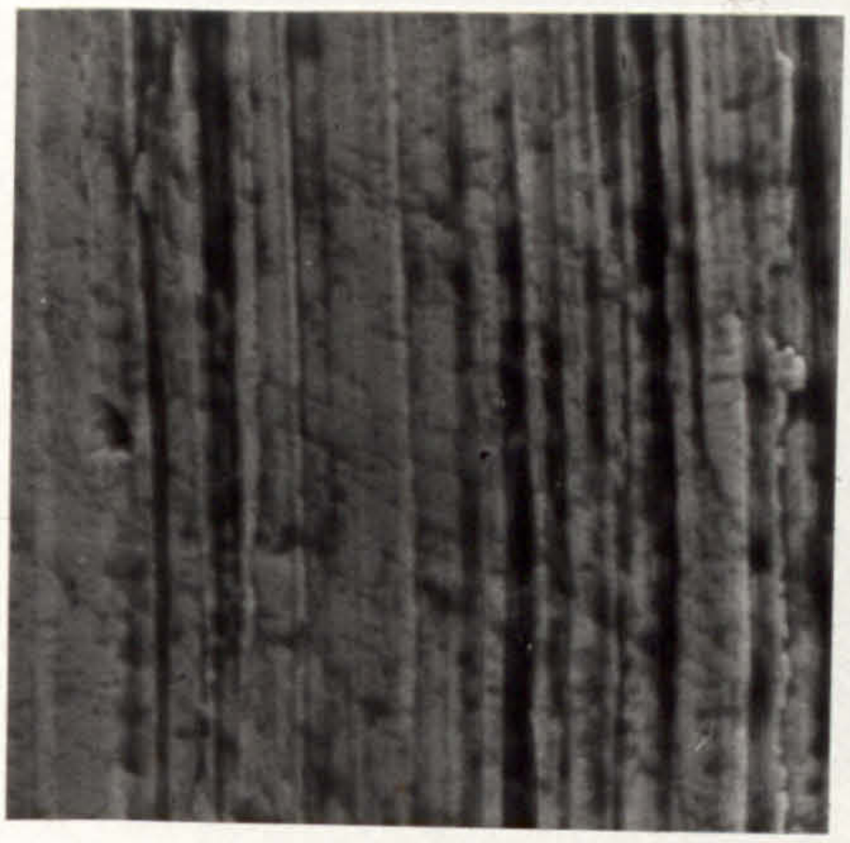

a)

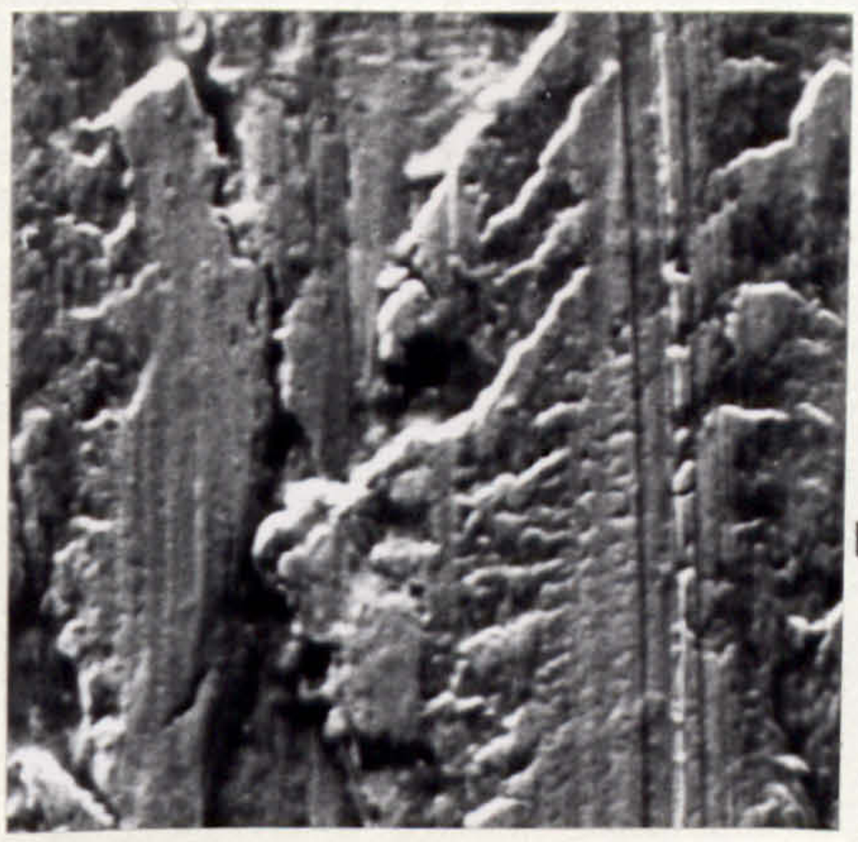

b)

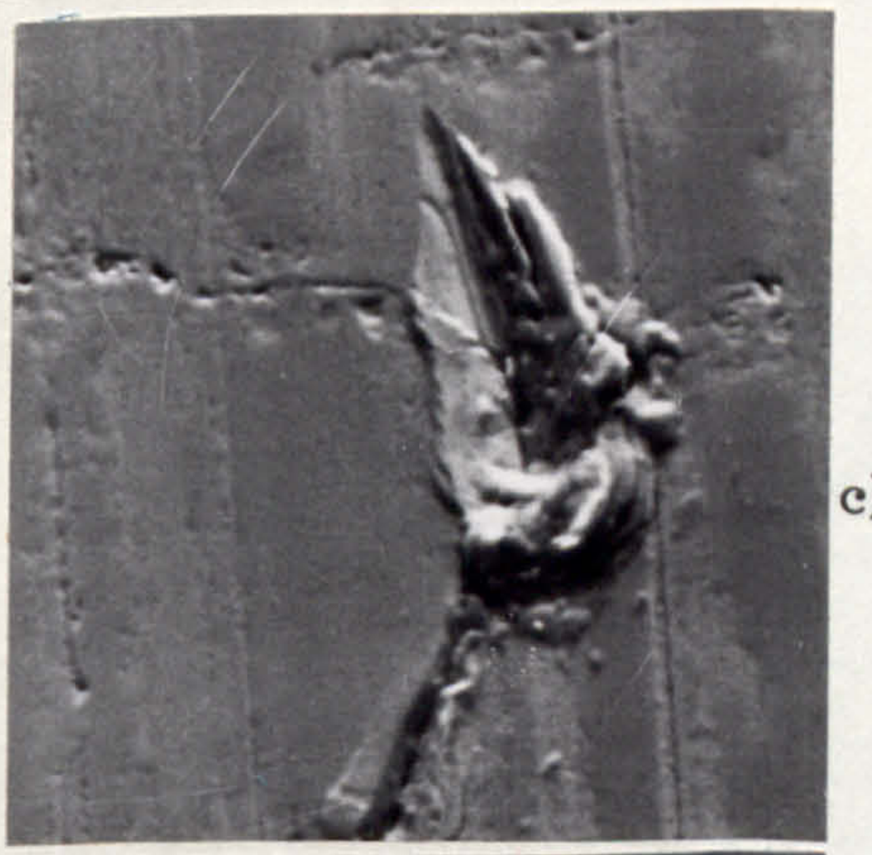

c)

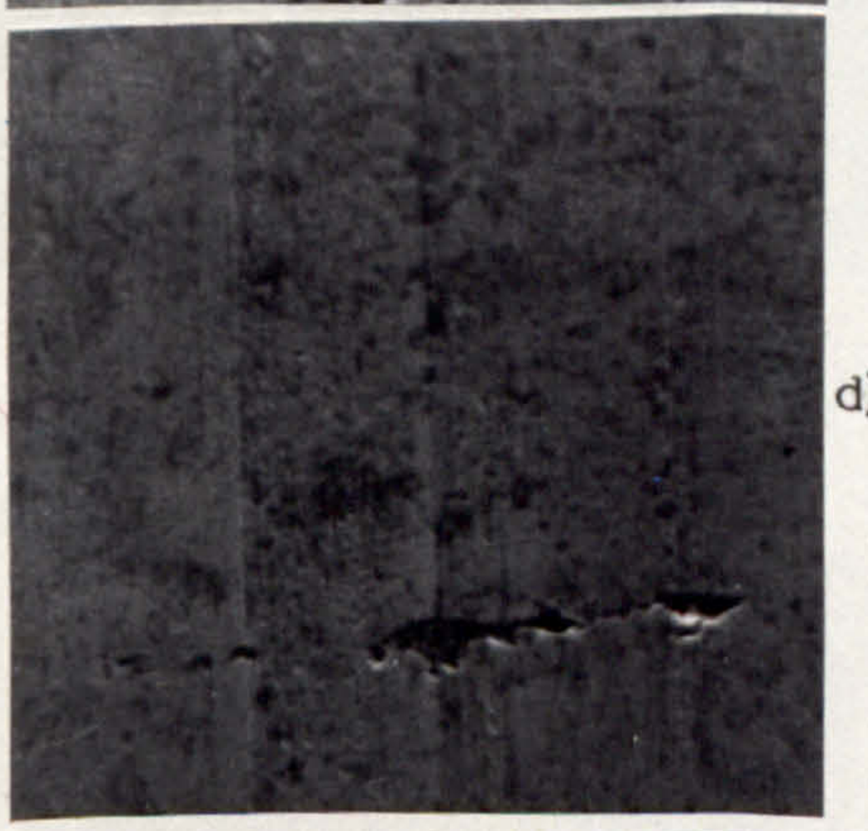

d)

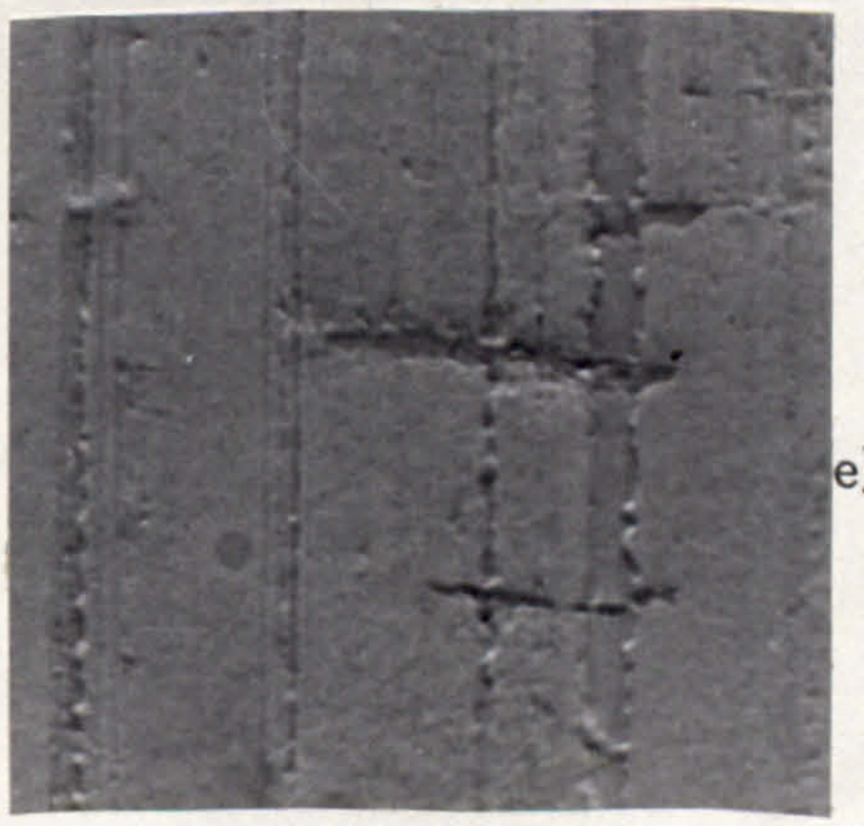

e)

20μ

FIG. 155. CAM SURFACES, S.E.M. EXAMINATION.

a) 'AS GROUND'

b) TEST 3A - WORN AGAINST A CHILLED WHITE IRON FOLLOWER

c) TEST 3B - WORN AGAINST A TOUGHENED ZIRCONIA FOLLOWER

d) TEST 3C - WORN AGAINST A SILICON CARBIDE FOLLOWER

e) TEST 3D - WORN AGAINST A SIALON FOLLOWER

a)

b)

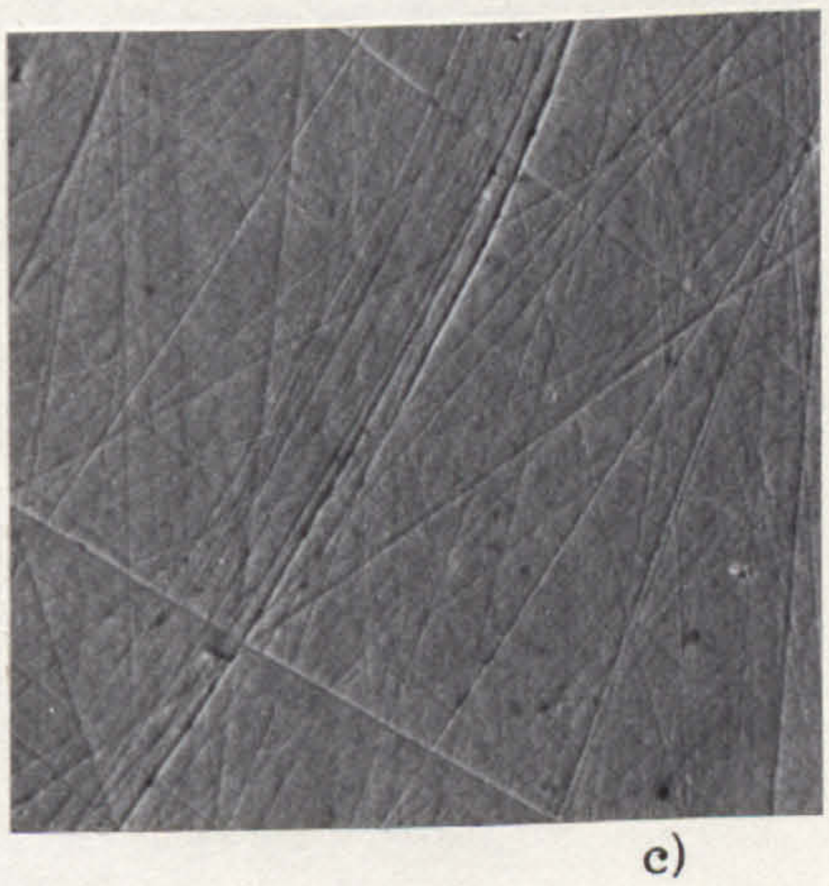

c)

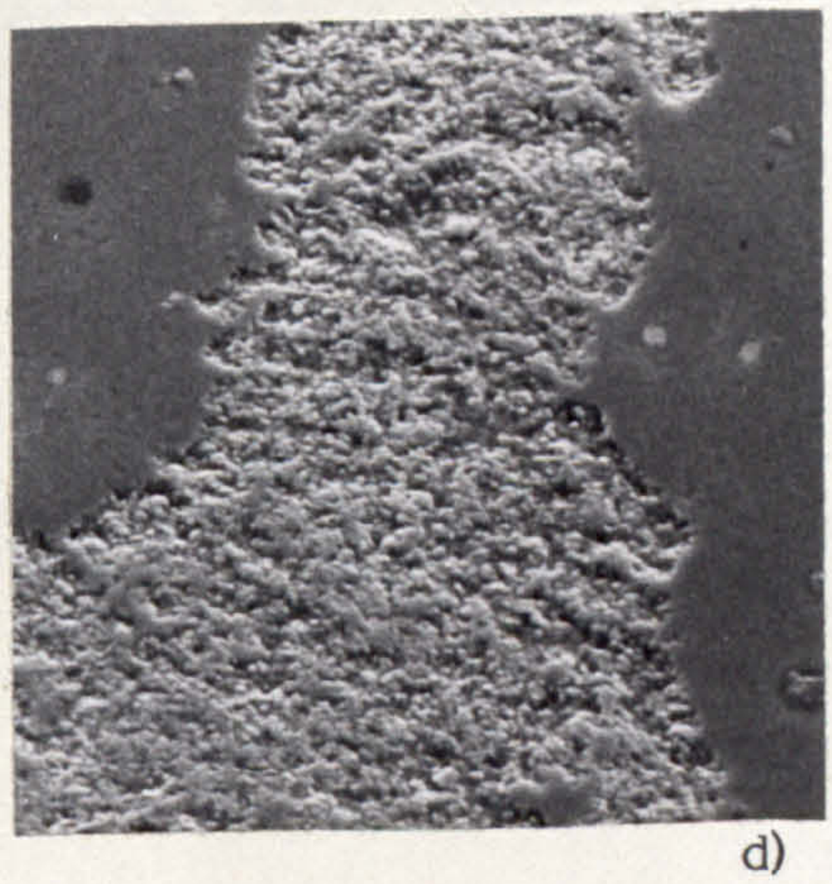

d)

20μ

FIG. 156. FOLLOWER SURFACES, S.E.M. EXAMINATION.

a) TEST 3A - CHILLED WHITE IRON, 'AS GROUND'.

b) TEST 3A - CHILLED WHITE IRON, 'WORN'.

c) TEST 3B - TOUGHENED ZIRCONIA, 'AS FINISHED'.

d) TEST 3B - TOUGHENED ZIRCONIA, 'WORN'.

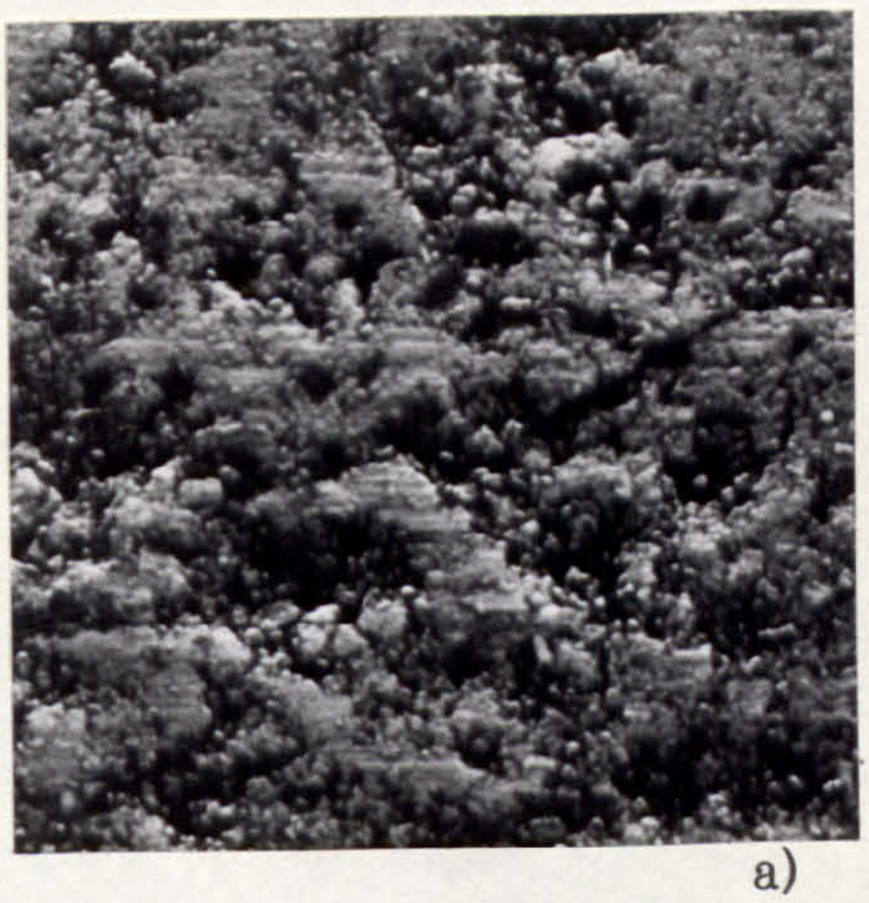

a)

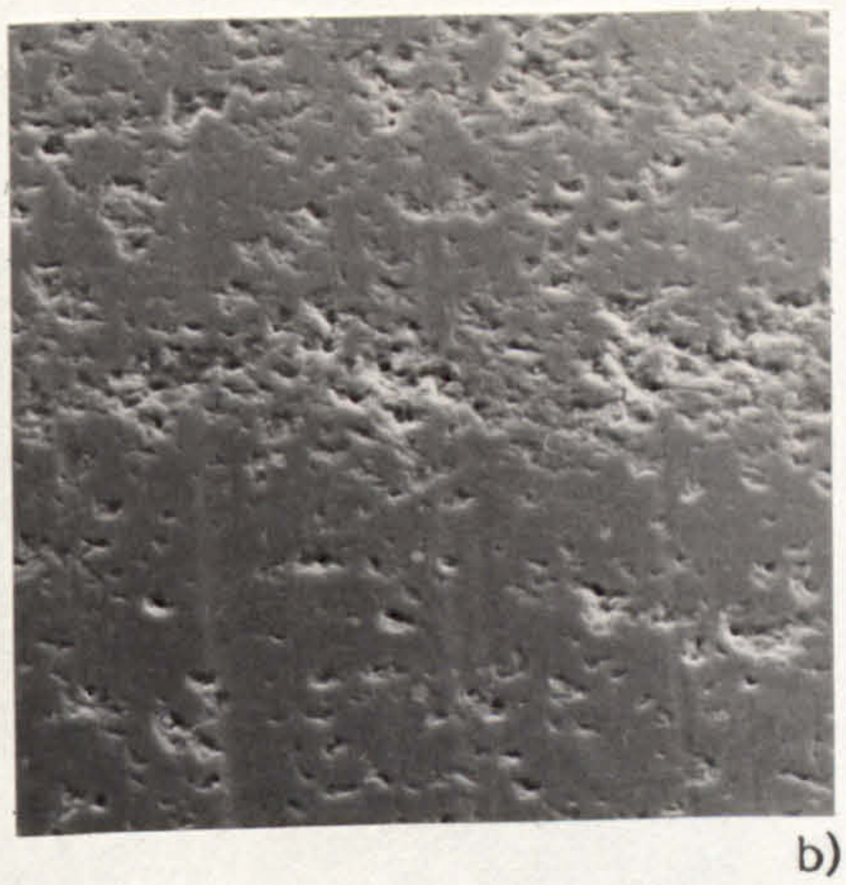

b)

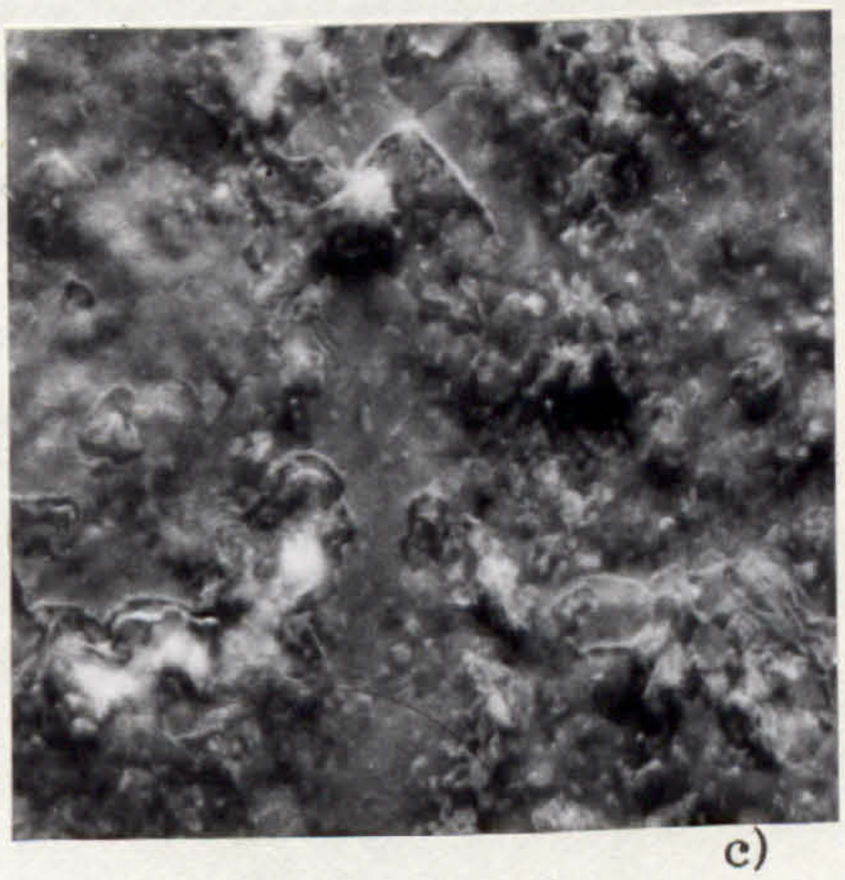

c)

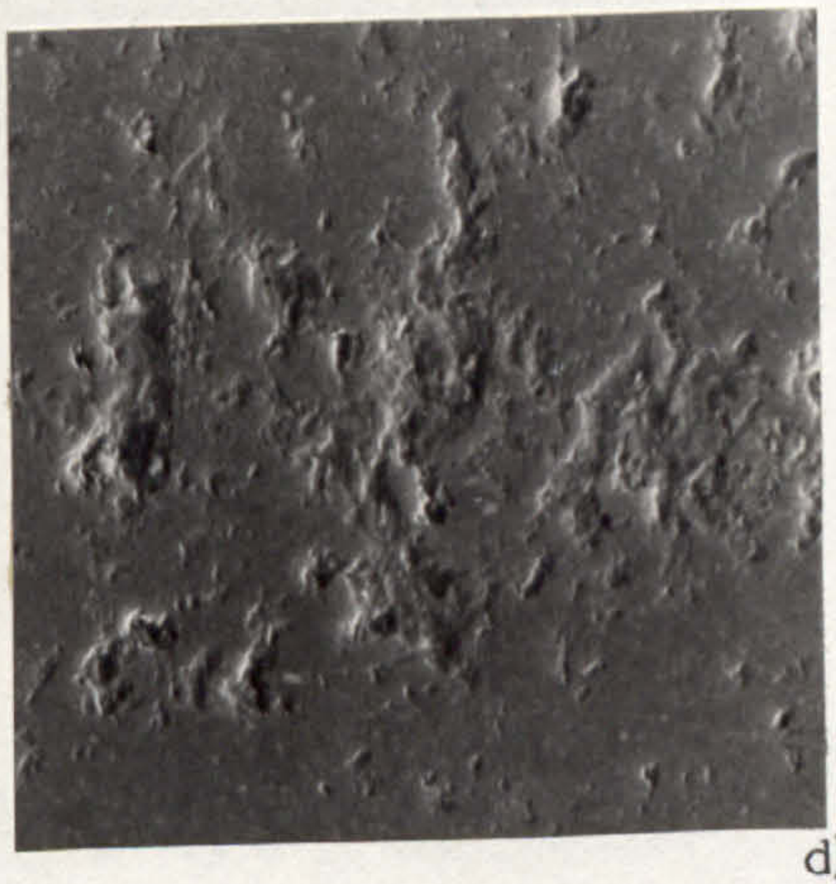

d)

20μ

FIG. 157. FOLLOWER SURFACES, S.E.M.

a) TEST 3C - SILICON CARBIDE, 'AS FINISHED'.

b) TEST 3C - SILICON CARBIDE, 'WORN'.

c) TEST 3D - SIALON, 'AS FINISHED'.

d) TEST 3D - SIALON, 'WORN'.

a)

b)

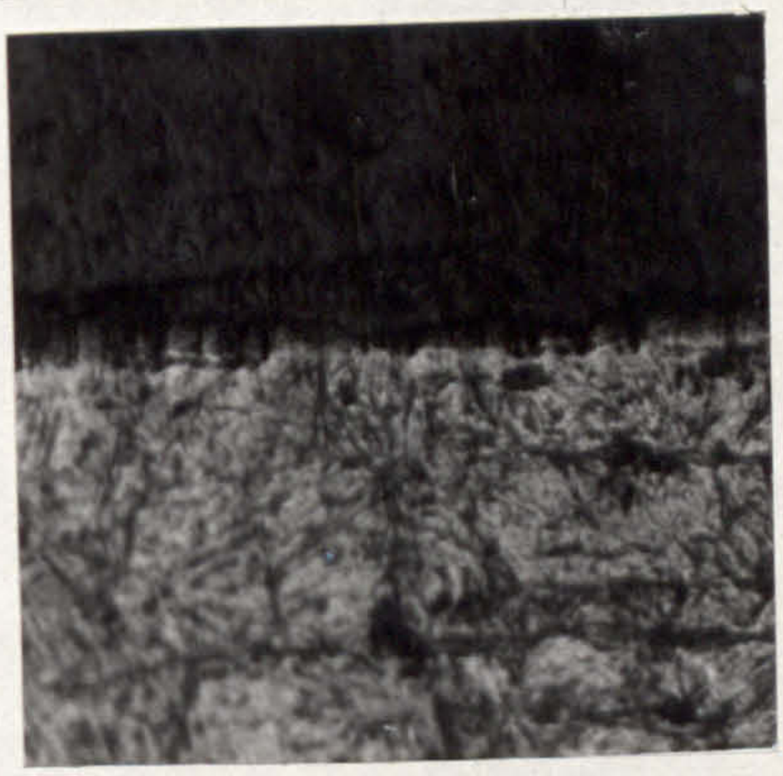

c)

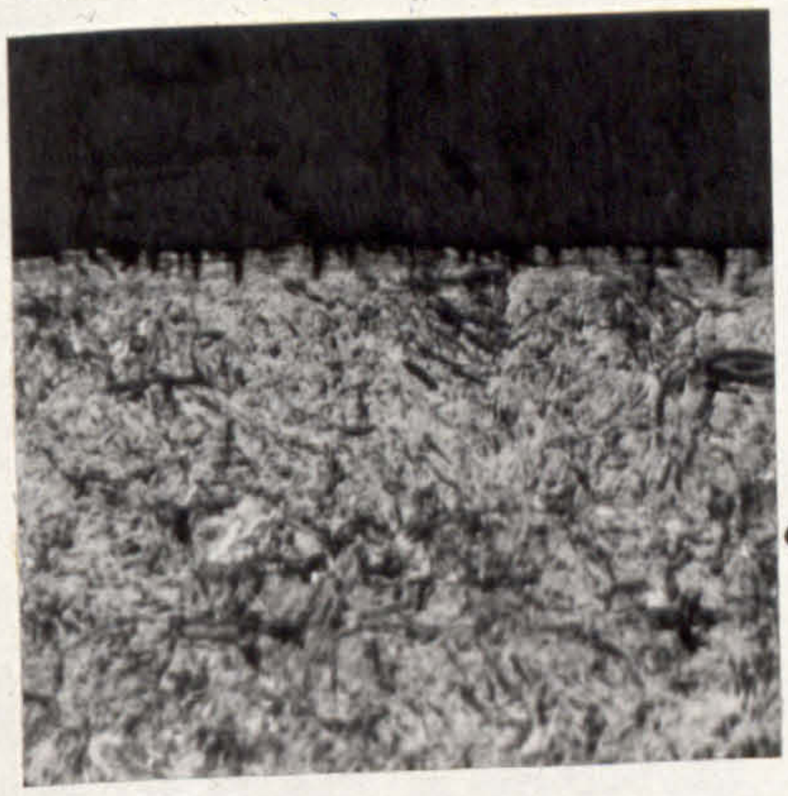

d)

100μ

FIG. 158. CAM SPECIMEN TAPERSECTIONS.

a) TEST 3A - WORN AGAINST A CHILLED WHITE IRON FOLLOWER.
b) TEST 3B - WORN AGAINST A TOUGHENED ZIRCONIA FOLLOWER.
c) TEST 3C - WORN AGAINST A SILICON CARBIDE FOLLOWER.
d) TEST 3D - WORN AGAINST A SIALON FOLLOWER.

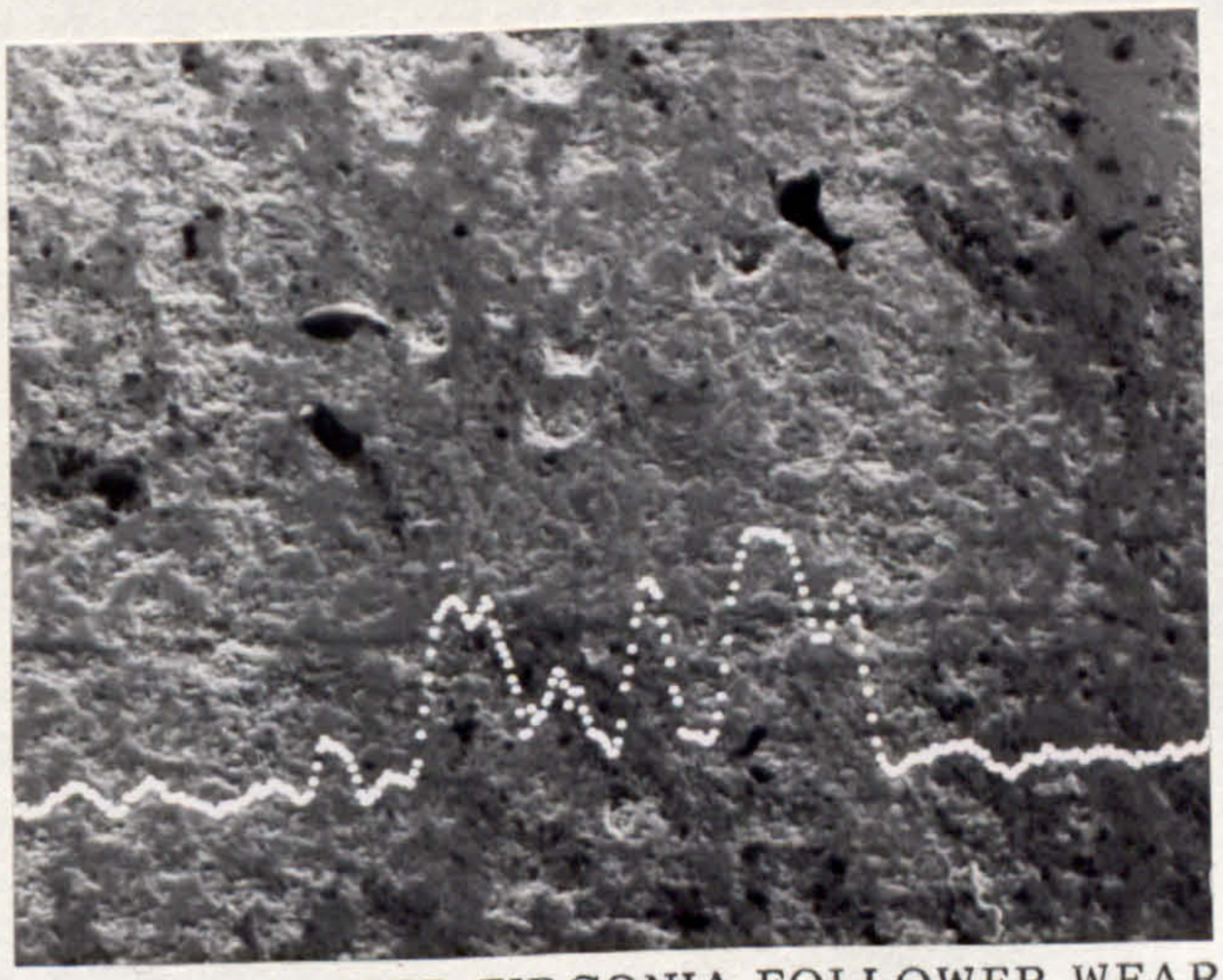

40μ

FIG. 159. TEST 3B. TOUGHENED ZIRCONIA FOLLOWER WEAR SURFACE. Fe LINE SCAN SHOWING MATERIAL TRANSFER.

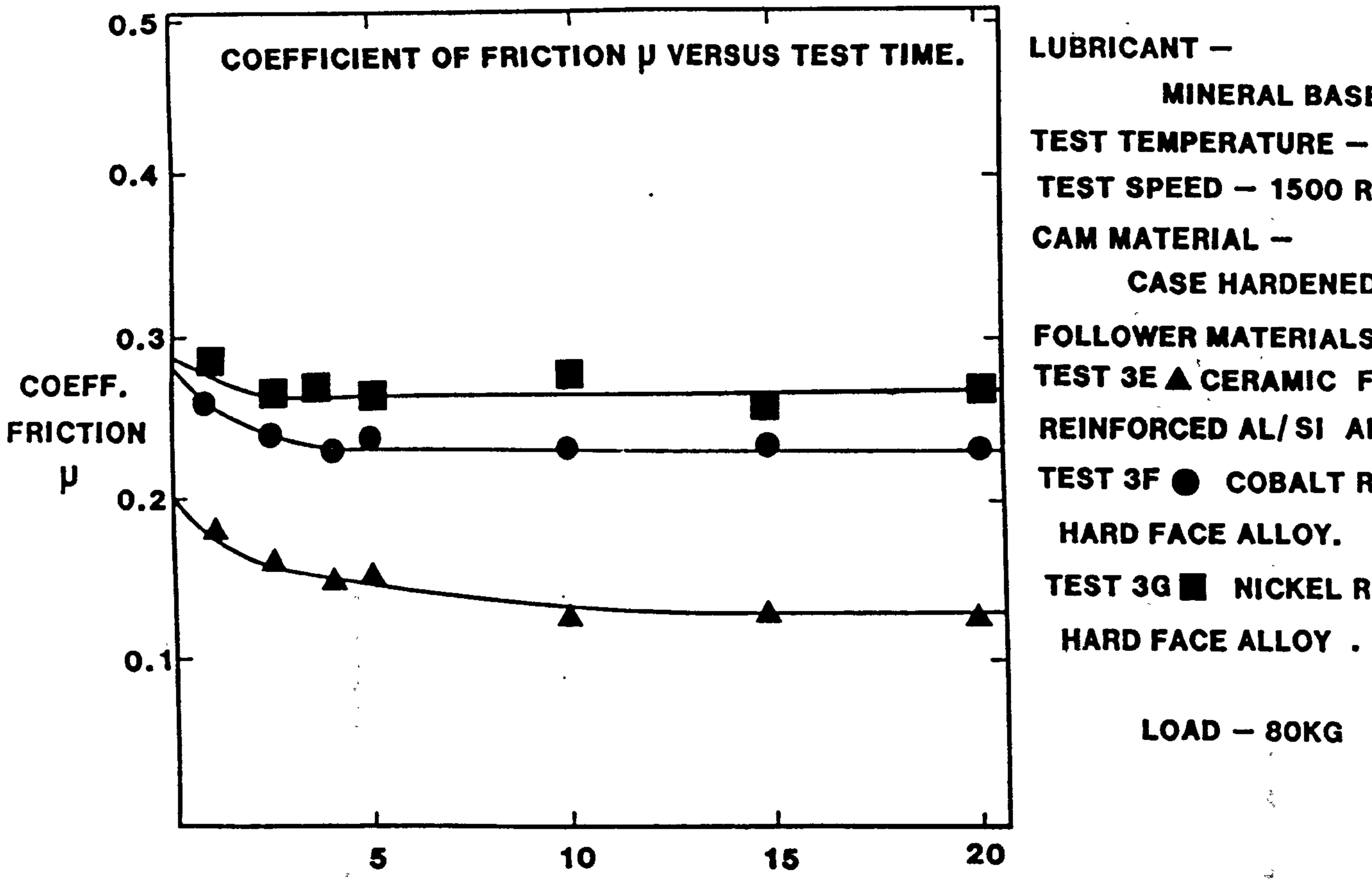

FIG. 160. GRAPH OF COEFFICIENT OF FRICTION VERSUS TEST TIME.

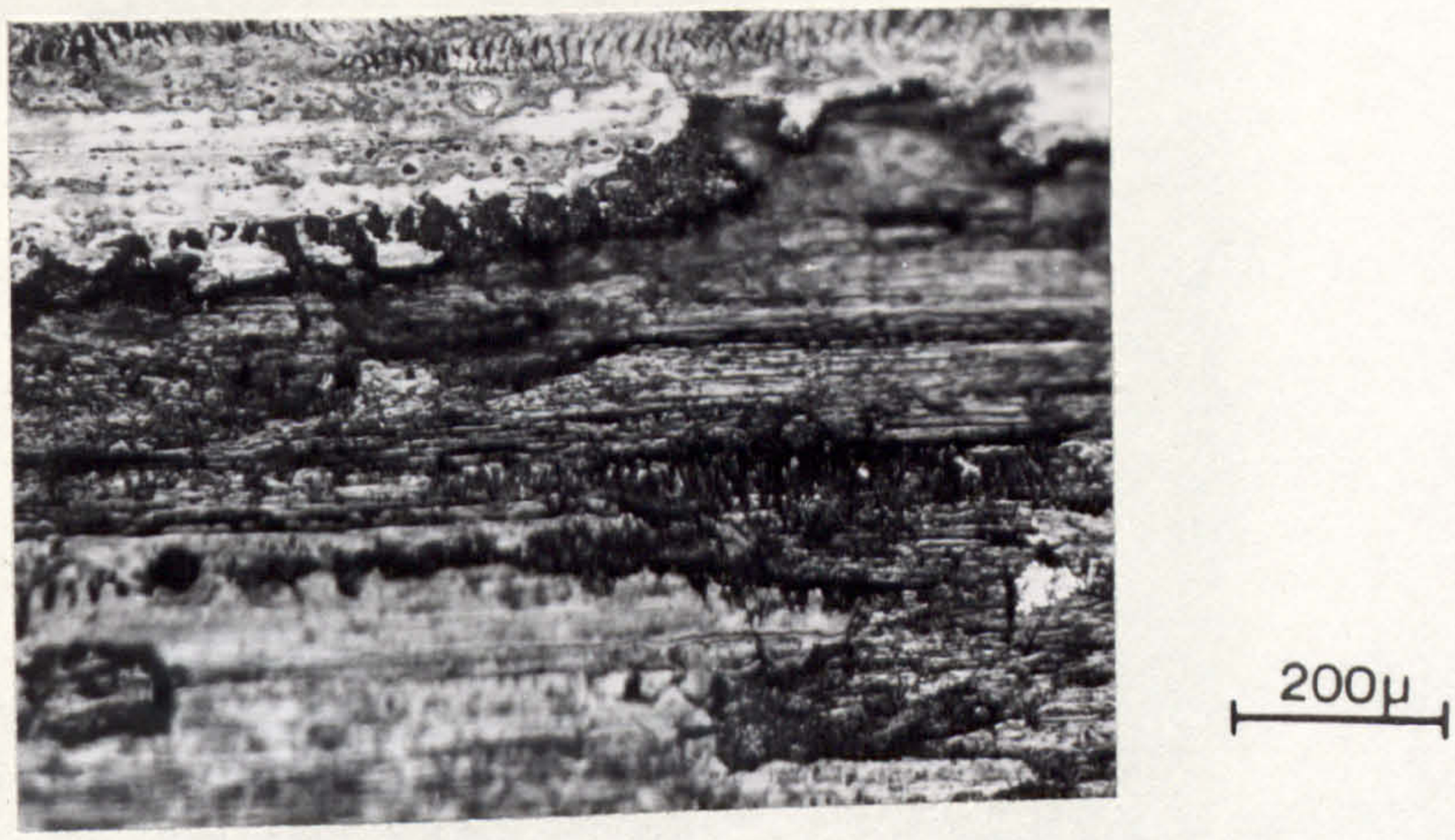

FIG. 161. TEST 3E, CAM WEAR SURFACE, OPTICAL.

FIG. 162. TEST 3E, FOLLOWER WEAR SURFACE, OPTICAL.

FIG. 163. TEST 3E, CAM WEAR SURFACE ELECTRON MICROGRAPH.

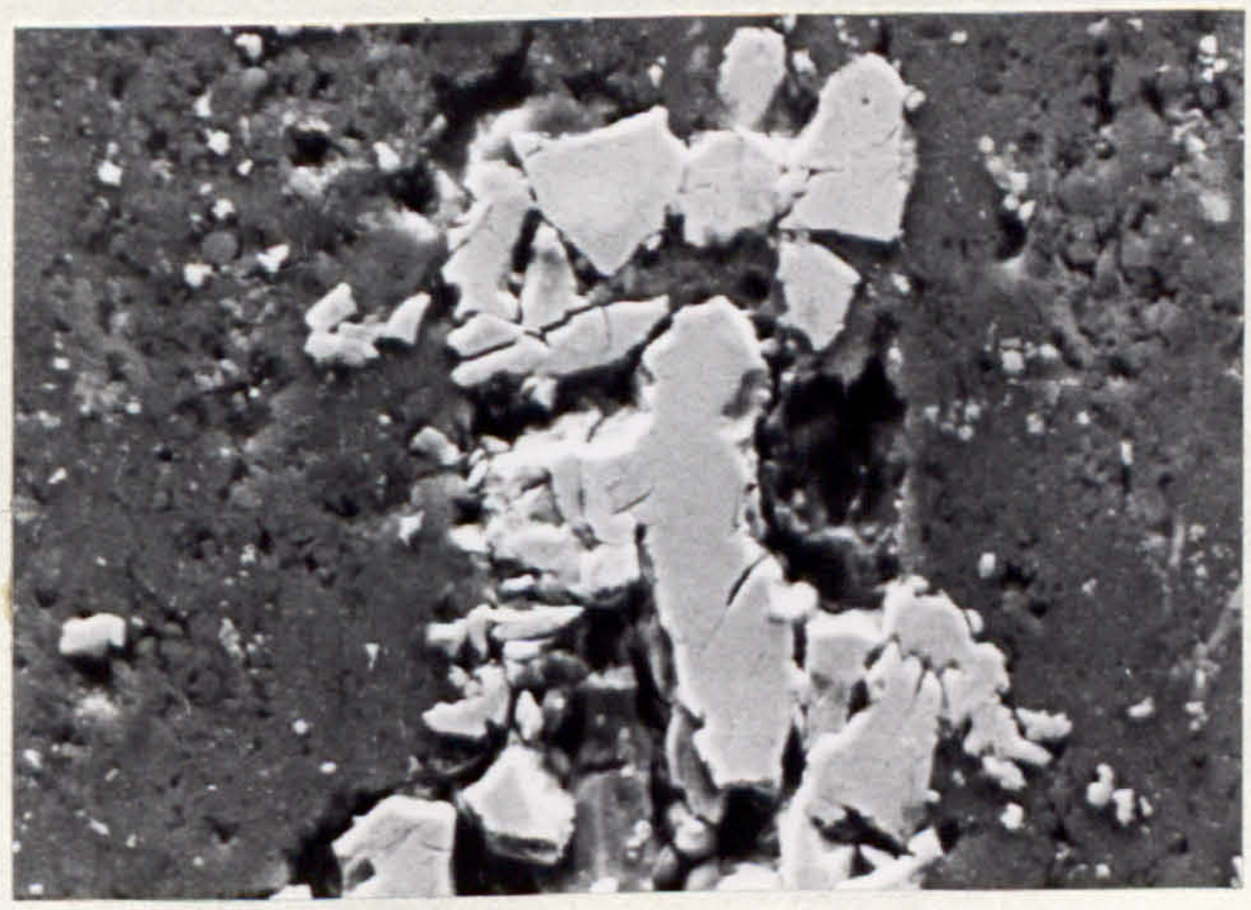

FIG. 164. TEST 3E, FOLLOWER WEAR SURFACE ELECTRON MICROGRAPH.

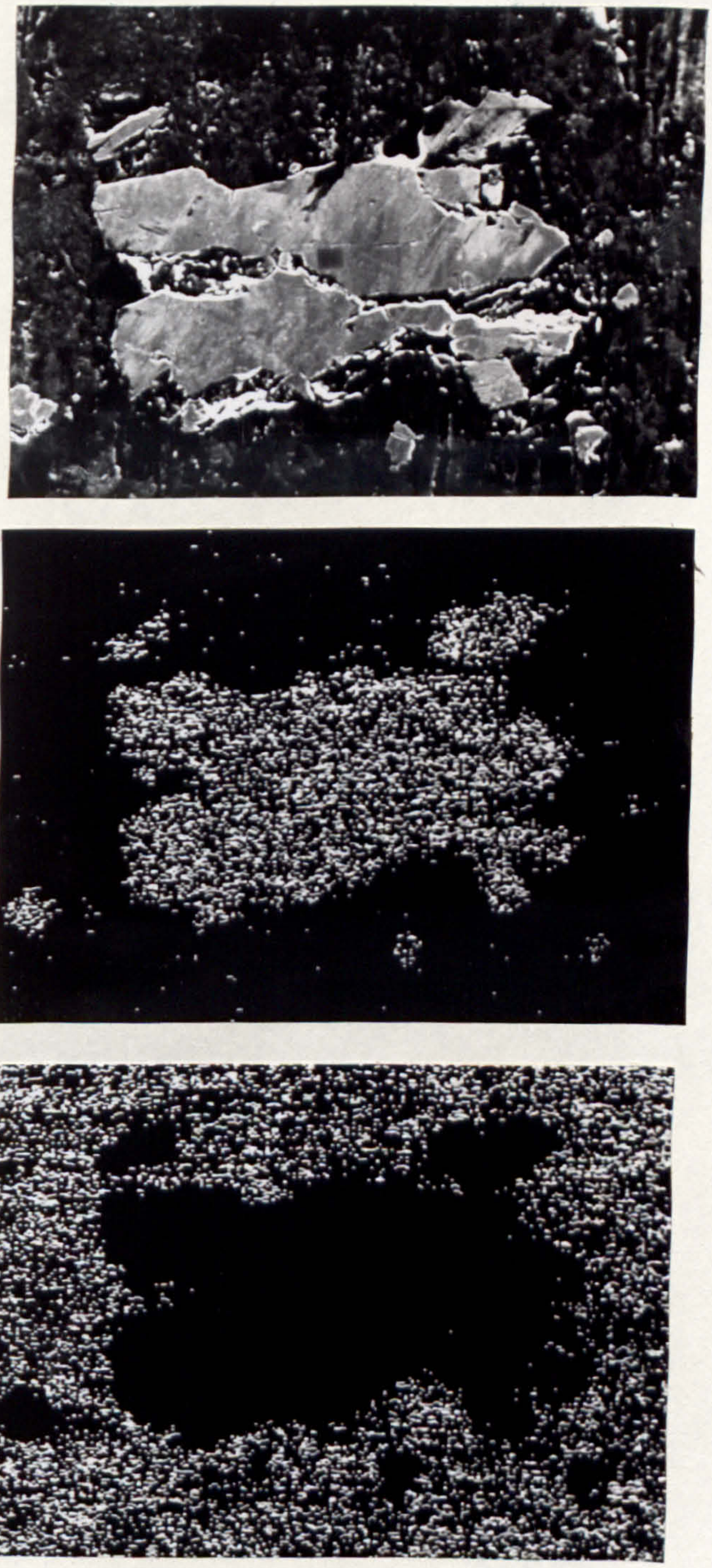

FIG. 165. TEST 3E, FOLLOWER WEAR SURFACE MICROGRAPH, AND X-RAY DOT IMAGE.

a) ELECTRON MICROGRAPH

b) X-RAY DOT IMAGE FOR IRON (Fe)

c) X-RAY DOT IMAGE FOR ALUMINIUM

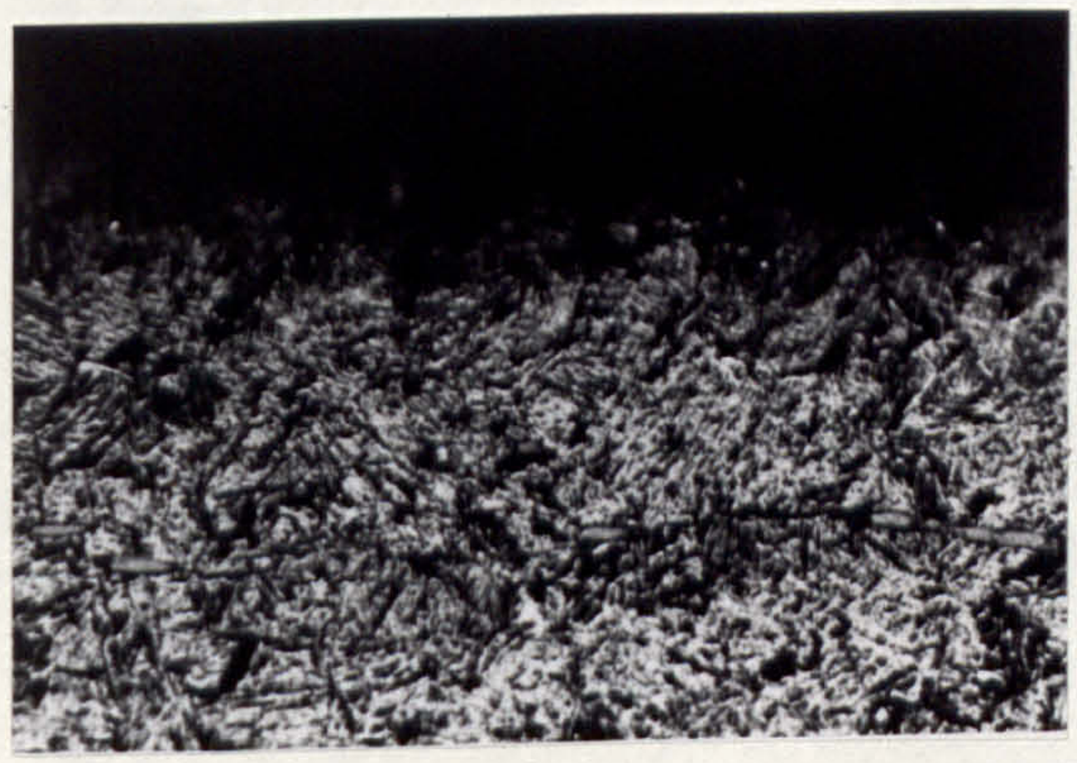

FIG. 166. TEST 3E, CAM SPECIMEN TAPERSECTION.

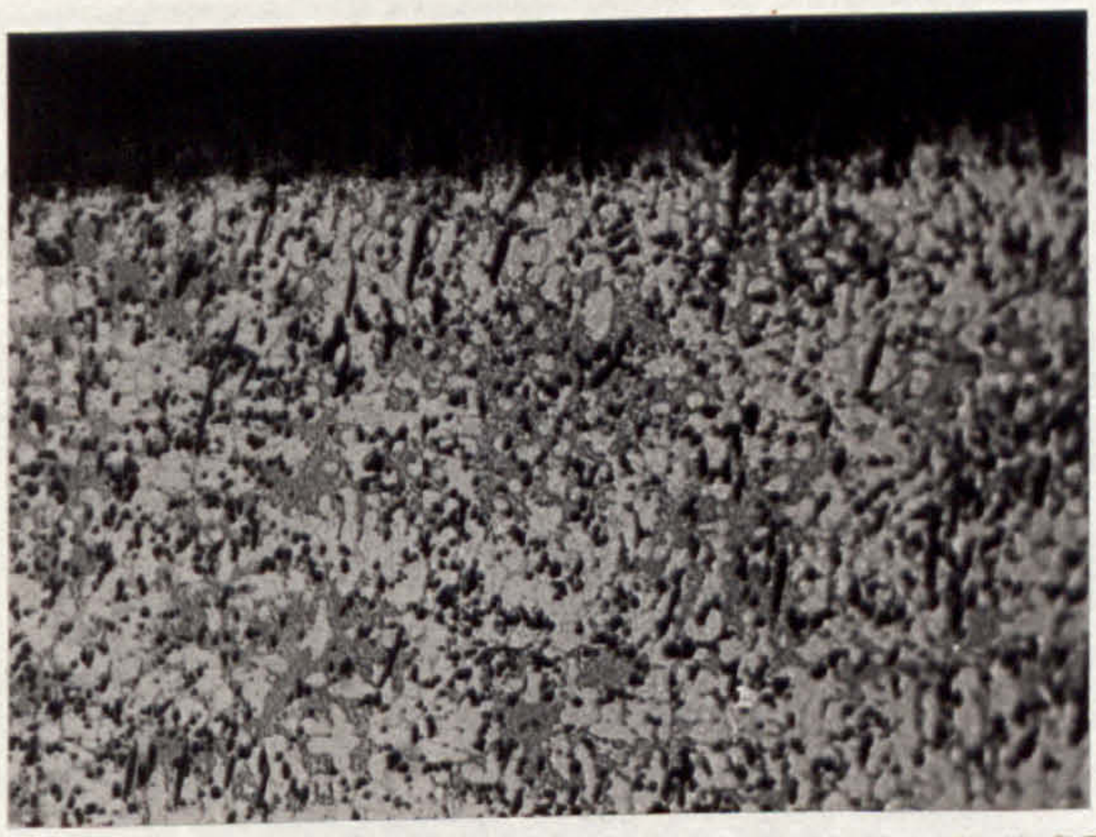

FIG. 167. TEST 3E, FOLLOWER SPECIMEN, TAPERSECTION.

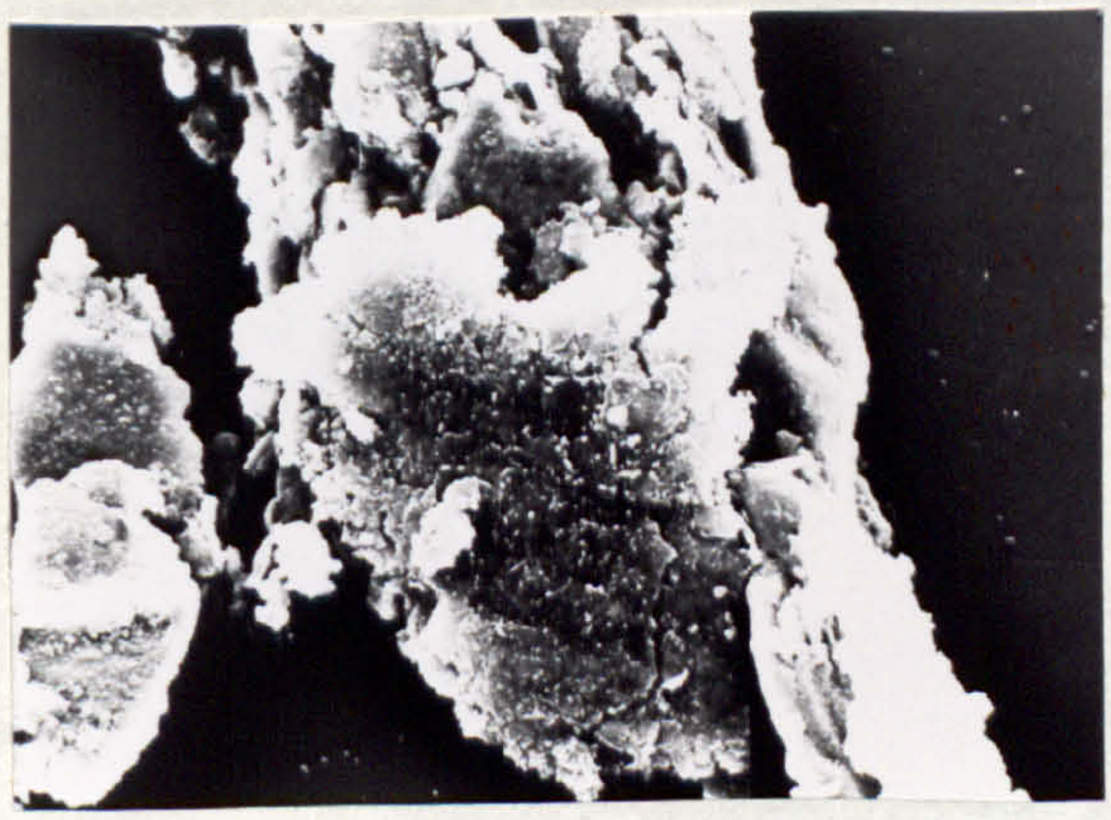

FIG. 168. TEST 3E, WEAR DEBRIS, ELECTRON MICROGRAPH.

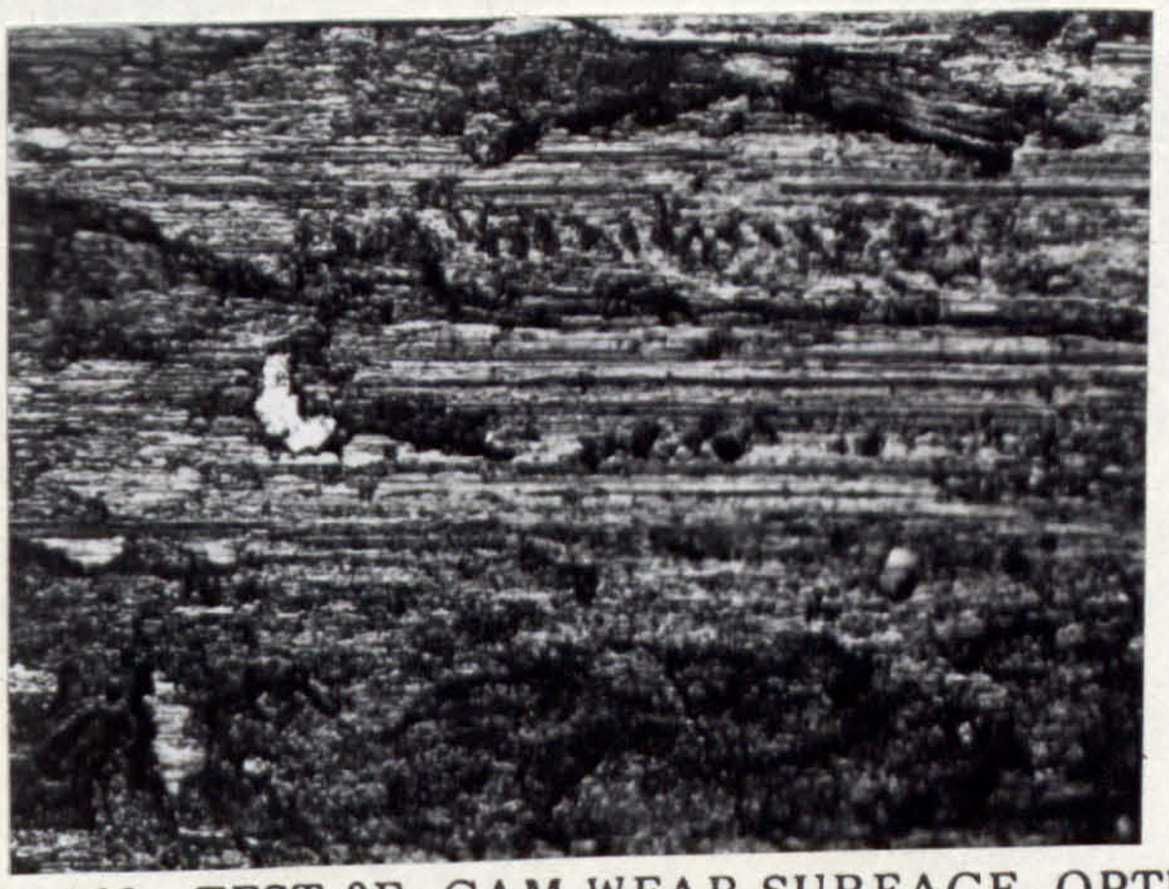

FIG. 169. TEST 3F, CAM WEAR SURFACE, OPTICAL.

FIG. 170. TEST 3F, CAM WEAR SURFACE, ELECTRON MICROGRAPH.

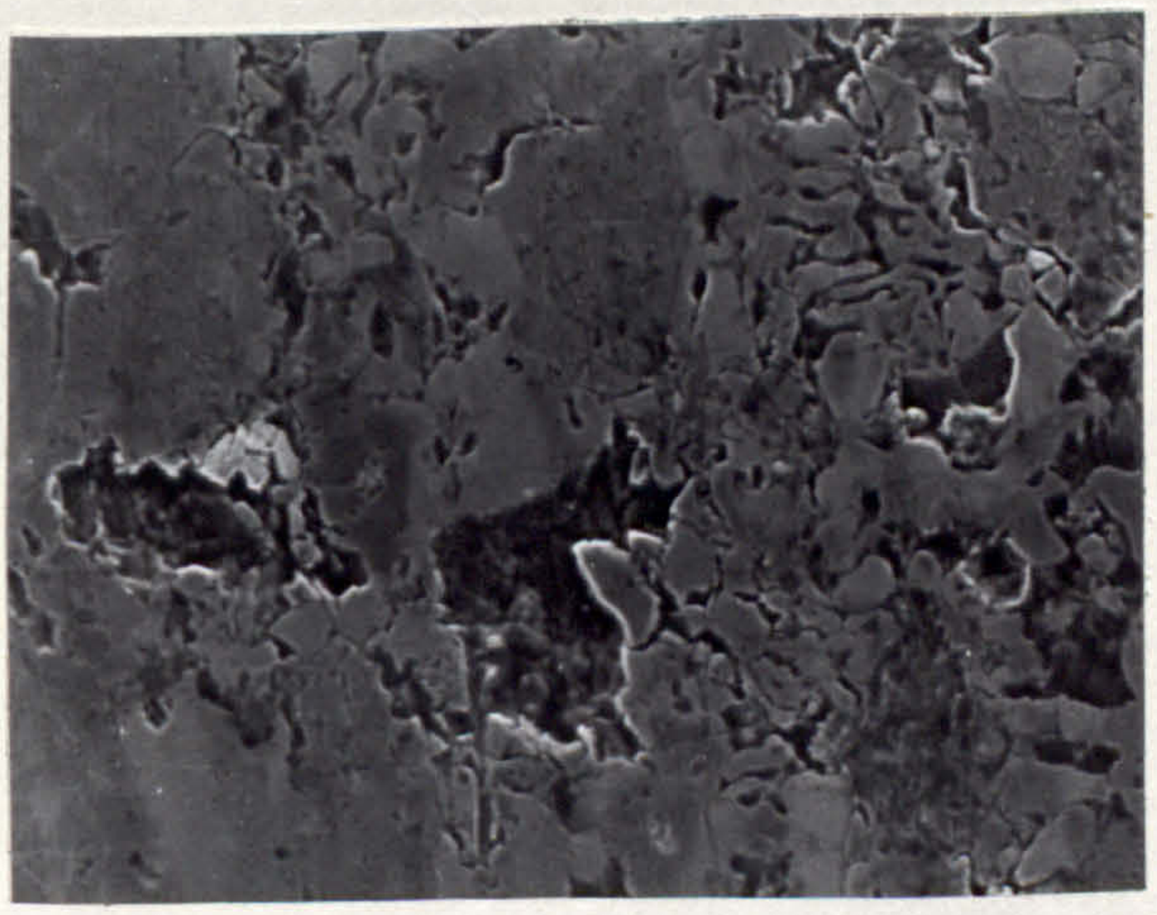

FIG. 171. TEST 3F, FOLLOWER WEAR SURFACE, ELECTRON MICROGRAPH.

Fig. 172. Test 3F, Cam Specimen Tapersection.

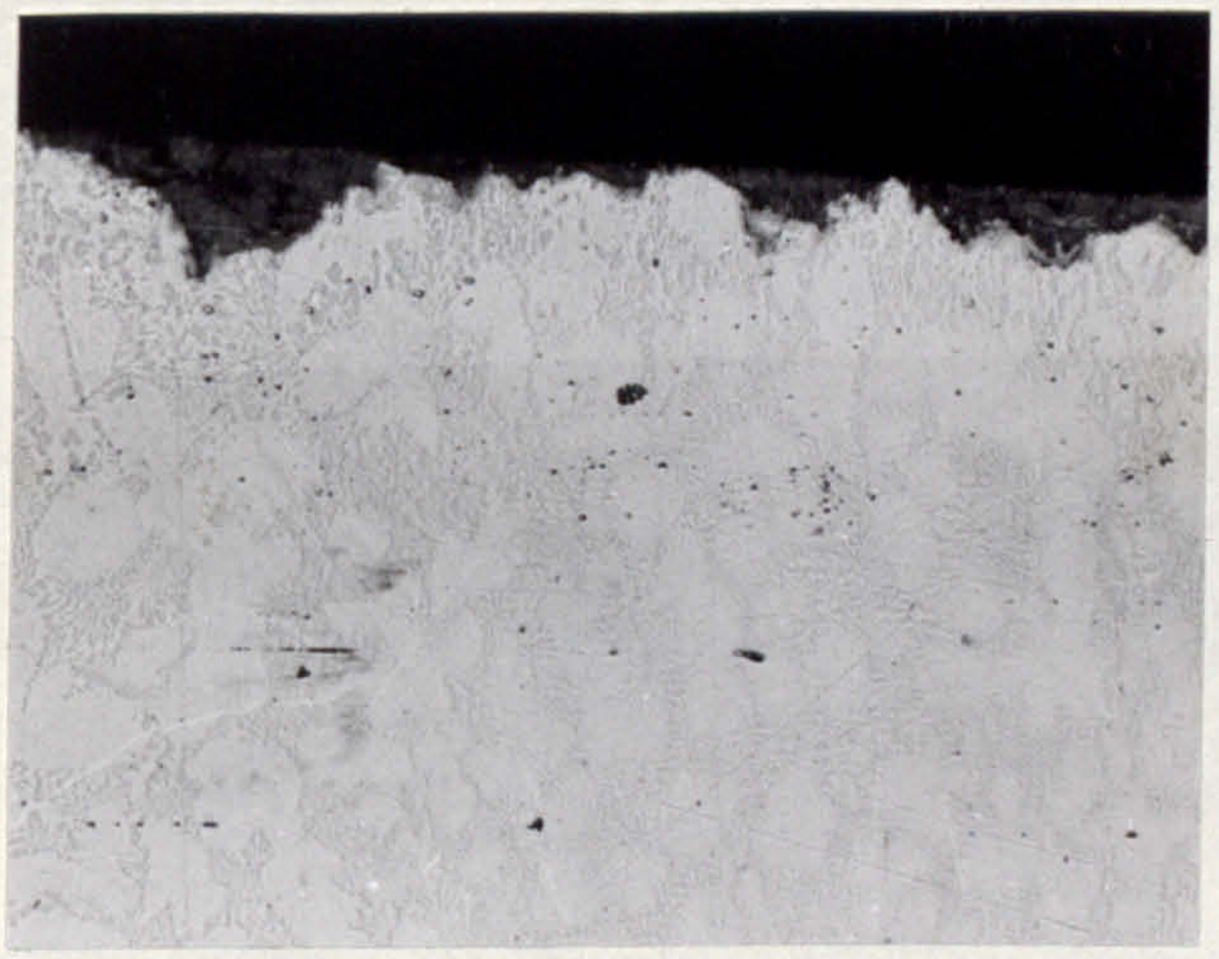

Fig. 173. Test 3F, Follower Specimen Tapersection.

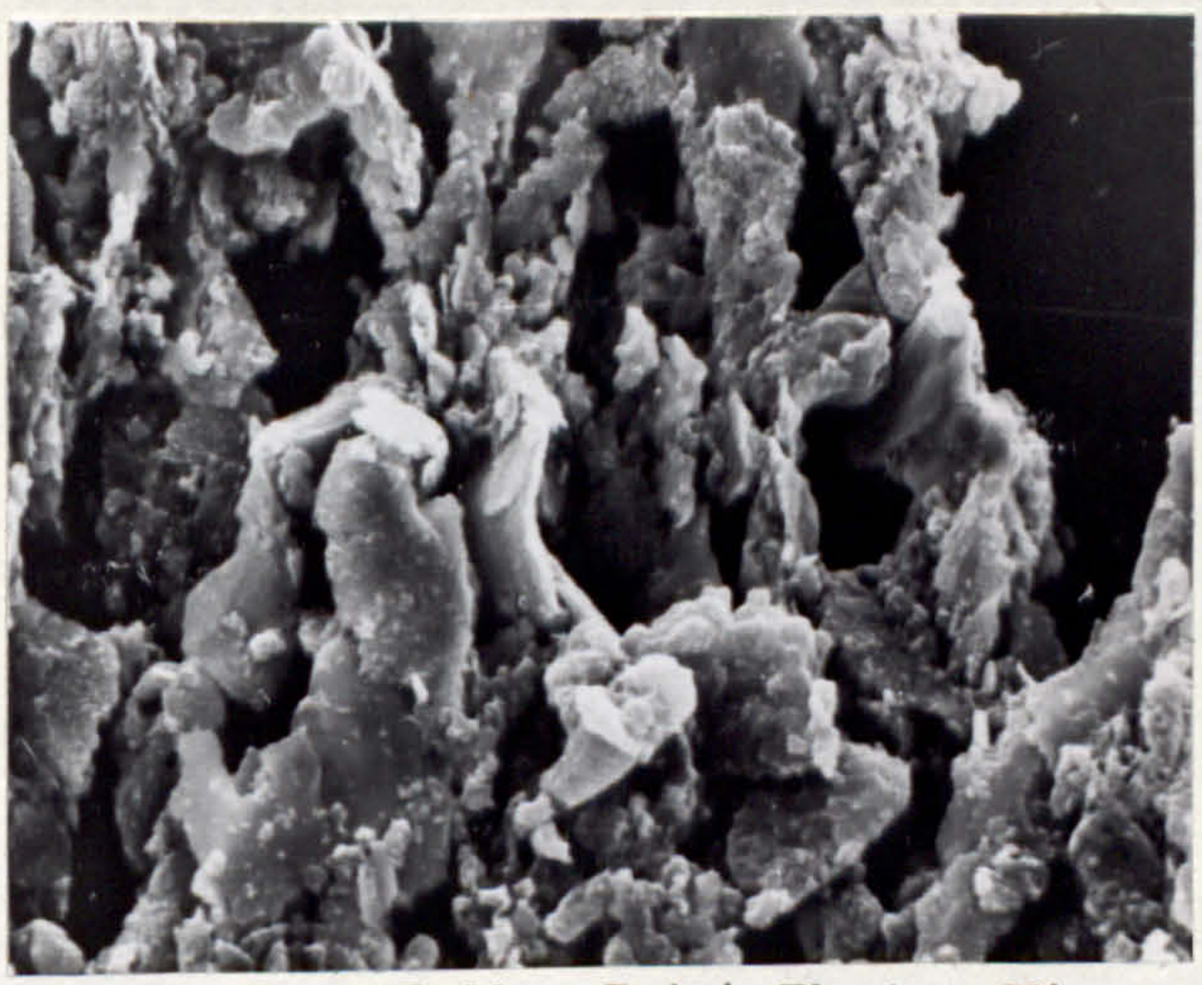

Fig. 174. Test 3F, Wear Debris, Electron Micrograph

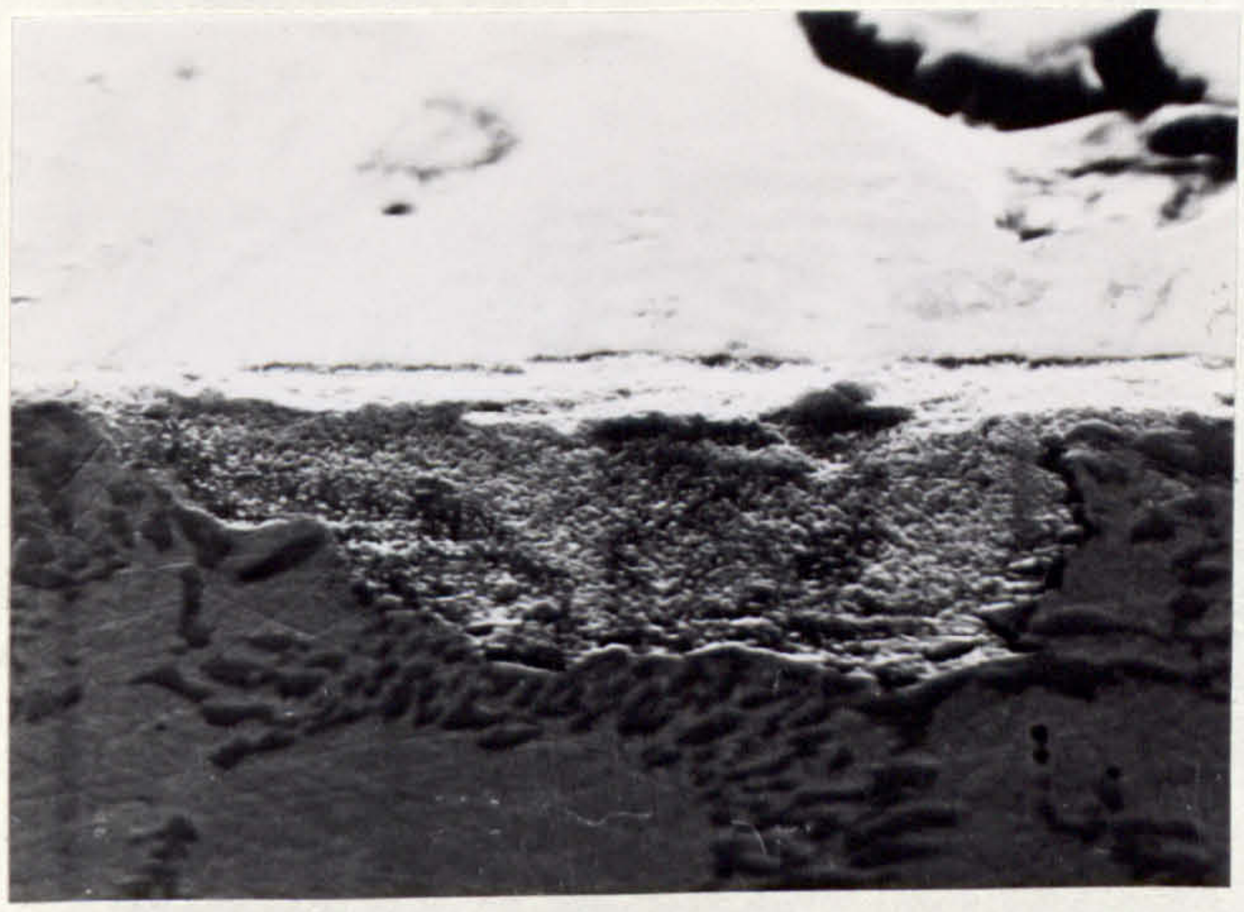

a)

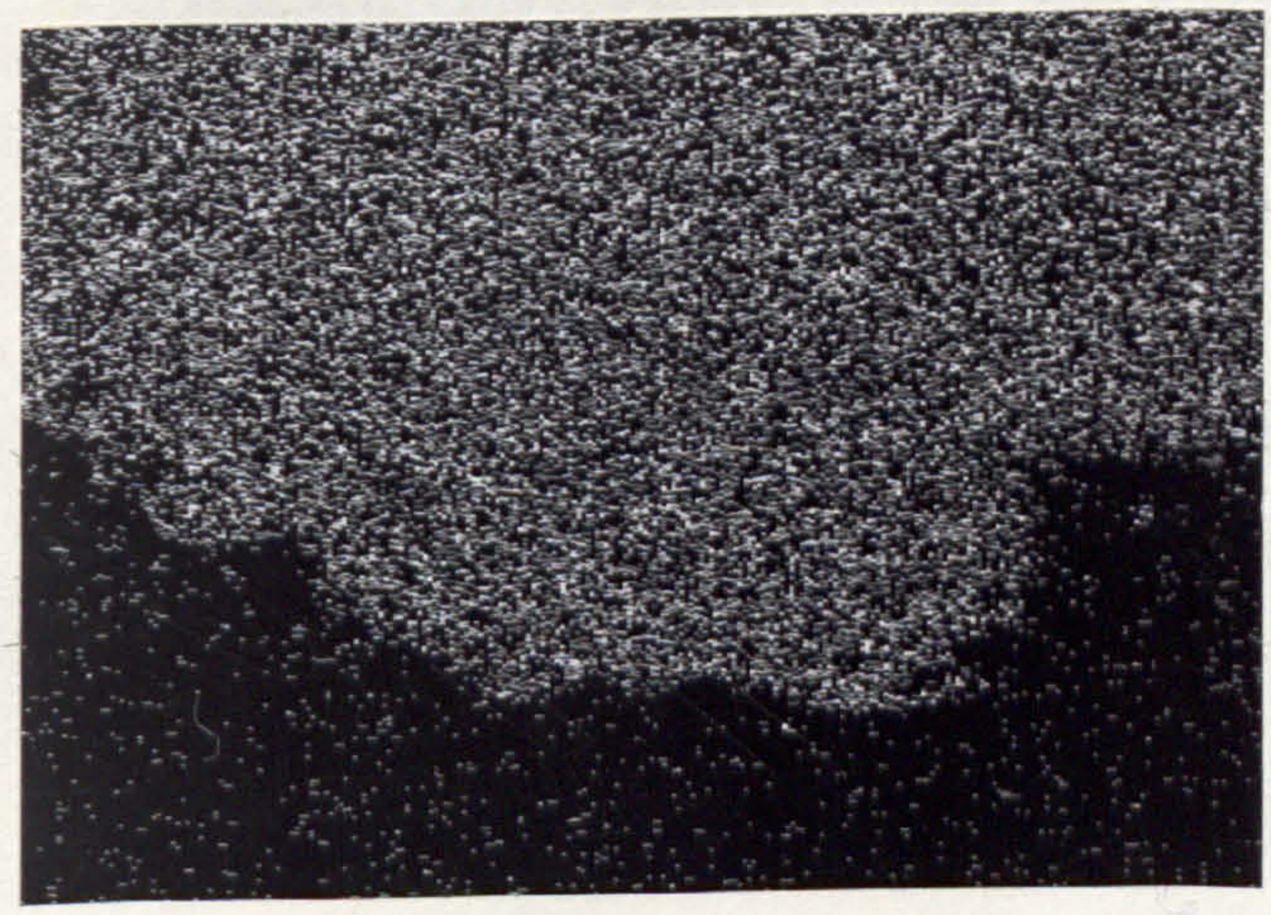

b)

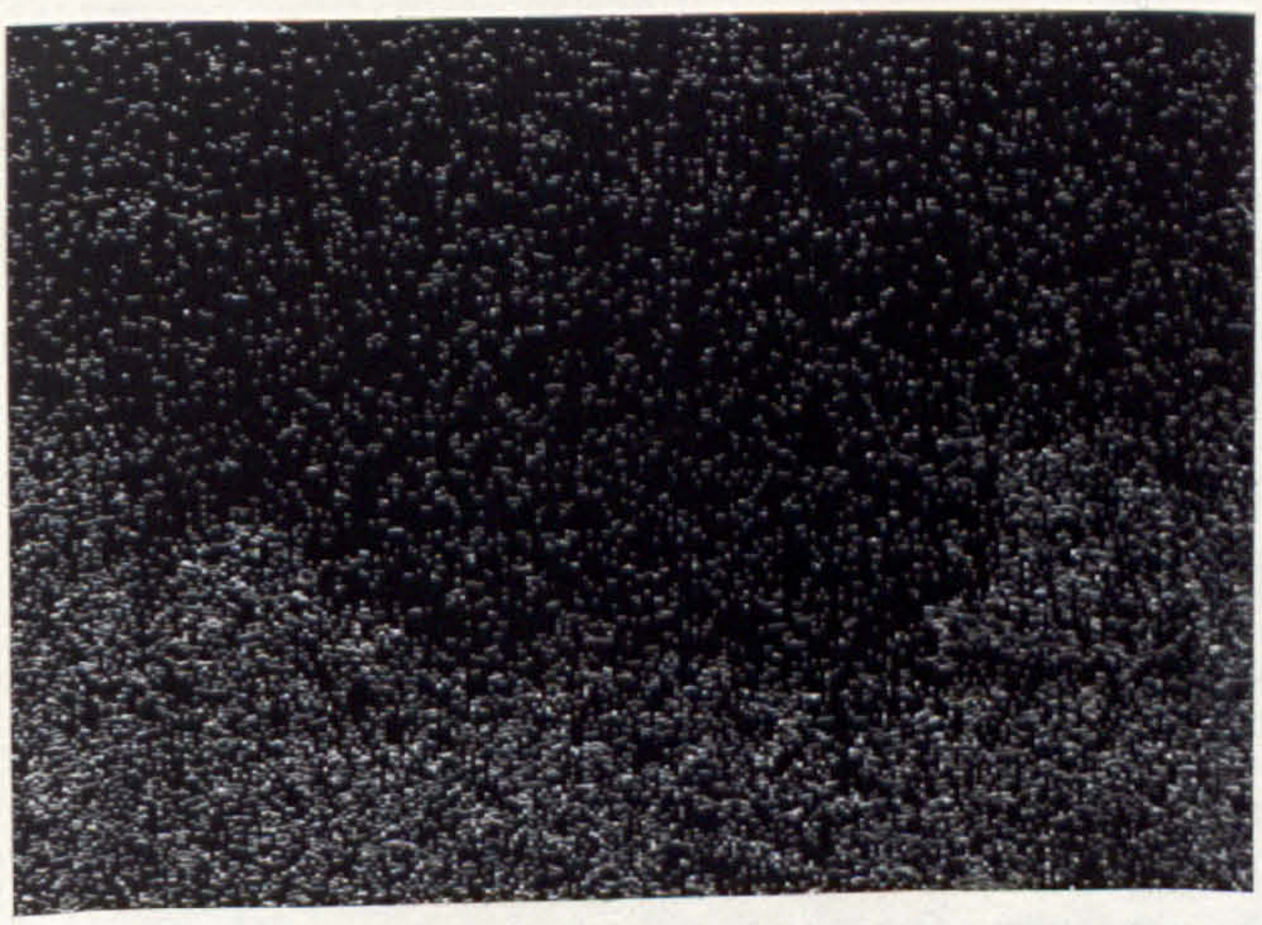

c)

20μ

FIG. 175. TEST 3F, FOLLOWER WEAR SURFACE, ELECTRON MICROGRAPH AND X-RAY DOT IMAGE.

a) ELECTRON MICROGRAPH
b) X-RAY DOT IMAGE FOR IRON
c) X-RAY DOT IMAGE FOR COBALT

FIG. 176. TEST 3G, CAM WEAR SURFACE, OPTICAL.

FIG. 177. TEST 3G, CAM WEAR SURFACE, ELECTRON MICROGRAPH.

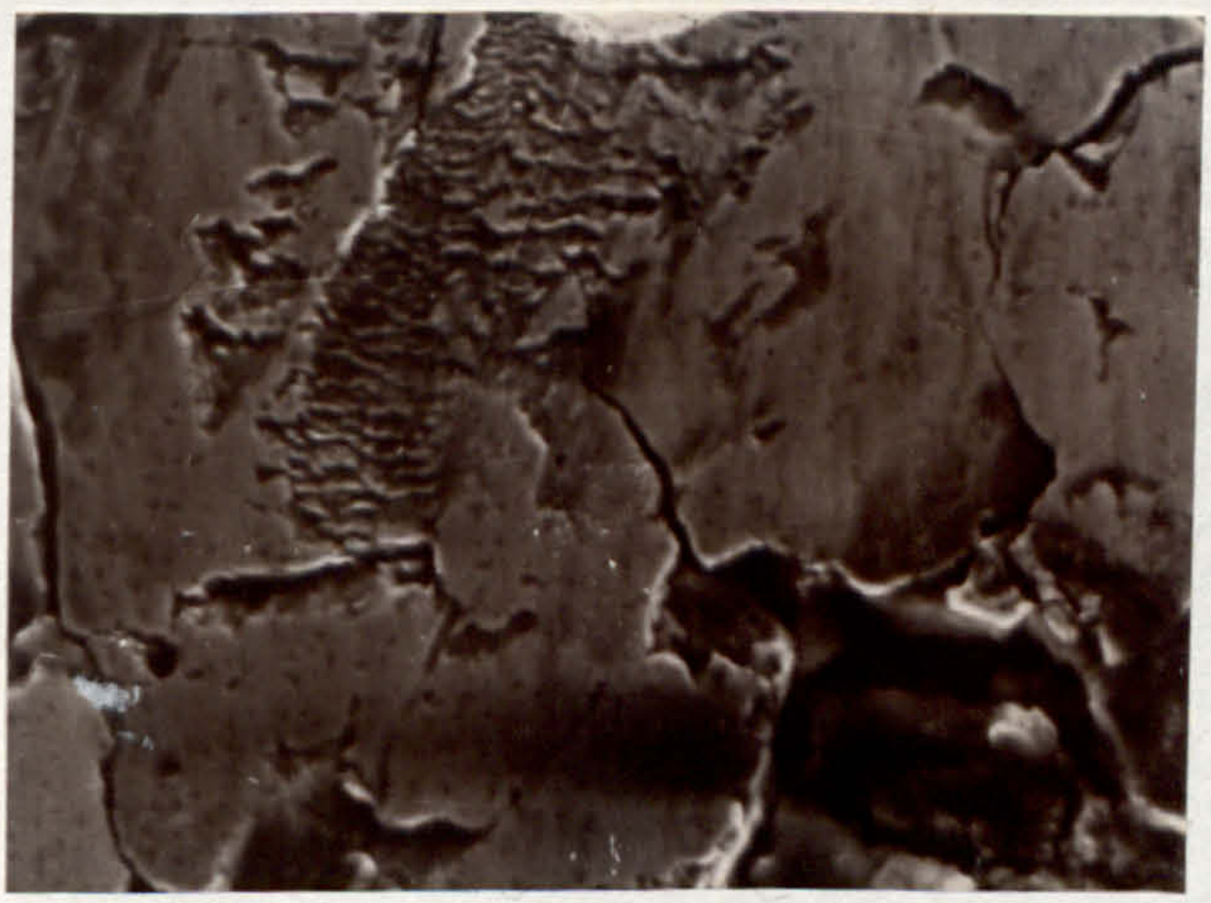

FIG. 178. TEST 3G, FOLLOWER WEAR SURFACE, ELECTRON MICROGRAPH.

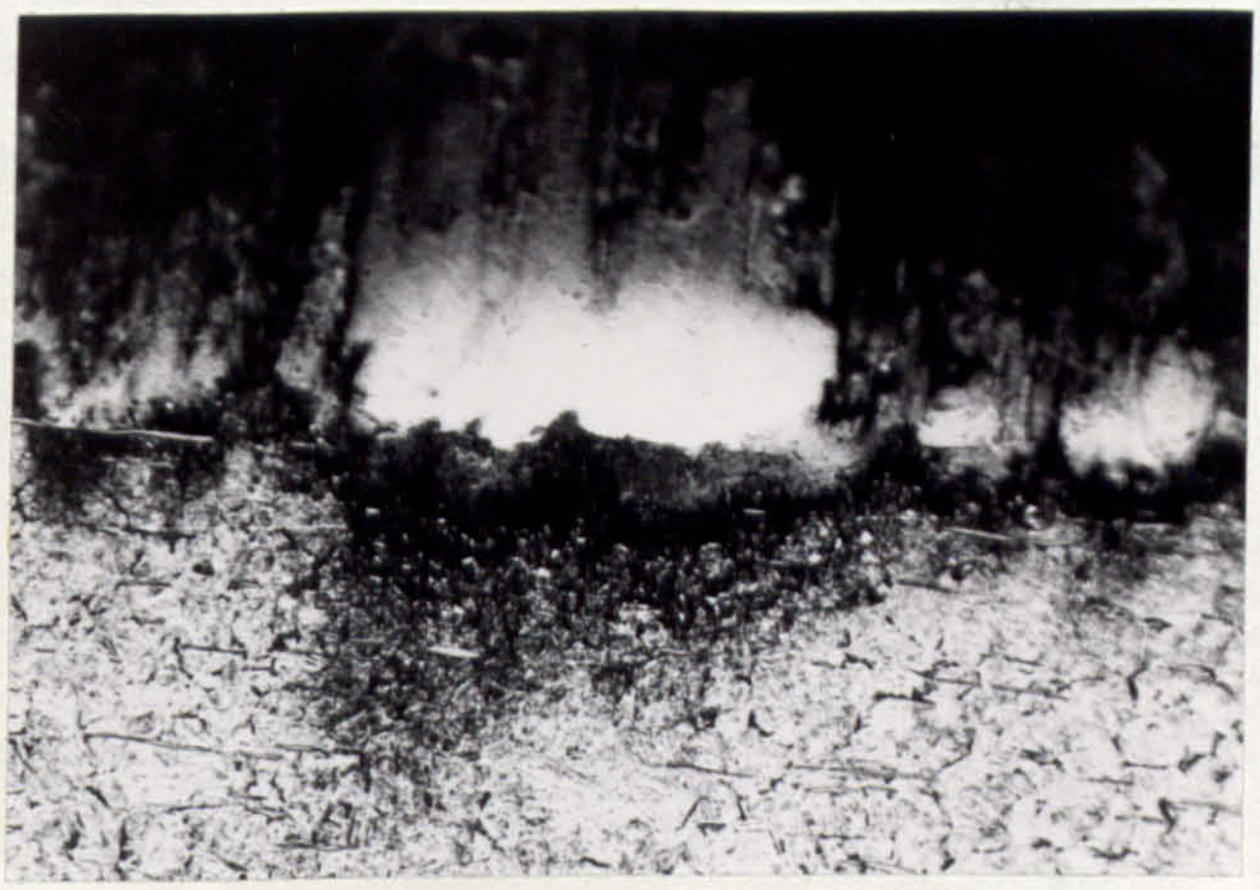

FIG. 179. TEST 3G, CAM SPECIMEN TAPERSECTION.

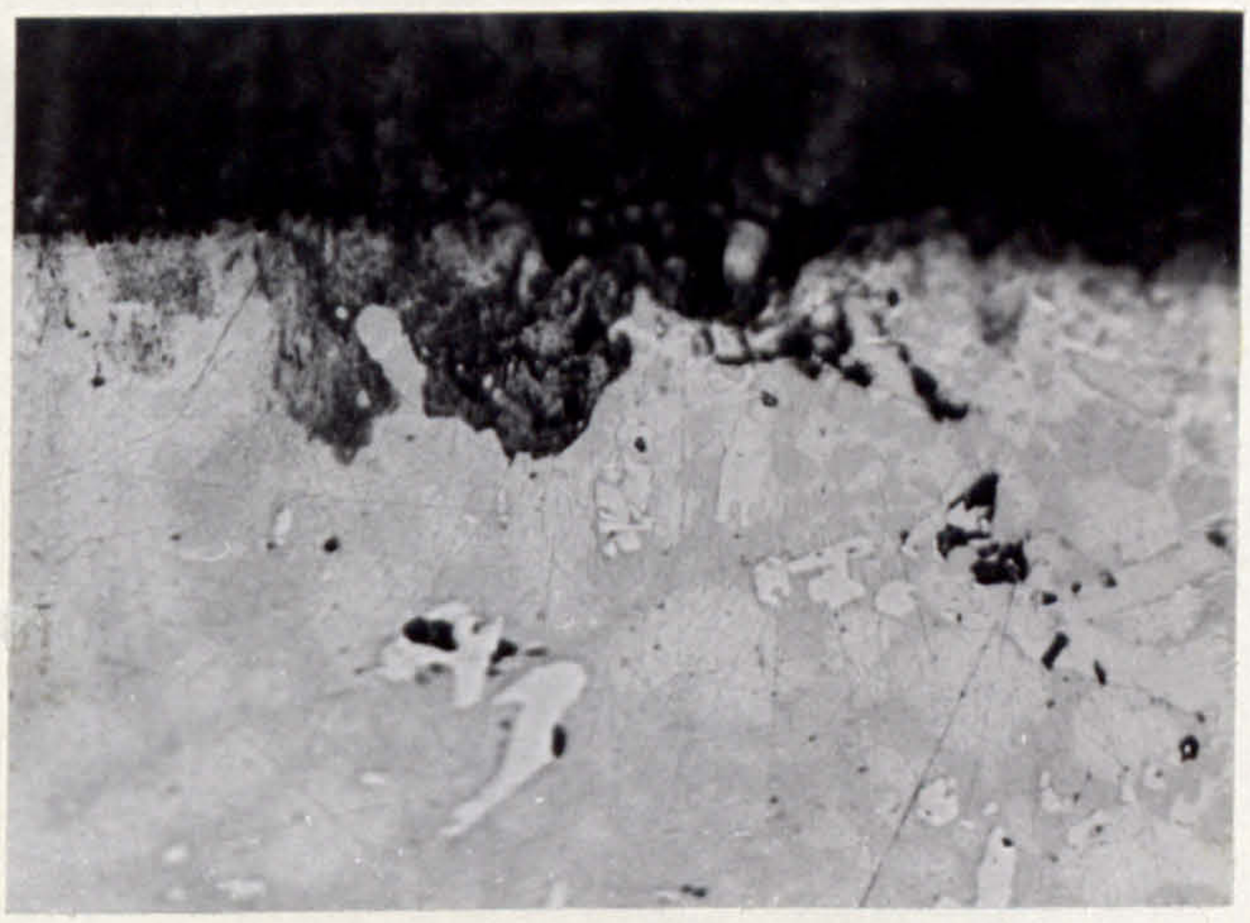

FIG. 180. TEST 3G, FOLLOWER SPECIMEN TAPERSECTION.

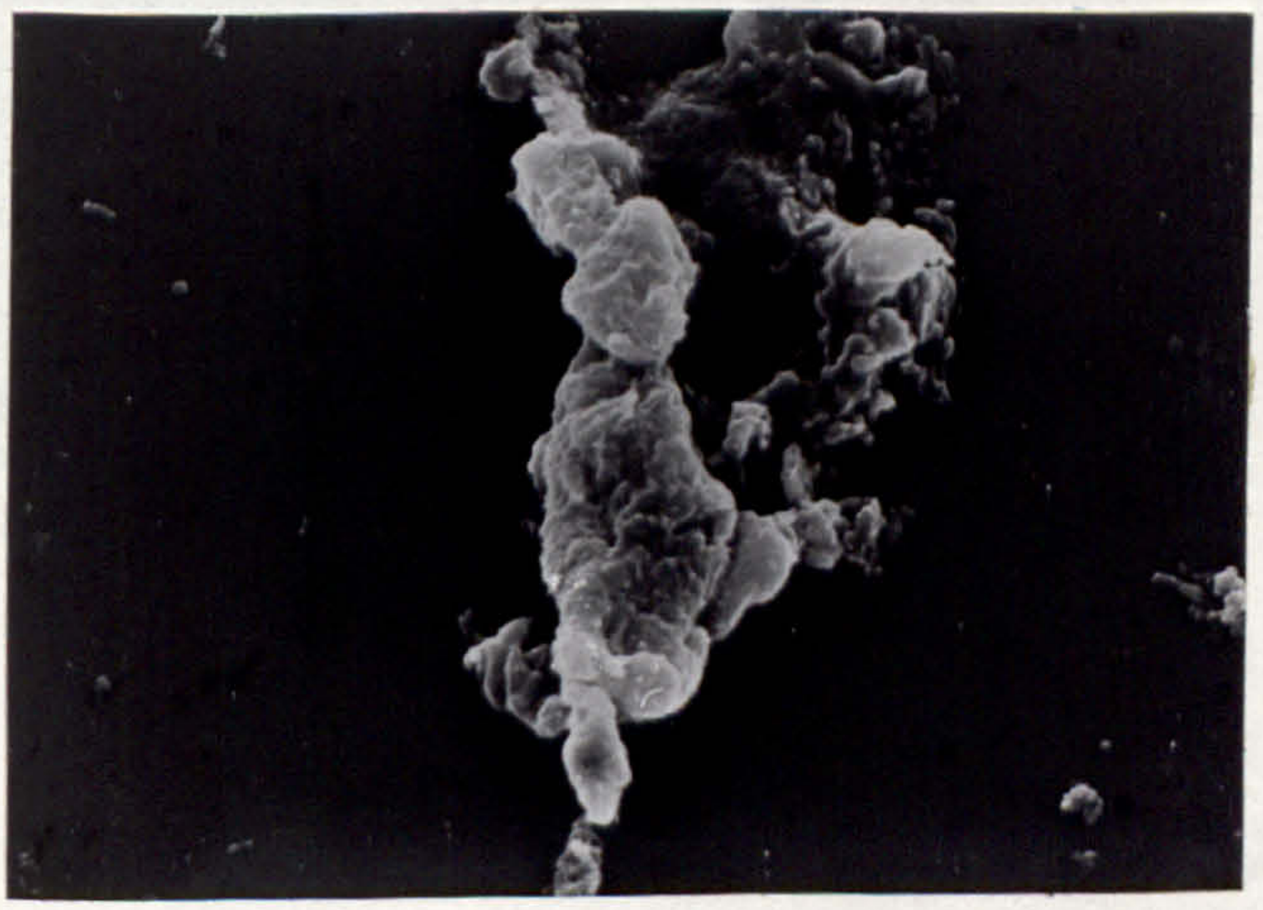

FIG. 181. TEST 3G, WEAR DEBRIS, ELECTRON MICROGRAPH.

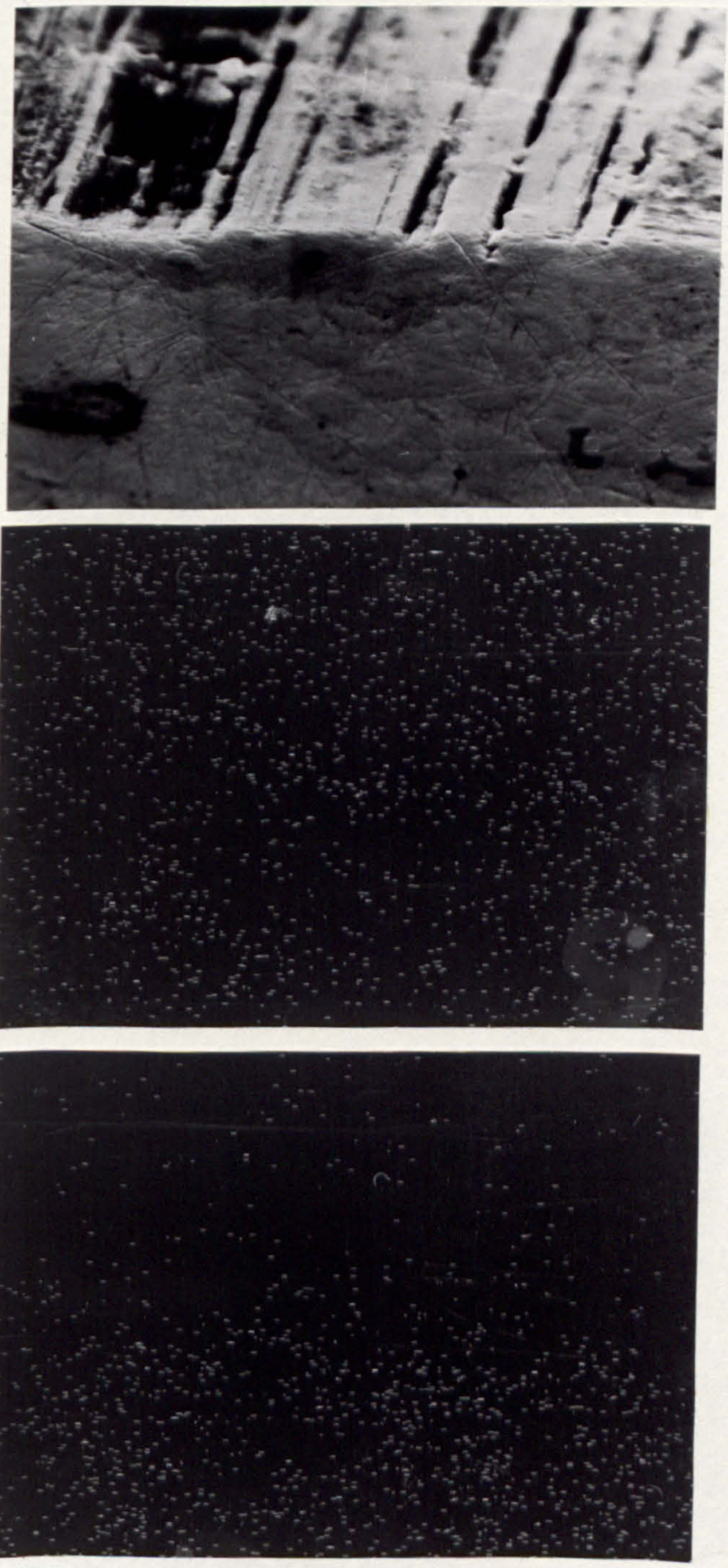

a)

b)

c)

20μ

FIG. 182. TEST 3G, FOLLOWER WEAR SURFACE, ELECTRON MICROGRAPH AND X-RAY DOT IMAGE.

a) ELECTRON MICROGRAPH

b) X-RAY DOT IMAGE FOR IRON

c) X-RAY DOT IMAGE FOR NICKEL

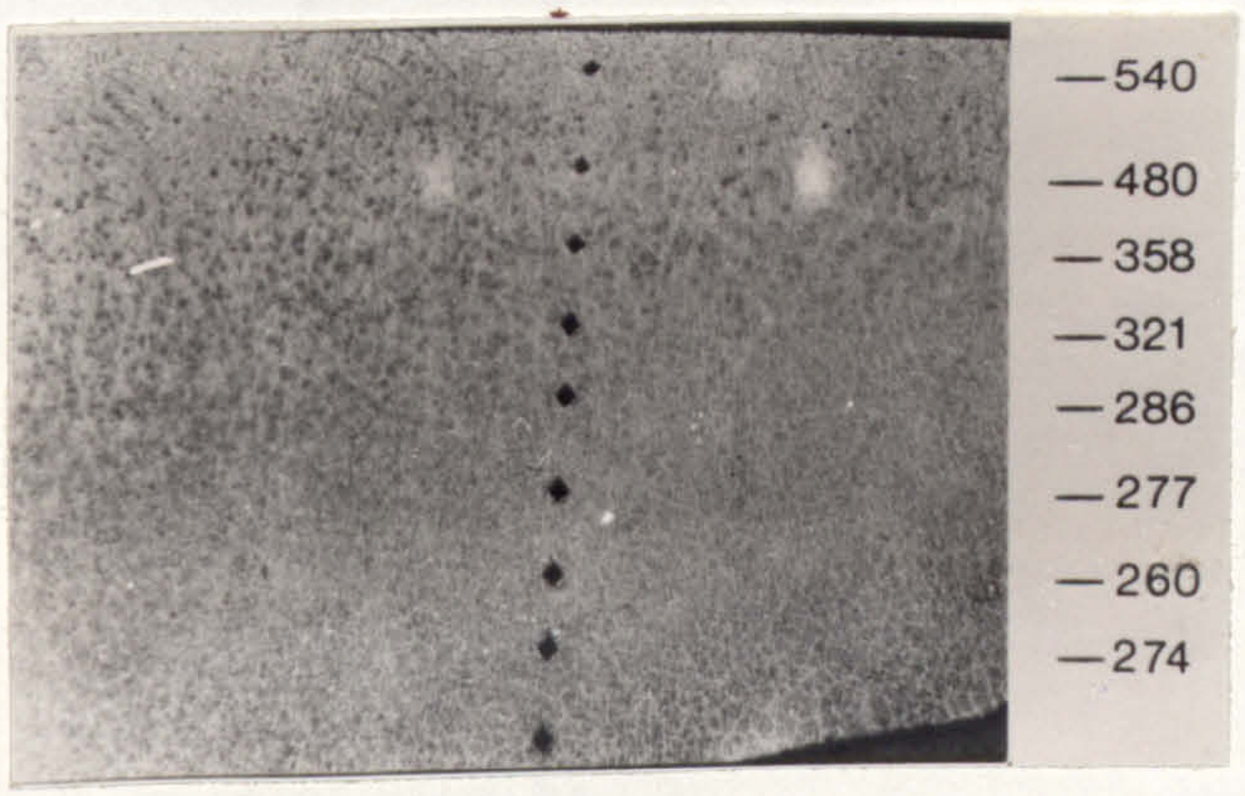

B.L.M.C. MINI

a)

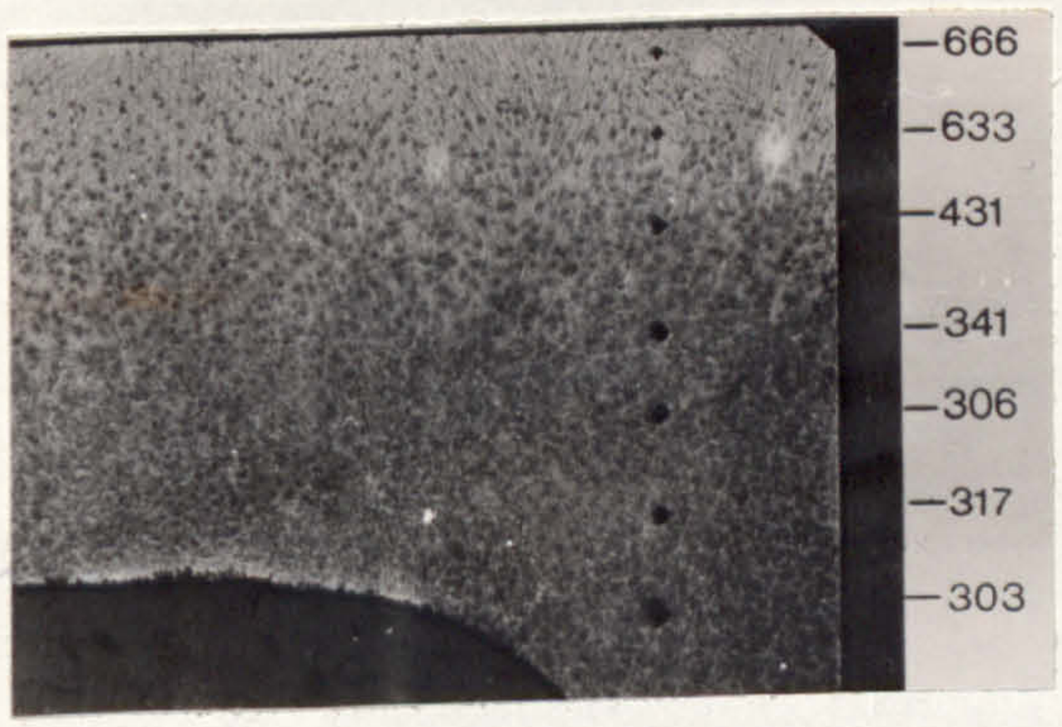

B.L.M.C. ROVER

b)

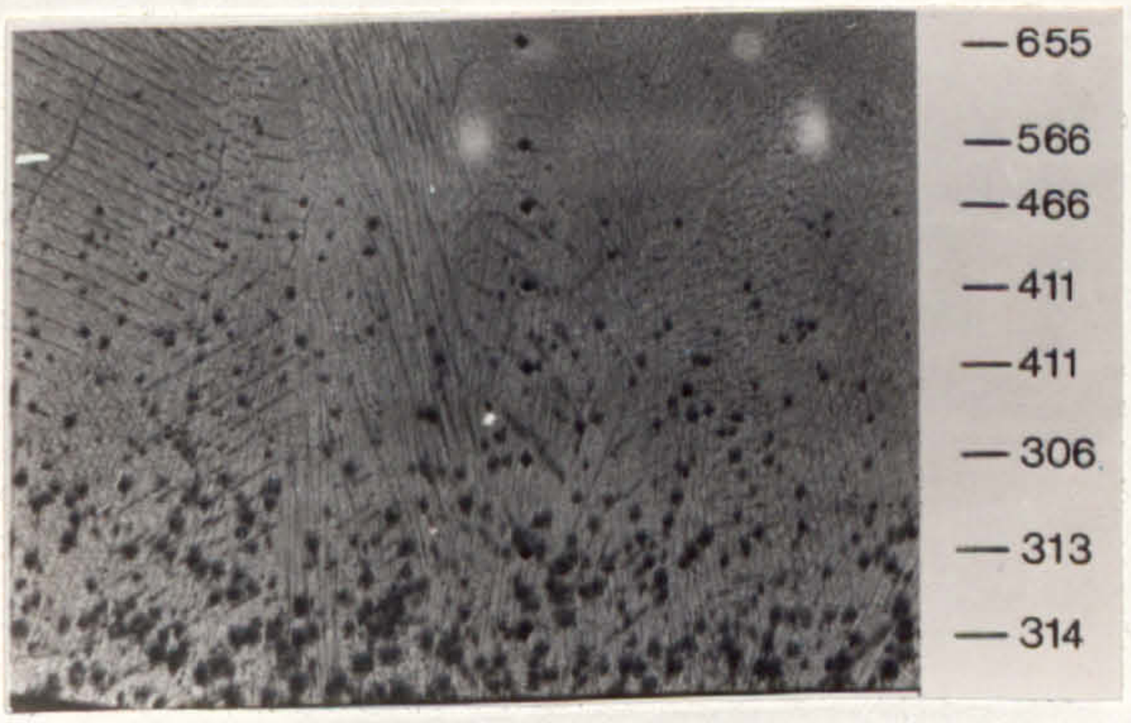

B.L.M.C. TRIUMPH

c)

4 mm

FIG. 183. a) B.L.M.C. 'MINI' TAPPET HARDNESS SURVEY

b) B.L.M.C. 'ROVER' TAPPET HARDNESS SURVEY

c) B.L.M.C. TRIUMPH TAPPET HARDNESS SURVEY

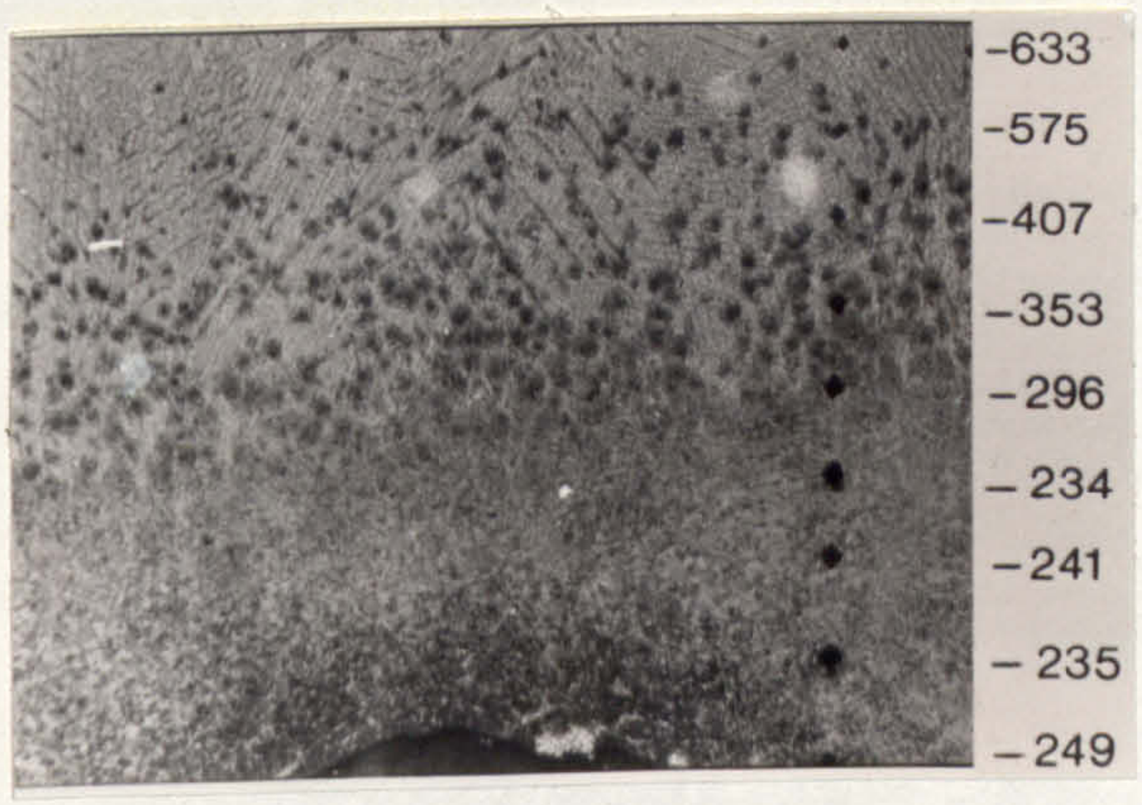

VAUXHALL VICTOR

a)

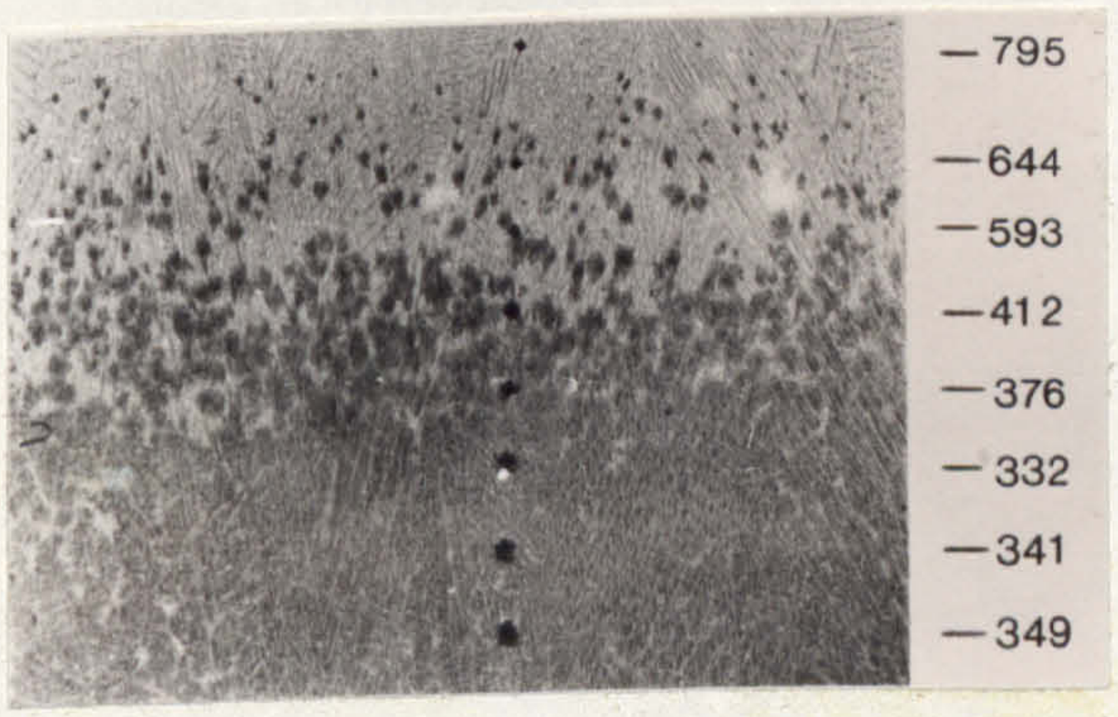

FORD DOVER

b)

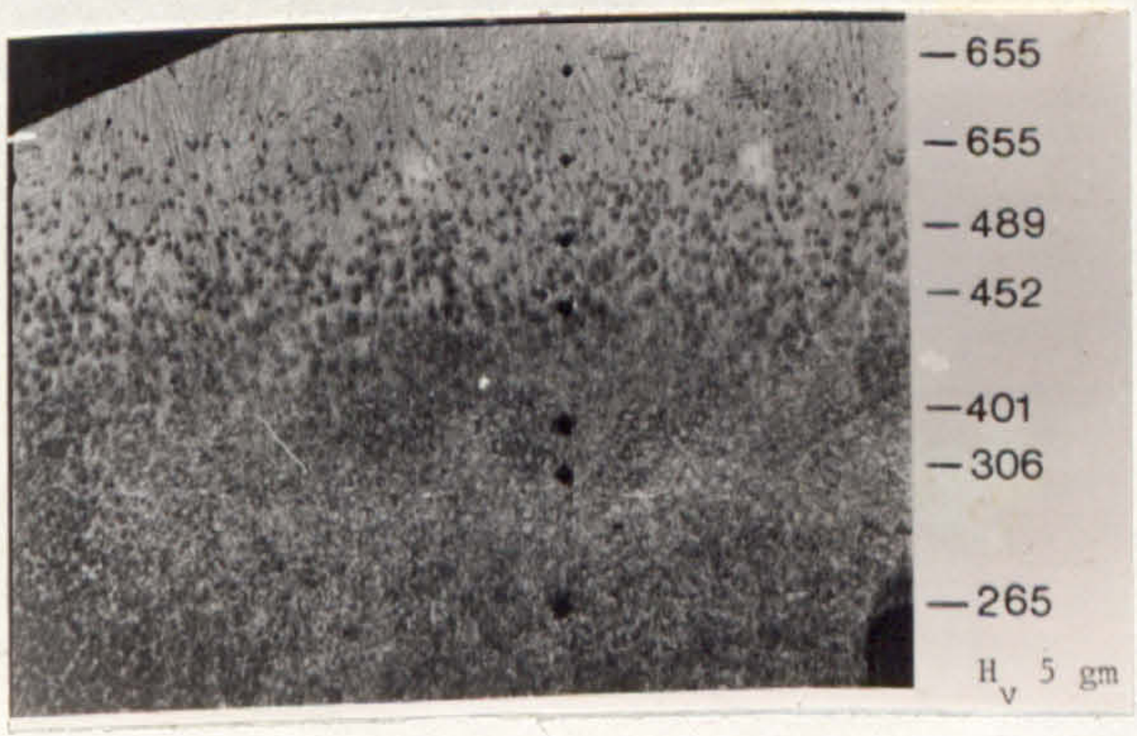

B.L.M.C. MAXI

c)

4mm

FIG. 184. a) VAUXHALL 'VICTOR' TAPPET HARDNESS SURVEY

b) FORD 'DOVER' TAPPET HARDNESS SURVEY

c) B.L.M.C. 'MAXI' TAPPET HARDNESS SURVEY

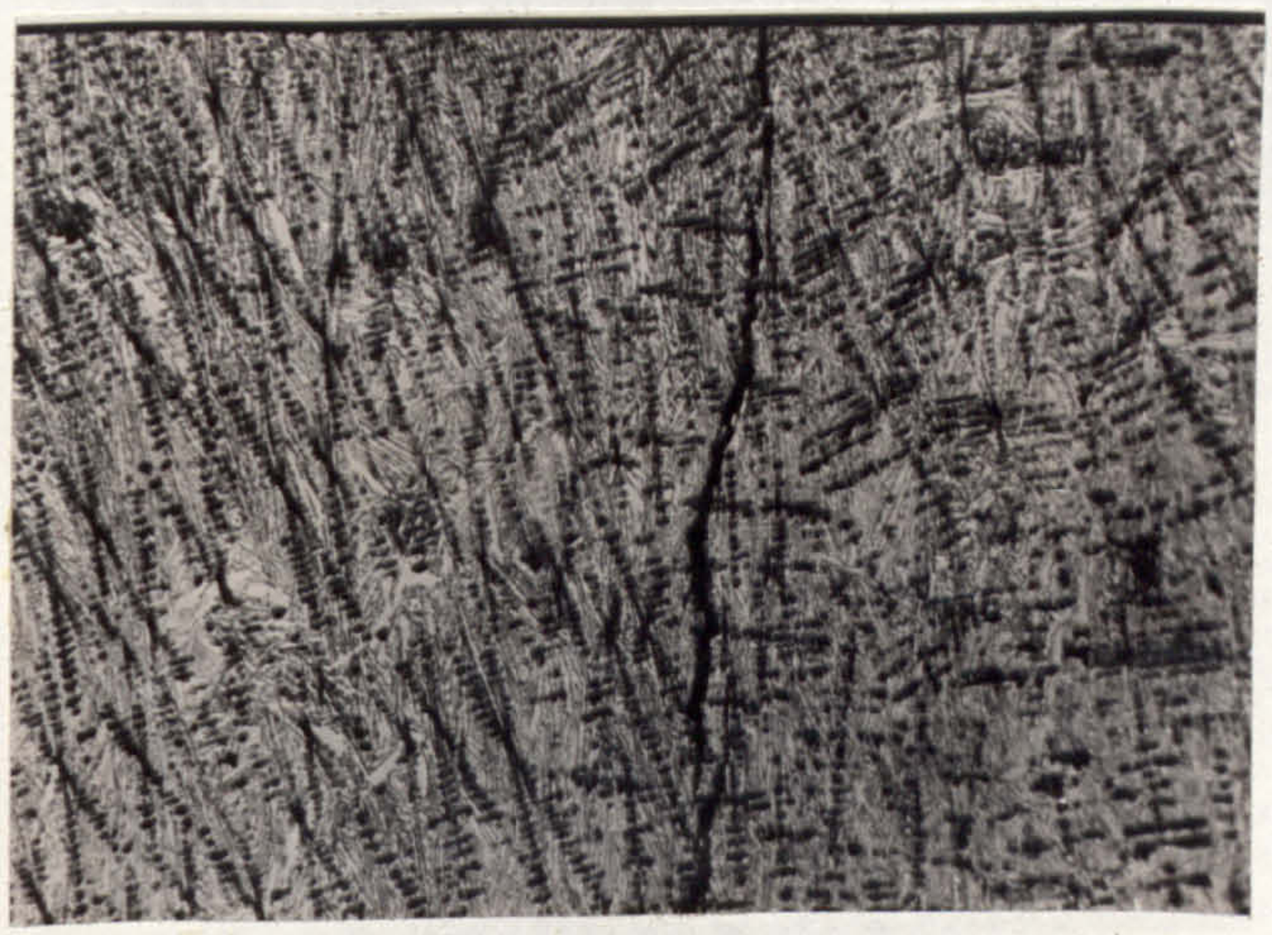

a)

200μ

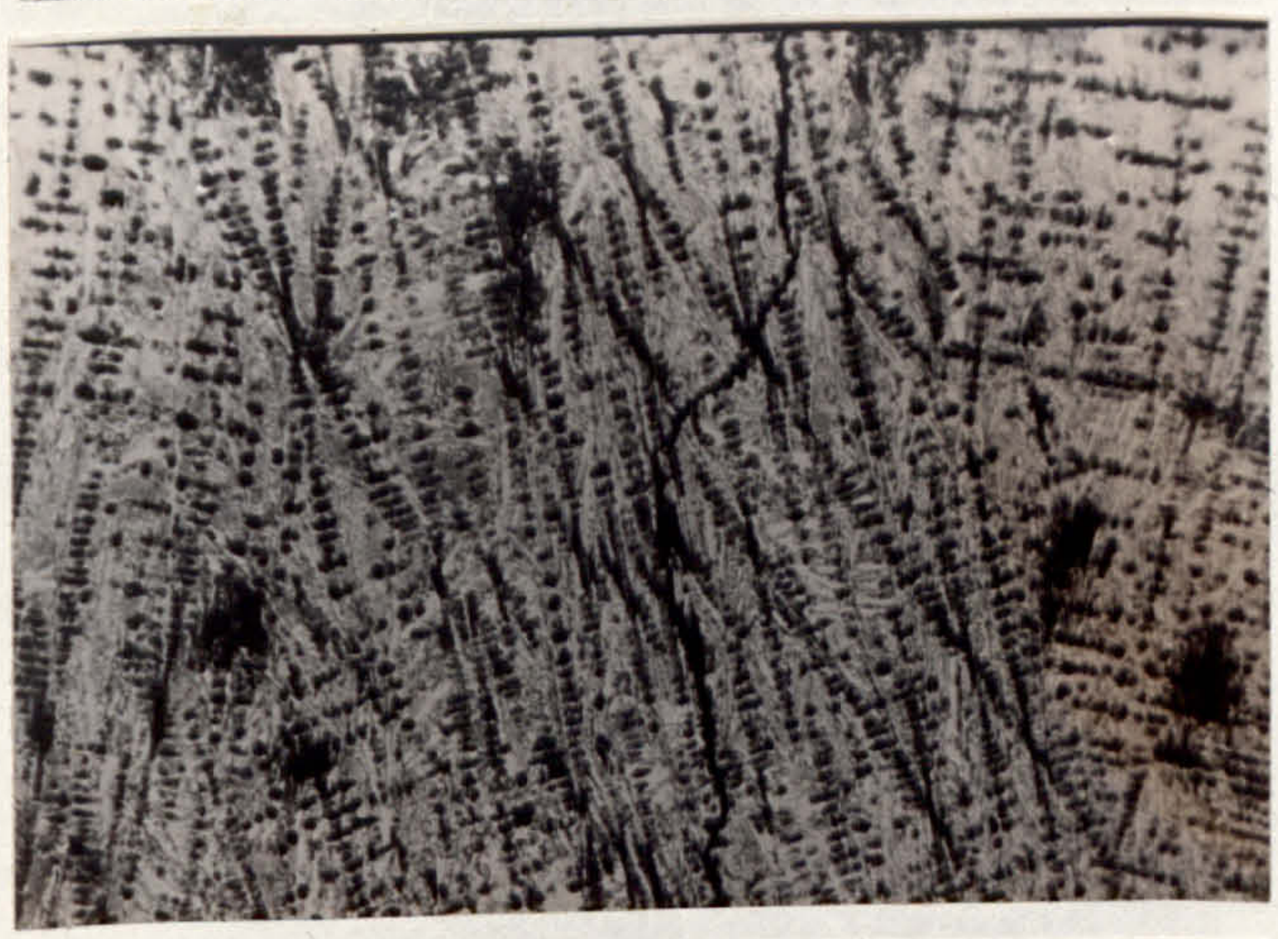

b)

200μ

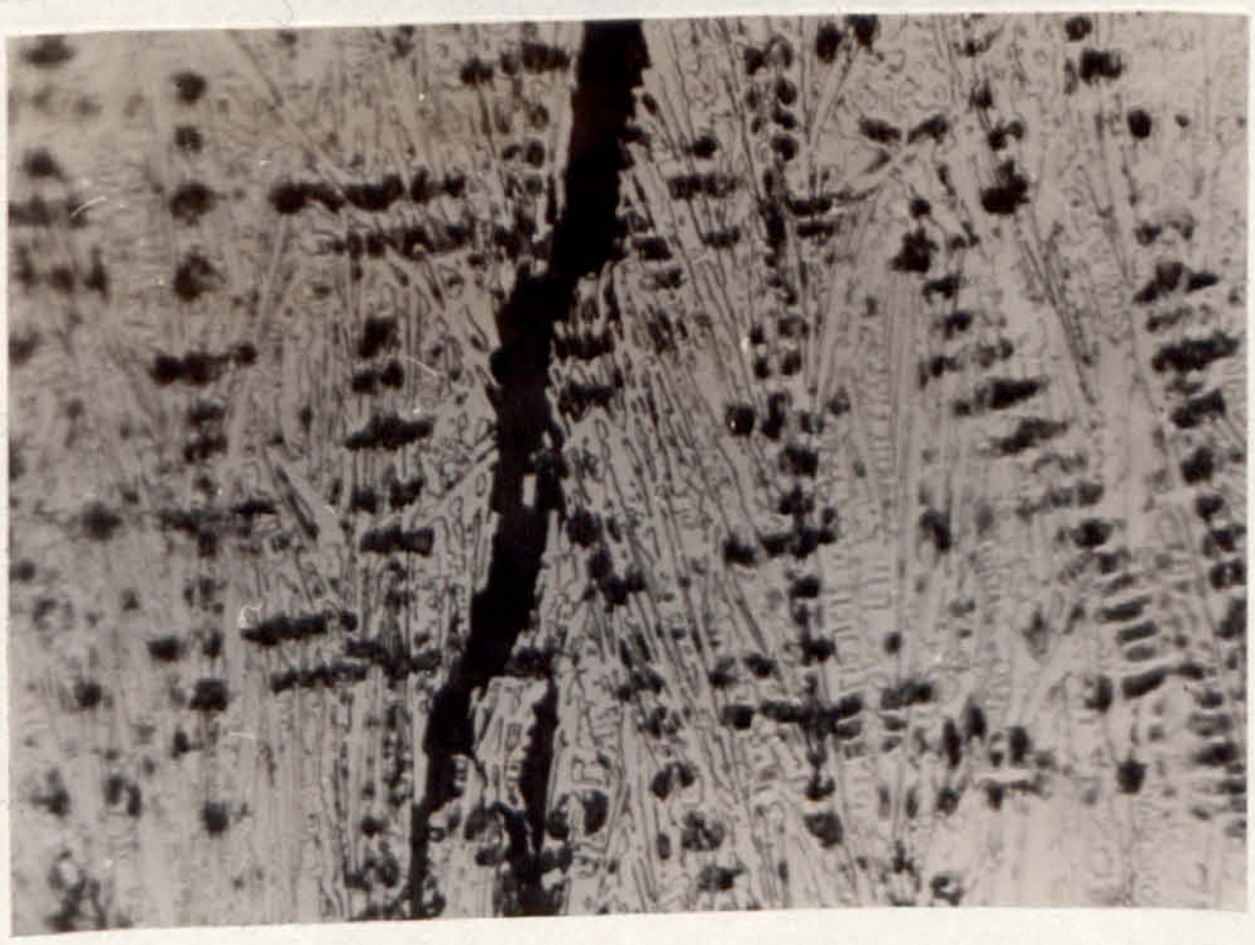

c)

40μ

FIG. 185. SHOWING CRACKS IN 'AS RECEIVED' CHILLED IRON TAPPET

a) CRACKS RUNNING AT 90° TO SURFACE

b) RANDOM ORIENTATION OF CRACK PATH

c) OXIDE FILLED CRACK

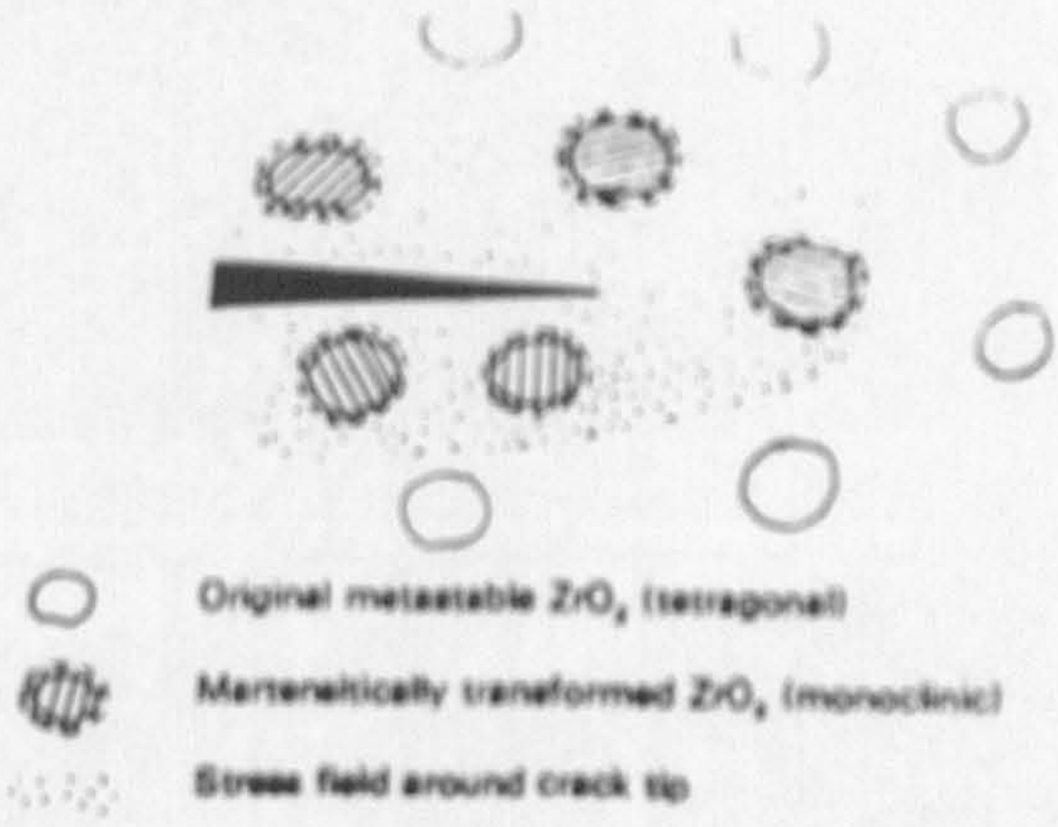

FIG. 186. STRENGTHENING MECHANISM OF TOUGHENED ZIRCONIA ARRESTING CRACK PROPOGATION.

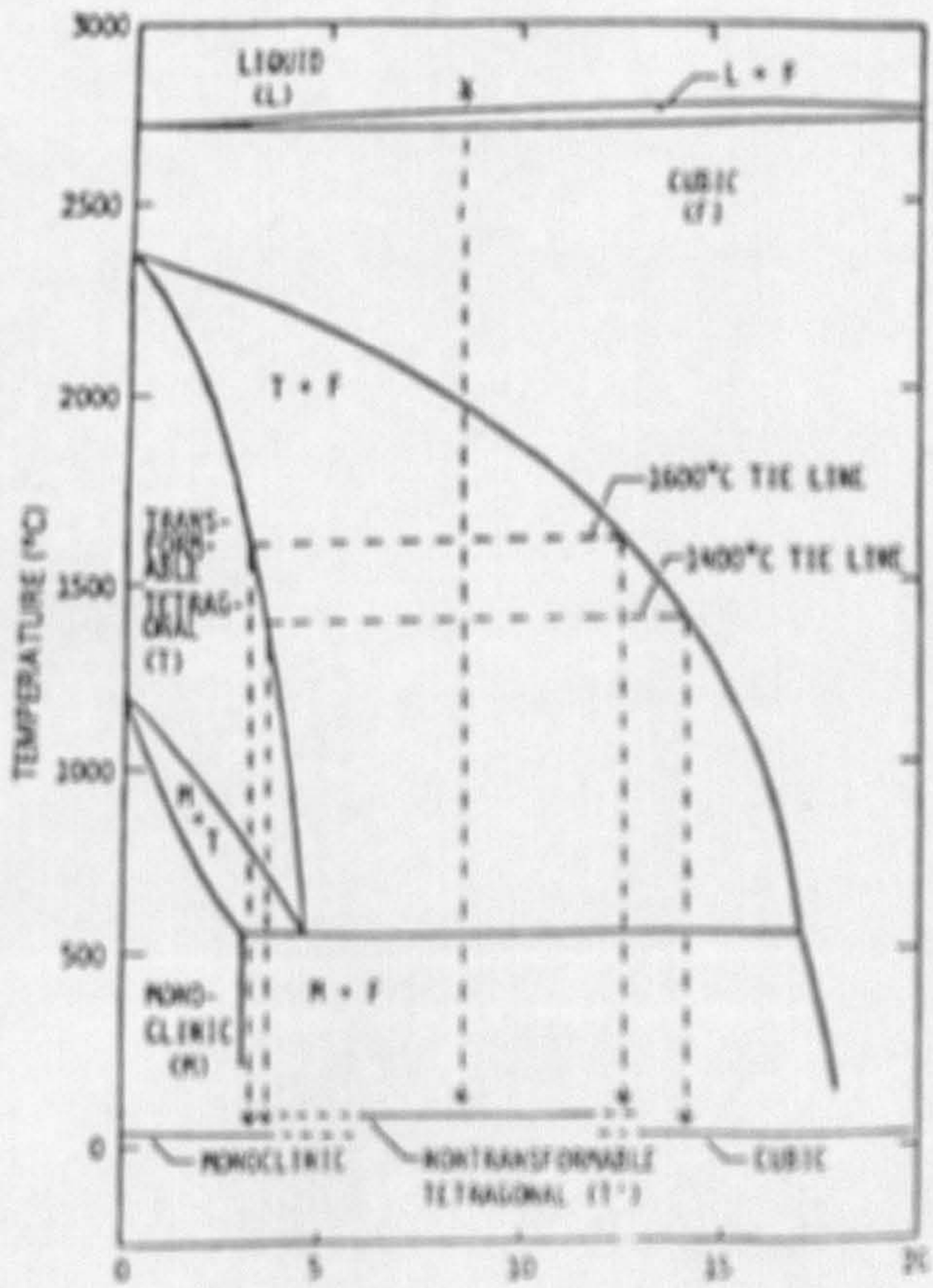

FIG. 187. ZIRCONIA/YTTRIUM PHASE DIAGRAM.

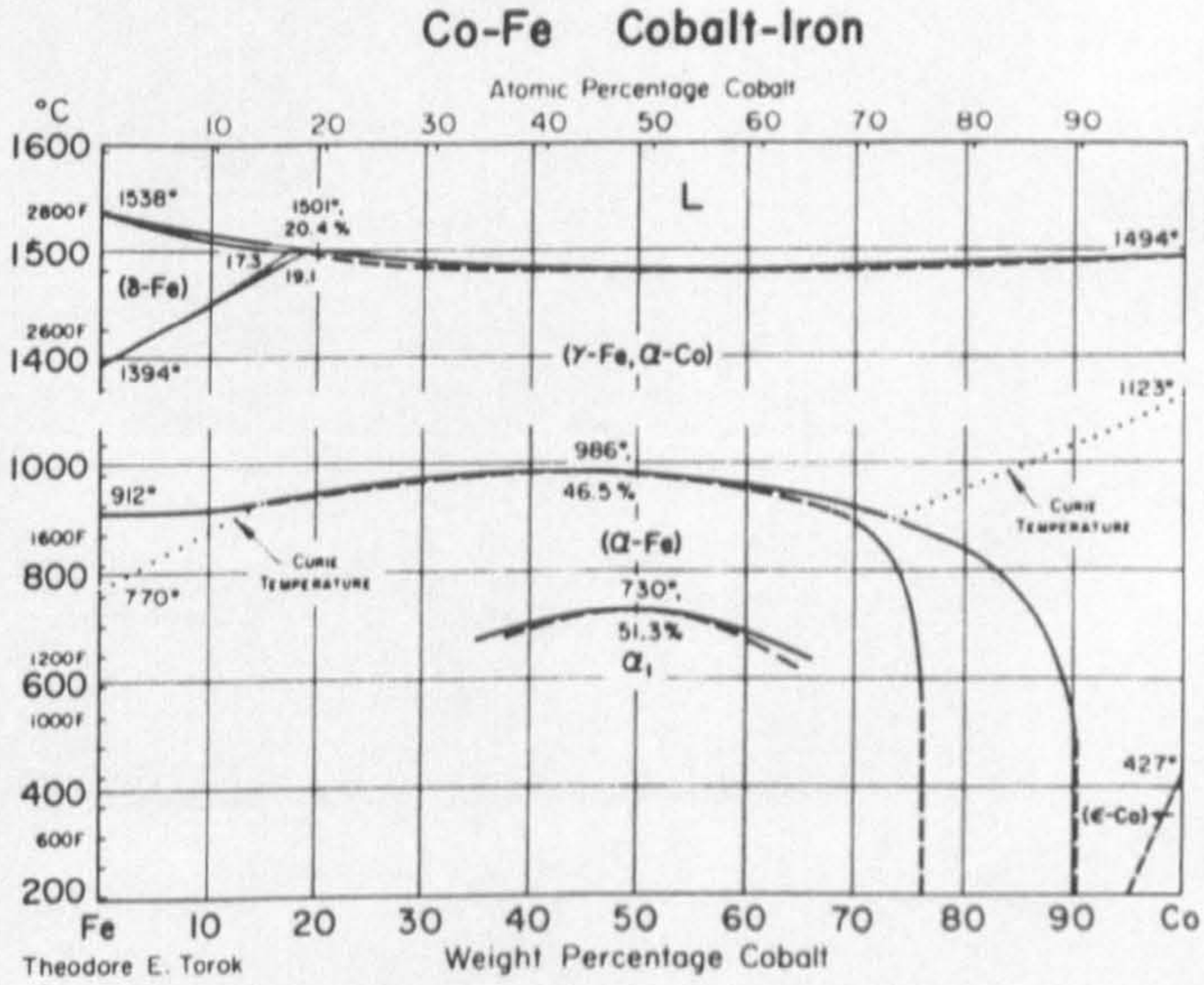

FIG. 188. IRON/COBALT PHASE DIAGRAM.

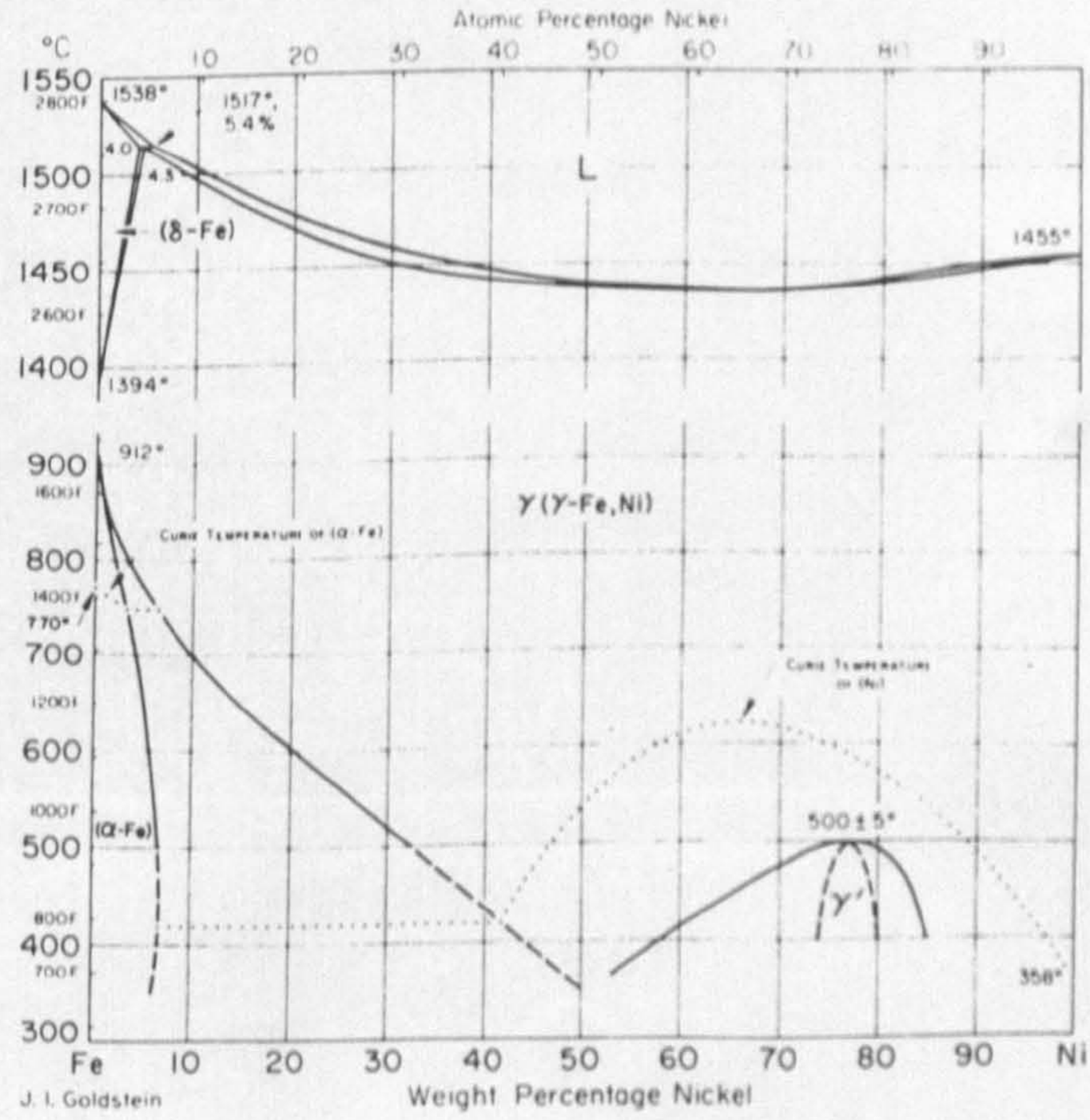

FIG. 189. IRON/NICKEL PHASE DIAGRAM.

```
>LIST
  232 MODE2 : *FX6,0
 1010 DIM GRAPHX(250) : DIM GRAPHY(250) : ARRAY=0 : M$=" "
 1020 PROCSTART
 1030 PRINT : PRINT "   CALL VARIABLES"
 1040 TEST = GET : IF TEST<>32 THEN 1040
 1050 MODE7
 1060 PRINT "Press RETURN after each entry"
 1070 VDU2 : PRINT : VDU1,27,64
 1080 INPUT "Date "V
 1090 INPUT "Test number "V
 1100 INPUT "Cam Material "V
 1110 INPUT "Follower Material "V
 1120 INPUT "Oil Type "V
 1130 INPUT "Oil Temp "V
 1140 INPUT "Test speed "V
 1150 INPUT "Test Duration "V
 1160 VDU3 : PRINT "Any additional information? "; :VDU2 : INPUT ""V
 1170 PRINT : PRINT "  Time     Oil C   Fir C  Friction u"
 1180 VDU1,27,65,8 : PRINT
 1190 VDU3
 1200 MODE2
 1210 PROCSTART
 1220 PRINT : PRINT "   START LOGGING"
 1230 PRINT : PRINT : PRINT "   *E TO END"
 1240 PRINT : PRINT "   *M FOR MARKER"
 1250 TEST = GET : IF TEST<>32 THEN 1250
 1260 MODE1
 1270 VDU23;8202;0;0;0;
 1280 VDU23,240,255,255,255,255,0,0,0,0
 1290 TM=TIME
 1300 VDU19,3,4,0,0,0 : COLOUR 129 : COLOUR 3
 1310 PRINT TAB(40)"";
 1320 PRINT "    Tribology of Overhead Cam Shafts    ";
 1330 PRINT"                                        ";
 1340 COLOUR 2
 1350 PRINT " Friction u";
 1360 COLOUR 0
 1370 PRINT "    Oil Temp   Follower temp ";
 1380 COLOUR 130 : COLOUR 1 : GCOL 0,129
 1390 FOR I=0 TO 11 : VDU240; : NEXT
 1400 VDU28,0,31,11,5 : VDU24,385;0;1279;895;
 1410 COLOUR 3 :CLS : CLG
 1420 REPEAT
 1430 T=TIME
 1440 PROCINPUT : PROCGRAPH : PROCPRINT : PROCOPTIONS
 1450 IF TIME-T<1000 THEN 1450
 1460 UNTIL TIME-TM>90000
 1470 REPEAT
 1480 T=TIME
 1490 PROCINPUT : PROCGRAPH : PROCPRINT : PROCOPTIONS
 1500 IF TIME-T<3000 THEN 1500
 1510 UNTIL TIME-TM>180000
 1520 REPEAT
 1530 T=TIME
 1540 PROCINPUT : PROCGRAPH : PROCPRINT : PROCOPTIONS
 1550 TI=TIME
 1560 IF TIME-TI<3000 THEN 1560
 1570 PROCGRAPH : PROCOPTIONS
 1580 IF TIME-T<90000 THEN 1550
 1590 UNTIL FALSE
 1600 END
 1620 DEF PROCSTART
 1630 COLOUR 130 : CLS
 1640 VDU23;8202;0;0;0;
 1650 PRINT : PRINT : PRINT
 1660 COLOUR 3
 1670 PRINT "  TRIBOLOGY GROUP"
 1680 PRINT : PRINT
 1690 COLOUR 1
 1700 PRINT "  Cam and Follower"
 1710 PRINT "  Rig Data logger"
```

APPENDIX 1. DATA LOGGING SYSTEM COMPUTER PROGRAM.

```
1720 PRINT : PRINT
1730 COLOUR 4
1740 PRINT "  Version 1.0 1984"
1750 PRINT
1760 COLOUR 15
1770 VDU28,0,31,19,12
1780 COLOUR 134 : CLS
1790 PRINT : PRINT : PRINT : PRINT
1800 PRINT " Press Space Bar To"
1810 ENDPROC
1820 DEF PROCINPUT
1830 FOR CHI=1 TO 4
1840 ACC=0
1850 FOR LOOP=1 TO 100
1860 ACC=ACC+ADVAL(CHI)
1870 NEXT
1880 ACC=ACC/1600
1890 IF CHI=1 THEN CH1=((ACC-1000)*0.025)/78
1900 IF CHI=2 THEN CH2=ACC*0.04+2.5
1910 IF CHI=3 THEN CH3=ACC*0.04+6.5 ELSE CH4=ACC*0.04
1920 NEXT
1930 ARRAY=ARRAY+1
1940 GRAPHY(ARRAY)=CH1*600+200
1950 GRAPHX(ARRAY)=(LOG((TIME-TM)/6000))*180+460
1960 IF GRAPHX(ARRAY) <460 THEN GRAPHX(ARRAY)=460
1970 @%=&20405 :COLOUR 3:PRINT TAB(3)CH1
1980 ENDPROC
1990 DEF PROCGRAPH
2000 HR=((TIME-TM) DIV 360000) MOD 24
2010 MIN=((TIME-TM) DIV 6000) MOD 60
2020 SEC=((TIME-TM) DIV 100) MOD 60
2030 VDU5 : GCOL 0,0 : CLG
2040 @%=&20105 : MOVE 480,880
2050 PRINT CH2;" C       ";CH3;" C"
2060 @%=&20002 : GCOL 0,0
2070 MOVE 450,100 : PRINT "Run Time ";HR;MIN;SEC;
2080 GCOL 0,3 : MOVE 450,800
2090 DRAW 1200,800 : DRAW 1200,200 : DRAW 450,200 : DRAW 450,800
2100 MOVE 450,180 : PRINT "1   10 Log Mins 1E3  1E4"
2110 GCOL 0,2
2120 MOVE 400,790 : PRINT "1"
2130 MOVE 400,530 : PRINT "u"
2140 MOVE 400,230 : PRINT "0"
2150 MOVE 460,GRAPHY(1)
2160 FOR DISPLY=1 TO ARRAY
2170 DRAW GRAPHX(DISPLY),GRAPHY(DISPLY)
2180 NEXT
2190 VDU4
2200 ENDPROC
2210 DEF PROCPRINT
2220 VDU2
2230 COLOUR 2
2240 DOT=CH1*575
2250 @%=&20000 :PRINT HR,MIN,SEC,;
2260 @%=&20108 :PRINT ,CH2,CH3,;
2270 @%=&20408 :PRINT CH1,M$;
2280 VDU1,27,1,76,1,63,1,2
2290 FOR I=0 TO DOT : VDU1,0 : NEXT
2300 VDU1,16,1,56,1,16
2310 FOR I=DOT TO 575 : VDU1,0 : NEXT
2320 PRINT :
2330 FOR I=1 TO 36 : VDU127 : NEXT
2340 VDU3
2350 ENDPROC
2360 DEF PROCOPTIONS
2370 M$=" "
2380 TEST=INKEY(10)
2390 IF TEST <> 42 THEN 2430
2400 TEST=INKEY(10)
2410 IF TEST = 77 THEN M$="*"
2420 IF TEST = 69 THEN PROCEND
2430 ENDPROC
2440 DEF PROCEND
2450 VDU2 : PRINT "END" : VDU3
2460 END
```

APPENDIX 1. DATA LOGGING SYSTEM COMPUTER PROGRAM.